Palaeomagnetic studies on rock formations in the High Atlas and Anti-Atlas regions of Morocco

NEWCASTLE UNIVERSITY LIBRARY

MS 084 10061 0 NR

A thesis submitted for the degree of

Doctor of Philosophy

at the

University of Newcastle upon Tyne

1972

BEST COPY

AVAILABLE

Poor text in the original thesis.
Some text bound close to the spine.
Some images distorted

I declare that non of the material contained in this thesis has previously been submitted for a degree at this, or any other University.



E.A. Hailwood

School of Physics

The University

Newcastle upon Tyne

Acknowledgements

I should like to thank my wife Vivienne for continual help and understanding during the preparations of this thesis. My sincere thanks are also due to Dr. D.H. Tarling for initiating the work, and for constant encouragement and guidance during the past three years, and to Mrs. M. Turner for sacrificing much of her spare time in order to type the manuscript.

I should like to thank Professor Runcorn for the use of the facilities of the School of Physics, and all members of the Geophysics Department with whom I have had helpful discussions at different times. In particular I should like to thank Dr. L. Molyneux for his interest and assistance in the work on asymmetrical alternating fields, Mrs. S. Hofmann for the use of her continental reconstruction computer programme, Mr. R. Thompson for kindly donating several rock samples for test purposes, and Mr. W.F. Mavor for his assistance with financial affairs.

My thanks are due to Mr. K. Sharp and the other members of the workshop staff, Mr. W. Rutherford, and to all other members of staff in the Computing Room, the Drawing Office and the General Office, for their assistance at various times over the past three years.

Finally I should like to thank Monsieur Ennadifi and other members of the Sérvice Géologique du Maroc, Mr. R.N. Gook and Mr. G.S. Hoye for assistance during the fieldwork in Morocco.

Financial assistance during the course of this work, from NERC and the Shell International Petroleum Co., is gratefully acknowledged.

Abstract

The first part of this thesis (Chapters 1 to 8) describes the results of palaeomagnetic studies on samples collected from the High-Atlas and Anti-Atlas regions of Morocco. New palaeomagnetic pole-positions are described from formations of Late Precambrian, Lower Cambrian, Devonian, Triassic, Jurassic and Cretaceous ages.

The new Moroccan Late Precambrian and Lower Cambrian poles are shown to be more consistent with reliable Lower Palaeozoic poles of the same age from North America than ones from Southeast Africa, when the two continents are plotted on a Bullard-type reconstruction. It is concluded that a small part of Northwest Africa, including Morocco, may originally have been attached to North America, and that the rest of Africa was widely separated from North America at that time. Collision between Africa and Eastern North America probably occurred during the Carboniferous period, resulting in the formation of the Hercynian fold-belts along the present-day North Atlantic margins of the two continents, and the welding of extreme Northwest Africa to the rest of the continent. Subsequent separation probably took place along a slightly different line, so that Morocco was left attached to Africa.

Radiometric dating results from Moroccan igneous intrusions paralleling the local coastline yielded a mean age of 183 my, i.e. Lower Jurassic. Other evidence suggests that the Mesozoic rifting between North America and Northwest Africa began at this time, and it is considered likely that the intrusion of the Moroccan Lower Jurassic igneous bodies was directly related to this event. Palaeomagnetic results from the Moroccan Cretaceous sediments indicate a gradual widening of the North Atlantic Ocean during the course of the Mesozoic.

There are no significant differences between mean Triassic, Jurassic and Cretaceous poles from Morocco, and corresponding poles from South-east and Central Africa, and it is concluded that no significant post-Triassic relative tectonic movement has occurred between North-west and South-east Africa.

The second part of the thesis (Chapters 9 and 10) describes an attempt at the AF demagnetisation of sediments by means of alternating fields of strengths up to 5000 Oe. Experiments were performed to investigate the effects of small asymmetries (up to 5%) in the waveform of the applied alternating field, and it was shown that asymmetries present in the natural AC mains supply at the Close House Laboratory at certain times of the day are sufficiently high to produce appreciable ARM's in rock samples, if no sample rotation system is used during the demagnetisation process.

Table of Contents

Part I : Palaeomagnetic results from Moroccan formations

		Page
Chapter 1.	**Introduction**	
1.1	Principal aims of research work undertaken for this thesis	1
1.2	Review of palaeomagnetic results from North Africa	1
1.3	Brief outline of the geology of Morocco	5
1.4	Collection and preparation of samples	7
1.5	Measurement of remanence	10
1.6	Stability tests	10
1.7	Other magnetic measurements	13
	1.7.1 Initial susceptibility	13
	1.7.2 Thermomagnetic analyses	14
1.8	Presentation and statistical treatment of results	17
	References	21
Chapter 2.	**Precambrian**	
2.1	Geology	
	2.1.1 Archaean	23
	2.1.2 Precambrian I	24
	2.1.3 Precambrian II	24
	2.1.4 Precambrian II-III	25
	2.1.5 Precambrian III	25
	2.1.6 Adoudounian	26
2.2	Location of sampling sites	27
2.3	NRM directions and intensities	28
2.4	Stability tests	29
2.5	Bulk demagnetisation	30
2.6	Thermomagnetic analyses and microscopic examination	31
2.7	Discussion	32
	References	38
Chapter 3.	**Cambrian**	
3.1	Geology	
	3.1.1 Identification of base of Cambrian	40
	3.1.2 Lower Cambrian	40
	3.1.3 Middle Cambrian	43
3.2	Location of sampling sites	44
3.3	Palaeomagnetic results from the Cambrian volcanic tuffs	
	3.3.1 NRM directions and intensities	44
	3.3.2 Stability tests	
	(a) Sites MB54 to 63	45
	(b) Sites MC18 to 23	46
	3.3.3 Bulk demagnetisation	46
	3.3.4 Thermomagnetic analyses and microscopic examinations	47
	3.3.5 Discussion	48
3.4	Palaeomagnetic results from the Cambrian red sediments	52
	References	

Page

Chapter 4. Devonian

4.1 Geology 55
4.2 Location of sampling sites 56
4.3 NRM directions and intensities 56
4.4 Stability tests 57
4.5 Bulk demagnetisation 58
4.6 Thermomagnetic analyses 59
4.7 Discussion 59
References 61

Chapter 5. Triassic

5.1 Geology
5.1.1 General sequence of Triassic deposits in Morocco 62
5.1.2 Distribution of Triassic deposits 63
5.1.3 Triassic igneous formations 63
5.2 Location of sampling sites 65
5.3 Palaeomagnetic results from the Ait Aadel dolerites
5.3.1 NRM directions and intensities 67
5.3.2 Pilot sample AF demagnetisation results 67
5.3.3 Bulk AF demagnetisation 68
5.3.4 Pilot sample thermal demagnetisation results 68
5.3.5 Bulk thermal demagnetisation 69
5.3.6 Thermomagnetic analyses 69
5.4 Palaeomagnetic results from the Issaldain dolerites
5.4.1 NRM directions and intensities 70
5.4.2 Pilot sample AF demagnetisation results 70
5.4.3 Bulk AF demagnetisation 71
5.4.4 Thermomagnetic analyses 72
5.5 Palaeomagnetic results from the Titchka sediments
5.5.1 NRM directions and intensities 72
5.5.2 Pilot sample thermal demagnetisation results 72
5.5.3 Bulk thermal demagnetisation 73
5.6 Palaeomagnetic results from the Oukaimeden sediments
5.6.1 NRM directions and intensities 74
5.6.2 Thermal demagnetisation results 75
5.7 Discussion 76
References 78

Chapter 6. Jurassic

6.1 Introduction 79
6.2 Geology
6.2.1 General Jurassic palaeogeography 79
6.2.2 Jurassic tectonic movements in the Central High Atlas 81
6.2.3 Jurassic igneous formations
(a) The Central Atlas Intrusives 81
(b) The Draa Valley Sills 82
(c) The Foum Zguid Dyke 82
6.2.4 Location of sampling sites 82

Page

6.3 Palaeomagnetic results from the Draa Valley sills
6.3.1 NRM directions and intensities 84
6.3.2 AF demagnetisation stability tests 84
6.3.3 Bulk AF demagnetisation 85
6.7.4 Thermomagnetic analyses and microscopic examinations 85
6.4 Palaeomagnetic results from the Foum Zgiud dyke
6.4.1 NRM directions and intensities 86
6.4.2 AF demagnetisation stability tests 86
6.4.3 Bulk AF demagnetisation 86
6.4.4 Thermomagnetic analyses 87
6.5 Palaeomagnetic results from the Central Atlas intrusives
6.5.1 NRM directions and intensities 88
6.5.2 AF demagnetisation stability tests 88
6.5.3 Bulk AF demagnetisation 89
6.5.4 Thermomagnetic analyses 89
6.6 Radiometric dating results 91
6.7 Discussion 91
References 95

Chapter 7. Cretaceous

7.1 Geology 96
7.2 Location of sampling sites 97
7.3 Palaeomagnetic results from the Infracenomanian red sandstones
7.3.1 NRM directions and intensities 97
7.3.2 Pilot sample demagnetisation results 98
7.3.3 Bulk thermal demagnetisation 98
7.4 Discussion 99
References 102

Chapter 8. Interpretation of results on a global scale

8.1 Introduction 103
8.2 The African polar-wander curve 104
8.3 Comparison of the African polar-wander curve with those of the other continents 107
8.3.1 Lower and Middle Palaeozoic 107
(a) Gondwanic continents 107
(b) Laurasian continents 110
(c) Comparison between Laurasian and Gondwanic Lower & Middle Palaeozoic polar-wander curves 112
8.3.2 Upper Palaeozoic 116
8.3.3 Mesozoic 117
(a) Separation of eastern North America from NW Africa 117
(i) Geological and other evidence 117
(ii) Palaeomagnetic evidence 119
(b) Separation of South America from Africa 122
(i) Geological evidence 122
(ii) Palaeomagnetic evidence 124
(c) Separation of Eastern Gondwanaland (India, Antarctica and Australia) from Africa 126
(i) Geological evidence 126
(ii) Palaeomagnetic evidence 127

Page

8.4 Polarities of Moroccan palaeomagnetic results 129
8.4.1 Palaeozoic 129
8.4.2 Mesozoic 130
8.5 Conclusions 131
References 132

Part II : Experiments on the alternating field demagnetisation of sediments, and investigations into the effects of asymmetries in the wave-form of the applied field

Chapter 9. The alternating field demagnetisation of sediments

9.1 The technique of A.F. demagnetisation 139
9.2 Theoretical treatment of AF demagnetisation
9.2.1 The Rayleigh laws 141
9.2.2 The Preisach diagram 142
9.2.3 Application to AF demagnetisation 145
9.3 Application of AF demagnetisation to sediments 146
9.4 Design of apparatus
9.4.1 General considerations 148
9.4.2 Design of coil 149
9.4.3 Practical details 153
9.4.4 Tuning of coil 154
9.4.5 Calibration 155
9.4.6 Field reduction mechanism 156
9.4.7 Performance of apparatus 157
9.5 Results of experiments on sediments 157
References 160

Chapter 10. Investigations into the effects of asymmetrical alternating fields on AF demagnetisation

10.1 Introduction 162
10.2 Measurement of asymmetry
10.2.1 Definition of percentage asymmetry 165
10.2.2 Asymmetry meter 167
10.2.3 Measurement of natural asymmetry of mains supply 169
10.2.4 Measurement of natural asymmetry in coil circuit 170
10.3 Production of artificial asymmetry 171
10.4 Attenuation of asymmetry by tuned coil circuit 172
10.5 Effect of varying asymmetry at constant peak field value 173
10.6 Effect of varying peak field value at constant asymmetry 175
10.7 Comparison between ARM's produced by asymmetry and by superimposed steady fields 177
10.8 Theoretical treatment of ARM's 180
10.9 Discussion of the peak-field equivalent of asymmetries 182
10.10 Conclusions 183
References 184

Abbreviations and symbols

The following is a short list of abbreviations and symbols used in this thesis.

N.R.M.	Natural remanent magnetisation
T.R.M.	Thermo-remanent magnetisation
C.R.M.	Chemical remanent magnetisation
A.R.M.	Anhysteretic remanent magnetisation
A.F.	Alternating field
D	Magnetic declination (measured in degrees E of N)
I	Magnetic inclination (regarded as positive downwards)
N	Number of samples averaged
R	Length of vector resultant of N unit remanence vectors
k	Precision parameter (Fisher, 1953)
α_{95}	Radius of 95 per cent confidence circle about mean direction
A_{95}	Radius of 95 per cent confidence circle about mean pole
σ_m	Standard error of mean
GT90	Greater than 90^o
G	Gauss
Oe	Oersted
γ	10^{-5} Oersted
M	Magnetic moment of sample
Mo	Magnetic moment of sample before A.F. or thermal treatment
J	Intensity of magnetisation of sample
Jo	Intensity of magnetisation of sample before AF or thermal treatment
My	Million years

N.B. In the bedding tilt corrections, the strike is given in degrees clockwise from North, and the dip in degrees from the horizontal, in a direction 90° clockwise from the strike.

Latitudes are denoted as positive, North; and negative, South, and longitudes as positive in degrees east of Greenwich, or negative in degrees west of Greenwich.

Part I

Palaeomagnetic results from Moroccan formations

CHAPTER 1 INTRODUCTION

1.1 Principal aims of research work undertaken for this thesis

The research work undertaken for this thesis had two main objectives. The first of these was to establish reliable palaeomagnetic pole-positions from North West Africa for as many different geological periods as possible. Since reliable palaeomagnetic results from North Africa were previously non-existent, it was considered important to obtain results which had world-wide as well as regional significance. Sampling was therefore confined as far as possible to the tectonically stable parts of Morocco. The results of this work are described and discussed in Part One of this thesis (Chapters 1 to 8).

The second main aim of this work was to design and construct equipment suitable for the A.F. demagnetisation of sediments. This required the production of alternating fields of at least 5000 Oe together with a mechanism for the smooth reduction of these fields to zero. This work led to a series of experiments concerning the response of different rock samples to asymmetrical alternating fields. The results of this work are described in Part Two of the thesis (Chapters 9 and 10).

1.2 Review of palaeomagnetic results from North Africa

During the last ten years a large amount of palaeomagnetic work has been carried out in East, Central and South Africa, but reliable palaeomagnetic results from the Northern and Western parts of this continent are virtually non-existent. This is surprising since the relationship between North West Africa and Europe is of considerable geological interest, and the unity of the

African continent throughout the whole of Phanerozoic time has yet to be firmly established, so that extrapolated results from South and East Africa are by no means unquestionably reliable. Furthermore, information concerning the separation of Western U.S.A. and Europe from N.W. Africa can be most reliably derived from a study of the previously adjacent portions of the original landmass. Reliable palaeomagnetic results from N.W. Africa are therefore likely to be of considerable interest in the study of the previous relationships of the major continents.

The first palaeomagnetic results from North Africa were obtained by Roche and Lepretre in 1955. These authors measured the natural remanent magnetisations (N.R.M.s) of sixty-one oriented samples of Tertiary and Quaternary lavas from the Ahaggar Massif in South Eastern Algeria. The Quaternary samples were all basalts, and the Tertiary samples included basalts, phonolites and trachytes.

The Tertiary samples yielded highly scattered directions of remanence, but the Quaternary samples, collected from six different sites in two volcanic series, showed fairly good grouping about a mean direction

$$D = 345^{\circ},\ I = 32^{\circ},\ \text{with}\ \alpha_{95} = 14^{\circ}$$

The scatter of the Tertiary directions of remanence is presumably due to secondary magnetisation, but partial demagnetisation cleaning techniques were not applied to these samples.

A gap of ten years followed before further palaeomagnetic results were published from North African rock formations. This work was carried out by Helsley (1965), who collected samples from two series of basic lava flows reported as being interbedded in the Middle

Cambrian sediments exposed in East Central Morocco. The first series gave widely scattered directions of remanence of reversed polarity, which clustered after partial A.F. demagnetisation. The samples from the second series were initially all of normal polarity, but partial A.F. demagnetisation caused two samples to reverse in polarity and become part of the reversed polarity group of the first series. A.F. demagnetisation produced no significant change in the directions of remanence of the other samples from the second series. The mean values of the normal and reversed groups differed by 6^{o}, and the virtual geomagnetic pole-positions calculated from the overall mean direction of remanence is 53^{o}N, 34^{o}E. Unfortunately this work was published only as an abstract, and details of the exact number of samples collected, the demagnetising fields at which scatter was reduced, the amount of scatter, and the exact locality and stratigraphic position of the sites are not known. The reliability of this result is therefore uncertain.

In anticipation of the more detailed survey described in this thesis, and to enable the planning of this work to include the most-suitable rock formations, a palaeomagnetic reconnaissance survey was carried out in Morocco by Tarling and Sutton (1967). Samples were collected from as great a range of time and area as possible, but only a few sites were samples in each formation. The authors found variable, but mostly good stability using thermal and A.F. demagnetising techniques, but generally poor agreement between directions of remanence in different samples from the same site, and different sites from the same formation. Three features of these results were considered to be significant. The first of these

is the general low inclination of the remanence directions. Such values are consistent with the remanences having been acquired in latitudes similar to, or slightly lower than the present latitude of Morocco, assuming a geocentric axial dipole field. The second feature is that 'reversals' of magnetisation were absent from all of the results. Finally, the direction of the Precambrian and Lower Cambrian remanence corresponds with a pole situated in the extreme East Central Pacific Ocean. This is contrary to results of this age obtained from other parts of Africa.

Following this reconnaissance survey, a more detailed survey was carried out by Hailwood (1968) in the Middle Atlas fold belt of Central Morocco. Forty one sites were sampled, thirteen of these being in Mesozoic sediments, twelve in Triassic dolerites and basalts, and sixteen in Quaternary basalts. All of the sediments were found to exhibit stability effects similar to those reported by Tarling and Sutton, and further study of these effects suggested that the sediments were unlikely to yield meaningful ancient pole-positions. Nine out of the twelve sites situated in Triassic dolerites and basalts were also rejected, because of high instability indicated by partial demagnetisation tests, and excessive between site scatter. Results from the remaining three sites appeared to indicate a post-Triassic rotation of the Middle Atlas region with respect to the rest of Africa.

Twelve out of the fifteen sites in Quaternary lavas were regarded as being sufficiently stable to yield a meaningful palaeomagnetic pole position, and results from these sites are consistent with a 15^{o} clockwise rotation of Africa during the last one million years.

1.3 Brief outline of the geology of Morocco

Morocco can be sub-divided into three distinct tectonic units, formed during three separate orogenic cycles (Choubert 1956). These units extend across the country in an E-W direction, and are referred to as the Rif Domain, the Atlas Domain and the Anti-Atlas Domain respectively (Fig 1.1). The three belts form a chronological sequence, the oldest lying to the south and the youngest to the north, and they appear to represent a progressive northward growth of the African continent since Precambrian times. During each successive cycle a thick sequence of sediments was laid down along the northern margin of Africa, and these were subsequently folded, granitised, uplifted, and finally embodied into the pre-existing continent.

The Anti-Atlas Domain is the oldest of these belts, and was formed by the deposition of a great thickness of geosynclinal sediments, followed by their folding and granitisation, during the late Precambrian. During the Palaeozoic era a thinner sequence of sediments was deposited over most of this region, but subsidence continued in the less-rigid NW part (the Sub Atlas synclinal zone). During the Hercynian orogeny (extending over most of the Carboniferous period) these cover rocks were crumpled, the fold-axes following local pre-existing basement fold-directions, and the region was uplifted to form a gigantic bulge which remained above sea-level during subsequent transgressions. This bulge was sufficiently strong to resist folding during the Alpine orogeny, and it has remained a permanent part of the African continent since this time.

The Anti-Atlas Domain is separated from the Atlas Domain by the prominent structural line of the South Atlas Fault. In the Atlas domain the effects of only two orogenic cycles are apparent, the Hercynian and the Alpine cycles, and the effects of the former are much more pronounced in this region than in the Anti-Atlas belt.

During the Palaeozoic era, while thin shallow-water sediments were being deposited in the relatively stable region to the South, a thick sequence of geosynclinal sediments were deposited in the Atlas domain. Folding of these sediments, and emplacement of granites occurred during the Hercynian orogeny, but the effects were less intense and more localised than those of the Precambrian orogeny in the Anti-Atlas belt. These characteristics seem to have determined the subsequent history of the region. During the Alpine lithogenesis (i.e. the Mesozoic and early Tertiary eras) the more rigid, partially granitised and metamorphosed zones remained emergent or were covered by a thin series of neritic deposits, whereas a thick sequence of limestones and marls was deposited in the weaker semi-plastic zones.

During the Alpine orogeny the latter zones were folded and uplifted to form the Middle- and High-Atlas fold-mountain belts, whereas the former zones remained relatively stable, undergoing only vertical uplift or depression.

In the Rif domain thick sequences of geosynclinal sediments were deposited during the Mesozoic and Tertiary eras, and during the Miocene were thrust southwards on to the African foreland to form a series of gigantic nappes. These overlie the autochthonous

Atlas structures, and mask the effects of earlier tectonic phases except where these have been exposed by subsequent erosion.

1.4 Collection and preparation of samples

The foregoing section indicates that samples collected from the Rif domain are likely to have undergone large-scale translations and rotations. Palaeomagnetic results from such samples may give information concerning the magnitude and nature of these displacements, and would therefore be of local interest, but they are unlikely to give results applicable to NW Africa or the African continent as a whole. The same argument applies to samples collected from the less-stable zones of subsidence and folding of the Atlas domain, e.g. the High and Middle Atlas fold belt, but the intervening more rigid and stable areas, e.g. the Moroccan and Oran Mesetas (Fig 1.1) may have escaped major tectonic movement.

The Anti-Atlas domain was not affected by post-Hercynian movements, and reliable post-Carboniferous palaeomagnetic results from this area will therefore have a regional rather than a local significance. Conversely pre-Carboniferous palaeomagnetic results from this area may reflect effects of Hercynian orogenesis and this must be taken into account in their interpretation.

Despite the latter qualification, the Anti-Atlas domain seems to offer the best prospects for obtaining palaeomagnetic results of more than local significance, and collection of samples was therefore concentrated in this region. Further advantages of this area are that rock-types suitable for palaeomagnetic work, viz red sandstones and basic igneous rocks, are relatively abundant, and that the Palaeozoic deposits are generally flat-lying or gently folded, whereas in the rest of Morocco they are intensely folded.

Although the bulk of sampling was carried out in the Anti-Atlas belt, some relatively undisturbed Mesozoic samples were collected from the High Atlas belt. Results from these samples were found to be in general agreement with those from the Anti-Atlas belt. Samples were collected during the course of two three-month field trips, in 1969 and 1970. In most cases sampling was performed by means of a portable gasoline-powered coring drill, or a portable heavy-duty electric drill. The latter was powered by a Kangol 2 KVA diesel generator mounted in a trailer. Water for cooling and lubrication purposes was drawn from a 30 gallon tank mounted in the trailer and was supplied by an electric pump powered from the generator. A 100 ft. length of water hose and power cable was found to be sufficient for sampling at most sites; where sampling had to be carried out at greater distances from the trailer a portable 1 gallon pressure-can was used.

Between four and six separately oriented cores, 2.5 cm in diameter and 15 to 20 cm in length were collected at each site. In the case of sedimentary formations sites were generally situated at least one foot apart in the stratigraphic sequence so that a sufficiently long time interval ($> 10^4$ years) could be sampled to allow the averaging out of secular variation effects.

In the case of thick igneous intrusions, sites were selected at intervals of several metres across the intrusion. It has been shown by Jaeger (1957) that a section through such an intrusion may provide a continuous record of the secular variation during the migration of the Curie temperature isotherm from the margin to the centre. The sampling scheme adopted should therefore at least partially average out the effects of secular variation.

In the case of single lava flows or thin igneous intrusions only one site was sampled in each flow or dyke, since in such a rock unit the time taken to cool through the range of blocking temperatures will be of the order of a year, and the field variations during such a period are likely to have been small. In order to average out the effects of secular variation a sequence of such rock units was sampled wherever possible.

Orientation of the cores was performed by means of the orientation table described by Hailwood (1968), and both magnetic and sun-compass bearings were taken. These usually agreed to within 1^{o} to 2^{o}, but occasional discrepancies of up to 8^{o} were observed. These were generally associated with very strongly magnetised rocks which apparently disturbed the magnetic compass bearings. Such local strong magnetic fields usually occurred at sites which were suspected of having been struck by lightning.

The advantages of field-drilling over the collection of oriented hand samples have been discussed elsewhere, e.g. Embleton (1966), and Helsley (1967). Although most of the sites were sampled by this method, occasionally, as in the case of the highly indurated Triassic red sediments, it was necessary to resort to the collection of hand-samples. The method used for collection and orientation of these samples is described by Hailwood (1968). Three separately oriented hand-samples were collected at each site, and three 2.5 cm diameter cores were subsequently drilled from each of these hand samples in the laboratory, yielding a total of nine cores per site.

Where formations had been tilted or folded, measurements were taken of the amount and direction of dip at each site so that the directions of magnetisation could be subsequently referred to the original horizontal. This also permitted the application of the 'fold-test' of stability outlined by Graham (1949).

In all cases one specimen, 2.5 cm in length, was cut from the lower portion of each core, where the effects of weathering were likely to be minimal, and this was used for measurements of remanence. The remainder of the core was used for thermomagnetic experiments, thin-section and reflection microscopic examinations etc.

1.5 Measurement of remanence.

All measurements of magnetic remanence were made on a PAR Model SM2 spinner magnetometer. This instrument is situated in the non-magnetic Nuffield Palaeomagnetic Laboratory at Close House, on the outskirts of Newcastle and remote from possible distrubances due to motor traffic, industrial machinery and other sources.

The basic igneous rocks sampled had intensities ranging from 10^{-1} to 10^{-4} gauss and these could be measured, using a 1 second time constant, to an accuracy of half a degree in an average time of 3 minutes per sample. The intensities of the acid volcanic rocks and red sediments ranged from 10^{-5} to 10^{-6} gauss, and a time constant of 10 secs. and occasionally 30 secs. was necessary to measure these to a comparable degree of accuracy. The average time of measurement of these weaker samples was 10 minutes per sample.

1.6 Stability tests

It is important in palaeomagnetic studies that the rock samples measured should be shown to have a sufficient degree of stability to be capable of retaining components of magnetisation over long periods of geological time. Furthermore it must be shown that the original primary component of remanence has not been replaced or swamped by a secondary component produced at

some later geological time, for example by heating or chemical weathering, and that the effects of magnetic anisotropy are negligible.

Only then can the direction of remanence carried by the rocks be taken with confidence to represent the direction of the geomagnetic field at the sampling locality at the time for formation of the rocks.

The most commonly used laboratory technique for testing the stability of remanence of rock samples is progressive partial demagnetisation. During such treatment stable components of remanence remain nearly constant in direction, whilst unstable components change continuously. The presence of an unstable secondary component superimposed on a more-stable primary component can be identified by a continuous change in direction as the unstable component is preferentially removed. When only the stable component remains the direction will stay constant and further treatment will result only in a decrease of intensity.

Two different methods of partial demagnetisation have been used; these are alternating field (A.F.) demagnetisation and thermal demagnetisation. The principles of these techniques have been described elsewhere (e.g. Thellier and Rimbert, 1954 and 1955, and Irving, 1961), & the alternating field technique is dealt with at length in Chapter 9 of this thesis.

As discussed in Chapter 9, the typical low coercivities of basic igneous rocks render them suitable for treatment by standard A.F. demagnetisation techniques. However the high coercive fields of sediments and acid igneous rocks are difficult to achieve with conventional A.F. demagnetisers, and in most cases the thermal technique is more effective in the treatment of these rock types.

The basic igneous rocks collected in Morocco were therefore subjected to partial A.F. demagnetisation, one pilot-sample from each site being treated at intervals of 75 to 100 Oe up to a maximum peak field of at least 500 Oe. The apparatus used was similar in design to the high-field apparatus described in Chapter 9. It was operated from the same power supply, and used the same field-reducing mechanism. However, unlike the latter apparatus, a three-axis specimen rotation system was used, so that all directions in the specimen could be demagnetised simultaneously. This system was not feasible for the high-field equipment because the limitations on the internal diameter of the demagnetising coil left insufficient room for the rotation mechanism.

The stability of the Moroccan acid igneous rocks and sediments was investigated by subjecting one pilot-sample from each site to progressive thermal demagnetisation, using the apparatus described by Stephenson (1967). Recent modifications to this equipment include a refined Helmholtz-coil system for the cancellation of the Earth's field at the centre of the furnace, and a Eurotherm solid-state temperature control unit, capable of maintaining extremely stable temperatures for long periods of time.

The pilot-sample results were examined to establish the alternating field value or temperature at which progressive changes in direction of remanence ceased, or at which within-site dispersion was a minimum. The remaining samples from each site were then treated at the appropriate field-value or temperature.

1.7 Other magnetic measurements

1.7.1 Initial susceptibility

The initial susceptibility, x, of a substance is defined as the intensity of magnetisation produced by unit applied magnetic field. In palaeomagnetic work the susceptibility per unit volume, or "volume susceptibility" of rock samples is of interest, and this is expressed as the induced moment in unit field per cm^3. The volume susceptibility depends on the amount and type of magnetic material present in the sample.

One of the main problems associated with the testing of stability of remanence by partial thermal demagnetisation is the possibility of chemical changes, e.g. oxidation of magnetite to haematite, occurring as a result of heating samples to temperatures of several hundred degrees centigrade. Since the susceptibility of rocks is very sensitive to changes in the nature and amount of the magnetic constituents, measurements of susceptibility after each increment in temperature will reveal the occurrence of such chemical changes. For this reason the susceptibility of the pilot-samples subjected to thermal demagnetisation was measured before heating, and then after each increment in temperature. The instrument used was the susceptibility bridge described by Collinson and Molyneux (1967) and built by de Sa and Noltimier.

This instrument consists basically of a balanced bridge circuit of coils wound on two ferrite rings, each with an equal air gap. Interaction between fields induced by the coils wound on each of the rings is eliminated by mounting them with their axes perpendicular to each other. Each ring carries a primary coil, and a split secondary coil with an equal number of windings either side of the air gap. The secondary coils are connected in series

opposition, and are adjusted so that when the primary coils are excited by a low frequency oscillator the outputs of the two secondary coils balance each other so that there is no net output. Ferrite and alloy trimmers situated near one of the gaps allow fine adjustment of this balance. Insertion of a rock sample into the other gap alters the reluctance of the gap and unbalances the bridge circuit. The amount of unbalance is proportional to the susceptibility of the sample, and the resultant signal from the secondary coils is amplified and read on an output meter.

The instrument is calibrated before use by placing a standard sample of accurately known susceptibility in the gap, and adjusting the gain of the amplifier so that the output meter gives the total susceptibility directly in units of gauss per oersted.

1.7.2 Thermomagnetic analyses

In thermomagnetic analyses the magnetisations of samples are measured continuously as the temperature is gradually increased to a maximum (usually of about 720°C) and then decreased again. As the Curie temperature of the magnetic constituents of a rock is approached, so the magnetisation drops off rapidly. At the Curie temperature of a particular mineral the net magnetisation in grains of that mineral is zero.

The Curie temperature measured in a rock sample depends therefore on the particular mineral species present. The two major magnetic constituents of rocks, magnetite and haemetite, have appreciably different Curie temperatures (580°C and 675°C respectively for pure compositions), so that in principle the presence of either

of these minerals can be identified by thermomagnetic analyses. In practice however the magnetic minerals are rarely pure magnetite or haemetite, but members of the two solid-solution series magnetite-ulvospinel and haemetite-ilmenite. The Curie temperatures of members of these two series overlap each other so that a unique magnetic mineral composition cannot always be deduced from thermomagnetic analysis alone, and information from the latter must be interpreted in conjunction with other observations, particularly microscopic examinations.

The most commonly used instrument for thermomagnetic analysis is the Curie balance, and two different versions of this instrument were used for investigating the Moroccan rocks. The principle of these instruments is the measurement of the force exerted on a specimen situated in an inhomogeneous magnetic field. This field gradient is produced by situating the sample in the fringing field of a high-power electromagnet.

The first instrument was an automatic translation balance, described by Creer and de Sa (1970), and this was used for measurements on the relatively strong igneous samples. In this instrument about 70 mg. of crushed rock powder is placed in a small quartz container attached to a beam. The latter is suspended horizontally, and is free to move only along the direction of its axis. The specimen is gradually heated by means of an element surrounding the quartz container, and the resulting change in magnetisation produces a change in the force acting on the sample. This is detected by a capacitance sensing device, and compensation is effected by a feed-back mechanism which produces a voltage proportional to the force. The voltage is fed to one channel of an XY recorder, while the other

channel records the temperature of the sample. This instrument is quick and convenient to use, and is ideal for routine measurements on strong igneous samples.

A more sensitive vertical torsion balance built by D.W. Collinson was used for the weaker red sediments and acid igneous rocks. In this instrument the specimen is situated at the lower end of a vertical suspension, and is surrounded by a cylindrically wound electric heating element. The upper end of the suspension is attached to a balance beam, pivoted about a horizontal torsion wire, and a restoring force is applied to the opposite end of the beam by means of two vertical soft-iron pole pieces, surrounded by vertical coils. As the specimen is heated the change in magnetisation alters the force acting on it due to the field gradient. As with the automatic translation balance the change in force is detected by a capacitance sensing device, and the corresponding compensation current, supplied by a feedback mechanism to the vertical coils, is passed through a standard resistance and monitored on a milli-voltmeter. In this instrument readings of the compensation voltage were taken manually at 20°C intervals, and these were subsequently plotted against the temperature. During heating the sample was kept at a temperature of 50 to 100°C for approximately half an hour to drive off any water present, so that subsequent changes in the vertical force exerted on the sample would be due only to changes in magnetisation, and not to loss of weight by evaporation of water.

1.8 Presentation and statistical treatment of results

The directions of magnetisation obtained from individual cores for each site were combined to give the mean site directions using a method developed by Fisher (1953). According to Fisher's analysis the best estimate of the true mean direction of N individual directions is given by the vector sum of the N individual directions. The declination, Dm, and the inclination, Im, of the mean direction are then given by:

$$\tan Dm = \frac{\sum_{n=1}^{N} m_i}{\sum_{n=1}^{N} l_i} \qquad (1.1)$$

and

$$\sin Im = \frac{\sum_{n=1}^{N} n_i}{R} \qquad (1.2)$$

where (l_i, m_i, n_i) are the direction cosines of the i th direction, with declination Di and inclination Ii, regarded as a unit vector. They are given by $l_i = \cos I_i \cos D_i$, $m_i = \cos I_i \sin Di$,

$$n_i = \sin I_i \qquad (1.3)$$

and

$$R^2 = \left(\sum_{n=1}^{N} l_i\right)^2 + \left(\sum_{n=1}^{N} m_i\right)^2 + \left(\sum_{n=1}^{N} n_i\right)^2 \qquad (1.4)$$

A measure of the scatter of individual directions about the mean direction is given by various statistical parameters. The most commonly used of these is the radius of the circle of 95% confidence (α_{95}). This is the semi-angle of the cone whose axis is the estimated mean direction, and within which there is a 95% probability of the true mean direction occurring. It is given by

$$\alpha_{95} = \frac{140}{(kN)^{\frac{1}{2}}} \text{ degrees} \qquad (1.5)$$

for large values of k and N, k being the precision parameter, given by

$$k = \frac{N - 1}{N - R} \qquad (1.6)$$

The circle of confidence is useful for comparing two mean directions, each having an associated error. If the circles do not intersect, the two mean directions may be considered to be significantly different. If the circles overlap a further test is required (Watson 1956).

A second frequently used statistical parameter is the Circular Standard Deviation (c.s.d.). This gives the radius of the circle whose centre is the true mean, and which contains 63% of the individual directions. It is given by

$$\text{c.s.d.} = 81\ k^{-\frac{1}{2}} \text{ degrees} \qquad (1.7)$$

The statistical treatment outlined above was used both for combining individual core directions giving unit weight to each, to find the mean site direction; and also for combining individual mean site directions from a particular formation to find the mean formation direction. This seemed to be the best procedure since each site represented effectively a spot reading in time of the geomagnetic field; and within-site scatter of directions will be due mainly to orientation errors and varying secondary components of magnetisation. The latter will also be an important element in between-site scatter, together with effects of secular variation of the geomagnetic field.

If partial demagnetisation procedures are successfully applied then the component of dispersion of directions due to varying secondary components of remanence will be reduced or eliminated. Combining the individual core directions from each site, giving unit weight to each should minimise the scatter in the mean-site direction due to orientation errors, so that the remaining scatter in the mean-formation direction should be due principally to secular variation.

Further sources of error which might contribute to scatter of directions are anisotropy effects in igneous rocks (e.g. Uyeda et al, 1963), inclination and compaction errors in sediments (e.g. Griffiths et al., 1957), and errors in the estimation of the original horizontal. The latter is likely to be most important in massive igneous rocks in which horizontal stratifications are absent and recourse has to be made to measurements on adjacent strata.

When the mean direction of magnetisation for each formation had been obtained, it was convenient for interpretation purposes to calculate the corresponding palaeomagnetic pole-positions, assuming an axial dipole field model. The validity of this assumption is discussed elsewhere (e.g. Irving, 1964).

If the direction of remanence obtained from a rock formation is specified by the declination, D, reckoned clockwise from true north, and inclination, I, reckoned as positive downward, and the mean locality of the collecting sites has a latitude of λ degrees and a longitude of ϕ degrees, then the coordinates (λ' , ϕ') of the palaeomagnetic pole position are given by:

$$\text{Sin } \lambda' = \sin \lambda \cos p + \cos \lambda \sin p \cos D \qquad (1.8)$$

where $(-90^\circ \leq \lambda' \leq 90^\circ)$

and $\phi' = \phi + \beta$

$$\text{for } \cos p \geqslant \sin \lambda \sin \lambda' \qquad (1.9)$$

or $\phi = \phi + 180 - \beta$

$$\text{for } \cos p < \sin \lambda \sin \lambda'$$

In these equations p is the palaeomagnetic colatitude, given by

$$2 \cot p = \tan I$$

and β is given by

$$\sin \rho = \sin p \sin D / \cos \lambda'$$

$$(-90 \leqslant \rho \leqslant 90)$$

The uncertainty in the position of the palaeomagnetic pole (λ' , ϕ') can be specified by an oval of 95% confidence, analagous to the circle of 95% confidence around the corresponding mean direction of magnetisation.

References

Choubert, G, 1956. Les grands traits de la géologie du Maroc. Introduction to the Lexique Stratigraphique International, Vol IV, fascicule 1a.

Collinson, D.W., and L. Molyneux, 1967. An instrument for the measurement of isotropic initial susceptibility of rock samples. Methods in Palaeomagnetism. Elsevier Pub. Co.

Creer, K.M., and A. de Sa., 1969. An automatic translation balance for recording variation of magnetisation. J. Phys. E; Sci. Instr. Vol. 3.

Embleton, B.J.J., 1966. M.Sc. Thesis. University of Newcastle upon Tyne.

Fisher, R.A., 1953. Dispersion on a sphere. Proc. Roy. Soc. London A, 217, 295-305.

Graham, J.W., 1949. The stability and significance of magnetism in sedimentary rocks. J. Geophys. Res., 54, 131-167.

Griffiths, D.H., R.F. King, and A.E. Wright, 1957. Some field and laboratory studies of the depositional remanence of recent sediments. Phil. Mag. Supp. Adv. Phys. 6, 306- 316.

Hailwood, E.A., 1968. A palaeomagnetic study of the Middle Atlas region of Morocco. M.Sc. Thesis, University of Newcastle upon Tyne.

Helsley, C.E., 1965. Palaeomagnetic results from the Middle Cambrian of N.W. Africa (abstract) Trans. A.G.U., 46, 67.

Helsley, C.E., 1967. Advantages of field drilling of samples for palaeomagnetic work. Methods in Palaeomagnetism. Elsevier Pub. Co.

Irving, E., P.M. Stott, and M.A. Ward, 1961. Demagnetisation if igneous rocks by alternating magnetic fields. Phil. Mag., 6, 225-241.

Irving, E., 1964. Palaeomagnetism and its application to geological and geophysical problems. Wiley.

Jaeger, J.C., 1957. The temperature in the neighbourhood of a cooling intrusive sheet. Amer. J. Sci., 255, 306-318.

Roche, A., and B. Leprêtre, 1955. Sur l'aimantation de roches volcaniques de l'Ahaggar, C.R. Acad. Sci. Paris, 240, 2002-2004.

Stephenson, A., 1967. Apparatus for thermal demagnetisation by the progressive method. Methods in Palaeomagnetism, Elsevier Pub. Co.

Tarling, D.H., and D.H. Sutton, 1967. Palaeomagnetic stability results of a reconnaissance survey of red sandstones in Morocco. Phys. Earth Planet Interiors, 1, 35-43.

Thellier, E., and F. Rimbert, 1954. Sur l'analyse d'aimantations fossiles par action de champs magnétiques alternatifs. C.R. Acad. Sci., Paris, 239, 1399-1401.

Thellier, E., and F. Rimbert, 1955. Sur l'utilisation en palaeomagnetism, de la désaimantation par champs alternatifs. C.R. Acad. Sci., Paris, 240, 1404-1406.

Uyeda, S., M.D. Fuller, J.C. Belshe, and R.W. Girdler, 1963. Anisotropy of magnetic susceptibility of rocks and minerals. J. Geophys. Res., 68, 279-291.

Watson, G.S., 1956. Analysis of dispersion on a sphere.Mon. Nat. Roy. Astr. Soc, Geophys. Supp., 7, 153-159.

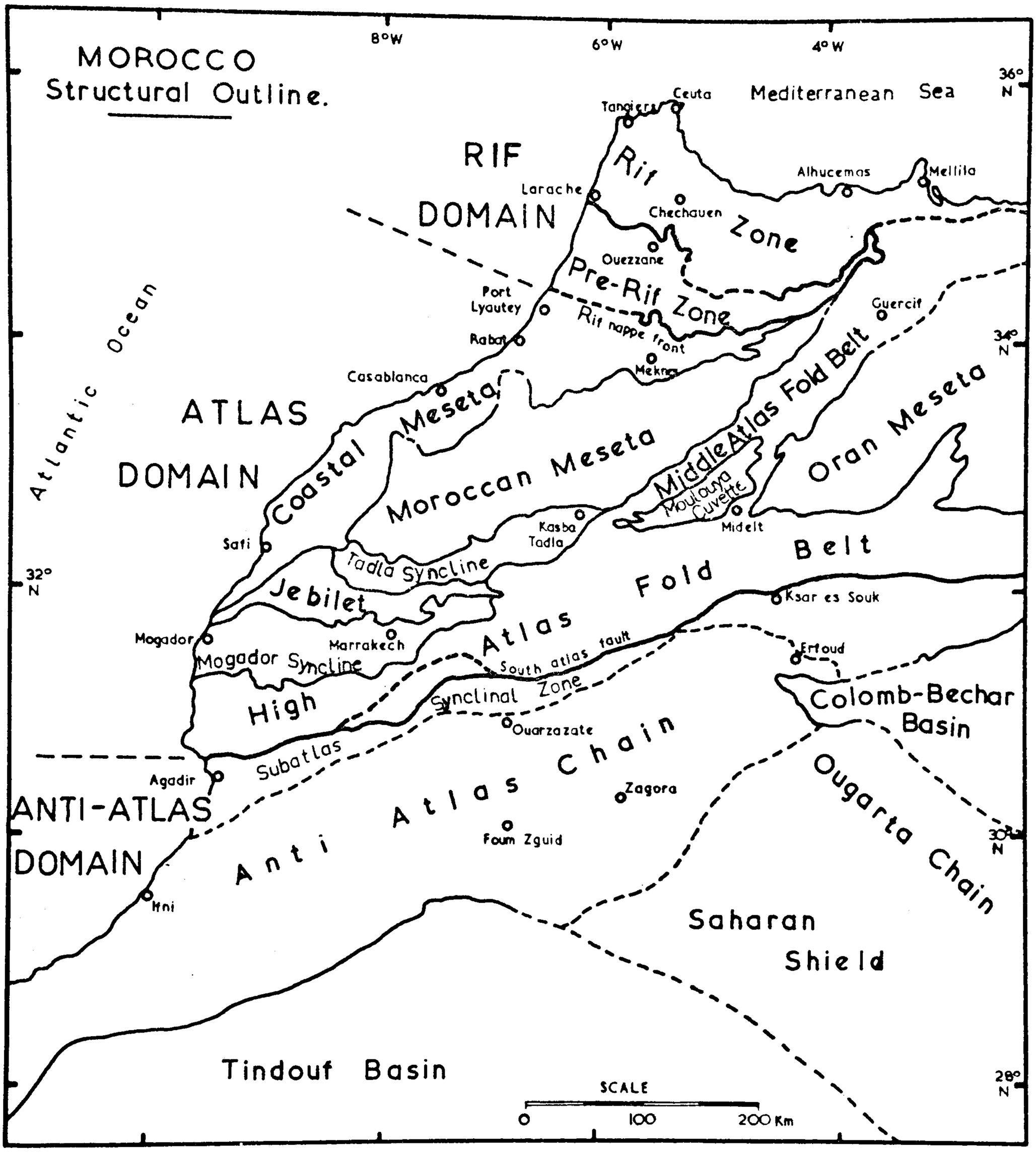


Fig 1.1 Principal structural elements of Morocco.

CHAPTER 2. PRECAMBRIAN

2.1 Geology and location of sampling sites

The Precambrian of the Anti-Atlas region of Morocco has been subdivided into five different systems (Choubert 1963), representing five successive geological cycles. These are:

1. Archaean (Precambrian 0)
2. Precambrian I
3. Precambrian II
4. Precambrian II-III
5. Precambrian III
6. Adoudounian (Infracambrian)

Samples were collected only from the Precambrian III, but a brief geological summary will be given of the whole Precambrian sequence. This will assist in evaluating the palaeomagnetic results in the context of the general Precambrian palaeogeographic and palaeoclimatologic environment, and also in assessing the suitability of the rest of the Moroccan Precambrian sequence for future palaeomagnetic work.

2.1.1. The Archaean

This system includes the oldest formations known in Morocco, and is comprised essentially of orthogneiss of variable facies containing recrys tallised potassium falspars. The mineral assemblage is characteristic of the high temperature and pressure condition of katazone metamorphism. Outcrops are confined to two Precambrian inliers (Bou Azzer and El Graara) in the axial part of the Anti-Atlas chain.

2.1.2. The Precambrian I

The Archaean rocks are overlain discordantly by the lower members of the Precambrian I system. A basal level of shales is followed by crystalline limestones and a complex series of basic and acid volcanics, followed in turn by a very thick series of locally migmatised shales. Outside the migmatitic zones the mineral assemblage is characteristic of mesozone metamorphism (high temperature and hydrostatic pressure, and intense stress). This sequence was subjected to two periods of granite intrusion. The first of these was closely associated with the migmatisation, and included calc-alkaline granites, whereas the second was characterised by alkaline granites and a network of leucocratic injections and pegmatites. These two episodes of granite intrusion were separated by an important period of intrusion of basic and ultrabasic rocks, especially serp entinites.

2.1.3. The Precambrian II

This system is comprised essentially of quartzites, followed by a thick series of shales of flysch-type facies. Limestones, sometimes containing micro-organisms (oolites) and basic flows, often occur at the base of the system. The intensity of metamorphism corresponds generally to that of the epizone (sericito-schists) although locally it reaches the mesozone. The orogenic belt established during the Precambrian II forms the main underlying framework of the present day Western Anti-Atlas. The exact extent of the magmatism which accompanied the folding of this belt is as yet uncertain, but there were at least two periods of granite intrusion, alternating with two episodes of basic vulcanicity.

2.1.4. The Precambrian II-II

The orogenic belt forming this system was originally regarded as part of the Precambrian II system, but has recently been identified as a separate sedimentary and orogenic cycle (Choubert 1963). In the NE Anti-Atlas the principal term of this series is a thick sequence of shales and sandstones of flysch facies (the Lizate series). Elsewhere it is preceded by a felspathic sandstone and arkose series (the Tidiline series), which includes rhythmic formations and pebbly shales. These have been interpreted as varves and tillites, and indicate a glaciation of the Anti-Atlas region during Precambrian II-III times (Choubert 1963). The base of the series comprises varied conglomerates accompanied by rhyolites and andesites, and in the south a continental facies is developed, including conspicuous pink and red sandstones and conglomerates.

This was the last major Precambrian orogenic cycle, and although regional metamorphism was feeble or non-existent, local granite emplacement was important. This was complex, and included calc-alkaline granites, alkaline granites and quartz diorites. The largest granitic area of Morocco, the Eastern Bloc of the High Atlas massif (the Ouzellarh promontary) is of this age.

2.1.5. The Precambrian III

The Precambrian III and Adoudounian together correspond to the interval of time between the last major Precambrian orogenic cycle and the appearance of the first Cambrian trilobite fauna. The Precambrian III is essentially a continental and volcanic series, whereas the Adoudounian is predominantly marine.

The Precambrian III differs in nature, attitude and facies from both the true Precambrian and the Palaeozoic. It corresponds

to the Katangan system, which is interposed between the Precambrian shield and the generally tabular Palaeozoic cover elsewhere in Africa. The Adoudounian forms part of the cover, and is distinguished from the overlying Palaeozoic series only by its lack of fossils.

The Precambrian III is characterised by a very thick, predominantly rhyolitic, volcanic series, associated with continental formations, conglomerates, sandstones, mudstones and stromatolitic calcareous lenses. The total thickness is variable, and locally reaches several thousands of metres. Local minor tectonic movements are evident, and successive volcanic complexes are separated by local weak discordances. Two of these are more important, apparently marking widespread palaeogeographic changes, and allow the separation of the Precambrian III into three stages:

1. The Lower Precambrian III, in which andesites are predominant and rhyolites subordinate.
2. The Middle Precambrian III, in which rhyolites are well developed, and andesites appear only as thin intercalations. Occasional continental deposits occur, including lacustrine sediments in the form of stromatolitic calcareous lenses.
3. The Upper Precambrian III, in which continental formations predominate. These appear to have been deposited in closed synclinal basins, and lacustrine limestones bearing remains of Collenia appear locally. Volcanic activity was less important, and is represented mainly by alkaline rhyolites and porphyritic andesites.

2.1.6. The Adoudounian

This system is weakly discordant on the Precambrian III and the basal series was deposited during a widespread marine transgression, which covered most of the Anti-Atlas region. This was followed

by the deposition of the "Lower Limestone" dolomitic series, which attains a local thickness of more than 2000 metres, and contains stromatolites (Collenia). The first sedimentary phase ended with a widespread regression, during which a continental formation, the "Lie de Vin" series was deposited. A conspicuous feature of this series is the frequence of ripple marks, mudcracks and pseudomorphs after salt, often occurring in plates of hardened mudstone and intercalations of limestone and dolomite. This series appears to have been deposited on a vast flood-plain, extending along the margin of a warm ocean, and submerged alternately by continental floodwater and marine incursions. It was followed by a second transgression, during which the "Upper Limestone" series was deposited, with a total thickness of some 1000 metres. A relatively important volcanic episode began during the Lower Adoudounian and continued intermittently throughout the Adoudounian and into the Lower Cambrian.

2.2. Location of sampling sites

Several of the sedimentary formations described above appear to be suitable for palaeomagnetic work, particularly the continental deposits of the Precambrian II-III, the Precambrian III, and the Adoudounian. However results of Tarling and Sutton (1967) from these rocks indicate generally poor magnetic stability and high scatter of remanence directions both before and after thermal treatment. It was therefore decided to concentrate on igneous formations.

The rock-types represented in the Archaean system are generally unsuitable for palaeomagnetic work, and although basic and acid volcanic rocks occur in the Precambrian I and Precambrian II system, they are usually highly deformed and metamorphosed, and were thought

unlikely to carry a primary remanence. However the thick series of rhyolites and andesites of Precambrian III age are generally undeformed and fresh in appearance, and eight sites were therefore sampled at the two localities in the Middle Precambrian III sequence of the Bou Azzer-Ouarzazate region (Fig. 2.1). One of these sites (MB70) was in an andesite dyke cutting a series of rhyolitic lavas, and two other sites (MB69 and MB71) were in the lavas immediately adjacent to the dyke and on either side of it. The other five sites were in different lava flows.

2.3. N.R.M. directions and intensities

The mean N.R.M. directions for the eight Precambrian sites are plotted in Fig. 2.2(a). Within-site scatter is variable, the values of α_{95} ranging from 5° to 19° (Table 2.5(a)). The mean-formation direction of remanence, giving unit weight to each site, and after correction for tilting, is

$$D = 117^{\circ}, \quad I = +56.5^{\circ}, \quad \alpha_{95} = 23^{\circ}$$

The value of α_{95} before correction for tilting (22°) is not significantly different from the value after correction. Three of the site mean directions (MB65, MB67 and MB70) are slightly displaced from the fairly close group formed by the other five sites. One of these (MB70) is the site situated in the andesite dyke, but the two sites situated in the baked lavas at the contact with the dyke (MB69 and MB71) form part of the main group.

The mean intensity of N.R.M., assuming a log-normal distribution is 4.87×10^{-6} gauss, and the mean susceptibility is 8.32×10^{-6} gauss per oersted.

2.4. Stability tests

One pilot sample, selected at random from each of the eight sites, was subjected to progressive thermal demagnetisation up to a maximum temperature of between 525°C and 700°C. The resulting changes in direction of remanence are plotted in Fig. 2.3, and intensity in Fig. 2.4.

In all cases except sample MB65.6 this treatment resulted in a progressive movement towards a shallow SE direction. In most samples, after initial changes of 20° to 40°, the direction of remanence remained approximately constant during heating from 200°C to at least 400°C, and sometimes up to 640°C. In sample MB65.6 the remanence vector moved in a SW direction on heating up to 175°C, after which it remained constant on further heating up to 550°C. In most samples heating at 640°C produced a further small change in direction of remanence, and heating at 700°C produced a large, apparently random change.

The intensities of magnetisation of pilot sample from sites MB65 to MB67 remained fairly constant on heating up to 640°C, sometimes after initial drops at 100°C. The intensities of pilot samples from sites MB64 and MB68 to MB71 began to decrease progressively at 100°C to 300°C, and in all cases heating at 700°C resulted in a drop to less than 10% of the initial intensity (Fig. 2.4).

During progressive demagnetisation the susceptibilities either remained constant or decreased slightly. No important chemical changes are therefore thought to have occurred as a result of heating.

The pilot-sample results indicate the presence of a stable component of remanence, having a shallow SE direction in all sites except MB65.6, in which it has a shallow SW direction. In all cases a less-stable secondary component is also present, and is removed by partial thermal demagnetisation at 200°C. The stable component is itself demagnetised at 640°C in some samples and 700°C in others, and the remaining magnetisation appears to have a random direction and a very low intensity. This agrees with the observations of several authors (e.g. As and Zijderveld, 1958, and Irving et al, 1961), who have noted the presence of residual magnetic moments with random directions in rocks which have been subjects to severe demagnetisation. These residual moments are thought to represent states of minimum magnetic energy (Irving, 1964).

2.5. Bulk demagnetisation

In order to remove the unstable secondary component of remanence detected in the pilot samples, all of the remaining samples were treated at 325°C. This value was selected as it lay approximately in the middle of the stable range. This treatment had a variable effect on the within-site dispersion of directions (Table 2.5(b). The value of α_{95} increased for two of the sites (MB64 and 65), but decreased for the other six, in some cases by a substantial amount.

The mean site directions of magnetisation after treatment at 325°C are plotted in Fig. 2.2(b). The mean formation direction after correction for tectonic tilting, and giving unit weight to each site, is

$$D = 128.5, \quad I = +10.0, \quad \alpha_{95} = 17^{\circ}$$

The value of α_{95} before correction for tilting is 20°.

It is difficult to judge whether the difference of 3° is significant, but if it is, then it implies that the stable component of magnetisation predates the (probably Carboniferous) folding of the rocks (Graham 1949), and quite possibly dates from their time of initial formation, i.e. late Precambrian.

Bulk thermal demagnetisation at 325°C resulted in a decrease in the mean intensity of magnetisation of the formation to 3.86×10^{-6} gauss.

There was no systematic difference between the mean site directions of the andesite dyke and the two sites in its baked contact with the lavas, compared with the other five sites in the lavas.

2.6. Thermomagnetic analyses and microscopic examination

Thermomagnetic analyses were carried out on crushed samples from four sites, viz MB64, MB69, MB70 and MB71. The thermomagnetic curves are either completely, or very nearly reversible (Figs.2.5 and 2.6), and in all cases a single Curie Point is indicated, in the range 650 to 700°C. This temperature is characteristic of haemetite. The blocky nature of most of the curves is consistent with the presence of a single magnetic phase with a narrow range of composition and grain size (Larson et al, 1968). Sample MB64.3 is particularly interesting, as the magnetisation decreases only very slightly on heating to 650°C, after which it suddenly drops to zero.

Microscopic examination of polished sections under reflected light revealed haematite as the only opaque mineral present, in agreement with the thermomagnetic analyses. A large number of

small grains were present, just visible under a X45 objective, and also several larger aggregates of crystals sometimes having apparently replaced ferromagnesian silicates (probably olivine). There was no sign of exsolution in any of the haemetite crystals observed.

2.7. Discussion

The palaeomagnetic pole position calculated by the method outlined in Section 1.8 of this thesis, corresponding to the mean Precambrian direction of magnetisation after bulk demagnetisation at 325°C and correction for tectonic tilting is

$$\text{Lat} = 30.5^{\circ}\text{S}, \quad \text{Long} = 57.0^{\circ}\text{E}, \quad A_{95} = 17^{\circ}$$

To enable comparison of this result with other Precambrian palaeomagnetic data from Africa it is important to establish the age of the formation as precisely as possible. This has been discussed by Choubert (1963).

All radiometric age determinations published so far on the Precambrian III of the Anti-Atlas region have been obtained by the K-Ar method, and these analyses have given ages in the range 392 to 215 my, reflecting effects of argon loss during the Hercynian orogeny.

The Rb-Sr method has been applied by Cahen et.al (1963) to samples from the Archaean and Precambrian I systems, and has yielded realistic values of 2600-1800 my for the Archaean, and 1670-1460 my for the Precambrian I.

This method is currently being applied to the Precambrian II and III, but until the results become available only approximate limits can be placed on the ages of these systems. The Precambrian III postdates the last Precambrian Anti-Atlas orogeny, and predates the base of the Adoudounian.

Choubert (1963) has correlated the last Anti-Atlas orogeny with the Kibara-Urundi-Karagwe-Muva-Ankola orogeny of Central Africa, which has been fairly reliably dated at about 1000 my (Holmes and Cahen, 1957). The overlying Adoudounian is separated from the Precambrian III by a discordance, thought to be contemporaneous with the Katangan orogeny of Central Africa. The date of this orogeny has been reliably established from radiometric measurements on the Katangan uraninites as 620 my. This is supported by K-Ar measurements on galena deposits in the Upper Adoudounian of the Western High Atlas, which give an age of 600 $\pm$ 70my.

Lower and upper limits of 1000 my and 620 my respectively can therefore be placed on the age of the Precambrian III system. Assuming an equal period of time for each of the three subdivisions of this system, the approximate limits of the Middle Precambrian III will be 750 to 870 my. An approximate age of 800 my can therefore be assigned to the samples collected, although this value may be in error by up to 100 my.

Unfortunately no palaeomagnetic results have yet been published for the interval between 1300 my and 600 my from other parts of Africa, but it is instructive to compare the Moroccan Precambrian pole with the results available for the interval 2000 to 1300 my. These results have been obtained from the Transvaal and Rhodesian shields, and are summarised by McElhinny et al (1968). They are listed in Table 2.6, and plotted in Fig. 2.7, together with the Moroccan Precambrian pole. The latter pole lies on a direct continuation of the polar-wander path plotted by McElhinny et al., and this may be taken as evidence in support of the validity of the Moroccan pole.

Although palaeomagnetic results covering the interval 1300 to 600my have not yet been published from other parts of Africa, work is currently in progress on rocks from the Bukoban system of East Africa. This system spans the interval from 1000 to 800 my, and is practically contemporaneous with the Moroccan Precambrian III system. Preliminary results (Dr. J.D.A. Piper, personal communication) yield a series of poles extending in a chronological sequence from the Central Atlantic to Mexico and then down to Peru. The pole lying closest to the Moroccan Precambrian III pole corresponds to an age of approximately 900 my, but is separated from the latter by an angular distance of some 40°.

Pending publication of Piper's results the reliability of the Bukoban poles is uncertain. However, if, as seems likely, they should turn out to be at least as reliable as the Moroccan pole, then this difference must be accounted for. Of the several possible factors which could influence the agreement of these results, two seem to be more likely.

The first is the possible occurrence of relative tectonic movement during the late Precambrian between the Anti-Atlas belt and the Saharan shield, or between the whole of the NW African craton and the East African craton. Movement between the Anti-Atlas belt and the Saharan shield at this time is unlikely, since the last major Precambrian orogenic phase in this region ended at about 1000 my. However the possibility of movement between the NW African and East African cratons cannot be completely ruled out.

The second factor is the possible effects of Hercynian orogenesis, as discussed in Section 1.3 and 1.4. Regional heating and deep burial during orogenesis may result in the original primary

components of remanence in rocks being replaced by stable secondary components. It has been demonstrated above that radiometric age determinations on the late Precambrian rocks of the Anti-Atlas region were affected by the Hercynian orogenesis, and it is possible that the remanent magnetism of these rocks may also have been affected. The palaeomagnetic pole position derived from this formation (30.5°S, 57.0°E) lies close to the Upper Carboniferous-Lower Permian pole (40°S, 64.5°E), and this is consistent with a remagnetisation of this formation during the (Carboniferous) Hercynian orogeny. Furthermore, the polarity of the magnetisation in the Moroccan Precambrian rocks is reversed, in agreement with the polarity of Upper Carboniferous and Permian formations from other parts of Africa (Opdyke, 1964 and McElhinny and Opdyke, 1968).

The fact that there is no systematic difference between the direction of remanence in the andesite dyke and its baked contacts, compared with the direction in the intruded lavas, even though there is clearly an age difference between these two rock units, may be due to "homogenisation" of the remanence in both units by later remagnetisation. However it is equally plausible that the difference in age of the two units is small, and that no significant "polar-wander" or continental movement occurred during this interval of time.

It has been observed by some authors (e.g. Chamalaun and Creer, 1964, and Chamalaun, 1964) that thermal demagnetisation at temperatures just below the Curie point of haemetite (670°C) sometimes reveals a primary component of remanence in rocks which have been severely remagnetised. The Moroccan Precambrian pilot-sample results were

therefore inspected to see if any common direction of magnetisation was revealed in different samples as a result of demagnetisation at 640°C to 700°C. No such component of remanence was detected.

The strongest evidence supporting the validity of the Moroccan Precambrian III pole-position is that correction for tilting reduces the between-site scatter, thereby implying that the time of magnetisation predates the time of folding. However, as discussed in Section 2.5, too much significance must not be attached to this, since the difference is only 3° in 17°, i.e. 16%.

Since two-thirds of the Anti-Atlas Precambrian III sequence is represented by volcanic rocks, and one-third by continental deposits, there is little direct evidence regarding the palaeoclimatic environment under which these rocks were formed. It can be stated with confidence that the glacial environment under which the Precambrian II-III tillites and varves were deposited had ceased to prevail by Precambrian III times, since there is no evidence of glacial deposits or structures in this sequence. The exact palaeoclimatic significance of the lacustrine sediments and thin stromatolitic limestones of the Precambrian III sequence is difficult to assess, but it is more probable that these were associated with a warm environment than with a cold one. There is little doubt that the thick dolomitic limestones, fossilised mudcracks and pseudomorphs after salt, of the overlying Adoudounian sequence were formed in a warm, possibly tropical or near-equatorial environment.

The palaeolatitude, λ , calculated from the mean palaeomagnetic inclination, I, of the Precambrian III rocks, from the formula

$$\text{Tan } I = 2 \tan \lambda \qquad (2.1)$$

is 5°, i.e. near equatorial, and is not at variance with the above remarks.

In conclusion it may be said that the fold-test and palaeoclimatic evidence seem to support the Moroccan Precambrian III pole-position, but reasons exist for doubting its validity, in particular the evidence of possible remagnetisation during the Hercynian orogeny.

The reliability of the Moroccan Precambrian results are discussed further, in conjunction with the Lower Cambrian results in Chapter three.

References

As, J.A. and J.D.A. Zijderveld, 1958. Magnetic cleaning of rocks in palaeomagnetic research. Geophys. J., 1, 308-319.

Cahen, L., G. Choubert and D. Ledant, 1963. Premiers résultats géochronologiques sur le Précambrien de l'Anti-Atlas (Sud-marocain) par la méthode strontium-rubidium. C.R. Acad. Sci. Paris, T 257

Chamalaun, F.H., 1964. Origin of the secondary magnetisation of the Old Red Sandstones of the Anglo-Welsh Cuvette. J. Geophys. Res., 69, 4327-4337

Chamalaun, F.H., and K.M. Creer, 1964. Thermal demagnetisation studies on the Old Red Sandstone of the Anglo-Welsh Cuvette. J. Geophys. Res., 69, 1607

Choubert, G. 1963. Histoire Géologique du Précambrien de l'Anti-Atlas. Notes et Mémoires du Service Géologique du Maroc. No.162.

Gough, D.I. 1956. A study of the palaeomagnetism of the Pilansberg dykes. Monthly Notices Roy.Astron. Soc., Geophys. Suppl.7,196-213

Gough, D.I., and C.B. van-Niekerk, 1959. On the palaeomagnetism of the Bushveld gabbro, Phil. Mag., 4, 126-136

Graham, J.W., 1949. The stability and significance of magnetism in sedimentary rocks. J. Geophys. Res., 54, 131-167

Holmes, A. and L. Cahen, 1957. Géochronologie africaine 1956. Résultats acquis au 1er juillet 1956. Mém. Ac. R. Sc. Col., Brussels 1957 (n.s.), 5, 1, 169pp

Irving, E., P.M. Stott, and M.A. Ward, 1961. Demagnetisation of igneous rocks by alternating magnetic fields, Phil. Mag., 6, 225-241.

Irving, E., 1964. Palaeomagnetism and its application to geological and geophysical problems. Wiley & Sons, New York.

Jones, D.L. and M.W. McElhinny, 1966. Palaeomagnetic correlation of basic intrusions in the Precambrian of southern Africa, J. Geophys. Res., 71, 543-552

Jones, D.L., 1968. A palaeomagnetic study of the Premier Mine Kimberlite, J. Geophys. Res. 73, No.22, 6937-6943

Larson, E., Mituko Ozima, Minoru Ozima, T. Nagata and D. Strangway, 1968. Stability of Remanent Magnetisation of Igneous Rocks. Geophys. J.R. astr. Soc., 17, 263-292

McElhinny, M.W., and N.D. Opdyke, 1964. The palaeomagnetism of the Precambrian dolerites of eastern Southern Rhodesia, an example of geologic correlation by rock magnetism. J. Geophys. Res., 69, 2465-2475

McElhinny, M.W. 1966. The palaeomagnetism of the Umkondo lavas, eastern Southern Rhodesia. Geophys. J. 10, 375-381

McElhinny, M.W., J.C. Briden, D.L. Jones and A. Brock, 1968. Geological and Geophysical Implications of Palaeomagnetic Results from Africa. Rev. Geophys. Vol. 6, No. 2.

McElhinny, M.W., and N.D. Opdyke, 1968. Palaeomagnetism of some Carboniferous glacial varves from central Africa. J. Geophys. Res., 73, 689-696.

Nicolaysen, L.O., J.W.L. de Villiers, A.J. Burger and F.W.E. Strelow, 1958. New measurements relating to the absolute age of the Transvaal system and of the Bushveld igneous complex. Trans. Geol. Soc. S. Africa, 61, 137-163

Opdyke, N.D. 1964. The palaeomagnetism of the Permian redbeds of southwest Tanganyika, J. Geophys. Res., 69, 2477-2487

Tarling, D.N., and D.H. Sutton, 1968. Palaeomagnetic stability results of a reconnaissance survey of red sandstones in Morocco. Phys. Earth Planet. Interiors 1, 35-43

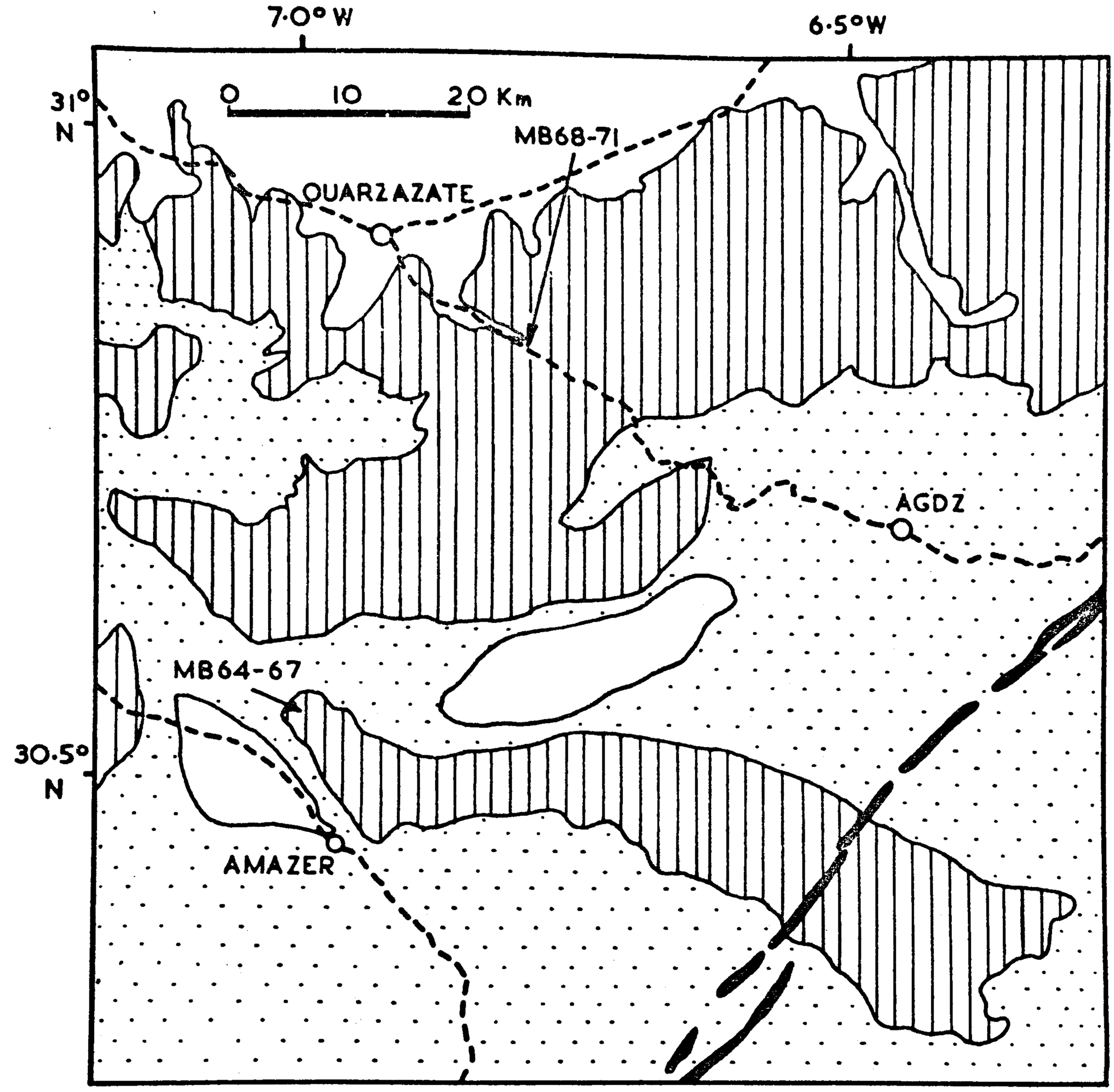


Fig 2.1 Outline geological map of the Ourzazate region, showing distibution of major outcrops of Precambrian rocks, and locations of sampling sites.

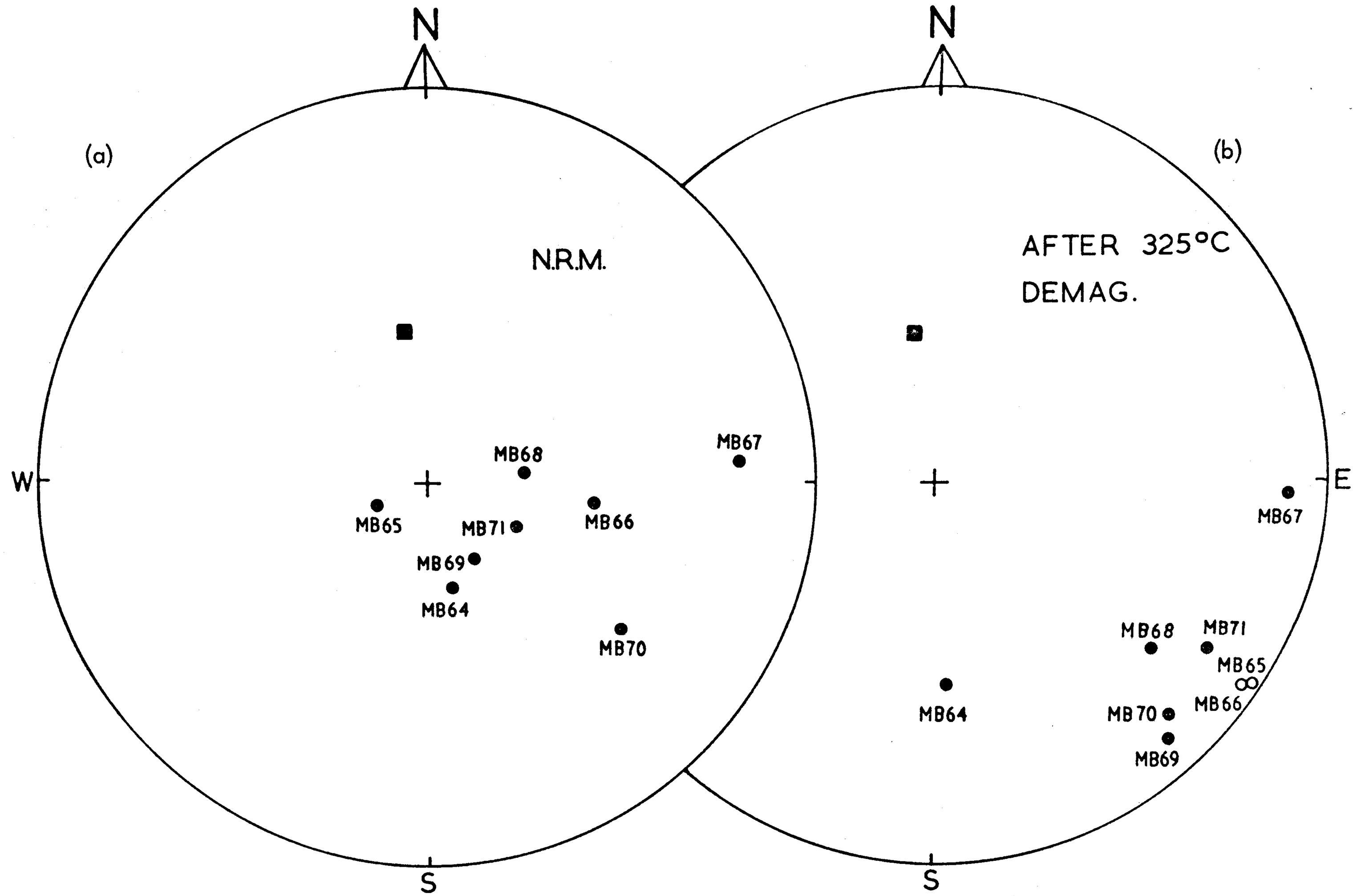


Fig 2.2 Precambrian mean site directions of magnetisation plotted on stereographic projections. (a) N.R.M. (b) After partial demagnetisation at 325° C.

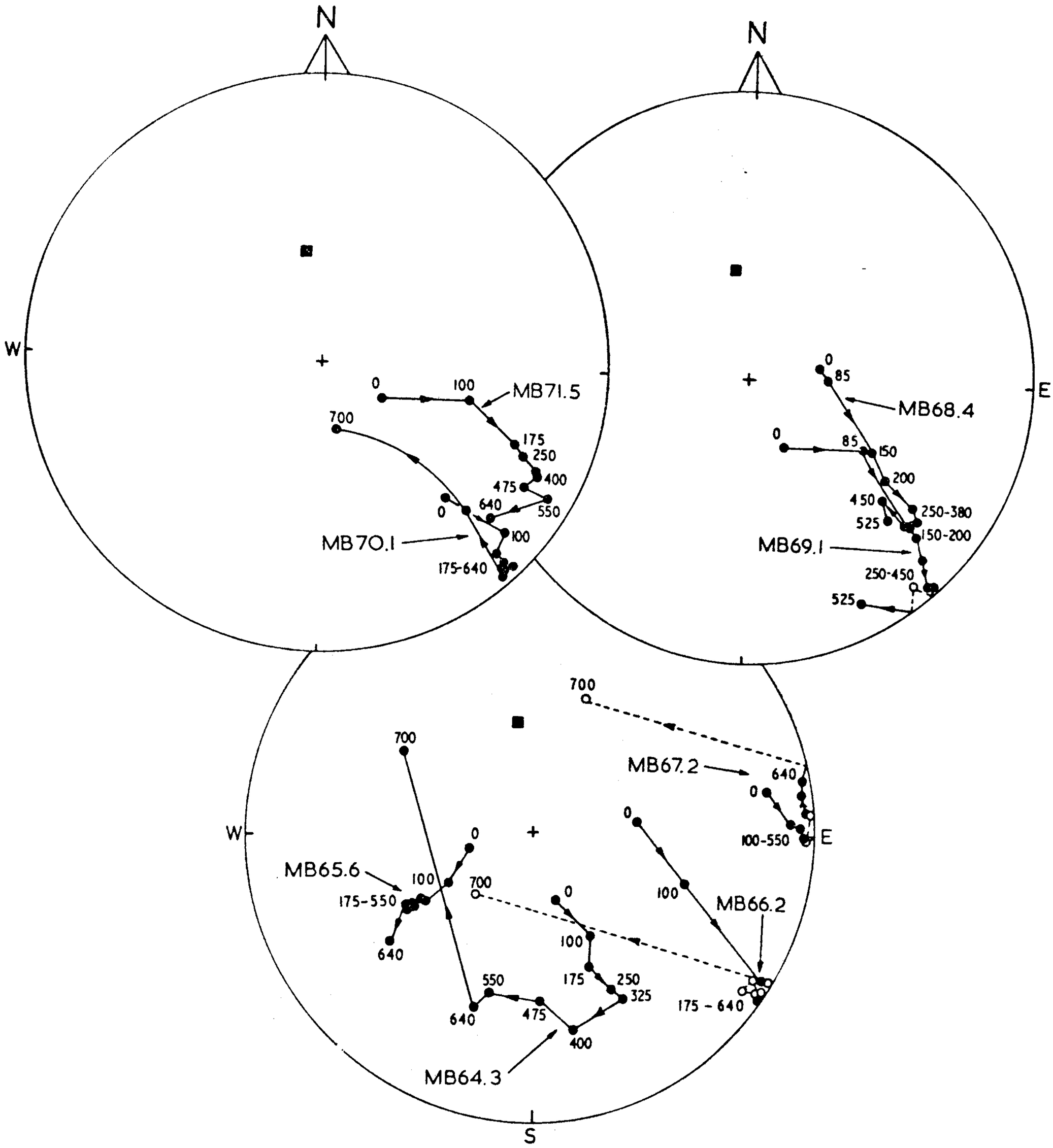
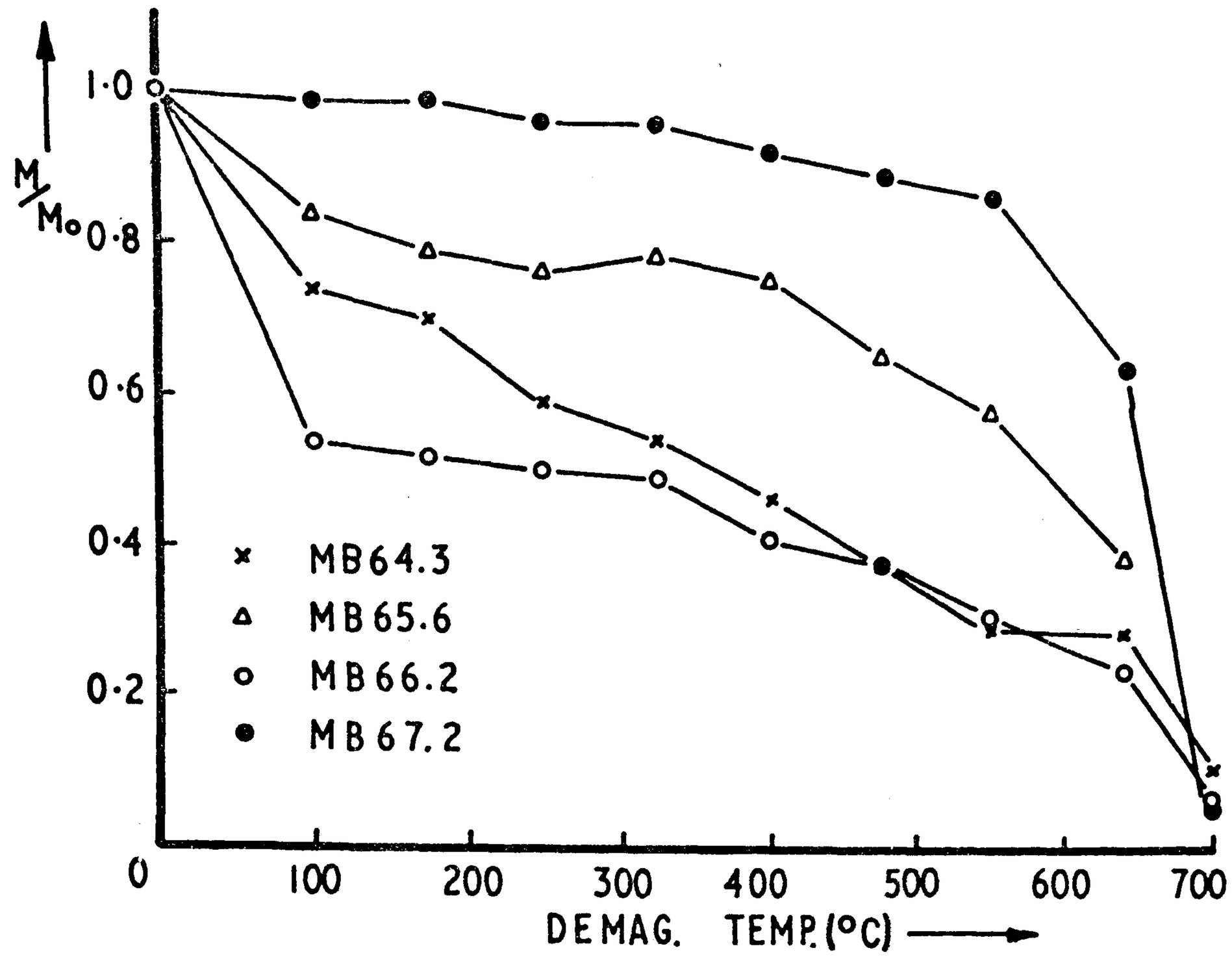


Fig 2.3 Changes in direction of magnetisation of Precambrian pilot samples during progressive demagnetisation, plotted on stereographic projections. Numbers against poles indicate temperatures.



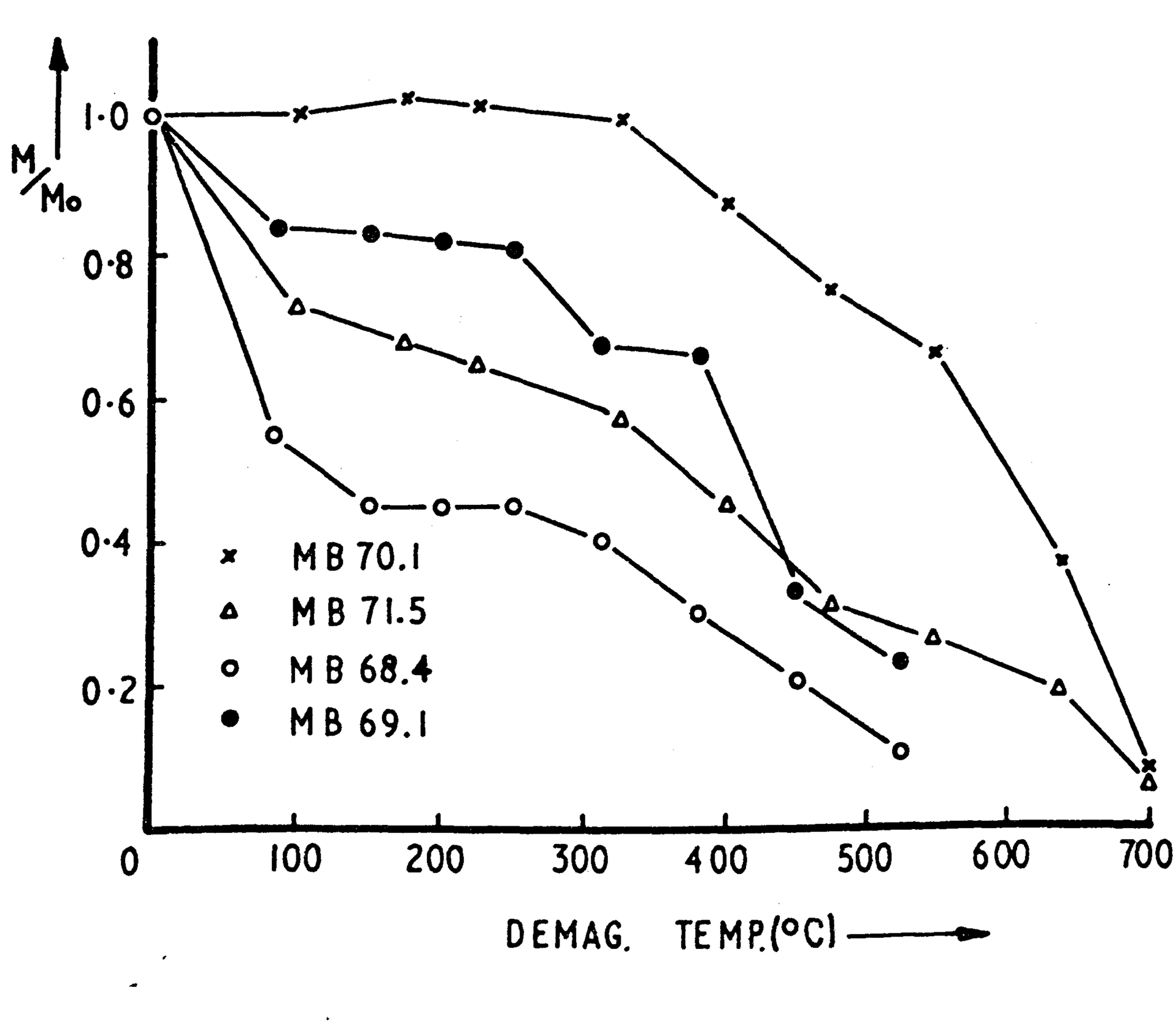


Fig 2.4 Changes in normalised intensity of magnetisation of Precambrian pilot [illegible] magnetisation.

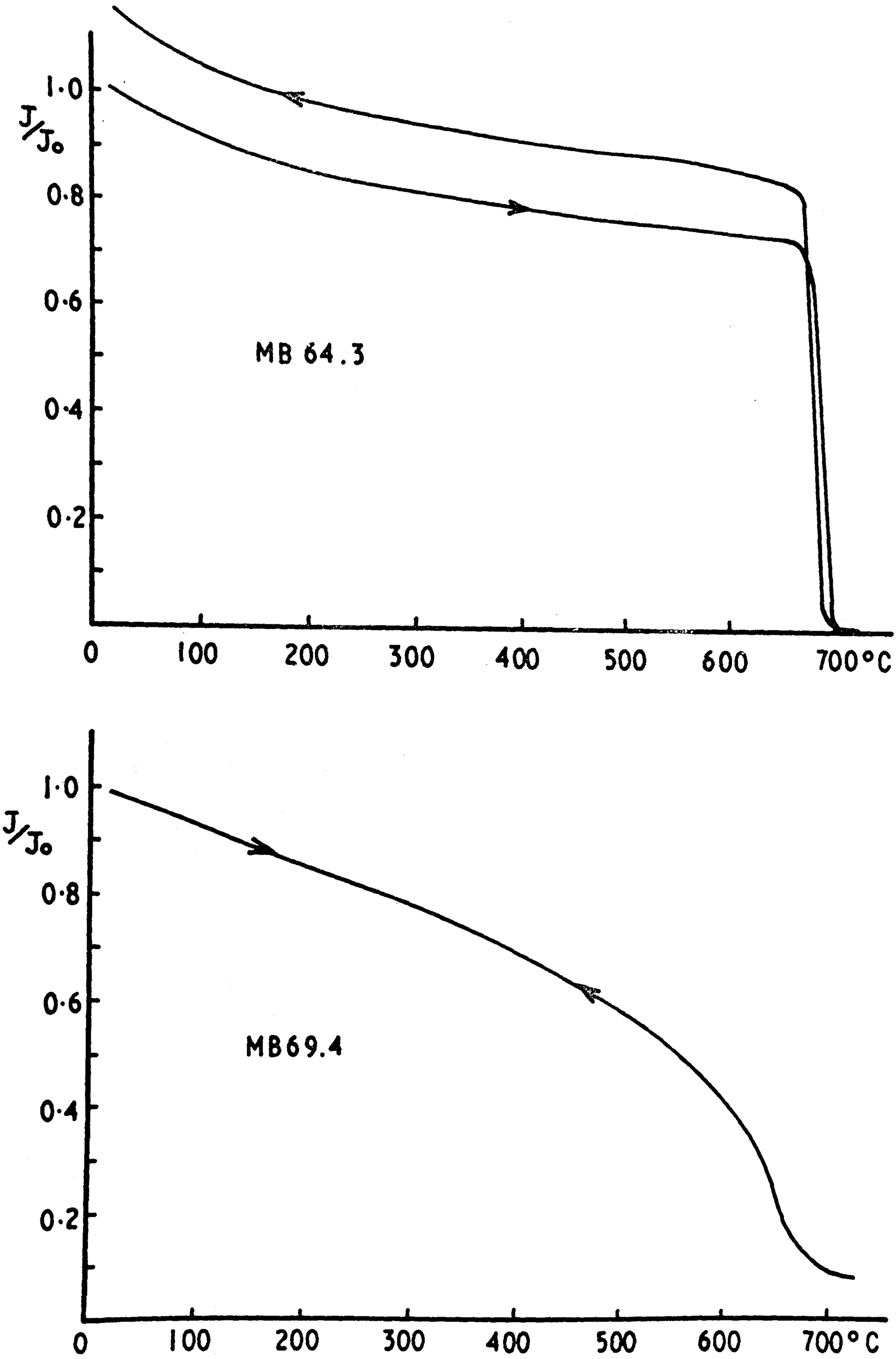


Fig 2.5 Results of thermomagnetic analyses on Precambrian samples MB64.3 and MB69.4.

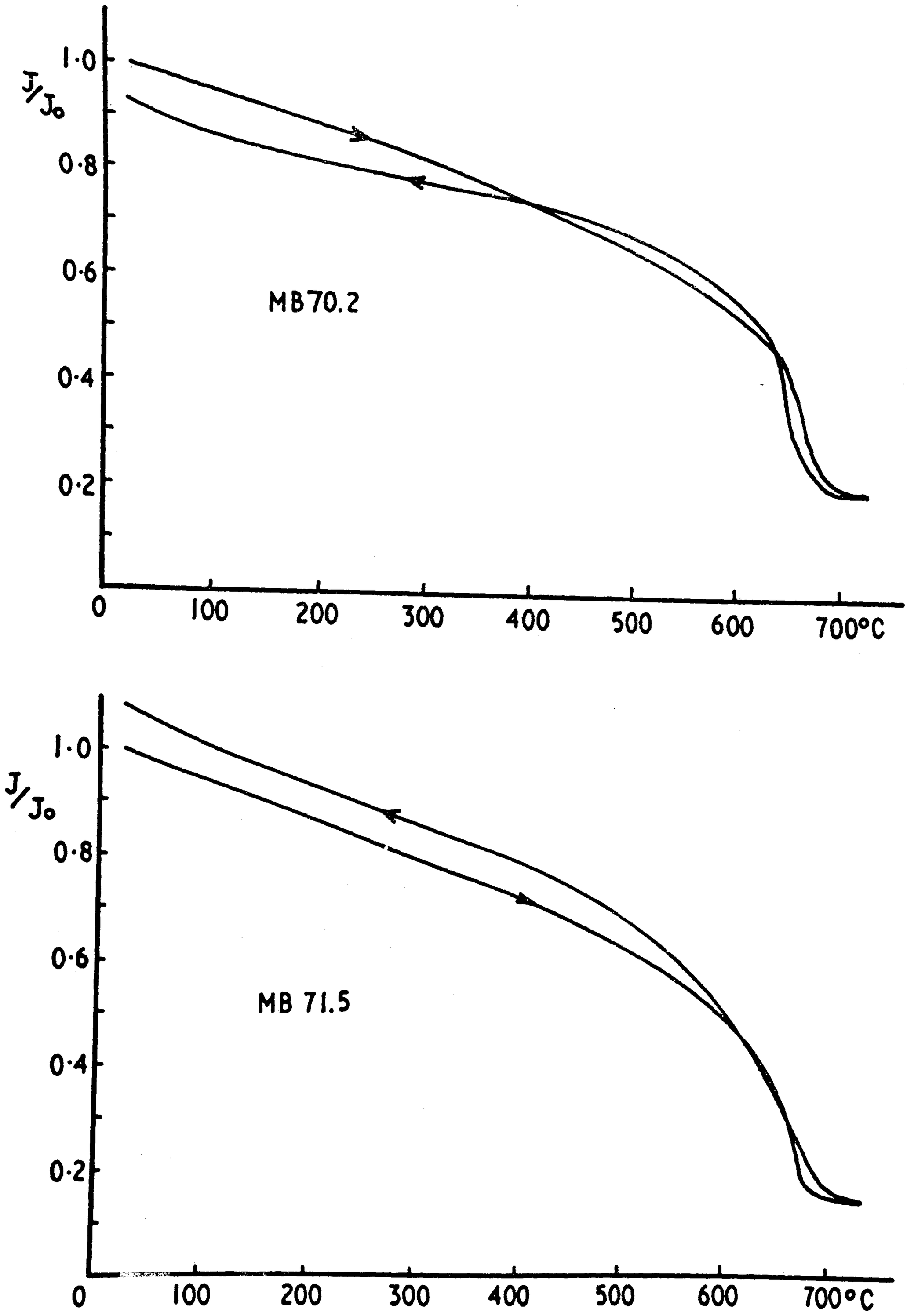


Fig 2.6 Results of thermomagnetic analyses on Precambrian samples MB70.2 and MB71.5.

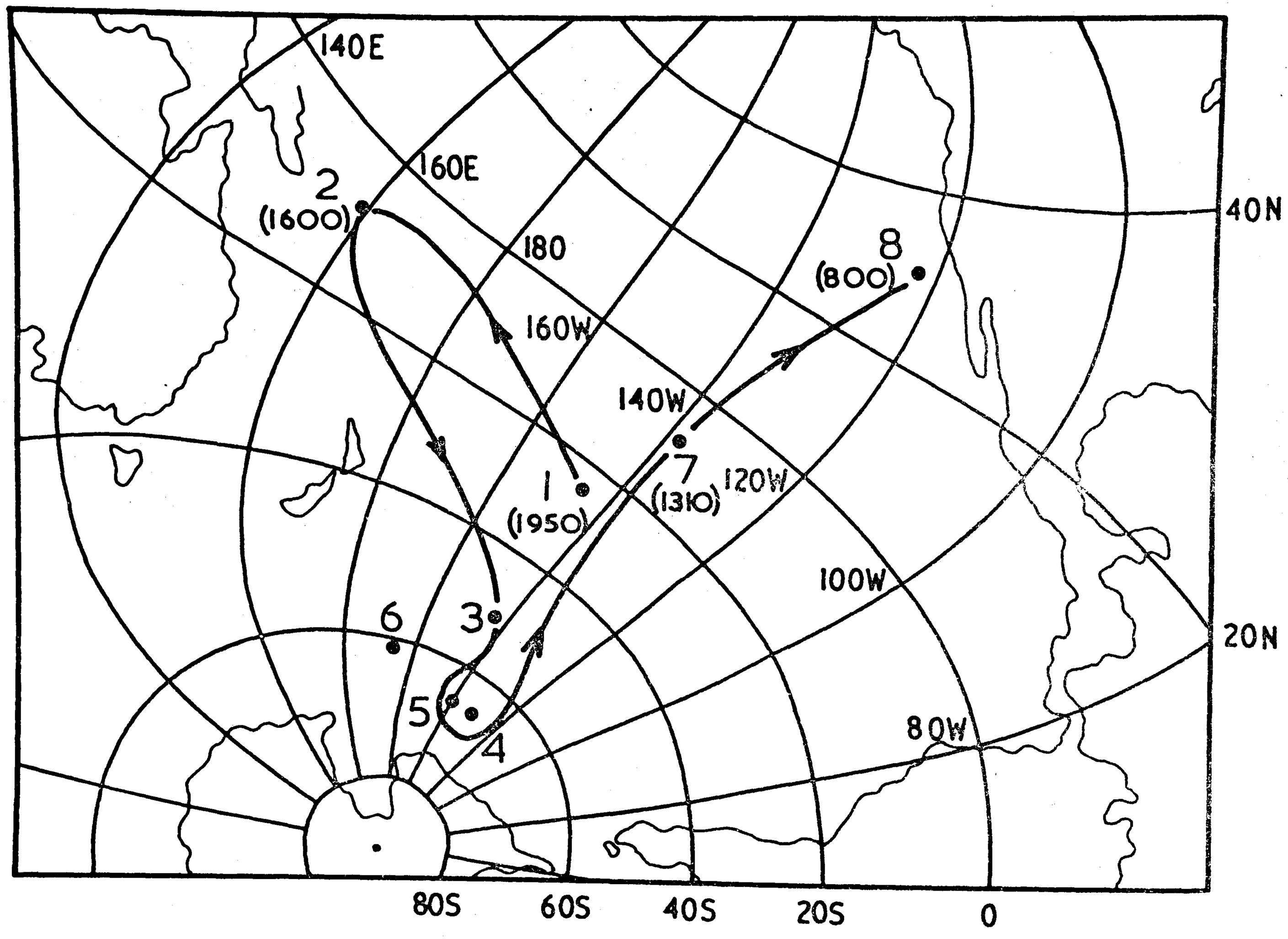


Fig 2.7 African Precambrian polar-wander curve. Pole numbers 1 to 7 refer to poles listed in Table 2.3. Pole 8 is the Moroccan Precambrian III pole. Figures in brackets refer to probable ages of poles.

TABLE 2.1 PRECAMBRIAN FIELD DATA

Site No.	Tilt Correction Strike	Dip	Location Lat.	Long.
MB64	61°	35°	30.51°	-7.00°
MB65	132°	11°	30.51°	-7.00°
MB66	37°	23°	30.51°	-7.00°
MB67	360°	10°	30.51°	-7.00°
MB68	45°	4°	30.71°	-6.63°
MB69	0	0	30.71°	-6.63°
MB70	0	0	30.71°	-6.63°
MB71	69°	8°	30.71°	-6.63°

TABLE 2.2 PRECAMBRIAN SAMPLE N.R.M.s AND INITIAL SUSCEPTIBILITIES

Site No.	Sample No.	Direction of Remanence* Dec	Inc	Int. ($\times10^{-6}$)	Suscept ($\times10^{-6}$)
364	1	168.0	+70.2	0.90	3.95
	2	178.1	+55.5	0.77	3.95
	3	170.8	+56.4	1.05	3.95
	5	169.6	+50.2	0.69	3.95
	6	147.5	+56.5	0.89	3.95
MB65	1	233.3	+76.6	6.86	4.74
	2	276.0	+77.9	8.74	4.70
	3	235.9	+74.7	5.39	4.70
	4	237.2	+71.7	4.41	4.74
	5	130.6	+64.4	1.26	4.74
	6	253.8	+66.4	1.51	4.74
MB66	1	80.3	+54.1	6.04	9.08
	2	93.7	+50.9	5.61	9.08
	3	95.3	+52.3	5.26	9.87
	4	21.4	+38.7	4.87	9.08
	5	104.0	+31.1	4.75	9.08
	6	108.0	+28.4	3.83	7.89
MB68	1	75.3	+59.2	15.0	21.71
	2	106.5	+55.3	14.0	17.76
	3	84.8	+58.7	16.0	20.36
	4	79.0	+60.9	20.0	20.36
	5	31.5	+72.4	19.0	23.68
	6	71.2	+63.3	19.0	23.68
MB69	1	150.1	+59.5	6.0	13.81
	2	114.6	+28.4	5.0	9.71
	3	170.9	+61.3	5.0	11.84
	4	182.2	+74.4	6.0	17.37
	5	175.3	+63.9	6.0	13.81
	6	143.5	+78.5	5.0	15.39
MB70	1	136.0	+24.7	5.75	8.22
	2	132.6	+20.3	5.75	8.63
	3	115.2	+26.1	5.31	7.89
	4	129.2	+31.7	5.20	8.22
	5	116.9	+21.6	5.52	9.04
	6	138.8	+26.6	5.69	8.22

Site No.	Sample No.	Direction of Remanence* Dec	Inc	Int. ($x10^{-6}$)	Suscept ($x10^{-6}$)	Site No.	Sample No.	Direction of Remanence* Dec	Inc	Int. ($x10^{-6}$)	Suscept ($x10^{-6}$)
[illegible]te [illegible]67	1	79.8	+17.3	6.09	4.29						
	2	84.1	+10.4	6.60	4.29	MB71	1	97.1	+67.8	6.97	14.39
	3	88.0	+15.2	7.02	4.74		2	101.5	+58.2	5.37	11.45
	4	90.8	+8.7	6.36	4.34		3	126.4	+47.0	5.53	12.92
	5	174.8	+20.3	7.04	4.74		4	137.0	+58.4	5.64	12.92
	6	87.5	+8.0	7.06	4.74		5	119.6	+63.1	5.92	13.03
							6	101.4	+67.4	5.37	11.84

* Corrected for tilting, where applicable

TABLE 2.3 PILOT SAMPLE DEMAGNETISATION RESULTS

Sample No. MB643				MB656			MB662			MB672		
Temp.	Dec.	Inc.	Int.+	Dec.	Inc.	Int.+	Dec.	Inc.	Int.+	Dec.	Inc.	Int.+
R.T.	162.9	+61.7	0.93	256.8	+63.5	1.65	85.3	+49.8	5.84	81.1	+10.2	6.18
100	151.9	+45.4	0.69	240.1	+51.9	1.39	109.2	+30.9	3.16	88.6	+4.7	6.13
175	158.4	+35.8	0.65	237.6	+42.0	1.30	122.6	+1.5	3.04	90.3	+3.3	6.11
250	154.5	+26.9	0.55	238.7	+37.7	1.25	125.8	-1.5	2.93	92.0	+1.8	5.92
325	152.4	+22.9	0.50	239.6	+40.6	1.28	127.0	-4.2	2.84	92.3	-1.3	5.94
400	169.3	+19.9	0.43	239.2	+35.5	1.24	123.7	-3.5	2.42	86.6	-0.5	5.71
475	178.0	+29.2	0.35	239.8	+37.5	1.08	126.9	+0.1	2.23	86.8	+1.7	5.48
550	195.7	+30.2	0.28	239.2	+35.5	0.96	125.3	-2.8	1.80	83.3	+2.5	5.33
640	198.9	+25.3	0.27	233.5	+26.3	0.64	123.4	-0.4	1.40	80.3	+2.3	3.98
700	302.4	+33.5	0.10				224.3	-57.2	0.39	21.0	-36.7	0.34

Sample No. MB684				MB691			MB701				MB715		
Temp.	Dec.	Inc.	Int.*	Dec.	Inc.	Int.*	Temp.	Dec.	Inc.	Int.+	Dec.	Inc.	Int+
R.T.	79.0	+60.9	2.0	150.1	+59.5	0.6	R.T.	136.0	+24.7	4.69	119.6	+63.1	6.34
85	88.2	+58.1	1.1	119.3	+38.8	0.5	100	131.5	+8.2	4.72	103.4	+34.5	4.66
150	117.8	+36.3	0.9	130.5	+15.5	0.5	175	136.4	+6.5	4.81	110.8	+18.1	4.31
200	124.5	+28.4	0.9	131.3	+12.4	0.5	250	135.3	-1.4	4.76	112.6	+15.0	4.13
250	126.5	+17.2	0.9	134.3	+7.4	0.5	325	136.0	+3.5	4.64	114.6	+10.5	3.64
310	128.0	+13.6	0.8	136.7	+1.7	0.4	400	136.8	+2.4	4.07	116.3	+9.5	2.85
380	131.3	+16.1	0.6	136.2	+1.0	0.4	475	137.7	+1.3	3.53	119.6	+11.1	2.00

Temp.	Dec.	Inc.	Int.*	Dec.	Inc.	Int.*	Temp.	Dec.	Inc.	Int.+	Dec.	Inc.	Int+
450	130.2	+24.8	0.4	138.6	-3.6	0.2	550	136.8	+2.4	3.09	119.4	+5.3	1.64
525	132.7	+19.9	0.2	150.7	+6.6	0.14	640	134.0	+18.9	1.75	130.8	+13.4	1.19
							700	165.6	+63.3	0.38	138.5	+0.4	0.35

* x 10^{-5} gauss cm^3

\+ x 10^{-6} gauss cm^3

TABLE 2.4. SAMPLE REMANENCE DIRECTIONS, INTENSITIES & SUSCEPTIBILITIES AFTER TREATMENT AT 325°C

Site No.	Sample No.	Direction of Remanence* Dec.	Inc.	Int. ($\times10^{-6}$)	Suscept ($\times10^{-6}$)
MB64	1	185.8	+50.8	0.55	3.55
	2	188.4	+31.8	0.57	3.16
	3	152.4	+22.9	0.50	3.16
	5	181.4	+25.6	0.71	3.16
	6	175.2	+29.2	0.67	3.55
MB65	1	225.5	+50.2	6.94	5.21
	3	221.4	+50.0	5.86	4.31
	4	219.7	+49.4	5.25	4.74
	5	(159.9	+37.7)	1.34	4.34
	6	239.6	+40.6	1.28	4.34
MB66	1	122.4	+6.3	4.03	8.68
	2	127.9	-6.1	3.59	9.47
	3	127.0	-4.2	2.84	9.47
	4	123.8	-5.5	4.15	9.47
	6	117.2	+6.7	3.70	7.89
MB68	1	126.2	+19.6	8.08	21.71
	2	126.3	+16.7	7.14	18.16
	3	134.8	+20.7	8.13	20.75
	4	128.0	+13.6	8.00	20.75
	5	121.8	+17.2	8.33	24.08
	6	128.9	+23.2	9.09	24.08
MB69	1	136.7	+1.7	4.00	13.81
	2	137.2	+3.4	5.15	9.32
	3	139.2	+3.2	4.74	11.84
	4	135.9	+5.4	4.98½	17.76
	5	144.9	+4.0	5.37	13.81
	6	136.0	+10.4	5.70	15.39
MB70	1	136.0	+3.5	4.64	8.29
	2	130.4	+7.6	5.32	7.89
	3	124.8	+10.7	4.36	7.89
	4	137.1	+10.8	5.08	7.10
	6	147.1	+4.8	5.64	7.89

Site No.	Sample No.	Direction of Remanence* Dec.	Inc.	Int. ($x10^{-6}$)	Suscept ($x10^{-6}$)	Site No.	Sample No.	Direction of Remanence* Dec.	Inc.	Int. ($x10^{-6}$)	Suscept ($x10^{-6}$)
MB67	1	85.4	+7.7	7.01	3.90	MB71	1	122.8	+10.3	4.78	13.42
	2	92.3	-1.3	5.94	4.34		2	126.4	+11.0	4.30	11.05
	3	98.6	+6.7	7.99	5.21		3	125.2	+3.4	5.15	12.53
	4	92.0	+7.2	7.59	4.34		4	121.8	+9.4	4.96	12.53
	5	183.7	+21.1	7.91	5.21		5	114.6	+10.5	3.64	13.03
	6	93.4	+6.8	8.00	4.34		6	123.7	+16.6	4.58	11.45

* Corrected for tilting, where applicable

TABLE 2.5(a) PRECAMBRIAN N.R.M. MEAN SITE DIRECTIONS, POLE POSITIONS AND STATISTICAL PARAMETERS

Site No.	D	I	N	R	k	α_{95}	c.s.d.	Pole position Lat.	Long.	α_{95}
MB64	166.9	+58.2	5	4.943	70	9.2	9.7	18.9S	3.7E	12.0
MB65	246.6	+74.0	5	4.975	158	6.1	6.4	15.8N	35.1W	10.4
MB66	96.6	+42.9	6	5.864	37	11.2	13.4	8.1N	57.8E	10.3
MB67	86.1	+11.9	5	4.979	194	5.5	5.8	6.5N	79.8E	4.5
MB68	83.8	+62.2	6	5.944	89	7.1	8.6	25.1N	45.7E	10.0
MB69	149.3	+63.7	6	5.638	14	18.7	21.9	31.5S	21.9E	16.8
MB70	128.1	+25.4	6	5.926	68	8.2	9.8	23.4S	49.9E	8.2
MB71	115.7	+61.1	6	5.908	54	9.2	11.0	7.9N	35.1E	10.8
Overall Mean	117.0	+56.5	8	6.934	7	23.0	32.0	1.4S	34.1E	30.5
							Antipole	1.4N	145.9W	30.5

TABLE 2.5(b) PRECAMBRIAN MEAN SITE DIRECTIONS, POLE POSITIONS & STATISTICAL PARAMETERS AFTER 325°C TREATMENT

Site No.	D	I	N	R	k	α_{95}	c.s.d.	Pole position Lat.	Long.	A_{95}
MB64	175.9	+32.7	5	4.833	24	15.9	16.6	41.0S	2.6W	15.2
MB65	122.8	-1.2	4	3.97	123	8.3	7.3	28.2S	65.4E	6.1
MB66	124.2	-1.4	6	5.970	168	5.2	6.2	29.4S	64.6E	3.9
MB67	92.3	+5.4	5	4.978	182	5.7	6.0	0.6S	79.4E	4.8
MB68	127.6	+18.5	6	5.979	237	4.4	5.3	25.7S	53.4E	3.8
MB69	138.3	+4.7	6	5.984	312	3.8	4.6	45.3S	65.6E	3.2
MB70	135.1	+7.5	5	4.952	83	8.4	8.9	35.0S	52.7E	8.0
MB71	122.4	+10.2	6	5.974	190	4.9	5.9	24.4S	60.8E	3.9
Overall Mean	128.5	+10.0	8	7.374	11	17.0	24.5	30.6S	57.2E	17.1
							Antipole	30.6N	122.8W	17.1

TABLE 2.6 PRECAMBRIAN POLE POSITIONS FROM THE TRANSVAAL AND RHODESIAN SHIELDS

Pole No.	Rock unit and Location	Age (M.y.)	Palaeomagnetic pole Lat.	Long.	A_{95}	Reference
1	Bushveld gabbro, Transvaal	1950 ± 50	23S	144W	12	Gough and van Niekerk, 1959 Nicolaysen et.al, 1958
2	Mashonaland dolerites, Rhodesia	1600	7S	160E	7.5	McElhinny and Opdyke, 1964
3	Premier Mine kimberlite, Transvaal	P.C.	51S	142.5W	7.5	Jones, 1968
4	Waterberg diabases, Botswana & Transvaal	P.C.	65S	129.5W	4.5	Jones & McElhinny, 1966
5	Umkondo dolerites, Rhodesia	P.C.	65.5S	140W	7.0	McElhinny & Opdyke, 1964
6	Umkondo lavas, Rhodesia	P.C.	61.5S	165W	12	McElhinny, 1966
7	Pilansberg dikes, Transvaal	1310 ± 60	7.5S	137.5W	10.5	Gough, 1956

TABLE 2.7 PRECAMBRIAN VOLCANICS. VARIATION OF SUSCEPTIBILITY WITH TEMPERATURE

Sample No.	RT	100°C	175°C	250°C	325°C	400°C	475°C	550°C
MB643	9.0	9.0	9.0	9.0	9.0	9.0	8.5	8.0
MB656	11.5	12.0	11.5	11.5	11.5	11.5	11.5	12.0
MB662	24.0	23.5	23.5	23.5	23.5	23.5	18.0	16.5
MB701	18.5	18.5	18.5	18.5	18.0	18.0	16.5	15.5
MB713	28.5	28.5	28.5	28.5	28.0	27.5	25.0	22.5
MB721	4.5	4.5	4.5	4.5	4.5	4.5	3.5	3.0

All values x 10^{-6} gauss per oersted

CHAPTER 3. CAMBRIAN

3.1. Geology

3.1.1. Identification of base of Cambrian

In the Anti Atlas region the upper Adoudounian (Infracambrian) sequence (section 2.1.6.) is terminated by an important regressive horizon. Although this regression was probably more widespread than that of the Lie de Vin series, no continental sediments were deposited.

The first term of the Lower Cambrian sequence is a limestone series of the same type as the underlying Upper Adoudounian, and the similarity of these two formations frequently makes it difficult to trace the intervening regressive horizon. However the base of the Lower Cambrian is marked locally by a weak discordance, appearing very clearly at certain localities in the southern flank of the Western Anti-Atlas.

3.1.2. Lower Cambrian

The Lower Cambrian transgression, like the preceding two Adoudounian transgressions, appears to have commenced in the Western Anti-Atlas, and to have progressively invaded the rest of the chain. The Cambrian sequence begins with a thin layer (20 to 30 metres) of dark, often oolitic, limestones (the "Calcaires de base" of Choubert, 1952), the upper-beds of which contain the first Archaeocyathids. The overlying sequence of shales, limestones, sandstones and volcanic tuffs has been sub-divided by Choubert (1952) into a series of lithological units, recognisable throughout the whole Anti-Atlas chain.

The first of these is a series of shales and limestones, the "série schisto-calcaire", having a total thickness of 300 to 450 metres, and containing the first trilobites. This is followed by the "série schisteuse", a sequence of shales with occasional beds of

cindery limestone, which varies in thickness from 400 metres in the West to 100 metres in the East. This series is overlain in turn by a sequence of beds, varying from a sandstone facies in the South to a predominantly pyroclastic facies in the North. The thickness of this formation is about 150 metres, and it is referred to as the "grés terminaux". It appears to mark the occurrence of a weak tectonic phase, and deposits of shallow water "pipe-rock" ("grès a tigillites") in the Western Anti-Atlas, and pink and chocolate sandstones with pebbles of red clay in the Central High Atlas, reflect continental influences associated with a regression.

The emergence of the High Atlas region soon afterwards, indicated by a widespread level of conglomerates, was accompanied by an episode of volcanic activity, marked by andesitic flows (spilites) in the Western High Atlas (de Koning, 1957). This volcanism was manifested in the Anti-Atlas region by the deposition of a series of volcanic ashes and tuffs, interbedded in the sandstones of the "grès terminaux" (Choubert and Faure-Muret, 1956).

The uppermost fossiliferous horizon of the Lower Cambrian sequence is represented by about 60 metres of shales, overlain by the basal Middle Cambrian beds containing Paradoxides.

Hupé (1952) attempted a subdivision of the above lithological sequence on the basis of trilobite zones, but later studies (Hupé, 1959) indicated that the palaeontological boundaries did not coincide exactly with the lithological boundaries. More recently Choubert (1963) has combined the two approaches, and recommended a subdivision into three stages, the Amouslek, Issafène and Asrir stages. The essential features of these three classifications are summarised in Fig. 3.1.

Fig 3.1. Subdivisions of the Anti Atlas Cambrian Sequence

Division	Trilobite zone (Hupe, 1952)	Zone fossil		Lithological subdivision (Choubert, 1952)	Stage (Choubert, 1963)
Middle Cambrian		Paradoxidae Protolenidae and Paradoxidae		Schistes des Feijas internes and basalts (E.Anti Atlas)	Middle Cambrian
					Regression
	VIII	Palaeolenus, Kingaspis etc.		Micmacca horizon	Ourmast horizon
	VII	Gentilaspis		"Grès terminaux" and volcanic tuffs	Asrir Stage
Lower Cambrian	VI	Longianda, Callavia, Gigantopygus		"Série schisteuse"	Issafene Stage
	V	Neltneria, Bondonella	Archaeocyathia		
	IV	Hebediscus, Pareops			
	III	Daguinaspis Marcaisia		"Série schisto-calcaire	Amouslek Stage
	II	Choubertella			
	I	Fallotaspis			
		First Archaeocyathids		"Calcaires de base"	
					Regression
Adoudounian (Infracambrian)		Collenia		"Série des Calcaires supérieurs" "Série Lie de Vin"	Upper Adoudounian
					Regression
				"Série des Calcaires inférieurs" "Série de Base"	Lower Adoudounian

3.1.3. Middle Cambrian

The regression which terminated the Asrir Stage is marked at some localities by a weak discordance between the "grès terminaux" and the base of the Paradozides beds (the "Ourmast horizon"). However in general the Middle Cambrian appears to be perfectly concordant on the Lower Cambrian throughout the whole of South Morocco.

The Middle Cambrian sequence consists of two terms, the Paradoxides Shales (or "schistes des Feijas internes") and the Conocoryphe and Lingula Sandstones (or "grès du Tabanit"). The thickness of the whole succession is about 1,000 metres, and the passage from the Paradoxides shales to the Lingula sandstones takes the form of a gradual enrichment of the shales in sandy material. This represents a gradual shallowing of water, reflected in the presence of tigillites (Scolythes) at several horizons.

The whole region was uplifted towards the end of the Middle Cambrian, and the uppermost Middle Cambrian, Upper Cambrian and Lower Tremadocian sequence is absent. A similar gap exists between the Middle Cambrian and Lower Ordovician throughout the whole Mediterranean region, and has been correlated with the Sarde tectonic phase. In the Eastern Anti-Atlas this emergence was preceded by an important episode of basaltic volcanism (Clariond and Gubler, 1937).

3.2. Location of sampling sites

In the palaeomagnetic reconnaissance survey of Tarling and Sutton (1967) results were obtained from five sites in Lower Cambrian sandstones, and ten sites in InfraCambrian sandstones. With a few exceptions, the stability of these rocks was found to be poor, and both within-site and between-site scatter of remanence directions was high. Partial demagnetisation increased the between-site scatter.

These results were not encouraging, and it was therefore decided to concentrate on collection of the Cambrian volcanic tuffs rather than sediments. As discussed above, these tuffs occur in the Asrir Stage (Gentilaspis zone), towards the top of the Lower Cambrian sequence.

During the 1969 field excursion ten sites were samples (MB54 to MB64) in the N.W. Anti-Atlas, in the region of Amouslek and Ait Baha (Fig. 3.2). During the 1970 field excursion a further six sites were sampled (MC18 to MC23) slightly further to the south west.

Two sites were also sampled in the coarse sandstones ("Grès terminaux") of the Central Anti-Atlas (Fig. 2.1), one near Amazer (MB72), and one near Agdz (MC17).

3.3. Palaeomagnetic results from the Cambrian volcanic tuffs

3.3.1. N.R.M. directions and intensities

The N.R.M. mean site directions of remanence all have a south to south-easterly declination, but the inclinations vary widely, from -38^{o} to $+71^{o}$ (Fig. 3.3(a)). Within-site scatter of remanence directions is small and most sites have an α_{95} of less than 10^{o}. The between-site scatter before correction for tilting is 17^{o}, whereas the value after correction is 25^{o}. This suggests that at least part of the remanence was produced in the rocks after they were folded

(Graham, 1949). In general the samples collected from the southern part of the region (sites MC18 to 23) seem to have a more westerly declination and steeper inclination than the samples from the north (sites MB54 to 63).

The mean intensity of magnetisation, assuming a log-normal distribution, is 2.82 x 10^{-6} gauss for sites MB54 to 63, and 1.10 x 10^{-6} gauss for sites MC18 to 23. The overall mean intensity of NRM is 1.98 x 10^{-6} gauss.

3.3.2. Stability tests

The results of progressive thermal demagnetisation stability tests, performed on one specimen from each site, are plotted in Figs. 3.4 and 3.5 for sites MB54 to 63 and Figs. 3.6 and 3.7 for sites MC18 to 23.

(a) Sites MB54 to 63

All pilot samples from these sites show a high degree of stability to thermal demagnetisation. In most cases, after initial changes of 10° to 40° towards the negative SE quadrant, the direction remains very constant during heating from 100°C to 525°C, and sometimes to 600°C (Fig. 3.4). Further heating to 675°C produces a random scatter of directions. In all of these samples the intensities of magnetisation decrease very gradually up to 600°C, after which they either decrease suddenly or change erratically (Fig. 3.5). The susceptibilities either remain constant or decrease gradually on heating to 525°C, and heating at 625°C and 650°C results in a sudden increase (Table 3.7).

(b) Sites MC18 to 23

The stabilities of samples from these sites are not as high as those from sites MB54 to 63. Initial changes of up to 90° occur towards the negative SE quadrant on heating to 200°C, after which the directions of remanence remain approximately constant, in most cases up to 400°C, and sometimes to 600°C (Fig. 3.6). Once again, heating at 650°C produces a random scattering of directions.

The intensities of magnetisation are more variable than those of sites MB54 to 63, and in two cases heating to 200°C results in a substantial increase in intensity. In all cases the intensity is reduced to 0.4 to 0.6 if the initial value on heating at 600°C (Fig. 3.7), after which it suddenly increases to several times its initial value (Table 3.3). As with sites MB54 to 63, the susceptibility either remains constant or decreases gradually on heating to 500°C, after which it suddenly increases.

These results indicate the presence of a stable component of remanence in samples from all sixteen sites. This component is isolated during thermal treatment from 100°C to 525°C in sites MB54 to 63 and 200°C to 400°C in sites MC18 to 23. In all cases a less-stable secondary component is also present, and is removed on heating at 100°C to 200°C.

Removal of the stable component of remanence at 600°C appears to leave only a component of random direction and intensity. The increase of susceptibility on heating at 600 to 650°C suggests the occurrence of a chemical change in all samples at these temperatures, and this may explain the sudden increase in intensity of samples from sites MC18 to 23.

3.3.3. Bulk demagnetisation

In order to isolate the stable component of remanence detected

in the pilot samples, the remaining samples from sites MB54 to 63 were heated at 250°C, and those from sites MC18 to 23 at 300°C. This resulted in a decrease in within-site scatter for eight of the sites and an increase in within-site scatter for the other eight. However the between-site scatter after correction for tilting was reduced substantially, from 25° to 13° (Fig. 3.3(b)), and the value before correction for tilting (12°) was not significantly different.

The reduction in between-site scatter after thermal treatment implies the successful removal of a less-stable component of remanence, and the fact that the between-site scatter is no longer significantly different before and after correction for tilting suggests that the component removed was probably impressed on the rocks after their (Carboniferous) time of folding.

The mean intensity of magnetisation of sites MB54 to 63 after bulk thermal treatment is 2.56×10^{-6} gauss, and that of sites MC18 to 23 is 1.00×10^{-6} gauss. The overall mean intensity is 1.78×10^{-6} gauss.

3.3.4. Thermomagnetic analyses and microscopic examinations

Thermomagnetic analyses were carried out on samples from sites MB54 to MB62. In both cases the curves were perfectly, or very nearly, reversible (Fig. 3.8), and showed a single Curie point in the vicinity of 670°C. This temperature is characteristic of haemetite.

Thin-section microscopic analyses revealed the presence of much calcite, possibly as an alteration product of calcic plagioclase, and sericite. The composition of the groundmass was difficult to assess, but several small crystals of altered clinopyroxene were identified.

In agreement with the thermomagnetic analyses, the only magnetic mineral present was haemetite. This was recognised under reflected light as small anhedral grains with high reflectivity, forming part of the groundmass. There were numerous grains just within the limit of visibility with a x_{45} objective, and presumably there were many more grains just below the limit of visibility. Such grains are likely to be close to single-domain size.

There were also many larger grains of haemetite, usually in aggregates which were pseudomorphic after olivine and pyroxene crystals, and presumably produced as a result of the breakdown of these minerals. There was no trace of exsolution in any of the grains of haemetite.

3.3.5. Discussion

The results described in Section 3.3.3. indicate the successful isolation of a stable component of remanence in the Lower Cambrian tuffs, and the palaeomagnetic pole position corresponding to the mean direction of stable remanence (Table 3.6) is

Lat = 41.5°S, Long = 69.5°E, with A_{95} = 10.5°.

As discussed in Section 3.2, these tuffs are situated in the Asrir stage, near the top of the Lower Cambrian sequence.

The ambiguous result of the fold test after bulk demagnetisation means that it is not possible to say with certainty whether the stable component was produced in the rocks before or after the Carboniferous folding (Section 1.4).

Since the polarity reversal sequence of the Earth's magnetic field is not accurately known for the Palaeozoic, it is uncertain whether the polarity at the time of formation of these rocks was normal or reversed. The polarity at this time cannot be inferred from

data from other continents, since normal, reversed and mixed polarities have all been reported from Lower Cambrian formations (Creer 1970).

Because of this it is difficult to establish which of the pole positions determined from the mean Lower Cambrian direction of magnetisation represents the palaeomagnetic "North" pole, and which represents the "South" pole. (In this usage "North" pole refers to the palaeomagnetic pole which can be traced in a continuous path to the present North pole, and is not necessarily the pole to which the north-seeking direction of remanent magnetisation points. Similarly for "South" pole). The usual procedure (e.g. McElhinny et al, 1968) is to adopt the designation which implies minimum continental movement or polar wander between successive geological periods for which poles have been determined. However the Moroccan Lower Cambrian poles are both situated approximately 90^{o} from the other African Lower Palaeozoic South poles, so that according to this criterion either pole may be taken to represent the South pole with equal validity. This means that two different interpretations can be placed on the Moroccan Lower Cambrian results.

The first of these is that the pole position quoted above (41.5^{o}S, 69.5^{o}E) represents the "South" pole. In this case the pole lies very close to the Upper Carboniferous to Permian pole-position derived from Tanzanian red beds (Opdyke, 1964). These poles are plotted, together with the Moroccan Upper Precambrian pole, in Fig 3.9. The other poles plotted are listed in Table 3.9.

If this interpretation is correct, then it suggests that the Upper Precambrian and Lower Cambrian formations were remagnetised

during the Hercynian orogeny, possibly as a result of deep burial and regional heating. As discussed in Section 3.3.4, there is evidence of chemical alteration and production of secondary haemetite in these rocks, but it is possible that this alteration occurred during, or soon after, their initial deposition. The mean direction of remanence, both before and after partial demagnetisation, is remote from the axial dipole field direction at the sampling localities, indicating that the secondary haemetite is not the result of recent chemical weathering. It seems likely that the stable component of remanence from which the Lower Cambrian pole-position was calculated resides in the small, apparently primary, single domain particles, whereas the larger secondary grains of haemetite carry the less-stable component, removed by partial demagnetisation.

If these formations were remagnetised as a result of being held at elevated temperature for long periods of time, then exsolution would be likely to have occurred in the magnetic phases. The complete absence of exsolution is evidence against this hypothesis.

The alternative interpretation of the Moroccan Lower Cambrian results is that the pole position quoted above represents the palaeomagnetic "North" pole. The corresponding "South" pole then lies at 41.5N, 110.5W, and is plotted, together with the Upper Precambrian pole in Fig. 3.10.

Pole B1 in this diagram representd the pole from the Ntonya Ring Structure (Briden, 1968), dated radiometrically as Upper Precambrian to Cambrian. The reliability of this pole with respect to NW Africa is questionable on palaeoclimatic grounds, since it implies that Morocco was situated very close to the South pole during

Infracambrian and Lower Cambrian times. This is difficult to reconcile with the presence of thick dolomitic limestone sequences with Archaeocyathids, and continental deposits with mudcracks and pseudomorphs after salt crystals, all indicators of a warm environment. Although the polar regions may not have always been glaciated, it seems highly improbable that the temperature at the poles would have remained sufficiently warm for a long enough period of time for these thick formations to accumulate.

The Moroccan late Precambrian and Lower Cambrian mean directions of magnetisation correspond to palaeolatitudes of 5^{o} and 10^{o} respectively, placing Morocco in near equatorial latitudes. These poles therefore agree with the palaeoclimatic evidence much more favourably than the Ntonya pole.

There is evidence of a widespread glaciation of NW Africa during the Ordovician and Silurian (e.g. Fairbridge, 1969, Arbey, 1968, and Destombes, 1968), and this is consistent with the positions of the Ordovician poles B2 and B3 (Table 3.9). A possible explanation of the anomalous pole B1 from the Ntonya Ring Structure is that the magnetisation dates from the Ordovician (or Silurian). Although the radiometric age determination is unlikely to be in error by this amount, there is the possibility of remagnetisation as a result of deep burial, local reheating or chemical weathering. If this explanation is correct, then the three poles B1, B2 and B3 can be grouped together to give the mean Ordovician pole denoted by "O" in Fig. 3.10. The corresponding Palaeozoic polar wander curve is shown by the solid black line.

Both of the above interpretations of the Moroccan late Precambrian and Lower Cambrian pole positions seem equally plausible, and final resolution of the problem must await determination of further African palaeomagnetic results of this age.

Finally, mention must be made of the pole "H" in Fig 3.10. This is the pole determined by Helsley (1965) from lavas of supposed Middle Cambrian age in east-central Morocco. These lavas may have been the ones mentioned in Section 3.1.3, and described by Clariond and Gubler,(1937), but since no details are available the reliability of this pole is uncertain. If it does represent a valid Middle Cambrian pole-position then the polar-wander curve in Fig 3.10 must be drawn from "B1" to "H", and then to "O". This implies an extremely large apparent polar movement ($\sim 140^{\circ}$) between the Lower and Middle Cambrian, in a time of at most 30 my. Such a rate seems unlikely when compared with the present-day time scale of continental movement ($\sim$1 to 10 cm per year).

3.4 Palaeomagnetic results from the Cambrian red sediments

The two sites situated in the coarse red sandstones of the Central Anti-Atlas (MB72 and MC17) had mean directions of NRM close to the present geomagnetic field direction at these localities (Fig. 3.11(a)), apparently reflecting either viscous effects, or recent chemical alteration. Progressive thermal demagnetisation of one sample from each site resulted in a movement towards a steep positive easterly direction on treatment at 150°C to 400°C (Fig 3.11(b)), but treatment of the remaining samples at 300°C resulted in a substantial increase in both within-site and between-site scatter (Table 3.8). These results are very similar to those of Tarling and Sutton (1968), and because of the very high scatter of directions of remanence they are thought unlikely to yield a meaningful palaeomagnetic pole-position.

References

Arbey, F., 1968. Structures et depots glaciaires dans l'ordovician terminal des chaines d'Ougarta (Sahara algerian). C.R. Acad. Sc. Paris, E.266, 76, D.

Briden, J.C., 1968. Palaeomagnetism of the Ntonya ring structure, Malawi, J. Geophys. Res., 73, 725-733.

Choubert, G. 1952. Le Precambrian III et le Georgien de l'Anti Atlas. Introduction stratigraphique; in P.Hupe. Contribution a l'etude du Cambrian inferieur et du Precambrian III de l'Anti-Atlas marocain. Notes et Mem. Serv. Geol. Maroc., No. 103, 39 pp.

Choubert, G., and A. Faure-Muret, 1956. L'activite volcanique de la fin du Georgien dans l'Anti-Atlas et le Haut Atlas occidentaux C.R. Acad. Sci., Paris, t242, pp 735-2, 738.

Choubert, G., 1963. Histoire geologique du Precambrian de l'Anti-Atlas Notes et Mem. Serv. Geol. Maroc. No. 162.

Clariond, L. and J. Gubler, 1937. Sur la presence des roches eruptives acadiennes et post-acadiennes au sud du Djebel Ougrat (Sud marocain). C.R. Acad. Sci. Paris, t.204, pp 706-708.

De Koning, G., 1957. Geologie des Ida ou Zal (Maroc). Stratigraphy, petrographie et tectonique de la partie S.W. du Bloc Occidental du Massif ancien du Haut Atlas. Eduard. Ijdo N.V. Leyde 270 pp.

Destombes, J. 1968. Sur la nature glaciaire des sediments du groupe du 2^{e} Bani, Ashgill superieur de l'Anti-Atlas, Maroc. C.R. Acad. Sc. Paris, t.267 pp.684-687 D.

Fairbridge, R.W., 1969. Early Palaeozoic South Pole in Northwest Africa. Geol. Soc. Am. Bull., 80 pp 113-114.

Graham, J.W., 1949. The stability and significance of magnetism in sedimentary rocks. J. Geophys. Res., 54,131-167.

Helsley, C.E., 1965. Palaeomagnetic results from the Middle Cambrian of Northwest Africa (abstract). Trans. Am. Geophys. Union, 46, 67.

Hupe, P. 1952. Contribution a letude du Cambrian inferieur et du Precambrian III de l'Anti Atlas marocain. Notes et Mem. Serv. Geol. Maroc. No. 103, 402 pp.

Hupe, P., 1959. Nouvelle contribution a l'etude du Cambrian marocain These, Paris.

Irving, E., 1964. Palaeomagnetism and its application to geological and geophysical problems. Wiley & Sons, New York.

McElhinny, M.W., J.C. Briden, D.L. Jones and A. Brock, 1968. Geological and Geophysical Implications of Palaeomagnetic Results from Africa. Rev. Geophys. Vol. 6, No. 2.

Opdyke, N.D., 1964. The palaeomagnetism of the Permian redbeds of southwest Tanganyika, J. Geophys. Res., 69, 2477-2487.

Tarling, D.H., and D.H. Sutton, 1968. Palaeomagnetic stability results of a reconnaissance survey of red sandstones in Morocco. Phys. Earth Planet. Interiors 1, 35-43.

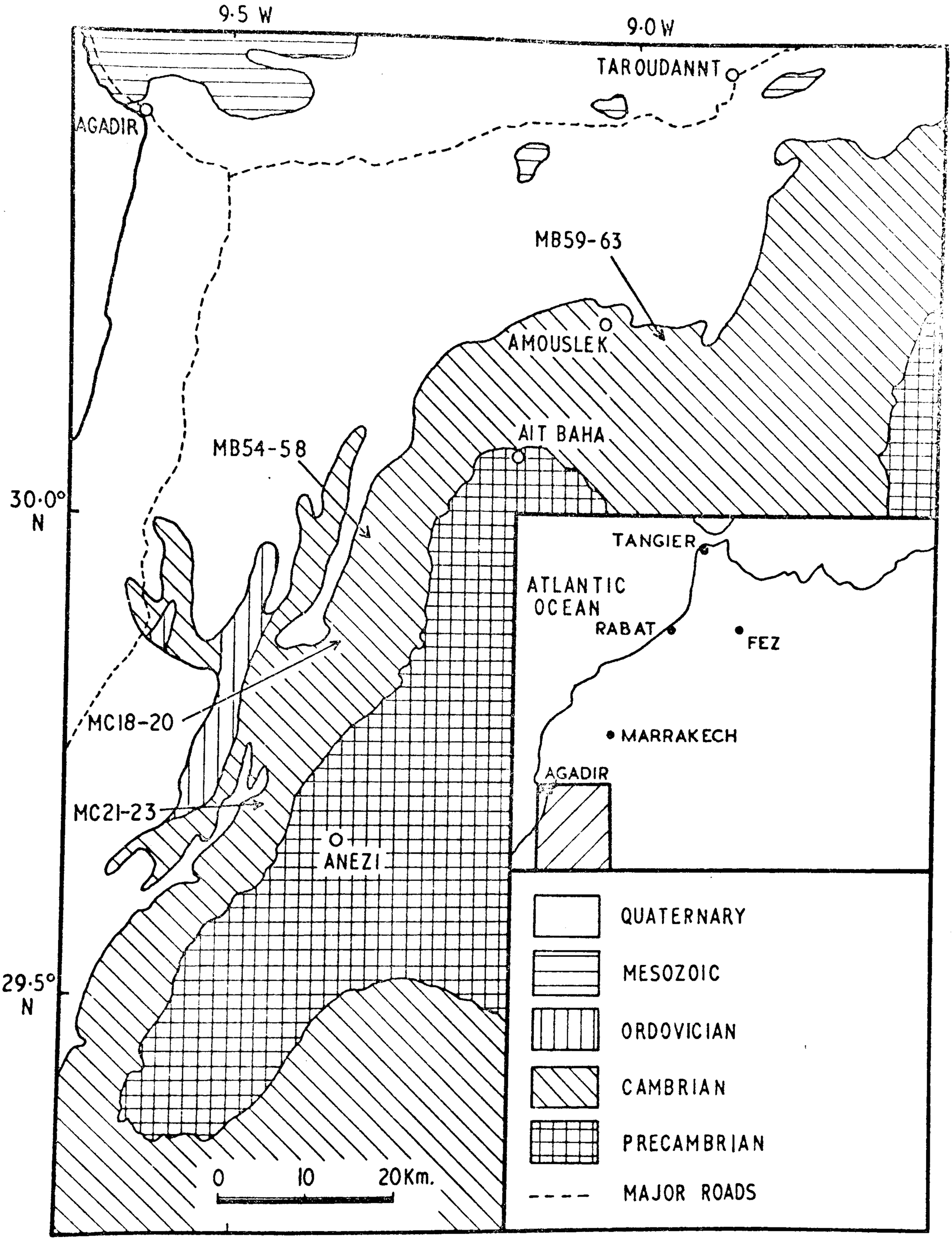


Fig 3.2 Outline Geological map of the NW Anti-Atlas, indicating Lower Cambrian sampling localities.

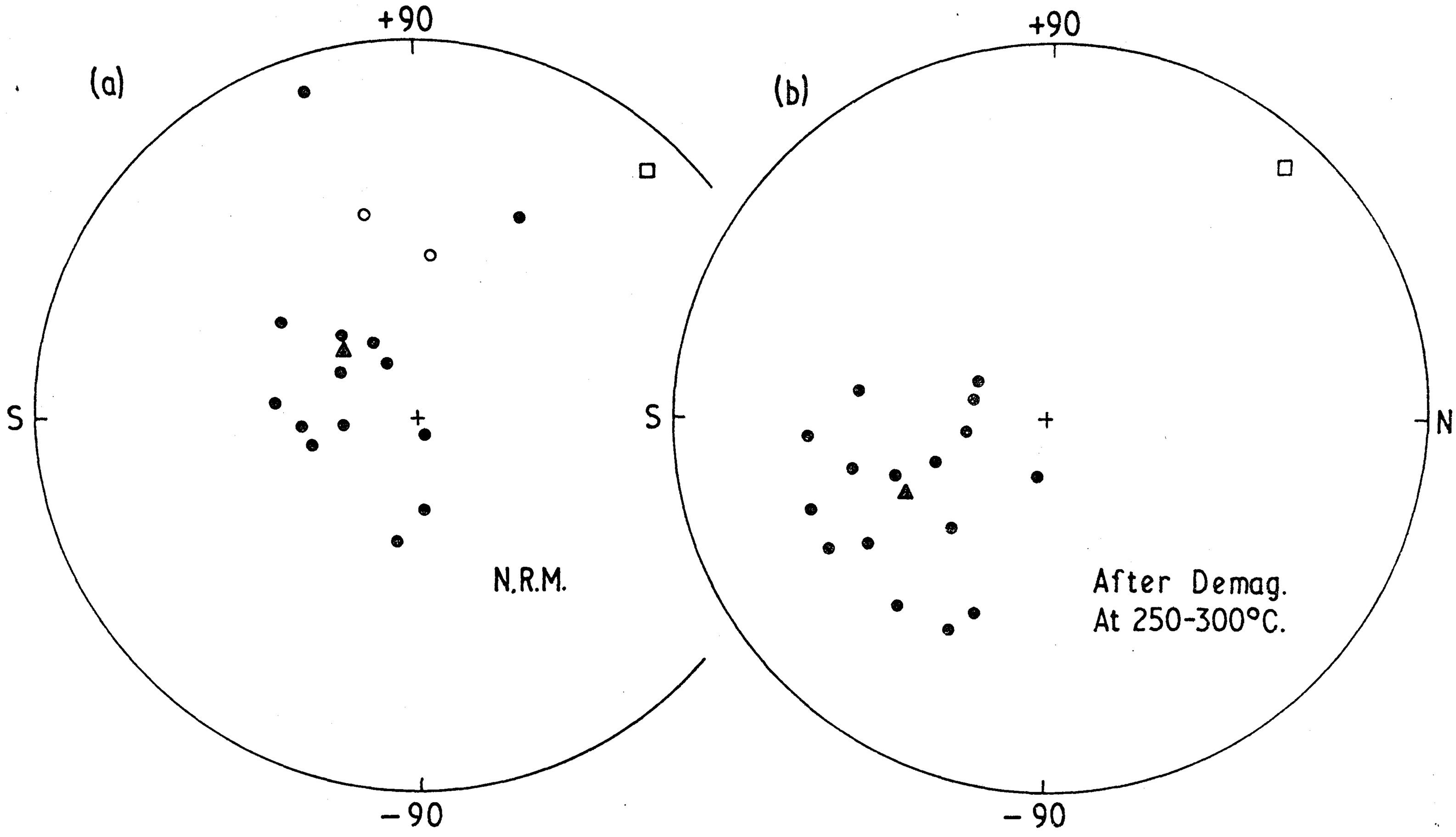


Fig 3.3 Mean site directions of magnetisation of Lower Cambrian volcanic tuffs, plotted on an equatorial stereographic projection. (a) N.R.M. (b) After demagnetisation at 250 to 300°C.

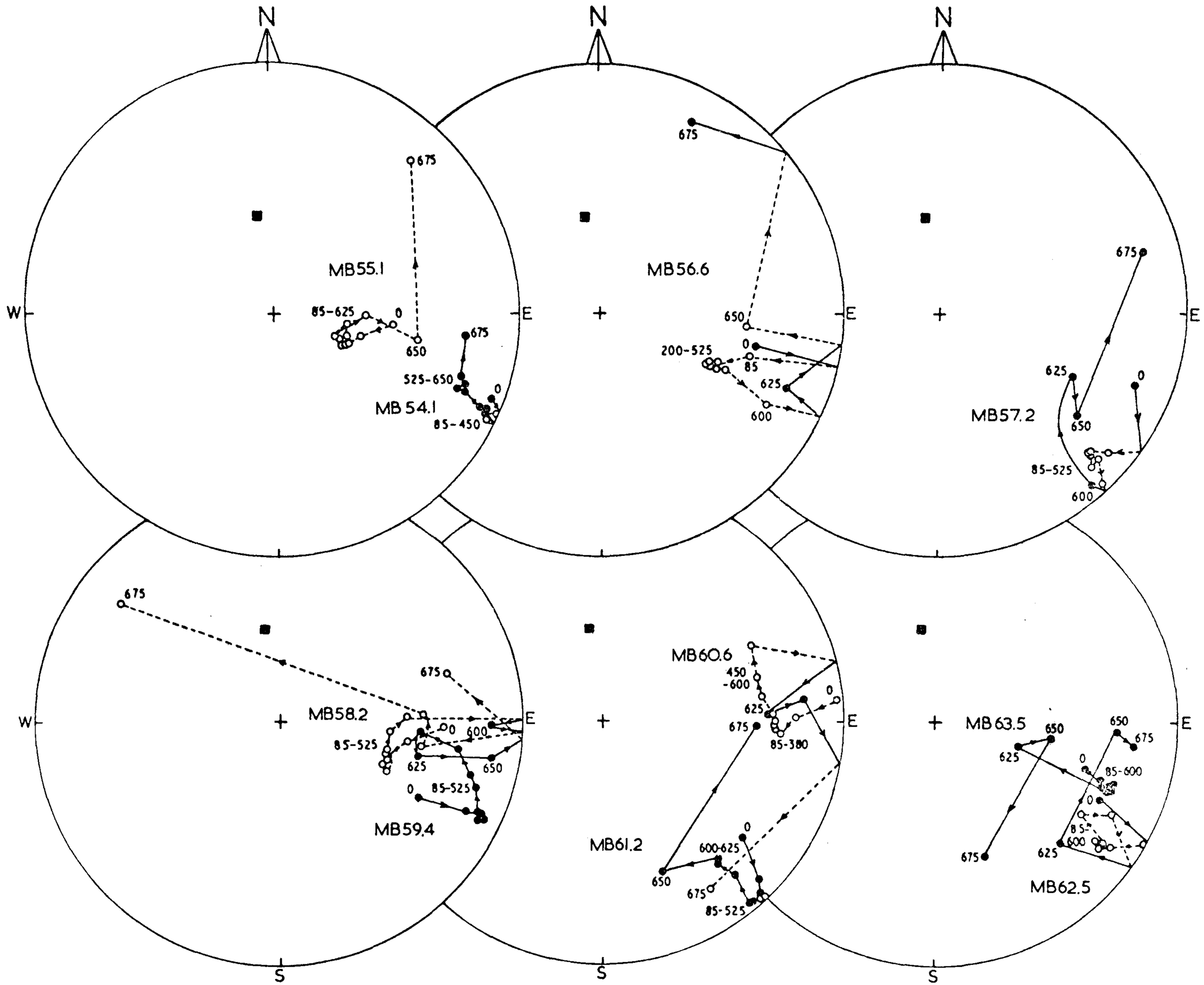


Fig 3.4 Lower Cambrian volcanic tuffs. Changes in direction of remanence of pilot samples from sites MB 54 to 63 during progressive thermal demagnetisation, plotted on polar stereographic projections.

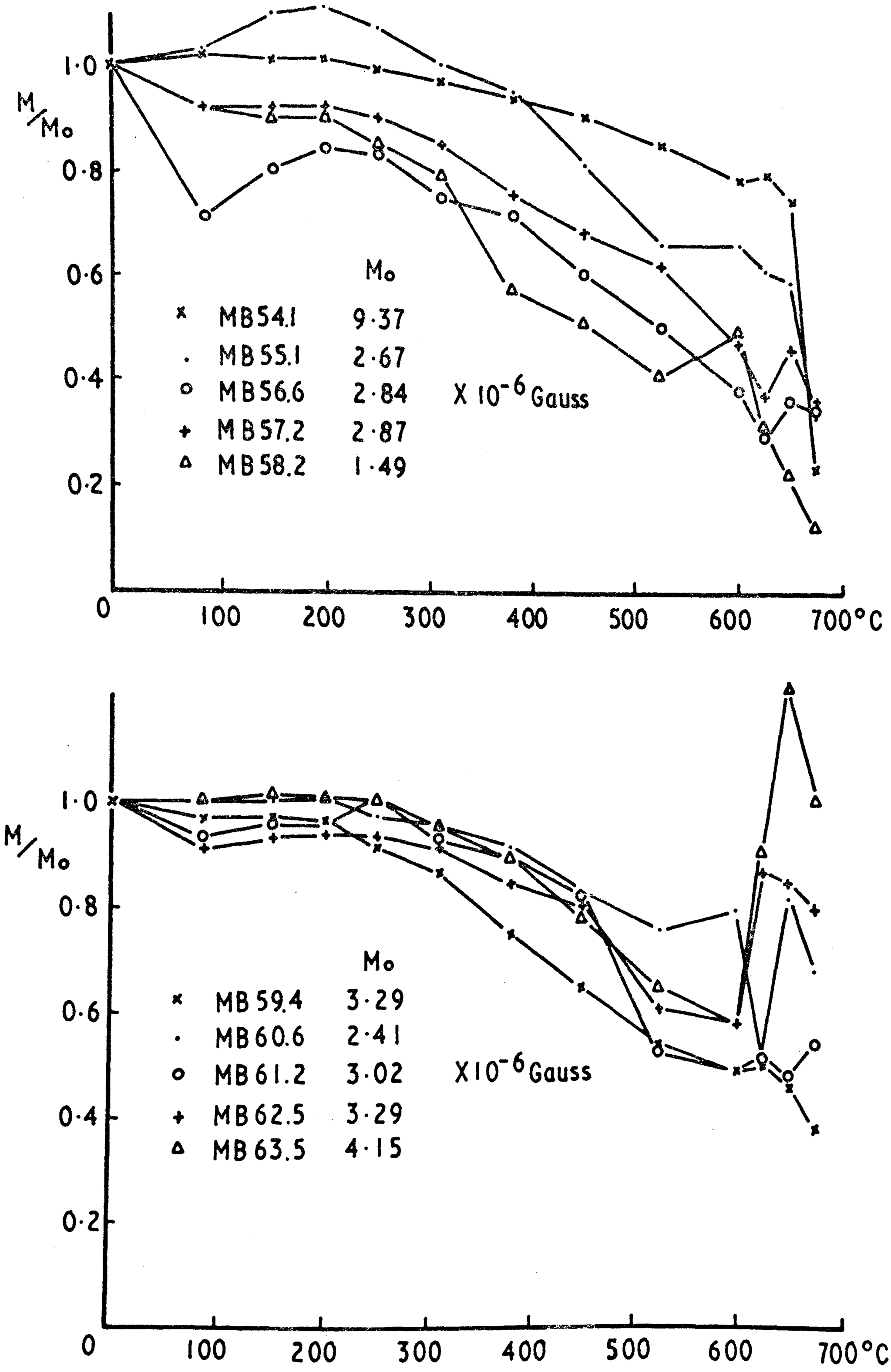


Fig 3.5 Lower Cambrian volcanic tuffs. Changes in intensity of magnetisation of pilot samples from sites MB 54 to 63 during progressive thermal demagnetisation.

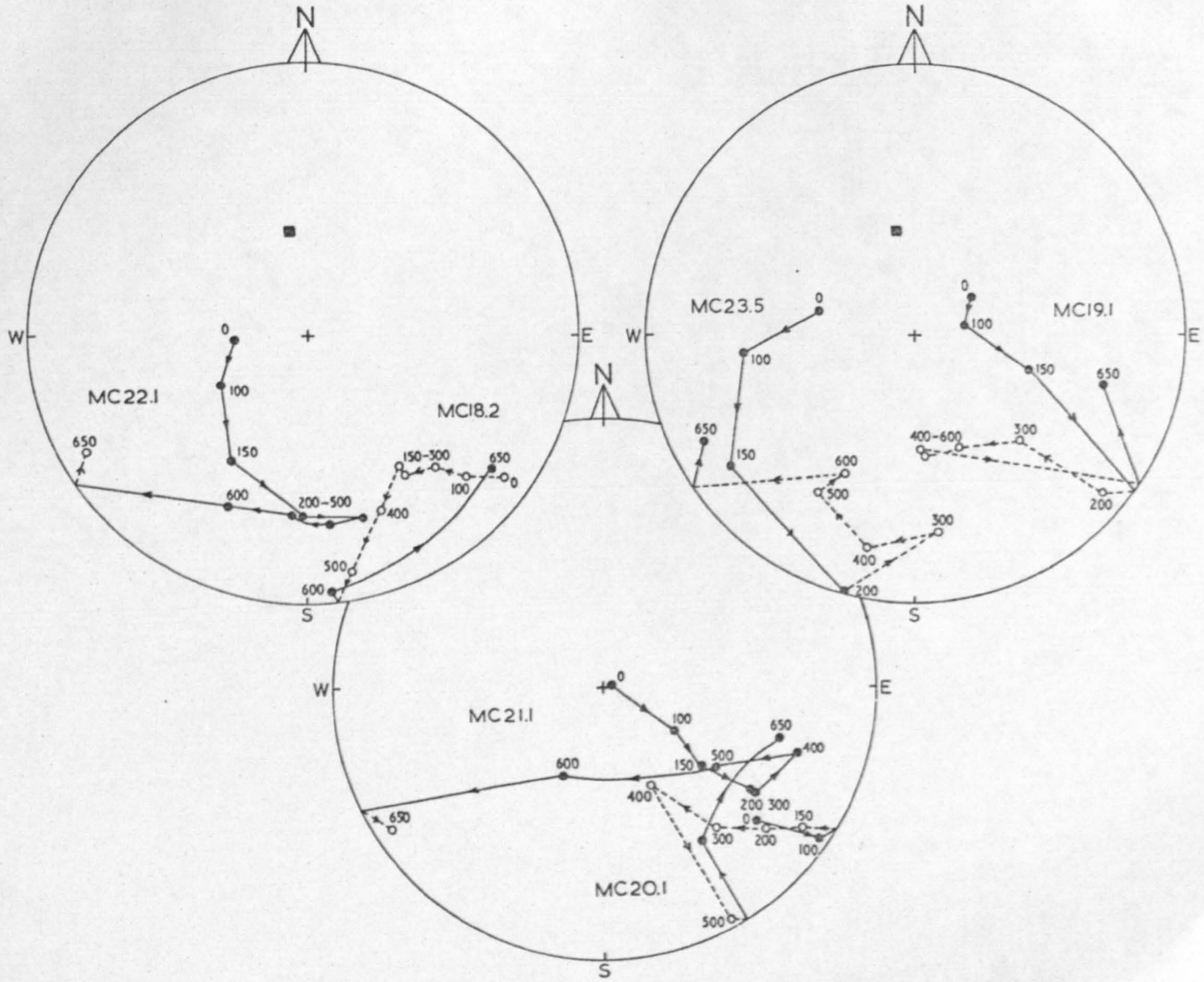


Fig 3.6 Lower Cambrian volcanic tuffs. Changes in direction of remanence of pilot samples from sites MC 18 to 23 during progressive thermal demagnetisation, plotted on polar stereographic projections.

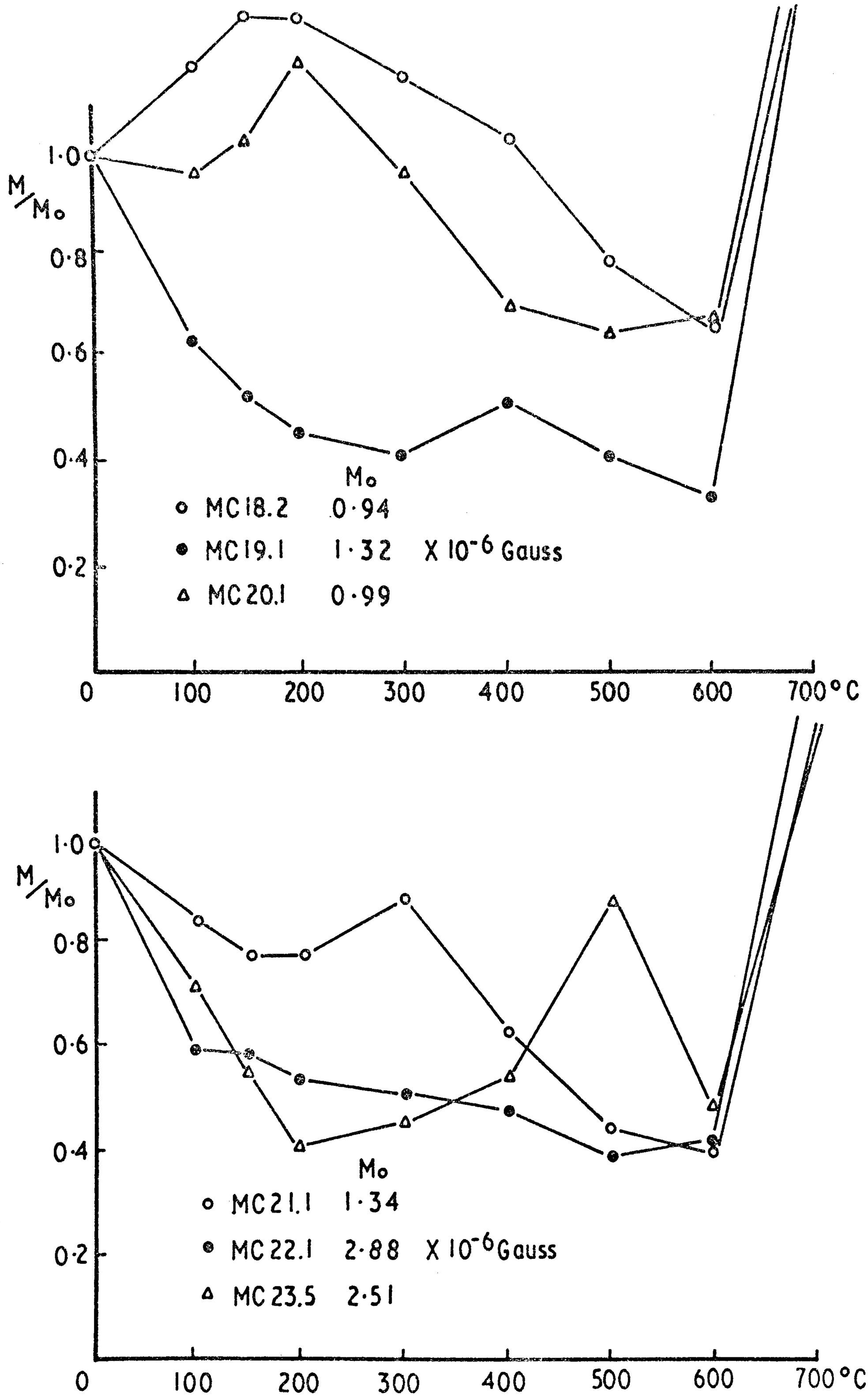
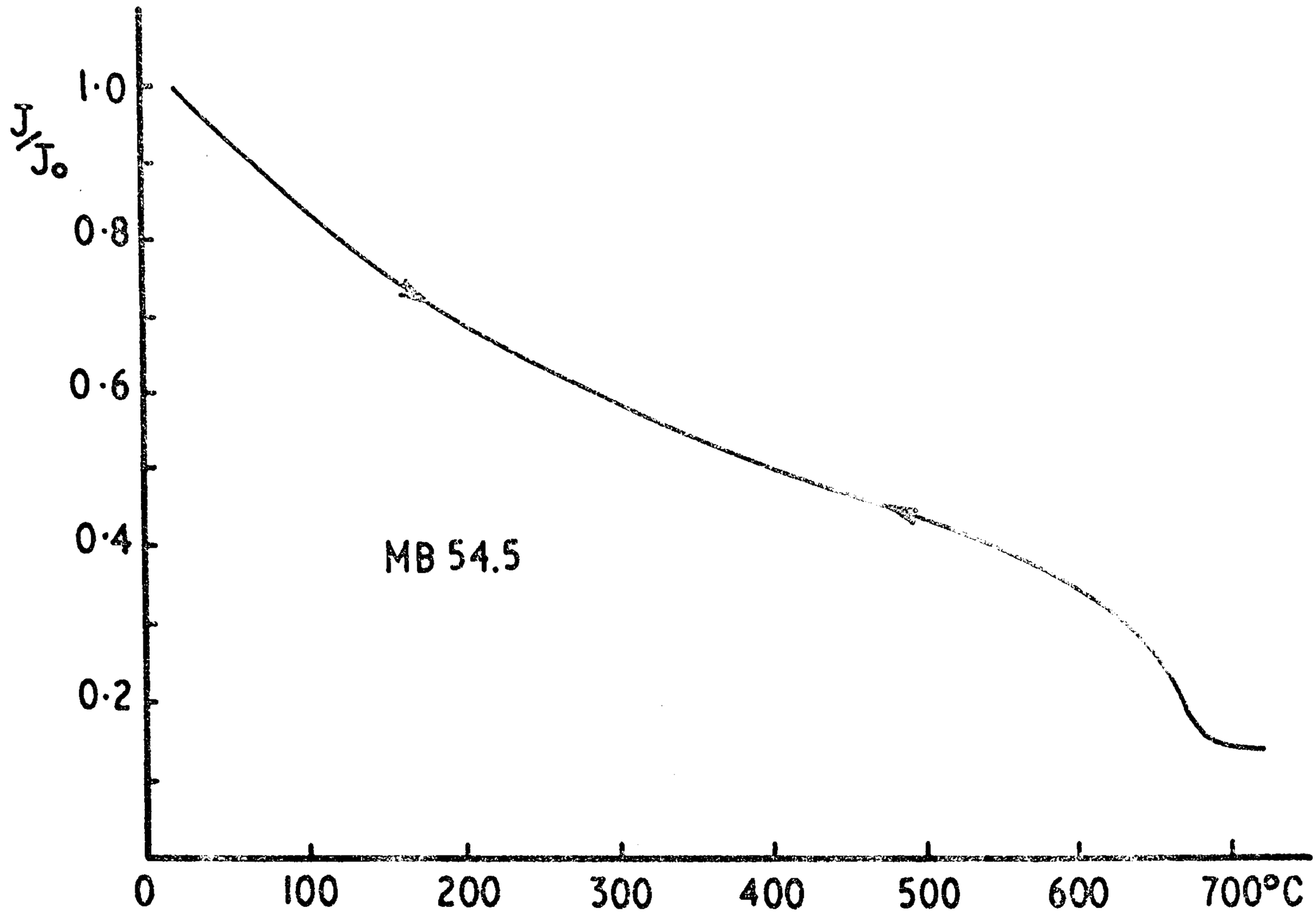


Fig 3.7 Lower Cambrian volcanic tuffs. Changes in intensity of magnetisation of pilot samples from sites MC18 to 23 during progressive thermal demagnetisation.



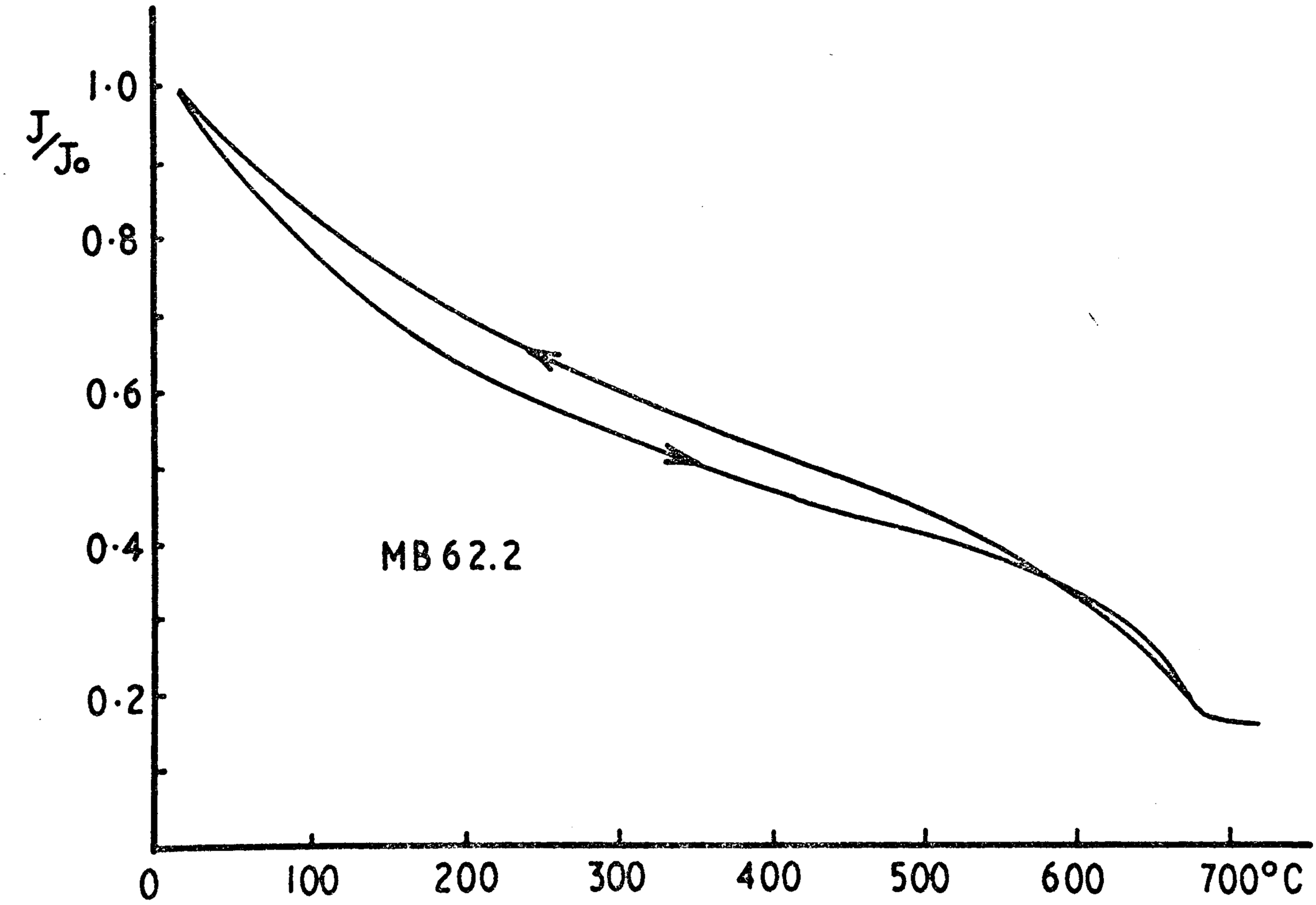


Fig 3.8 Results of thermomagnetic analyses on Lower Cambrian volcanic tuffs.

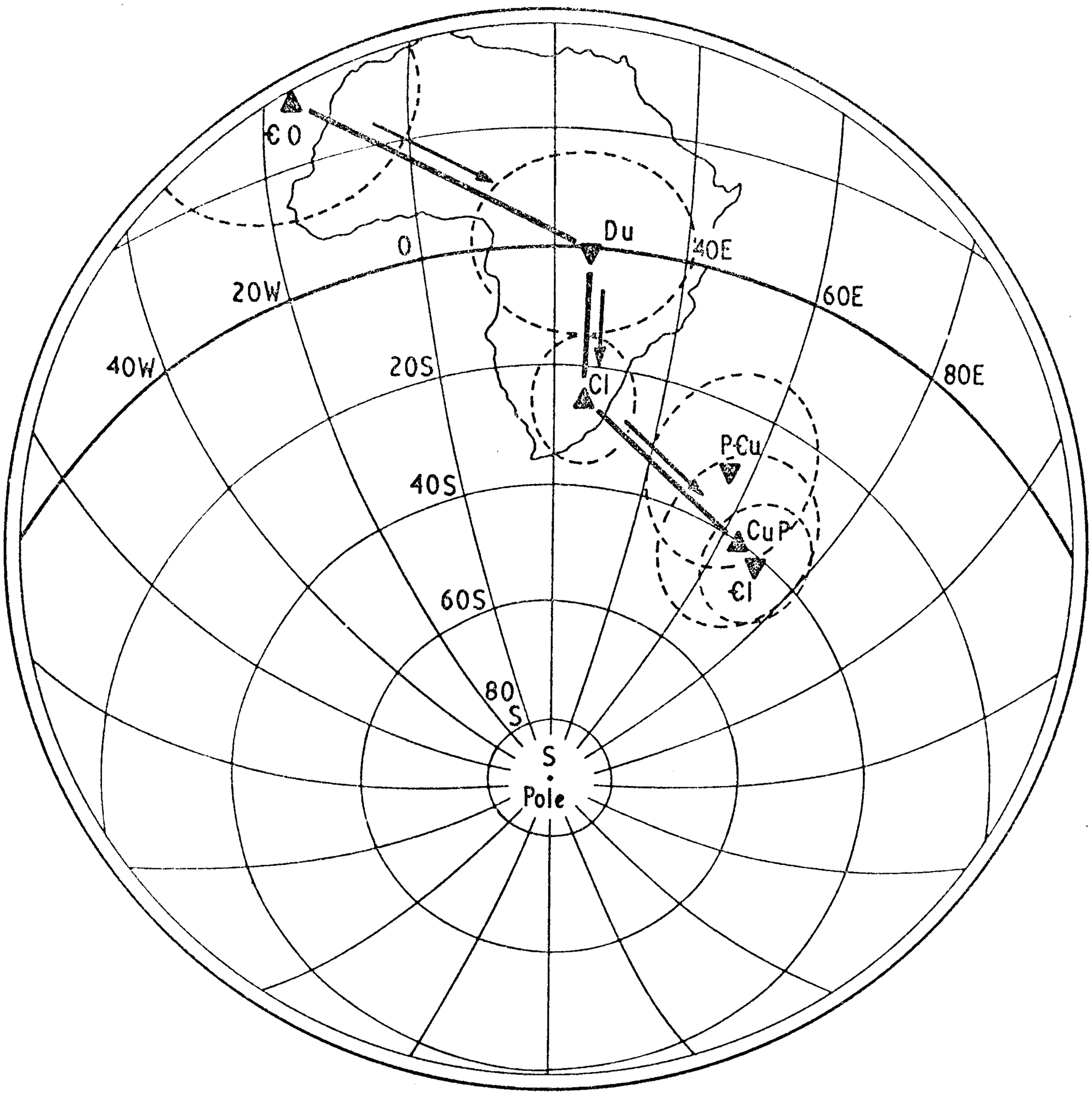


Fig 3.9 African Palaeozoic polar-wander curve, assuming that the Moroccan Precambrian and Cambrian poles represent reversed polarity epochs. Moroccan Devonian pole-position (discussed in Chapter 4) also plotted. Moroccan poles inverted triangles, other African poles upright triangles. €O is the mean Cambro-Ordovician pole from South and East African formations.

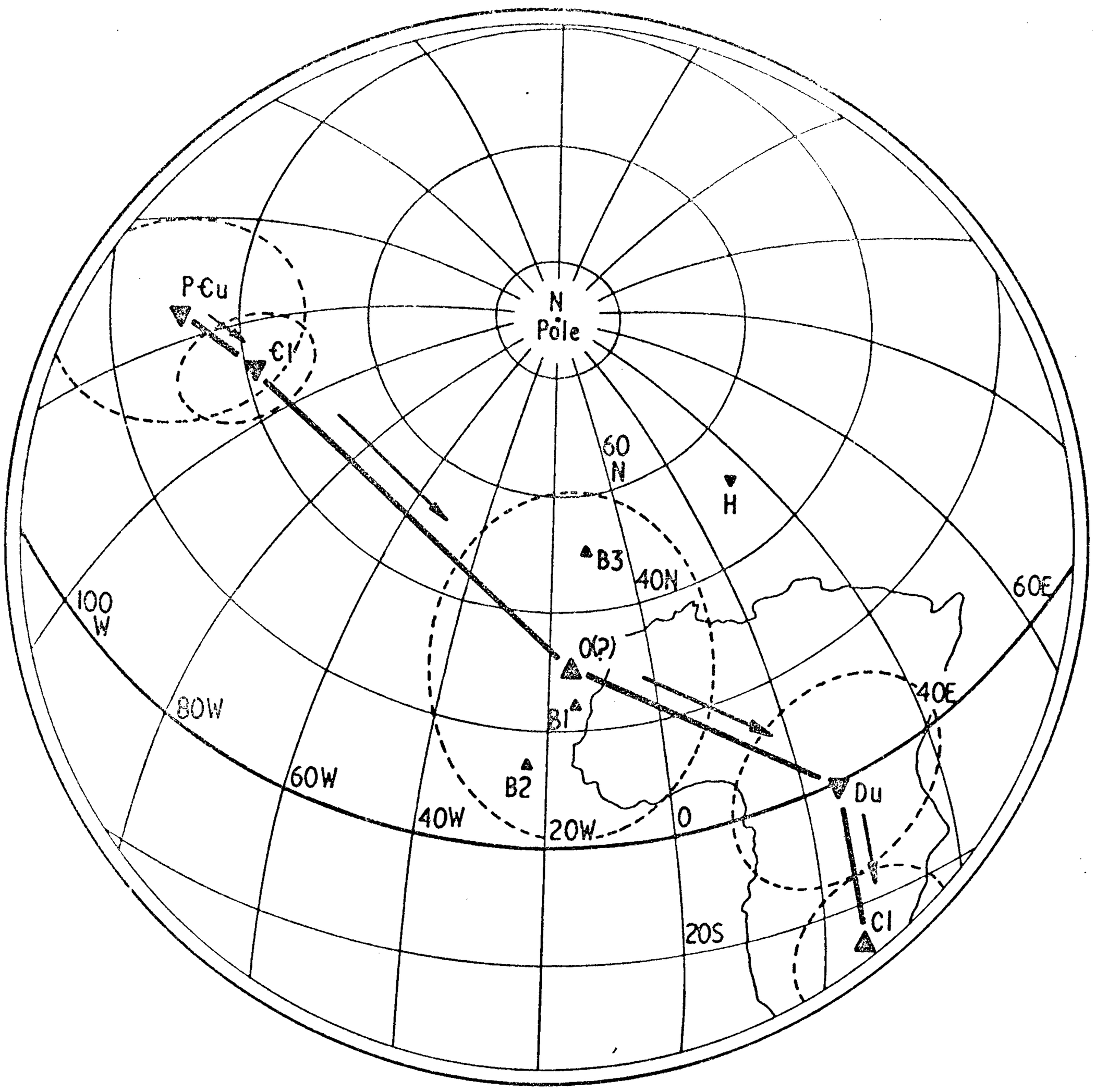


Fig 3.10 African Palaeozoic polar-wander, assuming that the Moroccan Precambrian and Cambrian poles represent normal polarity epochs. Nomenclature as in Fig 3.9. except O(?) which corresponds to €O in Fig 3.9.

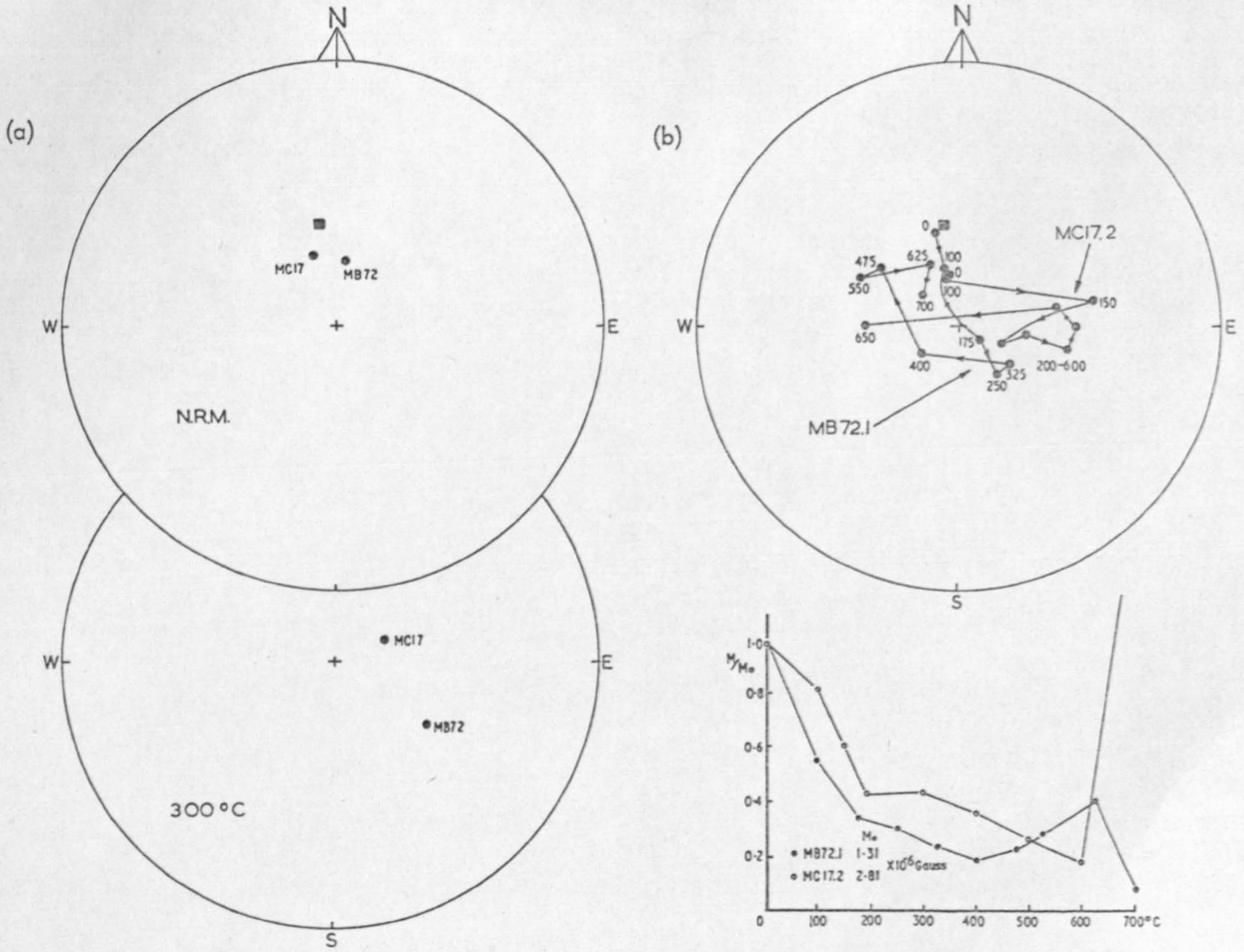


Fig 3.11 Lower Cambrian sediments. (a) Mean site directions of remanence before and after demagnetisation at 300 °C. (b) Pilot sample demagnetisation results. Plotted on polar stereographic projections.

Table 3.1. Cambrian sediments and tuffs. Field Data

Site No.	Tilt Correction Strike	Dip	Location Lat.	Long.	Site No.	Tilt Correction Strike	Dip	Location Lat.	Long.
MB54	23	39	29.80	-9.34	MC18	30	33	29.98	-9.35
MB55	10	40	29.80	-9.34	MC19	30	33	29.98	-9.35
MB56	37	31	29.80	-9.34	MC20	30	33	29.98	-9.35
MB57	25	21	29.80	-9.34	MC21	153	35	29.69	-9.48
MB58	2	29	29.80	-9.34	MC22	152	40	29.69	-9.48
MB59	116	22	30.18	-8.98	MC23	144	38	29.69	-9.48
MB60	346	17	30.18	-8.98					
MB61	7	22	30.18	-8.98					
MB62	3	21	30.18	-8.98					
MB63	279	20	30.18	-8.98					

Table 3.2. Cambrian N.R.M.s (relative to palaeo-horizontal)

Site No.	Sample No.	Dec	Inc	Int ($\times 10^{-5}$ gauss)
MB55	1	96.0	-37.7	0.27
	2	92.2	-33.8	0.21
	3	99.8	-32.6	0.25
	4	124.3	-46.8	0.20
	5	89.5	-39.4	0.20
	6	109.3	-36.3	0.18
MB56	1	106.0	+30.3	0.40
	2	84.2	+21.0	0.20
	3	96.2	-18.4	0.10
	4	100.9	+30.7	0.30
	5	108.7	+10.9	0.30
	6	102.5	+23.6	0.30
MB58	1	100.2	-11.7	0.17
	2	92.4	-21.9	0.15
	3	76.9	-35.1	0.13
	4	96.3	-25.7	0.13
	5	78.8	-31.6	0.14
	6	83.8	-33.3	0.13
MB59	1	103.3	+36.1	0.26
	2	118.0	+17.3	0.50
	3	108.8	+19.5	0.30
	4	118.6	+23.8	0.30
	5	113.5	+35.3	0.20
	6	121.5	+15.7	0.30
MB60	1	90.9	-16.0	0.30
	2	77.6	-7.2	0.30
	3	93.9	-6.1	0.20
	4	89.8	+5.4	0.30
	5	92.0	-1.6	0.20
	6	85.0	-1.2	0.20
MB62	1	115.7	+19.9	0.30
	2	104.0	+15.7	0.30
	5	114.9	+15.8	0.30
	6	118.3	+4.6	0.20
MB63	1	100.8	+23.7	0.40
	2	101.8	+22.3	0.40
	4	108.7	+25.5	0.50
	5	106.6	+24.3	0.40
	6	101.9	+18.8	0.40

MB57	1	130.6	-7.5	0.10
	2	120.1	+9.2	0.30
	3	128.9	-11.2	0.10
	4	125.0	+12.6	0.20
	5	126.8	-8.7	0.10
	6	113.3	-1.8	0.10

MB61	1	132.3	+30.2	0.30
	2	131.3	+20.6	0.30
	3	124.8	+29.0	0.30
	4	137.3	+26.6	0.40
	5	135.8	+28.0	0.40
	6	126.8	+21.0	0.40

Table 3.2 contd.

Site No.	Sample No.	Dec	Inc	Int($\times 10^{-6}$ gauss)	Site No.	Sample No.	Dec	Inc	Int($\times 10^{-6}$ gauss)
MC18	2	126.4	-5.6	0.94	MC21	2	198.4	+73.0	1.22
	3	109.0	-1.3	1.06		3	98.3	+84.0	0.52
	4	144.8	-16.5	0.60		4	176.4	+47.7	0.95
	5	47.7	+11.4	0.20		5	122.1	+68.6	1.20
	6	127.3	+8.1	1.26		6	170.3	+69.2	0.78
MC19	1	57.3	+60.8	1.32	MC22	1	266.2	+60.9	2.88
	2	62.5	+47.0	1.49		2	273.6	+57.1	1.38
	4	49.5	+40.5	1.58		3	283.6	+26.7	1.68
						4	212.0	+33.0	0.56
						5	227.3	+62.0	0.63
						6	198.7	+70.5	0.75
MC20	1	131.2	+16.0	0.99	MC23	1	271.3	+60.7	1.59
	2	133.2	+4.5	0.94		2	281.8	+53.0	1.52
	3	129.3	+4.4	0.76		3	251.9	+48.0	1.87
	4	130.4	+15.7	1.25		4	272.4	+41.4	2.44
	5	106.4	-20.2	0.39		5	285.0	+40.4	2.51
	6	153.7	+6.5	1.19		6	284.0	+39.7	2.91

Table 3.3. Pilot sample demagnetisation results

	MB541			MB551			MB566			MB572		
Temp	Dec	Inc	Int*	Dec	Inc	Int	Dec	Inc	Int	Dec	Inc	Int
R.T.	112.4	+3.2	9.37	96.0	-37.7	2.67	102.5	+23.6	2.84	120.1	+9.2	2.87
85	114.6	-0.2	9.60	104.7	-50.0	2.75	106.2	-24.7	2.01	128.7	-5.7	2.63
150	115.9	-2.6	9.50	113.2	-54.2	2.94	112.4	-35.5	2.27	131.8	-10.1	2.65
200	117.2	-2.4	9.46	113.7	-55.7	2.97	114.6	-38.7	2.38	132.7	-10.3	2.65
250	117.1	-0.8	9.30	115.9	-56.0	2.85	115.6	-39.1	2.35	133.0	-9.3	2.58
310	116.5	+0.7	9.11	115.3	-56.3	2.68	113.6	-37.9	2.14	135.1	-7.4	2.43
380	115.5	-3.2	8.78	112.3	-57.7	2.53	114.9	-37.2	2.05	131.6	-6.6	2.18
450	114.7	-5.2	8.53	107.9	-55.9	2.20	115.1	-33.8	1.73	136.0	-1.6	1.99
525	112.6	+10.1	8.07	99.1	-57.1	1.80	114.4	-30.7	1.45	135.4	+1.4	1.80
600	113.0	+12.7	7.44	111.1	-61.0	1.78	118.9	-14.1	1.11	137.8	+2.7	1.39
625	110.9	+11.2	7.50	91.7	-49.2	1.65	112.4	+10.7	0.85	115.0	+28.3	1.08
650	108.9	+12.6	7.05	101.1	-28.7	1.60	95.1	.28.0	1.05	126.2	+20.2	1.35
675	97.1	+14.5	2.29	43.3	-9.7	0.91	26.5	+8.9	0.99	72.8	+8.6	1.07

	MB582			MB594			MB606			MB612		
Temp	Dec	Inc	Int	Dec	Inc	Int	Dec	Inc	Int	Dec	Inc	Int
R.T.	92.4	-21.9	1.49	118.6	+23.8	3.29	85.0	-1.2	2.41	130.4	+16.4	3.02
85	99.0	-34.4	1.37	116.0	+9.3	3.18	89.1	-13.0	2.41	134.8	+4.9	2.80
150	106.8	-40.9	1.34	115.4	+6.0	3.19	93.7	-17.2	2.42	137.4	+1.5	2.89
200	109.6	-40.5	1.34	116.6	+5.1	3.16	92.8	-18.6	2.42	138.5	-0.6	2.87
250	112.8	-41.5	1.27	116.4	+4.3	2.98	89.9	-19.2	2.35	137.2	-0.4	2.81
310	114.8	-38.5	1.18	115.2	+5.4	2.83	91.0	-19.5	2.28	138.3	-0.7	2.79
380	105.0	-41.5	0.87	109.3	+9.2	2.45	87.8	-20.5	2.19	140.3	+1.5	2.52
450	95.5	-41.3	0.77	106.2	+11.7	2.11	80.8	-22.7	1.99	140.9	+2.0	2.43
525	88.4	-35.0	0.63	99.2	+17.3	1.75	74.1	-23.4	1.80	139.5	+9.7	1.58
600	91.0	+8.1	0.74	95.2	+28.7	1.59	62.9	-20.9	1.91	140.5	+17.0	1.45
625	100.0	-28.8	0.48	104.5	+28.8	1.61	87.8	+21.1	1.22	140.3	+16.2	1.52
650	87.3	-29.3	0.34	99.6	+6.9	1.49	84.0	+9.6	1.95	158.1	+22.9	1.42
675	307.7	-11.8	0.20	74.2	-18.9	1.23	147.0	-11.4	1.62	91.6	+25.3	1.60

* $\times 10^{-6}$ gauss

Table 3.3. contd.

	MB625			MB635			MC18.2				MC19.1		
Temp	Dec	Inc	Int	Dec	Inc	Int	Temp	Dec	Inc	Int	Dec	Inc	Int
R.T.	114.9	+15.8	3.29	106.6	+24.3	4.15	R.T.	126.4	-5.6	0.94	57.3	+60.8	1.32
85	120.1	-0.5	2.98	108.4	+17.8	4.14	100	131.7	-12.8	1.10	78.6	+58.1	0.83
150	125.5	-7.0	3.05	110.3	+15.0	4.20	150	135.6	-21.1	1.19	106.6	+42.3	0.69
200	125.3	-8.7	3.09	109.9	+14.3	4.17	200	144.9	-25.4	1.18	130.2	-4.6	0.59
250	126.9	-8.9	3.06	112.0	+14.8	4.17	300	145.4	-28.4	1.08	134.8	-31.9	0.55
210	126.0	-10.9	3.00	110.9	+13.8	3.93	400	156.9	-18.8	0.97	158.1	-41.0	0.68
380	124.9	-10.4	2.77	111.5	+13.8	3.70	500	168.9	-6.4	0.74	174.9	-40.5	0.56
450	125.1	-10.5	2.63	108.7	+13.8	3.24	600	174.1	+2.3	0.63	176.0	-42.6	0.45
525	121.9	-18.7	1.96	101.5	+15.1	2.66	650	126.0	+9.5	20.86	105.1	+18.4	12.23
600	117.1	-12.7	1.89	100.7	+17.2	2.38							
625	133.1	+19.1	2.84	106.4	+50.1	3.72							
650	93.0	+15.9	2.75	98.2	+37.6	5.06							
675	97.2	+10.9	2.60	159.4	+28.9	4.13							

	MC20.1			MC21.1			MC22.1			Mc23.5		
Temp	Dec	Inc	Int	Dec	Inc	Int	Dec	Inc	Int	Dec	Inc	Int
R.T.	131.2	+16.0	0.99	78.4	+85.6	1.34	266.2	+60.9	2.88	285.0	+40.4	2.51
100	124.9	+1.6	0.95	121.4	+65.7	1.13	239.4	+50.4	1.74	264.5	+24.6	1.80
150	125.1	-5.7	1.02	128.9	+40.4	1.04	210.5	+33.4	1.69	234.3	+10.1	1.39
200	131.2	-13.2	1.17	125.3	+23.4	1.04	181.5	+22.2	1.55	194.6	+0.5	1.01
300	141.0	-23.3	0.95	125.3	+21.2	1.19	162.6	+18.6	1.48	172.8	-17.4	1.14
400	154.0	-46.1	0.69	109.0	+16.0	0.85	172.3	+18.2	1.38	192.4	-12.3	1.36
500	151.5	-1.3	0.65	125.9	+35.9	0.59	183.7	+22.2	1.12	211.0	-21.5	2.21
600	146.9	+22.4	0.67	202.6	+51.2	0.53	204.0	+19.9	1.22	206.0	-30.5	1.20
650	106.2	+21.7	25.31	236.3	-3.7	51.82	240.9	-5.9	72.80	242.7	+7.6	46.04
650	106.8	+11.8	16.24	243.2	-25.6	22.21						

Table 3.4. Cambrian Remanence directions and intensities after treatment at 250°C (Sites MB54 to 63)

Site No.	Sample No.	Dec	Inc	Int(x10^{-6} gauss)	Site No.	Sample No.	Dec	Inc	Int(x10^{-6} gauss)	Site No.	Sample No.	Dec	Inc	Int(x10^{-6} gauss)
B54	1	117.1	-0.8	9.30	MB58	1	124.7	-39.8	0.99	MB62	1	129.6	-14.5	3.06
	2	117.3	+0.7	13.04		2	112.8	-41.4	1.27		2	139.6	-8.8	3.32
	3	111.6	-8.7	8.48		3	95.0	-55.0	1.06		5	101.3	-8.2	3.06
	4	111.7	-2.8	11.51		4	138.1	-37.8	1.21		6	141.0	-19.8	2.39
	5	112.5	-6.9	9.01		5	163.6	-83.4	0.87					
						6	101.4	-55.9	1.10					
MB55	1	115.9	-56.0	2.85	MB59	1	97.0	+6.3	2.43	MB63	1	108.6	+10.7	3.36
	2	118.1	-53.3	1.83		2	117.3	-6.6	4.46		2	113.7	+11.7	4.33
	3	138.2	-54.4	2.18		3	106.6	-0.4	2.99		4	112.0	+14.3	4.25
	4	137.6	-50.1	2.19		4	116.4	+3.9	2.98		5	112.0	+14.3	4.17
	5	135.6	-56.6	2.10		5	115.6	+25.4	2.03		6	109.5	+6.0	3.66
	6	132.5	-59.8	2.00		6	123.4	+7.9	3.21					
MB56	1	124.4	-20.8	1.97	MB60	1	97.2	-24.4	2.66					
	2	111.8	-34.2	2.01		2	86.5	-12.3	2.67					
	3	121.3	-37.7	2.10		3	92.1	-27.0	2.21					
	4	121.9	-17.4	1.73		4	98.4	-7.5	2.81					
	5	128.4	-32.7	2.64		5	91.1	-14.6	1.85					
	6	115.6	-39.1	2.35		6	89.8	-19.3	2.35					
MB57	1	135.9	-11.6	0.99	MB61	1	146.6	+15.3	1.93					
	2	133.0	-9.4	2.58		2	137.4	+3.1	2.85					
	3	143.1	-24.0	1.07		3	143.4	+5.4	2.05					
	4	139.7	-4.6	1.43		4	149.8	+16.9	3.04					
	5	136.4	-23.2	0.68		5	147.2	+17.6	3.70					
	6	120.5	-12.9	0.87		6	137.7	-16.8	2.17					

Table 3.4. contd. Cambrian remanence directions and intensities after treatment at 300°C (Sites MC18-23).

Site No.	Sample No.	Dec	Inc	Int*
MC18	2	145.4	-28.4	1.08
	3	132.6	-23.7	1.22
	4	176.0	-43.4	1.11
	5	145.6	-31.6	1.23
	6	133.7	-18.7	1.35
MC19	1	134.8	-31.9	0.55
	2	180.9	-59.8	0.50
	4	128.6	-38.9	0.41
MC20	1	141.0	-23.3	0.95
	2	160.5	-36.3	1.31
	3	152.3	-45.6	1.29
	4	160.2	-17.4	1.29
	5	158.5	-38.7	1.13
	6	156.5	-10.0	1.86
MC21	2	124.2	-30.3	1.17
	3	146.7	-13.1	1.14
	4	162.9	-3.1	1.55
	5	157.8	-5.8	0.93
	6	133.3	-7.0	0.92
MC22	1	162.6	+18.6	1.48
	2	133.6	-5.8	1.60
	3	179.0	-9.2	1.44
	4	139.5	-25.2	0.92
	5	170.8	+5.0	0.79
	6	144.1	-2.2	0.85
MC23	1	180.7	-15.1	1.05
	2	128.6	-6.2	1.18
	3	165.1	-5.9	0.92
	4	148.3	-24.3	1.31
	5	172.8	-17.4	1.14
	6	140.5	-39.2	0.93

Table 3.5. Cambrian N.R.M. mean site directions, pole positions and statistical parameters (data corrected for tectonic tilting)

Site No.	D	I	N	R	k	$_{95}$	c.s.d.	Pole Position Lat.	Long.	A_{95}
MB654	112.3	-1.3	5	4.991	438	3.7	3.9	19.5S	69.7E	1.9
MB55	101.2	-38.3	6	5.907	54	9.2	11.0	20.2S	94.7E	10.4
MB56	99.7	+16.8	6	5.693	16	17.1	20.2	3.9S	68.2E	10.9
MB57	124.1	-1.3	6	5.894	47	9.9	11.8	29.5S	62.6E	6.8
MB58	88.6	-26.8	6	5.885	44	10.3	12.3	5.6S	94.1E	8.8
MB59	114.2	+24.7	6	5.910	55	9.1	10.9	13.2S	57.0E	7.1
MB60	88.2	-4.5	6	5.934	75	7.8	9.3	0.4N	83.9E	5.8
MB61	131.4	+26.0	6	5.972	181	5.0	6.0	25.8S	45.1E	4.4
MB62	113.3	+14.1	4	3.963	81	10.2	9.0	16.0S	62.5E	8.1
MB63	103.9	+23.0	5	4.990	391	3.9	4.1	5.7S	63.6E	3.5
MC18	121.5	-6.8	5	4.756	16	19.5	20.1	28.8S	66.9E	17.5
MC19	49.4	+53.0	3	2.899	20	28.4	18.2	49.8S	59.8E	34.3
MC20	130.9	+4.7	6	5.707	17	16.7	19.7	33.0S	55.1E	13.7
MC21	164.4	+71.0	5	4.818	22	16.7	17.3	1.1S	0.5W	25.7
MC22	247.9	+56.4	6	5.443	9	23.6	27.3	2.7N	54.5W	28.3
MC23	274.9	+47.8	6	5.892	46	10.0	11.9	17.7N	75.2W	11.1
Overall Mean No tilt correction	103.9	+39.9	16	13.280	5	17.3	35.0			
Overall Mean Tilt correction applied	112.7	+20.4	16	11.104	4	25.5	47.6	11.9S	56.0E	25.5

Table 3.6. Cambrian Mean Site Directions of Remanence, pole positions and statistical parameters, after thermal demagnetisation at 250 to 300°C

Site No.	D	I	N	R	k	α_{95}	c.s.d.	Pole Position Lat.	Long.	A_{95}
MB54	114.0	-3.7	5	4.985	269	4.7	4.9	21.7S	69.8E	3.4
MB55	129.7	-55.4	6	5.966	149	5.5	6.6	47.8S	102.9E	7.3
MB56	120.7	-30.4	6	5.918	61	8.6	10.4	34.5S	81.1E	6.6
MB57	134.7	-14.4	6	5.911	56	9.0	10.8	42.1S	62.2E	7.2
MB58	117.8	-53.3	6	5.683	16	17.4	20.5	83.3S	106.2E	22.7
MB59	112.7	+6.1	6	5.846	32	11.9	14.3	17.8S	66.3E	9.1
MB60	92.5	-17.6	6	5.944	89	7.2	8.6	6.7S	87.7E	5.0
MB61	143.6	+7.0	6	5.850	33	11.8	14.1	41.6S	43.3E	7.0
MB62	122.8	-11.3	4	3.880	25	18.8	16.3	31.1S	68.5E	18.8
MB63	111.2	+11.4	5	4.990	418	3.7	4.0	15.0S	64.9E	2.5
MC18	145.1	-30.0	5	4.822	22	16.5	17.1	56.1S	64.9E	16.9
MC19	142.8	-45.4	3	2.837	12	36.8	23.3	59.8S	86.4E	43.6
MC20	154.8	-28.7	6	5.823	28	12.8	15.3	63.0S	55.0E	9.2
MC21	145.6	-12.2	5	4.781	18	18.4	19.0	49.8S	52.0E	16.5
MC22	155.0	-3.3	6	5.588	12	20.0	23.4	53.3S	35.6E	16.9
MC23	156.5	-18.9	6	5.607	13	19.5	22.8	60.4S	44.0E	17.9
Overall Mean No tilt correction	130.7	-0.2	16	14.555	10	12.0	25.3			
Overall Mean tilt correction applied	131.3	-19.6	16	14.340	9	13.0	27.2	41.6S	69.5E	10.7

Table 3.7. Lower Cambrian volcanic tuffs. Variation of susceptibility with temperature

Spec No.	R.T.	85°C	150°C	200°C	250°C	310°C	380°C	450°C	525°C	625°C	650°C
MB541	169	175	169	175	175	169	162	150	140	180	220
MB551	162	156	156	162	162	163	162	150	140	180	260
MB566	188	188	188	189	189	195	189	163	150	240	360
MB572	150	150	150	143	150	143	143	130	120	180	240
MB582	46	45	45	45	45	45	42	40	38	50	60
MB594	110	110	110	110	117	110	117	98	80	320	260
MB606	110	110	104	110	104	104	110	104	96	440	320
MB612	123	123	123	123	124	117	124	124	120	380	260
MB625	260	254	254	254	254	254	266	260	260	440	1100
MB635	280	280	266	266	273	273	280	273	273	540	1660

Spec No.	R.T	100°C	150°C	200°C	300°C	400°C	500°C	600°C	650°C
MC17.2	30	45	40	40	40	40	25	35	50
MC18.2	30	30	30	30	30	30	30	35	55
MC19.1	35	35	35	35	35	35	25	30	50
MC20.1	30	30	25	30	25	25	25	40	55
MC21.1	65	65	60	65	60	60	50	75	155
MC22.1	120	115	115	115	105	120	65	100	245
MC23.5	105	100	100	105	100	110	65	70	190

All values x 10^{-6} gauss per oersted

Table 3.8. Lower Cambrian sediments, sites MB72 and MC19

(i) Pilot sample demagnetisation results

Sample No.	MB72.1			Sample No.	MC17.2		
Temp	D	I	Int($\times10^{-6}$ gauss)	Temp	D	I	Int($\times10^{-6}$ gauss)
R.T.	346.4	48.8	1.31	R.T.	343.9	70.4	2.81
100	346.8	63.8	0.74	100	349.2	67.9	2.38
175	115.7	78.7	0.45	150	34.5	80.3	1.72
250	139.3	64.2	0.39	200	113.9	69.5	1.14
325	122.8	63.0	0.30	300	97.1	59.9	1.21
400	235.2	70.8	0.23	400	102.8	43.1	1.01
475	308.5	48.9	0.29	500	40.8	41.2	0.74
550	301.4	44.1	0.37	600	80.5	47.6	0.50
640	336.0	60.2	0.53	650	269.4	41.0	17.09
700	313.9	58.8	0.09				

(ii) Mean site directions and pole positions

(a) N.R.M.

Site No.	D	I	N	R	k	A_{95}	c.s.d.
MB72	8.0	62.2	6	5.905	52	9	11
MC17	343.1	59.1	3	2.941	34	21	14

(b) After bulk demagnetisation (200°C)

MB72	124.5	44.5	6			37	
MC17	65.3	67.2	3	2.917	24	26	17

Table 3.9. African Palaeozoic palaeomagnetic pole positions

Age	Description	Ref (McElhinny, 1968)	Formation mean pole position Lat.	Long	α_{95}	No Samples	No Sites	Age of Mean pole	Symbol	Mean Palaeomagnetic pole position Lat	Long	α_{95}
Precambrian III	Moroccan rhyolites & andesites	-	30.5S	57.0E	17°	46	8	Late Precambrian	PEu	30.5S	57.0E	17°
Lower Cambrian	Moroccan volcanic tuffs	-	41.5S	69.5E	10.5°	87	16	Lower Cambrian	€1	41.5S	69.5E	10.5°
Upper Precamb. to Lower Camb.	Ntonya Ring Structure Malawi	B1	27.5N	15.0W	2°	-	7	Ordovician(?) (see text)	O(?)	31.0N	17.0W	29.5°
Ordovician	Hook intrusives Zambia	B2	14.0N	23.5W	36°	-	3					
Lower Ordovician	Table Mt.Series, Cape Town	B3	50.0N	11.0W		8						
Upper Devonian	Msissi norite, Morocco	-	0.5S	25.0E	16.5°	42	8	Upper Devonian	Du	Du	0.5S	25.0E	16.5°
Lower Carboniferous	Dwyka varves, Central Africa	B4	26.5S	26.5E	10.5°	23	5	Lower Carboniferous	C1	26.5S	26.5E	10.5°
Upper Carboniferous	K3 Beds, Galula coalfield	B5	45.5S	40.0E	8°	34	5					
Lower Permian	Ecca Redbeds Tanzania	B6	27.0S	89.0E	15.5°	27	4	Upper Camb to Lower Permian	CuP	40.0S	64.5E	16.5

CHAPTER 4. DEVONIAN

4.1 Geology

The Devonian sequence of the NE Anti Atlas is characterised by a greater diversity than the preceding Lower Palaeozoic deposits. However there is a predominance of neritic sediments, and limestones are frequent, usually containing corals, crinoids, brachyopods, and occasional trilobites. The overall palaeoclimatic and palaeogeographic environment indicated by these deposits is one of warm, clear, relatively shallow seas, marking a return to warmer conditions following the Ordovician and early Silurian glacial period (Hollard, 1968).

In the Eastern Anti-Atlas region Devonian outcrops are confined to synclinal basins between Zagara and Erfoud (Fig. 1.1), bounded to the North and West by the Precambrian and Lower Palaeozoic massifs.

The Lower Devonian sequence begins with a series of dark shales and limestones, containing Orthocerids and graptolites, and local basaltic horizons (e.g. at Hammar Laghdad). The well-known highly fossiliferous Devonian coral reef of Hammar Laghdad was formed at this time, indicating local shallow, warm waters, and possible subsidence.

The base of the Middle Devonian is marked by 50 metres of grey limestones with gonatite-bearing nodules. This is followed by some 200 metres of reef-limestone deposits, with an abundant neritic fauna (brachyopods, crinoids, corals etc), and stromatoporitic reefs in the more turbulent zones.

The Upper Devonian sequence begins with deposits of fine, pink, possibly continental, sandstones, often with ferruginous cement. These are followed by biostromatic deposits (bedded structures composed of

shell, crinoid and coral beds, lacking reef-like structure), indicating a continuation of warm, shallow water conditions, and passing upwards into a transgressive sequence. The uppermost Devonian (Famenian) series begins with deeper water deposits, rich in gonatites, in the East (Erfoud), and shallower, sandy deposits to the West (towards Zagora). An important tectonic phase occurred during this stage (Choubert, 1963), resulting in the subsidence of an E-W elongated trough, which was filled with a thick sequence of some 2000 metres of flysch deposits. This tectonic phase appears to have been accompanied by magmatic activity, represented by the norite intrusion to the south of Msissi (Between Erfoud and Zagora). Finally the whole area was submerged by a widespread transgression resulting in the deposition of sandstones and limestones containing Upper Famenian fossils.

4.2 Location of sampling sites

An attempt was made to sample the Lower Devonian basalts in the vicinity of Hammar Laghdad, but bad-weather conditions prevented this. It would probably be profitable to sample this formation on any future palaeomagnetic survey of the region. A visit to the Famenian norite to the south of Msissi was more fruitful, and eight sites were sampled, covering the whole area of outcrop of this intrusion (approx. 5 sq.km). The mean location of these sites is 30.93°N, 4.71°W, and the immediately overlying Upper Famenian deposits are horizontal and undisturbed, so that no tilt correction is considered necessary.

4.3 N.R.M. directions and intensities

With the exception of sites MB43 and MB48, the mean site NRM directions are distributed close to the present geomagnetic field direction at the collecting sites (Fig. 4.1(a) and Table 4.5). The within-site scatter of remanence directions is highly variable, from

2^{o} to 35^{o}, and between-site scatter is high (approx. 30^{o}).

The intensities of NRM range from 0.5 to 0.8 x 10^{-3} gauss at all sites except MB43 and MB48, at which the values are 5 x 10^{-3} and 70 x 10^{-3} gauss respectively.

4.4 Stability tests

Pilot-samples from two sites (MB42 and MB44) were subjected to progressive A.F. demagnetisation at 75 Oe. intervals, and the results are plotted in Fig 4.2.

In both samples the direction of remanence progressively moves towards a steep negative north-westerly direction on treatment up to 300 Oe, and this direction is maintained on further treatment up to 450 Oe. Yet further treatment up to 900 Oe produces a random scattering of directions. The intensities of magnetisation decrease on treatment up to 300 Oe, after which they remain approximately constant, and treatment above 500 Oe results in erratic changes.

These results indicate the isolation of a stable component of remanence with a steep negative north-westerly direction during treatment from 300 to 450 Oe. At higher fields this component is either destroyed, or swamped by a spurious random moment introduced by the demagnetising apparatus. (Chapter 8).

This conclusion was verified by subjecting all five samples from a third site (MB49) to stepwise demagnetisation up to a maximum field of 600 Oe., and examining the within-site dispersion of directions after each stage of treatment. The results are plotted in Fig 4.3, in which each point on the stereogram represents the mean of the five individual sample directions after treatment at the value indicated,

and the graph shows the circular standard deviation of these five directions plotted against the demagnetising field. The within-site dispersion of directions remains low ($< 20^{o}$) on treatment up to 450 Oe, after which it increases rapidly, and the mean remanence vector after treatment at 300 to 450 Oe has a steep negative inclination and north-westerly declination, in agreement with the pilot samples from sites MB42 and MB44.

4.5 Bulk demagnetisation

The remaining samples from the other sites were demagnetised at 300 Oe, in order to isolate the stable component of remanence detected in the pilot samples. This resulted in a decrease in within-site scatter for half of the sites and an increase for the other half (Table 4.6), and a substantial decrease in the between-site scatter, from 31^{o} to 15^{o}.

The intensities of magnetisation of all sites except MB48 decreased to 0.2 to 0.3 x 10^{-3} gauss after bulk demagnetisation, but the intensity of site MB48 remained two orders of magnitude higher. Inspection of the field data revealed that whereas at all the other sites the sun-compass and magnetic-compass orientation values agreed to within 2^{o}, in the case of site MB48 they differed by up to 7^{o}. This appears to indicate the presence of a strong local magnetic field, which influenced the magnetic compass bearing, and was probably produced by a lightning strike.

The mean direction of magnetisation of site MB48 remained slightly displaced from the other sites after bulk demagnetisation at 300 Oe (Fig 4.1(b)), and further treatment of a pilot-sample from thissite up to 600 Oe resulted in little change in direction. Treatment at 750 Oe produced a movement away from the other mean site directions

(Table 4.2). Since the effects of the lightning strike are apparently not completely removed by partial demagnetisation this site was eliminated from the final statistical analysis.

4.6 Thermomagnetic analyses

A thermomagnetic analysis was carried out on one sample from each site, and typical results are plotted in Fig 4.4. For all sites except MB48 and MB49 these curves are irreversible, and similar to that of MB42, the cooling curves being downshifted with respect to the heating curves. This behaviour may be due to the occurrence of any one of several reactions during heating, e.g. decomposition of a metastable phase, reduction of a partially oxidised phase, or internal homogenisation or ordering by diffusion processes (Larson et al, 1969).

In all cases only single Curie points are indicated by the heating and cooling curves, implying the presence of a single magnetic phase only. For the heating curves these are in the range 500 to 540°C, and for the cooling curves 480 to 530°C. These values are consistent with titanomagnetite of composition approx. 15% Fe_3O_4 and 75% Ti Fe_2O_3 (Nagata, 1961).

4.7 Discussion

The distribution of the mean site NRM directions close to the present earth's field direction suggests the presence of a secondary component of remanence in these samples. The good grouping of seven of the mean site vectors (excluding site MB48) around a steep north westerly direction, remote from the present earth's field direction, after A.F. treatment indicates the successful removal of this secondary component, and the isolation of a stable underlying component, probably of primary origin.

Thus the mean direction of stable remanence obtained from these seven sites is thought to represent a good approximation to the

geomagnetic field direction with respect to N.W. Africa during the Upper Devonian. The sampling sites are evenly distributed throughout the total area of exposure of this formation, and since the coarse grain-size indicates a slow rate of cooling it is probable that these results at least partially average out the effects of secular variation of the geomagnetic field (Jaeger, 1957).

The mean pole-position derived from these rocks after A.F. cleaning is plotted on the Palaeozoic polar wander curve in Figs. 3.9 and 3.10. It lies between the mean Lower Palaeozoic pole and the Lower Carboniferous pole derived from elsewhere in Africa, and this may be taken as evidence both for the validity of the Devonian pole and for the unity of the African continent since at least Devonian times. The palaeolatitude corresponding to the mean direction of remanence is 45^{o}, and is consistent with the palaeoclimatic evidence indicating a return to warmer conditions following the Ordovician-Silurian glaciation.

This pole-position, and the general Palaeozoic polar-wander curve derived from the Moroccan late Precambrian and Lower Cambrian poles described in the previous two chapters, is compared with results from other continents in Chapter 8.

References

Choubert, G., 1963. Histoire géologique du Précambrian de l'Anti Atlas. Notes et Mém. Serv. Géol. Maroc., No. 162.

Hollard, H. 1970. Silurian-Devonian-Carbonifère. Extrait de : Colloque international sur les Correlations du Précambrian. Notes et Mém. Serv. Géol. Maroc, No. 229. pp 161-188

Jaeger, J.C. 1957. The temperature in the neighbourhood of a cooling intrusive sheet, Am. J. Science, 255, 306-318.

Larson, E., Mituko Ozima, Minoru Ozima, T. Nagata and D. Strangway, 1969. Stability of remanent magnetisation of igneous rocks. Geophys. J.R. astr. Soc. 17, 263-292

Nagata, T. 1961. Rock Magnetism. Maruzen Co., Ltd., Tokyo.

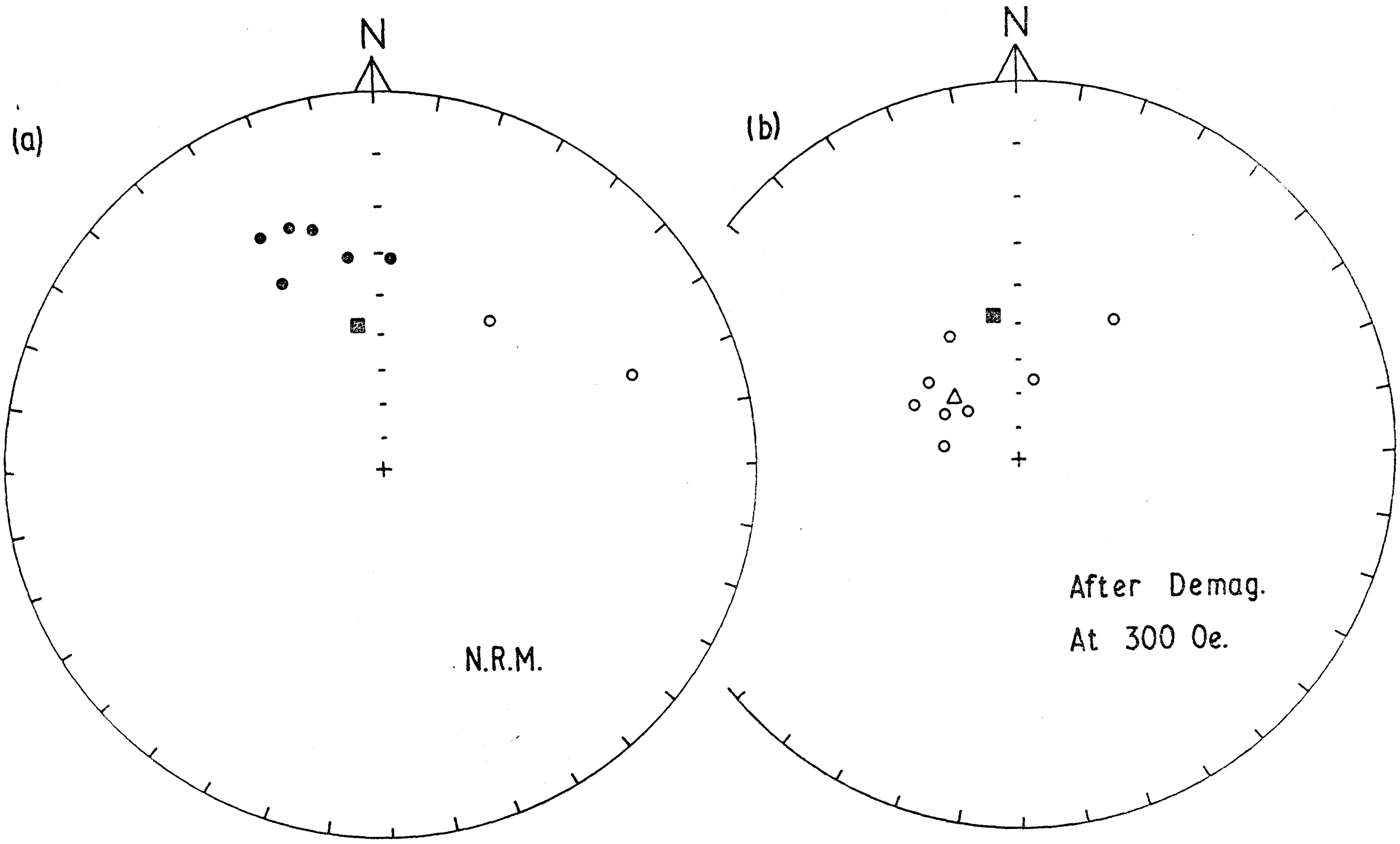


Fig 4.1 Devonian norite. Mean site directions of remanence plotted on stereographic projections.
(a) N.R.M. (b) After AF demagnetisation at 300 Oe.

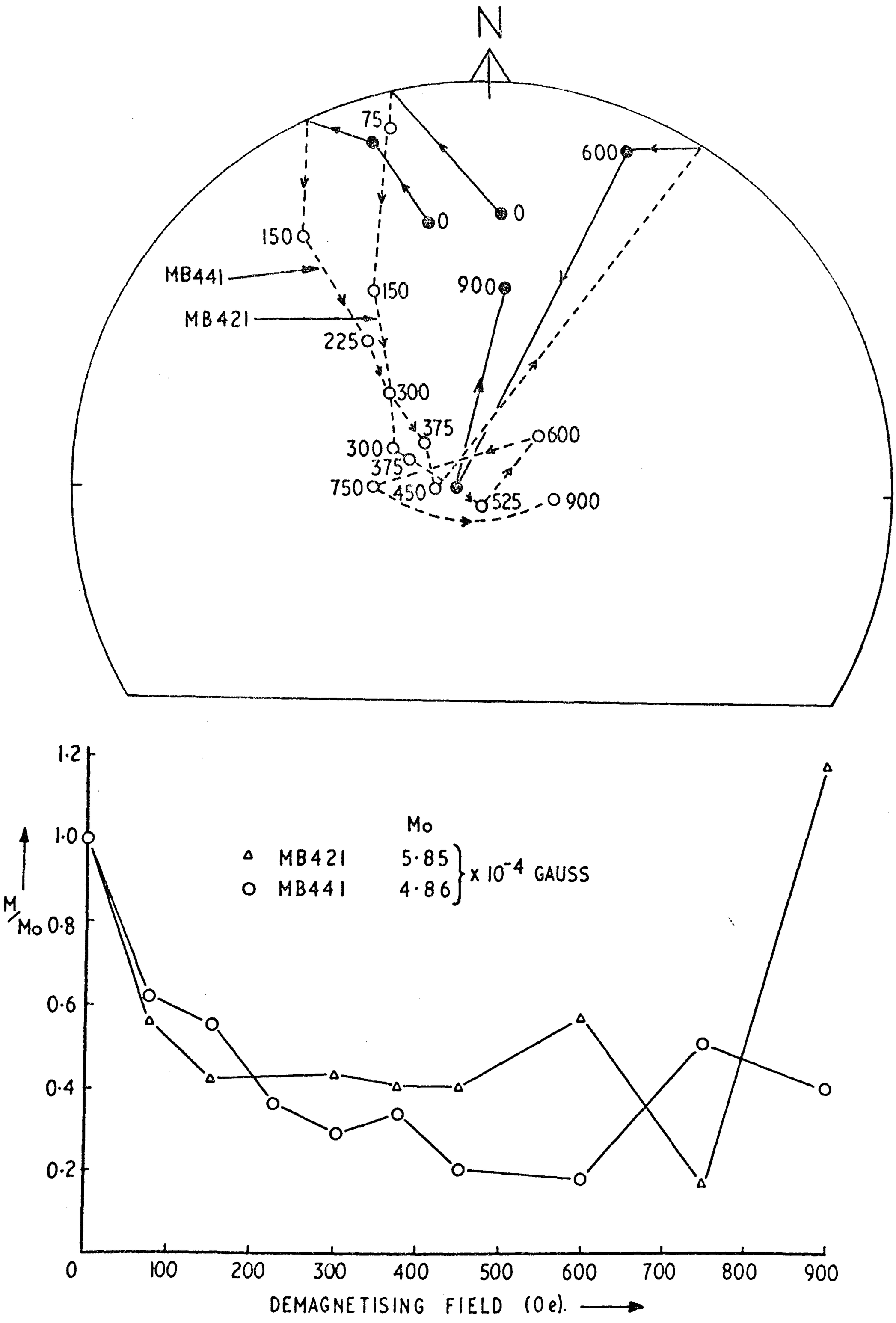


Fig 4.2 Devonian norite. Pilot sample demagnetisation results from sites MB42 and MB44..

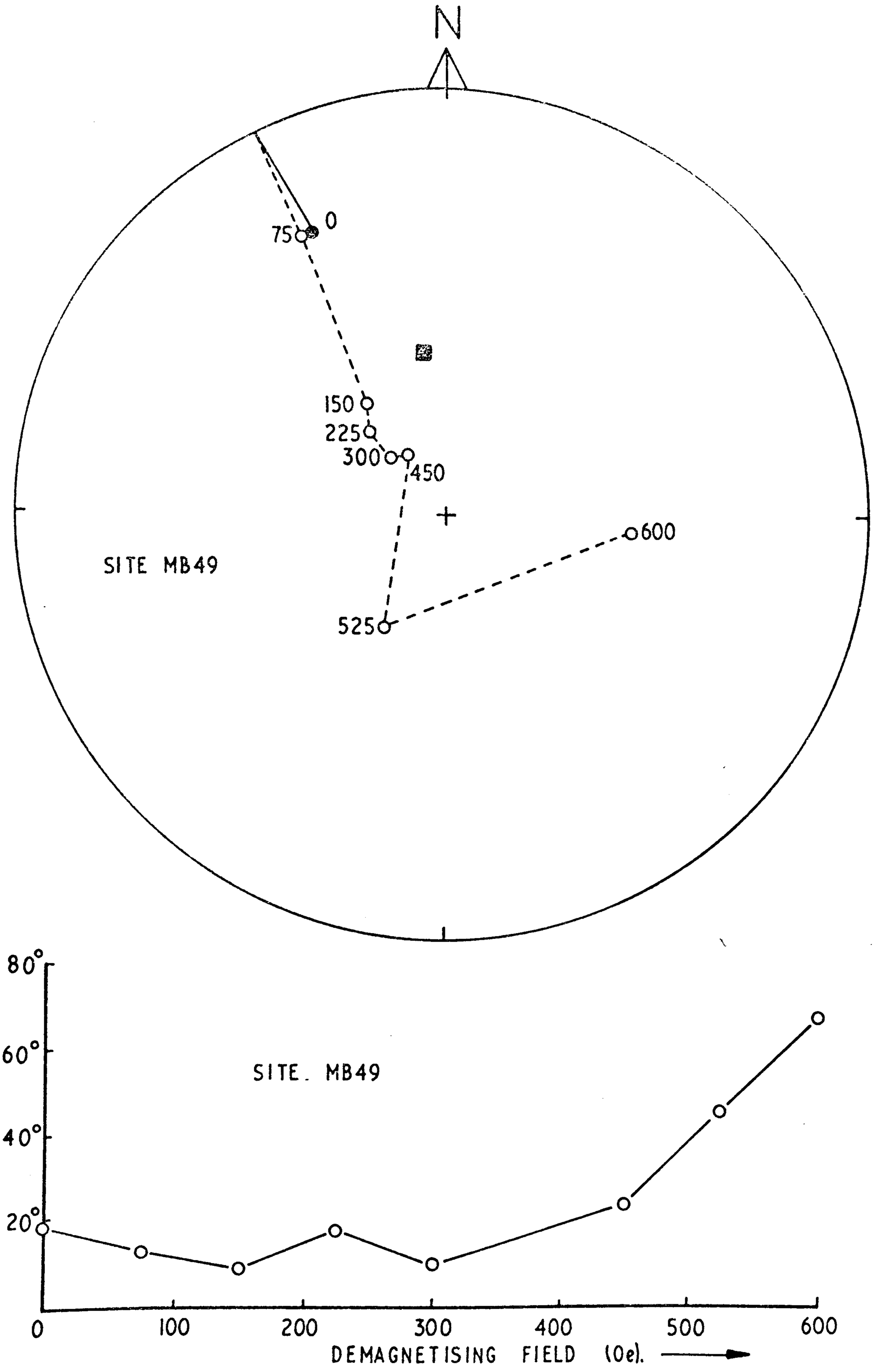
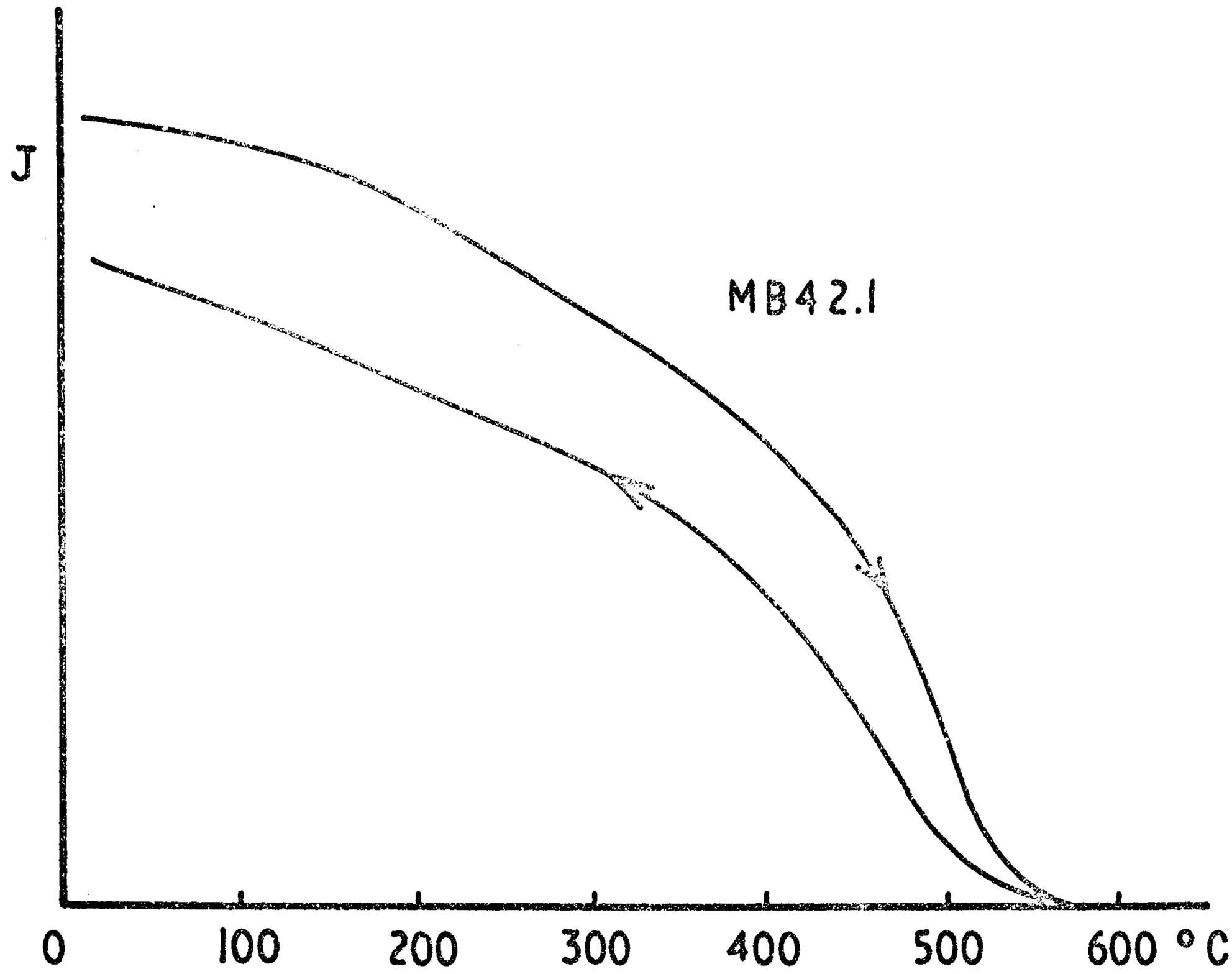


Fig 4.3 Devonian norite. Results of subjecting all five samples from site MB49 to stepwise demagnetisation. Each pole represents the mean of the five separate directions after each stage of treatment. Numbers indicate peak field in Oe. The graph shows the circular standard deviation (C.S.D.) of these five directions plotted against demagnetising field.



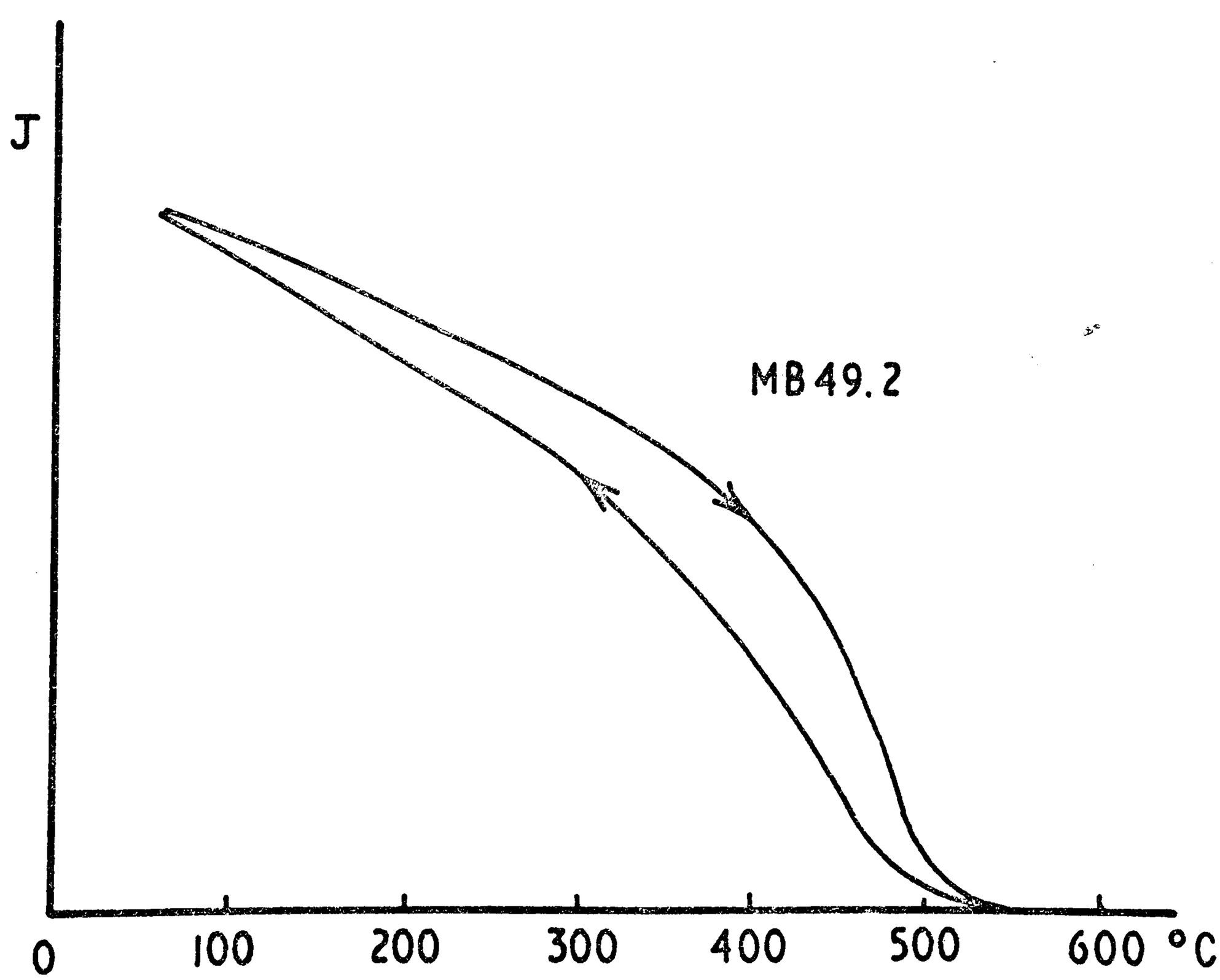


Fig 4.4 Devonian norite. Thermomagnetic results from sites MB42 and MB49. Intensity, J, in arbitrary units.

Table 4.1 Devonian norite. Individual sample N.R.M.'s

Site No.	Sample No.	Direction of remanence D	I	Int ($x10^{-3}$) gauss	Site No.	Sample No.	Direction of remanence D	I	Int ($x10^{-3}$) gauss
MB42	2	12.6	+12.5	0.60	MB46	1	337.9	+20.8	0.70
	4	0.9	+23.6	0.60		2	341.3	+23.0	0.70
	5	0.7	+26.2	0.60		3	338.9	+19.6	0.60
	6	354.6	+65.4	0.80		4	344.5	+20.9	0.60
						5	338.9	+20.6	0.70
MB43	1	70.5	+18.6	4.45		6	339.2	+20.4	0.70
	2	68.9	-18.0	4.90					
	3	69.6	-19.1	5.95	MB47	1	349.4	+31.9	0.80
	4	69.0	-16.5	4.88		2	356.1	+30.4	0.80
	5	73.0	-20.0	5.52		3	0.9	+30.8	0.90
	6	73.4	-21.3	5.86		4	352.8	+29.8	0.80
						5	348.0	+30.4	0.90
MB44	2	332.9	+25.3	0.60		6	346.3	+28.6	0.80
	3	342.0	+21.6	0.50					
	4	352.8	+20.9	0.50	MB48	3	34.6	-40.0	66.8
	5	345.9	+22.6	0.50		4	39.0	-31.0	68.5
	6	351.0	+23.0	0.50		5	31.9	-41.6	80.8
						6	41.3	-38.3	62.8

Site No.	Sample No.	Direction of Remanence D	I	Int ($x10^{-3}$) gauss	Site No.	Sample No.	Direction of Remanence D	I	Int($x10^{-3}$) gauss
MB45	1	334.2	+25.4	0.50					
	2	351.1	+29.8	0.50	MB49	2	345.3	+52.7	0.50
	3	346.0	+21.6	0.50		3	337.7	+17.2	0.40
	4	340.2	+23.2	0.50		4	327.9	+11.3	0.60
	5	226.5	+28.0	0.50		5	321.8	+7.7	0.70
	6	346.6	+24.2	0.50		6	338.5	+14.3	0.50

Table 4.2 Devonian norite. Pilot sample demagnetisation results

Demag field.	D	I	Int ($\times 10^{-3}$ gauss)	Demag field	D	I	Int ($\times 10^{-3}$ gauss)	Demag field	D	I	Int
0	3.0	+21.0	0.58	0	347.5	+22.0	0.49	0	34.6	-40.0	
75	345.0	-4.3	0.33	75	341.4	+6.2	0.30	300	33.3	-41.3	7.0
150	330.6	-31.5	0.24	150	324.1	-14.8	0.27	375	33.0	-42.1	4.0
300	264.6	-61.1	0.25	225	321.7	-39.7	0.18	450	32.6	-42.8	2.3
375	256.2	-64.4	0.23	300	315.0	-52.3	0.14	525	38.6	-44.4	1.3
550	198.2	-86.1	0.28	375	307.8	-67.9	0.16	600	38.7	-49.1	0.8
600	41.9	-68.7	0.33	450	273.1	-75.7	0.10	675	40.5	-40.1	0.55
750	272.5	-48.8	0.10	600	21.3	+5.0	0.09	750	21.4	-44.3	0.40
900	94.0	-70.4	0.70	750	276.9	+83.2	0.25				
				900	5.4	+36.2	0.19				

Table 4.3. Devonian norite. Site MB49 stability test demagnetisation results

Treatment	Mean direction of remanence D	I	c.s.d.
0	334.3	+17.2	19.4
75	334.2	-16.5	13.4
150	323.9	-52.2	8.9
225	317.5	-60.2	18.5
300	314.6	-69.1	10.4
450	325.8	-71.4	24.3
525	207.9	-56.2	50.8
600	95.4	-42.2	68.3

Table 4.4 Devonian norite. Remanence directions and intensities after demagnetisation at 300 Oe.

Site No.	Sample No.	Direction of remanence D	I	Int($\times 10^{-3}$) gauss
MB42	2	319.1	-61.4	0.25
	4	297.2	-65.4	0.24
	5	301.7	-63.2	0.26
	6	289.9	-64.8	0.25
MB43	1	349.2	-64.7	0.20
	2	12.7	-73.6	0.18
	3	20.2	-66.1	0.21
	4	350.9	-67.8	0.20
	5	31.4	-48.7	0.20
	6	11.1	-66.1	0.20
MB44	2	293.7	-55.5	0.28
	3	299.3	-56.6	0.19
	4	322.9	-56.1	0.17
	5	305.9	-47.3	0.18
	6	329.8	-54.3	0.18
MB46	1	285.6	-53.7	0.26
	2	298.6	-54.1	0.27
	3	302.9	-56.8	0.27
	4	304.5	-57.7	0.25
	5	293.4	-50.0	0.29
	6	306.7	-55.2	0.27
MB47	1	326.4	-49.0	0.19
	2	336.8	-46.1	0.23
	3	347.4	-53.7	0.20
	4	325.2	-49.4	0.26
	5	325.9	-42.9	0.25
	6	329.8	-48.1	0.25
MB48	3	33.3	-41.9	7.00
	4	36.4	-39.6	15.00
	5	30.8	-43.2	9.00
	6	39.9	-40.8	14.00

Site No.	Sample No.	Direction of remanence D	I	Int($x10^{-3}$) gauss	Site No.	Sample No.	Direction of remanence D	I	Int($x10^{-3}$) gauss
MB45	1	292.7	-58.9	0.18					
	2	310.6	-59.5	0.17	MB49	2	271.2	-74.7	0.20
	3	304.6	-70.2	0.18		3	313.2	-65.9	0.20
	4	247.4	-47.9	0.30		4	316.6	-59.2	0.19
	5	191.1	-63.2	0.17		5	339.3	-75.0	0.19
	6	327.7	-62.7	0.19		6	323.7	-65.1	0.19

Table 4.5 Devonian norite. N.R.M. mean site directions and statistical parameters

Site No.	D	I	N	R	k	α_{95}	c.s.d.
MB42	3.5	+31.5	4	3.745	12	28	
MB43	70.5	-19.0	6	5.995	1044	2	2.5
MB44	345.0	+23.0	5	4.966	117	7	
MB45	332.5	+31.5	6	4.907	5	35	
MB46	340.0	+21.0	6	5.995	1025	2	2.5
MB47	352.0	+30.5	6	5.982	276	4	5.0
MB48	37.0	-38.0	4	3.985	200	6.5	5.5
MB49	333.5	+20.5	5	4.759	17	19.5	
Overall Mean	359.5	+16.0	8	6.249	4	31.5	41.5
Overall Mean excl. Site MB48	354.0	+23.5	7	5.887	5	28.5	35.5

Table 4.6. Devonian norite. Mean site direction, pole positions and statistical parameters after 300 Oe treatment

Site No.	D	I	N	R	k	α_{95}	c.s.d.	Pole position Lat.	Long.	A_{95}
MB42	302.5	-64.0	4	3.984	193	6.5		3S	211.5E	10
MB43	11.5	-65.5	6	5.905	52	9.5		10N	168.5E	13
MB44	312.0	-55.0	5	4.927	55	10.5		9.5S	213E	14
MB45	281.0	-67.5	6	5.603	13	19.5		16.5S	214.5E	31
MB46	298.5	-55.0	6	5.978	230	4.5		2N	221E	6
MB47	331.5	-48.5	6	5.966	148	5.5		23.5N	202E	7
MB48	35.0	-41.5	4	3.995	596	4.0		25.5N	139.5E	4
MB49	314.5	-69.0	5	4.935	61	10.0		3.5S	200.5E	16
Overall Mean	328.5	-64.0	8	7.488	14	15.5		4N	162W	22
							Antipole	4S	18E	22
Overall Mean excl.site MB48	315.5	-63.0	7	6.797	29	11.5		0.5N	155W	16.5
							Antipole	0.5S	25E	16.5

CHAPTER 5. TRIASSIC

5.1. Geology

5.1.1. General sequence of Triassic deposits in Morocco

Permian deposits are poorly developed in Morocco, and in most areas Triassic deposits rest directly on Carboniferous or older formations. In the few localities where Permian deposits are present, they are of Middle Autunian age (i.e. Lower Permian) and pass conformably downwards into Stephanian deposits. This 'Stephano-Autunian' group was folded during the Saalian tectonic phase, and is overlain discordantly by red continental Triassic deposits.

The Triassic sequence can be subdivided into two main lithological groups (Choubert & Faure-Muret, 1962).

1. A Lower Series of red sandstones, commencing with a conglomerate horizon, and including several pelitic bands.

2. An Upper Series of red clays, often saliferous, and including towards the centre of the sequence a thick series of basaltic lava flows. Sandstones are also sometimes present, but are of only subsidiary importance.

An important marine incursion occurred during the eruption of the basalts, and is marked by a limestone intercalation containing a fauna characteristic of the German Middle Triassic Letterkohle (upper Muschelkalk) stage. The Triassic sequence is otherwise poorly fossiliferous, and this bed forms an important reference horizon, recognisable particularly in NE Morocco and at various localities in the High Atlas (e.g. S.W. of Talsinnt). Triassic salt deposits are also very widespread, and occur as continuous beds or lenses throughout the whole sequence.

5.1.2. Distribution of Triassic deposits

The distribution of the Lower Series of red sandstones is relatively limited, and they are confined mainly to basins of subsidence. In the central part of the High Atlas belt two principal basins can be distinguished. The Westerly Basin extends from the Sous valley in the south to Safi in the north, and is bounded to the west by the Mesetian branch of the Hercynian chain (Fig 1.1). The total thickness of sediments in this basin reaches 4 to 5000 metres. The Easterly Basin extends over the Precambrian part of the Central High Atlas belt between Marrakech and Ouarzazate.

In all cases the Upper Series of red clays and basaltic lava flows is transgressive over the Lower Series, and in the easterly basin the junction of the two series is slightly discordant. The deposits of the Upper Series are much more widely distributed than those of the Lower Series, and occur over most of the Atlas domain. They indicate a widespread area of lagunal and lacustrine sedimentation extending over most of Central Morocco during Middle Triassic times. The source of sediments appears to have been the Hercynian chains lying to the south, and the sandy deposits of the Lower detrital series are best developed in the southern part of the region. Tectonic activity continued over the whole of this period, represented by repeated subsidence in the Lower Series and the widespread volcanic phase of the Upper Series.

5.1.3. Triassic igneous formations

As discussed above, the thick sequence of dolerites and basalts occurring in the middle of the Upper Series have been dated from fossils contained in a thin limestone intercalation as Middle Triassic. In the Central High Atlas the volcanic series reaches a thickness of 200 metres, and comprises a sequence of continuous flows interstratified

with clays formed by erosion of the basalts, and baked red mudstones. The whole sequence is highly altered and has an overall dark green colour. The rocks can be classified petrologically into two categories:

(i) Microgabbros, with ophitic structure, in which glass is practically non-existent, and the grains are visible to the naked eye. These occur mainly at the base of the flows, indicating a slower rate of crystallisation, and are very solid and relatively fresh.

(ii) Doleritic basalts, consisting of a single phase, and devoid of phenocrysts.

Broussé (1966) has determined the mineralogical composition of these rocks as follows:

Phenocrysts	pyroxene	0 to 6%
	olivene	0 to 4%
	plagioclase	0 to 8%
Matrix	labradorite	22 to 44%
	pyroxene	6 to 25%
	olivene	0 to 10%
	glass	2 to 16%
	sphene	0 to 1%
	chlorite (produced by alteration	5 to 25%
	limonite	10 to 45%
	chalcedony and chlorite	0 to 25%

This analysis indicates a predominantly tholeütic composition, and the abundance of vacuoles, filled with chalcedony and chlorite indicates extrusion in an aqueous medium. Further evidence of this mode of emplacement includes the presence of glass, very small grains

of minerals in the form of 'spherulites', characteristic of rapid crystallisation, the absence of fluid structures, and the frequent presence, especially in fractured zones, of ferriferous jaspers, formed during the eruption of the lavas, by water highly charged with silica.

The whole of the volcanic series is highly altered, and it seems probable that this was a palaeoalteration, produced during, or soon after the emplacement of the rocks, as a direct result of extrusion in the sub-aqueous environment. The alteration products, determined by X-ray, thermal and chemical analyses (Broussé, 1966) are:

(i) fine-grained chlorite, generally in fissures

(ii) illite, kaolinite, montmorillonite and calcite, all in very small amounts

(iii) limonite

The alteration is most pronounced in the fractured zones and along faults, due to the easy penetration of water along the numerous tectonic joints, shear joints and fissures formed during cooling and contraction of the lava. The highly altered parts frequently resemble true sediments, and in some cases even exhibit a 'pseudo-bedding'.

5.2 Location of sampling sites

The alteration of the Middle Triassic dolerite series probably occurred penecontemporaneously with its emplacement, in which case, the magnetic constituents of the alteration products should still reflect the ambient geomagnetic field direction at these localities during Middle Triassic times.

The series was sampled at a total of 24 sites at two localities on the northern and southern flanks respectively of the Central High

Atlas belt, in the easterly basin of subsidence described in Section 5.1.2. The first locality, on the northern flank of the High Atlas was situated at the site of a new dam (Ait Aadel), under construction across the river Tessaout in the vicinity of Tamelelt, to the East of Marrakech (Fig 5.1). To eliminate the possibility of recent weathering effects the sites were situated in deep horizontal tunnels, cut during the course of the dam construction up to a hundred meters into the walls of a gorge, itself several hundred meters deep. At these sites orientation of the cores was performed by sighting to the tunnel entrance, where sun compass and magnetic oompass bearings were taken. A total of sixteen sites were sampled at this locality (MB1-16).

The second locality was situated on the southern flanks of the Central High Atlas, near the village of Issaldain on the Marrakech-Ouarzazate road, and eight sites were sampled over the total thickness of the volcanic series (MB28-30 and 32-36). At both localities individual sites were situated as far as possible in separate lava flows.

A series of red sandstones lying in the Upper detrital series, immediately below the Middle Triassic volcanic sequence, were sampled at six sites situated near the Tizi 'n' Titchka pass on the Marrakech-Ouarzazate road (sites MB22 to 27), and a similar sequence of red sandstones, in the same stratigraphic position, but situated 50 km to the SW, was sampled at two sites near the summit of Jebel Oukaimeden (sites MB81 and 82).

5.3. Palaeomagnetic results from the Ait Aadel dolerites

5.3.1. N.R.M. directions and intensities

The mean site NRM directions of the sixteen sites situated at the Ait Aadel dam are plotted in Fig 5.2(a). The within-site scatter is generally fairly high (10^{o}-40^{o}) and the between-site scatter is also large (24^{o}). (Table 5.2). The formation is mainly horizontal, and small tilt-corrections were necessary at only two sites (Table 5.1). Application of these tilt-corrections did not significantly affect the between-site scatter.

The intensities of N.R.M. were very variable, ranging from 0.5 to 20 x 10^{-4} gauss. In general low intensities were associated with the more highly weathered samples.

5.3.2. Pilot sample A.F. demagnetisation results

One pilot sample from each site was subjected to partial A.F. demagnetisation stability tests, at 85 Oe intervals up to a maximum field of between 700 and 900 Oe. The resultant changes in direction of remanence are plotted in Fig 5.3, and intensity in Fig 5.4.

There appears to be no overall consistent pattern of behaviour of these pilot samples. In some cases (e.g. samples MB3.1; MB13.4 and MB15.2) the directions of remanence remained close to the earth's present field direction at these localities on treatment up to 450 Oe, after which they scattered randomly. In other cases (e.g. samples MB6.2, 7.1, 8.6, 9.4 and 11.2) the remanence vectors changed to a shallow negative NE or SE direction, and then underwent little change on further treatment to 850 Oe, and in yet other samples (e.g. MB2.3, 4.2 and 12.4) the remanence vectors remained constant along some other apparently arbitrary direction during treatment over a range of several hundred oersteds.

After treatment at 700 to 900 Oe, the intensity decreased to less

than 10% of its original value in only five samples (MB3.1, 12.4, 13.4, 14.1 and 15.2). In the other eleven samples the intensity remained above 50% of its original value, over the whole range of treatment (Table 5.3).

5.3.3. Bulk A.F. demagnetisation

The pilot sample A.F. demagnetisation results showed no definite evidence of the isolation of a common stable direction of magnetisation in all sites. However, since a few samples showed apparent indications of the presence of a stable component the remaining samples from six sites (MB3 to 8) were subjected to bulk A.F. demagnetisation at what appeared to be the most appropriate field from an inspection of the pilot-sample results. The results are listed in Tables 5.5 and 5.6, and the mean site directions after treatment are plotted in Fig 5.2(c).

In all cases this treatment resulted in a substantial increase in within site scatter, but the mean-site directions were only slightly better grouped then in the case of the initial N.R.Ms.

5.3.4. Pilot sample thermal demagnetisation results

In view of the unsatisfactory results of partial A.F. demagnetisation, the stability of the Ait Aadel samples was further investigated by thermal demagnetisation tests. Pilot samples from five sites (MB2.1, 9.2., 12.5, 14.3 and 16.1) were subjected to progressive thermal demagnetisation up to a maximum temperature of 650^{o}C, and the results are listed in Table 5.7, and plotted in Figs 5.5 and 5.6.

In all cases the remanence vector moved to a positive northwesterly direction on treatment at 100^{o}C, after which it remained approximately constant on further treatment up to 500^{o}C. Above this temperature the directions scattered randomly. In all samples except MB2.1 the intensity

of magnetisation decreased progressively on treatment up to the maximum temperature of 650°C. In sample MB2.1 treatment at 650°C resulted in a slight increase of intensity.

5.3.5. Bulk thermal demagnetisation

The pilot sample results described above appear to indicate the isolation of a stable component of remanence over the range 100 to 500°C in all of the samples studied. The remaining samples from these five sites, and from the other eleven sites, were therefore subjected to bulk thermal demagnetisation at 300°C, and the results are listed in Table 5.8. The mean site directions after this treatment are listed in Table 5.2 and plotted in Fig 5.2(c). In two-thirds of the sites the within-site scatter was substantially increased and in one-third it was reduced as a result of this treatment. However the between-site scatter was substantially reduced, from 24° to 7.5°, indicating the successful isolation of an underlying stable component. One site (MB4) was eliminated from the final statistical analysis because of its excessively high within-site scatter (> 90°).

The palaeomagnetic south pole-position corresponding to the mean direction of remanence after thermal cleaning is

$$72.0^{\circ}S,\ 74.5^{\circ}E,\ A_{95} = 7.5^{\circ}$$

5.3.6. Thermomagnetic analyses

Thermomagnetic analyses were carried out on samples from sites MB4, MB6 and MB11. In all three cases the shape of the curve was very similar (Fig 5.7) and indicated a Curie Point in the range 470 to 570°C. The curves were all irreversible, the cooling curve being downshifted with respect to the heating curve, indicating the possible occurrence of phase changes or internal homogenisation as a result of heating (Larson et al, 1969).

The positive response of these samples to thermal demagnetisation, compared with their general negative response to A.F. demagnetisation, indicates the presence of magnetic grains with high coercive forces and blocking temperatures. This suggests that the magnetic constituents are unlikely to be members of the titanomagnetite series, but are more likely to be members of the ilmeno-haemetite series, possibly resulting from the high-temperature oxidation conditions associated with their mode of emplacement (Section 5.1.3.)

The thermomagnetic curves showed only one Curie point, indicating the presence of a single magnetic phase only.

5.4. Palaeomagnetic results from the Issaldain dolerites

5.4.1. N.R.M. directions and intensities

The mean site NRM directions of the eight sites sampled at this locality are listed in Table 5.9, and plotted in Fig 5.8. With the exception of sites MB28 and MB32 the within-site scatter is small ($< 10^{o}$), and the maximum value (site MB32) is only 16^{o}. The between-site scatter is also small, and the mean direction of N.R.M., giving unit weight to each site is

$$D = 3.6, \quad I = +4.2, \quad \alpha_{95} = 6^{o}$$

This direction is situated very close to the direction of the present earth's field at these localities (D = 351.5, I = 47.5).

The intensities of NRM were very similar to those of the Ait Aadel dolerites, i,e. of the order of 10^{-3} gauss.

5.4.2. Pilot sample A.F. demagnetisation results

Pilot samples were selected at random from four of the eight sites, and subjected to progressive A.F. demagnetisation upto a maximum peak field of 900 Oe. The results are listed in Table 5.11, and plotted in Figs 5.9 and 5.10.

In two of the samples (MB28.2 and 30.3) the direction of remanence remained virtually unchanged over the whole range of treatment. A third sample (MB29.2) showed similar behaviour, apart for a brief movement away from the main groups of directions at 750 Oe, probably due to a measurement or instrumental error. The direction of remanence of the fourth sample (MB35.1) remained close to the main group on treatment up to 300 Oe, after which it moved progressively away.

In all four samples the intensity of magnetisation decreased progressively over the whole range of treatment, reaching a minimum value of 10 to 20% of the original value, after treatment at 900 Oe.

5.4.3. Bulk A.F. demagnetisation

The pilot sample demagnetisation results indicate the presence of a stable component of remanence, existing over the whole range of treatment from 0 to 900 Oe in three of the samples, and 0 to 300 Oe in the fourth. The remaining samples from the first three sites were accordingly demagnetised at 450 Oe, and the samples from the other five sites at 300 Oe. The results are presented in Table 5.12.

This treatment resulted in a general increase of within-site scatter, as with the sites situated at the Ait Aadel locality, but the between-site scatter remained unchanged (6^{o}). The mean site directions after treatment are plotted in Fig 5.8(b), and in general they are situated further from the present direction of the geomagnetic field at these localities than the corresponding NRM mean-site directions. This is interpreted as being due to the removal of a weak viscous component by partial A.F. demagnetisation.

The pole-position calculated from the mean direction of remanence after cleaning is

$$77.3S,\quad 39.4W,\qquad A_{95} = 6.5^{o}$$

This is significantly different from the pole-position obtained from the Ait Aadel dolerites, and the possible reasons for this difference will be discussed at the end of this chapter.

5.4.4. Thermomagnetic analyses

Thermomagnetic analyses were carried out on samples from sites MB28 and MB35. The results are broadly similar to those from the Ait Aadel dolerites, discussed in Section 5.3.6., and a typical curve is plotted in Fig 5.11. The downshift of the cooling curve is more pronounced than in the Ait Aadel samples, and the Curie Point of the cooling curve is 100°C lower than that of the heating curve. The reasons for this are thought to be the same as those mentioned in Section 5.3.6.

5.5. Palaeomagnetic results from the Titchka sediments

5.5.1. N.R.M. directions and intensities

The intensities of NRM of the sediments were very weak, lying in the range 0.1 to 0.7 x 10^{-5} gauss (Table 5.14). The mean site directions are plotted in Fig 5.12(a), and listed in Table 5.13. With the exception of site MB22, the within-site scatter of directions is high ($> 30^{o}$), and the between-site scatter is greater than 90^{o}.

5.5.2. Pilot sample thermal demagnetisation results

One sample from each site was subjected to progressive thermal demagnetisation at 50 or 100°C intervals, up to a maximum temperature of 700°C, and the results are plotted in Figs 5.13 and 5.14. The remanence vectors of the pilot samples from all sites except MB23 and MB27 moved towards a steep negative direction, in most cases with

an easterly or south easterly declination, on treatment up to 650 or 700°C. The pilot samples from sites MB23 and 27 retained a positive easterly direction over the whole range of treatment. The changes in intensity of magnetisation of the pilot samples were much more variable (Fig 5.14). In three of the samples the intensities decreased progressively over the whole range of treatment, in two samples they increased on treatment up to 500°C, after which they rapidly decreased, and in one other sample an initial decrease was followed by an increase or treatment up to 500°C, and then a rapid decrease. In all cases the intensity decreased to less than 10% of the initial value after treatment at 700°C.

5.5.3. Bulk thermal demagnetisation

The pilot sample results indicate the presence of an underlying component of remanence with a steep negative direction in at least four of the sites, and the remaining samples from all six sites were therefore demagnetised at both 300°C and 650°C. The results are listed in Table 5.16, and the mean-site directions after treatment are plotted in Fig 5.12(b) and (c), and listed in Table 5.13.

Treatment at 300°C did not significantly reduce the between-site scatter, and the within-site scatter increased in four out of the six sites. However treatment at 650°C resulted in movement of the mean direction of remanence of four of the sites (excluding sites MB22 and 27) to the negative southeasterly quadrant, and those of the other two sites to the negative northeasterly and northwesterly quadrants respectively. The within-site scatter remained high, but the values were less than those after treatment at 300°C.

It is considered that a common stable direction of remanence was isolated in the four sites MB23 to 26, after treatment at 650°C

and the corresponding mean direction of remanence, giving unit weight to each site is

$$D = 165^{o}, \quad I = -23^{o}, \quad \alpha_{95} = 22^{o}$$

The mean palaeomagnetic pole position calculated from this direction of remanence is

$$68.5^{o}S, \quad 87.0E, \quad A_{95} = 22.5^{o}$$

The between-site scatter before correction for tilting is 24^{o}, compared with the value of 22^{o} after correction. It is difficult to judge whether this 10% difference is significant, but if it is, then it implies that the stable component of remanence of the rocks was acquired prior to the folding, and is evidence of long-term stability (Graham, 1949).

5.6. Palaeomagnetic results from the Oukaimeden sediments

5.6.1. N.R.M. directions and intensities

Because of their relative hardness, the Oukaimeden sediments were sampled by collection of three oriented blocks at each site, instead of by the usual field-drilling technique. Two or three cores were subsequently drilled from each block in the laboratory. (Section 1.4), yielding a total of eight specimens from site MB81 and nine specimens from site MB82.

The intensities of NRM of the samples from site MB82 are comparable to those of the Titchka sediments (0.1×10^{-5} gauss), but those of the samples from site MB81 were an order of magnitude higher. There appears to be no obvious petrological difference between the samples from the two sites. The directions of N.R.M. of individual specimens are plotted in Fig 5.15(a), and listed in Table 5.17. The between-specimen and between-site scatter are both greater than 90^{o}, but there appears to be an approximately bipolar distribution of of directions between the positive northwesterly quadrant and the negative southeasterly quadrant.

5.6.2. Thermal demagnetisation results

Three pilot samples were selected at random from each site, and subjected to progressive thermal demagnetisation at 50 or 100°C intervals up to a maximum temperature of 650°C. The corresponding changes in direction of remanence are plotted in Fig 5.16, and in intensity of magnetisation in Fig 5.17.

The directions of remanence of four of the samples remained in, or moved towards the negative southeasterly quadrant during the course of this treatment. However the scatter of the six specimen directions after treatment at both 300 and 650°C remained greater than 90° (Fig 5.15(b) and (c)). A further six specimens were demagnetised at 650°C, but the scatter of the twelve directions was still greater than 90° (Fig 5.15(c)).

Since the directions of magnetisation isolated in the Ait Aadel dolerites and the Titchka sediments lie in the positive northwest and negative southeast quadrants respectively, it is possible that the bipolar distribution of specimen directions observed in the NRMs of the Oukaimeden sediments represents a Triassic direction of magnetisation. However, due to the closeness of the Triassic direction to the present geomagnetic field direction (and also to the axial dipole field direction) at these localities, this distribution may also represent viscous magnetisation or recent weathering effects. Because of the very high scatter of directions it is not considered possible to distinguish between these two possible explanations.

No palaeomagnetic pole position was therefore calculated for the Oukaimeden sediments.

5.7. Discussion

The results described in Sections 5.3. to 5.6 indicate that stable components of magnetisation were isolated in three out of the four Triassic formations studied. The mean directions of magnetisation and corresponding palaeomagnetic south pole positions derived from these three formations are summarised in Table 5.19, and the Triassic pole positions derived from rocks of similar age in South and East Africa (McElhinny et al, 1968) are listed in Table 5.20. All of these poles are plotted in Fig 5.18, in which the black triangles represent poles from Moroccan formations and the black squares poles from South and East African formations. It can be seen from this diagram that the poles from the Ait Aadel dolerites (pole 2) and the Titchka sediments (pole 3) lie close to the main group of poles from South and East African formations, whereas the pole from the Issaldain dolerites (pole 1) lies remote from this group, but very close to the pole from the Tanzanian Songwe Rift sandstones (pole 4).

The Issaldain and Songwe Rift poles both lie very close to the mean Upper Tertiary pole (81.5S, 48.5W), listed in table 8.1. The most likely explanation for the discrepancy between the former two poles and the other five Triassic poles plotted in Fig 5.18 is that the Issaldain and Songwe Rift formations were both remagnetised during the Upper Tertiary, possibly as a result of chemical weathering. This explanation is supported by the fact that the Issaldain samples were collected from roadside exposures, whereas the Ait-Aadel samples, which occupy an identical stratigraphic position, were collected from deep underground tunnels.

An alternative explanation is that the Issaldain and Songwe Rift formations have both recorded a brief and temporary excursion of the pole away from the mean position which it occupied for the rest of the Triassic period. This explanation seems unlikely in view of the fact that the Ait Aadel dolerites occupy a similar stratigraphic position, but show no evidence of such an excursion.

The mean pole corresponding to the Ait Aadel dolerites and the Titchka sediments is plotted as an open triangle in Fig 5.18, and the mean pole calculated from the South and East African formations, excluding the Songwe Rift sandstones is plotted as an open square. The corresponding ellipses of 95% confidence are plotted around these mean poles, and it is clear that no significant difference exists between the two. It is concluded that no significant relative tectonic motion has occurred between NW and SE Africa since Triassic times.

The new Moroccan Triassic pole-positions will be compared with data from other continents in Chapter eight.

References

Broussé, 1966. Étude minéralogique et pétrographic des roches du site d'Ait Aadel, Maroc. Faculté des Sciences, Orsay

Choubert, G. and Anne Faure Muret, 1962. Évolution du domaine Atlasique marocain depuis les temps Palaeozoiques. In Livre a la mémoire du Professeur Paul Fallot, Societé Géologique de France

Graham, J.W., 1949. The stability and significance of magnetism in sedimentary rocks. J. Geophys. Res., 54, 131-167.

Larson, E., Mituko Ozima, Minoru Ozima, T. Nagata and D. Strangway, 1969. Stability of remanent magnetisation of igneous rocks. Geophys. J.R. astr. Soc. 17, 263-292.

McElhinny, M.W., J.C. Briden, D.L. Jones and A. Brock. Geological and geophysical implications of palaeomagnetic results from Africa. Rev. Geophys. 6, 2, 201-238.

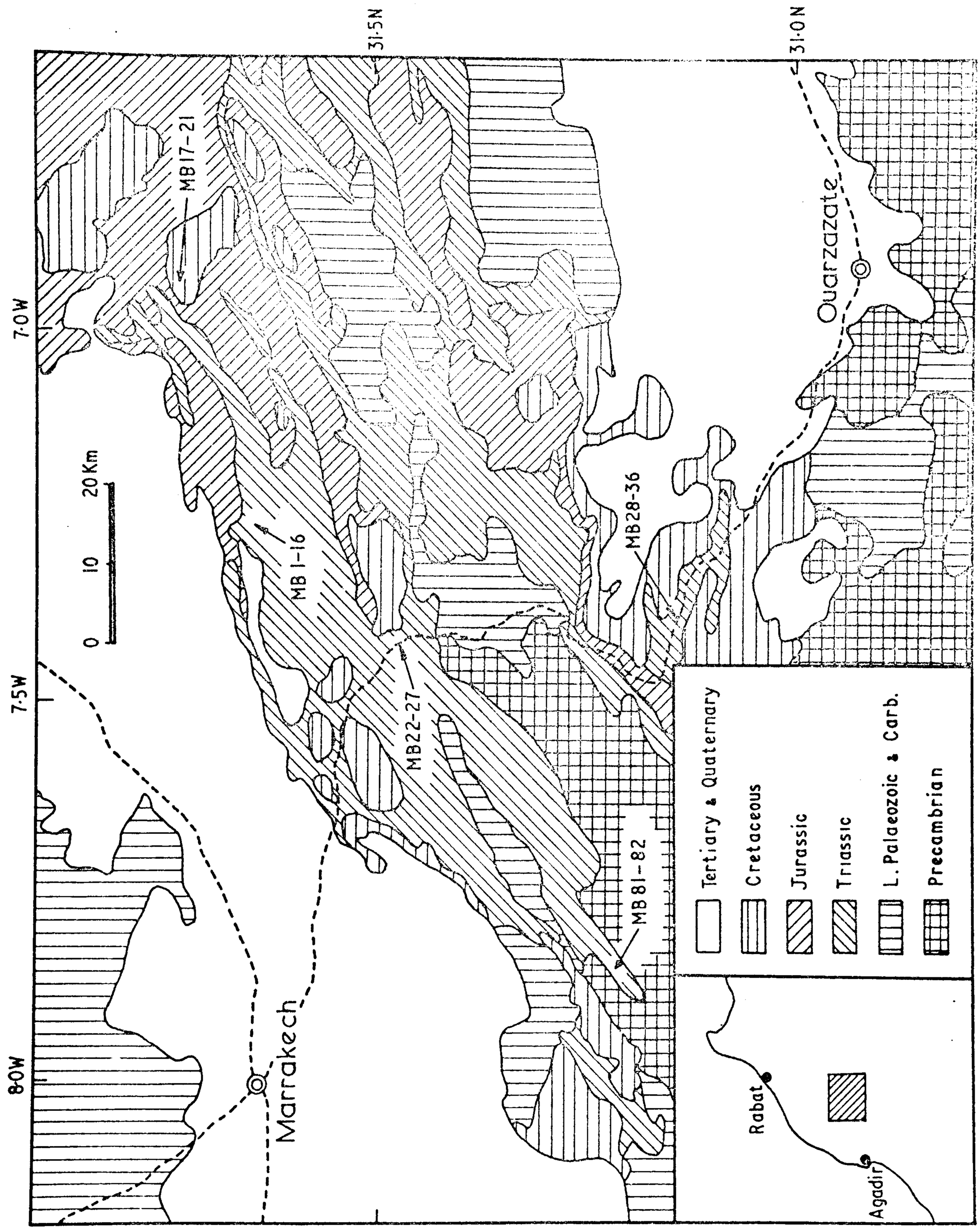


Fig 5.1 Outline geological map of the Central High Atlas region, showing location of Triassic and Cretaceous sampling sites.

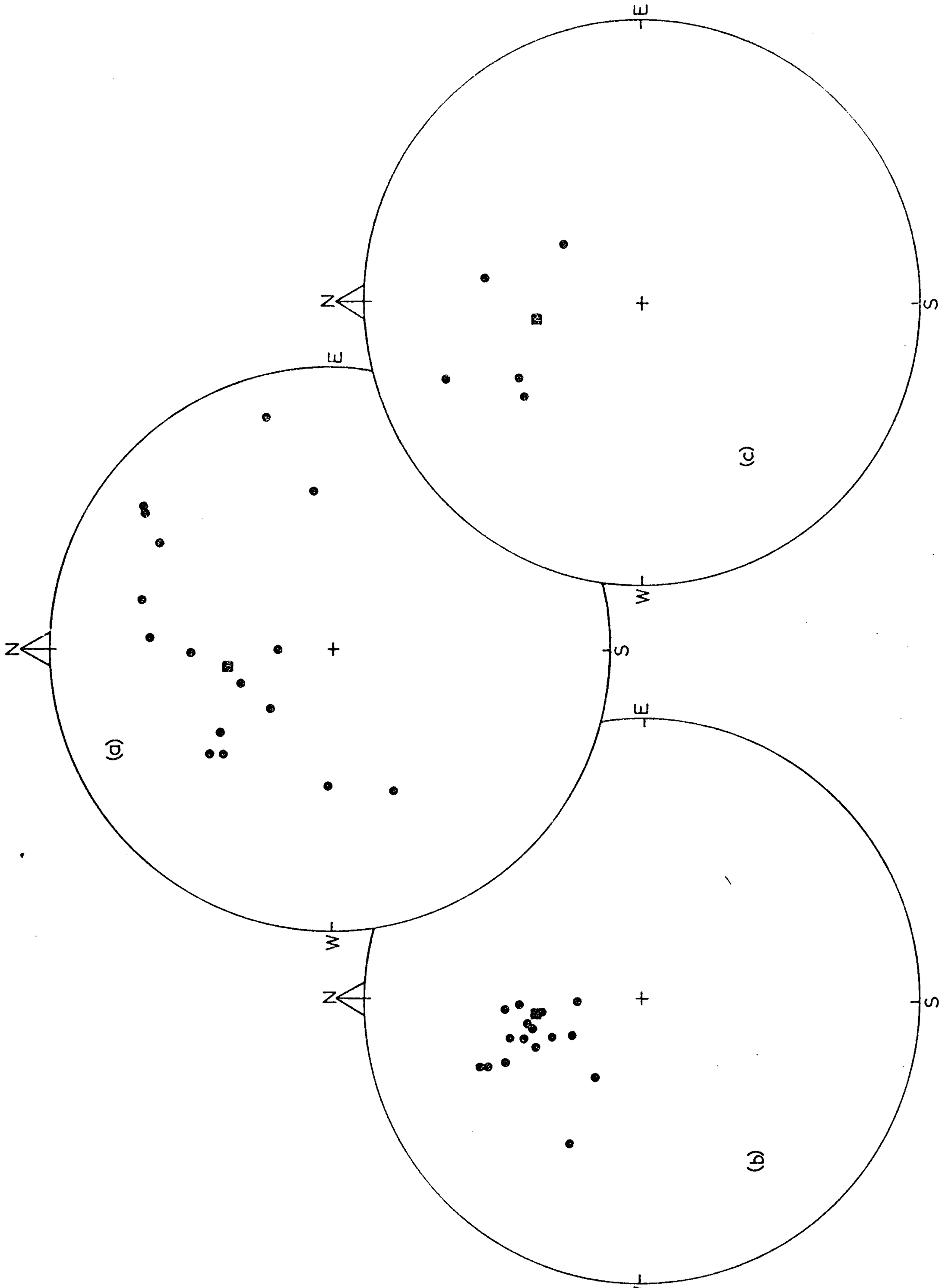


Fig 5.2 Ait Aadel dolerites. Mean site directions (a) N.R.M. (b) After thermal demagnetisation at 300°C. (c) After AF demagnetisation at 300 to 525 Oe. (Sites MB3 to MB8 only).

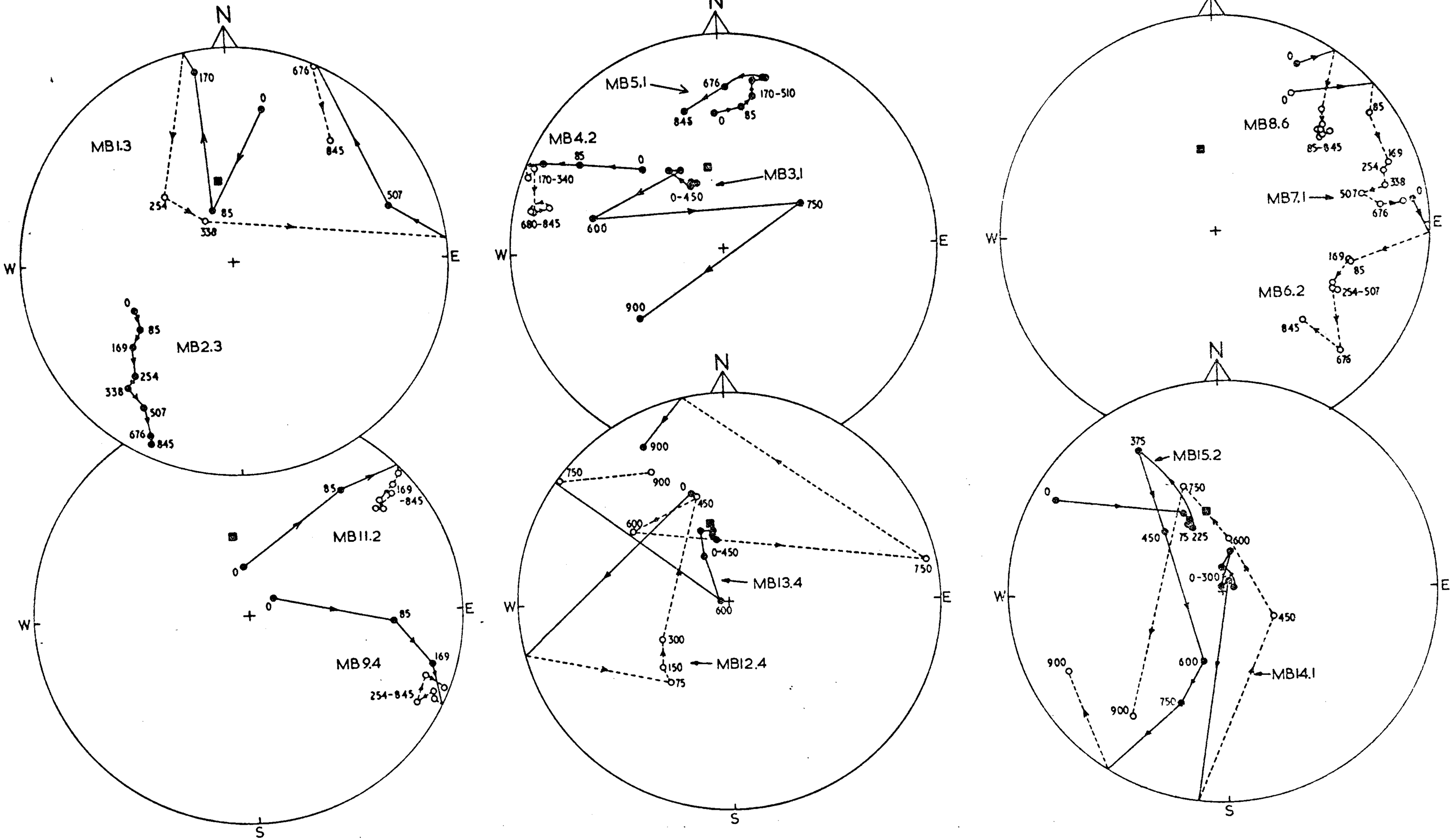
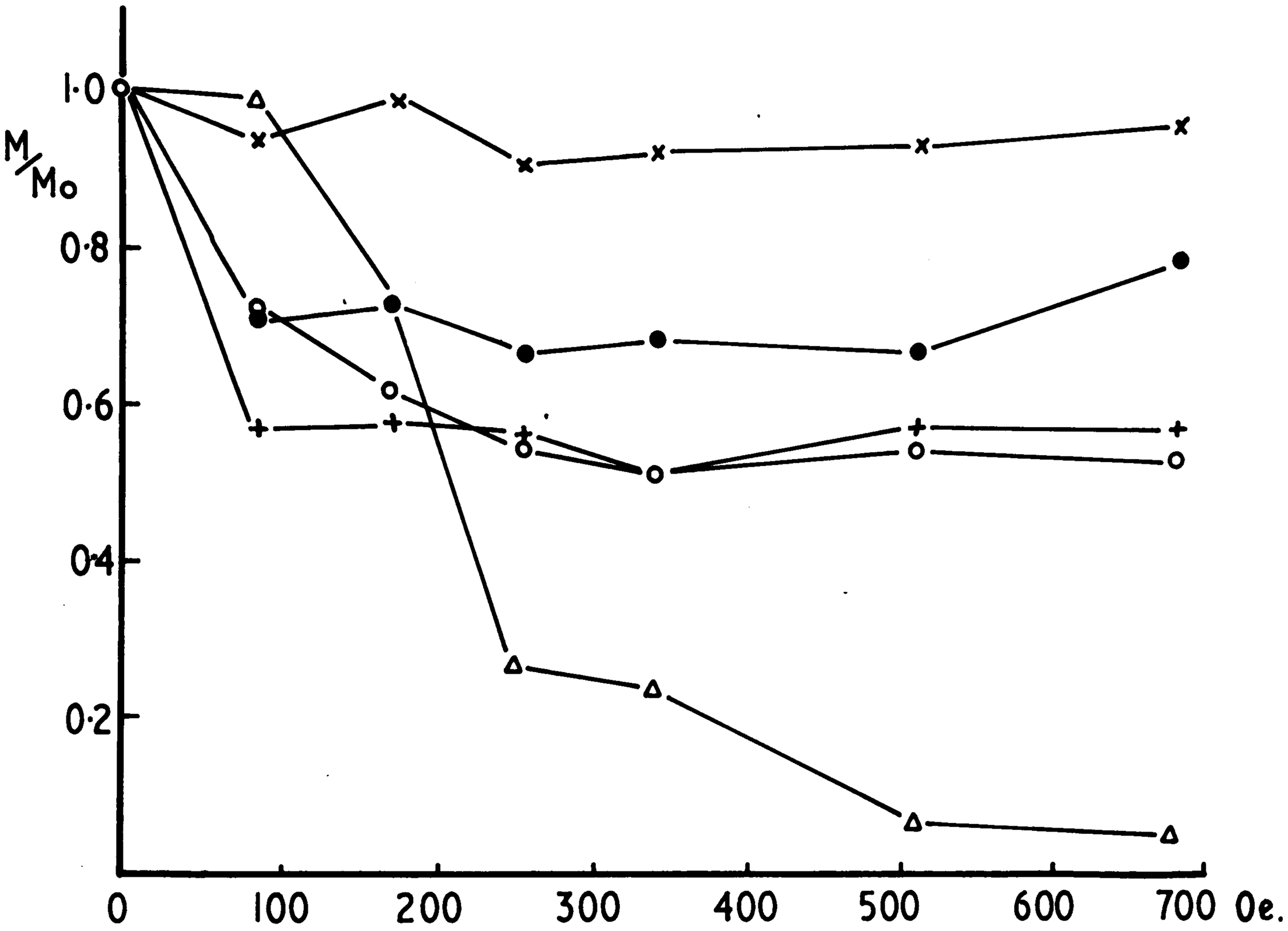


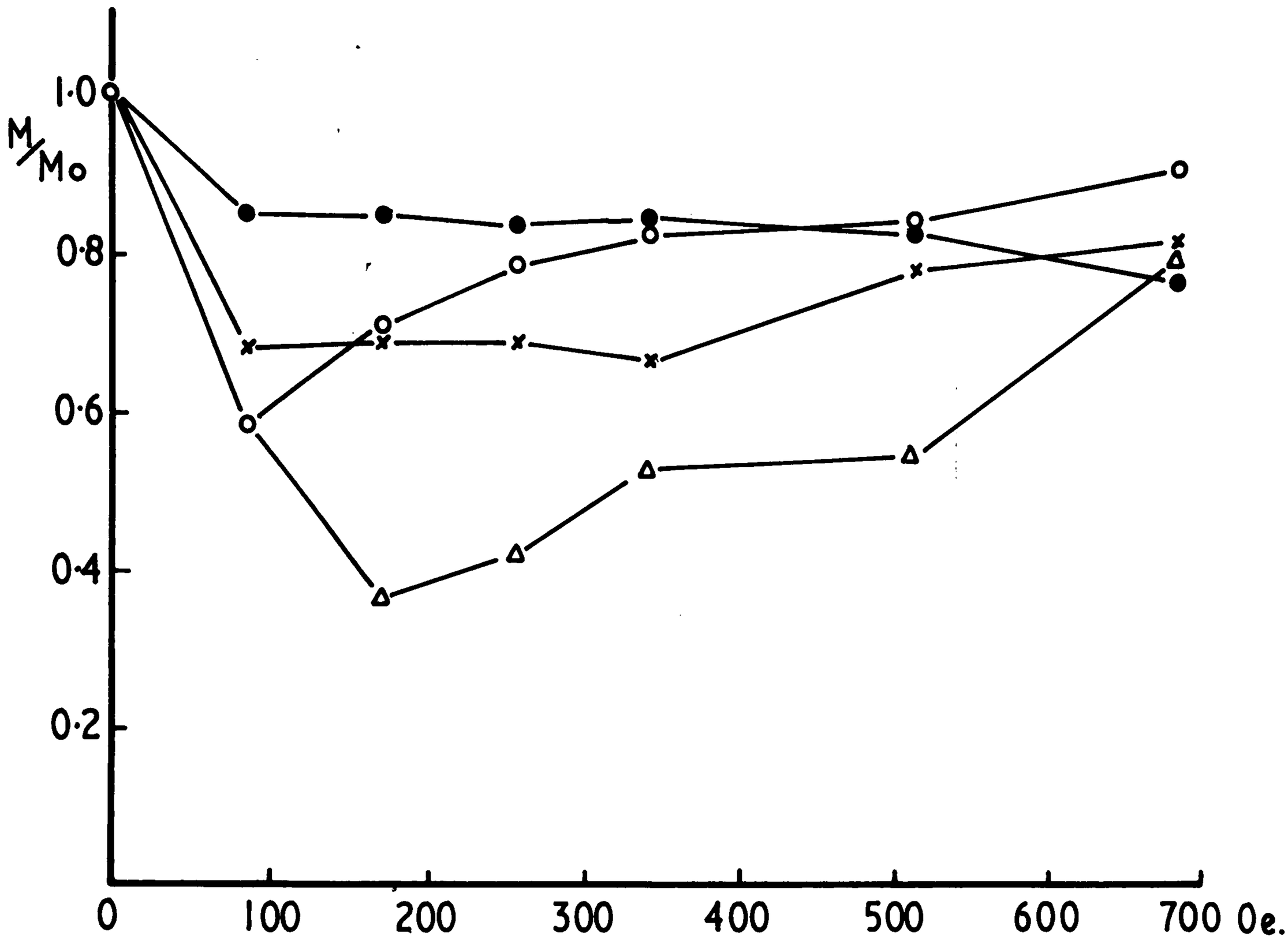
Fig 5.3 Ait Aadel dolerites. Changes in direction of remanence of pilot samples during progressive AF demagnetisation.



		Mo
△	MB 3.1	0·16
●	MB 2.3	3·13
○	MB 4.2	9·04
×	MB 5.1	7·11
+	MB 7.1	0·57

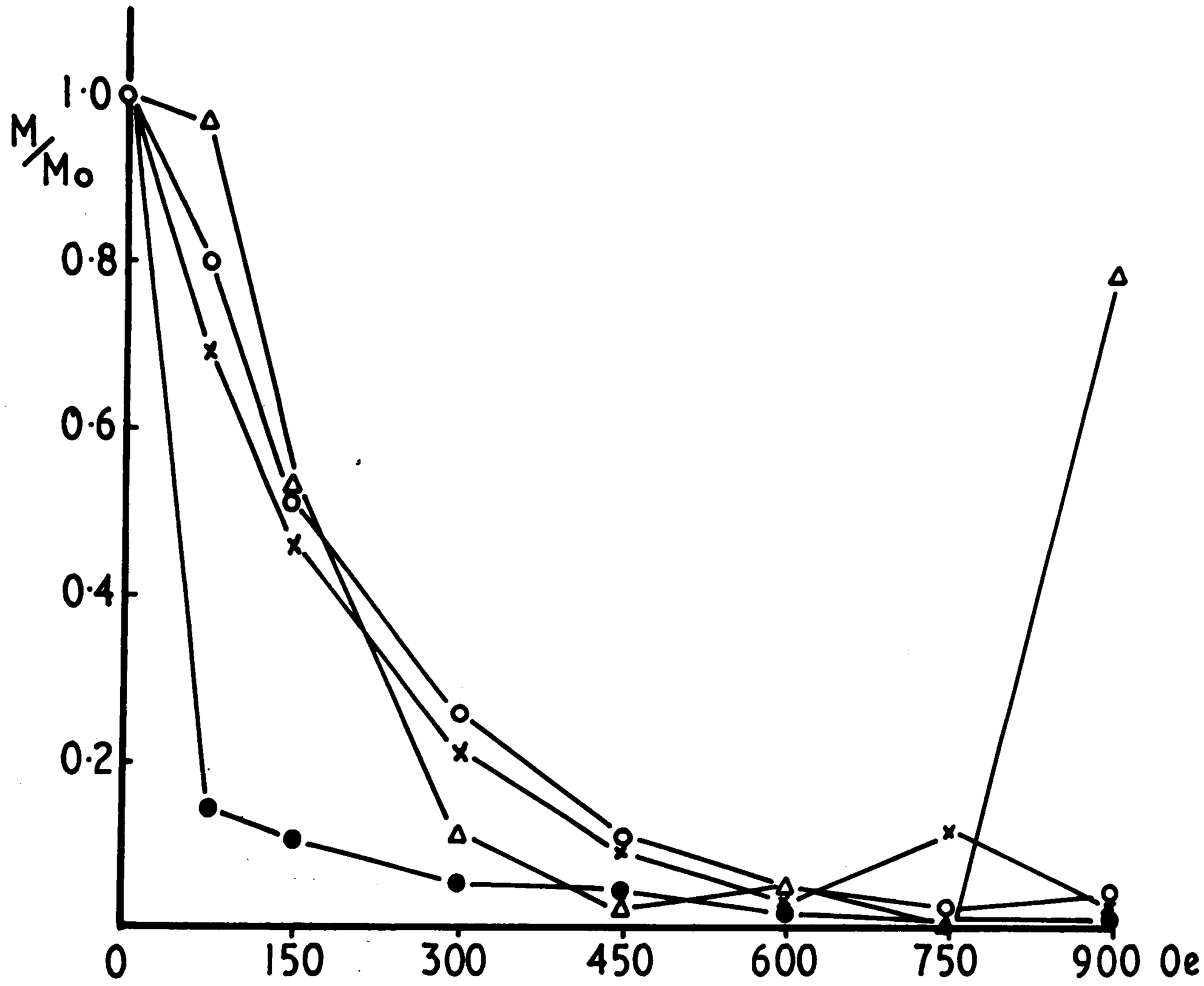
$\times 10^{-4}$ Gauss

Fig 5.4(a) Ait Aadel dolerites. Changes in intensity of magnetisation of pilot samples from sites MB3 to MB7 during progressive AF demagnetisation.



		Mo	
●	MB 8.6	10·81	
o	MB 9.4	5·29	X 10^{-4} Gauss
x	MB 10.5	6·24	
Δ	MB 11.2	6·03	

Fig 5.4(b) Ait Aadel dolerites. Changes in intensity of magnetisation of pilot samples from sites MB8 to MB11 during progressive AF demagnetisation.



		Mo
●	MB12·4	7·77
o	MB13·4	1·28
x	MB14·1	1·57
Δ	MB15·2	4·00

X 10^{-4} Gauss

Fig 5.4(c) Ait Aadel dolerites. Changes in intensity of magnetisation of pilot samples from sites MB12 to MB15 during progressive AF demagnetisation.

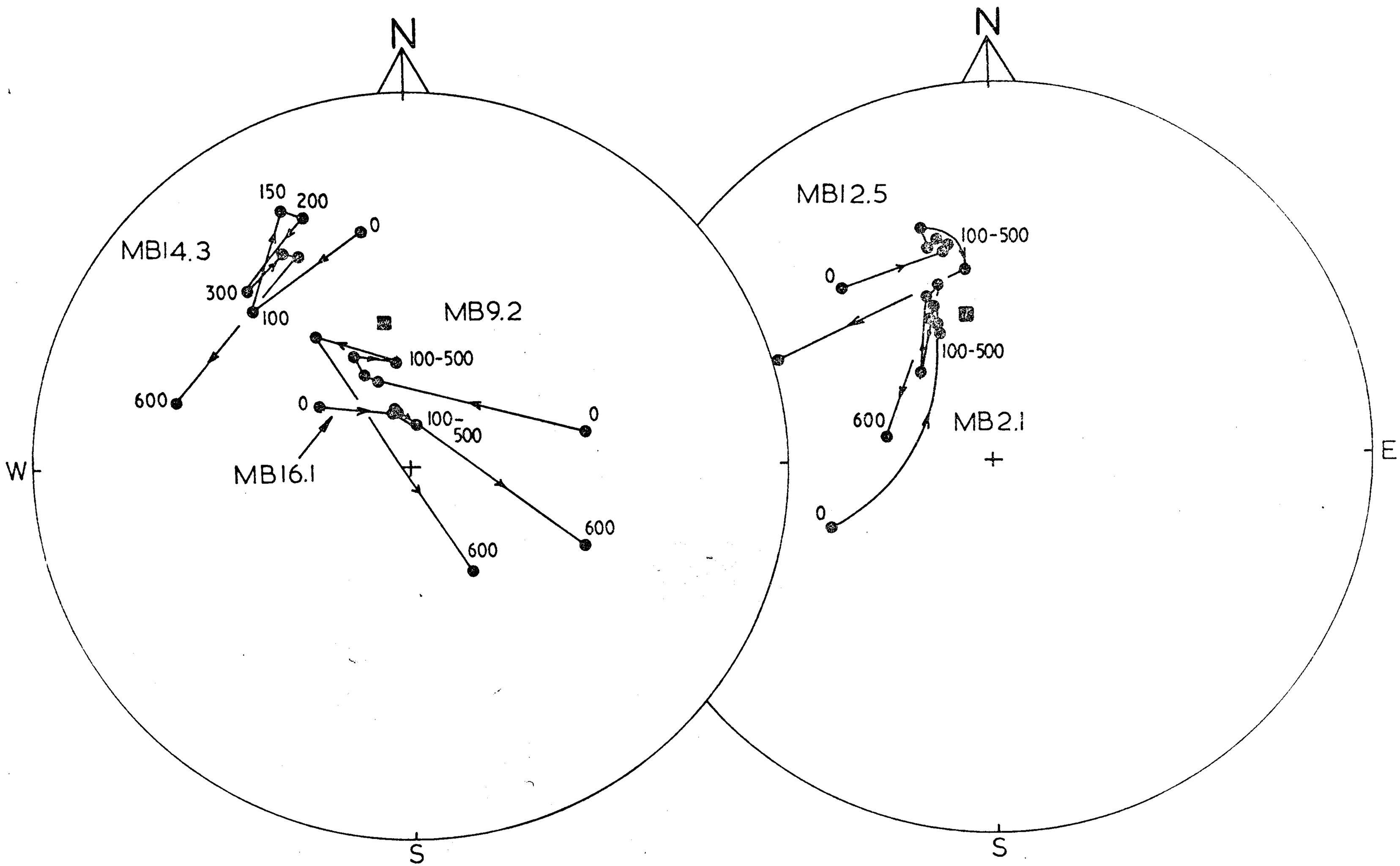
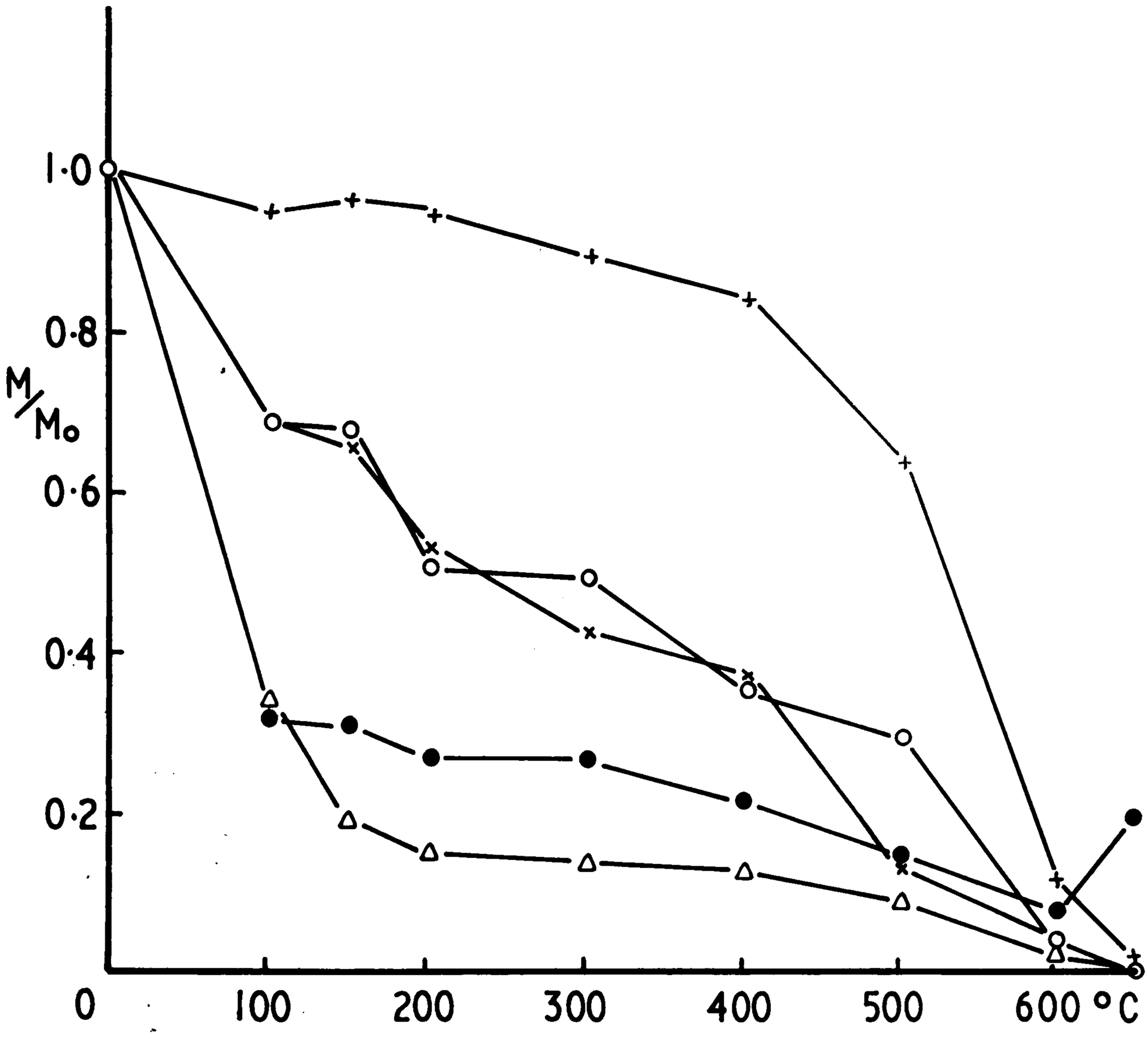


Fig 5.5 Ait Aadel dolerites. Changes in direction of remanence of pilot samples during progressive thermal demagnetisation.



	Mo	
● MB 2·1	3·98	
o MB 9·2	5·25	
× MB12·5	6·76	X 10^{-4} Gauss
△ MB 14·3	3·50	
+ MB16·1	0·40	

Fig 5.6 Ait Aadel dolerites. Changes in intensity of magnetisation of pilot samples from sites MB2, MB9, MB12, MB14, and MB16 during progressive thermal demagnetisation.

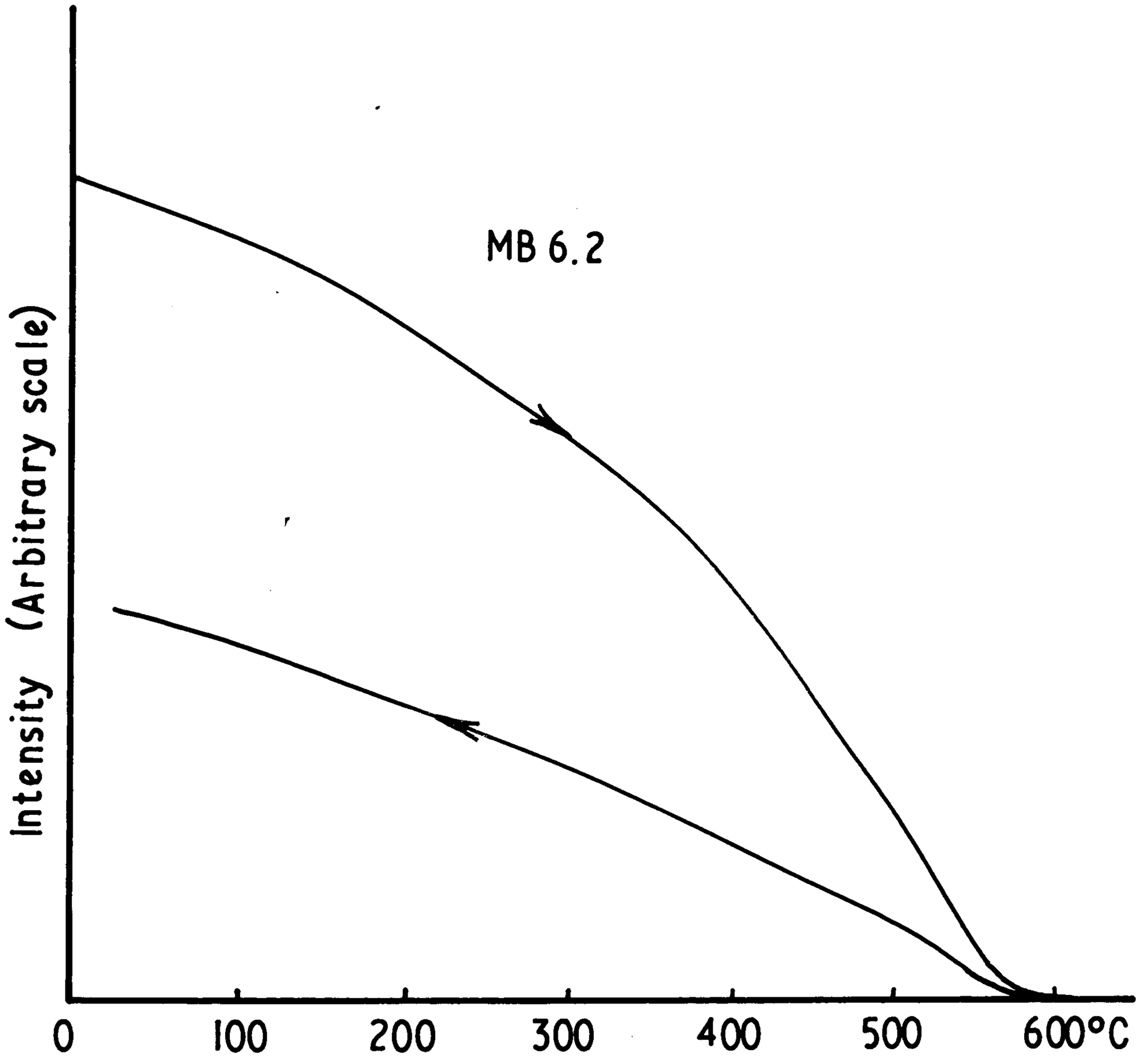


Fig 5.7 Ait Aadel dolerites. Thermomagnetic analysis of sample MB6.2

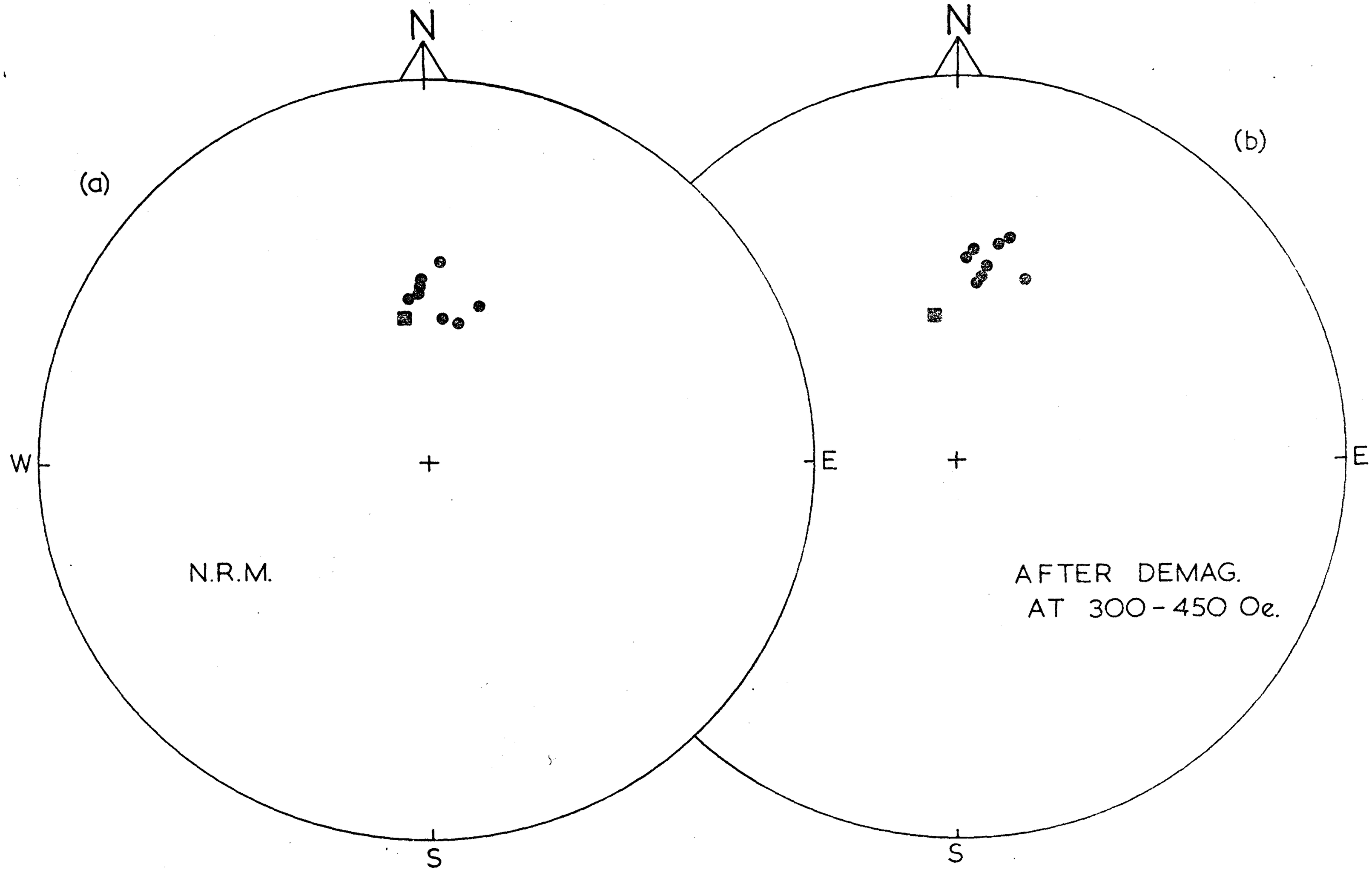


Fig 5.8 Issalain dolerites. Mean site directions of remanence (a) N.R.M. (b) After demagnetisation at 300 to 450 Oe.

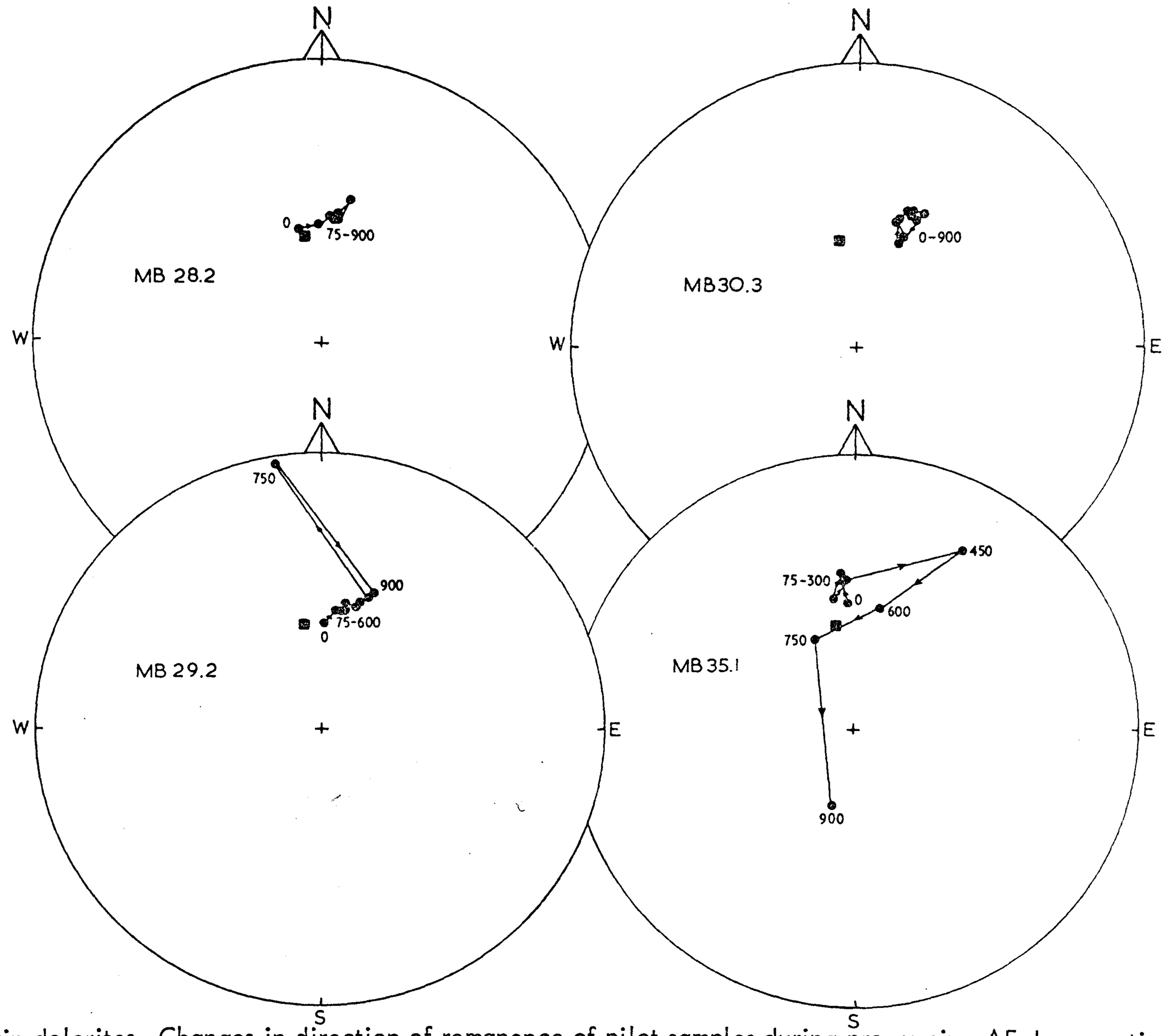
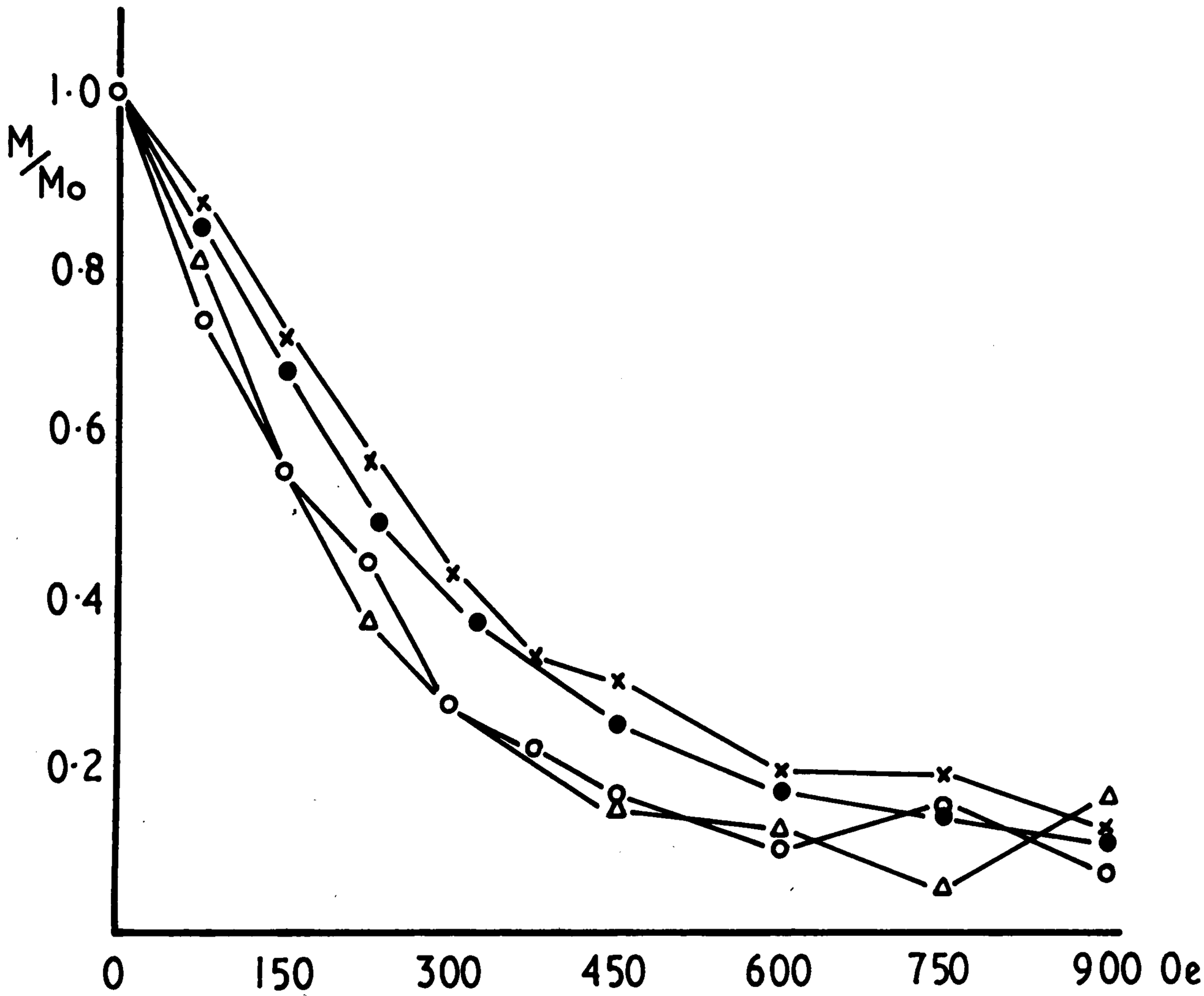


Fig 5.9 Issaldain dolerites. Changes in direction of remanence of pilot samples during progressive AF demagnetisation.



		Mo
●	MB 28.2	12·11
o	MB 29.2	12·91
x	MB 30.3	13·75
Δ	MB 35.1	9·00

X 10^{-4} Gauss

Fig 5.10 Issaldain dolerites. Changes in intensity of magnetisation of pilot samples during progressive AF demagnetisation.

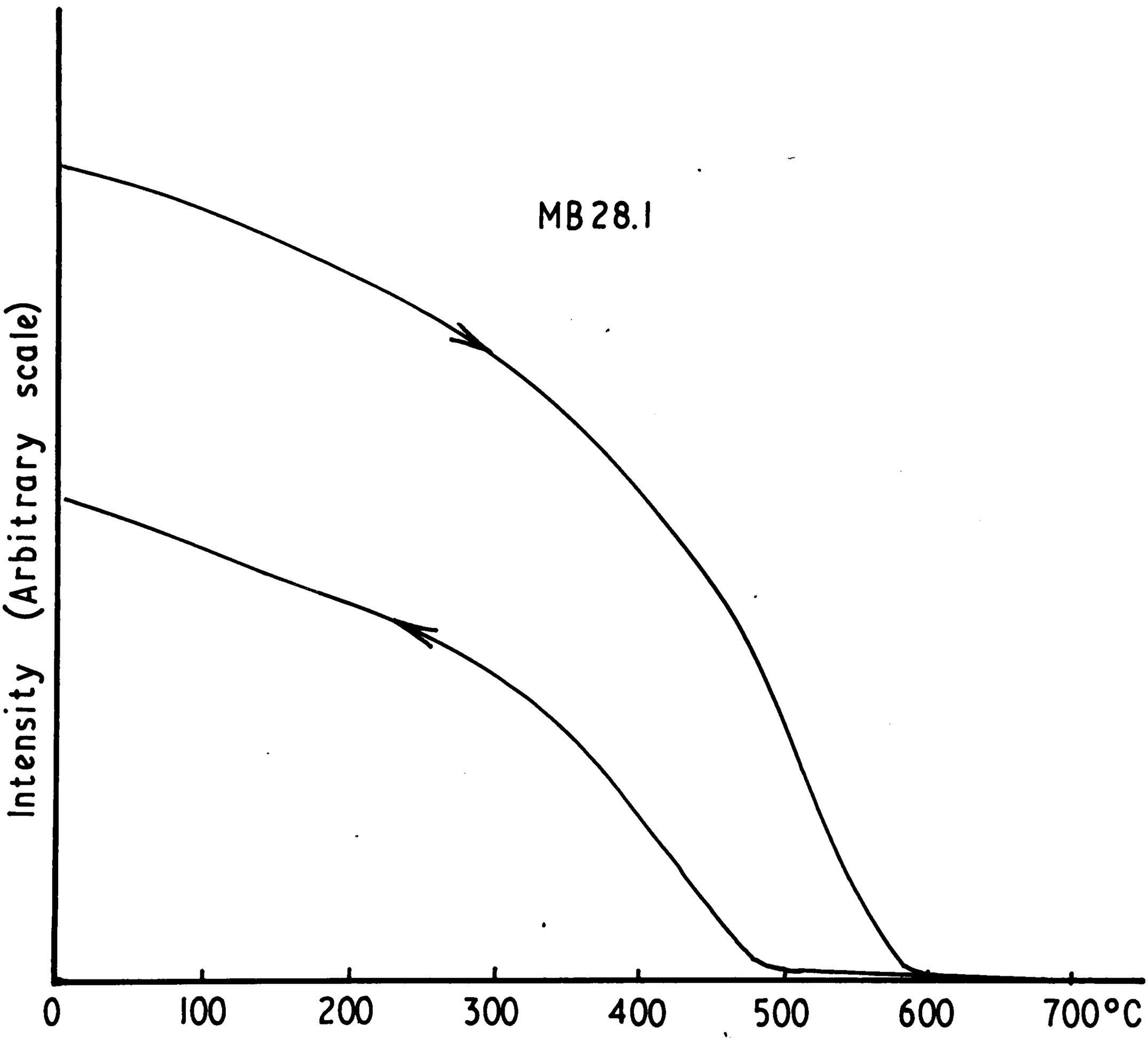


Fig 5.11 Issaldain dolerites. Thermomagnetic analysis of sample MB28.1.

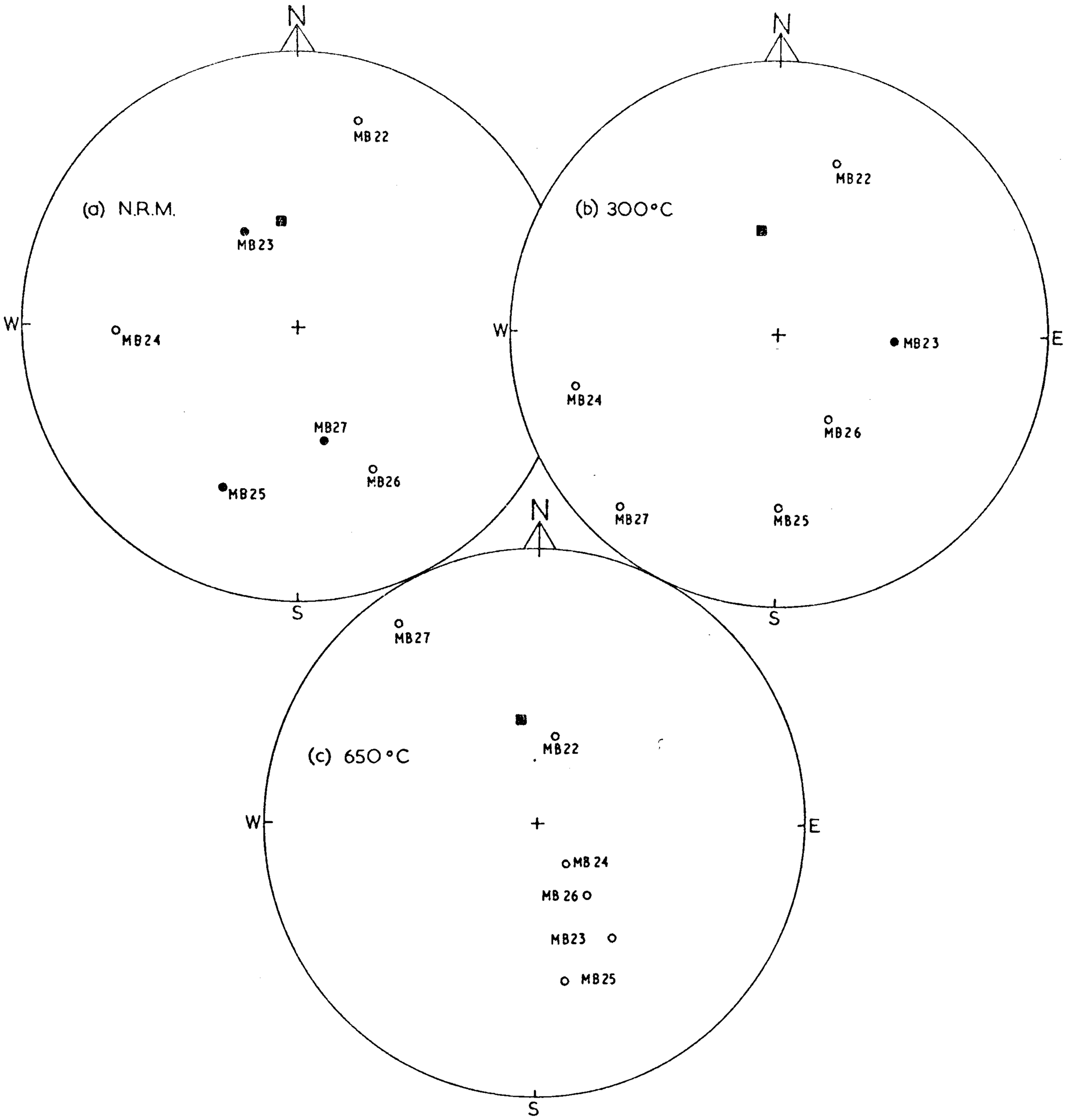


Fig 5.12 Titchka sediments. Mean site directions of remanence (a) N.R.M. (b) After demagnetisation at 300°C. (c) After demagnetisation at 650°C.

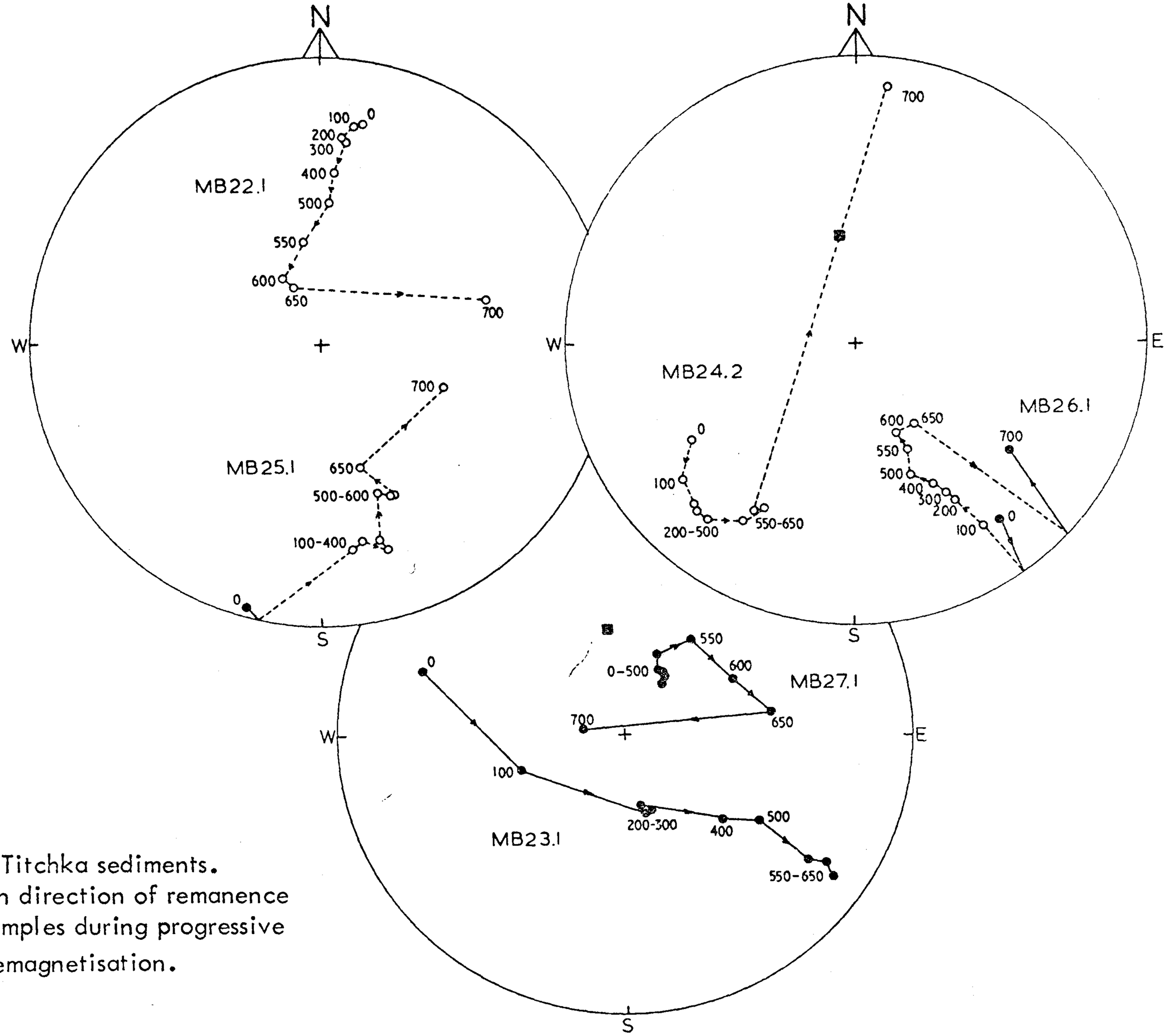
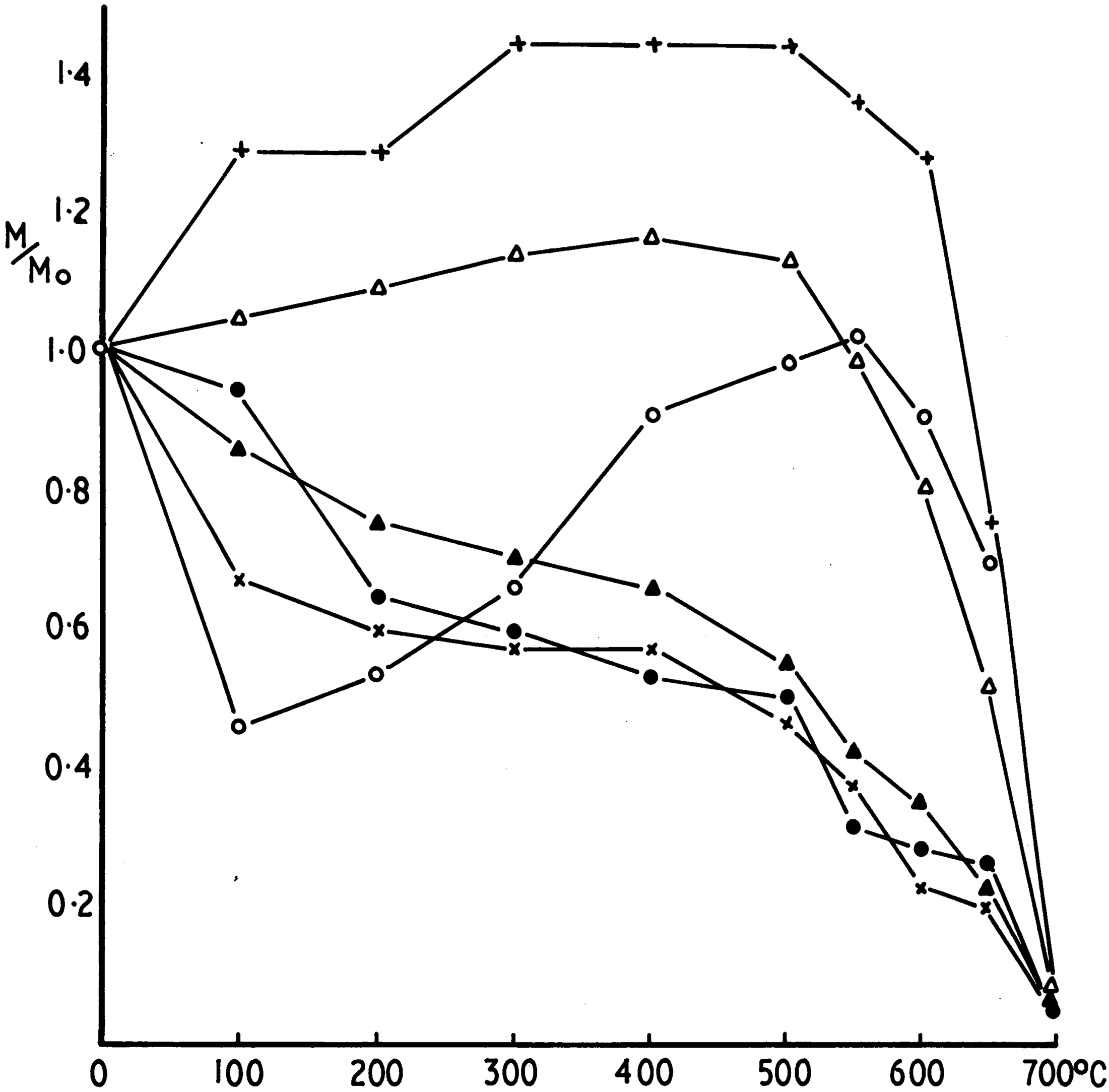


Fig 5.13 Titchka sediments. Changes in direction of remanence of pilot samples during progressive thermal demagnetisation.



	Mo
• MB 22.1	0·65
o MB 23.1	0·24
× MB 24.1	0·60
+ MB 25.1	0·13
Δ MB 26.1	0·38
▲ MB 27.1	0·70

X 10^{-5} Gauss

Fig 5.14. Titchka sediments. Changes in intensity of magnetisation of pilot samples during progressive thermal demagnetisation.

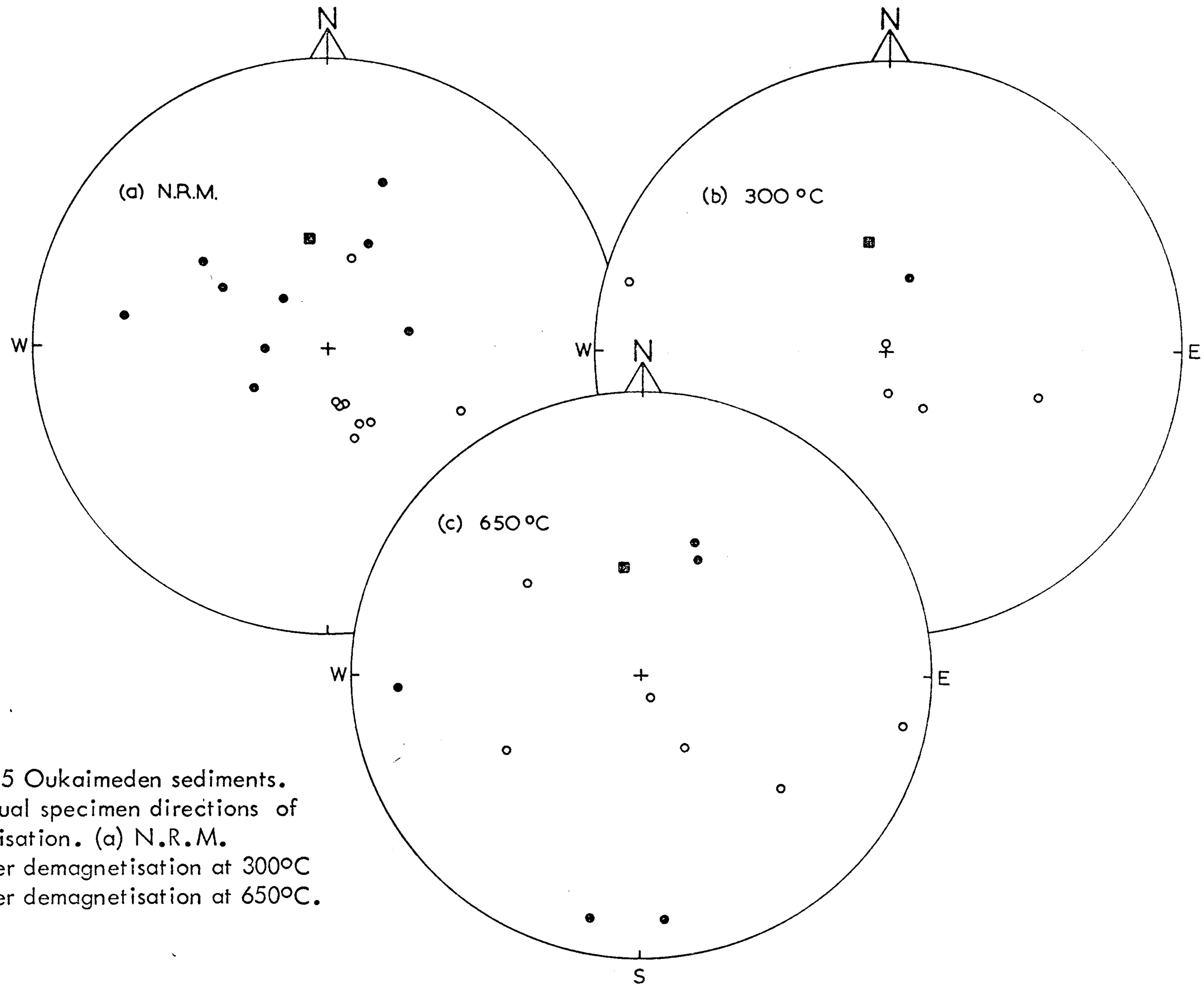


Fig 5.15 Oukaimeden sediments.
Individual specimen directions of magnetisation. (a) N.R.M.
(b) After demagnetisation at 300°C
(c) After demagnetisation at 650°C.

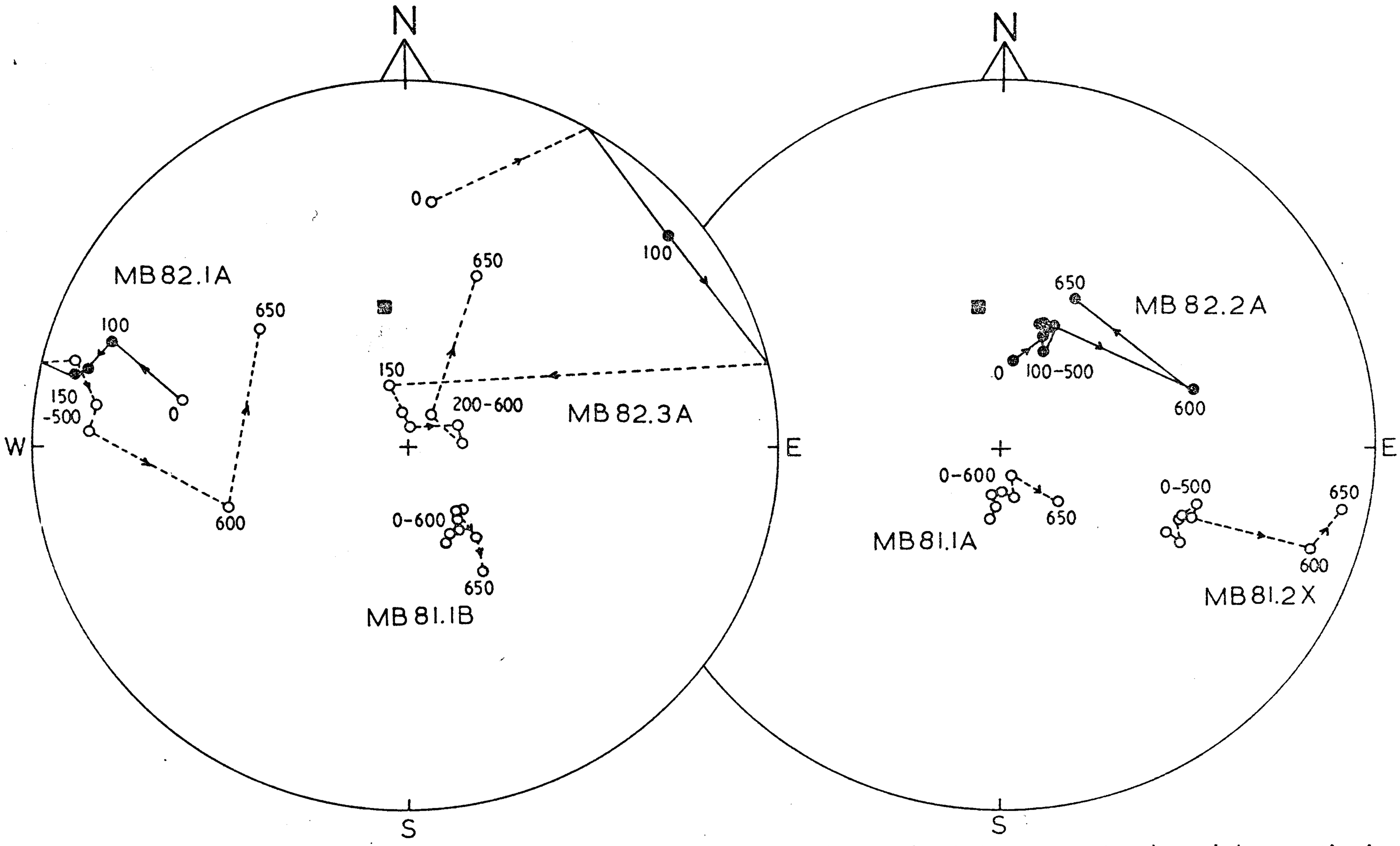
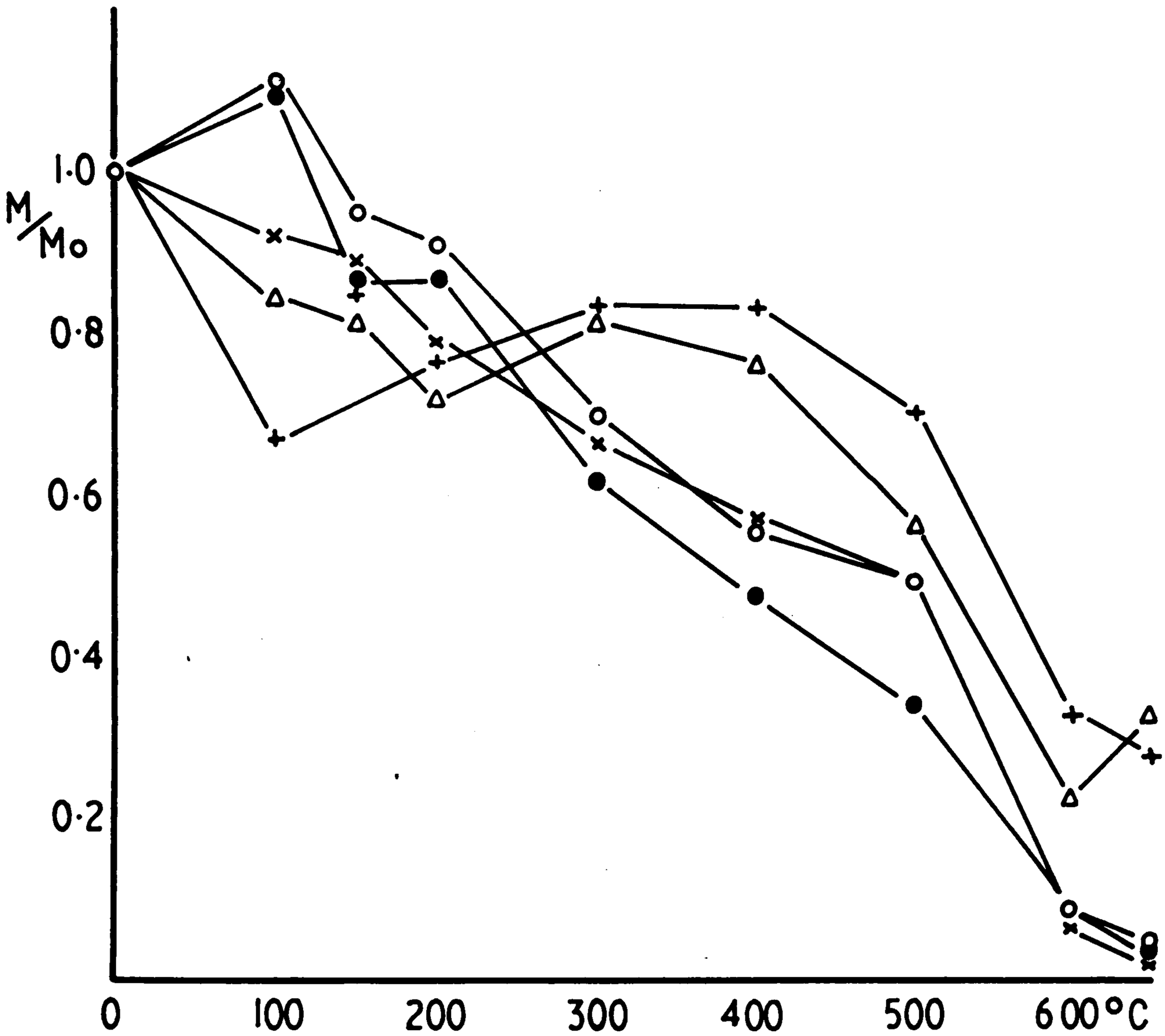


Fig 5.16 Oukaimeden sediments. Changes in direction of remanence of pilot samples during progressive thermal demagnetisation.



•	MB 81.1A	3·56	
o	MB 81.1B	3·41	
x	MB 81.2X	3·23	X 10^{-5} Gauss
+	MB 82.1A	10·07	
Δ	MB 82·2A	15·90	

Fig 5.17 Oukaimeden sediments. Changes in intensity of magnetisation of pilot samples from sites MB81 and MB82 during progressive thermal demagnetisation.

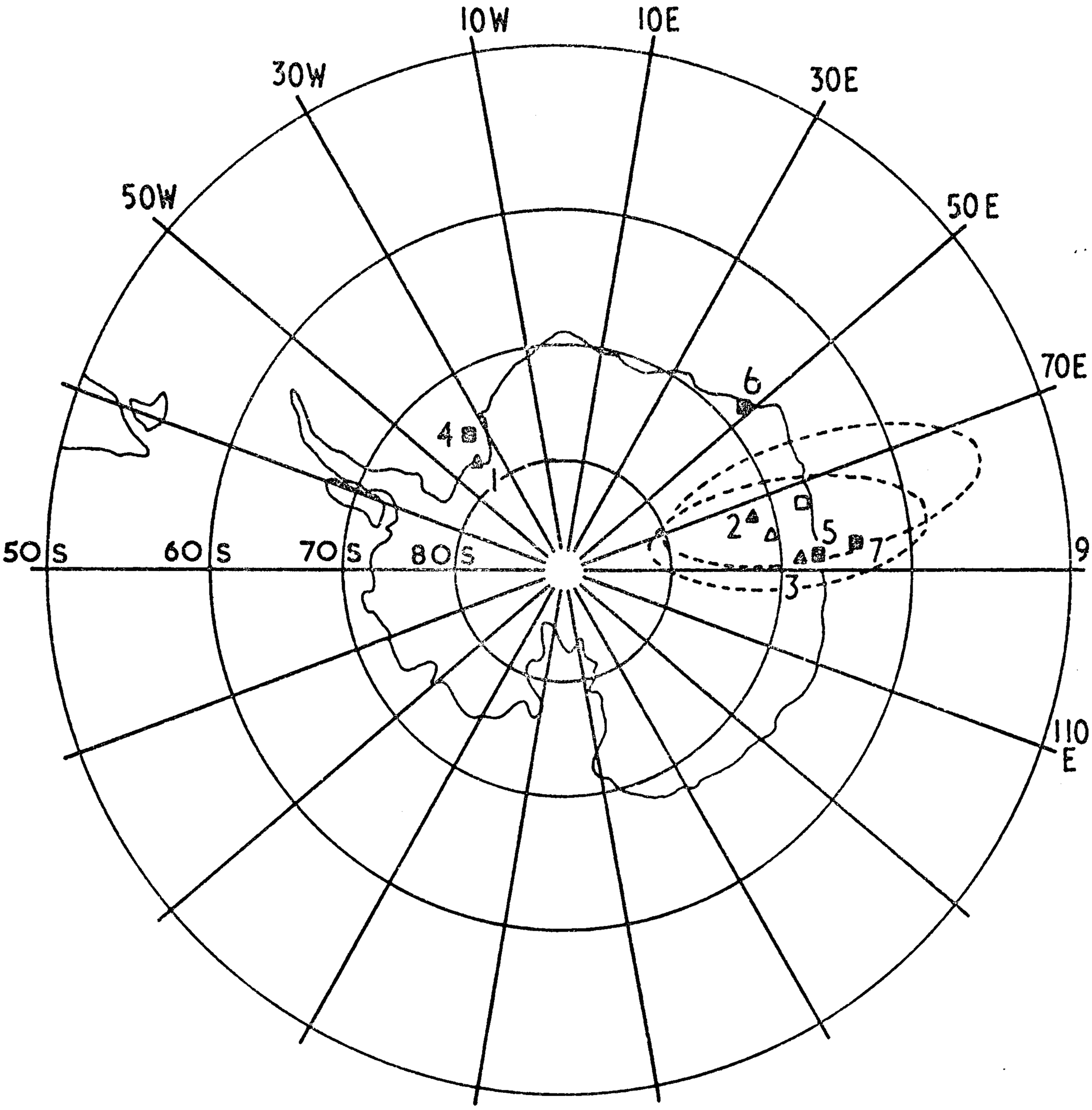


Fig 5.18 African Triassic pole positions. Black triangles, poles from Moroccan formations; black squares, poles from South and East African formations. Open triangle, mean of Moroccan poles 2 and 3; open square, mean of South and East African poles 5 to 7. For pole reference numbers see Tables 5.19 and 5.20.

Table 5.1 Triassic Field Data

(a) Ait Aadel dolerites

Mean location	Lat.	Long
	31.63N	7.25W

Tilt correction	Stike	Dip
Sites MB3, MB4	118	17
Sites MB1, MB2, and MB5 to MB16	None	

(b) Issaldain dolerites

Mean location	Lat.	Long
	31.13N	7.38W

Tilt correction	Strike	Dip
Sites MB28-36	None	

(c) Titchka sediments

Mean location	Lat.	Long
	31.46N	7.41W

Tilt correction		Strike	Dip
Site	MB22	105	26
	MB23	105	26
	MB24	114	29
	MB25	114	19
	MB26	90	31
	MB27	90	31

(d) Oukaimeden sediments

Mean location	Lat.	Long
	31.20N	7.81W

Tilt correction		Strike	Dip
Site	MB81	211	16
	MB82	214	9

Table 5.2 Ait Aadel Triassic dolerites. Mean site directions, pole positions and statistical parameters

Site No.	N.R.M. D	I	N	R	k	α_{95}	After thermal demag. at 300°C D	I	N	R	k	α_{95}	Lat.	Long	A_{95}
MB1	14.6	+18.9	6	5.706	17	17	341.3	+41.0	4	3.904	31	17	72.2N	115.9W	15
MB2	245.9	+31.9	6	5.220	6	29	344.5	+45.2	4	3.977	129	8	75.7N	112.2W	7
MB3	315.9	+55.6	5	4.670	12	33	336.8	+24.6	4	2.865	3	71	66.5N	124.6W	58
MB4	316.9	+32.7	5	4.934	61	10	300.1	+54.0	5	2.443	2	GT90	22.5N	62.0W	GT90
MB5	4.0	+22.8	5	4.758	16	19	337.4	+51.5	5	3.686	3	53	66.9N	69 5W	71
MB6	73.8	+8.0	6	4.895	4	35	296.5	+30.2	6	4.905	4	35	32.3N	93.9W	34
MB7	32.5	+17.4	6	4.639	4	41	354.6	+37.0	4	3.218	4	54	80.1N	124.1W	62
MB8	36.0	+10.4	5	4.917	48	11	332.0	+58.1	4	3.134	4	58	70.5N	66.5W	82
MB9	83.0	+29.6	6	5.675	15	18	357.3	+41.7	3	2.976	83	14	82.2N	166.8W	12
MB10	37.5	+9.0	6	5.858	35	11	343.0	+37.4	4	3.927	41	14	71.3N	126.1W	12
MB11	271.9	+38.5	6	5.660	15	18	335.4	+32.9	4	3.992	371	5	63.9N	123.0W	3
MB12	320.4	+30.0	3	2.996	556	5	346.7	+44.0	1	1.000	-	-	76.9N	120.4W	-
MB13	339.7	+51.5	5	4.957	94	8	351.9	+49.0	4		71	11	83.2N	103.9W	11
MB14	358.6	+35.6	4	3.510	6	40	336.0	+27.2	2	1.963	27	50	62.3N	128.9W	32
MB15	323.0	+35.4	6	5.410	8	24	335.5	+43.6	4	3.963	82	10	67.8N	106.6W	11
MB16	0.0	+68.2	5	4.931	58	10	357.1	+64.2	5	4.917	48	11	74.0N	17.8W	15
Overall Mean.	0.0	+43.2	16	11.497	3	24	339.7	+42.8	15	14.482	27	7.5	72.0N	105.5W	7.5
												Antipole	72.0S	74.5E	7.5

Table 5.3. Ait Aadel Triassic dolerites N.R.M.s

Site No.	Sample No.	D	I	Int($\times 10^{-4}$ gauss)
MB1	1	349.1	+25.2	22.02
	2	1.8	+17.1	13.40
	3	12.9	+17.2	8.04
	4	21.9	+14.1	5.07
	5	13.4	+11.1	8.26
	6	49.6	+23.1	4.47
MB2	1	246.7	+40.9	3.98
	2	239.1	+20.2	5.06
	3	244.8	+34.5	3.07
	4	252.1	+12.9	2.16
	5	204.2	+14.6	12.26
	6	316.8	+46.0	9.88
MB3	1	339.4	+53.3	0.16
	2	323.0	+55.5	0.14
	3	5.2	+56.6	0.19
	4	288.2	+34.1	2.69
	5	277.9	+56.2	3.58
MB4	1	300.5	+22.1	9.39
	2	315.9	+34.4	8.85
	3	324.8	+35.6	5.33
	4	323.4	+34.4	7.81
	5	321.9	+35.3	6.92
MB5	1	358.5	+25.4	7.11
	2	13.0	+16.3	7.14
	3	11.7	+5.9	8.26
	5	7.7	+15.8	7.21
	6	340.1	+49.6	6.14
MB6	1	73.7	-25.4	1.80
	2	82.9	+3.4	2.53
	3	43.1	+1.8	0.75
	4	56.8	-9.7	4.97
	5	130.4	+26.3	3.30
	6	64.7	+47.8	3.89
MB7	1	26.7	+43.6	2.87
	2	42.2	+2.0	2.67
	3	38.0	+39.9	0.57
	4	336.1	+49.6	0.82
	5	17.5	-21.9	1.60
	6	73.6	-21.4	1.47
MB8	1	34.6	-1.3	6.05
	2	51.3	+17.8	7.08
	4	32.9	+7.4	8.61
	5	29.9	+18.3	5.50
	6	31.9	+9.2	9.78

Site No.	Sample No.	D	I	Int($\times 10^{-4}$ gauss)
MB9	1	76.1	+2.9	5.96
	2	79.5	+38.8	5.25
	3	84.3	+12.5	8.60
	4	96.4	+31.3	5.34
	5	67.7	+36.5	6.39
	6	98.5	+52.9	4.23
MB10	1	28.7	+13.9	7.94
	2	48.9	-6.6	8.18
	3	43.9	+6.9	5.56
	4	42.2	+24.5	5.61
	5	34.8	+11.7	6.68
	6	26.8	+3.0	6.54
MB11	1	244.9	+44.8	4.16
	2	275.9	+37.1	4.15
	3	247.6	+16.2	3.63
	4	292.0	+34.8	6.13
	5	303.3	+44.7	8.11
	6	272.5	+41.7	3.73
MB12	1	323.9	+32.2	8.03
	4	317.6	+29.7	7.77
	5	319.9	+28.1	6.76
MB13	1	342.1	+45.0	0.36
	3	334.4	+58.4	0.15
	4	326.5	+58.1	
	5	341.8	+46.8	
	6	349.6	+48.0	
MB14	1	57.8	+55.8	
	2	354.8	+6.5	
	3	348.9	+24.8	3.50
	5	337.5	+43.3	
MB15	1	7.2	+23.0	
	2	301.0	+5.5	
	3	305.1	+41.2	
	4	298.2	+33.3	
	5	335.3	+45.9	
	6	336.9	+46.0	
MB16	2	343.8	+49.4	0.25
	3	355.1	+57.0	0.27
	4	1.4	+64.9	0.29
	5	339.5	+75.9	0.23
	6	36.4	+68.2	0.20

Table 5.4 Ait Aadel dolerites. Pilot sample A.F. demagnetisation results

Field (Oe)	Sample No. MB1.3			MB2.3			MB4.2		
	D	I	Int*	D	I	Int*	D	I	Int*
0	12.9	+17.2	8.57	244.8	+34.5	3.13	315.9	+34.4	9.04
85	341.3	+60.5	53.93	235.2	+33.0	2.23	302.5	+13.8	6.47
169	351.0	+5.0	37.95	231.3	+25.7	2.30	296.7	+4.2	5.62
254	316.1	-41.9	27.09	222.5	+19.5	2.10	292.5	-1.4	4.90
338	326.6	-64.2	10.63	221.4	+14.2	2.17	296.9	-4.0	4.71
507	72.5	+13.6	3.69	212.9	+11.8	2.13	282.7	-5.2	4.97
676	25.4	-0.2	3.45	206.6	+5.0	2.49	285.4	-9.8	4.85
845	40.6	-16.8	3.77	205.9	+3.0	2.86	282.6	-4.7	4.41

	Sample No. MB5.1			MB6.2		
	D	I	Int*	D	I	Int*
0	358.5	+25.4	7.11	82.9	+3.4	2.53
85	9.4	+22.2	6.71	105.5	-23.3	2.98
169	13.1	+18.2	7.05	104.3	-23.0	3.58
254	12.4	+13.0	6.34	116.1	-27.1	4.29
338	16.4	+10.6	6.60	118.1	-26.4	3.95
507	14.8	+11.0	6.66	118.1	-24.5	4.09
676	3.1	+16.1	6.88	134.8	-10.9	2.99
845	346.1	+23.0	6.20	136.7	-27.9	3.88

* $x10^{-4}$ gauss

Field (Oe)	Sample No. MB7.1			MB8.6			MB9.4		
	D	I	Int*	D	I	Int*	D	I	Int*
0	30.5	+16.8	3.80	28.0	+7.8	10.81	55.0	+73.7	5.29
85	53.6	-5.1	2.17	92.8	-16.5	9.14	94.1	+20.8	3.10
169	70.0	-7.3	2.20	47.1	-19.3	9.13	107.2	+6.2	3.78
254	72.3	-9.4	2.17	48.5	-21.2	9.07	117.2	-2.3	4.21
338	77.2	-10.4	1.97	50.2	-22.8	9.23	114.6	-3.2	4.39
507	77.5	-18.8	2.19	50.1	-22.4	9.03	119.6	-6.0	4.52
676	82.8	-13.0	2.20	51.1	-19.4	8.44	111.1	-7.4	4.90
845	83.3	-5.7	1.91	46.8	-21.7	8.79	113.7	-0.7	4.43

Field (Oe)	Sample No. MB10.5			MB11.2			Field (Oe)	MB3.1		
	D	I	Int*	D	I	Int*		D	I	Int+
0	357.3	+63.3	6.24	30.5.5	+18.3	6.03	0	339.4	+53.3	16.00
85	37.7	+16.4	4.22	287.3	+15.5	3.49	75	335.4	+51.6	15.93
169	47.8	-0.4	4.30	251.2	-6.9	2.15	150	334.2	+52.7	11.62
254	49.0	-4.1	4.29	219.9	-10.4	2.54	300	326.6	+41.7	4.35
338	50.2	-10.2	4.17	193.6	-22.2	3.21	450	332.6	+44.5	3.88
507	52.7	-11.5	4.93	192.5	-23.0	3.31	600	283.9	+25.5	1.07
676	50.8	-12.7	5.17	185.2	-28.8	4.83	750	62.2	+43.9	0.88
845	51.2	-5.9	4.52	184.8	-14.0	4.04	900	230.1	+34.9	0.83

*$x10^{-4}$ gauss

+ $x10^{-6}$ gauss

Field (Oe)	Sample No. MB12.4			MB13.4		
	D	I	Int*	D	I	Int
0	317.6	+29.7	7.77	350.9	+57.0	1.28
75	335.4	+51.6	1.12	350.2	+52.0	1.02
150	334.2	+52.7	0.81	348.1	+53.8	0.66
300	326.6	+41.7	0.42	341.0	+50.0	0.33
450	332.6	+44.5	0.29	332.4	+63.3	0.14
600	283.9	+25.5	0.07	274.0	+87.0	0.08
750	62.2	+43.9	0.07	308.3	-0.5	0.02
900	230.1	+34.9	0.05	331.4	-18.2	0.05

	Sample No. MB14.1			MB15.2		
	D	I	Int	D	I	Int
0	72.1	+82.9	1.57	301.0	+5.5	4.00
75	2.3	+77.5	1.10	335.7	+44.5	3.86
150	13.5	+68.0	0.74	337.7	+48.7	2.14
225.	0.6	+87.8	0.46	338.5	+52.8	0.89
300	37.4	+83.3	0.34	335.8	+50.6	0.46
450	117.2	-58.9	0.16	318.7	+47.2	0.07
600	9.5	-61.2	0.06	194.4	+51.7	0.21
750	342.0	-32.6	0.20	200.0	+30.7	0.01
900	215.7	-18.4	0.03	243.3	-12.0	3.31

* x 10^{-4} gauss

Table 5.5. Ait Aadel dolerites. Sites MB3 to 8, bulk A.F. demagnetisation results

Treatment (Oe)	Site No.	Sample No.	D	I	Int($\times 10^{-4}$ gauss)
375	MB3	1	326.6	+41.7	4.35
		2	342.3	+32.1	
		3	336.4	+43.7	
		4	350.2	+48.0	
		5	300.3	-11.5	
525	MB4	1	13.1	-38.5	
		2	282.7	-5.2	4.97
		3	193.3	+60.0	
		4	328.6	+51.6	
		5	284.1	-0.1	
300	MB5	1	16.4	+10.6	6.60
		2	311.7	+32.5	
		3	306.6	+27.4	
		5	322.5	+23.7	
		6	280.0	+51.6	
300	MB6	1	352.4	+39.2	
		2	118.1	-26.4	3.95
		3	308.4	-15.8	
		4	325.9	-32.8	
		5	0.7	+84.3	
		6	331.6	+21.0	
350	MB7	1	77.2	-10.4	1.97
		2	341.1	+29.5	
		4	244.4	+61.7	
		5	333.7	+3.3	
		6	37.4	+13.5	
300	MB8	1	353.8	+42.8	
		2	269.0	+88.0	
		4	129.9	+45.4	
		5	5.7	+36.5	
		6	50.2	-22.8	

Table 5.6 Ait Aadel Triassic dolerites. Sites MB3 to 8. Mean site directions after bulk A.F. demagnetisation

Treatment (Oe)	Site No.	D	I	N	R	k	α_{95}
375	MB3	328.7	+34.9	5	4.437	7	31
525	MB4	299.8	+20.2	5	2.711	2	87
300	MB5	322.1	+33.1	5	4.338	6	34
300	MB6	339.0	+14.8	6	2.836	2	85
350	MB7	9.0	+30.3	5	2.937	2	77
300	MB8	36.0	+51.5	5	3.318	2	64
Overall Mean		338.6	+34.4	5.320		7	26.5

Table 5.7 Ait Aadel Triassic dolerites. Thermal demagnetisation pilot sample results

	Sample No.	MB2.1		MB9.2			MB12.5		
Temp.	D	I	Int*	D	I	Int	D	I	Int
0	246.7	+40.9	3.98	78.9	+39.0	5.25	320.4	+28.1	6.76
100	340.2	+47.8	1.27	333.9	+62.6	3.62	347.9	+30.6	4.65
150	340.1	+42.7	1.23	334.5	+60.4	3.58	350.2	+30.5	4.43
200	338.1	+45.8	1.06	332.9	+54.3	2.66	346.7	+28.0	3.61
300	322.5	+57.5	1.06	353.2	+59.0	2.61	344.4	+29.8	2.89
400	343.6	+38.1	0.86	339.3	+50.8	1.90	344.3	+24.7	2.48
500	339.0	+40.1	0.59	324.5	+44.3	1.56	352.7	+35.9	0.94
600	282.7	+57.7	0.32	149.6	+53.7	0.22	295.9	+23.8	0.30
650	168.2	+54.6	0.79	32.4	+57.5	0.09	318.2	-54.9	0.04

	Sample No.	MB14.3		MB16.1		
Temp	D	I	Int*	D	I	Int
0	348.9	+24.8	3.50	343.8	+69.4	0.40
100	312.9	+29.8	1.21	303.4	+58.5	0.38
150	333.9	+15.7	0.67	348.8	+73.3	0.39
200	338.2	+19.5	0.53	347.7	+71.9	0.38
300	318.3	+26.3	0.48	345.9	+72.7	0.36
400	329.6	+24.4	0.45	12.6	+77.4	0.34
500	332.8	+26.4	0.34	343.2	+72.1	0.26
600	285.9	+25.0	0.11	114.9	+36.1	0.05
650	170.9	+48.2	0.05	15.4	-18.3	0.01

* $x10^{-4}$ gauss

Table 5.8 Ait Aadel Triassic dolerites. Bulk thermal demagnetisation results (300°C)

Site No.	Sample No.	D	I	Int
MB1	1	332.4	+28.5	9.16
	2	343.2	+40.8	4.10
	5	350.2	+34.7	2.48
	6	339.7	+59.3	1.60
MB2	1			
	2	343.5	+54.6	0.89
	4	344.2	+42.3	0.94
	5	348.8	+44.9	5.01
	6	341.5	+38.8	4.00
MB3	2	352.8	+30.4	0.03
	4	339.8	+76.9	0.33
	5	296.2	+9.4	0.57
	6	2.9	-26.9	0.40
MB4	1	15.7	-30.7	0.68
	2	217.2	+41.3	0.18
	3	190.8	+60.8	0.86
	4	320.7	+69.5	0.28
	5	280.8	-3.0	1.01
MB5	1	285.1	+35.9	1.27
	2	2.4	+10.7	3.59
	3	7.9	+21.4	0.39
	5	308.8	+55.7	0.34
	6	153.9	+67.1	0.31
MB6	1	338.5	+40.8	0.52
	2	240.8	+41.4	0.55
	3	309.7	+1.6	0.34
	4	266.4	+5.4	0.24
	5	310.4	+61.0	0.62
	6	312.4	+8.9	0.36
MB7	2	339.8	+20.9	0.41
	4	273.0	+73.3	0.30
	5	346.4	+17.6	0.35
	6	38.7	+18.7	0.49
MB8	1	70.3	+52.5	0.14
	2	266.0	+26.3	0.19
	3	340.2	+49.6	0.17
	5	341.6	+41.5	0.19
MB9	1	2.7	+36.1	1.97
	2			
	5	356.8	+38.1	1.79
	6	351.0	+50.5	2.09
MB10	2	349.2	+33.5	1.77
	3	336.0	+43.4	1.60
	4	333.9	+48.0	1.62
	6	349.5	+23.7	1.46
MB11	1	336.7	+39.1	2.77
	3	334.8	+31.3	3.15
	4	335.2	+30.5	4.98
	5	335.1	+30.7	5.56
MB12	1	346.7	+44.0	4.70
	5			
MB13	1	349.5	+48.5	0.29
	3	358.0	+62.3	0.12
	5	350.3	+43.2	0.78
	6	351.9	+41.9	1.58
MB14	2	239.2	+16.6	0.88
	3			
	5	332.2	+37.8	0.63
MB15	1	337.9	+34.6	3.06
	4	324.6	+43.3	1.97
	5	334.1	+45.8	1.93
	6	346.0	+49.7	1.32
MB16	1			
	2	343.1	+67.6	0.22
	3	1.1	+51.2	0.24
	4	349.0	+69.2	0.24
	5	350.7	+76.7	0.20
	6	9.4	+54.6	0.15

Table 5.9 Issaldain Triassic dolerites. Mean site directions, pole positions and statistical parameters

Site No.	N.R.M. D	I	N	R	k	95	After bulk A.F. demag. D	I	N	R	k	95	Lat.	Long	A_{95}
MB28	356.9	+41.8	5	4.896	38	12	9.2	+37.2	6	5.727	18	16	+77.7	+130.0	14
MB29	12.7	+47.9	6	5.948	96	7	3.3	+33.4	6	5.865	37	11	+77.1	+158.8	10
MB30	18.9	+42.5	6	5.991	564	3	20.6	+35.6	6	5.979	234	4	+68.2	+109.2	5
MB32	4.1	+32.8	5	4.840	25	16	10.2	+34.8	5	4.849	26	15	+75.4	+134.5	16
MB33	359.0	+38.5	6	5.982	279	4	14.3	+27.9	6	5.965	145	6	+69.2	+130.6	4
MB34	357.6	+40.4	6	5.996	1162	2	5.2	+32.0	6	5.981	258	4	+75.5	+152.4	4
MB35	354.8	+42.6	6	5.985	334	4	347.9	+36.3	5	4.929	57	10	+74.6	+221.3	10
MB36	6.1	+48.1	6	5.927	69	8	10.8	+40.0	5	4.273	5	36	+82.8	+111.5	33
Overall Mean	3.6	+42.1	8	7.933	104	6	7.8	+35.0	8	7.921	88	6	+77.3	+140.6	6.5

Table 5.10 Issaldain Triassic dolerites. NRM directions and intensities

Site No.	Sample No.	D	I	Int*
MB28	1	5.7	+20.1	19.20
	2	351.8	+47.3	12.11
	3	355.5	+51.5	
	4	352.3	+44.6	
	5	355.9	+44.5	
MB29	2	6.1	+54.5	12.91
	3	17.2	+50.0	
	4	9.7	+44.5	
	5	357.0	+51.5	
	6	22.7	+42.7	
MB30	1	15.1	+38.1	
	2	24.4	+40.9	
	3	19.2	+44.4	13.75
	4	17.8	+42.7	
	5	18.2	+44.6	
	6	18.5	+43.9	
MB32	2	359.2	+34.7	
	3	27.6	+13.1	
	4	358.9	+35.3	
	5	355.4	+38.0	
	6	355.0	+39.3	
MB33	1	2.2	+30.1	
	2	2.0	+42.4	
	3	359.1	+39.3	
	4	354.4	+39.7	
	5	357.6	+39.2	
MB34	1	355.3	+37.6	
	2	356.2	+42.2	
	3	357.0	+38.6	
	4	357.8	+40.6	
	5	359.4	+41.1	
	6	0.3	+42.1	
MB35	1	357.9	+40.5	
	2	358.0	+39.4	
	3	352.8	+40.8	
	4	355.1	+42.4	
	5	356.4	+49.4	
	6	348.8	+42.9	
MB36	1	13.9	+48.2	
	2	9.1	+50.4	
	3	15.5	+51.3	
	4	10.2	+45.0	
	5	8.6	+52.1	
	6	343.5	+38.4	

* $\times 10^{-4}$ gauss

Table 5.11 Issaldain Triassic dolerites. Pilot A.F. demagnetisation results

Field	Sample No. MB28.2 D	I	Int*
0	349.5	+45.3	12.11
75	359.2	+43.8	10.26
150	4.2	+41.0	8.15
250	6.8	+40.4	5.95
340	5.6	+41.3	4.49
450	8.0	+39.5	3.09
600	6.9	+40.8	2.07
750	11.8	34.4	1.66
900	8.5	+42.2	1.37

Field	Sample No. MB29.2 D	I	Int*
0	0.3	+47.5	12.91
75	6.4	+41.7	9.48
150	10.8	+38.8	7.11
225	15.8	+39.7	6.65
300	10.3	+41.7	3.49
375	16.7	+37.5	2.83
450	10.4	+41.7	2.06
600	19.4	+35.3	1.35
750	350.8	+0.6	1.95

Field	Sample No. MB30.3 D	I	Int*
0	18.5	+38.5	13.75
75	21.7	+35.7	11.97
150	20.4	+35.4	9.83
225	22.0	+35.4	7.68
300	22.0	+35.4	5.86
375	27.3	+33.8	4.59
450	25.0	+37.1	4.18
600	22.3	+46.6	2.60
750	16.6	+39.7	2.60
900	23.1	+43.5	1.60

Field	Sample No. MB35.1 D	I	Int*
0	357.9	+40.5	9.00
75	355.8	+31.7	7.23
150	356.2	+30.5	4.98
225	351.9	+38.2	3.29
300	357.3	+31.9	2.46
450	30.7	+15.2	1.38
600	11.7	+40.6	0.95
750	338.3	+49.5	0.41
900	195.1	+58.2	1.46

* $x10^{-4}$ gauss

Table 5.12 Issaldain Trassic dolerites. Bulk A.F. demagnetisation results

Treatment (Oe)	Site No.	Sample No.	D	I	Int($\times 10^{-4}$ gauss)	Treatment (Oe)	Site No.	Sample No.	D	I	Int($\times 10^{-4}$ gauss)
450	MB28	1	34.5	+28.0		300	MB33	1	15.6	+16.1	13.45
		2	8.0	+39.5	3.09			2	14.2	+32.2	10.98
		3	352.0	+47.2				3	12.8	+26.4	12.01
		4	9.1	+54.6				4	9.3	+33.4	11.72
		5	355.9	+13.6				5	16.3	+29.8	22.09
		6	13.6	+35.2				6	17.2	+29.2	23.73
450	MB29	1	9.2	+36.2		300	MB34	1	3.0	+29.3	9.30
		2	10.4	+41.7	2.06			2	4.2	+29.3	9.93
		3	351.7	+41.5				3	12.9	+30.9	11.52
		4	347.6	+25.5				4	6.6	+34.9	10.25
		5	2.8	+33.6				5	358.7	+30.6	9.63
		6	17.2	+19.1				6	6.0	+36.6	9.83
450	MB30	1	13.9	+31.9		300	MB35	1	357.3	+31.9	2.46
		2	29.1	+36.2				3	332.7	+44.1	2.23
		3	25.0	+37.1	4.18			4	349.3	+42.6	1.64
		4	16.9	+36.3				5	355.6	+34.3	2.06
		5	21.1	+38.8				6	343.0	+26.9	1.29
		6	18.3	+32.5							
						300	MB36	1	13.6	-19.1	1.26
300	MB32	2	8.9	+32.8	12.47			2	358.1	+44.5	1.38
		3	37.0	+21.3	10.98			3	332.0	+54.0	2.02
		4	3.4	+37.3	11.21			4	20.0	+8.0	1.14
		5	3.1	+37.3	10.86			5	38.0	+7.8	2.69
		6	354.2	+40.5	10.78			6	352.9	+74.1	2.34

Table 5.13. Titchka Triassic sediments. Mean site directions

Site No.	N.R.M. D	N.R.M. I	N.R.M. α_{95}	300°C D	300°C I	300°C α_{95}	650°C D	650°C I	650°C α_{95}	Lat.	Long	A_{95}
MB22	17.0	-13.1	13.5	19.4	-22.6	40.4	339.9	-80.4	38.8	16.9N	172.1E	52.3
MB23	331.5	+46.7	33.1	92.5	+42.2	83.7	148.5	-11.9	35.8	51.9S	69.0E	34.7
MB24	268.8	-22.8	38.4	247.5	-14.3	38.7	185.7	-37.0	38.8	69.9S	141.2E	53.3
MB25	203.8	+24.3	33.2	175.0	-23.3	30.3	172.8	-15.4	18.7	73.8S	30.8E	17.4
MB26	151.7	-29.4	48.2	147.1	-43.9	34.1	156.8	-26.1	23.3	61.1S	103.7E	31.2
MB27	167.5	+43.8	65.8	222.5	-9.2	GT90	325.1	-6.4	82.0	53.2N	237.0E	80.1
Overall Mean	223.9	+33.4	GT90	181.4	-34.2	GT90	173.5	-46.7	63.5	57.5S	139.0E	81.9
				Mean of sites MB23-26 only			165.1	-23.2	21.8	68.5S	86.8E	22.5

Table 5.14 Triassic sediments (Titchka) N.R.M. direction and intensities*

Site No.	Sample No.	D	I	Int(x10^{-5} gauss)
MB22	1	11.0	-13.4	0.65
	2	12.4	-18.9	0.52
	3	22.1	-30.4	0.50
	4	4.3	-18.4	0.70
	5	19.6	+4.9	0.70
	6	32.6	-1.6	0.80
MB23	1	287.7	+16.6	0.24
	2	287.2	+69.3	0.20
	3	37.6	+53.4	0.26
	4	5.3	+19.8	0.30
	5	331.8	+52.5	0.29
	6	320.7	+29.2	0.47
MB24	1	265.0	-27.1	0.60
	2	239.0	-22.7	0.50
	3	342.6	+22.0	0.40
	4	232.0	-45.9	0.70
	5	269.2	-12.5	0.40
	6	271.0	-26.2	0.50
MB25	1	195.5	+1.6	0.13
	2	140.2	+56.7	0.15
	3	229.7	+14.9	0.18
	4	233.4	-5.1	0.16
	5	204.9	+47.1	0.10
	6	186.1	+12.0	0.36
MB26	1	141.1	+12.0	0.38
	2	139.4	-37.0	0.22
	3	237.9	-68.4	0.43
	4	185.6	-18.6	0.37
	6	117.4	-14.4	0.36
MB27	1	36.8	+66.1	0.70
	2	103.9	-19.7	0.40
	3	243.8	+19.9	0.17
	4	164.0	+21.2	0.34
	5	159.1	+15.8	0.17
	6	226.8	+59.7	0.16

* Corrected for tilting

Table 5.15 Titchka Triassic sediments. Pilot sample demagnetisation results *

Temp.	Sample No. MB22.1			MB23.1			MB24.2		
	D	I	Int($\times 10^{-5}$ gauss)	D	I	Int	D	I	Int
0	11.0	-13.4	0.65	287.7	+16.6	0.24	239.0	-22.9	0.50
100	4.3	-13.6	0.62	249.6	+48.2	0.11	231.0	-15.3	0.40
200	6.2	-16.6	0.42	164.5	+56.7	0.13	224.3	-12.6	0.36
300	7.2	-17.7	0.39	167.4	+60.1	0.16	222.0	-11.8	0.35
400	4.7	-27.2	0.35	131.0	+39.7	0.22	218.9	-11.6	0.35
500	4.1	-36.4	0.33	122.6	+30.4	0.24	216.3	-1.0	0.28
550	351.2	-48.7	0.21	125.0	+13.3	0.25	211.3	-16.6	0.23
600	336.0	-65.5	0.19	122.7	+9.0	0.23	207.9	-22.7	0.14
650	330.9	-60.5	0.17	125.0	+6.0	0.17	210.2	-21.0	0.12
700	73.9	-27.6	0.03				7.0	-4.8	0.03

	Sample No. MB251			MB26.1			MB27.1		
	D	I	Int($\times 10^{-5}$ gauss)	D	I	Int	D	I	Int
0	195.5	+1.6	0.13	141.1	+12.0	0.38	36.8	+66.1	0.70
100	170.8	-16.7	0.17	144.9	-13.4	0.40	35.6	+63.6	0.60
200	167.9	-19.5	0.17	148.0	-23.2	0.42	34.8	+61.1	0.53
300	161.8	-15.1	0.19	148.9	-25.9	0.44	30.7	+60.5	0.50
400	163.3	-17.7	0.19	151.0	-30.5	0.45	28.2	+60.2	0.47
500	158.6	-30.9	0.19	157.1	-36.2	0.44	22.1	+55.1	0.39
550	155.4	-29.5	0.18	153.7	-43.9	0.38	35.0	+44.5	0.30
600	154.3	-28.8	0.17	154.9	-51.5	0.31	62.1	+43.3	0.25
650	161.6	-40.8	0.10	144.0	-51.4	0.20	81.0	+34.5	0.16
700	109.1	-41.4	0.01	124.6	-23.1	0.03	279.5	+73.7	0.04

* Corrected for tilting

Table 5.16 Tichka Triassic sediments. Bulk demagnetisation results*

Site No.	Sample No.	300°C D	300°C I	300°C Int(x10^{-5} gauss)	650°C D	650°C I	650°C Int
MB22	1	7.2	-17.7	0.39	330.9	-60.5	0.17
	2	349.9	-52.8	0.20	290.1	-63.4	0.20
	3	97.0	-42.0	0.20	125.2	-55.6	0.20
	4	345.9	-25.9	0.40	333.5	40.7	0.20
	5	23.8	+16.9	0.30	27.3	-17.1	0.11
	6	30.7	+7.6	0.50	21.3	-21.8	0.20
MB23	1	146.1	+52.5	0.18	125.0	+6.0	0.17
	2	141.8	-17.8	0.20	139.4	-34.9	0.20
	3	95.4	-32.2	0.06	136.1	-52.2	0.20
	4	38.9	+23.1	0.18	98.7	-28.1	0.10
	5	118.8	+75.1	0.17	148.2	-5.3	0.20
	6	325.7	+38.3	0.15	213.9	-31.2	0.10
MB24	1	242.1	-23.4	0.29	215.7	-58.3	0.10
	2	222.0	-11.8	0.35	210.2	-21.0	0.12
	4	211.2	-43.7	0.49	163.0	-53.5	0.30
	5	266.5	+19.1	0.18	31.7	-50.7	0.10
	6	286.6	-3.7	0.15	114.2	-70.9	0.08
MB25	1	161.8	-15.1	0.19	161.6	-40.8	0.10
	2	129.6	-5.7	0.19	156.0	-29.8	0.20
	3	195.3	-42.4	0.24	182.0	-27.5	0.20
	4	222.5	-51.7	0.31	203.4	-57.4	0.30
	5	180.9	-2.1	0.17	155.6	-17.3	0.10
	6	181.4	-10.4	0.41	165.9	-10.4	0.30
MB26	1	148.9	-25.9	0.44	144.0	-51.4	0.20
	2	125.1	-42.0	0.29	132.3	-47.2	0.20
	3	234.8	-70.3	0.51	215.7	-80.0	0.50
	4	173.5	-27.5	0.51	165.9	-38.5	0.40
	6	113.6	-29.8	0.41	118.9	-37.8	0.30
MB27	1	30.7	+60.5	0.50	81.0	-34.5	0.16
	2	119.9	-47.4	0.48	24.3	+21.9	0.26
	3	242.1	-27.3	0.28	268.5	-22.1	0.13
	4	184.1	-5.7	0.34	353.3	+41.7	0.20
	5	225.4	-24.1	0.19	271.4	-10.1	0.38
	6	294.2	+28.7	0.36	299.9	-5.8	0.21

* Corrected for tilting

Table 5.17 Oukaimeden Triassic sediments. Remanence directions and intensities

Site No.	Sample No.	NRM D	NRM I	NRM Int($\times10^{-5}$ gauss)	300°C D	300°C I	300°C Int($\times10^{-5}$ gauss)	650°C D	650°C I	650°C Int($\times10^{-5}$ gauss)
MB81	1A	156.8	-58.1	3.56	173.7	-73.5	0.80	152.7	-80.2	0.09
	1B	163.5	-56.4	3.41	145.7	-62.7	2.40	149.3	-45.8	1.40
	1C	150.0	-57.3	3.10				267.3	+9.6	0.07
	2X	114.8	-36.3	3.23	106.6	-32.5	2.15	101.4	-4.5	1.11
	2Y	304.7	+35.5	0.02				128.9	-24.7	0.08
	3A	170.8	-69.4	3.30						
	3B	167.4	-67.0	2.88						
	3C	164.4	-66.9	3.89						
MB82	1A	279.4	+20.1	0.11	285.4	-5.0	0.09	309.7	-35.7	1.03
	1B	318.1	+64.4	0.07				240.0	-34.1	0.03
	1C	298.8	+44.9	0.01				267.3	+9.6	0.02
	2A	21.1	+47.1	0.16	17.3	+59.7	0.13	26.2	+41.0	0.05
	2B	18.4	+26.6	0.15				173.9	+7.6	0.04
	2C	241.3	+58.2	0.14				190.6	+6.6	0.05
3A	3A	15.2	-54.3	0.03	7.7	-83.9	0.07	22.5	-35.6	0.02
	3B	270.4	+66.1	0.09						
	3C	77.0	+59.3	0.01						

Table 5.18 Oukaimeden Triassic sediments. Pilot sample demagnetisation results

Temp.	Sample No. MB81.1A D	I	Int*	MB81.1B D	I	Int*	MB81.2X D	I	Int*
0	156.8	-58.1	3.56	161.0	-58.3	3.41	118.5	-36.4	3.23
100	187.1	-67.0	3.90	160.8	-58.0	3.80	118.9	-32.3	2.96
150	184.4	-70.9	3.10	151.8	-59.9	3.25	112.6	-34.8	2.87
200	173.7	-73.5	8.10	147.8	-60.0	2.65	111.6	-35.1	2.56
300	178.4	-75.8	2.20	145.7	-62.7	2.40	106.6	-32.5	2.15
400	177.0	-76.0	1.70	141.3	-64.6	1.90	108.8	-31.8	1.85
500	189.1	-74.6	1.20	143.7	-64.9	1.72	110.8	-32.2	1.60
600	158.7	-80.5	0.30	144.5	-54.7	0.27	108.6	-6.7	0.21
650	133.3	-65.1	0.09	149.3	-45.8	0.14	101.4	-4.5	0.11

Temp.	Sample No. MB82.1A D	I	Int+	MB82.2A D	I	Int+	MB82.3A D	I	Int+
0	281.6	+26.8	1.07	8.6	+62.8	1.59	6.4	-21.7	0.28
100	290.0	+9.6	0.72	21.2	+63.7	1.34	50.6	+4.7	0.17
150	284.0	+7.3	0.91	22.2	+61.5	1.28	344.4	-70.2	0.46
200	282.8	+5.4	0.82	18.9	+60.3	1.14	351.3	-79.2	0.59
300	285.4	-5.0	0.90	17.3	+59.7	1.30	7.7	-83.9	0.71
400	277.6	-10.0	0.90	24.0	+58.5	1.23	65.6	-73.0	0.93
500	272.6	-9.?	0.76	22.6	+60.4	0.91	86.8	-73.2	1.10
600	251.4	-35.8	0.35	73.1	+33.3	0.35	37.1	-77.1	0.65
650	309.7	-35.7	0.30	26.2	+41.0	0.52	22.5	-35.6	0.25

* x 10^{-5} gauss
+ x 10^{-6} gauss

Table 5.19 Summary of Triassic pole-positions from Moroccan formations

Pole Ref No.(Fig 5.18)	Formation	Mean direction of magnetisation D	I	α_{95}	No. Samples	No. Sites	Palaeomagnetic south pole position Lat.	Long	A_{95}	Mean pole position Lat.	Long	A_{95}
1	Issaldain dolerites	8.0	+35.0	6	45	8	77.5S	39.5W	6.5			
2	Ait Aadel dolerites	339.5	+43.0	7.5	63	15	72.0S	74.5E	7.5	70.5S	81.0E	12
3	Titchka sediments	165.0	-23.0	22	22	4	68.5S	87.0E	22.5			

Table 5.20 Summary of Triassic pole-positions from S.E. African formations

4	K5 redsand-stones Songwe Rift, Tanzania	14.0	-27.0	10	5	1	75.0S	36.0W				
5	Upper Beaufort sediments, S. African				19	4	67.0S	87.0E				
6	Red sandstone formation Zambia	350.5	-55.5	4.5	-	6	68.0S	49.5E	5	67.5S	75.0E	13
7	Shawa ijolite Rhodesia	335.5	-51.5	11.5	13	5	64.0S	85.5E	14			

CHAPTER 6. JURASSIC

6.1 Introduction

In this chapter palaeomagnetic results are described from three igneous formations:

(i) The Draa Valley sills

(ii) The Foum Zguid dyke

(iii) The Central Atlas intrusives

Stratigraphic evidence indicates that the first two of these formations are post-Stephanian and pre-Lower Cretaceous in age, and previous authors (e.g. Choubert & Faure-Muret, 1962, Hollard, 1970) have referred to them as "Hercynian", implying an Upper Palaeozoic age. However radiometric dating results performed on these rocks at Newcastle, and described in this chapter, indicate that they are in fact Upper Triassic to Lower Jurassic, having a mean age of approximately 183 m.y.

6.2. Geology

6.2.1. General Jurassic palaeogeography

A major transgression occurred at the beginning of the Jurassic period, in the Lower Lias, and the sea rapidly invaded the whole of the Atlas domain. This transgression spread as far as the line of the South Atlas fault zone, which formed the southern shore of the ocean during most of the Jurassic. An area to the north, including the Moroccan Meseta (Fig 1.1) remained emergent or was only partially covered by the sea, whereas the Oran Meseta was entirely submerged by a shallow sea, and received a cover of neritic sediments. In the weaker belts between these stable zones troughs of subsidence developed, and the largest of these, the High Atlas trough, was established along the northern margin of the Anti Atlas, immediately adjacent to the shore-

line of the African continent. To the north of this the Middle Atlas trough developed between the Moroccan and Oran Mesetas (Fig 1.1) and further still to the north the Prerif and Rif troughs were established. Thick sequences of sediments were deposited in the latter, and folded and thrust southwards to their present position during the Alpine orogenesis. This trough resembles a classical geosyncline, whereas the Middle and High Atlas belts were subjected to less intense folding, confined mainly to the cover rocks.

Because of the contrasting environments of deposition between the stable mesetas and intervening subsiding troughs, Jurassic sedimentation was very variable. However an overall pattern of deposition is evident, consisting predominantly of limestones, dolomites and clayey marns in the Liassic, limestones and marns in the Bajocian and Bathonian, sandstones in the Upper Bathonian and Callovian, and limestones and dolomites in the Kimmeridgian and Portlandian. In general the sedimentation was more calcareous and less varied in the rigid zones of the Mesetas than in the intervening subsident zones, and sediments continued to accumulate in the latter zones during most of the Jurassic.

A separate basin of deposition, the 'Haha basin', began to develop along the present day Atlantic coast of Morocco between Agadir and Safi during the Middle Jurassic, but sedimentation did not become completely marine in this basin until the Callovian. The Haha basin is very similar in character to the other late Mesozoic marginal Atlantic basins, e.g. the Tarfaya-Rio de Oro, Dakar, Ivory Coast and Middle Congo basins, and probably developed during the separation of Africa and North America (Reyment 1969).

6.2.2. Jurassic tectonic movements in the Central High Atlas

Following the major Lower Liassic (Upper Sinemurian) transgression three major tectonic events occurred during the Jurassic. The first of these was marked by a major regression during the Toarcian (Upper Lias), followed very rapidly by a second transgression in the Aalenian. The second, and most important tectonic event was a period of uplift during the Mid Bathonian, during which the sea retreated from most of the Atlas domain, and deposition ceased in the Atlas trough. During this phase the principal anticlinal axes of the High Atlas were defined, and the intervening synclinal basins were filled with continental sediments.

During the third event, in the Upper Jurassic, the sea finally retreated from the Middle Atlas belt, and the region to the NE became stabilised.

A fourth tectonic phase occurred at the end of the Portlandian, and resulted in the emergence of almost all of the Atlas domain. This event was more important than any of the preceding three Jurassic events, and produced a radical change in the palaeogeography of the Atlas domain. It has been termed the "post-Portlandian, pre-Cretaceous phase" (Choubert and Faure-Muret, 1962), and will be referred to later in this chapter.

6.2.3. Jurassic igneous formations

(a) The Central Atlas intrusives

The Central Atlas intrusives outcrop in the axial zone of the calcareous High Atlas, in the cores of Liassic and Jurassic anticlines (Fig 6.1). In general the rocks are of gabbroic and dioritic composition, accompanied by basic types enriched in olivene (troctolites), and more acid types having the composition of syenites. An important

alkaline complex (Bou Agrao) near Midelt (Fig 1.1), comprises a wide variety of nepheline syenites.

Certain of these igneous rocks are overlain discordantly by continental Infracenomanian deposits, and Choubert and Faure-Muret have suggested that they were intruded during the important post-Portlandian, pre-Cretaceous tectonic phase referred to in Section 6.2.2. This suggestion is supported by the radiometric age determinations described later in this chapter.

(b) The Draa Valley sills

The Draa Valley sills are a set of very fresh and well-exposed dolerites, injected at various levels into the Devonian and Carboniferous sedimentary sequence in the southern part of the Anti-Atlas belt (Fig 6.1). They outcrop discontinuously over an area of some 20,000 sq.km along the NW rim of the Sahara, and were previously regarded as Hercynian, i.e. Upper Palaeozoic. Radiometric dating results, described later in this chapter, indicate that they are in fact Lower Jurassic in age.

(c) The Foum Zguid dyke

This is a large quartz dolerite body, approximately 100 metres wide, and extending in an almost continuous line in a NE-SW direction for some 200 km across south Morocco (Fig 6.1). The Foum Zguid dyke is associated with several smaller dykes, and whereas the Draa Valley sills were folded with the country rocks which they intrude, the dykes are straight and practically vertical. At several localities they cross beds which have been previously folded, and cut through the sills. They must therefore be, in part at least, younger than the sills.

6.2.4. Location of sampling sites

Most of the Jurassic sedimentary sequence consists of limstones and marls, and is unsuitable for palaeomagnetic work. The only sandstones

in the sequence are those of Bathonian and Callovian age, which are poorly consolidated, and impossible to sample by normal collecting techniques. Collection was therefore confined to the three igneous formations described in section 6.2.3.

The Draa Valley sills were sampled at a total of sixteen sites distributed along the northernmost outcrops of this formation, and the Foum Zguid dyke was sampled at five sites, approximately evenly distributed across its total width of outcrop. The Central Atlas intrusives were sampled at six sites, three of these being in a single gabbro intrusion, the Tassent gabbro, and three inrelated dykes (one site per dyke).

6.3. Palaeomagnetic results from the Draa Valley sills

6.3.1. N.R.M. directions and intensities

The intensities of NRM of samples from this formation were generally high, ranging from 0.1 to 6.0 x 10^{-2} gauss (Table 6.3). Within-site scatter of NRM directions was variable, but less than 20^{o} at all sites except two, at which it exceeded 40^{o} (Table 6.2), and the between-site scatter was high (20^{o}). The mean site directions are plotted in Fig 6.2, and listed in Table 6.2(a). The overall mean direction of NRM, giving unit-weight to each site, is

$$D = 343.5, \quad I = 36.5, \quad \alpha_{95} = 20^{o}$$

6.3.2. A.F. demagnetisation stability tests

One pilot sample from each site was subjected to partial A.F. demagnetisation at 750e intervals upto a maximum peak field of between 450 and 750 Oe. In all cases treatment was discontinued as soon as excessive scatter began to occur.

The results are plotted in Fig 6.3(a) and (b), which demonstrate two differing types of behaviour. Approximately half of the samples (e.g. MC5.1, 7.1, 9.1, 15.1 etc) underwent initial, often large, changes in direction of remanence on treatment up to 150 to 225 Oe, after which the latter remained approximately constant on further treatment up to 450 to 525 Oe. Above 525 Oe the directions began to scatter. In all of these samples the constant direction maintained over the range 150 to 525 Oe had a NNW declination and a steep positive inclination. This behaviour indicates the removal of a less-stable component of remanence on treatment at 150 to 225 Oe, and the isolation of a more-stable underlying component, which was itself destroyed on treatment at 450 to 525 Oe.

The other half of the pilot samples (e.g. MC1.3, 2.2, 13.1 etc) carried an NRM with a steep positive NNW direction, which remained unchanged on treatment up to 375 to 450 Oe, after which scatter occurred. This indicates the presence of a single stable component of remanence in these samples, requiring fields of 375 to 450 Oe for its destruction.

6.3.3. Bulk A.F. demagnetisation

The remaining samples from each site were demagnetised at fields of between 225 and 335 Oe, and the results are listed in Table 6.5. The mean site directions of remanence after treatment are listed in Table 6.2(b), and plotted in Fig 6.2(b). This treatment resulted in a general reduction of within-site scatter (maximum value 12^{o}), and a considerable improvement in between-site scatter (reduced to 4.5^{o}). The mean direction of remanence after treatment, giving unit weight to each site, is

$$D = 339, \quad I = 27.5, \quad \alpha_{95} = 4.5$$

The corresponding palaeomagnetic south pole position is

$$65.5S, \ 50.5E, \ A_{95} = 3.5$$

6.3.4. Thermomagnetic analyses and microscopic examinations

Microscopic examination of polished sections of samples of the Draa Valley sills revealed the presence of an opaque phase which was tentatively identified as maghemite.

Thermomagnetic analyses were carried out on samples from sites MC1, 4, 9, 11 and 16. In all cases the shape of the curve was similar to that illustrated in Fig 6.5(a). Curie points on the heating curves varied from 480 to $500^{o}C$, and on the cooling curves from 430 to $470^{o}C$, The cooling curve was always down shifted with respect to the heating curve. This behaviour may be due to decomposition of a metastable phase, reduction of a partially oxidised phase, or internal homogenisation (Larson et al, 1969). In this case the most plausible explanation, consistent with the microscopic observations, is the decomposition of a titanomaghemite component to

the antiferromagnetic stable phase haemetite (Ozima & Larson, 1967).

6.4. Palaeomagnetic results from the Foum Zguid dyke

6.4.1. N.R.M. directions and intensities

N.R.M. intensities of samples from the five sites situated in the Foum Zguid dyke ranged from 0.3 to 1.2 x 10^{-3} gauss, and were an order of magnitude lower than those of the Draa Valley sills. Within-site scatter was low ($<6^{o}$) for three sites (MB37 to 39) but very high for the other two (35 and 45^{o} respectively). The mean remanence vectors of the first three sites were well grouped around a positive NNW direction, whereas those of the other two sites were more highly scattered (Fig 6.6(a) and Table 6.6(a).

6.4.2. A.F. demagnetisation stability tests

One pilot sample from each site was subjected to progressive A.F. demagnetisation at 75 Oe intervals up to a maximum peak field of between 600 and 900 Oe. The results are plotted in Figs. 6.7 and 6.8, and listed in Table 6.8.

In all five pilot samples the intensity decreased progressively during treatment up to 450 Oe, but in the samples from sites MB37, 38 and 39, subsequent treatment up to 900 Oe caused an increase in intensity. The reason for this increase is uncertain, but it may be due to spurious magnetisation being introduced in the samples by the demagnetising apparatus (Chapter 10). The remanence vectors of the pilot-samples either remained close to, or moved towards a positive NW direction on treatment up to 300 Oe, after which they moved away in apparently random directions.

6.4.3. Bulk A.F. demagnetisation

The pilot sample results indicate the presence of a stable component of remanence with a positive NW direction at all sites, over the range of treatment from 150 to 300 Oe. The remaining samples from each site were

demagnetised in the appropriate field, and the results are listed in Table 6.9. This treatment caused a substantial decrease in within-site scatter of remanence directions for sites MB40 and 41, and a slight increase for sites MB37 to 39 (Table 6.6(a). The mean site directions after treatment are plotted in Fig 6.6(b), from which it can be seen that the two mean site directions which originally differed significantly from the others become part of the main group after treatment.

The mean direction of magnetisation after treatment, giving unit weight to each site, is

$$D = 325, \quad I = 40, \quad \alpha_{95} = 4$$

The corresponding palaeomagnetic south pole position is

$$58S, \quad 79E, \quad A_{95} = 4$$

This pole is significantly different from that derived from the Draa Valley sills, and the possible reasons for this discrepancy will be discussed at the end of this chapter.

6.3.4. Thermomagnetic analyses

Thermomagnetic analyses were carried out on one sample from each site, and the general form of the curves is illustrated in Fig 6.5(b). The Curie points of the heating curves varied from 500 to 530°C, and those of the cooling curves from 480 to 510°C. In all cases only a single Curie point was present, indicating the presence of only one magnetic phase.

The general shape of the curves is similar to that of the curves derived from the Draa Valley sills, and it is possible that, like the latter, the Foum Zguid dyke curves indicate the presence of titanomaghemite. However no microscopic studies were performed on these samples to complement the thermomagnetic analyses.

An alternative possible explanation is that the observed Curie points represent titanomagnetite of approximate composition 15% Fe_3O_4, 75% $TiFe_2O_4$.

6.5. Palaeomagnetic results from the Central Atlas Intrusives

6.5.1. N.R.M. directions and intensities

The intensities of NRM of samples from the three sites situated in the gabbro intrusion (MB76, 79 and 80) were fairly weak, ranging from 0.07 to 0.16 x 10^{-3} gauss. Two of the dykes (MB75 and 78) had slightly stronger intensities, in the range 0.16 to 0.90 x 10^{-3} gauss, and that of the third dyke (site MB77) was an order of magnitude higher still.

The within-site dispersion of NRM directions was fairly low ($<10^{o}$) at all sites except MB78 and 80, at which it approached 30^{o}. The NRM between-site scatter was very high (56^{o}), indicating the presence of a component of remanence with random orientation (Table 6.10 and Fig 6.9(a)).

6.5.2. A.F. demagnetisation stability tests

One pilot sample from each site was progressively demagnetised at 75 Oe intervals up to a maximum peak field of 600 Oe. The results are listed in Table 6.12, and plotted in Fig 6.10 and 6.11.

The remanence vectors of the pilot samples from sites situated in dykes either retained a positive northerly direction with intermediate inclination (e.g. samples MB75.3 and 80.3), or else moved towards such a direction during treatment up to 150 Oe. (Sample MB77.1) This direction was retained during further treatment up to 300-450 Oe, after which scatter began to occur. Two of the pilot samples from sites situated in the gabbro intrusion (MB76.6 and 79.2) retained a positive northerly, shallow to intermediate, direction of remanence over the whole range of treatment, while the remanence vector of the third pilot sample moved away from this direction after treatment above 230 Oe.

The intensities of magnetisation of all pilot-samples except MB79.2 decreased progressively over the whole range of treatment. The latter sample showed a slight increase during treatment from 450 to 600 Oe.

6.3.3. Bulk A.F. demagnetisation

The pilot demagnetisation results described above indicate the presence of a component of remanence with a positive northerly direction in all six samples during treatment over at least the range 150 to 225 Oe. The remaining samples from each site were accordingly demagnetised at the most appropriate field value in this range, and the results are listed in Table 6.13. This treatment produced a decrease of within-site scatter for four of the sites, and a slight increase for the other two. It also resulted in a substantial reduction of between-site scatter, from 56° to 22° (Table 6.10(b) and Fig 6.9(b)).

The mean direction of remanence after treatment, giving unit weight to each site, is

$$D = 318.5, \quad I = 38.5, \quad \alpha_{95} = 22^{\circ}$$

and the corresponding palaeomagnetic southpole position is

$$53^{\circ}S, \quad 81.5^{\circ}E, \quad A_{95} = 24^{\circ}$$

This is in good agreement with the pole obtained from the Foum Zguid dyke.

6.3.4. Thermomagnetic analyses

Thermomagnetic analyses were carried out on one sample from each site, and typical curves for the gabbro and dyke samples are shown in Figs 6.12 and 6.13 respectively.

The gabbro samples showed two Curie points on the heating curves, in the ranges 510 to $530^{\circ}C$ and 560 to $580^{\circ}C$ respectively, representing two distinct magnetic phases. The cooling curves also showed two Curie

points, but this time in the ranges 470 to 530°C and 630 to 670°C, the highest of these being typical of haemetite. These results may be interpreted as representing oxidation of one of the original phases to haemetite (or a member of the ilmeno-haemetite series), and decomposition of the other to a phase with a lower Curie point.

The thermomagnetic results from the three Central Atlas dykes are similar to those from the Foum Zguid dyke and Draa Valley sills, and are thought to represent similar magnetic mineral compositions.

6.6. Radiometric dating results

Potassium-argon age determinations were performed by Dr. J.G. Mitchell at the University of Newcastle, on cores chosen from those used for palaeomagnetic measurements. Selection was carried out after consideration of a thin section of each core sample, and according to the criteria outlined by Dalrymple & Lanphere (1969). Whole rock analyses were performed on the 16-30 gauge (B.S.410) fraction from the crushed cores of the fine-grained rocks. In the case of the coarser-grained samples from the Tassent gabbro, biotite was separated from the 85-100 gauge (B.S.410) fraction using a shaking table.

Triplicate potassium analyses were performed by flame photometry using a lithium internal standard, and duplicate argon analyses were performed by the isotope dilution method on an Omegatron mass spectrometer (Grasty & Miller, 1965), using an argon extraction system similar to that described by Miller & Brown (1965)). The results are listed in Table 6.14.

6.7. Discussion

The mean radiometric age determined for the Draa Valley sills, assigning unit weight to each sample, is 183 my, and that determined for the Foum Zguid dyke is 184 my. These results indicate that the two formations are contemporaneous within the range of experimental error (Table 6.14).

The radiometric results obtained from the Central Atlas intrusives are more variable. The mean value derived for the Tassent gabbro is 156 my, and for the two dykes is 126 my (132 and 120 my respectively). This variability may represent a real difference in age between the gabbro and the dykes, or may reflect the relatively complex tectonic history of this region, during which argon loss could have occurred. In this case the results obtained may be considered as a stratigraphic minimum age of intrusion.

As discussed in section 6.2.3., other geological evidence indicates that this formation is post-Liassic and pre-Infracenomanian, and Choubert & Faure-Muret (1962), have suggested a post-Portlandian, pre-Cretaceous age, in the range 141 to 136 my (Geol. Soc. Phanerozoic time-scale, 1964). This is in general agreement with the radiometric results.described above.

Although the radiometric dating results from the Draa Valley sills and Foum Zguid dyke are identical, within the range of experimental error, geological evidence (Section 6.2.3.) indicates that the dyke is in fact slightly younger than the sills, and that a significant episode of folding occurred between the intrusion of these two formations. The date of this tectonic phase is now accurately defined as 183 to 184 my.

The palaeomagnetic pole positions derived from the three Moroccan Jurassic igneous formations are listed in Table 6.15, and those derived from South & East African Jurassic formations are listed in Table 6.16. All of these poles are plotted in Fig 6.14, together with the ovals of 95% confidence around the Moroccan poles. It is clear from this diagram that there is a significant difference between the pole from the Draa Valley Sills (pole 1) and that from the Foum Zguid dyke (pole 2), but no significant difference between the latter and the pole from the Central Atlas intrusives (pole 3).

This difference is puzzling since the radiometric ages obtained for the first two formations are identical to each other, but substantially different from that of the Central Atlas intrusives. Furthermore these two formations lie in the stable Saharan Shield-Anti Atlas region, whereas the Atlas Intrusives lie in a fold belt which was affected by post-Jurassic orogenic movements. The anomalous pole from the Draa

Valley sills is based on a large number of sites, and is considered to be substantially more reliable than the other two Moroccan poles.

One pole from East Africa (pole 4), that from the Zambian red sandstone formation (Opdyke 1964) agrees with the pole from the Draa Valley sills, whereas the other five poles from SE Africa are in better agreement with those from the Foum Zguid dyke and Central Atlas intrusives. The age of the Zambian red sandstone formation is quoted as 180 to 200 my (McElhinny et al, 1968), and it is possible that this formation and the Draa Valley sills have recorded the same small temporary excursion of the pole away from the mean position which it occupied with respect to Africa for the rest of the Mesozoic. Since this excursion is not recorded in the Foum Zguid dyke, the time taken to return to the mean Mesozoic position must have been less than the range of uncertainty in the age determinations ($\sim$ maximum 3 my). The geological evidence cited above indicates that the intrusion of these two formations was separated by a period of time of sufficient length for a significant folding episode to have occurred.

The mean Moroccan Jurassic pole, calculated by assigning unit weight to each formation, is plotted in Fig 6.14, together with the mean SE African pole, and the corresponding ovals of 95% confidence. There is no significant difference between these two poles, and this confirms the conclusion drawn in chapter 5, that no significant relative tectonic movement has occurred between North-west and South-east Africa since at least Triassic times.

The palaeolatitude, λ, calculated from the inclination, I, of the mean remanence vector of the three Moroccan Jurassic formations, by means of the formula

$$\tan I = 2 \tan \lambda$$

is 20^{o}.

The present-day latitude of the sampling sites is approximately 31°N, and this indicates that during the Jurassic this region was situated at least 10° closer to the equator than at present. This conclusion is supported by the palaeoclimatological evidence of thick limestones and evaporite sequences, indication of a warm environment of deposition.

References

Choubert, G. and A. Faure-Muret, 1962. Évolution du domaine Atlasique Marocain depuis les temps Palaeozoiques. In Livre a la mémoire du Professeur Paul Fallot, Sociéty Géologique de France.

Dalrymple, G.B. and Lamphere, M.A. 1969. Potassium-Argon Dating. W.H. Freeman & Co., San Fransisco

Geol. Soc. Phanerozoic time scale, 1964. Quat. J. geol. Soc. London 120 S 260-2

Grasty, R.L. & Miller, J.A. 1965. The Omegatron, a useful tool for argon isotope studies. Nature, 207, 1146-1148

Hollard, H. 1970. Silurian-Devonian-Carbonifère. Extrait de Colloque international sur les Corrélations du Précambrian. Livret-guide de l'éxcursion: Anti-Atlas occidental et central. Notes et M. Serv. géol. Maroc No. 229 pp 161-188

Larson, E. Mituko Ozima, Minoru Ozima, T. Nagata and D. Strangway 1969. Stability of remanent magnetisation of igneous rocks. Geophys. J.R. astro. Soc. 17, 263-292.

McElhinny, M.W. Briden, J.C. Jones, D.L. & Brock, A., 1968. Geological and geophysical implications of palaeomagnetic results from Africa Rev. Geophys. 6, 2, pp 201-238

Miller, J.A. & Brown, P.E., 1965. Potassium-Argon age studies in Scotland. Geol. Mag. 102, 106-134

Opdyke, N.D. 1964. The palaeomagnetism of some Triassic redbeds from Northern Rhodesia. J. Geophys. Res., 69, 2495-2497

Ozima, M. and E.E. Larson, 1967. Study on irreversible change of magnetic properties of some ferromagnetic minerals. J. Geomag. Geoelect. 19, 117-127

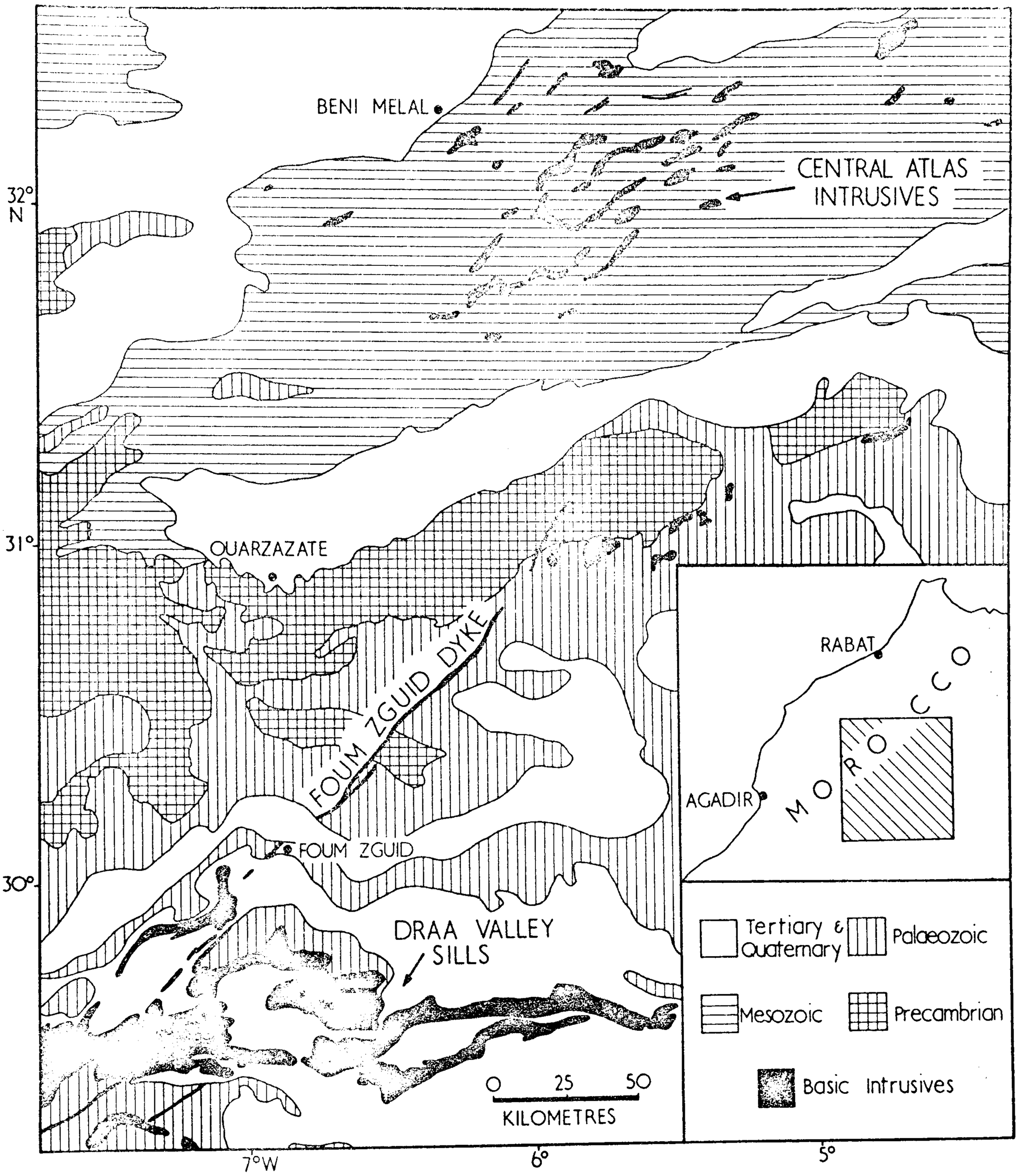


Fig 6.1 Outline geological map of South Morocco, showing locations of the three Jurassic igneous formations studied.

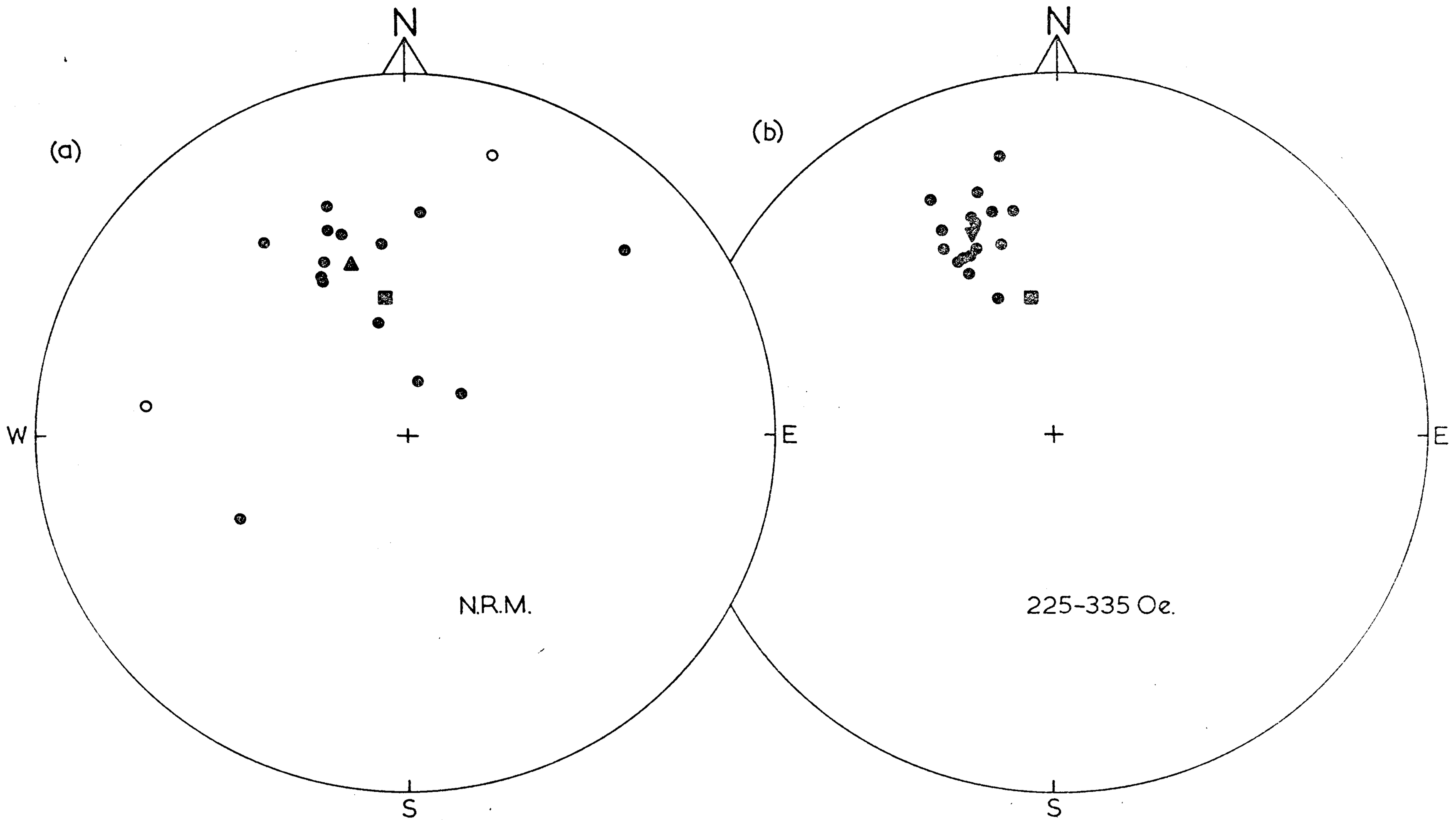


Fig 6.2 Draa Valley Sills. Mean site directions of remanence. (a) N.R.M. (b) After demagnetisation at 225 to 335 Oe.

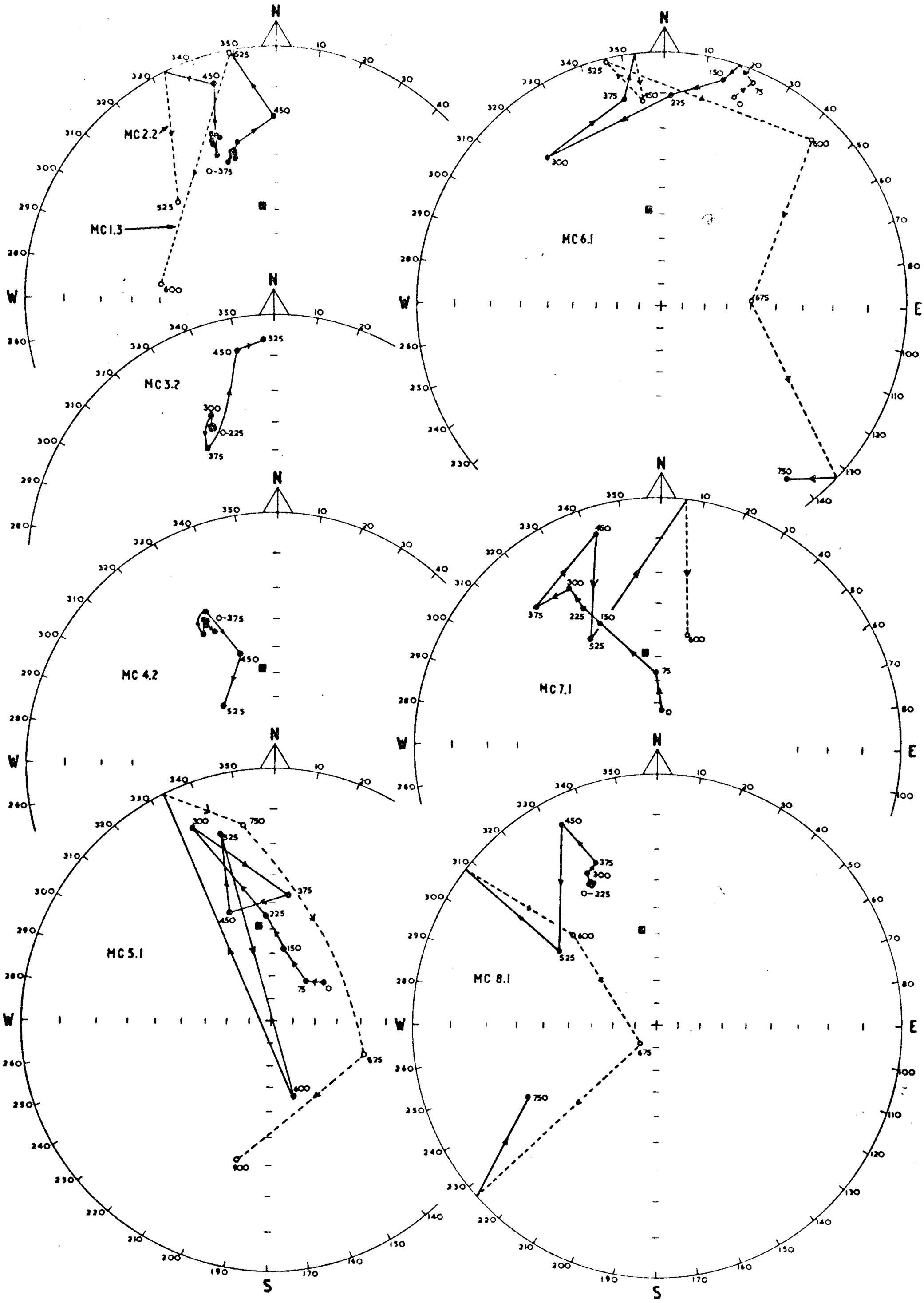


Fig 6.3(a) Draa Valley Sills. Changes in direction of remanence of pilot samples from sites MC1 to MC8 during progressive demagnetisation.

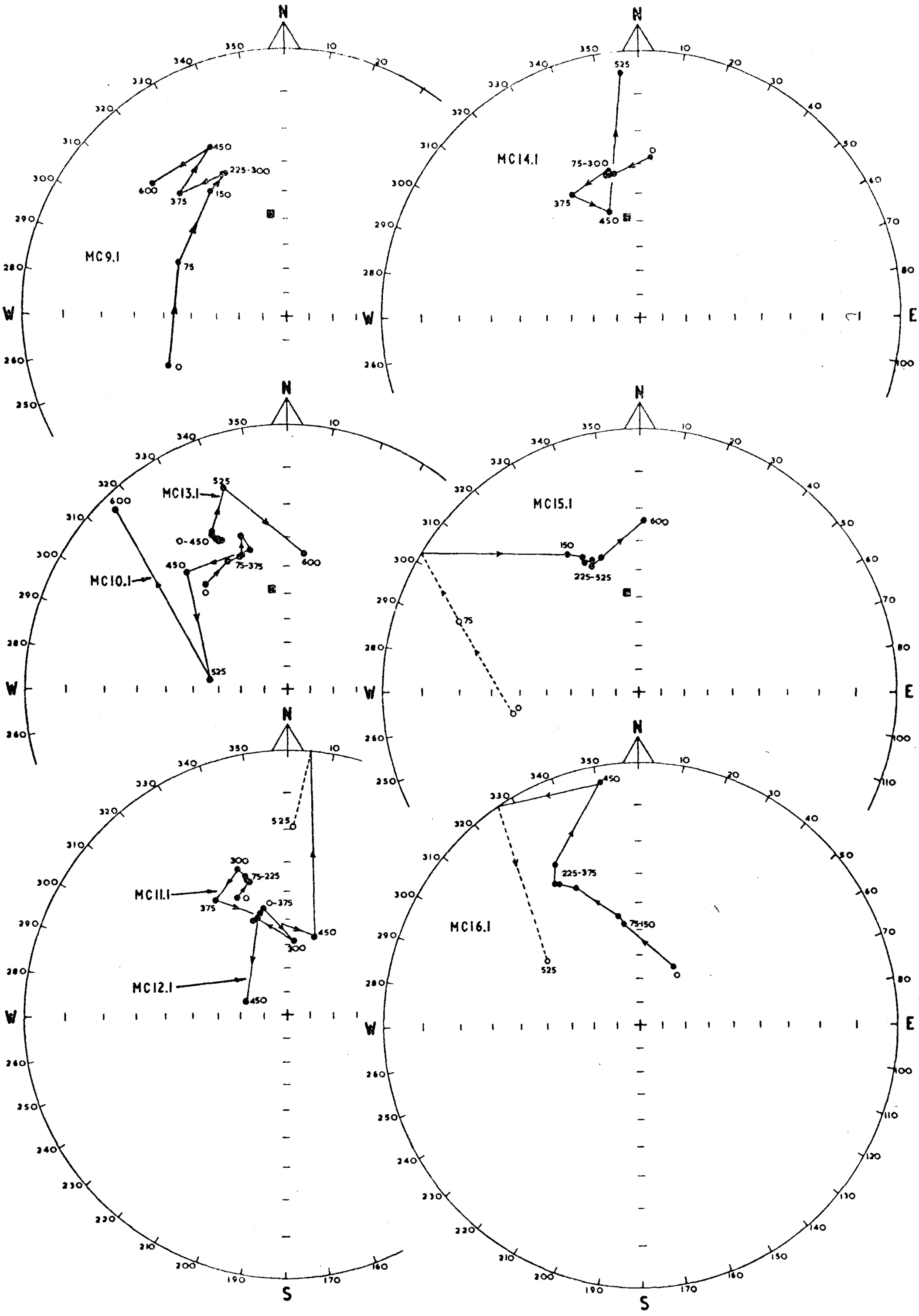
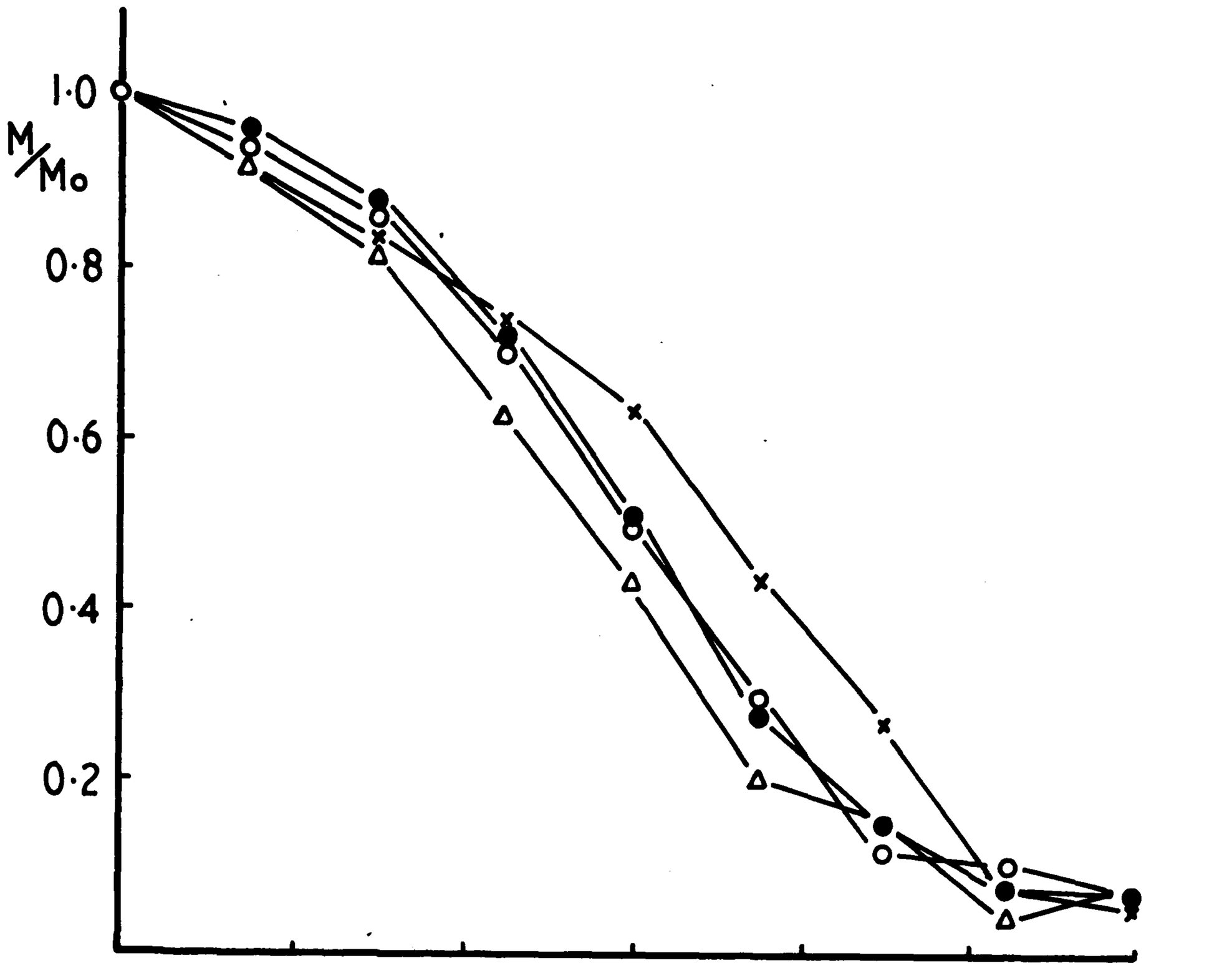
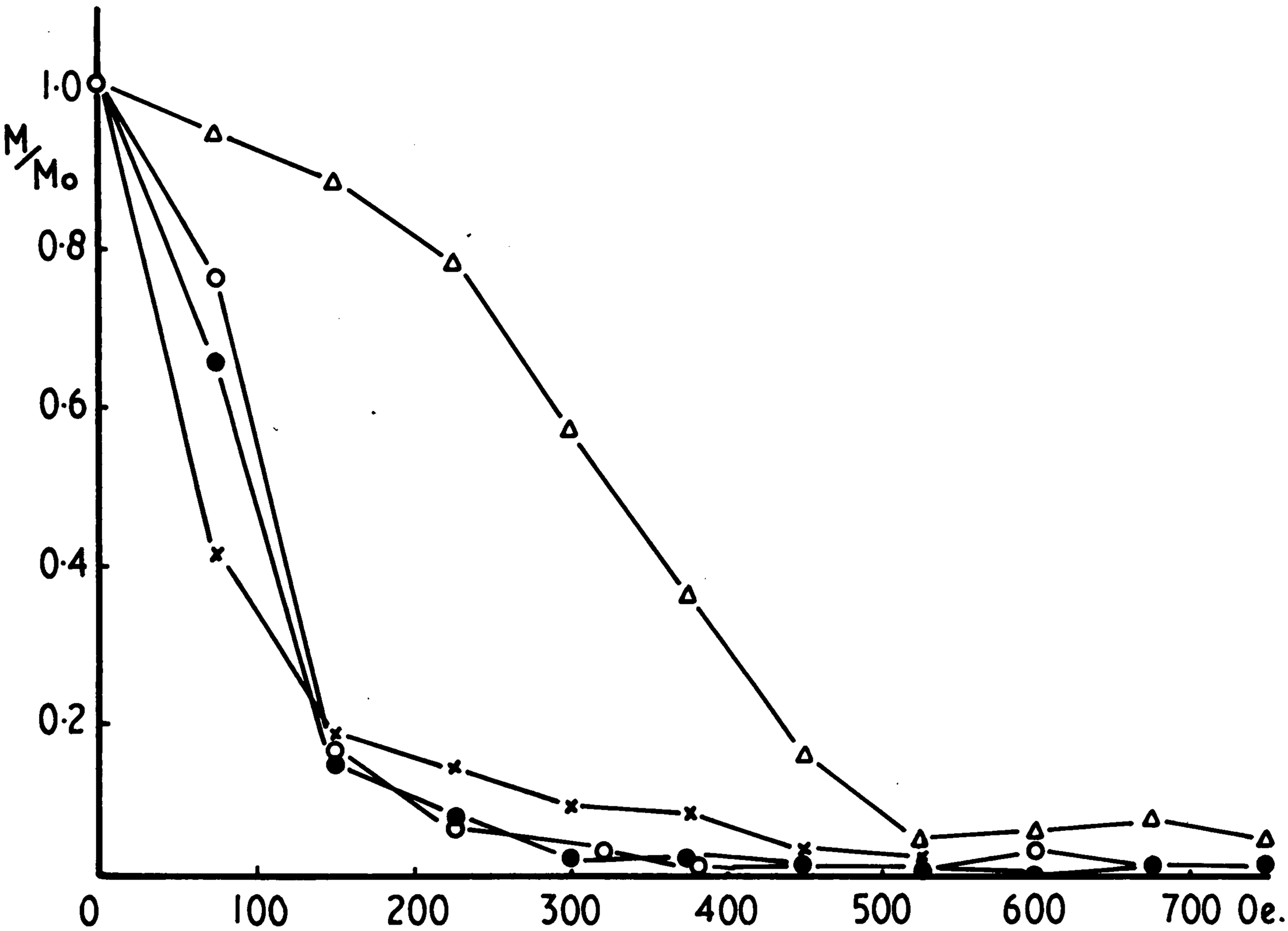


Fig 6.3(b) -Draa Valley Sills. Changes in direction of remanence of pilot samples from sites MC9 to MC16 during progressive demagnetisation.



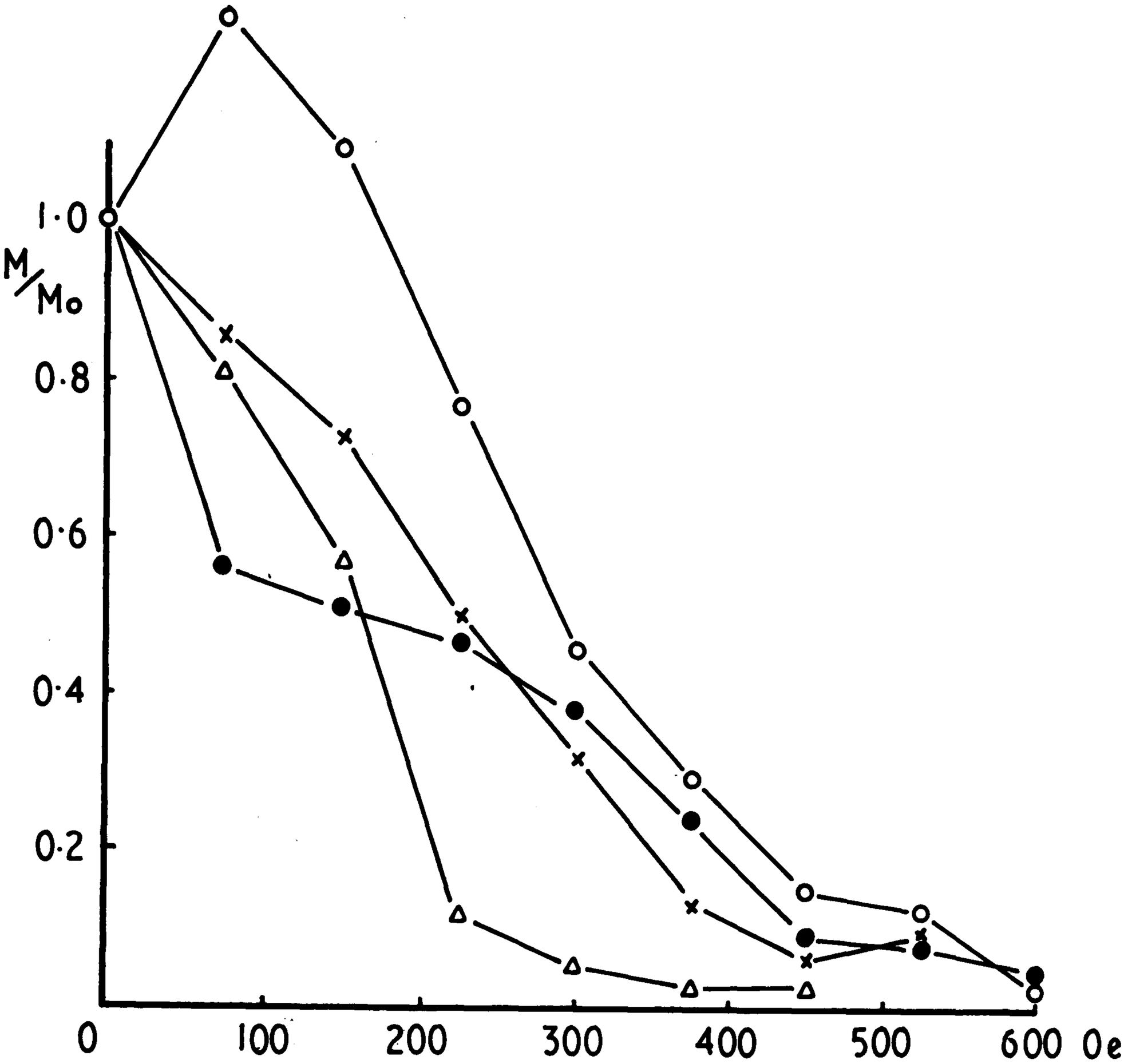
		Mo	
●	MC1.3	0·34	
o	MC2.2	0·35	X 10^{-2} Gauss
x	MC3.2	0·30	
Δ	MC4.2	0·27	

Fig 6.4(a) Draa Valley sills. Changes in normalised intensity of magnetisation of pilot samples from sites MC1 to MC4 during progressive AF demagnetisation.



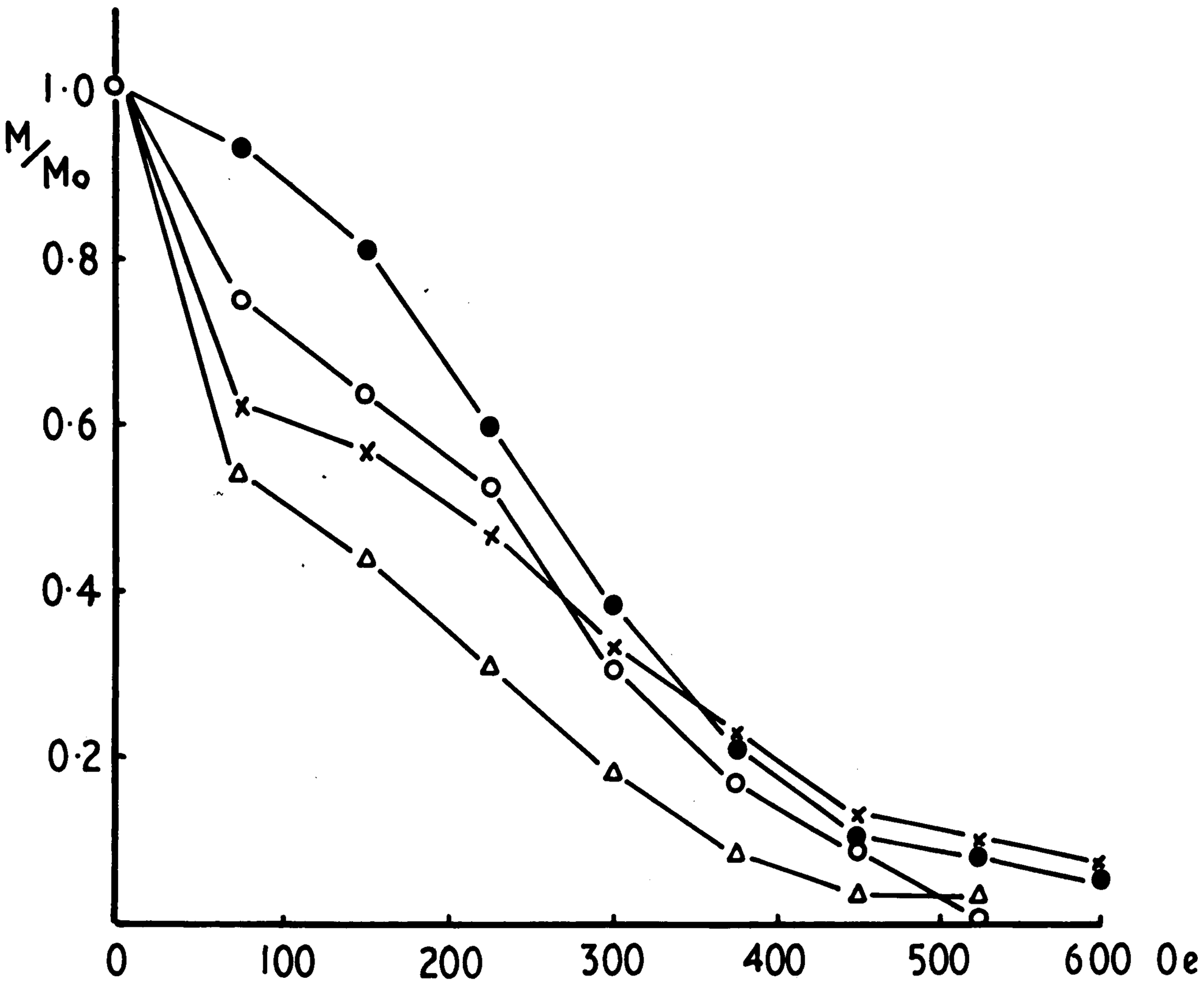
		Mo	
●	MC 5.1	2·60	
o	MC 6.1	5·00	X 10^{-2} Gauss
x	MC 7.1	0·90	
Δ	MC 8.1	0·32	

Fig 6.4(b) Draa Valley sills. Changes in normalised intensity of magnetisation of pilot samples from sites MC5 to MC8 during progressive AF demagnetisation.



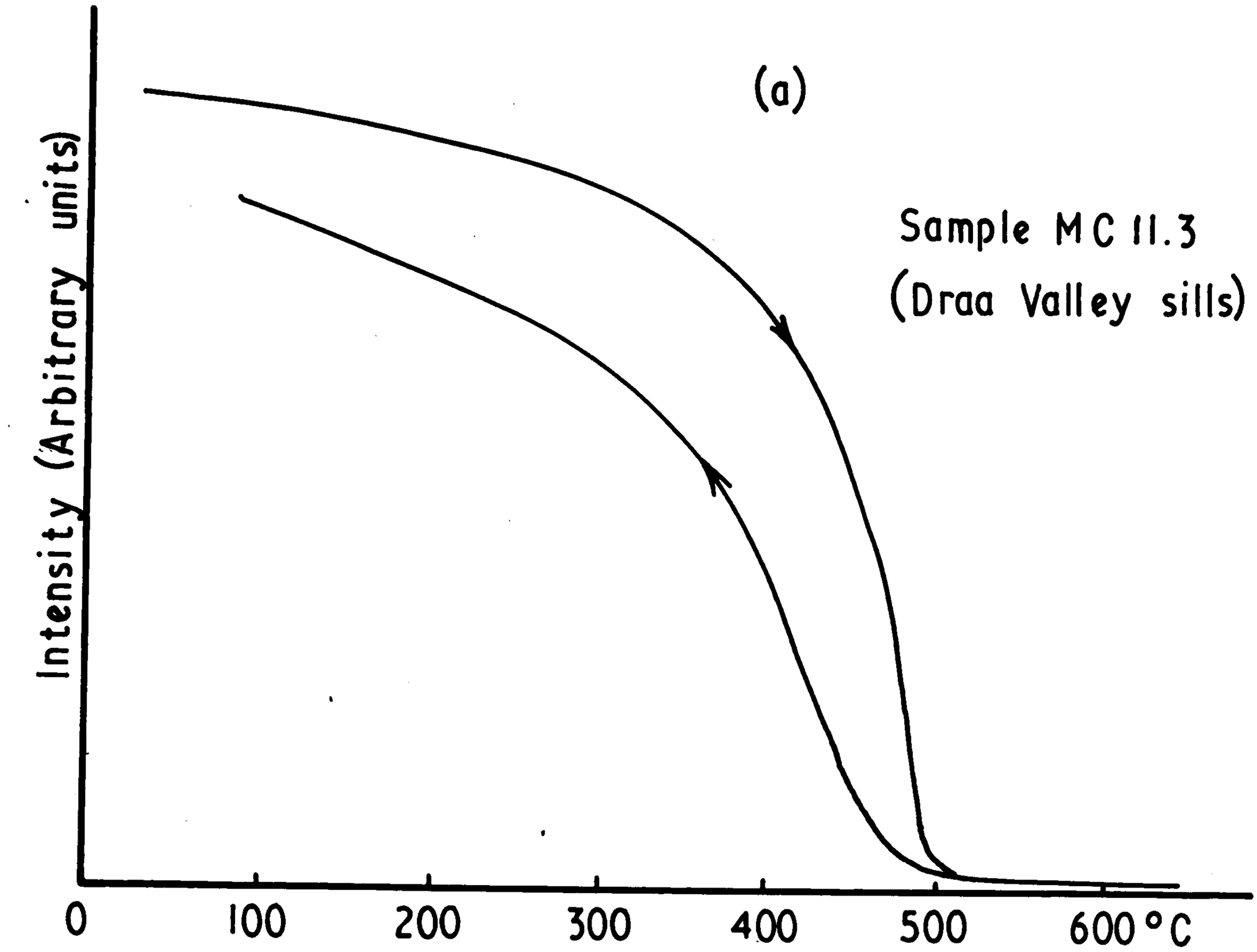
		Mo	
●	MC 9.1	0·58	
o	MC 10.1	0·17	X 10^{-2} Gauss
x	MC 11.1	0·22	
Δ	MC 12.1	0·13	

Fig 6.4(c) Draa Valley sills. Changes in normalised intensity of magnetisation of pilot samples from sites MC9 to MC12 during progressive AF demagnetisation.



		Mo	
●	MC 13.1	0·30	
o	MC 14.1	0·36	X 10^{-2} Gauss
×	MC 15.1	0·60	
Δ	MC 16.1	0·39	

Fig 6.4(d) Draa Valley sills. Changes in normalised intensity of magnetisation of pilot samples from sites MC13 to MC16 during progressive AF demagnetisation.



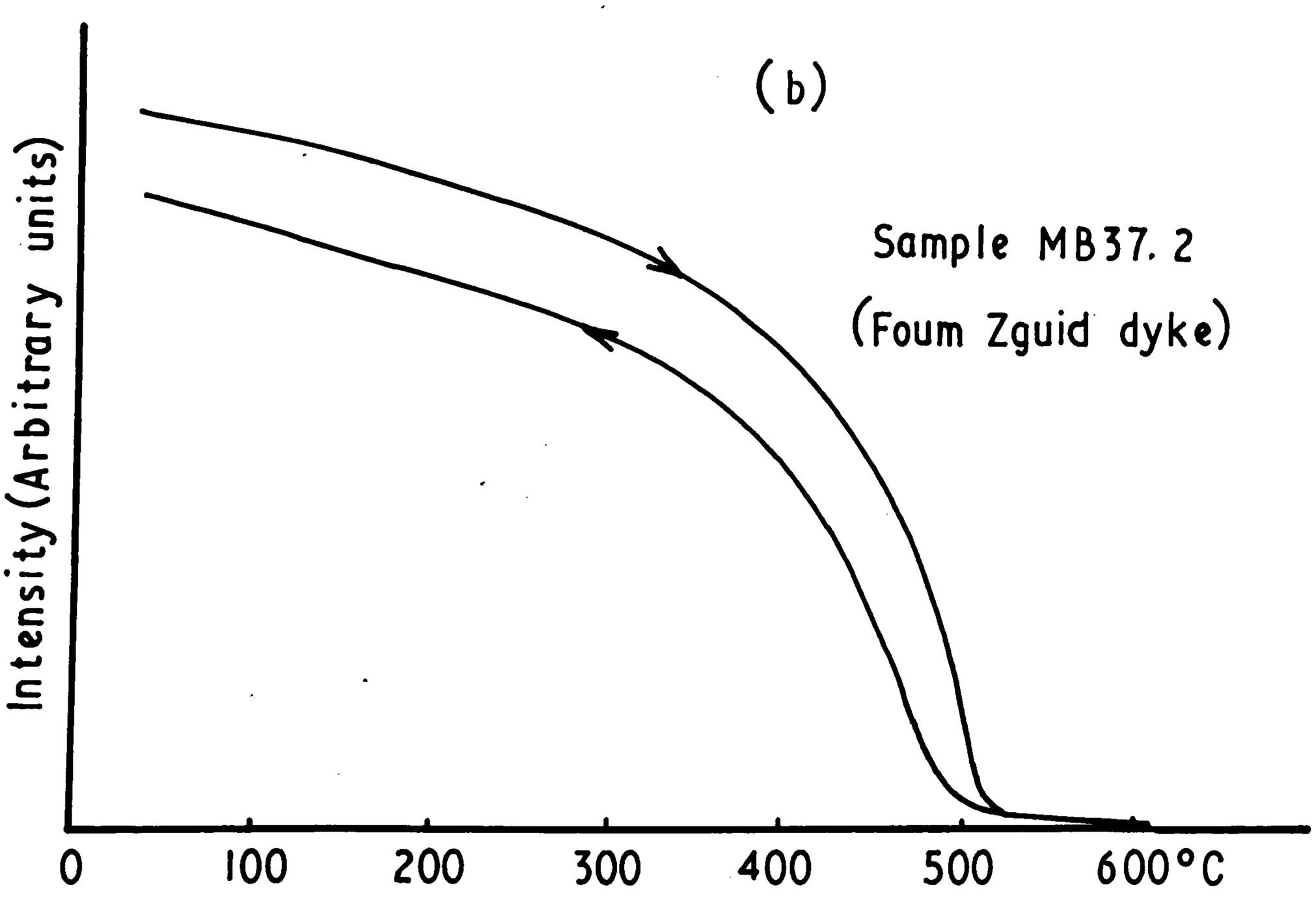


Fig 6.5 Thermomagnetic analyses on sample MC11.3 from the Draa Valley sills and sample MB37.2 from the Foum-Zguid dyke.

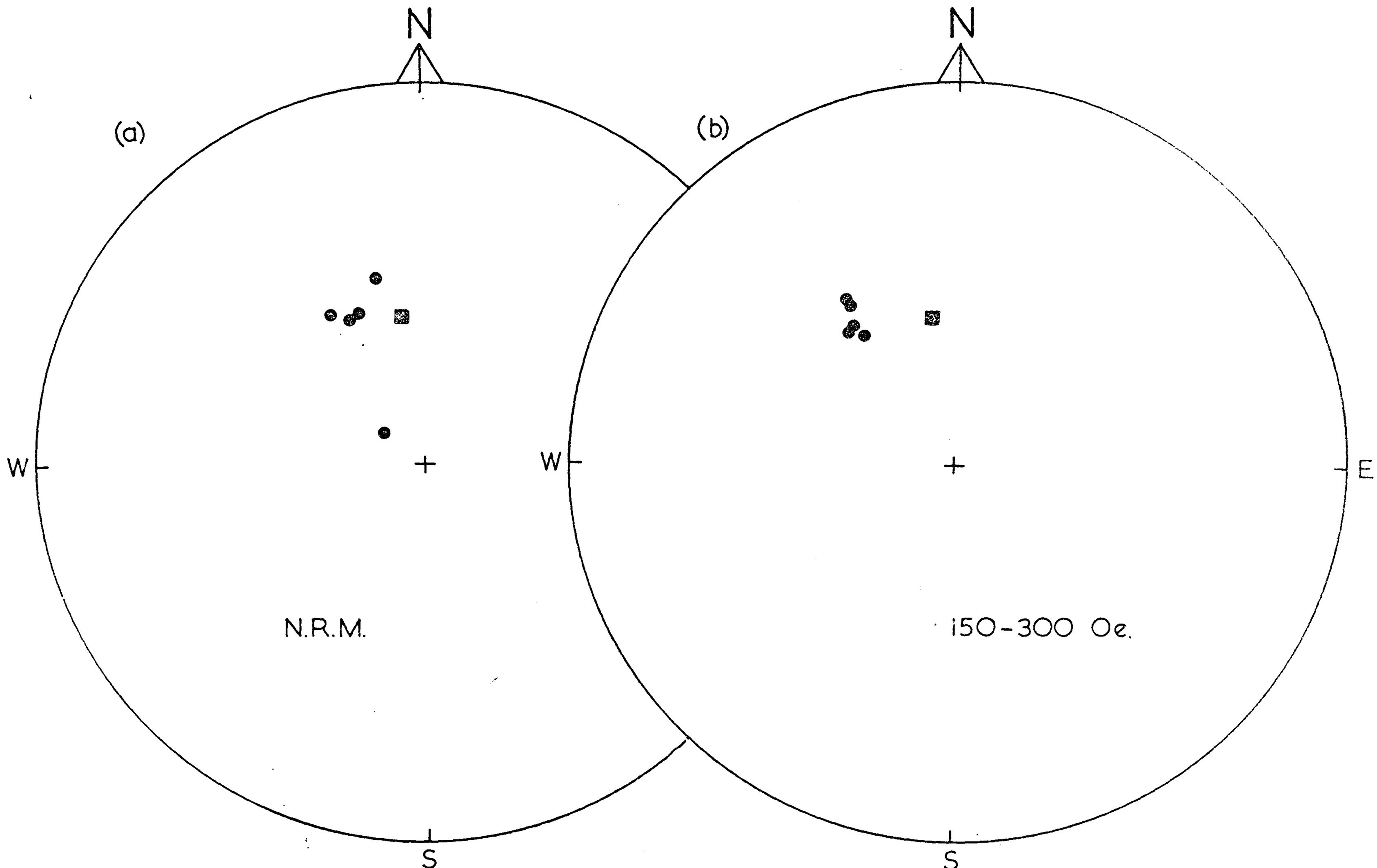


Fig 6.6 Foum-Zguid dyke. Mean site directions of remanence (a) N.R.M. (b) After demagnetisation at 150 to 300 Oe.

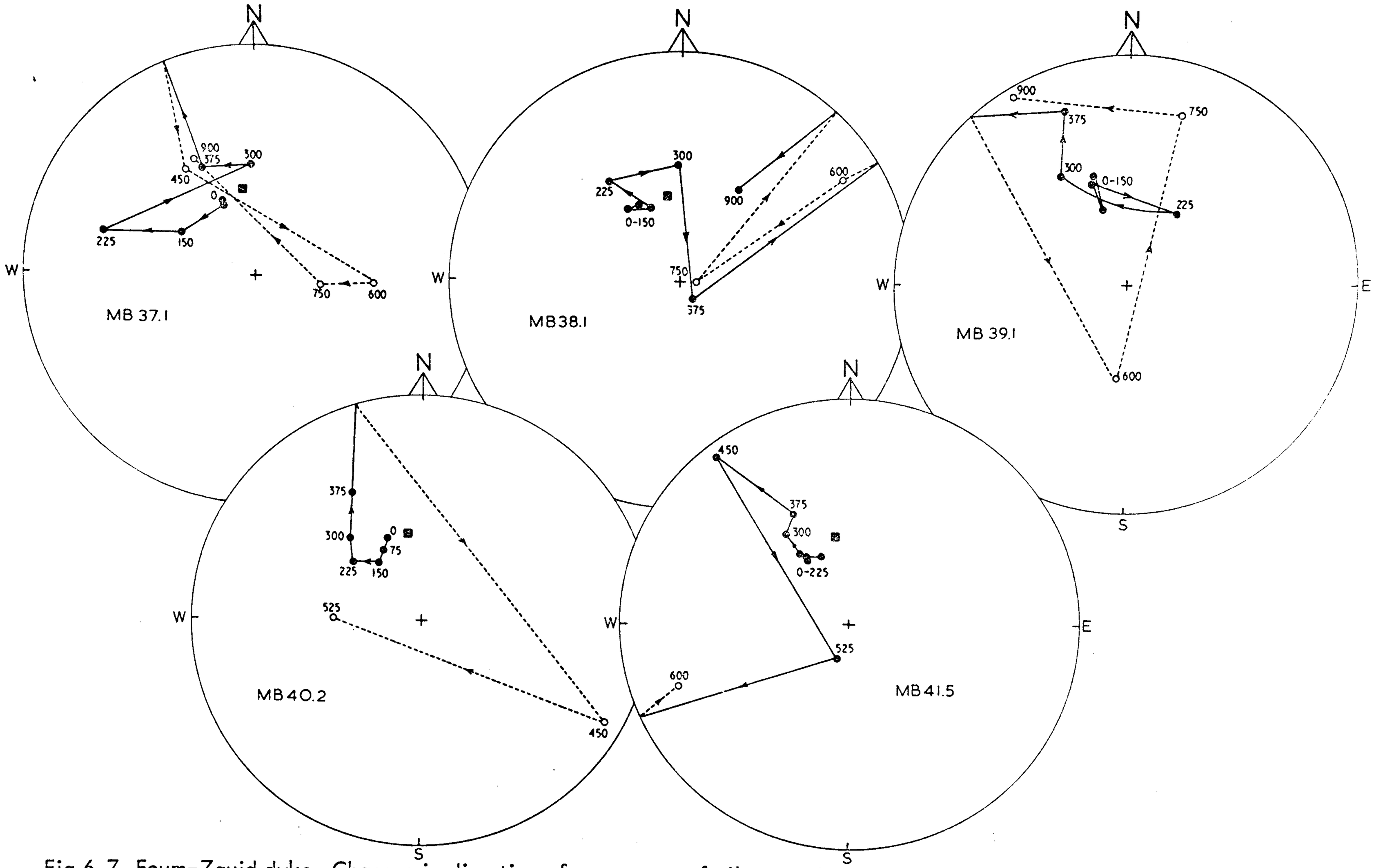
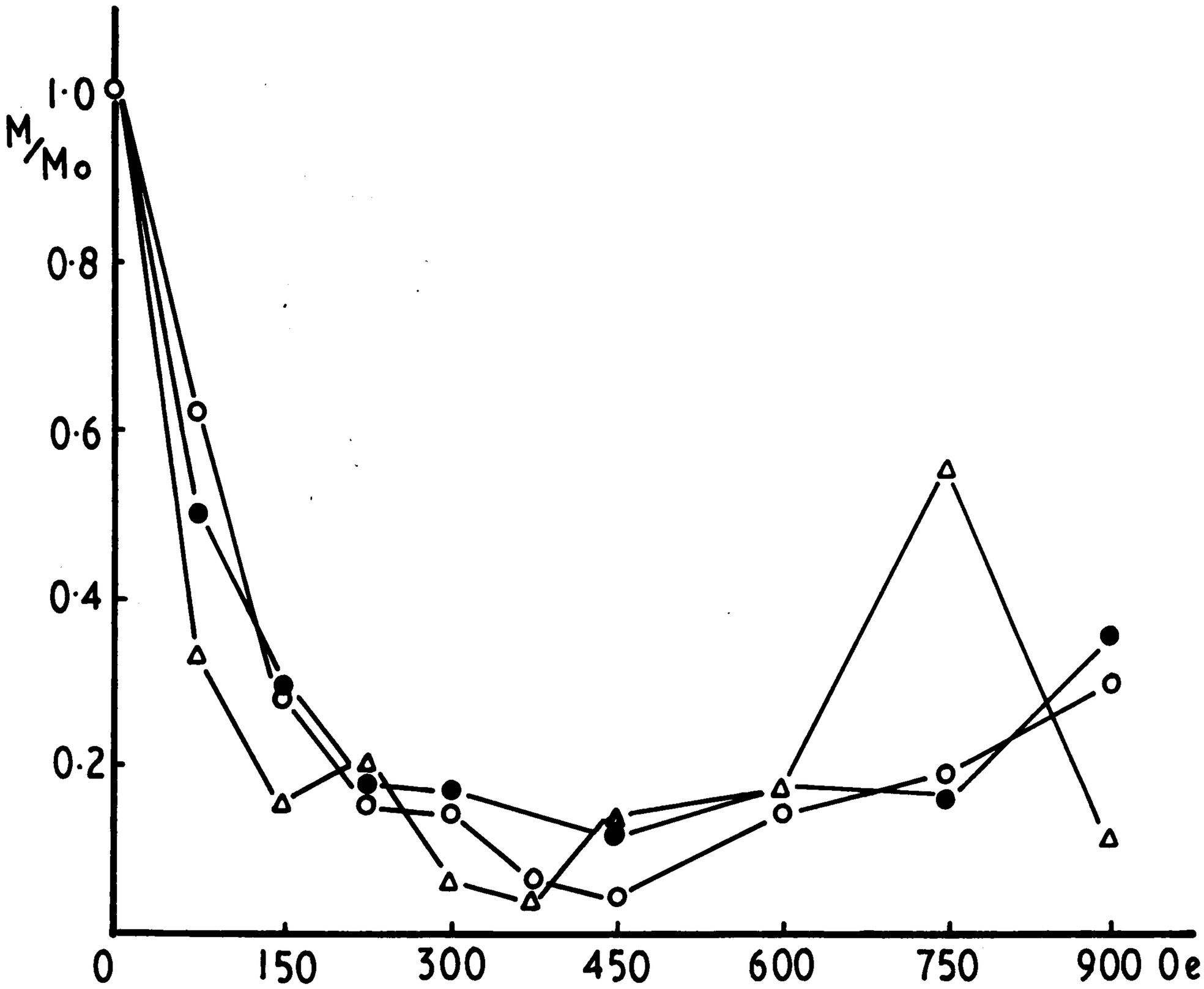


Fig 6.7 Foum-Zguid dyke. Changes in direction of remanence of pilot samples during progressive AF demagnetisation.



		Mo
●	MB 37.1	10·31
o	MB 38.1	9·93 X 10^{-4} Gauss
△	MB 39.1	2·21

Fig 6.8(a) Foum-Zguid dyke. Changes in intensity of magnetisation of pilot samples from sites MB37 to MB39 during progressive AF demagnetisation.

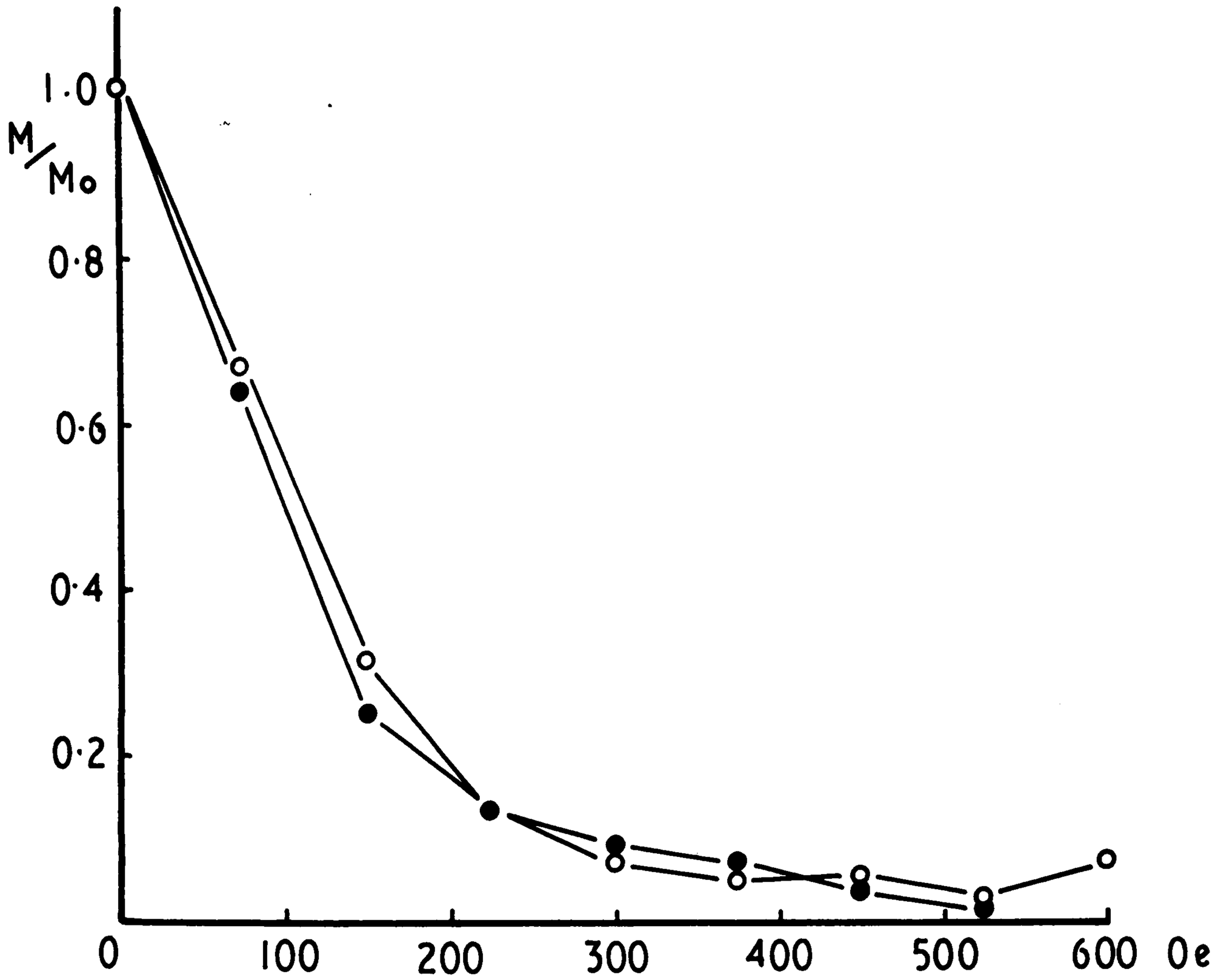


Fig 6.8(b) Foum-Zguid dyke. Changes in intensity of magnetisation of pilot samples from sites MB40 and MB41 during progressive AF demagnetisation.

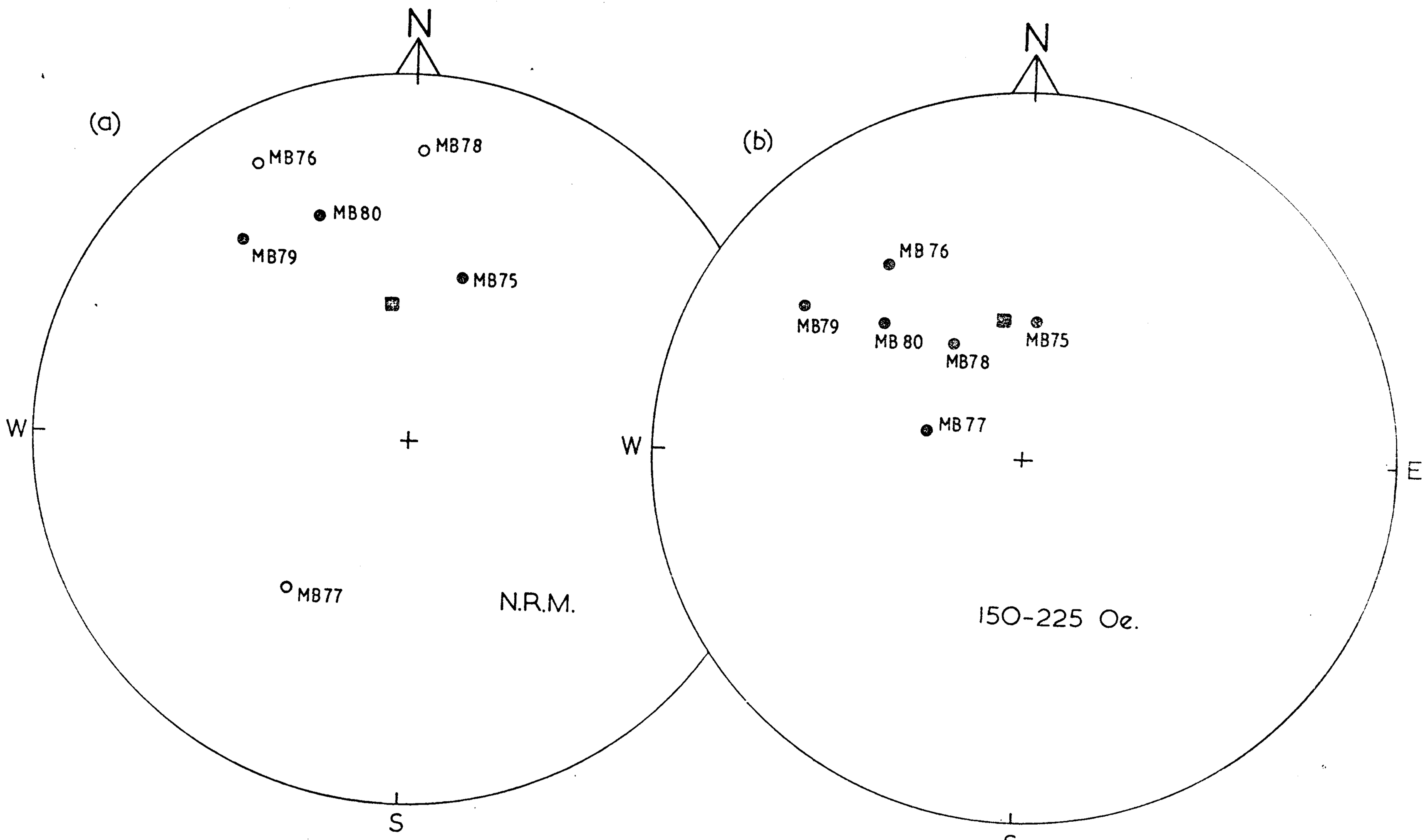


Fig 6.9 Central Atlas Intrusives. Mean site directions. (a) N.R.M. (b) After demagnetisation at 150 to 225 Oe.

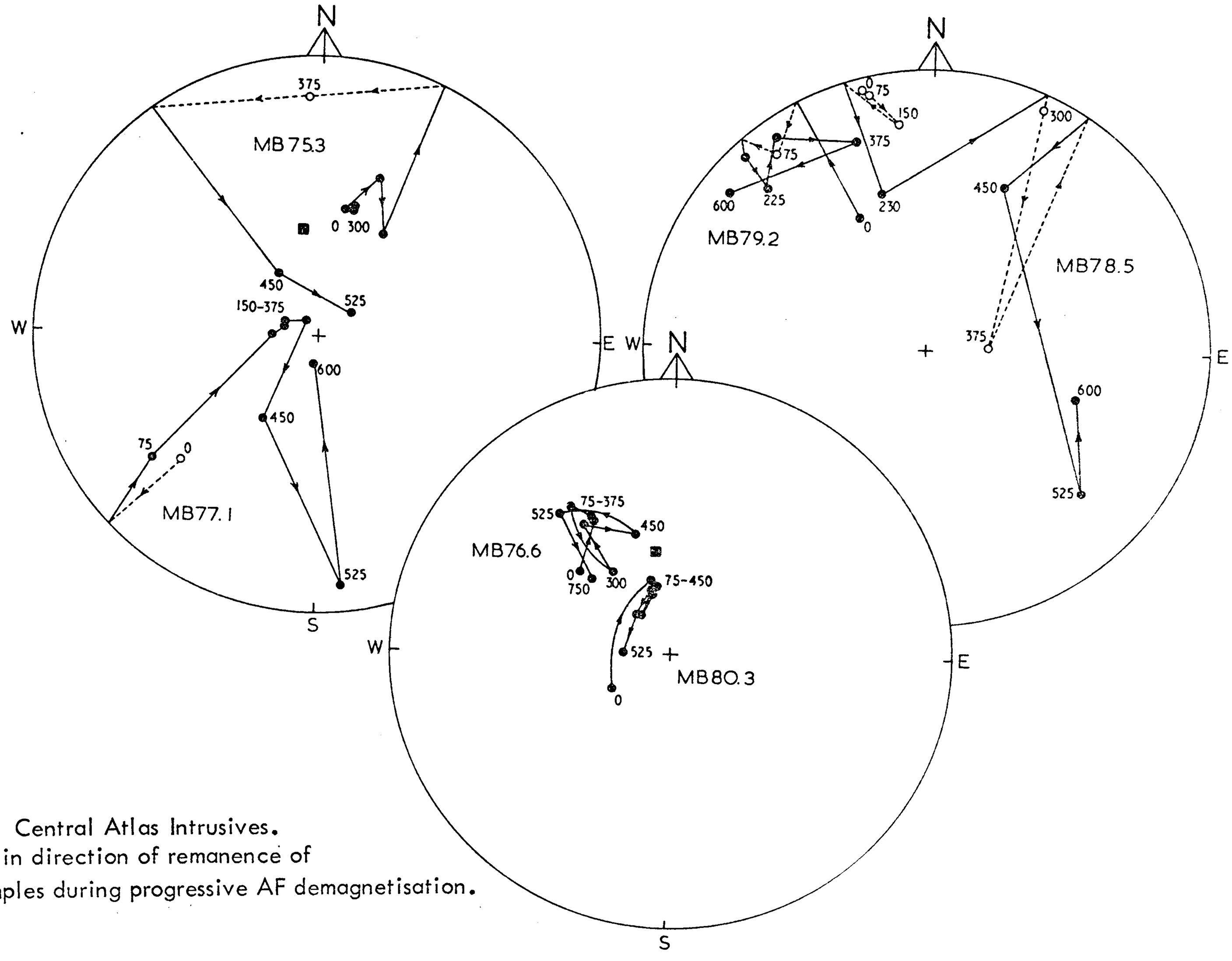
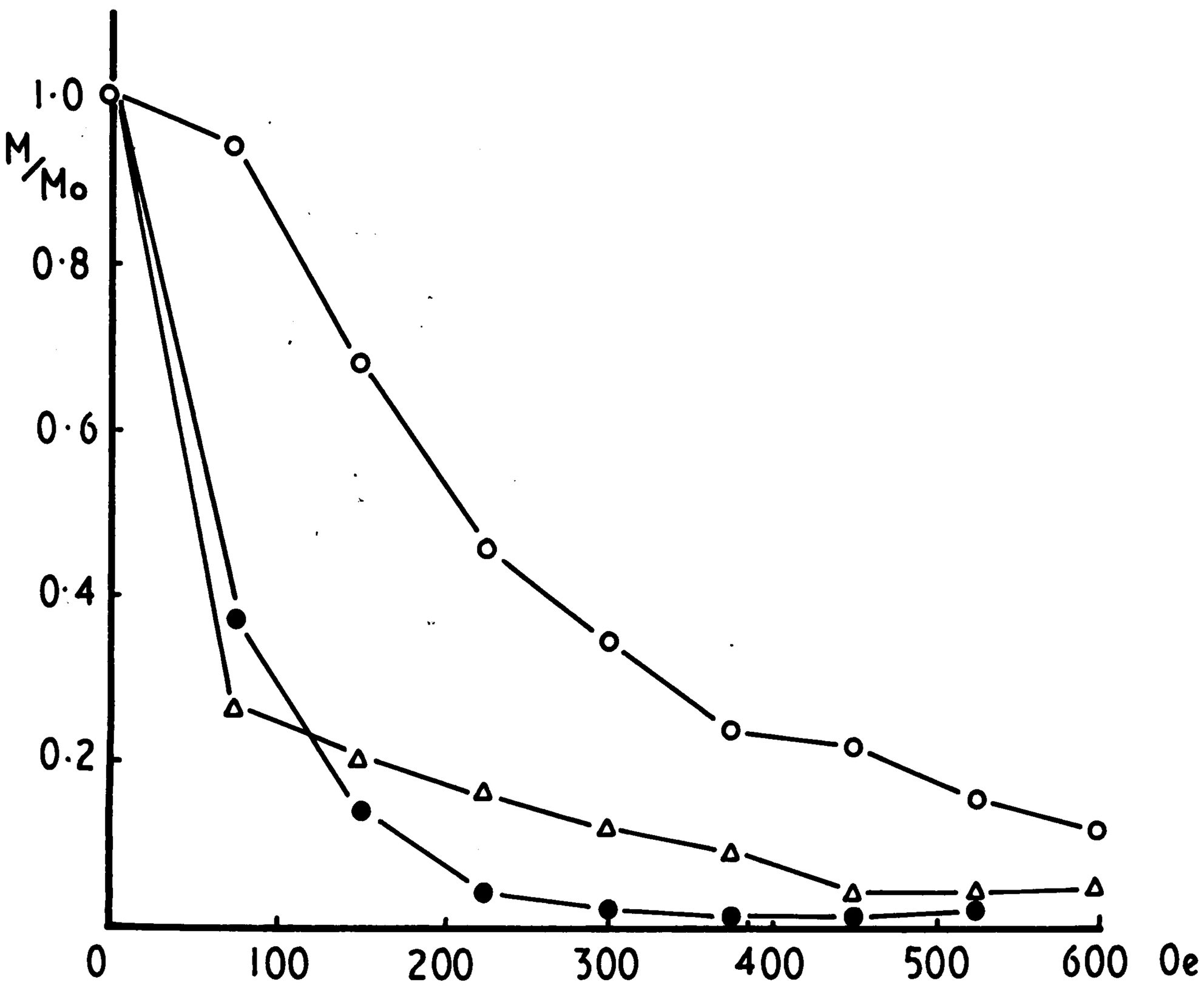


Fig 6.10 Central Atlas Intrusives.
Changes in direction of remanence of
pilot samples during progressive AF demagnetisation.



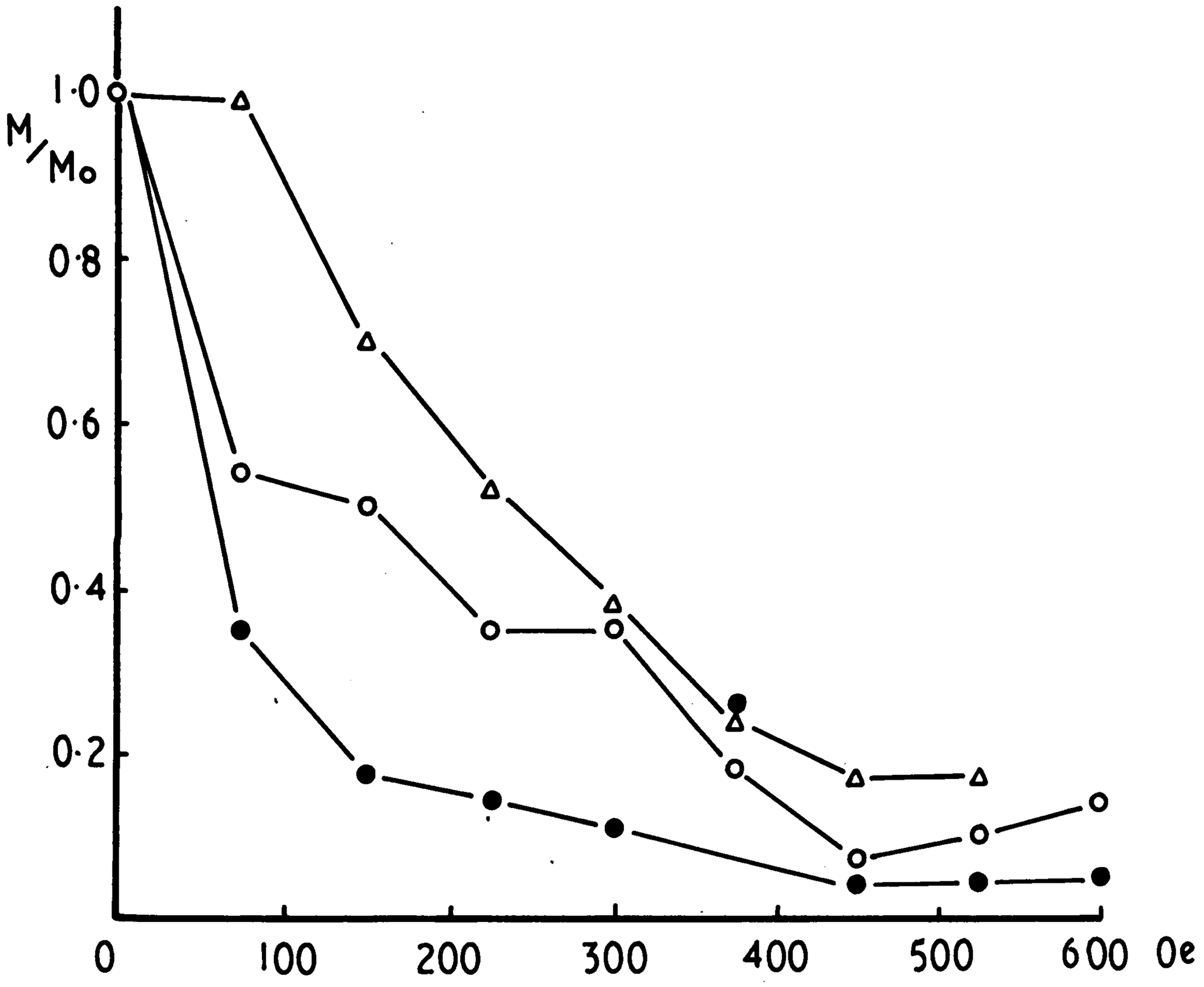
Mo

● MB 75.3 8·00

○ MB 76.6 1·47 X10^{-4} Gauss

△ MB 77.1 80·00

Fig 6.11(a) Central Atlas Intrusives. Changes in normalised intensity of magnetisation of pilot samples from sites MB75 to MB77 during progressive AF demagnetisation.



Mo

●	MB 78.5	2·96	
o	MB 79.2	1·27	X 10^{-4} Gauss
Δ	MB 80.3	0·87	

Fig 6.11(b) Central Atlás Intrusives. Changes in normalised intensity of magnetisation of pilot samples from sites MB78 to MB80 during progressive AF demagnetisation.

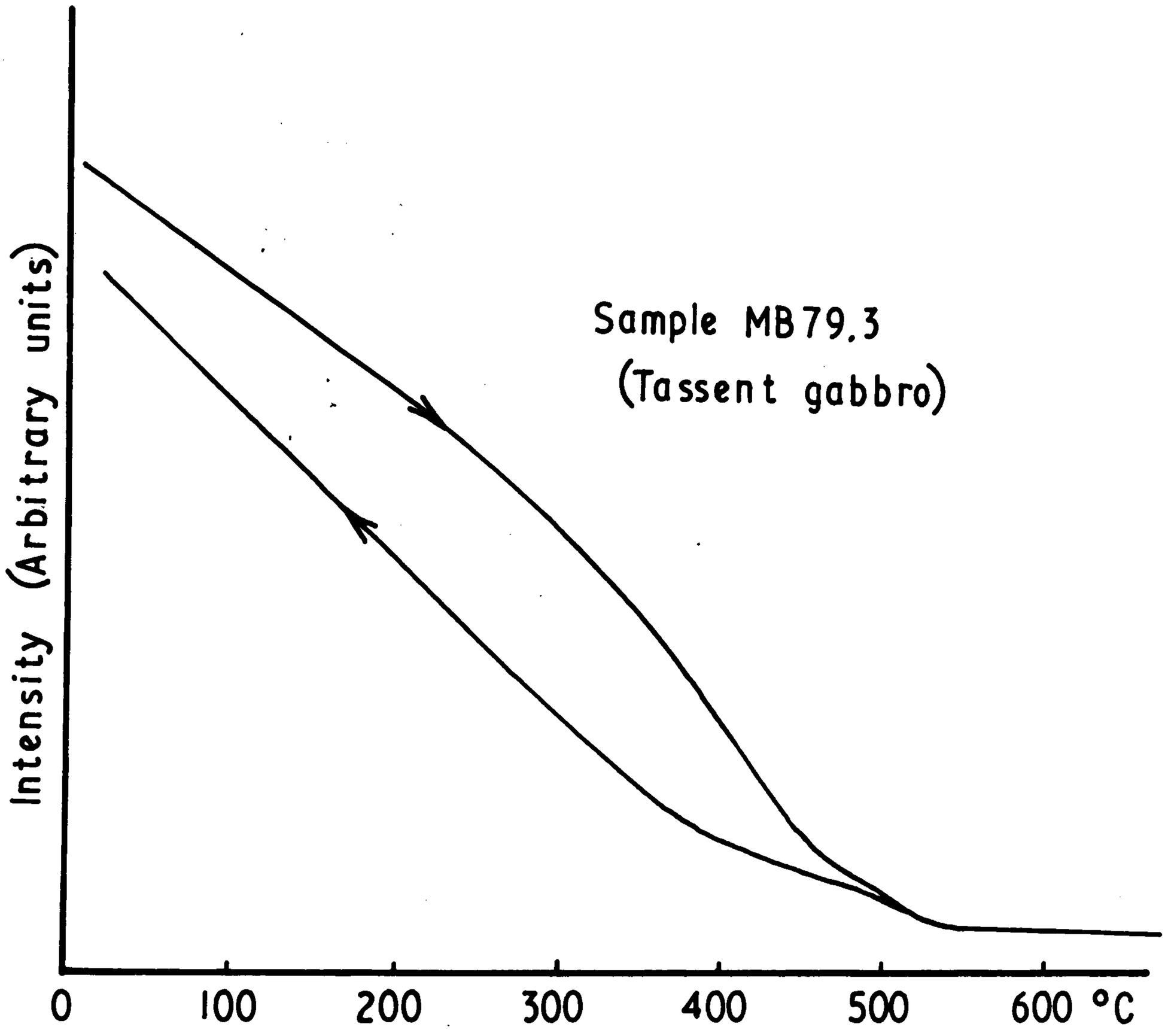


Fig 6.12 Thermomagnetic analyses on sample MB79.3 from the Tassent gabbro.

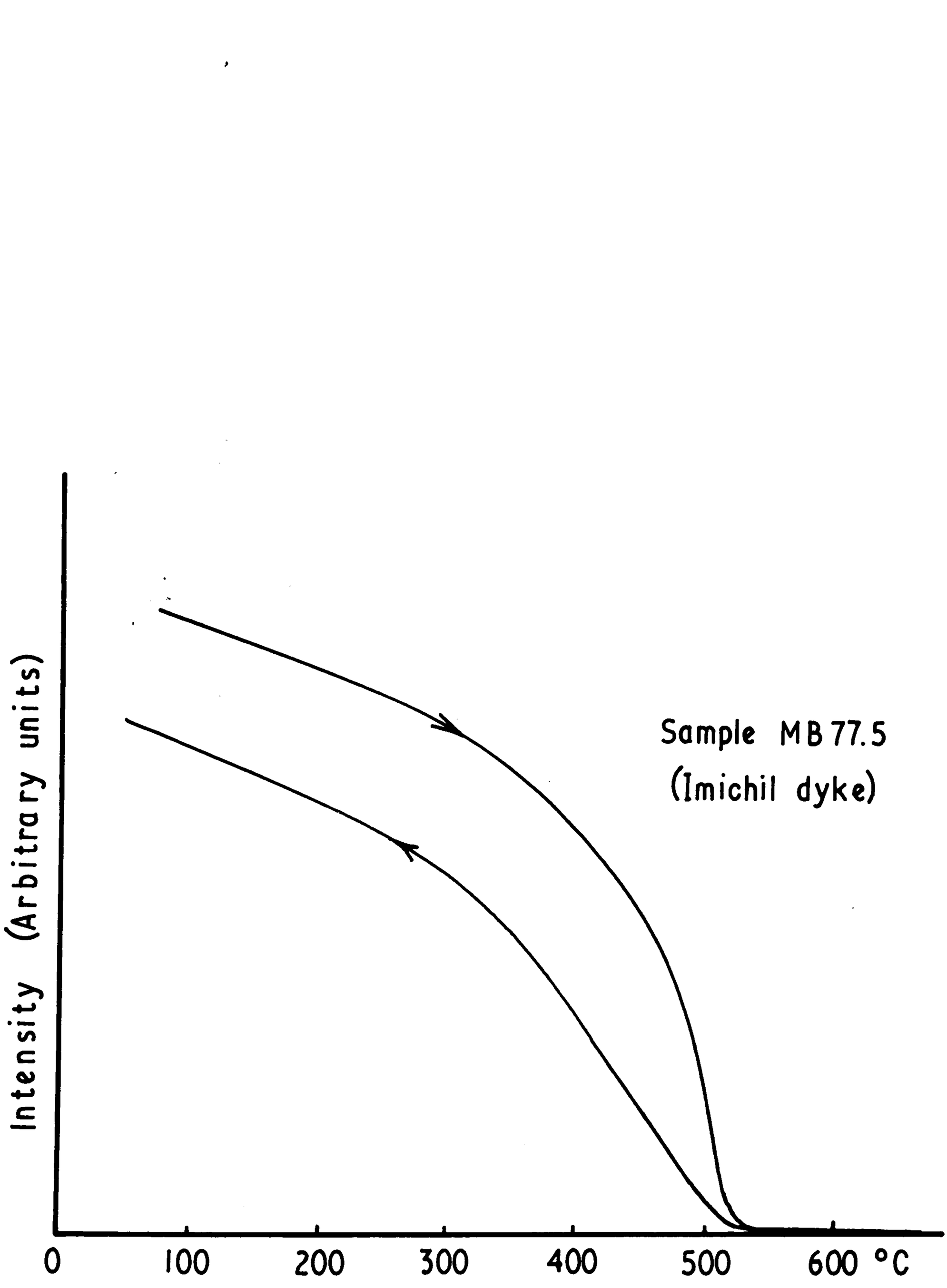


Fig 6.13 Thermomagnetic analysis on sample MB77.5 from the Imichil dyke.

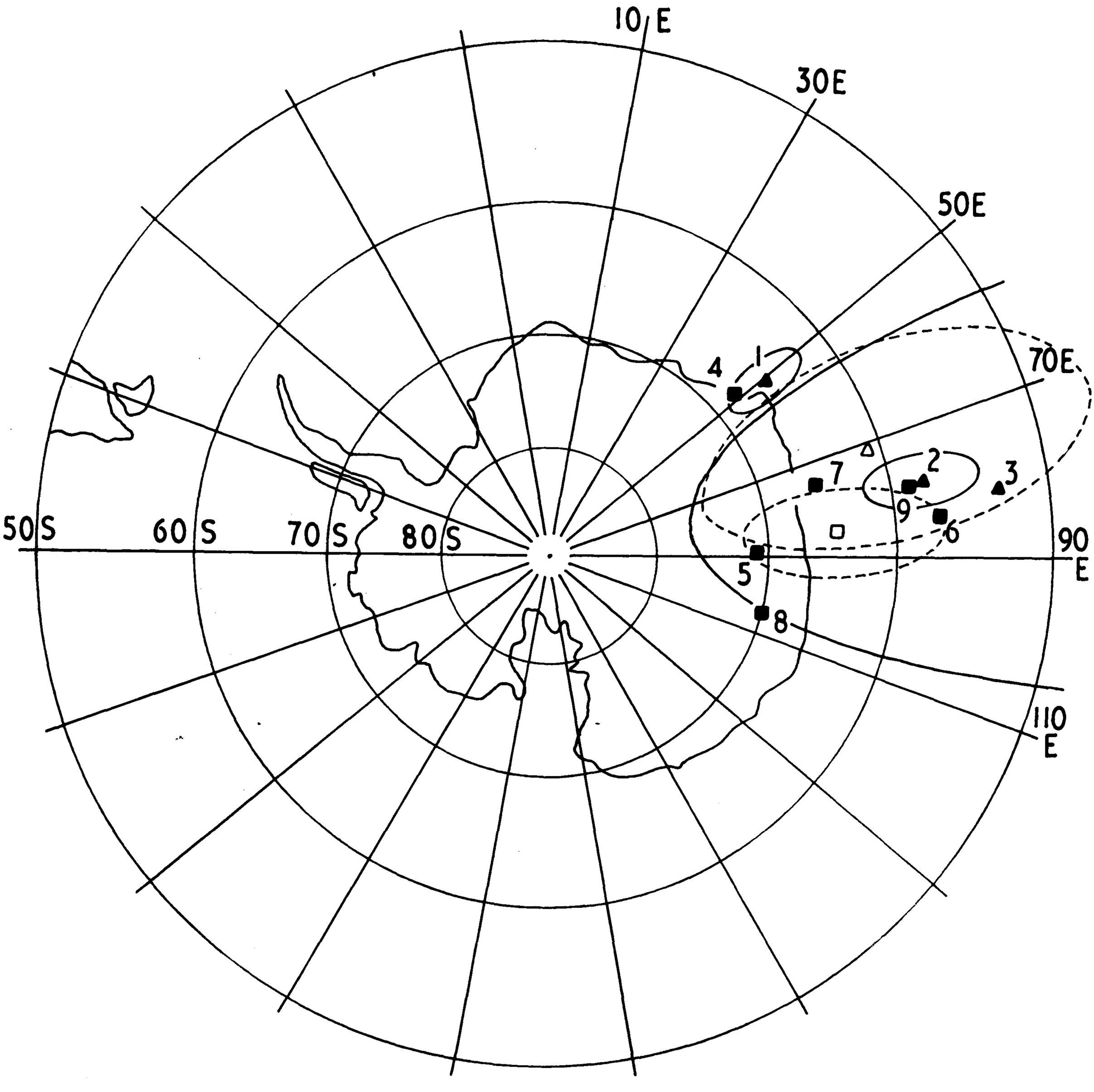


Fig 6.14 African Jurassic pole positions. Solid triangles, poles from Moroccan formations; solid squares, poles from South and East African formations. Open triangle, mean Moroccan Jurassic pole; open square, mean South and East African pole. Ovals of confidence shown around Moroccan poles (solid lines) and S.E. African poles (broken lines).

Table 6.1. Jurassic Field Data

(a) Draa Valley sills

Site locations

Sites	Lat.	Long
MC1-9	29.79N	6.92W
MC10-12	29.77N	6.96W
MC13	29.83N	7.12W
MC14	29.81N	7.16W
MC15	29.91N	7.06W
MC16	29.90N	7.08W

Tilt corrections

Sites	Strike	Dip
MC1-2	209	4
MC3-9	0	0
MC10-11	17	11
MC12-16	0	0

(b) Foum Zguid dyke

Mean location	Lat.	Long
Sites MB37-41	30.11N	6.87W

Tilt correction None

(c) Central Atlas intrusives

Site locations

Site	Lat.	Long
MB75	32.50N	6.02W
MB76	31.21N	5.62W
MB77	32.17N	5.57W
MB78	31.21N	5.62W
MB79-80	32.21N	5.62W

Tilt correction

Sites	Strike	Dip
MB75, 77 & 78	None	
MB76, 79 & 80	118	73

Table 6.2. Draa Valley (Jurassic) sills. Mean site directions, pole positions and statistical parameters

(a) N.R.M.

Site No.	D	I	N	R	k	α_{95}
MC1	343.0	+28.5	6	5.959	122	6
MC2	342.0	+22.0	6	5.990	503	3
MC3	340.0	+27.5	6	5.983	303	4
MC4	352.4	+33.5	6	5.654	15	18
MC5	48.5	+13.0	6	4.339	3	47
MC6	16.5	-10.5	6	5.959	122	6
MC7	13.5	+72.5	6	5.989	453	3
MC8	325.5	+23.0	6	5.663	15	18
MC9	242.0	+36.0	6	5.993	716	2.5
MC10	333.0	+37.0	6	5.877	40	11
MC11	333.0	+38.5	6	5.991	562	3
MC12	346.5	+54.5	6	5.887	44	10
MC13	336.5	+33.5	6	5.979	239	4
MC14	4.0	+25.5	6	5.990	516	3
MC15	277.0	-19.0	6	4.608	4	41
MC16	51.0	+68.5	6	5.800	25	14
Overall mean	343.5	+36.5	16	12.522	4	20

Table 6.2 (contd)

(b) After A.F. demagnetisation

Site No.	Peak Field (Oe)	D	I	N	R	k	α_{95}	Palaeomagnetic South Pole Lat.	Long	A_{95}
MC1	335	345.0	+24.0	5	4.993	596	3	68.0S	35.0E	3
MC2	330	343.5	+19.5	5	4.976	165	6	64.5S	35.0E	6
MC3	300	339.5	+24.0	5	4.994	735	3	64.5S	45.5E	3
MC4	250	340.0	+25.0	4	3.971	105	9	65.5S	45.0E	10
MC5	330	350.5	+25.0	6	5.882	42	10	71.5S	23.5E	8
MC6	330	348.5	+13.0	6	5.844	32	12	64.5S	20.0E	12
MC7	330	333.5	+16.5	6	5.973	188	5	57.5S	48.0E	3
MC8	300	332.0	+24.0	6	5.991	536	3	59.0S	55.5E	2
MC9	300	330.5	+28.0	6	5.944	89	7	58.5S	61.5E	7
MC10	300	338.0	+31.0	6	5.990	489	3	66.0S	54.5E	3
MC11	300	335.0	+31.5	6	5.976	212	5	64.0S	59.5E	5
MC12	225	338.0	+45.5	5	5.979	192	5	70.5S	80.5E	6
MC13	225	334.0	+32.0	6	5.980	256	4	63.0S	61.0E	4
MC14	225	345.5	+32.0	6	5.993	771	2	71.5S	42.5E	2
MC15	300	332.0	+32.0	6	5.954	110	6	61.5S	63.0E	7
MC16	300	333.0	+36.5	6	5.960	125	6	63.5E	68.0E	4
Overall Mean		339.0	+27.5	16	15.785	70	4.5	65.5S	50.5E	3.5

Table 6.3. Draa Valley sills. N.R.M.s

Site No.	Sample No.	D	I	Int($x10^{-2}$ gauss)
MC1	1	358.0	+31.2	0.34
	2	340.9	+26.6	0.35
	3	344.8	+28.4	0.34
	4	341.9	+30.2	0.35
	5	334.6	+24.5	0.33
	6	340.1	+29.3	0.35
MC2	1	337.3	+20.9	0.35
	2	340.8	+20.7	0.35
	3	341.2	+22.8	0.35
	4	340.9	+22.4	0.37
	5	341.8	+22.0	0.27
	6	348.5	+21.5	0.39
MC3	1	340.4	+28.1	0.29
	2	335.7	+26.8	0.30
	3	344.1	+26.7	0.31
	4	344.7	+28.2	0.32
	5	343.1	+26.9	0.30
	6	331.8	+27.0	0.33
MC4	1	348.2	+33.2	0.30
	2	334.4	+27.9	0.27
	3	45.6	+33.6	0.25
	4	341.0	+31.0	0.25
	5	344.2	+31.1	0.26
	6	350.9	+31.0	0.26
MC5	1	44.8	+59.0	2.60
	2	38.9	+45.9	2.90
	3	58.8	+42.8	2.10
	4	2.4	-30.6	0.60
	5	68.0	-15.9	2.00
	6	71.1	-29.7	3.10
MC6	1	18.2	-6.6	5.00
	2	19.5	-7.8	6.00
	3	17.1	-7.9	4.10
	4	25.4	-12.9	4.10
	5	13.3	-13.7	3.50
	6	5.7	-14.6	3.90
MC7	1	8.4	+73.4	0.90
	2	6.5	+70.6	0.90
	3	14.0	+71.9	1.20
	4	12.3	+71.0	1.20
	5	35.8	+71.9	2.10
	6	2.2	+73.6	2.60
MC8	1	334.1	+24.3	0.32
	2	293.6	+40.6	0.26
	3	329.5	+26.6	0.31
	4	327.5	-9.9	0.26
	5	328.0	+26.6	0.31
	6	332.6	+25.4	0.31

Site No.	Sample No.	D	I	Int($\times 10^{-2}$ gauss)
MC9	1	247.3	+37.9	0.58
	2	244.6	+37.2	0.58
	3	243.7	+36.8	0.60
	4	239.3	+34.7	0.67
	5	239.2	+35.8	0.68
	6	239.1	+37.2	0.69
MC10	1	323.7	+34.8	0.17
	2	318.3	+35.6	0.14
	3	325.9	+40.0	0.11
	4	329.6	+33.1	0.13
	5	2.0	+38.8	0.09
	6	338.9	+34.6	0.10
MC11	1	335.4	+37.3	0.22
	2	330.8	+38.2	0.22
	3	331.7	+37.3	0.23
	4	330.0	+39.3	0.21
	5	329.7	+38.6	0.21
	6	340.4	+40.0	0.23
MC12	1	340.9	+47.7	0.13
	2	337.5	+56.1	0.12
	3	22.5	+46.9	0.13
	4	341.9	+59.0	0.12
	5	341.0	+53.9	0.12
	6	332.7	+55.1	0.12
MC13	1	336.3	+25.1	0.30
	2	330.2	+35.6	0.32
	3	334.7	+36.1	0.28
	4	342.0	+34.2	0.30
	5	337.4	+35.4	0.29
	6	336.9	+34.7	0.35
MC14	1	2.5	+27.1	0.36
	2	1.5	+28.7	0.36
	3	2.5	+25.5	0.29
	4	10.5	+23.5	0.41
	5	3.1	+25.5	0.41
	6	4.1	+23.8	0.39
MC15	1	259.6	-37.2	0.60
	2	256.2	-28.2	0.83
	3	234.6	-28.4	2.50
	4	313.1	+16.8	0.28
	5	263.9	-35.4	0.49
	6	330.8	+19.9	0.29
MC16	1	30.4	+60.2	0.39
	2	33.6	+44.9	0.70
	3	63.5	+65.5	0.55
	4	85.6	+71.7	0.82
	5	67.2	+75.5	0.90
	6	82.6	+84.5	1.70

Table 6.4. Draa Valley sills. Pilot sample A.F. demagnetisation results

Field(Oe)	Sample No. MC1.3			MC2.2			MC3.2			MC4.2		
	D	I	Int*	D	I	Int*	D	I	Int*	D	I	Int*
0	344.4	+28.7	35.66	340.7	+21.9	34.29	336.0	+27.4	30.40	334.9	+28.7	27.53
75	343.6	+26.8	34.21	340.0	+19.7	32.08	335.7	+26.5	28.03	333.4	+25.8	25.39
150	343.1	+26.4	31.27	339.3	+19.2	29.52	335.8	+25.9	25.41	334.4	+25.2	22.45
225	344.1	+25.8	25.75	338.2	+20.6	23.98	336.1	+25.7	19.48	332.9	+24.4	17.45
300	34.13	+29.3	18.08	338.4	+21.7	17.03	337.4	+22.9	13.48	331.5	+28.0	12.02
375	346.2	+23.6	10.16	337.7	+26.1	10.25	330.4	+31.8	8.30	335.3	+22.2	5.42
450	358.7	+17.3	5.44	343.6	+6.4	4.01	349.7	+7.3	2.86	341.6	+40.3	4.24
525	348.7	-0.1	2.93	314.8	-32.6	3.39	356.8	+5.5	1.97	317.5	+55.0	1.16
600	297.8	-38.9	2.41									

	Sample No. MC5.1			MC6.1			MC7.1			MC8.1		
	D	I	Int*	D	I	Int*	D	I	Int*	D	I	Int*
0	53.7	+60.3	26.00	18.3	-6.5	50.00	7.1	+73.4	93.80	344.4	+24.7	31.30
75	41.1	+65.5	17.00	22.2	-1.7	38.00	359.5	+56.5	38.65	335.4	+25.1	29.35
150	8.6	+56.8	3.70	14.6	+3.7	8.00	334.3	+32.4	16.98	335.6	+25.6	27.70
225	355.6	+43.8	1.90	2.2	+9.7	2.90	330.7	+24.9	13.06	334.8	+25.3	24.50
300	336.8	+10.0	0.60	320.6	+16.1	1.40	329.7	+16.9	8.54	335.5	+22.4	17.95
375	7.0	+35.5	0.50	349.1	+10.2	0.70	318.1	+15.8	7.24	338.9	+20.5	11.23
450	338.1	+39.6	0.33	353.7	-10.8	0.33	343.1	+5.6	2.96	334.2	+6.1	4.77
525	343.6	+14.2	0.15	346.0	-0.5	0.12	326.6	+35.4	1.91	306.9	+36.9	1.32
600	162.0	+54.7	0.11	41.9	-5.9	1.50	14.6	-39.0	1.06	316.7	-37.3	1.71
675	-	-	-	85.8	-49.6	0.43	279.0	+62.5	0.81	221.4	-78.7	2.22
750	351.3	-13.4	0.14	141.6	+8.0	0.26	34.2	+84.3	1.39	241.2	+28.3	1.15

Table 6.4 (contd)

Field (Oe)	Sample No. MC9.1 D	I	Int*	MC10.1 D	I	Int*	MC11.1 D	I	Int*	MC12.1 D	I	Int*
0	247.2	+38.0	58.20	322.0	+35.9	16.65	337.2	+37.6	21.43	331.9	+40.3	12.33
75	296.4	+41.0	32.55	335.3	+32.9	21.18	343.7	+33.6	18.52	336.8	+39.3	9.99
150	329.5	+31.9	29.67	340.3	+33.2	18.25	343.0	+32.6	15.56	339.6	+38.3	7.00
225	336.5	+28.9	27.47	341.4	+32.9	12.90	343.2	+31.7	10.72	349.4	+53.9	1.37
300	337.0	+28.6	22.35	342.9	+27.3	7.62	341.1	+28.8	6.79	334.7	+40.3	0.58
375	319.3	+27.5	14.10	345.4	+32.3	4.86	328.1	+34.6	2.69	287.9	+59.8	0.20
450	335.6	+19.6	5.10	319.2	+29.0	2.50	19.7	+55.1	1.39			
525	99.0	-0.6	4.50	276.5	+56.8	2.07	1.3	-18.5	2.01			
600	315.1	+18.8	2.44	316.3	+3.2	0.26						

	Sample No. MC13.1 D	I	Int*	MC14.1 D	I	Int*	MC15.1 D	I	Int*	MC16.1 D	I	Int*
0	336.0	+25.8	29.74	4.6	+27.2	36.00	260.2	-37.0	60.00	31.3	+60.7	39.00
75	335.0	+24.6	27.61	350.5	+32.0	27.00	291.0	-16.2	37.00	348.6	+44.3	21.00
150	334.5	+24.5	24.03	348.0	+32.1	23.00	332.1	+27.7	34.00	334.8	+30.1	17.00
225	335.0	+24.8	17.99	346.9	+32.3	19.00	336.6	+30.6	28.00	329.7	+26.2	12.00
300	335.4	+23.5	11.32	347.6	+31.1	11.00	337.4	+32.8	20.00	328.7	+25.6	7.00
375	334.5	+21.8	6.31	331.5	+34.3	6.00	339.6	+33.2	13.00	332.3	+20.0	3.00
450	333.6	+22.9	3.11	343.8	+45.3	3.00	339.4	+34.7	8.00	351.2	+3.4	1.00
525	342.2	+12.3	2.33	355.8	+4.2	1.00	343.8	+33.0	6.00	303.6	-43.1	1.00
600	6.8	+33.9	1.34									

* x 10^{-4} gauss

+ x 10^{-3} gauss

Table 6.5. Draa Valley sills. Bulk A.F. demagnetisation results

Demag field(Oe)	Site No.	Sample No.	D	I	Int*
335	MC1	1	341.0	+22.4	14.15
		3	346.2	+23.6	9.75
		4	347.9	+26.9	12.81
		5	342.7	+23.7	12.21
		6	347.4	+22.4	10.63
330	MC2	2	338.4	+21.7	17.17
		3	338.4	+23.6	16.27
		4	343.3	+18.0	15.82
		5	343.5	+17.3	12.03
		6	352.4	+15.8	12.73
300	MC3	2	337.5	+22.9	13.48
		3	341.2	+22.3	11.52
		4	342.1	+24.8	11.83
		5	340.6	+26.3	12.68
		6	335.5	+24.4	14.86
250	MC4	2	332.9	+24.3	17.45
		4	337.3	+26.0	11.26
		5	338.0	+25.6	14.68
		6	352.7	+23.7	13.09
330	MC5	1	336.9	+10.0	5.67
		2	343.7	+37.6	11.57
		3	353.7	+31.4	7.55
		4	358.1	+28.3	6.60
		5	352.7	+23.8	6.46
		6	357.8	+19.0	5.63
330	MC6	1	320.7	+16.1	13.57
		2	355.7	+7.0	10.78
		3	350.1	+15.4	11.55
		4	2.1	+15.8	12.20
		5	351.7	+10.8	10.88
		6	350.6	+9.6	12.76
330	MC7	1	329.7	+16.9	8.61
		2	331.1	+14.3	8.21
		3	334.9	+13.3	5.82
		4	335.4	+10.1	6.07
		5	338.0	+24.1	5.79
		6	332.3	+20.7	6.79
300	MC8	1	335.5	+22.4	18.67
		2	333.6	+23.5	18.03
		3	332.5	+29.1	18.55
		4	332.6	+23.8	18.11
		5	327.5	+23.3	17.58
		6	331.4	+22.6	17.02

* $x10^{-4}$ gauss

Table 6.5 (contd)

Treatment	Site No.	Sample No.	D	I	Int*
300	MC9	1	337.1	+28.6	22.35
		2	332.5	+25.0	18.95
		3	331.4	+24.5	16.20
		4	314.9	+38.6	12.01
		5	333.7	+24.6	16.35
		6	330.1	+24.8	13.63
300	MC10	1	342.9	+27.3	7.62
		2	338.4	+31.1	6.73
		3	335.4	+33.5	6.78
		4	333.2	+30.7	6.90
		5	338.8	+32.7	6.35
		6	339.8	+29.9	7.38
300	MC11	1	341.1	+28.8	7.20
		2	330.1	+35.8	5.64
		3	334.4	+28.3	6.02
		4	338.2	+31.2	5.51
		5	327.4	+31.8	4.57
		6	340.6	+33.2	5.57
225	MC12	1	339.6	+38.3	7.42
		2	346.3	+50.0	2.99
		3	17.7	+45.5	3.03
		4	337.1	+48.7	2.85
		5	336.2	+45.2	3.22
		6	331.7	+45.0	2.76
225	MC13	1	335.0	+24.9	18.14
		2	325.9	+33.9	17.59
		3	332.7	+34.1	15.21
		4	337.1	+33.0	16.64
		5	338.2	+32.6	15.95
		6	335.0	+32.5	19.92
225	MC14	1	346.9	+32.3	19.01
		2	342.6	+34.1	19.27
		3	343.2	+32.8	9.09
		4	349.5	+28.3	17.83
		5	345.3	+31.9	17.24
		6	345.2	+31.0	15.22
300	MC15	1	337.4	+32.8	19.55
		2	319.9	+25.1	18.49
		3	325.2	+32.7	15.34
		4	334.5	+33.5	20.66
		5	334.4	+33.1	18.15
		6	342.1	+32.8	19.87
300	MC16	1	328.7	+25.5	6.76
		2	334.8	+35.7	8.33
		3	332.6	+34.3	7.18
		4	336.0	+36.3	7.48
		5	333.9	+38.7	7.76
		6	331.1	+46.9	9.54

Table 6.6. Foum Zguid dyke. Mean site directions, pole positions and statistical parameters

(a) N.R.M.

Site No.	D	I	N	R	k	α_{95}
MB37	334.0	+44.0	5	4.989	357	4
MB38	337.5	+43.5	5	4.991	460	4
MB39	329.0	+40.5	5	4.974	157	6
MB40	308.5	+74.5	6	4.413	3	45
MB41	346.5	+36.0	6	4.913	5	35
Overall Mean	334.5	+48.0	5	4.826	23	16

(b) After A.F. demagnetisation

Site No.	Peak field(Oe)	D	I	N	R	k	α_{95}	Palaeomagnetic south pole Lat.	Long	A_{95}
MB37	250	327.0	+35.0	5	4.952	84	8	58.5S	71.0E	7
MB38	225	327.0	+36.5	5	4.992	502	3	58.5S	72.5E	3
MB39	150	321.5	+42.0	6	5.920	63	8	55.0S	83.5E	8
MB40	300	325.0	+45.0	3	2.983	118	11	59.5S	85.5E	10
MB41	300	324.0	+41.5	4	3.945	54	12	58.0S	81.0E	14
Overall Mean		325.0	+40.0	5	4.987	316	4	58.0S	79.0E	14

Table 6.7. Foum Zguid dyke N.R.M.s

Site No.	Sample No.	D	I	Int($x10^{-2}$ gauss)
MB37	1	331.4	+46.2	1.00
	2	327.8	+40.2	1.10
	3	336.5	+44.3	1.80
	4	333.9	+42.8	1.10
	5	340.5	+46.0	1.40
MB38	1	338.6	+43.2	1.10
	2	331.3	+41.1	1.00
	3	344.2	+43.3	1.10
	4	335.5	+44.3	1.10
	5	338.2	+45.2	0.60
MB39	2	332.7	+39.3	0.30
	3	325.7	+38.6	0.60
	4	338.7	+43.4	0.40
	5	316.9	+39.5	0.50
	6	330.5	+30.5	0.40
MB40	1	313.2	+52.5	1.10
	2	338.4	+46.7	1.00
	3	43.9	+45.3	0.80
	4	191.2	+35.0	0.70
	5	212.3	+42.0	0.90
	6	344.8	+50.8	1.60
MB41	1	333.8	+48.5	1.50
	2	339.8	+45.7	0.80
	3	339.2	+45.5	1.20
	4	341.5	+40.4	0.90
	5	31.0	-42.9	0.80
	6	336.6	+48.3	0.90

Table 6.8. Foum Zguid dyke. Pilot sample A.F. demagnetisation results

Field (Oe)	Sample No. 37.1 D	I	Int*	MB38.1 D	I	Int*	MB39.1 D	I	Int*
0	335.7	+49.9	10.31	332.1	+47.8	9.93	343.0	+36.0	2.21
75	334.6	+52.0	5.18	324.8	+47.2	6.16	343.0	+51.0	0.73
150	300.1	+48.9	3.02	339.4	+51.5	2.77	340.6	+39.0	0.34
225	286.4	+20.8	1.86	325.0	+33.1	1.46	33.7	+47.6	0.45
300	356.7	+37.1	1.80	359.2	+35.2	1.39	329.3	+30.5	0.13
375	334.4	+32.9	0.45	139.9	+79.5	0.57	340.0	+11.0	0.08
450	327.3	-31.9	1.21	194.8	+73.7	0.40			
600	92.5	-35.1	1.74	66.8	-25.0	1.41	184.6	-45.0	0.29
750	96.7	-57.9	1.63	177.6	-70.3	1.87	17.5	-13.7	0.37
900	331.6	-29.7	3.69	35.7	+17.8	2.94	328.9	-1.6	1.23

Field (Oe)	Sample No.MB40.2 D	I	Int*	MB41.5 D	I	Int*	D	I	Int*
0	338.3	+46.7	9.57	338.3	+53.8	8.67			
75	331.8	+50.6	6.08	328.7	+50.7	5.79			
150	324.1	+54.7	2.37	327.8	+52.9	2.66			
225	311.0	+46.7	1.21	325.8	+47.6	1.11			
300	320.5	+37.6	0.90	326.1	+38.4	0.58			
375	332.4	+24.1	0.68	334.0	+31.6	0.40			
450	119.5	-3.9	0.25	322.5	+2.6	0.39			
525	271.2	-47.9	0.14	197.0	+71.7	0.19			
600				248.8	-13.0	0.60			

Table 6.9 Foum Zguid dyke. Bulk A.F. demagnetisation results

Demag field(Oe)	Site No.	Sample No.	D	I	Int*
250	MB37	1	334.4	+32.9	0.45
		2	316.1	+25.4	0.61
		3	328.4	+34.2	0.83
		4	331.1	+42.8	1.43
		5	327.3	+39.3	1.17
225	MB38	1	325.0	+33.1	1.46
		2	329.2	+34.0	1.13
		3	326.7	+36.8	0.88
		4	328.7	+41.4	1.21
		5	324.9	+36.3	0.95
150	MB39	1	329.3	+30.5	0.13
		2	306.0	+43.6	0.22
		3	326.0	+50.0	0.45
		4	328.9	+46.7	0.32
		5	315.6	+44.8	0.42
		6	321.1	+33.6	0.32
300	MB40	1	325.2	+47.4	0.17
		2	320.5	+37.6	0.90
		6	330.4	+50.1	0.20
300	MB41	1	310.9	+34.2	0.77
		3	321.3	+42.6	0.52
		5	326.1	+38.4	0.58
		6	340.3	+49.0	0.97

* x 10^{-4} gauss

Table 6.10. Central Atlas intrusives. Mean site directions, pole positions and statistical parameters

(a) N.R.M.

	Site No.	D	I	N	R	k	α_{95}
	MB75	8.0	+47.0	6	5.986	351	4
MB76	MB76	331.0	-8.0	6	5.958	120	6
	MB77	209.0	-29.5	5	4.949	78	9
	MB78	2.0	+26.0	6	5.223	6	29
	MB79	320.0	+19.5	6	5.962	131	6
	MB80	337.5	+22.5	6	5.266	7	28
	Overall Mean	332.0	+19.0	6	3.895	2	56

(b) After A.F. demagnetisation

Site No.	Peak field(Oe)		D	I	N	R	k	α_{95}	Palaeomagnetic south pole Lat.	Long	A_{95}
MB75	150	6.	6.5	+48.0	3	2.996	494	6	83.5S	66.0W	7
MB76	150		324.5	+23.5	4	3.990	305	5	52.0S	61.0W	5
MB77	225		284.0	+59.5	4	3.982	167	7	30.0S	116.0E	11
MB78	225		330.0	+43.5	3	2.938	32	22	64.0S	78.0E	22
MB79	225		301.0	+20.0	4	3.974	114	9	32.0S	76.5E	5
MB80	225		308.5	+23.5	3	2.998	1144	4	39.0S	73.5E	2
Overall Mean			318.5	+38.5	6	5.494	10	22	53.0S	81.5E	24

Table 6.11 Central Atlas intrusives N.R.M.s

Site No.	Sample No.	D	I	Int*
MB75	1	16.6	+46.2	0.46
	2	3.3	+50.7	0.58
	3	1.7	+45.0	0.63
	4	11.2	+47.7	0.51
	5	7.5	+48.3	0.80
	6	7.6	+44.8	0.90
MB76+	1	332.0	+3.1	0.15
	2	325.5	-8.5	0.15
	3	336.9	-15.2	0.13
	4	332.7	-11.7	0.16
	5	326.8	-7.0	0.15
	6	331.3	-9.0	0.16
MB77	1	221.0	-19.5	7.9
	3	205.9	-34.3	17.0
	4	211.5	-32.5	14.0
	5	203.4	-32.3	21.0
	6	201.8	-27.2	20.0
MB78	1	12.6	-24.1	0.16
	2	319.0	+23.9	0.29
	3	1.0	+44.1	0.28
	4	29.4	+37.0	0.30
	5	353.8	+29.5	0.26
	6	15.7	+30.0	0.32
MB79+	1	306.8	+23.4	0.14
	2	319.9	+20.8	0.12
	3	326.3	+19.4	0.12
	4	323.3	+16.5	0.14
	5	324.9	+17.0	0.14
	6	319.5	+18.5	0.14
MB80+	1	308.8	+32.0	0.11
	2	328.4	+14.1	0.10
	3	353.9	+28.8	0.05
	4	324.2	+15.0	0.09
	5	318.3	+24.2	0.07
	6	35.4	+4.1	0.12

* x 10^{-3} gauss

+ tilt correction not applied

Table 6.12 Central Atlas intrusives. Pilot sample A.F. demagnetisation results

Field (Oe)	Sample No. MB75.3 D	I	Int*	MB76.6 D	I	Int*	MB77.1 D	I	Int*
0	5.5	+46.5	8.00	312.6	+42.6	1.47	220.5	-20.2	80.00
75	5.0	+47.1	3.00	329.9	+31.1	1.38	236.2	+17.0	21.00
150	0.1	+47.0	1.10	330.2	+30.1	1.00	293.5	+60.8	16.00
225	14.8	+36.1	0.30	325.7	+24.4	0.68	309.8	+61.6	13.00
300	21.7	+54.2	0.18	326.4	+50.3	0.52	303.0	+63.1	10.00
375	358.4	-2.1	0.08	327.3	+31.4	0.35	322.0	+67.8	7.00
450	305.6	+56.5	0.07	344.5	+41.1	0.32	228.8	+54.0	3.00
525	27.2	+86.0	0.13	322.4	+24.1	0.24	175.3	+16.9	3.00
600				245.0	+5.1	0.18	267.3	+80.4	4.00

Field (Oe)	Sample No. MB78.5 D	I	Int*	MB79.2 D	I	Int*	MB80.3 D	I	Int*
0	341.4	+34.7	2.96	268.2	+37.0	1.27	237.0	+62.9	0.87
75	342.7	+33.9	1.04	312.4	+21.0	0.69	345.2	+57.8	0.86
150	351.3	+26.7	0.49	300.8	+17.9	0.63	349.5	+62.3	0.61
225	324.0	+63.7	0.41	291.4	+19.8	0.45	344.4	+64.5	0.45
300	28.6	+32.2	0.34	301.7	+26.1	0.45	323.6	+69.6	0.33
375	36.6	-43.9	0.77	296.4	+44.5	0.23	343.6	+63.2	0.21
450	42.1	+57.0	0.11	117.5	-24.3	0.09	317.9	+68.6	0.15
525	132.6	-10.6	0.12	295.2	+11.3	0.13	270.8	+60.7	0.15
600	121.9	+14.5	0.14	246.0	+12.0	0.18			

* x 10^{-4} gauss

Table 6.13. Central Atlas intrusives. Bulk A.F. demagnetisation results

Demag. field(Oe)	Site No.	Sample No.	D	I	Int*	Demag. field(Oe)	Site No.	Sample No.	D	I	Int*
150	MB75	1	11.9	+46.9	0.27	225	MB78	1	321.5	+30.4	0.27
		2	3.9	+49.9	0.53			2	326.3	+49.4	0.32
		6	3.1	+47.4	0.15			3	345.7	+49.2	0.27
150	MB76	1	321.4	+21.6	0.98	225	MB79	1	302.1	+23.1	0.48
		2	321.9	+22.2	0.99			3	303.8	+27.3	0.49
		3	331.2	+26.3	0.96			4	298.4	+10.2	0.49
		4	323.7	+23.7	1.16			6	300.9	+19.6	0.49
225	MB77	3	289.6	+59.9	10.16	225	MB80	1	307.3	+21.5	0.69
		4	397.2	+60.1	10.28			2	309.4	+25.8	0.78
		5	279.2	+57.3	9.24			4	309.0	+23.2	0.73
		6	269.8	+58.5	10.62						

* x 10^{-5} gauss

Table 6.14. Radiometric dating results from Jurassic igneous formations

Site No.	Percentage of K_2O	Radiogenic argon ($mm^3\ gm^{-1}$)	Atmospheric contamination (%)	Age
(a) Draa Valley sills				
MC14 (whole rock)	0.16	$(3.87 \pm 0.07)10^{-3}$	73.0	180 ± 4
		$(3.94 \pm 0.07)10^{-3}$	69.6	183 ± 4
MC15 (whole rock)	0.56	$(3.62 \pm 0.05)10^{-3}$	60.2	186 ± 3
		$(3.55 \pm 0.05)10^{-3}$	57.4	183 ± 3
MC16 (whole rock)	0.57	$(3.62 + 0.05)10^{-5}$	65.4	183 + 3
		$(3.58 \pm 0.08)10^{-3}$	60.8	181 ± 4
(b) Foum Zguid dyke				
MB47 (whole rock)	1.03	$(6.62 \pm 0.09)10^{-3}$	51.1	186 ± 3
		$(6.47 \pm 0.08)10^{-3}$	54.9	182 ± 3
MB38 (whole rock)	0.53	$(3.42 \pm 0.07)10^{-3}$	64.4	187 ± 4
		$(3.32 \pm 0.08)10^{-3}$	71.3	182 ± 4

Table 6.14 (contd)

Site No.	Percentage of K_2O	Radiogenic region ($mm^3\ gm^{-1}$)	Atmospheric contamination (%)	Age
(c) Central Atlas intrusives				
Tassent gabbro				
MB76 (biotite)	6.01	$(3.22 \pm 0.06)10^{-2}$	29.0	155 ± 3
		$(3.14 \pm 0.05)10^{-2}$	25.5	152 ± 3
MB79 (biotite)	6.80	$(3.67 \pm 0.05)10^{-2}$	26.8	157 ± 2
		$(3.62 \pm 0.07)10^{-2}$	26.8	154 ± 2
MB80 (biotite)	5.51	$(3.05 \pm 0.05)10^{-2}$	24.9	160 ± 3
		$(3.00 \pm 0.06)10^{-2}$)	28.4	158 ± 3
Dykes				
MB77 (whole rock)	0.80	$(3.28 \pm 0.06)10^{-3}$	40.6	121 ± 3
		$(3.22 \pm 0.05)10^{-3}$	42.9	119 ± 3
MB78 (whole rock)	0.51	$(2.36 \pm 0.04)10^{-3}$	54.9	134 ± 3
		$(2.31 \pm 0.04)10^{-3}$	56.1	131 ± 3

$\lambda_e = 0.584 \times 10^{-10}\ yr^{-1}$
$\lambda_\beta = 4.72 \times 10^{-10}\ yr^{-1}$
$^{40}K/_K = 1.19 \times 10^{-2}$ atom per cent

Table 6.15. Summary of Jurassic pole-positions from Moroccan formations

Pole Ref No. (Fig6.14)	Formation	Mean direction of magnetisation D	I	α_{95}	No samples	No sites	Palaeomagnetic south pole position Lat	Long	A_{95}	Mean pole position Lat	Long	A_{95}
1	Draa Valley sills	339	+27.5	4.5	90	16	65.5S	50.5E	3.5			
2	Foum Zguid dyke	325	+40.0	4	23	5	58.0S	79.0E	4	61.0S	71.0E	14
3	Central Atlas intrusives	318.5	+38.5	22	21	6	53.0S	81.5E	24			

Table 6.16 Summary of Jurassic pole-positions from S.E. African formations

Pole Ref. No.(Fig6.14)	Formation	Mean direction of magnetisation D	I	α_{95}	No samples	No sites	Palaeomagnetic south pole position Lat	Long	A_{95}	Mean pole position Lat	Long	A_{95}
4	Red sst.formation Zambia	350.5	-55.5	4.5		6	68.0S	49.5E	5			
5	Stormberg lavas	338.0	-56.0	-	74	4 localities	71.0S	89.0E	15			
6	Karoo lavas,Cent.Afr.	-	-	-	-	9 flows	57.0S	84.0E	8			
7	Karoo dolerites	-	-	-	-	N = 10	65.5S	75.0E	12.5	64.5S	85.0E	7.5
8	Marangudzy ring	159.5	+43.5	8.5		8	70.0S	105E	9			
9	Mateke Hills ring complex	149.5	+58.5	6.5		6	58.5S	79.5E	8.5			

CHAPTER 7. CRETACEOUS

7.1. Geology

Most of the important present-day structural features of South and Central Morocco developed during Upper Cretaceous and Lower Tertiary times, and were only slightly modified during the Alpine orogeny.

During the Lower Cretaceous (Infracenomanian) widespread continental deposits of Saharan origin were laid down, as a result of erosion of the high lands to the south. At the beginning of the Cenomanian (Middle Cretaceous) a very important marine transgression occurred. The sea spread from the West over a vast area of Morocco, to the North of the High Atlas, and between the High- and Anti-Atlas (Choubert & Faure Muret, 1962). For a brief period it connected with the Mediterranean via the Algerian High Plateau to the East, and passed around the eastern end of the Anti-Atlas to submerge the Colomb-Bechar and Tindouf basins (Fig 1.1). The Moroccan palaeogeography remained broadly similar to this during the Lower Turonian, but further to the east the sea which connected with the Mediterranean linked up with a transgression, spreading from the Gulf of Guinea, northwards through the Sahara (Reyment, 1969). In the Upper Turonian and Senonian the sea progressively retreated again. The Haha coastal basin, which had developed during the course of the Jurassic and Lower Cretaceous gradually disappeared during the Senonian, as a result of the progressive uplift of the Western High Atlas.

The first effects of the Alpine orogeny appeared in the Maestrichtian (Uppermost Cretaceous), and deposits of this age lie discordantly on top of Senonian deposits, and are themselves covered discordantly by Eocene deposits.

During the two major Alpine tectonic phases (Upper Eocene-Lower Oligocene, and Neogene) the regions to the north (Rif and Pre rif zones) were highly deformed and thrust southwards, but in the High Atlas deformation was confined to relatively mild warping of the cover rocks. The Anti Atlas remained unaffected by the Alpine orogeny.

7.2. Location of sampling sites

A small number of localised basaltic lava flows are inter-stratified with the continental Infracenomanian deposits of the High Atlas regions However, due to very bad weather conditions the roads providing access to these outcrops were impassible at the time of the field work in this region, and attempts to sample the lavas were unsuccessful. These rocks are considered to be worthwhile sampling on any future field work in the area.

The continental Infracenomanian deposits were more accessible, and five sites were sampled over a total stratigraphic thickness of some 100 metres in these coarse-grained red sandstones.

7.3. Palaeomagnetic results from the Infracenomanian red sandstones

7.3.1. N.R.M. directions and intensities

The intensities of N.R.M. of these samples were generally higher than those of the Triassic red sediments, and varied from 0.5 to 1.7 $\times 10^{-5}$ gauss. This may possibly be correlated with the much darker red colouration of the former. Both the between-site and the within-site scatter of N.R.M. directions were small, the former being 6^{o}, and the latter ranging from 5^{o} to 11^{o} (Table 7.2(a)). Small tilt corrections of up to 8^{o} were applied to the remanence vectors of all sites, but had no significant effect on the between-site scatter. The mean site NRM directions all lie

just to the NW of the present field direction at these localities (Fig 7.1(a)), and the latter lies within the 95% confidence limit of the overall mean direction. The value of the overall mean, giving unit weight to each site, is

$$D = 347.5, \quad I = 39.0, \quad \alpha_{95} = 6.0,$$

and the corresponding palaeomagnetic south pole position is

$$75^{\circ}S, \quad 36.5^{\circ}E, \quad A_{95} = 5.5^{\circ}$$

7.3.2. Pilot sample demagnetisation results

The results obtained by subjecting one sample from each site to progressive thermal demagnetisation up to a maximum temperature of 675°C are plotted in Figs 7.2 and 7.3. In all cases the direction of remanence underwent little change on treatment up to 600°C, after which a random scatter of directions occurred. The intensities of magnetisation decreased progressively over the whole range of treatment.

The susceptibilities decreased during treatment up to 600°C, after which they began to increase again. This suggests the occurrence of a chemical change, involving the magnetic phase, at some temperature between 600 and 675°C. The destruction or modification of an original magnetic phase would explain the sudden random change in direction of remanence after heating the samples to 675°C.

7.3.3. Bulk thermal demagnetisation

Although the NRM within-site and between-site scatter of directions was small, all of the samples were demagnetised at 300°C, to see if any slight improvement in scatter could be obtained. However this treatment resulted instead in a slight increase of between-site scatter (from 6° to 7°) and a general small increase of within-site scatter (Table 7.2(b)).

The mean direction of remanence after treatment is identical to that before treatment, but there seems to be a tendency towards 'stringing' along a great circle through the present earth's field direction at these localities after treatment. This suggests that there might be a small component of remanence, of variable magnitude, directed along the earth's present field direction in these samples, which is not removed by treatment at 300°C. The pilot sample results indicate that such a component is unlikely to be removed by further treatment at higher temperatures.

7.4. Discussions

The pole position from the Moroccan Infracenomanian sandstones is plotted in Fig 7.4 (pole 1), together with poles derived from Cretaceous formations elsewhere in Africa. (poles 2 to 4). Since the mean direction of magnetisation of the Moroccan sandstones is not significantly changed by demagnetisation at 300°C, but the within-site scatter is smaller before treatment, the mean pole position before treatment (Table 7.2) is plotted in Fig 7.4.

Poles 3 and 4, from the Lupata volcanic series, and Mlanje Massif syenite respectively, lie close to the mean Mesozoic position (c.f. figs 5.18 and 6.14), whereas the poles from the Moroccan Infra-cenomanian sandstone and the Mozambique red siltstone (poles 1 and 2) lie close together, but some 30° away from the mean Mesozoic position.

Although the two deviant poles (1 and 2) were derived from formations situated at either extremity of the African continent, they still agree closely with each other, and it therefore seems unlikely that the discrepancy between these poles and poles 3 and 4 is due to

relative tectonic displacement. It is more likely to be due to one of the following:

(i) a temporary excursion of the pole away from the mean Mesozoic position, similar to the Jurassic excursion suggested in Chapter 6.

(ii) poles 1 and 2 representing an intermediate position of the south pole during its movement from the mean Mesozoic position to the Lower Tertiary position, close to the present South pole, or

(iii) the presence of a secondary component of remanence directed along the Earth's present field direction in both the Moroccan sandstones and the Mozambique siltstones.

Although the bulk demagnetisation results indicate the possible presence of a small component of remanence aligned along the Earth's present field direction in the Moroccan sediments, it is considered that the magnitude of this component is too small to account for the observed discrepancy.

Radiometric age determinations on the Lupata volcanic series (Gough et al, 1964) yielded ages of 107 and 110 my, and on the Mlanje Massif (Briden, 1967) 116 $\pm$ 6 and 128 $\pm$ 6 my. Both of these formations are therefore Lower Cretaceous in age and are Aptian or older (Geol. Soc. Phan. time-scale, 1964). The Mozambique red siltstones have been correlated with the Lupata volcanic series (Gough & Opdyke, 1963), but it is possible that they are slightly younger than this formation. It is also possible that the Moroccan Cretaceous sandstones are younger than Aptian, since they are known only to be pre-Cenomanian. If this interpretation is correct, then the pole-position derived from these two formations may represent an intermediate position of the South pole, during its movement from the mean Mesozoic position to the Lower Tertiary position.

There are no other African palaeomagnetic results to suggest that it remained in the mean Mesozoic position later than the Lower Cretaceous.

If the Mozambique red siltstones and Moroccan Infracenomanian red sandstones should turn out to be older than Albian, then this explanation will become untenable, and the only alternative is that they represent a temporary excursion of the pole away from the mean Mesozoic position.

References

Briden, J.C. 1967. A new palaeomagnetic result from the Lower Cretaceous of east-central Africa, Geophys. J., 12, 375-380

Choubert, G. and A. Faure-Muret, 1962. Évolution du domaine Atlasique Marocain depuis les temps Palaeozoiques. In Livre a la mémoire du Professeur Paul Fallot, Society Géologique de France

Geol. Soc. Phanerozoic time-scale, 1964. Quart. J. geol. Soc. London, 120 S, 260-2

Gough, D.I. & N.D. Opdyke, 1963. The palaeomagnetism of the Lupata alkaline volcanics. Geophys. J., 7, 457-468.

Gough, D.I. & N.D. Opdyke and M.W. McElhinny, 1964. The significance of palaeomagnetic results from Africa. J. Geophys. Res., 69, 2509-2519.

Reyment, R.A., 1969. Ammonite biostratigraphy, continental drift and oscillatory transgressions. Nature, Vol 224, pp137-140.

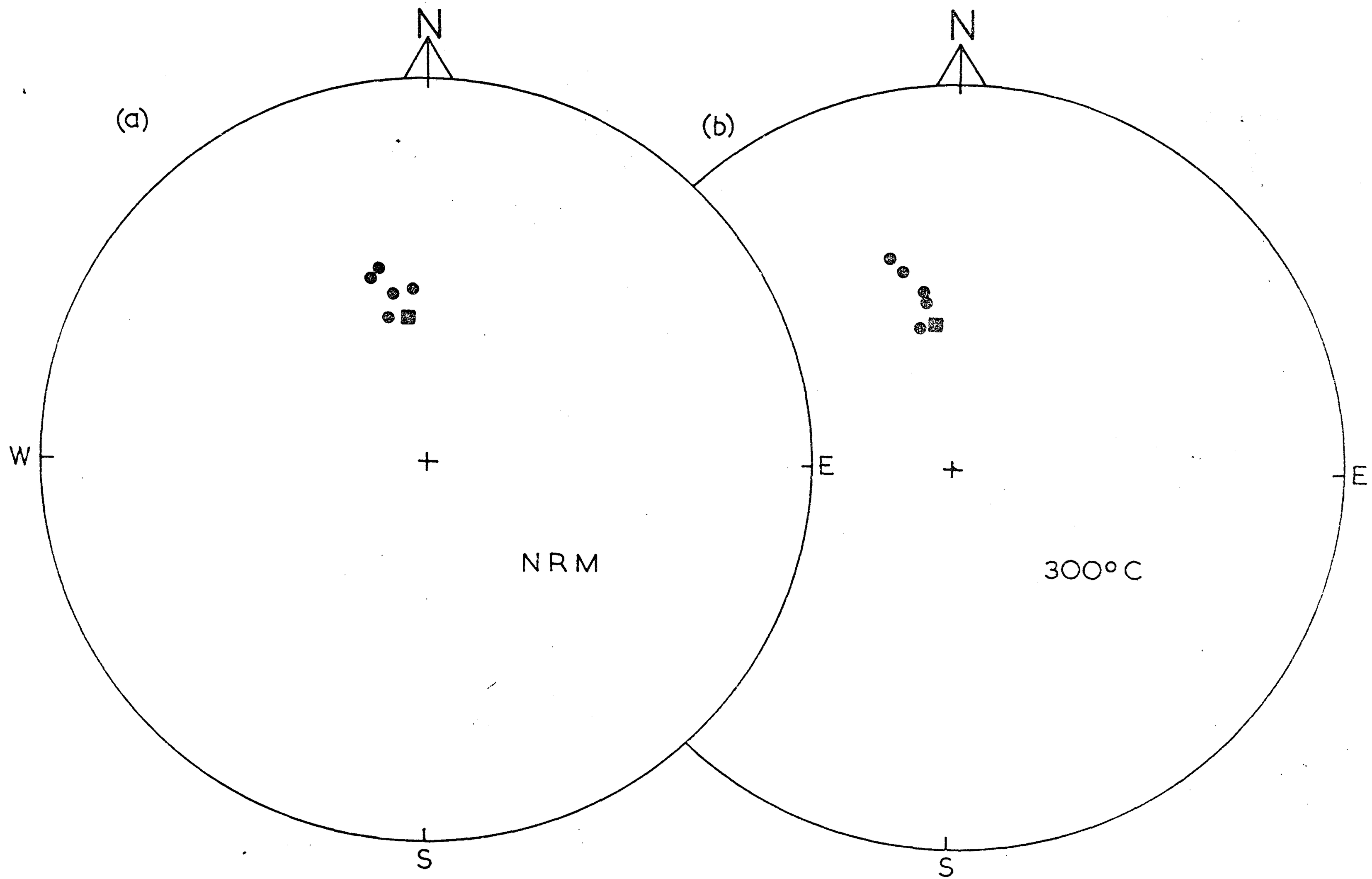


Fig 7.1 Cretaceous sediments. Mean site directions (a) N.R.M. (b) After 300°C treatment.

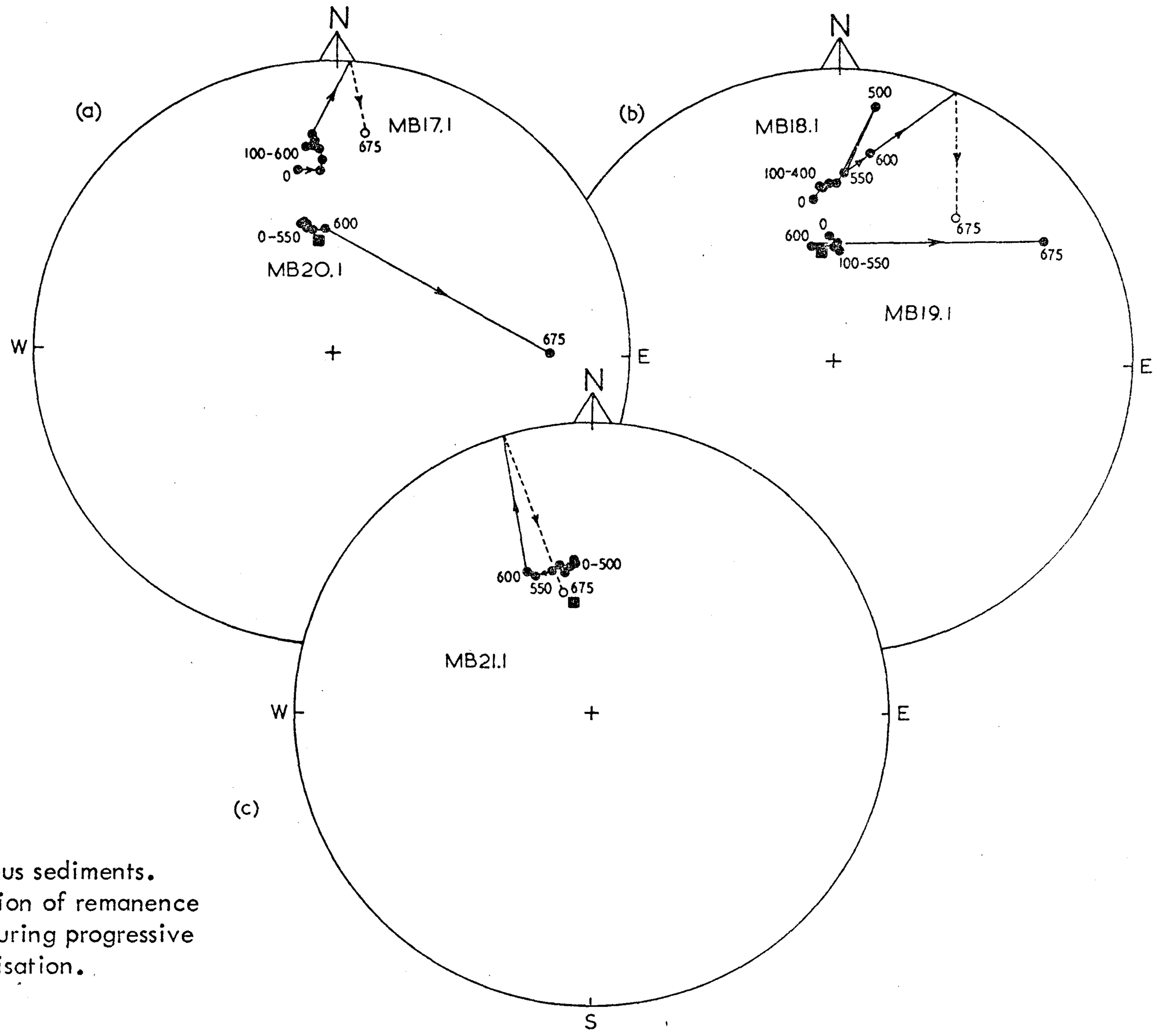
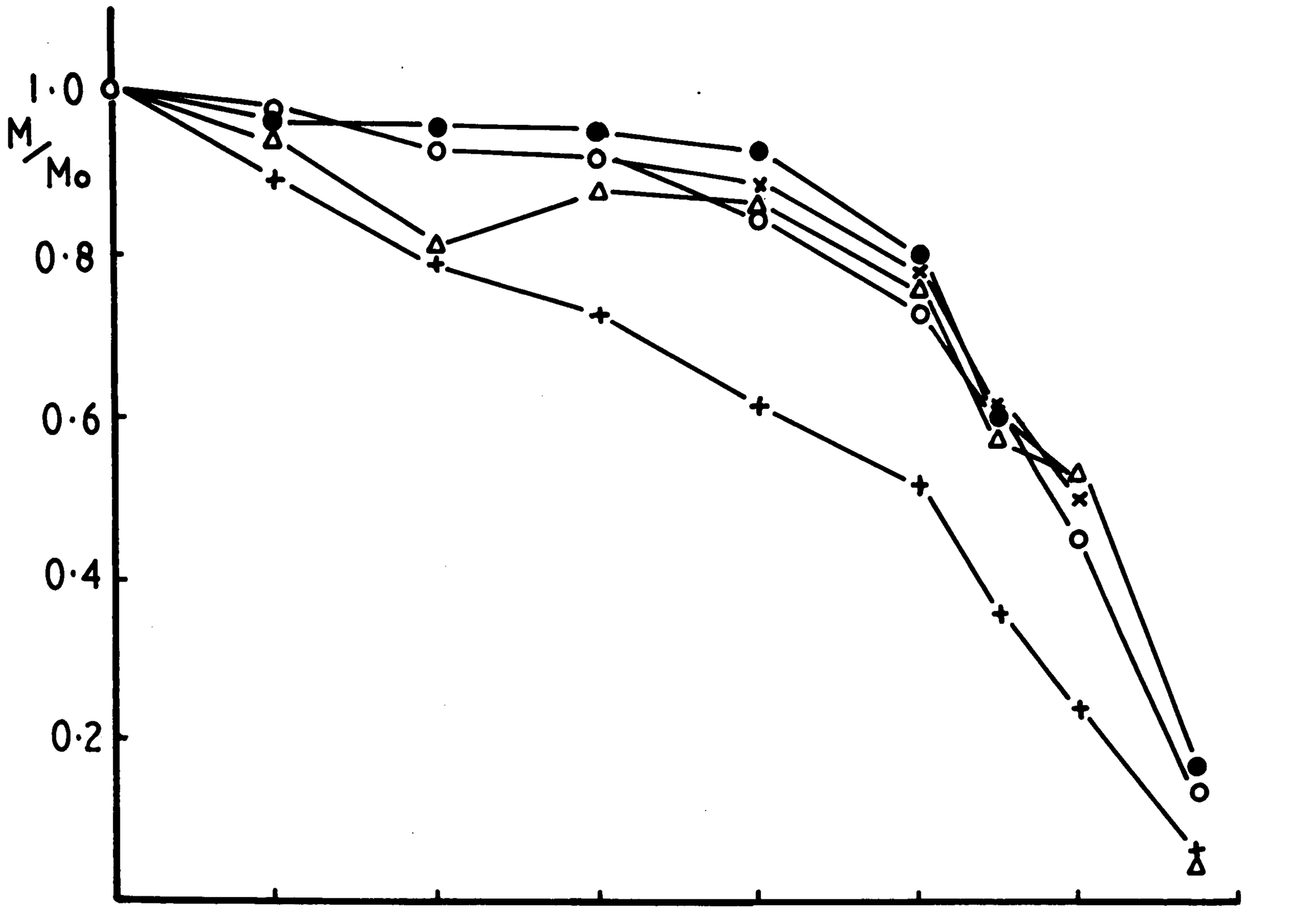


Fig 7.2 Cretaceous sediments. Changes in direction of remanence of pilot samples during progressive thermal demagnetisation.



		Mo	
●	MB 17.1	0·75	
o	MB 18.1	0·63	
×	MB 19.1	0·61	X10^{-5}Gauss
+	MB 20.1	1·16	
Δ	MB 21.1	1·72	

Fig 7.3 Cretaceous sediments. Changes in intensity of magnetisation of pilot samples during progressive thermal demagnetisation.

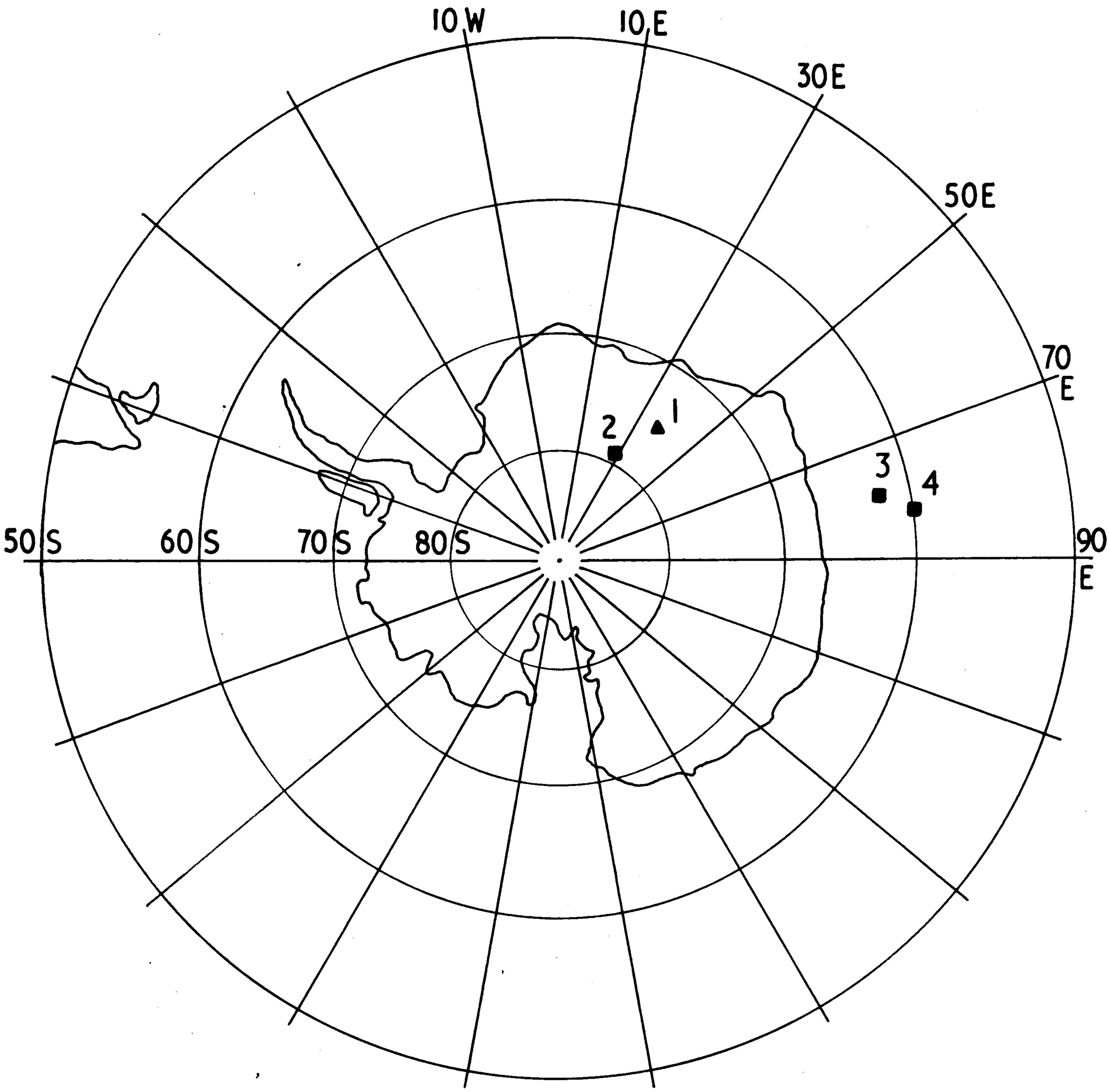


Fig 7.4 African Cretaceous palaeomagnetic pole positions. Black triangle, Moroccan pole; black squares, poles from South and East African formations.

Table 7.1. Cretaceous field data

(a) Mean location of sampling sites

Lat.	Long
31.71N	6.91W

(b) Tilt corrections

Sites	Strike	Dip
MB17-18	237	8
MB19	312	4
MB20-21	237	8

Table 7.2. Cretaceous mean site directions, pole positions and statistical parameters

(a) N.R.M.

Site No.	D	I	N	R	k	α_{95}	Palaeomagnetic pole position Lat.	Long	A_{95}
MB17	346.5	+34.0	6	5.882	42	10.5	72.3N	140.0W	11
MB18	342.5	+35.0	6	5.926	67	8	69.9N	130.0W	8.5
MB19	345.0	+45.5	5	4.919	49	11	75.9N	121.5W	14.0
MB20	348.0	+39.5	6	5.971	174	5	75.9N	133.5W	4.5
MB21	355.5	+40.0	5	4.964	113	7	80.5N	162.5W	6.5
Overall Mean	347.5	+39.0	5	4.978	183	6.0	75.5N	143.5W	5.5
							Antipole 75.5S	36.5E	

(b) After thermal demagnetisation at 300°C

MB17	343.2	+29.6	6	5.878	41	10.5	68.6N	137.5W	9.5
MB18	345.5	+33.5	6	5.922	64	8.5	71.5N	137.0W	8.5
MB19	346.4	+47.9	5	4.887	35	13	77.7N	103.0W	16.5
MB20	349.8	+38.8	6	5.965	141	5.5	77.1N	139.5W	5.0
MB21	350.8	+41.5	5	4.953	84	8.5	79.5N	136.0W	8.0
Overall Mean	347.0	+38.5	5	4.966	117	7.0	75.0N	133.0W	5.5
							Antipole 75.0S	47E	

Table 7.3. Cretaceous N.R.M.s

Site No.	Sample No.	D	I	Int($\times 10^{-5}$ gauss)
MB17	1	353.9	+27.8	0.70
	2	4.6	+29.4	0.70
	3	347.0	+39.1	1.00
	4	324.9	+30.7	0.60
	5	344.9	+41.6	0.70
	6	342.9	+32.4	0.80
MB18	1	352.0	+30.4	0.63
	2	333.0	+41.8	0.47
	3	328.0	+39.8	0.56
	4	354.3	+29.0	0.66
	5	345.2	+34.9	0.58
	6	339.9	+32.7	0.50
MB19	1	358.2	+45.8	0.61
	2	327.4	+43.9	1.50
	4	326.6	+49.4	1.70
	5	355.0	+42.3	0.70
	6	354.9	+42.7	0.80
MB20	1	346.8	+40.8	1.16
	2	350.7	+40.1	1.38
	3	347.8	+36.7	1.10
	4	342.4	+41.1	1.29
	5	352.7	+31.4	1.20
	6	346.0	+47.9	1.28
MB21	1	353.9	+33.2	1.70
	2	357.2	+42.5	1.70
	3	0.6	+50.0	1.20
	4	359.0	+36.5	1.10
	5	347.6	+37.5	1.20

Table 7.4. Cretaceous pilot-sample thermal demagnetisation results

Temp(°C)	Sample No. MB17.1 D	I	Int*	MB18.1 D	I	Int*	MB19.1 D	I	Int*
0	353.9	+27.8	0.75	352.0	+30.4	0.63	358.2	+45.8	0.61
100	355.9	+25.9	0.72	355.3	+28.2	0.61	1.2	+46.3	0.54
200	357.1	+23.0	0.71	356.1	+28.2	0.59	359.7	+47.6	0.48
300	355.8	+20.3	0.71	358.5	+27.2	0.58	0.1	+47.6	0.44
400	354.4	+18.5	0.70	360.0	+27.4	0.54	3.1	+48.8	0.38
500	354.7	+17.7	0.60	7.8	+7.1	0.47	2.3	+47.7	0.32
550	352.4	+19.4	0.45	2.2.	+24.2	0.37	359.2	+47.1	0.22
600	353.9	+15.7	0.40	9.3	+18.3	0.29	349.2	+45.9	0.14
675	7.5	-15.4	0.12	38.6	-25.0	0.08	59.4	+11.6	0.04

Temp(°C)	Sample MB20.1 D	I	Int*	MB21.1 D	I	Int*	D	I	Int*
0	346.8	+40.8	1.16	353.9	+33.2	1.72			
100	346.8	+40.9	1.12	354.0	+34.4	1.62			
200	347.4	+41.2	1.08	350.1	+36.6	1.37			
300	347.9	+40.9	1.06	352.5	+34.8	1.51			
400	348.1	+42.0	1.03	349.3	+34.0	1.49			
500	347.7	+42.9	0.90	344.9	+35.0	1.32			
550	351.3	+44.3	0.71	339.0	+35.3	1.02			
600	357.1	+43.8	0.58	336.6	+32.9	0.91			
675	88.9	+17.2	0.06	344.7	-43.5	0.85			

* x 10^{-5} gauss

Table 7.5. Cretaceous bulk thermal demagnetisation results (300°C)

Site No.	Sample No.	D	I	Int($\times 10^{-5}$ gauss)	Site No.	Sample No.	D	I	Int($\times 10^{-5}$ gauss)
MB17	1	355.8	+20.3	0.70	MB20	1	347.9	+40.9	1.10
	2	341.1	+20.5	0.70		2	354.3	+38.8	1.20
	3	344.8	+37.7	0.90		3	348.0	+35.0	1.00
	4	325.0	+25.3	0.50		4	343.5	+39.9	1.10
	5	347.5	+41.3	0.70		5	354.9	+30.0	1.10
	6	345.5	+30.7	0.80		6	349.7	+47.6	1.20
MB18	1	358.5	+27.2	0.60	MB21	1	352.5	+34.8	1.50
	2	335.9	+39.2	0.40		2	350.0	+45.3	1.40
	3	333.0	+39.3	0.50		3	357.2	+52.5	1.10
	4	355.1	+28.8	0.60		4	355.0	+37.4	1.00
	5	347.6	+33.8	0.50		5	340.7	+36.8	1.00
	6	340.4	+30.3	0.40					
MB19	1	0.1	+47.6	0.40					
	2	324.0	+45.2	1.00					
	4	326.1	+54.8	1.00					
	5	356.5	+40.7	0.60					
	6	1.0	+44.9	0.60					

Table 7.6. Cretaceous sediments. Variation of susceptibility during thermal demagnetisation of pilot samples

Treatment (^{o}C)	0	100	200	300	400	500	550	600	675
MB17.1	81	71	71	78	73	57	57	52	60
MB18.1	73	71	65	65	65	52	47	45	52
MB19.1	65	58	52	58	53	47	47	45	52
MB20.1	68	65	71	71	65	57	47	47	57
MB21.1	95	91	85	97	94	73	58	58	57

Figures refer to total susceptibility in units of 10^{-6} gauss cm^{3} Oe^{-1}

Table 7.7. African Cretaceous palaeomagnetic pole positions

Pole Ref No.(Fig7.4)	Formation	Mean direction of magnetisation D	I	α_{95}	No Samples	No Sites	Palaeomagnetic south pole position Lat.	Long	A_{95}	Mean pole position Lat.	Long	A_9
1	Infracenomanian ssts, Morocco	347.5	+39.0	6	28	5	75.0S	36.5E	5.5			
2	Red siltstones, Mozambique	359.0	-46.0	6	5	-	79.0S	28.0E	-	61.0S	81.0E	5
3	Lupata volcanic Series, Mozambique	336.0	-54.5	3	-	7	62.0S	79.5E	4	77.0S	33.0E	9.5
4	Mlanje Massif Syenite, Malawi	333.0	-54.0	9.5	8	-	60.0S	82.0E	12			

CHAPTER 8. INTERPRETATION OF RESULTS ON A GLOBAL SCALE

8.1. Introduction

Differences in palaeomagnetic pole-positions from formations of different geological age, situated on the same continent, can arise from any one, or combination of, the following three processes (assuming an average geocentric dipole field, and internal rigidity of the continent).

(i) Movement of the continent relative to the geomagnetic dipole axis, which itself remains fixed, and approximately coincident with the rotation axis.

(ii) Movement of the geomagnetic dipole axis relative to the continent, which itself remains stationary with respect to the rotation axis.

(iii) Movement of the whole earth, or an outer shell of the earth, relative to the geomagnetic dipole axis, which itself remains stationary and coincident with the rotation axis.

The first of these processes is usually referred to as 'continental drift', and the second two as different forms of 'polar wander'.

A chronological sequence of palaeomagnetically determined pole-positions from a continent defines an 'Apparent polar-wander curve' for that continent. If polar-wander curves from different continents have significantly different shapes, then relative movement between the continents, and hence continental drift, is implied. However some element of polar-wander may also be present, and can sometimes be detected by means of additional information from sea-floor magnetic anomalies (e.g. McElhinny & Wellman, 1969).

In this chapter the new palaeomagnetic results from Morocco described in chapters 2 to 7 will be combined with results from other parts of Africa, and the general form of the new Phanerozoic apparent polar-wander curve for Africa will be discussed. This new African polar-wander curve will then be compared with curves from the other Gondwanic continents (South America, Australia, Antarctica & India), and the Laurasian continents (North America & Eurasia). Similarities and differences between these curves will be interpreted in terms of motions of the continents, and/or polar-wander, taking into account other factors, particularly geological and sea-floor spreading evidence.

8.2. The African polar-wander curve

A complete list of African Upper Precambrian to Recent palaeomagnetic pole-positions is given in Table 8.1. In this table the reference numbers refer to McElhinny et al,(1968). Where formations are thought to span similar age-ranges, mean pole-positions have been calculated, and are listed in the last three columns of the table. The African polar-wander curve derived from these mean poles is plotted in Fig 8.1. In this diagram open triangles refer to poles derived exclusively from Moroccan formations, solid triangles to poles from South and East African formations, and half-solid triangles to poles calculated from combined Moroccan and South-east African data.

The Upper Precambrian to Devonian pole-positions have been discussed in chapters 2 to 4. In Fig 8.1 the Moroccan Upper Precambrian (P.Cu) and Lower Cambrian (€1) poles are plotted in positions corresponding to magnetisation during 'normal'magnetic intervals. The alternative possibility, discussed in Section 3.3.5, of magnetisation during 'reversed' magnetic intervals is equally plausible, and reasons are given later

in this chapter for considering this to be a more valid interpretation.

The "Lower Carboniferous" pole, Cl, is derived from the Dwyka varves of Central Africa. Palaeontological age determinations on this formation are poor, and indicate only that it is 'probably Carboniferous'. A lower Carboniferous age was suggested by McElhinny & Opdyke (1968) on the basis of a comparison with palaeomagnetic results for the Carboniferous of Australia (Irving 1966). More recently this suggestion has been supported by Plumstead (quoted in McElhinny et al, 1968), who cites evidence from plant fossils in an overlying bed, but the true age of this formation remains uncertain. According to Robinson (personal communication) the Dwyka glaciation may have continued through to Lower Permian times.

The formations yielding the "Upper Carboniferous" (Cu) and "Lower Permian"(Pl) poles are both commonly regarded by geologists as being Lower Premian in age. However the two poles are significantly different from one another, and McElhinny & Opdyke (1968) suggest that this may be due to a difference in age between the two formations. They point out that according to this interpretation the Permo-Carboniferous palaeomagnetic results from Africa are consistent with those from Australia on King's (1962) reconstruction of Gondwanaland. The alternative possibility, that the two formations are of the same age, must also be considered, and in this case the difference between the two poles may be due to incomplete averaging of palaeosecular variation (Opdyke, 1964). (This interpretation is still the one favoured by Opdyke (personal communication)). The polar-wander curve then follows the solid line in Fig 8.1 from the "Lower Carboniferous" position, through the mean "Upper Carboniferous-Lower Permian" position (Cu-Pl), to the Triassic position (Tr).

Two mean poles are listed in Table 8.1 for each of the Triassic, Jurassic and Cretaceous periods. Pole Tr1, from two Moroccan and two Southeast African formations, is considered to represent the true Triassic pole-positions with respect to Africa, whereas pole Tr2, from one Moroccan and one Tanzanian formation, is thought to reflect Tertiary remagnetisation effects (Section 5.7).

Pole J1, from one Moroccan and one Zambian formation, is thought to represent a temporary westward excursion of the pole during the Lower Jurassic, and to avoid confusing the diagram, neither this pole nor pole Tr2 are plotted. Pole J2, from two Moroccan and five East African formations, represents the position of the pole with respect to Africa during the rest of the Lower Jurassic (Section 6.7).

The Cretaceous pole, k1, from two East African formations, is considered to represent the pole-position at the beginning of the Cretaceous, and k2, from one Moroccan and one East African formation, an intermediate position during movement of the pole from k1 to the Lower Tertiary position, T1.

McElhinny and Wellman (1969) cite evidence from Africa and the other Gondwanic continents of a westward excursion of the pole during the Tertiary. This is reflected in the shape of the Tertiary part of the African polar-wander curve shown in Fig 8.1. The Lower Tertiary pole, T1, is calculated from a single formation, the Ethiopian traps, of Eocene to Oligocene age, and the Upper Tertiary pole Tu, is very well defined from six formations, ranging in age from Miocene to Plio-Pleistocene.

The mean Quaternary pole, Q, has a large error circle, but lies close to the present South pole.

8.3. Comparison of the African polar-wander curve with those of the other continents

Several different syntheses of world-wide palaeomagnetic results have recently been published (e.g. Creer, 1970a, and Tarling, 1971), and a general review of the data will not therefore be given here. A list of pole-positions derived from recent reviews is given in Table 8.2, together with the sources of the data, and only those poles which are considered to be immediately relevant to the interpretation of the African polar wander curve will be discussed in the following sections.

8.3.1. Lower & Middle Palaeozoic

Using the data listed in Table 8.2, the Lower & Middle Palaeozoic apparent polar-wander curves of all the major Gondwanan continents are plotted in Fig 8.2 and Laurasian continents in Fig 8.3. In these diagrams the continents and their polar-wander curves have been rotated by appropriate amounts about the poles listed in Bullard et al (1965), and Smith & Hallam (1970), by means of a computer map-plotting program written by Mrs. S. Hofmann of the University of Newcastle.

(a) Gondwanic continents

All Gondwanic Lower Palaeozoic poles except the Moroccan Lower Cambrian pole described in Chapter 2 lie in the ganeral region of Northwest Africa, when plotted on a Smith-Hallam reconstruction. The South American Lower Palaeozoic pole spans a wide age range, from Cambrian to Lower Devonian, but the lower age limit, that of the Argentinian red beds (Creer, 1970b), is not precisely known. This mean pole includes results from the Urucum Formation (Jacadigo series) of Brazil, which although generally considered to be Silurian, is thought by some geologists to be Precambrian, because of similar lithology to the Precambrian banded iron ores of Minas Gerais State, Brazil (Oliveira, 1956).

The Indian pole, from the Salt Range purple sandstones (McElhinny, 1970) is more precisely dated as Lower Cambrian from diagnostic Redlichiid trilobites in overlying shales and dolomites (Schindewolf and Seilacher, 1955). The Australian Lower Palaeozoic pole, quoted in McElhinny & Briden, 1971, was derived from the Antrim Plateau volcanics (McElhinny and Luck, in press) and the Jinduckin Formation (Luck, 1970). The Antrim volcanics are quoted as being Precambrian to Lower Cambrian, but the reliability of this age determination is uncertain. The mean African Cambro-Ordovician pole is calculated from three formations (Table 8.1), one of which (the Ntonya Ring Structure) has yielded a radiometric age determination of 630 my (McElhinny et al, 1968).

Thus at least three independent palaeomagnetic studies from Gondwanic continents span the Lower Cambrian period, and indicate that if the Smith-Hallam reconstruction is valid, then the pole was situated in the region of NW Africa at this time. However this conclusion is not supported by the new Moroccan Lower Cambrian pole position, which implies that Northwest Africa was situated in low palaeolatitudes at this time. As discussed in chapter 3, the presence in this region of thick carbonate sequences containing archaeocyathids, and continental deposits with mudcracks and pseudomorphs after salt crystals, indicates a predominantly warm environment, and supports the new Moroccan Lower Cambrian pole position, rather than those from the other Gondwanic continents and East Africa.

An alternative explanation is that the Smith-Hallam reconstruction is not correct. A different reconstruction of Gondwanaland has been suggested by Tarling (1971), in which India is fitted to Australia, and Australia to Antarctica, and these three combined continents are then fitted to Africa by rotating Antarctica through some 60° anticlockwise from the position shown in Fig 8.2. On Tarling's reconstruction the pole from the Australian Lower Cambrian Antrim volcanics lies further

to the west than in Fig 8.2, and slightly nearer to the Moroccan Lower Cambrian pole, but the Indian pole is just as remote from the latter as on the Smith-Hallam reconstruction. Both reconstructions are therefore equally inconsistent with the position of the new Moroccan Lower Cambrian pole. If this pole is valid, then the only other plausible explanation is that part of NW Africa, including Morocco was detached from the rest of Gondwanaland at that time. The Moroccan formation which yielded this pole is situated to the south of the South Atlas Fault, so that the line of suture must lie even further to the south than this, and may be represented by the southern boundary of the Hercynian fold belt (Sougy, 1962), which coincides approximately with the northern rim of the Tindouf Basin (Fig 1.1).

On the Smith-Hallam reconstruction (Fig 8.2) the Mid-Palaeozoic poles tend to group in the region of South Africa, and the new Moroccan Upper Devonian pole is broadly consistent with this pattern. The polar shift from NW Africa to South Africa was originally thought to have occurred during the Mid-Devonian (Briden, 1967), but McElhinny & Briden (1971) have recently suggested that it took place in the late Ordovician. This conclusion is difficult to reconcile with the position of South American Ordovician to Mid-Devonian poles recently published by Creer (1970b) from Bolivian formations. These poles are not plotted in Fig 8.2, but lie off the south coast of NW Africa, in the vicinity of the Indian Lower Cambrian pole.

The new Moroccan Upper Devonian pole lies slightly to the north of Upper Devonian and Lower Carboniferous poles from the other continents, and this may be due to the polar shift having occurred in two stages; from NW Africa to a position in Central Africa just south of the present equator in the Late Ordovician, and thence to its position in South Africa some time between the Upper Devonian and Lower Carboniferous.

An alternative to this 'two-stage shift' explanation is that NW Africa was still detached from the rest of the continent in the Upper Devonian, but had moved closer to the latter, resulting in a smaller difference between the poles from NW and SE Africa in the Devonian than in the Lower Cambrian. This explanation is consistent with the age of folding of the Hercynian belt (Choubert, 1963 and Sougy, 1962), which indicates that the two units may not have finally combined until the Carboniferous.

(b) Laurasian continents

There are very few fully reliable Lower Palaeozoic pole determinations from the Laurasian continents, since most results are from rocks affected by later orogenic movements, but there is evidence to suggest that Western Europe may have been detached from the Russian platform during this period, and that the two continents were united along the line of the Urals during the Hercynian orogeny (Hamilton, 1970, and Tamrazyan, 1971). This situation is exactly analogous to that suggested above for the relationship between part of NW Africa and the rest of the African continent.

The polar-wander curve for Western Europe shown, in Fig 8.3, suggests that the pole remained in essentially the same position throughout the Lower Palaeozoic and Devonian, undergoing a westerly excursion of some 40^{o} during the Lower Devonian.

The North American Ordovician to Devonian pole position plotted in Fig 8.3 is derived from the Onondaga Limestone (Graham, 1956), the Bloomsburg redbeds (Creer, 1969) and the Trenton Group sediments (Graham, 1954 and 1956). There is evidence that the remanence of these formations is post-depositional, but some authors, e.g. Creer (1971a), consider that it still dates from Lower Palaeozoic times. However this pole conflicts

with results from other North American formations on which stability tests have been carried out. In a recent study on isotopically dated Cambro-Ordovician intrusives from Colorado, involving comprehensive sta bility tests, Larson and Mutschler (1971) obtained a palaeopole (pole ~~G~~ O in Fig 8.3) close to the North American late Palaeozoic pole positions. This result agrees with several other studies on North American Lower Palaeozoic formations, e.g. the Cambrian Sawatch formation (Howell & Martinez, 1957), the Silurian Clinton iron ores (Irving, 1964), and the Devonian Perry lavas (Phillips & Heroy, 1966) and sediments (Robertson et al, 1968). Larson & Mutschler present strong and convincing arguments against the possibility of the Coloradan intrusives having been remagnetised in the Upper Palaeozoic, and consider the likelihood of incomplete averaging of palaeosecular variation, or the occurrence of local tectonic rotation, to be small. They conclude that either little polar movement occurred relative to North America between the early and late Palaeozoic, or, if substantial movement did occur, then by late Palaeozoic times the palaeopole had returned to a position nearly coincident with that of the early Palaeozoic.

According to this interpretation both the North American and the European polar wander curves show possible westward or north westward excursions during the Ordovician or Lower Devonian. The proximity of the Middle to Upper Carboniferous poles indicates that these continents occupied the relative positions shown in Fig 8.3 during the Middle Palaeozoic. However the angular distance of some 30° between the Cambro-Ordovician poles implies movement of the continents towards each other during the Lower Palaeozoic. This is probably related to the existence of the Caledonian fold-belt between them at this time (Dewey, 1969; Dewey and Horsfield, 1970).

(c) Comparison between Laurasian and Gondwanic Lower & Middle Palaeozoic polar-wander curves

The African, North American and Western European polar-wander curves are plotted on a Bullard reconstruction of these continents in Fig 8.4. In this diagram the pole plotted for the Moroccan Lower Cambrian formation is the antipole of that shown in Fig 8.1. This pole is situated some 90° from the mean Cambro-Ordovician pole for Southeast Africa, but less than 30° from Larson & Mutschler's North American Cambro-Ordovician pole.

It was suggested in section (b) above that part of NW Africa, including Morocco, was detached from the rest of Africa during the Lower Palaeozoic. It seems likely that this part of NW Africa was in fact attached to North America at this time.

Reliable Lower & Middle Carboniferous poles from all continents lie in the general region of South Africa when the continents are reassembled on the combined Smith-Hallam-Bullard reconstruction (Figs 8.2 & 8.4). This indicates that by the Carboniferous the three separate supercontinents, Gondwanaland (comprising South America, Australia, India, Antarctica and most of Africa), Western Laurasia (comprising North America, Western Europe and possibly also part of NW Africa), and Eastern Laurasia (Eurasia to the east of the Urals), had combined to form a single supercontinent (Pangaea).

Evidence for the fusion of Western and Eastern Laurasia along the line of the Ural mountains during the Hercynian orogeny has been discussed in detail by Hamilton (1970) and Tamrazyan (1971). Evidence for the fusion of Laurasia and Gondwanaland will be examined below.

Sougy (1962) has demonstrated that a belt of folded early and middle Palaeozoic rocks extends along the Atlantic coast of Africa from

Morocco at least as far south as Senegal. The belt comprises a bordering folded zone and an inner zone exhibiting strong deformation, dynamic metamorphism and igneous intrusion. There is evidence of minor tectonism associated with the Caledonian orogeny, but the main fold movements occurred during the Carboniferous and Permian. The evolution of the northern part of this belt has been described in detail in the geological sections of chapters 1 to 4 of this thesis.

The eastern coast of North America is bordered by the Appalachian Mountains, in which Caledonian and Hercynian orogenic belts are closely inter-related (e.g. Holmes, 1965). The Caledonian belt can be traced northwards to link up with the European and Greenland Caledonides on the reconstruction shown in Fig 8.3, and is crossed by the Hercynian belt in the region of Cape Hatteras. When North America and Africa are reassembled in the positions shown in Fig 8.4 the Hercynian belt forms a continuous link between the two continents. The principles phases of folding occurred in the North American part of the belt during the Carboniferous and Permian, i.e. at the same time as the principle phases in NW Africa.

It therefore seems likely that the Hercynian orogenic belts of NW Africa and the eastern coast of North America were produced as a result of the collision of these two continents during the Carboniferous period. If Morocco originally formed part of the North American plate, as suggested above, then this hypothesis is consistent, in general terms, with the Moroccan late Precambrian and Lower Cambrian pole-positions described in this thesis.

Palaeoclimatic evidence, (particularly the presence of limestones with extensive coral reefs), from the eastern coast of North America indicates a warm environment of deposition during the Cambrian period, in agreement with evidence from Morocco. The palaeomagnetically determined palaeolatitudes of the two regions are also in close agreement, so that the difference of approximately 30° between the Lower Palaeozoic poles from the two regions is likely to be due mainly to differences in magnetic declination rather than inclination. Since the Moroccan formations were situated within the Hercynian belt this difference in declination may reflect local rotation of the region during collision of the two continents. An interesting corollary to this hypothesis follows from the shape and orientation of the polar-wander curves of the Gondwanic continents. These indicate that the latter were moving in a predominantly northwestward direction during the Lower & Middle Palaeozoic. In order for the two supercontinents to collide in the Mid-Palaeozoic, Western Laurasia must have been either nearly stationary, or else moving in such a direction, and at such a rate, that its north westward component of velocity was less than that of Gondwanaland during the same period. Between the Cambrian and the Carboniferous periods (a total time of some 250 my) Gondwanaland moved through an angular distance of some 50° in a northwestward direction. This corresponds to an angular velocity of approximately 1° per 50 my, i.e. a linear velocity of 0.2 cm per year in this direction (assuming no change in the radius of the Earth since Lower Palaeozoic times).

If the Moroccan late Precambrian and Lower Cambrian rocks were magnetised during "normal" magnetic intervals, so that the combined North American-Moroccan South pole was situated in the vicinity of 35°N,

120°W then a total north westward movement of some 180° is implied for Western Laurasia between the late Precambrian and the Carboniferous. This corresponds to a linear velocity of approximately 7 cm per year in a northwestward direction, so that clearly the two supercontinents could not have collided. Thus if the above hypothesis is valid, the Moroccan late Precambrian and Lower Cambrian formations must have been magnetised during "reversed" magnetic intervals, so that the South pole was situated in the vicinity of 35°S, 60°E as indicated in Fig 8.4. The direction of movement of Western Laurasia is then reversed over much of the Lower Palaeozoic, and collision becomes possible.

The poles plotted in Figs 8.2 and 8.3 are shown in the combined reconstruction of Fig 8.7. To avoid overcrowding, the pole age reference symbols have not been plotted, but the ages of the poles can be found by direct comparison with Figs 8.2 and 8.3. The postulated shapes of the mean polar wander curves are shown schematically for Western Laurasia (white curve) and Gondwanaland (black curve). These curves are separate in the Lower Palaeozoic, and meet in the Mid-Palaeozoic, when the two supercontinents collided. The Upper Palaeozoic and Mesozoic parts of the curves will be discussed in the following sections.

The sequence of Moroccan Precambrian orogenic belts described in chapter 2 requires detailed study before interpretation in terms of plate tectonics is possible. However, according to the above hypothesis they were situated near the leading margin of the spreading North American plate, and may therefore represent 'orthotectonic' orogens (Dewey, 1969).

Finally, it is clear that according to this interpretation the shapes of the Lower and Middle Palaeozoic polar-wander curves from the northern and southern continents are markedly different. This indicates that the most important process operating at this time was continental drift, and if true polar-wander did occur at all, it was only a subsidiary

8.3.2. Upper Palaeozoic

In section 8.2, mention was made of the two alternative Upper Palaeozoic polar-wander paths for Africa shown in Fig 8.1. On the Smith-Hallam reconstruction of Gondwanaland (Fig 8.2) the only pole lying in the immediate vicinity of the African "Lower Permian" pole is the Indian upper Carboniferous to Permian pole, calculated by McElhinny & Briden (1971). This pole is the mean of the Talchir Series pole (Wensink & Klootwijk, 1968) and the Kamthi beds pole (Wensink, 1968). Upper Carboniferous to Permian poles from all other continents lie much closer to the African mean Upper Carboniferous-Lower Permian pole than to the separate Lower Permian pole. The Upper Palaeozoic polar-wander path indicated by the solid line in Figs 8.2.and 8.5 is therefore considered to be more valid than that shown by the broken line. This conclusion is consistent with the lack of geological evidence for an age difference between the formations from which the separate African "Upper Carboniferous" and "Lower Permian" poles were derived (section 3.2).

McElhinny and Briden (1971) preferred the alternative interpretation, shown by the broken line in Figs 8.2 & 8.5, largely because of the close grouping of the Indian & Australian Upper Carboniferous to Permian poles with the African "Lower Permian" pole on their reconstruction. However, on the reconstruction shown in Figs 8.2 & 8.5 these three poles are considerably more scattered. Rotation of these poles was performed by means of a computer map-plotting program, and was subsequently checked by manual rotation on a stereographic net. The discrepancy between these positions and those shown by McElhinny & Briden must therefore be due to either the use of different rotation angles and/or poles, or to an error in the rotation technique of these authors.

8.3.3. Mesozoic

In this section evidence relating to the history of the break-up and dispersal of the fragments of Pangaea, from sources other than palaeomagnetic studies, will be examined first. This evidence will then be compared with palaeomagnetic evidence, derived from a comparison of the new African polar-wander curve with those of the other continents.

(a) Separation of eastern North America from NW Africa

(i) Geological and other evidence

The North Atlantic between eastern North America and NW Africa displays a pattern of magnetic anomalies similar to those observed in other oceans (Heirtzler and Hayes, 1967, Rona et al, 1969). A conspicuous feature of this area is the presence of a distinct boundary between seaward regions in which anomalies are observed, and landward regions, parallel to both coastlines, with hardly any anomalies. The latter regions are some 500 km wide, and have been termed "Magnetic Quiet Zones" (MQZ's). The magnetic anomalies seaward of the MQZ's can be correlated on either side of the Mid Atlantic Ridge (Pitman et al, 1971), according to the Vine-Matthews sea floor spreading hypothesis (Vine & Matthews 1963).

The age of the sediment/basement interface at the western MQZ boundary has been determined from a JOIDES drill hole (No.105) as 155 my i.e. Mid Jurassic (Ewing et al, 1970). This implies that by Mid Jurassic times a basin some 1000 km across had developed between N.America and N.W. Africa. An extrapolation, using the oldest westerly dated anomaly (120my) yields an age of separation of North America from NW Africa of 180 my, i.e. Lower Jurassic. This is consistent with the occurrence of a widespread marine transgression over Morocco during the Lower Lias (Section 6.2.1), followed by a period of tectonic instability. A complete change in the palaeogeography of the region resulted in the development of coastal

basins, in which sedimentation did not become completely marine.until the Callovian (Section 6.2.1). This indicates that final submergence may not have occurred until Mid Jurassic times.

In chapter 6 of this thesis radiometric age determinations were described from extensive dolerite intrusions in South Morocco. The mean age of intrusions in the Anti Atlas region is 183 my, and the general trend of dykes and related tectonic features in this area is NE-SW, i.e. parallel to the local coastline and MQZ. It is therefore suggested that the intrusion of these bodies was related to the initial rifting of North America away from NW Africa during late Triassic-early Jurassic times. The possible relationship between such intrusive features and the early phases of rifting has been suggested by several other workers (e.g. Siedner & Miller, 1968; Coney, 1970, and Behrendt & Wotorson, 1970).

May (1971) has shown that the parallel sets of late Triassic to early Jurassic dolerite dykes in eastern North America, West Africa, and northeastern South America form a radial pattern when the continents are reassembled on a reconstruction similar to that shown in Fig 8.4. The orientations of the Moroccan Lower Jurassic dolerite dykes are in good agreement with this pattern. May interprets the pattern as representing lines of tension in a net of principal stress trajectories, describing a stress field imposed on the continental crust by movements in the upper mantle at the onset of North Atlantic sea floor spreading. At this stage imperfect coupling between the mantle and crust allowed the stress to be distributed over a wide area, and the resultant strain is represented by the dykes and associated intrusives. With the onset of rifting the stress on the continental crust was relieved, and further displacements of the mantle resulted only in the production of new oceanic crust in the rift.

Both of the above lines of evidence therefore indicate that the initial rifting between North America and NW Africa occurred at a time close to the Triassic/Jurassic boundary, and interpretation of the MQZ boundary as a remanent magnetic anomaly implies that by the Mid Jurassic a basin some 1000 km across existed between the two continents. Rona (1969) has identified possible salt diapirs penetrating the sediments of the lower continental rise up to 1300 km seaward of the present NW African coast, indicating the presence of thick evaporite deposits in this region. According to the above evidence these deposits cannot be older than Mid Jurassic (Rona considered them to be late Triassic to early Jurassic), and their existence implies that the basin between North America and NW Africa must have had a limited connection with an external ocean at this time, in order to provide a saline source. The presence of a thick carbonate sedimentary sequence on the Bahama platform, spanning the Tertiary, Cretaceous, and probably a large part of the Jurassic period (Dietz et al, 1970), indicates that this restricted channel may have been situated between North & South America. This would result from the initial opening of the North Atlantic by sinistral rotation of Laurasia about a pivot point in Spain. The thick sequence of Upper Jurassic marine limestones in Moroccan (section 6.2.1) and other NW African coastal basins (Querol, 1966) implies that the restricted channel had opened by Upper Jurassic times. Open ocean must have been present to the west of Morocco during the Cretaceous, since all Cretaceous marine transgressions came from this direction (section 7.1).

(ii) Palaeomagnetic evidence

The African and Western Laurasian polar-wander curves are superimposed on a Bullard reconstruction in Fig 8.4, and as discussed above,

the close grouping of the Lower to Middle Carboniferous poles indicates that these continents occupied the approximate relative positions shown, at this time. Although the Upper Carboniferous and Permian poles from North America and Western Europe lie close to the African Upper Carboniferous pole, Cu, the African Lower Permian pole, Pl is remote from this group. In section 8.3.2. it was shown that data from the other Gondwanic continents are more consistent with the African mean pole, Cu - Pl, than with the separate poles, Cu and Pl. However best agreement is obtained with the North American and Western European data by ignoring the African pole, Pl, altogether, and drawing the polar wander curve direct from Cu to the Triassic pole, Tr. This interpretation may be considered as equally valid, since the African pole Pl was derived from only one formation (the Tanzanian Eca redbeds), and only four sites were sampled.

If this interpretation is accepted, then the African, North American and Western European polar-wander curves are practically coincident up to the Triassic, and the three Triassic poles are distributed at intervals along the mean curve (Fig 8.4). This distribution may reflect age differences in the three poles, the African pole being younger than the North American pole, which in turn is younger than the Western European pole, but geoldgical evidence for the age of these poles does not support this suggestion.

The Western European mean Triassic pole is derived from three sedimentary and one volcanic formation, and Van Andel & Hospers (1966) and Hospers (1967) consider that the mean direction of magnetic remanence of the sedimentary formations may contain an inclination error. Using a method of triangulation, in which inclination of magnetic remanence is ignored, they calculate a mean pole position from the intersection of

Palaeomeridians. Their Eurasian Triassic pole position (64S, 38W) coincides almost exactly with the North American Triassic pole plotted in Fig 8.4, after appropriate rotation. Triassic sedimentary formations from North America are also suspected of containing inclination errors (Creer, 1970a), and the North American Triassic pole plotted in Fig 8.4 is therefore calculated exclusively from igneous formations.

The position of the European and North American Triassic poles to the north of the African pole cannot be interpreted in terms of continental movement in any meaningful way. Superimposition of these poles requires either considerable overlap of the continents, or else large-scale E-W movements (the "Tethys shear" of some authors, e.g. Van Hilten, 1964, de Boer, 1965 & Irving, 1967) for which there is little geological evidence. The discrepancies in the Triassic pole-positions plotted in Fig 8.4 are represented as differences in palaeoisoclines in Fig 8.8. If Van Andel & Hosper's Eurasian Triassic pole, derived by triangulation, is used instead of the pole listed in Table 8.2, then the palaeolatitudinal difference between Eurasia & Africa is reduced to less than 10°, and lies within the range of experimental error of the latitude determinations. The continents may therefore have maintained the relative positions shown in Fig 8.4 until Triassic times, in agreement with the geological evidence described in the previous section.

The relative positions of the North American and African Jurassic poles, compared with those of the Triassic poles (Fig 8.4), are consistent with the opening of the North Atlantic by a sinistral rotation of North America away from Africa, as indicated by geological evidence. The reconstruction obtained by superimposing the Jurassic poles is shown in Fig 8.9, in which the initial opening of the restricted Atlantic basin in the vicinity of the Bahamas is evident. Again in agreement with

geological evidence, the palaeomagnetic data indicate that by Cretaceous times the North Atlantic had developed from a restricted sea into an extensive ocean basin (Fig 8.10).

The reconstructions shown in Figs 8.9 and 8.10 indicate the presence of a wide sea (the "Tethys") between Africa and Europe during the Jurassic and Cretaceous. Although the African poles are reliable, those from Europe are more dubious. Out of a total of thirteen studies on Eurasian Jurassic formations outside the Alpine belt only three have been subjected to adequate stability tests. The mean Cretaceous pole plotted in Fig 8.4 was derived from these three formations, but since two of them (both from Spitzbergen) are highly scattered, with magnetic declinations some 180° apart, the reliability of this pole is questionable. The European Cretaceous pole is better defined from a total of seven formations, and evidence for the existence of the Tethys sea during the Cretaceous is therefore more reliable. Geological evidence concerning the development of this sea in the Atlas region has recently been summarised by Kanes & Conolly (1971). It was in this sea that the sediments now forming the Rif-Baetic-Alpine belt were deposited prior to their deformation and uplift during the Tertiary orogenies. The intense folding and thrusting in this belt was probably due to relative motion between the African and Eurasian plates, involving a net northward movement of Africa.

(b) Separation of South America from Africa

(i) Geological evidence

There is now a considerable body of geological evidence supporting the former juxtaposition of South America and Africa according to the reconstruction shown in Figs 8.2 and 8.5 (Smith & Hallam, 1970). Of particular importance are several transverse structures, e.g. an age-province

boundary connecting West Africa with NE Brazil (Hurley et al, 1967), an E-W Precambrian geosyncline, linking the Bahia region of Brazil with Gabon (Allard & Hurst, 1969), and the late-Palaeozoic to early Mesozoic "Gondwanide" fold belt, linking South Africa with SE South America (Du Toit, 1937). A continental connection across at least part of the South Atlantic until Middle Cretaceous times is implied by the existence of identical species of ostracods in late Jurassic and early Cretaceous deposits of Brazil and West Africa (Krommelbein and Wenger, 1966; and McKenzie and Hussainz, 1968).

On the basis of detailed studies of ammonite faunas Reyment (1969) considers the fracture between Africa and South America to have grown simultaneously from the north and south. He has shown that there was no exchange of ammonites between the north and South Atlantic during the Upper Albian and Lower Turonian (Mid Cretaceous), but that by Upper Turonian times exchange had occurred. He concludes that final separation of the two continents took place in late Lower Turonian times (approximately 90 my ago).

Further evidence relating to the date of separation of South America from Africa has been deduced from a study of the Benue trough (Wright, 1968), a NE-SW structure situated in West Africa on the bend between the E-W and N-S trending coastlines. Wright considers that as South America and Africa were wedged apart from the south, they remained connected along the present E-W coastal segment of Africa, so that the African continental plate was subjected to slight, but increasingly significant distortion. He suggests that the Benue trough and its sediment filling of Mid Albian to Senonian deposits, originated as a tensional graben system, resulting from partial relief of the distorting stresses. When Africa and South America finally separated the southern half of Africa tended to swing back so that the hitherto stretched Benue trough region was

transformed into a minor compressional belt. The sediments in this trough were folded in the Upper Senonian, indicating that the final closure of the trough, and separation of Africa from South America probably occurred approximately 80 my ago. This is slightly younger than Reyment's estimate. Available sea-floor spreading data indicates that dispersal was definitely in progress by Late Cretaceous times.

(ii) Palaeomagnetic evidence

The South American and African polar-wander curves are superimposed on a Bullard reconstruction in Fig 8.5. These two curves follow approximately parallel paths from the Lower Palaeozoic through to the Triassic, and the South American mean Upper Carboniferous to Lower Permian pole is in slightly better agreement with the African mean Upper Carboniferous to Lower Permian pole than with the separate Upper Carboniferous pole.

The South American mean Upper Carboniferous to Lower Permian pole was derived from four formations, the Argentinian redbeds, the Piaui Formation (Creer, 1965), and the Paganzo formation at Los Colorados and Huaco Gorge (Creer et al, 1969). Creer (1970a) has calculated separate Upper Carboniferous and Lower Permian poles for South America, taking into account new data from the Taiguati and Piaui formations (Creer 1970b) and the Argentinian La Colina basalt (Embleton, 1970). However both of these poles lie on the curve plotted in Fig 8.5, after rotation, and so do not alter the above conclusions.

The South American Permo-Triassic pole plotted in Fig 8.5 was derived exclusively from igneous formations of Lower Triassic, possibly Upper Permian age. Poles derived from sedimentary formations of the same age are systematically displaced away from this pole, and may therefore contain inclination errors.

The angular difference of some 15° between the South American and African Triassic poles is similar to that between the Eurasian and African poles. It is comparable with the range of uncertainty in the two pole determinations (A_{95} of 10° and 5° respectively) and may therefore be attributed to experimental error. On the Bullard reconstruction of these continents plotted in Fig 8.8, this difference is shown to represent a rotational error of approximately 16° between South America and Africa.

The South American Jurassic pole-position plotted in Fig 8.5 is derived from only one formation, the Chon Aike lavas (Valencio and Vilas, 1970), and is not supported by results from Kimmeridgean sediments (one site) exposed in Neuquen province (Creer, 1962). Its reliability is therefore uncertain, and the difference between this pole and the reliable African Jurassic pole may not be significant.

Out of a total number of eight palaeomagnetic studies on South America Cretaceous rocks, only one, that on the Serra Geral formation of southern Brazil (Creer, 1962) has included comprehensive stability tests. Consequently the South American Cretaceous pole plotted in Fig 8.5 is subject to similar uncertainties to the Jurassic pole.

The South American and African Jurassic and Cretaceous poles have been superimposed to yield the reconstructions shown in Figs 8.9 and 8.10 respectively. Reconstructions of this type determine the palaeolatitudes and relative orientations of the continents, but not the palaeolongitudes. Consequently the relative longitudinal positions of the continents in these diagrams are arbitrary. However both diagrams indicate the presence of an opening between the southern parts of South America and Africa, and the Triassic results (Fig 8.9) suggest that this opening might have begun as early as Triassic times.

The geological evidence described in the previous section implies a continental connection between Brazil and West Africa until Mid-Cretaceous times, but it is possible that the initial opening between the two continents commenced further to the south in the Triassic. Because of the uncertainty in the South American pole determinations this suggestion is only tentative, but it may be significant that consistent differences between Triassic, Jurassic and Cretaceous poles from the two continents all imply an opening rather than an overlap of the continents.

The South American and African Tertiary poles are situated some 50° apart, and this indicates that the two continents were widely separated by this time.

(c) Separation of Eastern Gondwanaland (India, Antarctica and Australia) from Africa

(1) Geological evidence

Geological evidence for the former positions of India, Australia and Antarctica relative to Africa is more ambiguous than that for South America. This evidence has recently been discussed by Smith & Hallam, (1970), and Tarling (1971).

The oldest post-Palaeozoic marine sediments between Eastern Gondwanaland and Africa range in age from late Triassic/early Jurassic in North Kenya and North Madagasgar to Upper Liassic/Mid Jurassic in Tanzania and Central Madagasgar (Arkell, 1956). Because of this, several authors (e.g. King, 1959), have suggested that the initial split between Eastern Gondwanaland and Africa occurred in the late Triassic, and spread down the east coast of Africa to reach southern Africa in Neocomian (Lower Cretaceous) times. However Dingle and Klinger (1971a) have recently reported marine Upper Jurassic sediments from the Knysna Outlier of the Cape Province,

South Africa. They conclude (Dingle & Klinger, 1971b) that the southern part of the East Gondwana/Africa split cannot be younger than early Upper Jurassic.

(ii) Palaeomagnetic evidence

The polar-wander curves for Africa, India and Australia are superimposed on a Smith-Hallam reconstruction in Fig 8.6. Two poles from Antarctica are also plotted. As discussed in section 8.3.2, the Australian mean Upper Carboniferous to Permian pole, calculated from six separate Kiaman poles (McElhinny & Luck, 1970) agrees better with the African mean Upper Carboniferous to Lower Permian pole than with the separate Lower Permian pole. However the Indian Upper Carboniferous to Permian pole lies some 30° to the east of these two poles. The Indian pole is derived from two apparently reliable determinations which are in reasonable agreement with each other. The discrepancy with the Australian and African data may therefore represent actual movement of India relative to the rest of Gondwanaland at this time, but the lack of Permian compressional structures between these continents makes this interpretation doubtful.

This situation is reversed for the Triassic data. The Indian mean Permo-Triassic pole, derived from the Godavary Valley Kamthi sandstones (Verma and Bhalla, 1968), the Parsora formation (Bhalla and Verma, 1969), the Mangli Beds, and the Pachmarhi Beds (Wensink, 1968) lies fairly close to the African mean Triassic pole, whereas the Australian Triassic pole is remote from the latter. Thus Australia may have begun to drift away from the rest of Gondwanaland during the Triassic, but this suggestion is contrary to the interpretation of sea floor magnetic anomalies by Le Pichon (1968), who considers that Australia did not separate from Antarctica until anomaly 18 time (Late Eocene).

All Gondwanic Jurassic poles except that from Antarctica are significantly different from the African Jurassic pole. This suggests that the break-up and dispersal of Gondwanaland proceeded during the Jurassic period, but that Antarctica remained close to Africa through to Mid-Jurassic times, in agreement with the geological evidence described above.

In the preceding sections it has been observed that although the Laurasian polar-wander curves agree well with the African Upper Carboniferous pole, the Gondwanic polar-wander curves (with the exception of India) are in better agreement with the African mean Upper Carboniferous to Lower Permian pole. Clearly these two alternatives cannot both be correct, and relative movement between Laurasia and Gondwanaland during the Upper Carboniferous and Lower Permian must therefore be suspected. Since the principal phases of folding in the Hercynian orogenic belt between these two continents extended well into the Permian, it is possible that the collision between them was complex, and involved a rebound during Lower Permian times.

Finally it may be remarked that although the positions of the four circum-Atlantic continents in the Jurassic and Cretaceous, shown in Figs 8.9 and 8.10 are compatible with each other, the positions in the Triassic (Fig 8.8) are not. As discussed above, this may be due to errors in the pole determinations, but an alternative possibility is that the form of the geomagnetic field departed from that of an axial geocentric dipole during this period. In a recent analysis of all available reliable Permo-Triassic data, Briden et al (1970) concluded that to a first approximation the Permo-Triassic geomagnetic field can be represented by that of a geocentric dipole. However they consider that the observed second-order departures from this field cannot easily

be accounted for by errors in the palaeomagnetic data, and the possibility of multipole components must therefore be considered. Briden et al do not comment on the timing of the appearance of these multipole components, and the suggestion is made here that their occurrence immediately prior to the break-up and dispersal of the continents may be highly significant.

Analyses of the geomagnetic field have not yet been performed for other geological periods, but since realistic continental reconstructions based on palaeomagnetic data, and agreeing with geological and palaeogeographical evidence, can be made for most periods, it seems probable that if non-dipole components did exist, they were much smaller than in Permo-Triassic times. A possible connection between the build-up of stress in the Upper Mantle prior to continental fragmentation, and the presence of non-dipole or non-axisymmetric fields at this time implies effective core/mantle coupling. This could result from the presence of relatively long-lived irregularities in the figure of the core/mantle interface.

8.4. Polarities of Moroccan palaeomagnetic results

8.4.1. Palaeozoic

Various attempts have been made (e.g. Khramov et al, 1965, and Khramov, 1967) to correlate field reversals detected at different localities by palaeomagnetic studies on Lower Palaeozoic rocks. However the small number of reliable Lower Palaeozoic results so far available makes it extremely difficult to erect a meaningful polarity time-scale for this interval.

Results from the Middle and Upper Palaeozoic are more reliable, and Khramov has suggested the occurrence of a predominantly reversed magnetic interval extending over some 50 my from Mid-Devonian to Mid-Visean times. This is in agreement with the reversed polarity observed in the Moroccan Upper Devonian formation (chapter 4 of this thesis).

8.4.2. Mesozoic

Several attempts have been made to establish a world-wide polarity time-scale for various parts of the Mesozoic period (e.g. Burek, 1970, and Helsley and Steiner, 1969), and recently McElhinny & Burek (1971) have proposed a polarity time-scale for the whole of the Mesozoic, based on a synthesis of palaeomagnetic results from all continents. Their results suggests the occurrence of a predominantly normal period (the "Graham" interval) extending from the Upper Triassic (about 200my ago) to the Upper Jurassic (about 150 my). This was preceded by a period of some 30 my during which regular polarity changes occurred, and during the Middle Triassic there were at least two normal and two reversed periods.

Of the three Moroccan Triassic formations studied, two were definitely of Middle Triassic age, and one of these had a normal polarity (the Ait Aadel dolerites), and the other a reversed polarity (the Titchka sediments) in agreement with McElhinny & Burek's proposed mixed polarity interval. The third Moroccan Triassic formation (the Issaldian dolerites) was suspected of having suffered remagnetisation as a result of weathering during Upper Tertiary times. Since both the Middle Triassic and the Upper Tertiary periods correspond to intervals of mixed polarity, the polarity of the Issaldian dolerites (normal) is inconclusive.

The three Moroccan Jurassic formations all had normal polarities, in agreement with the suggested "Graham" interval of normal polarity covering most of the Jurassic period.

According to McElhinny & Burek's analysis the "Graham" interval was followed by another period of mixed polarity, extending from the Upper Jurassic to the Lower Cretaceous. The Moroccan Lower Cretaceous Central Atlas sediments, of normal polarity, correspond to this interval.

Thus the magnetic polarities of the one Devonian and seven Mesozoic Moroccan formations described in this thesis are in general agreement with McElhinny & Burek's proposed polarity time-scale.

8.5 Conclusions

It has been shown in this chapter that the new Moroccan Late Precambrian and Lower Cambrian palaeomagnetic pole-positions are more consistent with reliable Lower Palaeozoic poles from North America than ones from Southeast Africa, when the two continents are plotted on a Bullard-type reconstruction. It is concluded that a small part of Northwest Africa, including Morocco, may originally have been separate from the rest of the continent, and may have been attached to Eastern North America. Collision between Northwest Africa and Eastern North America probably occurred during the Carboniferous, resulting in the formation of the Hercynian fold-belt between the two continents, and subsequent separation may have taken place along a slightly different line, so that Morocco was left attached to the African continent.

Radiometric dating results from Moroccan igneous intrusions paralleling the coastline yield a mean age of 183 my. Other evidence suggests that the initial rifting between North America and Northwest Africa occurred at this time, and it is suggested that the intrusion of the Moroccan igneous bodies was directly related to this event. Palaeomagnetic results from the Moroccan Cretaceous formation indicate a gradually widening of the North Atlantic during the course of the Mesozoic. There is no significant difference between mean Triassic, Jurassic and Cretaceous poles from Morocco and those from Southeast and Central Africa, and it is concluded that no significant post-Triassic relative tectonic movement has occurred between NW and SE Africa.

REFERENCES

Allard, O., & V.J. Hurst, 1969. Brazil-Gabon geologic link supports continental drift. Science, V. 163, pp 528-532

Arkell, W.J., 1956. Jurassic geology of the world. New York, Hafner Publishing Co., 806p.

Behrendt, J.C. and C.S. Wotorson, 1970. Aeromagnetic and gravity investigations of the coastal area and continental shelf of Liberia, West Africa, and their relation to continental drift. Geol. Soc. Amer. Bull., vol 81, p3563-3574.

Bhalla, M.S. and Verma, R.K. 1969. Palaeomagnetism of the Triassic Parsora Sandstones from India. Phys. Earth Planetary Interiors, 2 pp138-146.

Briden, J.C. 1967a. A new palaeomagnetic result from the Lower Cretaceous of east-central Africa. Geophys. J, 12, 375-380.

Briden, J.C. 1967b. Recurrent continental drift of Gondwanaland. Nature, Vol.215, No. 5108, pp 1334-1339.

Briden, J.C., 1968. Palaeomagnetism of the Ntonya ring structure, Malawi. J. Geophys. Res., 73, 725-733.

Briden, J.C., A. Gilbert Smith & J.T. Sallomy, 1970. The geomagnetic field in Permo-Triassic time. Geophys. J.R. astr. Soc., 23, pp 101-117.

Brock, A. 1967. Palaeomagnetic result from the Hook intrusives, Zambia. Nature, 216, 359-360.

Brock, A. 1968., Palaeomagnetism of the Nuanetsi igneous province and its bearing upon the sequence of Karroo igneous activity in southern Africa. J. Geophys. Res., 73, 1389-1397.

Bullard, E.C., J.E. Everitt, & A.G. Smith, 1965. The fit of the continents around the Atlantic. Phil. Trans. Roy. Soc. London, Ser A., 258, pp41-51.

Burek, P.J. 1970.
Amer. Assoc. Petr. Geol. Bull., 54, 1120.

Choubert, G., 1963. Histoire géologique du Précambrian de l'Anti Atlas. Notes Mém. Serv. Géol. No. 162. Éditions du Serv.Géol. du Maroc.

Creer, K.M., 1962a. Palaeomagnetic data from South America. J. Geomagn. Geoelect., 13, pp154-165.

Creer, K.M. 1962b. Palaeomagnetism of the Serra Geral formation. Geophys. J. Roy. Astro. Soc. 7., pp1-22.

Creer, K.M. 1965. Palaeomagnetic data from the Condwanic continents. Phil. Trans. Roy. Soc. London, Ser A, 258, pp27-40.

Creer, K.M. 1967. Palaeomagnetism of some Lower Palaeozoic South American rocks. UNESCO/IUGS Symposium on Continental Drift, Montevideo.

Creer, K.M. 1968. Palaeozoic palaeomagnetism. Nature 219, p246.

Creer, K.M. 1969. Comments on paper by J.L. Roy, N.D. Opdyke & E. Irving. Further palaeomagnetic results from the Bloomsburg formation. J. Geophys. Res., 74, pp3299-3302.

Creer, K.M., 1970a. A review of palaeomagnetism. Earth-Sci. Rev., 6, pp369-466.

Creer, K.M., 1970b. A palaeomagnetic survey of South American rock formations. Phil. Trans. Roy. Soc. London A., 267, pp457-558.

Creer, K.M., B.J.J. Embleton & D.A. Valencio., 1969. Permo-Triassic and Triassic palaeomagnetic data for South America. Earth Planetary Sci. Letters, 8. pp173-178.

de Boer, J., 1965. Palaeomagnetic indications of megatectonic movements in the Tethys. J. Geophys. Res., 70, pp931-944.

de Boer, J., 1968. Palaeomagnetic differentiation and correlation of the Late Triassic volcanic rocks in the central Appalachians (with special reference to the Connecticut Valley). Geol. Soc. Amer. Bull., Vol.79, No. 5, pp609-626.

Dewey, J.F., 1969. Continental margins: A model for conversion of Atlantic type to Andean type. Earth planet. Sci. Letters, 6, 189-197.

Dewey, J.F. & Horsfield, B., 1970. Plate tectonics, orogeny and continental growth. Nature, 225, pp521-525.

Dietz, R.S., J.C. Holden and W.P. Sproll., 1970. Geotectonic evolution and subsidence of the Bahama platform. Geol. Soc. Amer. Bull, Vol.81, pp1915-1928.

Dingle, R.V. & H.C. Klinger, 1971a. Trans. Geol. Soc. South Africa (in press)

Dingle, R.V. and Klinger, 1971b. Significance of Upper Jurassic sediments in the Knysna Outlier (Cape Province) for timing of the breakup of Gondwanaland. Nature (Physical Science) Vol.232, p37-38.

Du Toit, A.L., 1937. Our wandering continents. (Oliver & Boyd, Edinburgh & London).

Embleton, B.J.J., 1970. Resultadas palaeomagneticas del Basalto basal de la Formacion La Colina, Paganzo medio, Argentina. Rev. Assoc. Geol. Arg., in press.

Ewing, J., et al, 1970. Deep sea drilling project : Leg 11. Geotimes, Vol. 15, No. 7, pp14-16.

Gough, D.I. & A. Brock,,1964. The palaeomagnetism of the Shawa ijolite. J. Geophys. Res., 69, 2489-2493.

Gough, D.I. & N.D. Opdyke, 1963. The palaeomagnetism of the Lupata alkaline volcanics. Geophys. J., 7, 457-468.

Gough, D.I., N.D. Opdyke & M.W. McElhinny, 1964. The significance of palaeomagnetic results from Africa. J. Geophys. Res., 69, 2509-2519.

Graham, J.W., 1949. The stability and significance of magnetism in sedimentary rocks. J. Geophys. Res., 54, pp131-167.

Graham, J.W., 1954. Rock magnetism and the Earth's magnetic field during Palaeozoic time. J. Geophys. Res., 59, pp215-222.

Graham, J.W., 1956. Palaeomagnetism and magnetostriction. J. Geophys. Res., 61, pp735-739.

Graham, K.W.T., 1961. Palaeomagnetic studies on some South African rocks, Ph.D. thesis, University of Cape Town.

Graham K.W.T., & A.L. Hales, 1961. Preliminary palaeomagnetic measurements on Silurian sediments from South Africa. Geophys. J., 5, 318-325.

Grekoff, N., 1963.
Rev. Inst. Franc. Petrol. 18, p1709.

Hailwood, E.A., 1968. A palaeomagnetic study of the Middle Atlas region of Morocco. M.Sc. thesis, University of Newcastle upon Tyne.

Hallam, A., 1969. Re-evaluation of the palaeogeographic argument for an expanding Earth. Nature, 232 pp180-182.

Hamilton, W., 1970. The Uralides and the motion of the Russian & Siberian platforms. Bull. Geol. Soc. Amer. 81, p2553.

Heirtzler, J.R. & D.R. Hayes, 1967. Magnetic boundaries in the North Atlantic Ocean. Science, V.157, p185-187.

Helsley, C.E., 1965. Palaeomagnetic results from the Middle Cambrian of northwest Africa (abstract). Trans. Am. Geophys. Union, 46, 67.

Helsley, C.E. & M.B. Steiner, 1969.
Earth Planet. Sci. Lett., 7, 325.

Holmes, A., 1965. Principles of Physical Geology. (Thomas Nelson, London, 1288p).

Hospers, J., 1967. Review of palaeomagnetic evidence for the displacement of the continents. In: S.K. Runcorn (Editor), Mantles of the Earth & Terrestrial Planets. Interscience, London, pp331-349.

Howell, L.G., & J.D. Maritinez, 1957. Polar movement as indicated by rock magnetism. Geophysics, Vol.22, p384-397.

Hurley, P.M., F.F.M. de Almeida, G.C. Melcher, V.G. Cordani, J.R. Rand, K. Kawashita, P. Vandoros, W.H. Pinson & H.W. Fairburn, 1967. Test of continental drift by comparison of radiometric ages. Science, v.157, pp495-500.

Irving, E., 1964. Palaeomagnetism, and its application to geological and geophysical problems. John Wiley & Sons, London.

Irving, E., 1966. Palaeomagnetism of some Carboniferous rocks from New South Wales and its relation to geological events. J. Geophys. Res., 71, 6025-6051.

Irving, E., 1967. Palaeomagnetic evidence for transcurrent movements along Tethys. Aspects of Tethyan Biogeography (eds. C.G. Adams & D.V. Ager), Systematics Assoc. Publ. No. 7, 59-78.

Kanes, W.H., and J.R. Conolly, 1971. Rifting of Europe from Africa : Triassic to Jurassic history of the Moroccan Atlas Mountains. Geol. Soc. Am. Abstracts, p617.

Khramov, A.N., 1967. The Earth's magnetic field in the Late Palaeozoic. Akad.Nauk, SSSR Izv., Earth Phys. Ser., pp86-108.

Khramov, A.N., V.P. Rodionov, & R.A. Komissarova, 1965., in 'The Present & Past of the Geomagnetic Field', 206 (Nauka Press, Moscow).

King, L.C., 1961. The palaeoclimatology of Gondwanaland during the Palaeozoic & Mesozoic eras. Descriptive Palaeoclimatology (ed. A.E.M. Nairn), Interscience, New York, 307-339.

King, L.C., 1962. The Morphology of the Earth. Oliver & Boyd, Edinburgh.

King, P.B., 1959. The evolution of North America. Princeton Univ. Press, 190p.

Krommelbein, K. & R. Wenger, 1966., in Sedimentary basins of the African coast, part 1. (Union Inst. Sci. Geol. Ass. Serv. Geol. Afr., Paris) p193.

Larson, E.E. & F.E. Mutschler, 1971. Anomalous palaeomagnetic pole from isotopically dated Cambro-Ordovician intrusives in Colorado. Geol. Soc. Am. Bull., 82, pp1657-1666.

Luck, G.R., 1970. The palaeomagnetism of some Cambrian and Ordovician sediments from the Northern Territory, Australia. Geophys. J. Roy. Astr. Soc., 20, 31.

May, P.R. 1971. Pattern of Triassic-Jurassic diabase dykes around the North Atlantic in the context of predrift positions of the continents. Geol. Soc. Amer. Bull., v82 pp1285-1292.

McElhinny, M.W., 1970. Palaeomagnetism of the Cambrian Purple Sandstone from the Salt Range, West Pakistan. Earth Planet, Sci. Letters, 8, 149.

McElhinny, M.W., & J.C. Briden, 1971. Continental drift during the Palaeozoic. Earth planet. Sci. Letters., Vol. 10. No.4, pp407-416.

McElhinny, M.W., J.C. Briden, D.L. Jones & A. Brock, 1968. Geological and geophysical implications of palaeomagnetic results from Africa. Rev. Geophys. Vol.6, No.2, pp201-238.

McElhinny, M.W., & P.J. Burek, 1971. Mesozoic palaeomagnetic stratigraphy. Nature, 232, pp98-102.

McElhinny, M.W., & D.L. Jones, 1965. Palaeomagnetic measurements on some Karoo dolerites from Rhodesia, Nature, 206, 921-922.

McElhinny, M.W., & G.R. Luck, 1970. The palaeomagnetism of the Antrim Plateau Volcanics of Northern Australia. Geophys. J. Roy. Astr. Soc., (in press).

McElhinny, M.W., & N.D. Opdyke, 1968. Palaeomagnetism of some Carboniferous glacial varves from central Africa. J. Geophys. Res., 73, 689-696.

McElhinny, M.W. & P.Wellmann, 1969. Polar wandering and sea-floor spreading in the Southern Indian Ocean. Earth Planet. Sci. Latters, Vol.6, No.3, pp198-204.

McKenzie, K.G., & S.U. Hussainy, 1968. Nature, 220, p.806.

Nairn, A.E.M., 1964. Palaeomagnetic measurements on Karroo and post-Karroo rocks, a second progress report. Overseas Geol. Mineral Resources, Gt. Brit., 9,302-320.

Oliveira, A.I., 1956. Handbook of South American Geology (ed.,W.F. Jenks) : Brazil, Mem. Geol. Soc. Amer., 65, 1-62.

Opdyke, N.D., 1964a. The palaeomagnetism of some Triassic redbeds from Northern Rhodesia. J. Geophys. Res., 69, pp2495-2497.

Opdyke, N.D., 1964b. The palaeomagnetism of the Permian redbeds of southwest Tanganyika. J. Geophys. Res., 69, pp2477-2487.

Phillips, J.C. & P.B. Heroy, 1966. Palaeomagnetic results from the Devonian Perry lavas near East-port, Maine. Amer. Geophys. Union, Trans. (abstr), Vol 47, p80.

Pitman, W.C., M. Talwani & J.R. Heirtzler, 1971. Age of the North Atlantic Ocean from magnetic anomalies. Earth. Planet. Sci. Letters, 11. pp195-200.

Querol, R., 1966. Regional geology of the Spanish Sahara, p27-38 in D. Reyre, ed., Sedimentary basins of the African coasts, part 1. Atlantic Coast. Paris, Assoc. African Geol. Surveys, 304p.

Reyment, R.A., 1969. Ammonite biostratigraphy, continental drift and oscillatory transgressions. Nature, 224 pp137-140.

Robertson, W.A., J.L. Roy and J.K. Park, 1968. Magnetism of the Perry formation of New Brunswick and the rotation of Newfoundland. Can. J. Earth. Sci. Vol. 5, p1175-1182.

Roche, A., & B. Leprêtre, 1955. Sur l'aimantation de roches volcaniques de l'Ahaggar. Compt. Rend., 240, 2002-2004.

Rona, P.A., 1969. Possible salt domes in the deep Atlantic off northwest Africa. Nature, V.224, p141-143.

Rona, P.A., J. Brakl &J.R. Heirtzler, 1969. Magnetic anomalies between the Canary and Cape Verde Islands (abs). Am. Geophys. Union. Trans. V.50, p189.

Schneider, E.D., P.R. Vogt & A. Lowrie, 1969. Diapiric structures and magnetic anomalies of the Pre-Cenozoic Atlantic Ocean (abs). Am. Geophys. Union. Trans., V.50, p212.

Siedner, G. & J.A. Miller, 1968. K-Ar age determinations on basaltic rocks from South-west Africa and their bearing on continental drift. Earth. Planet. Sci. Letters., V.4, pp451-458.

Smith, A.G., and A. Hallam, 1970. The fit of the Southern Continents. Nature, Vol.225, No.5228, pp139-144.

Sougy, J., 1962. West African fold belt. Geol. Soc. Amer. Bull., V.73., pp871-876.

Temrazyan, G.P., 1971. Siberian continental drift. Tectonophysics, 11, pp433-460.

Tarling, D.H., 1971. Gondwanaland, Palaeomagnetism and Continental drift. Nature, Vol.229, No.5279, pp17-21.

Thellier, E., & O. Thellier, 1951. Sur la direction du champ magnétique terrêstre, rétrouvée sur des parfois de fours des époques puniques et romaine, á Carthage. Compt. Rend., 233, 1476-1478.

Valencio, D.A., & J.F. Vilas, 1970. Palaeomagnetism of some Middle Jurassic lavas from southwest Argentina. Nature, 225, pp262-264.

Van Andel, S.I. & J. Hospers, 1966., Systematic errors in the palaeomagnetic inclination of sedimentary rocks. Nature, 212. pp891-893.

Van Hilten, D., 1964. Evaluation of some geotectonic hypotheses by palaeomagnetism. Tectonophysics, 1, 1-71.

van Zijl, J.S.V., K.W.T. Graham & A.L. Hales, 1962a. The palaeomagnetism of the Stormberg lavas of South Africa I., Evidence for a genuine reversal of the Earth's magnetic field in Triassic-Jurassic times. Geophys. J., 7, 23-39.

van Zijl, J.S.V., K.W.T. Graham & A.L. Hales, 1962b. The palaeomagnetism of the Stormberg lavas, II, the behaviour of the magnetic field during a reversal. Geophys. J., 7, 169-182.

Verma, R.K., & Bhalla, M.S., 1968. Palaeomagnetism of Kamthi sandstones of Upper Permian age from Godavary valley, India. J. Geophys. Res., 73, pp709-763.

Vine, F.J., & D.H. Matthews, 1963. Magnetic anomalies over oceanic ridges. Nature, V.199, p947-949.

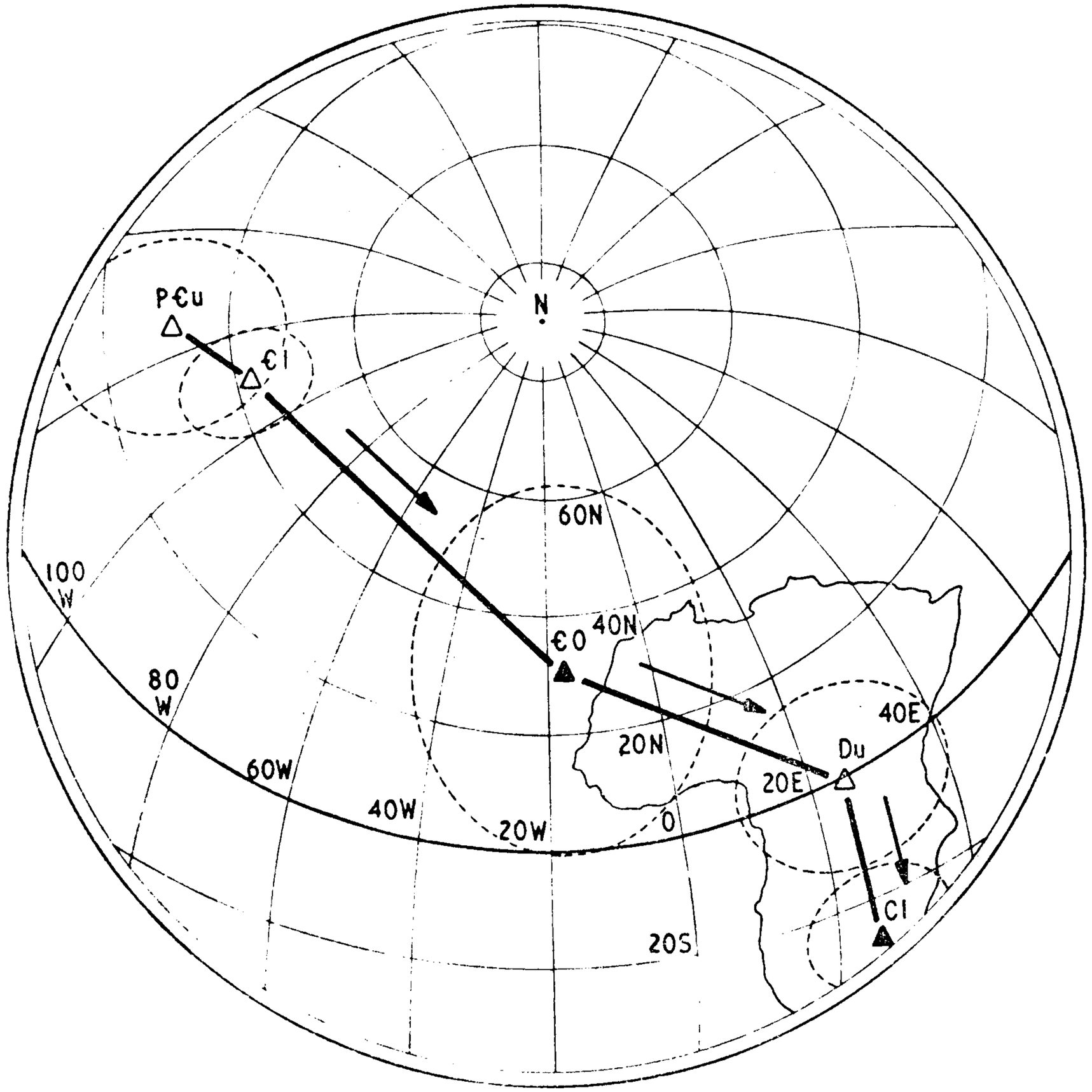
Watkins, N.D., A. Richardson & R.G. Mason, 1968. Palaeomagnetism of the Macaronesian insular region : the Cape Verde Islands. Geophys. J., 16, 119.

Wensink, H., 1968. Palaeomagnetism of some Gondwana Red Beds from Central India, Palaeogeog.Palaeoclim. Palaeoecol. 5, 323.

Wensink, H., & C.T. Klootwijt, 1968. The palaeomagnetism of the Talchir Series of the Lower Gondwana System, Central India. Earth Planet. Sci. Letters, 4, 191.

Wilson, J.T., 1966. Did the Atlantic close and then re-open? Nature, 211, pp676-681.

Wright, J.B., 1968. South Atlantic continental drift and the Benue trough. Tectonophysics, 6, p301-310.



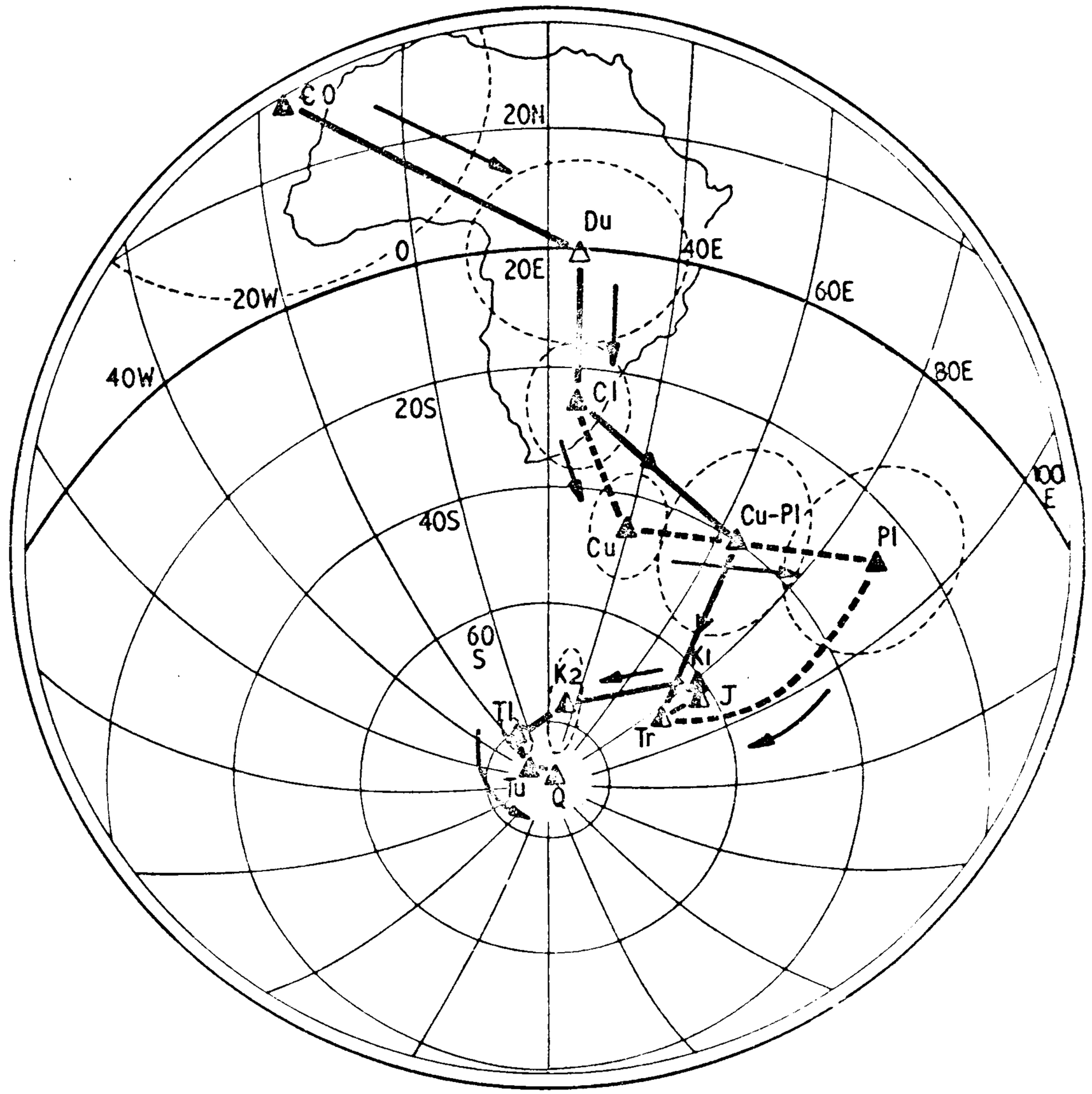


Fig 8.1 African Phanerozoic polar-wander curve

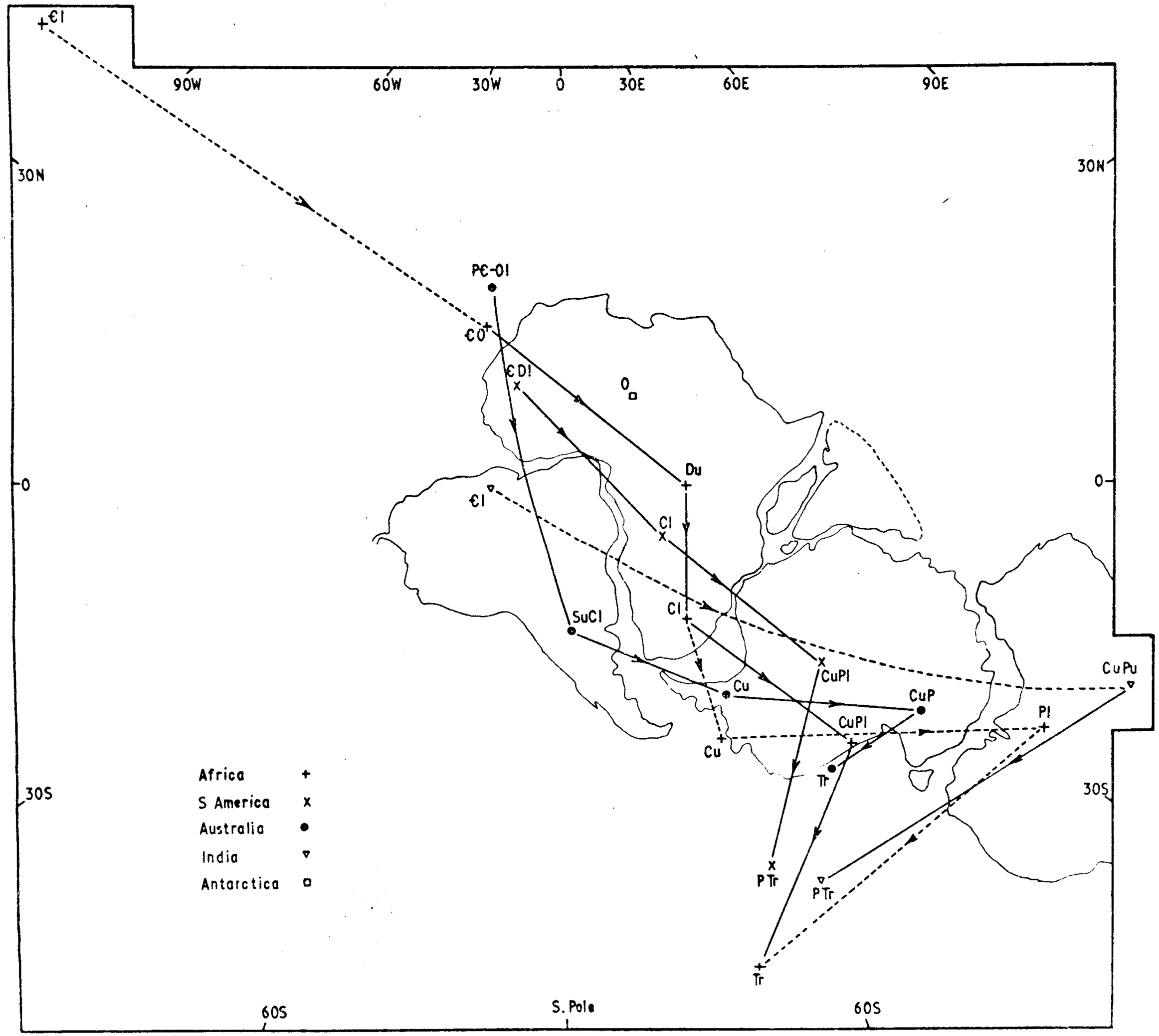


Fig 8.2 Mean Palaeozoic pole-positions for the Gondwanic continents, plotted on a Smith-Hallam reconstruction (stereographic projection)

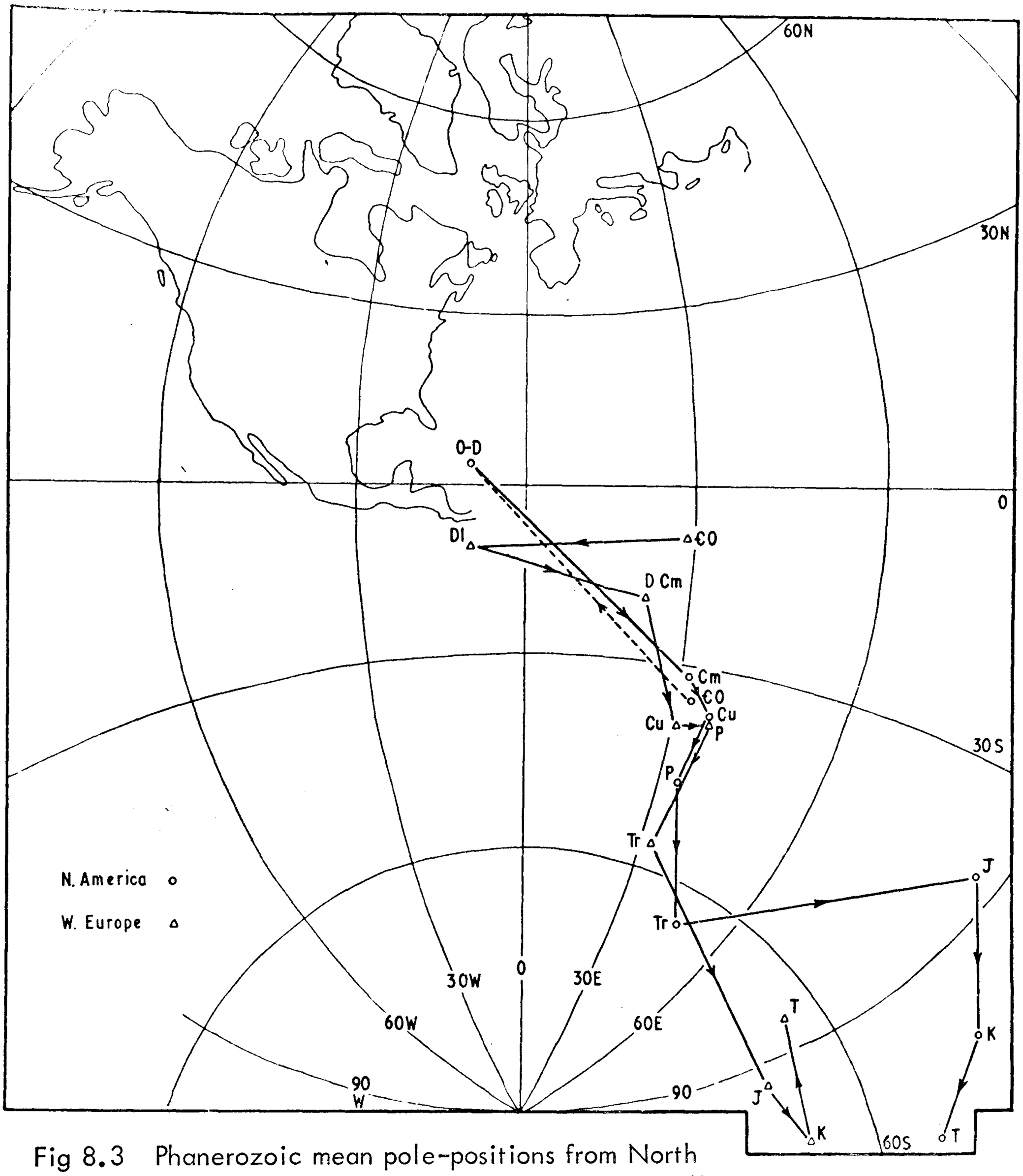


Fig 8.3 Phanerozoic mean pole-positions from North America & Western Europe, plotted on a Bullard reconstruction (stereographic projection)

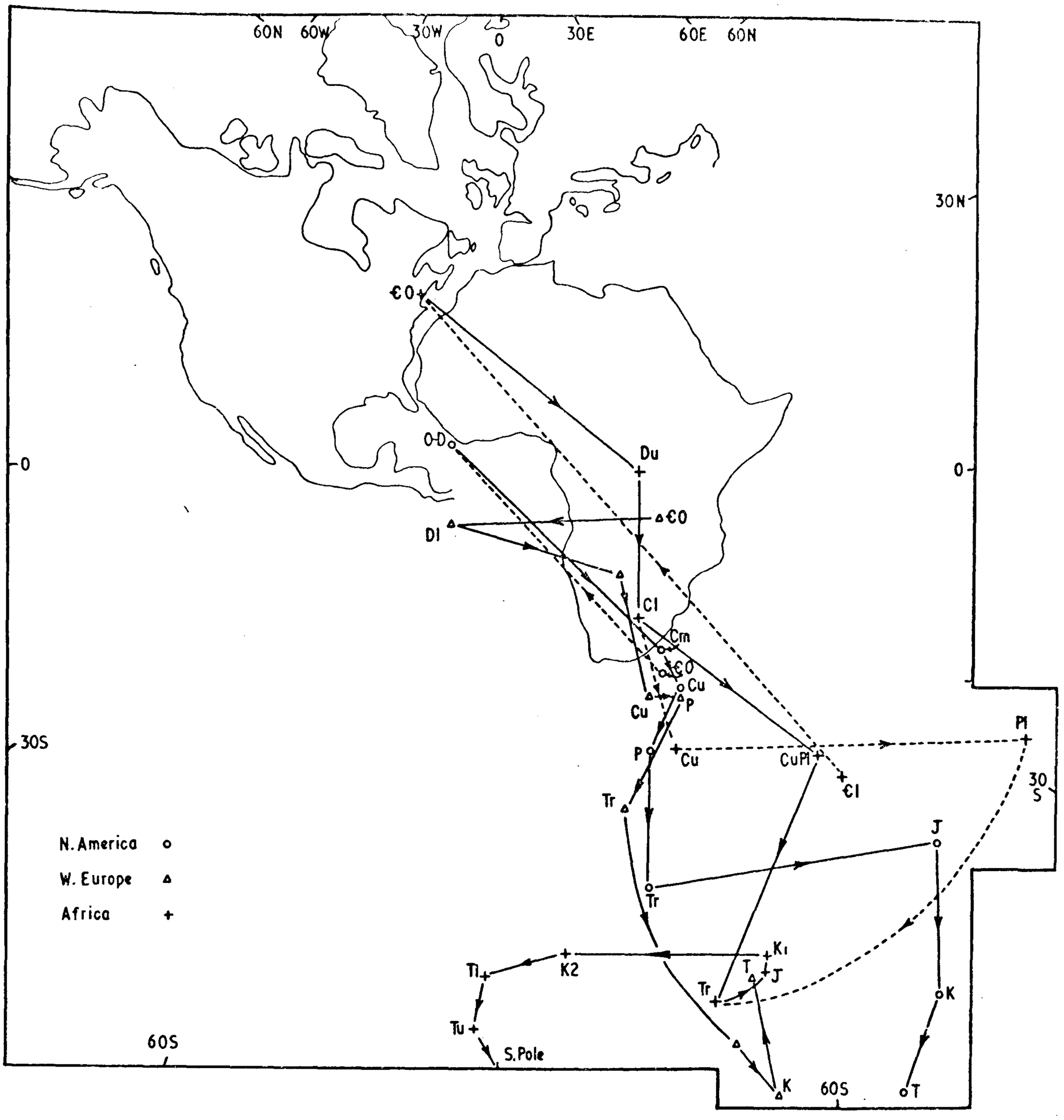


Fig 8.4 Superimposition of African & Western Laurasian polar-wander curves on a Bullard reconstruction (stereographic projection)

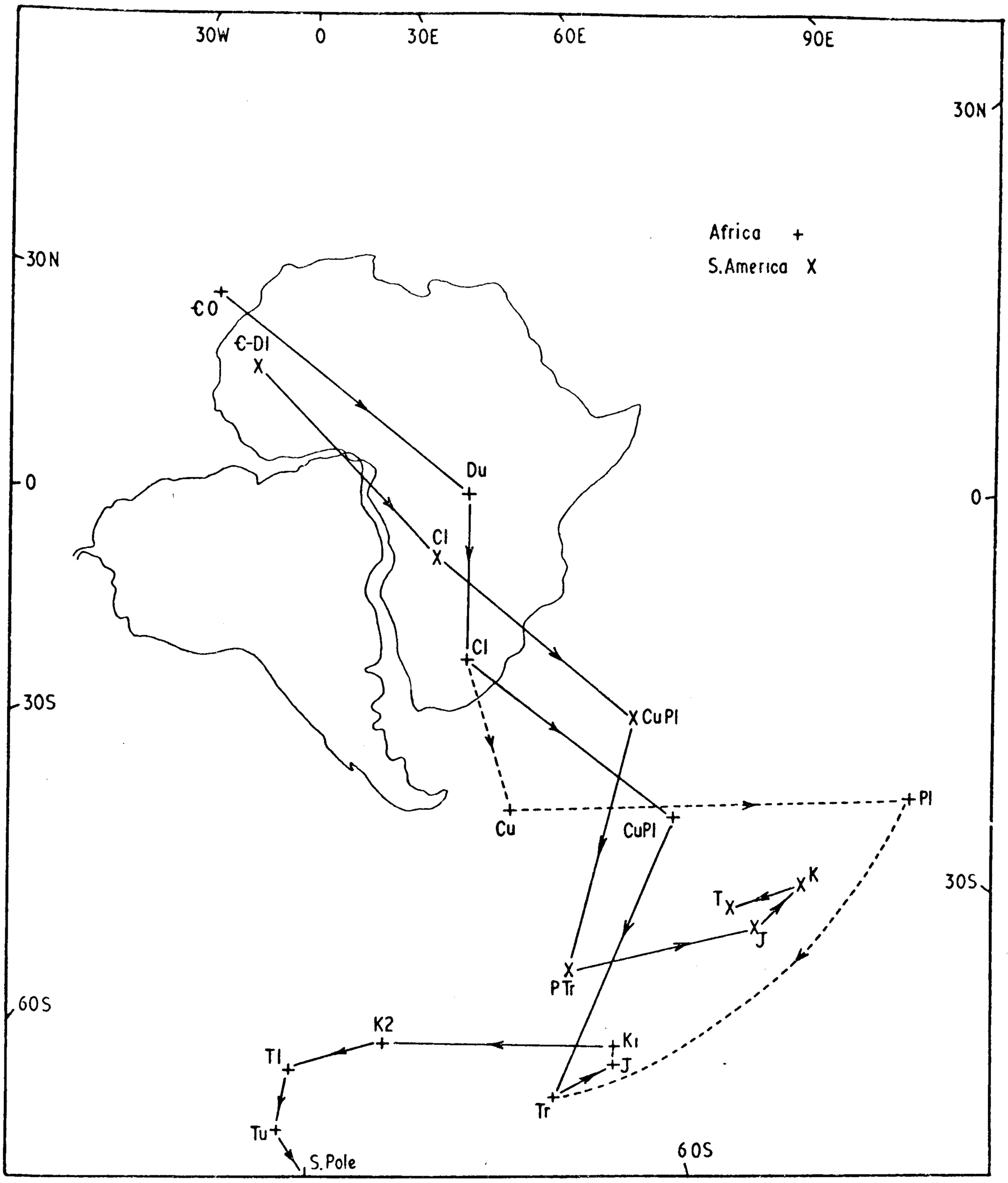


Fig 8.5 Superimposition of African & South American polar-wander curves on a Bullard reconstruction

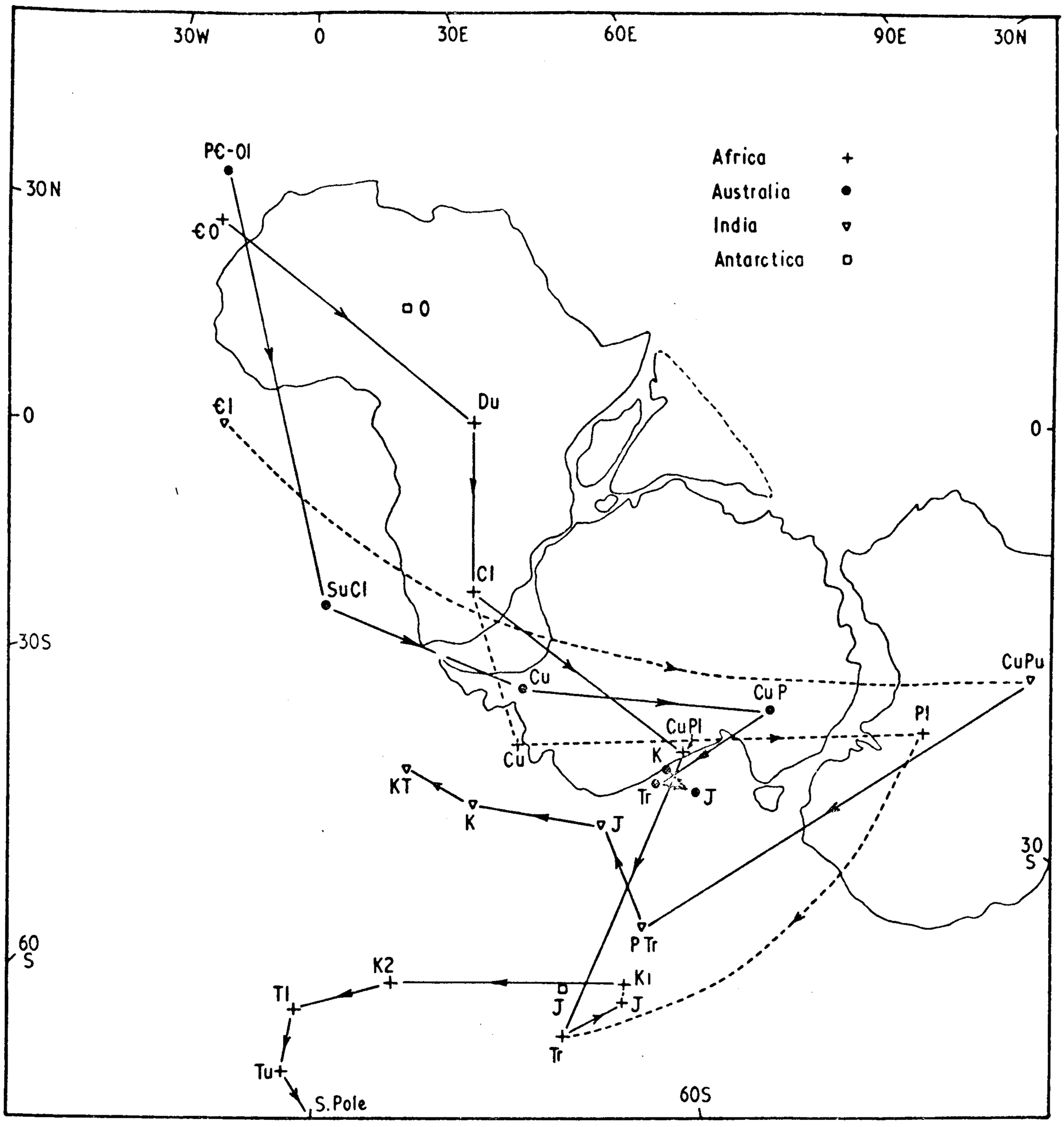


Fig 8.6 Superimposition of African & Eastern Gondwanaland polar-wander curves on a Bullard reconstruction

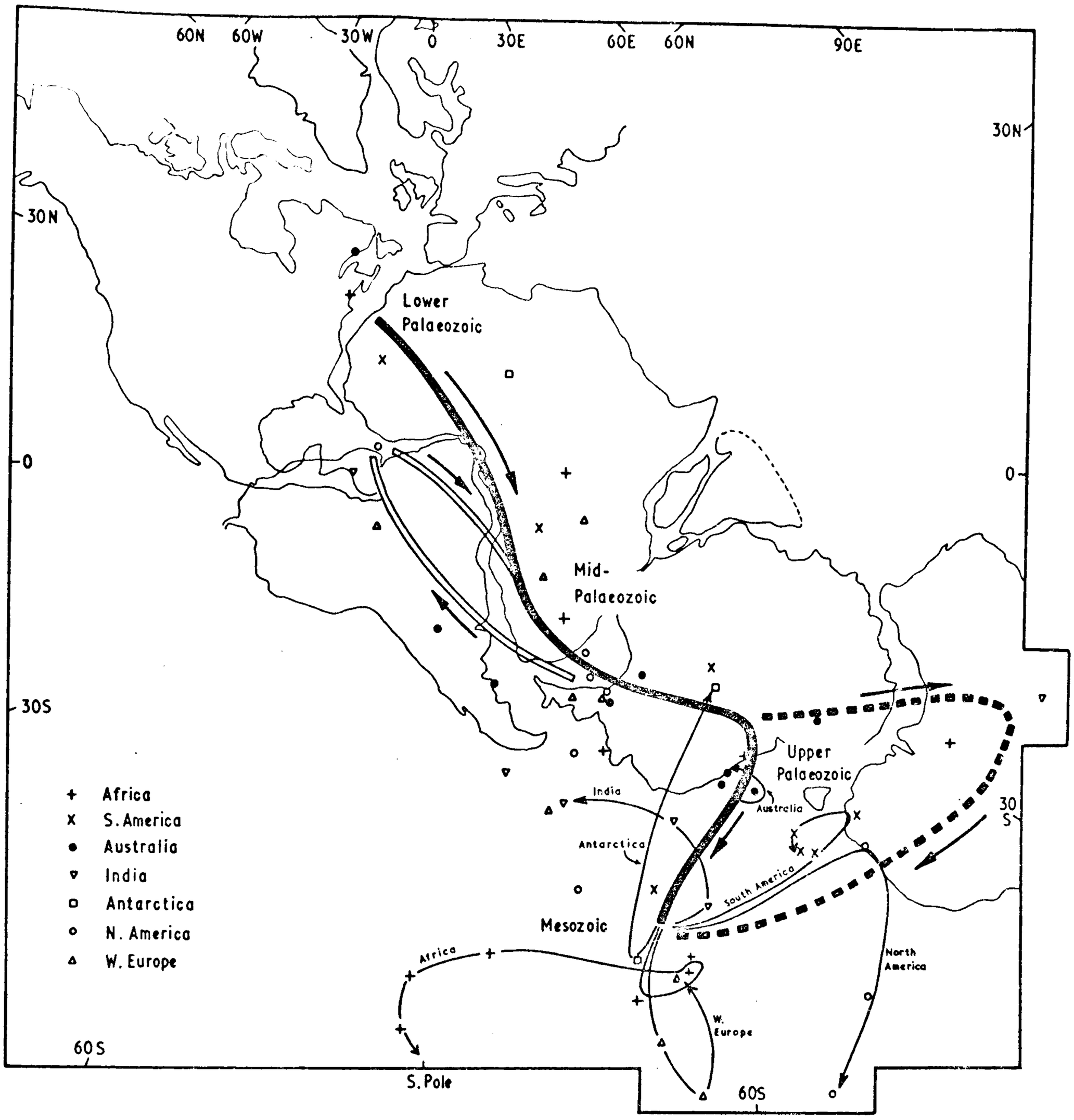


Fig 8.7 Schematic representation of proposed mean polar-wander curves for Western Laurasia (white curve) and Gondwanaland (black curve). Broken curve represents possible alternative Upper Palaeozoic path

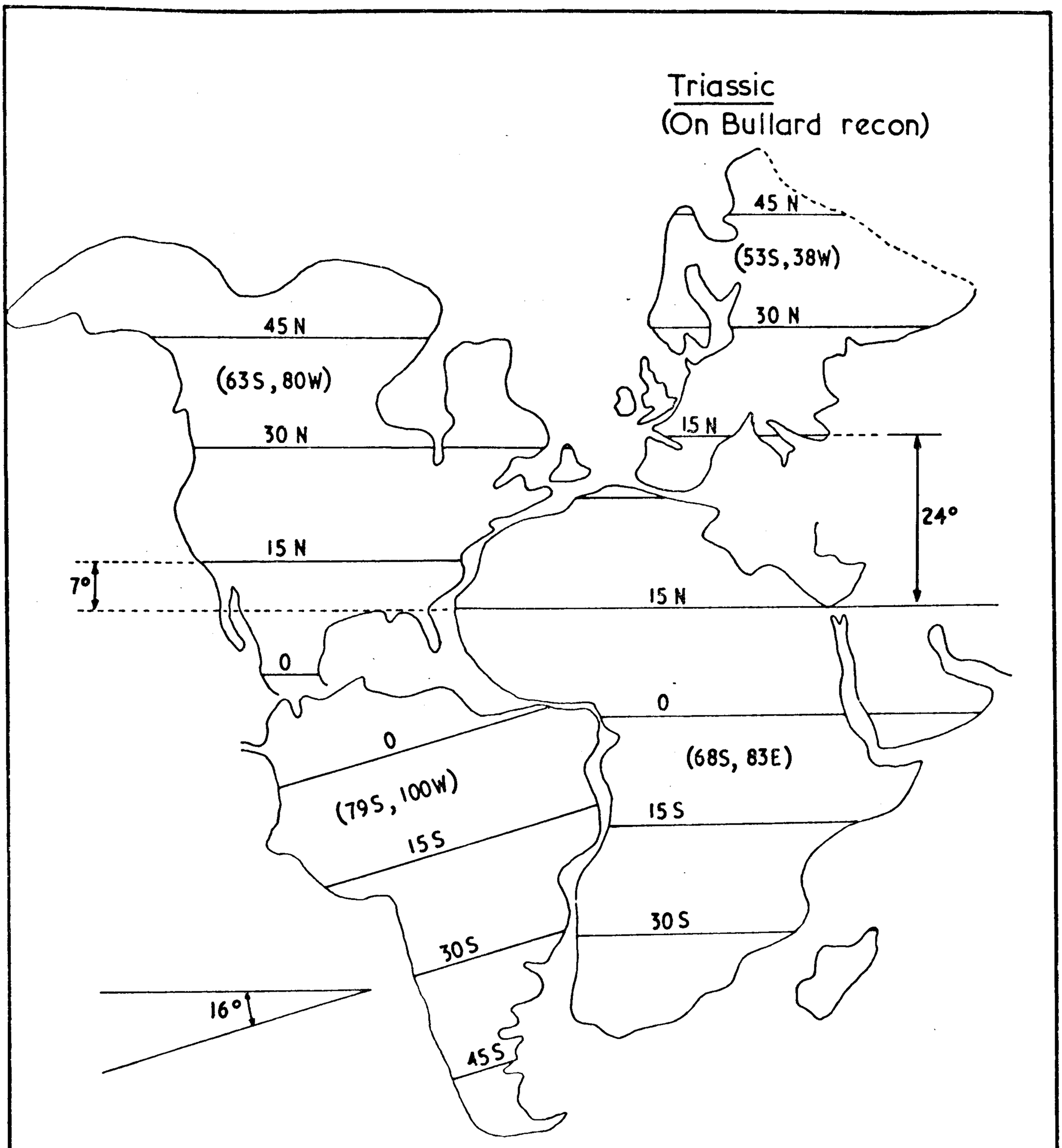


Fig 8.8 Discrepancies in Triassic pole positions from circum-Atlantic continents represented as differences in palaeoisoclines on a Bullard reconstruction

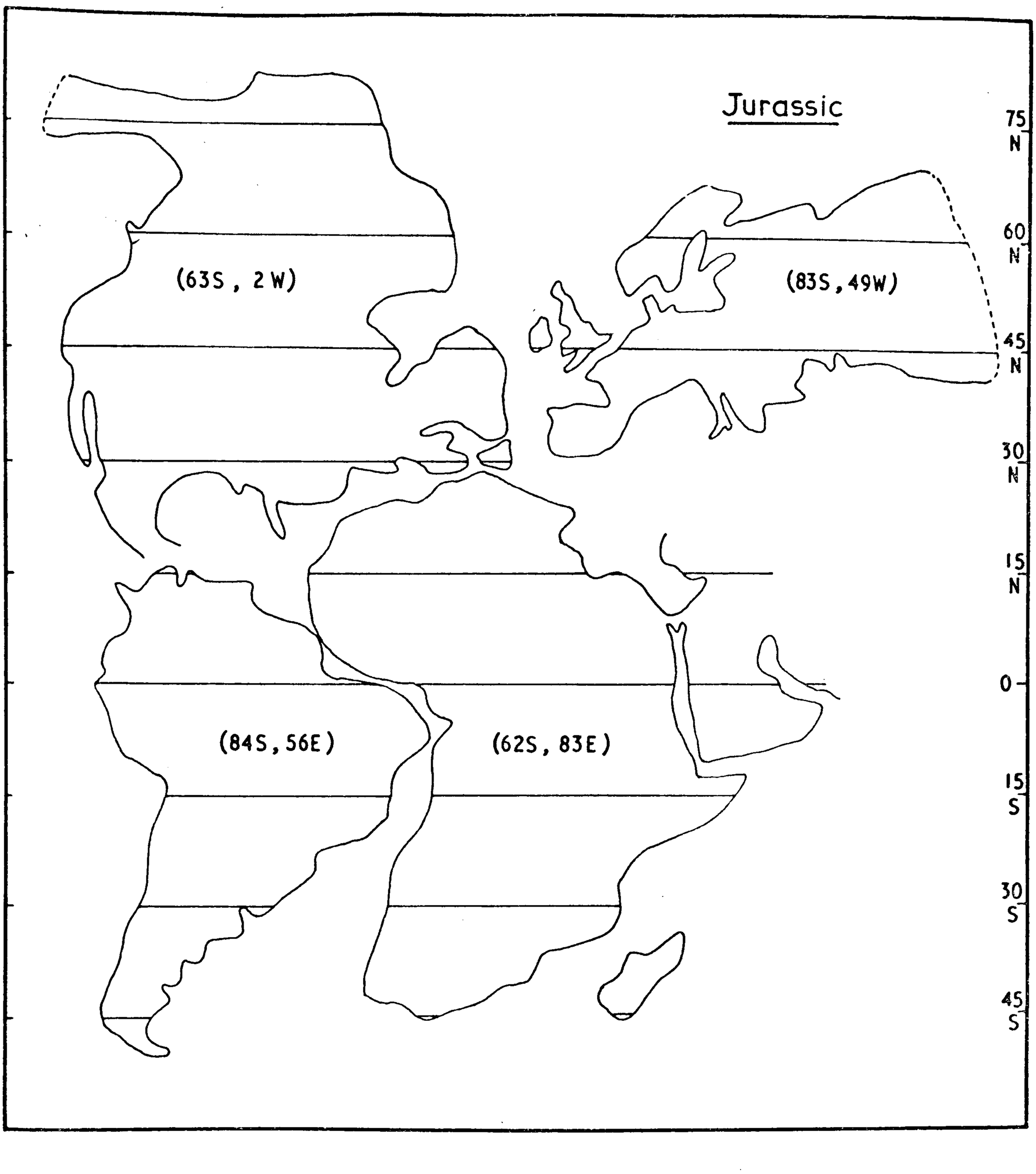


Fig 8.9 Jurassic palaeolatitudinal positions of the circum-Atlantic continents, plotted on a Platt-Carey projection

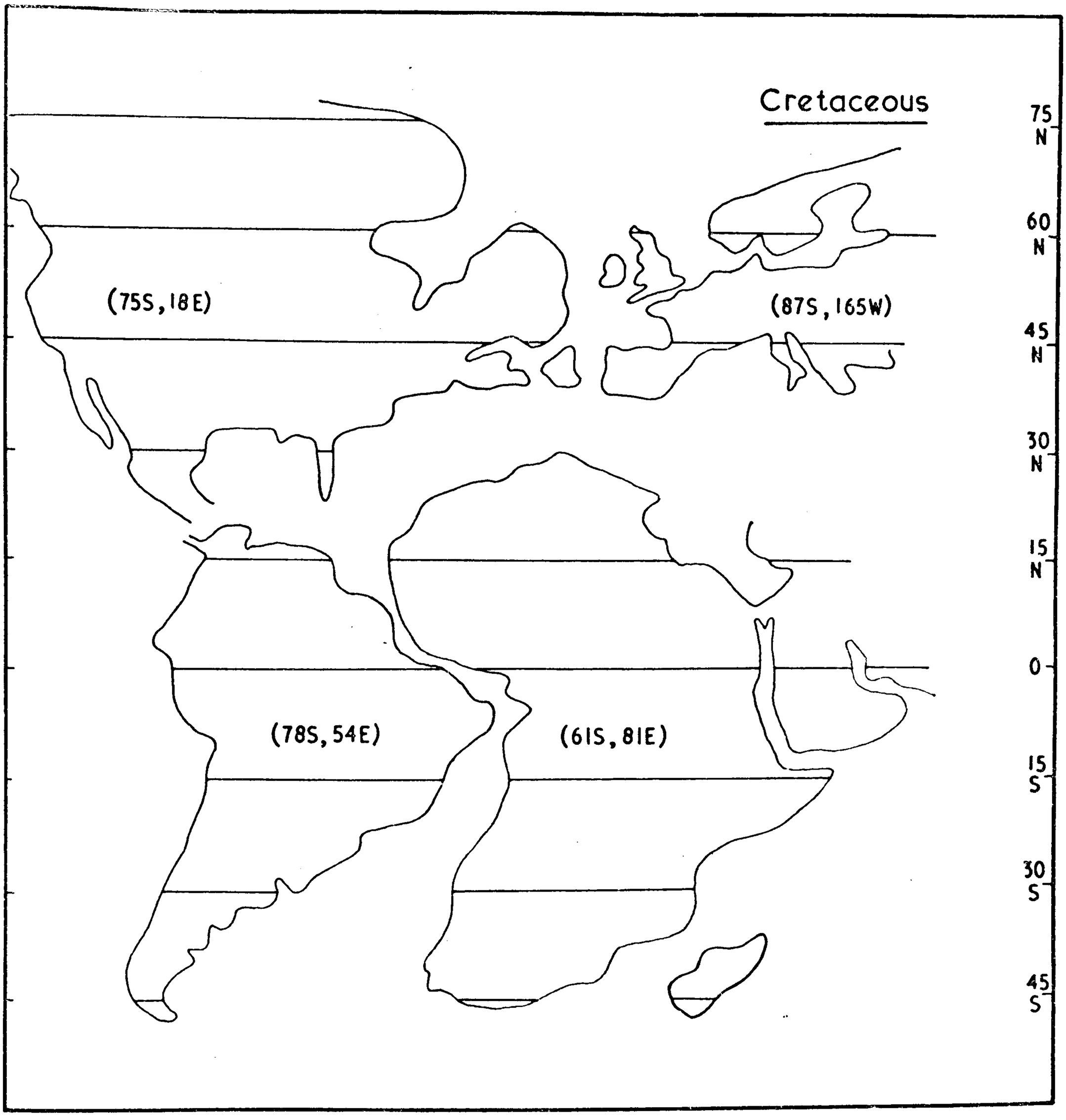


Fig 8.10 Cretaceous palaeolatitudinal positions of the circum-Atlantic continents, plotted on a Platt-Carey projection

Table 8.1. African Upper Precambrian to Recent palaeomagnetic pole positions

Formation age	Description	McElhinny Ref.No.	Formation palaeomagnetic pole position						Mean palaeomagnetic pole position			
			Lat	Long	A_{95}	No samples	No sites	Reference	Age	Lat	Long	A_{95}
P6u	Anti-Atlas volcanics, Morocco	-	30.5N	123W	17	43	8	This thesis	P6u	30.5N	125W	17
€1	Anti-Atlas tuffs, Morocco	-	41.5N	110.5W	10.5	87	16	This thesis	€1	41.5N	110.5W	10.5
€m	Lavas, east-central Morocco	2.1	53N	34E	-	-	-	Helsley,1965				

Table 8.1 contd

Formation Age	Description	McElhinny Ref.No	Formation palaeomagnetic pole position Lat	Long	A_{95}	No samples	No sites	References	Mean palaeomagnetic pole position Age	Lat	Long	A_{95}
P€-€1	Ntonya Ring Structure, Malawi	B1	27.5N	15W	2	-	7	Briden, 1968				
€u-O1	Hook Intrusives, Zambia	B2	14N	23.5W	36	-	3	Brock, 1967	€-O	31N	17W	29.5
O	Lower Table Mt Series shales Cape Town	B3	50N	11W	-	8	-	Graham & Hales, 1961				
D	Msissi norite, Morocco	-	0.5S	25E	16.5	38	7	This thesis	D	05.S	25E	16.5
C1	Dwyka varves, Central Africa	B4	26.5S	26.5E	10.5	23	5	McElhinny & Opdyke, 1968	C1	26.5S	26.5E	10.5
Cu	K3 beds, Galula coalfield, Tanzania	B5	45.5S	40E	8	34	5	Opdyke, 1964	Cu-P1	40S	64.5E	16.5
P1	Ecca redbeds, Tanzania	B6	27S	89E	15.5	27	4					
Tr m	Ait Aadel dolerites Morocco	-	72S	74.5E	7.5	63	15	This thesis				
Tr m	Titchka sediments Morocco	-	68.5S	87E	22.5	22	4	This thesis				
Tr l	Upper Beaufort sediments, S.Africa	2.19	67S	87E	-	19	4	Graham 1961	Tr_1	68S	84E	4.5
Tr	Shawa ijolite, Rhodesia	B7	64S	85.5E	14	13	5	Gough & Brock, 1964				

Table 8.1 contd

Formation Age	Description	McElhinny Ref.No	Formation palaeomagnetic pole position Lat	Long	A_{95}	No samples	No sites	References	Mean palaeomagnetic pole position Age	Lat	Long	A_{95}
Tr m	Issaldain dolerites Morocco	-	77.5S	39.5W	6.5	45	8	This thesis	Tr_2 (Remag.in Tertiary)	76.5S	37.5W	5.5
Tr	K5 redsandstones, Songwe,Tanzania	2.23	75S	36W	-	5	1	Nairn, 1964				
Tru-J1	Red sandstone formation,Zambia	B8	68S	49.5E	5	-	6	Opdyke, 1964	J_1	67S	50E	5.5
J1(183my)	Foum Zguid dyke, S.Morocco	-	58S	79E	4	23	5	This thesis				
J(120-160 my)	Central Atlas intrusives,Morocco	-	53S	81.5E	24	21	6	This thesis				
Tru-J1 (200-150 my)	Stormberg lavas Lesothe	B12	71S	89E	15	74	4	van Zyl et al, 1962a, b	J_2	62S	83.5E	6
Tru-J1 (200-150 my)	Karoo lavas Central Africa	B13	57S	84E	8	-	9	McElhinny et al 1968				
Tru-J1	Karoo dolerites, Rhodesia	B11	65.5S	75E	12.5	-	10	McElhinny & Jones 1965				
J1(190±5 my)	Marangudzi Ring Complex,Rhodesia	B9	70S	105E	9	-	8	Gough et al,1964; Brock, 1968				
J1(168±4 my)	Mateke Hills Ring Complex, Rhodesia	B10	58.5S	79.5E	8.5	-	6	Gough et al, 1964				

Table 8.1 contd

Formation Age	Description	McElhinny Ref.No	Formation palaeomagnetic pole position Lat	Long	A_{95}	No samples	No sites	Reference	Mean palaeomagnetic pole position Age	Lat	Long	A_{95}
K1(111-106 my)	Lupata volcanic series, Mozambique	B15	62S	79.5E	4	-	7	Gough & Opdyke, 1963	K_1	61S	81E	5
K1(116-128 my)	Mlanje Massif syenite, Malawi	B14	60S	82E	12	8	-	Briden, 1967				
K1(?)	Red siltstones, Mozambique	2.51	79S	28E	-	5	-	Gough & Opdyke, 1963	K_2	77S	33E	9.5
K1(?)	Central Atlas sediments Morocco	-	75S	47E	4	30	5	This thesis				
Te-To	Ethiopian traps	-	81S	12W	4.5	-	20	McElhinny & Wellman 1969	T1	81S	12W	4.5
Tm	Turkana lavas	-	85S	17W	2.5	-	62	McElhinny & Wellman 1969	Tu	86.5S	32.5W	1.5
Tm	Cavallo massif lavas, Algeria	-	88S	26W	3	51	13					
Tm	Cape Verde Island lavas	-	85S	43W	3	-	138	Watkins et al, 1968				
Tm(7-14my)	Rift valley volcanics	-	85S	40W	3.5	-	43	Quoted in McElhinny & Wellman, 1969				
Tp(2.5-7 my)	Rift valley volcanics	-	88S	27W	3	-	60					
Tp1(0-2.5 my)	Rift valley volcanics	-	88S	36W	3	-	60					
Quat	Ahaggar basalts, Algeria	2.68	74S	76E	-	22	6	Roche & Leprêtre, 1955	Q	88.5S	64E	22
Quat	Archaeological baked clays	-	88S	25E	-	-	3	Théllier, 1951				
Quat	Middle Atlas basalts Morocco	-	77S	107W	19	96	16	Hailwood, 1968				

Table 8.2 World wide mean pole position

	Age	Lat	Long	Source
1. Africa				
	€1	+41.5	-110.5	Summary of Table 8.1
	CO	+31	-17	
	Du	-0.5	+25	
	C1	-26.5	+26.5	
	Cu	-45.5	+40	
	P1	-27	+89	
	Tr	-68	+83	
	J	-62	+83.5	
	K_1	-61	+81	
	K_2	-77	+33	
	T1	-81	-12	
	Tu	-86.5	-32.5	
	Q	-88.5	+64	
2. South America				
	€-D1	+15	-38	McElhinny & Briden, 1971
	C1	-28	-34	
	Cu-P1	-62	-14	
	PTr	-79	-100	Creer, 1970
	J	-84	+56	
	K	-78	+54	
	T	-84	+26	
	Q	-85	+45	

	Age	Lat	Long	Source
3. North America				
	€-O	-36.5	-57.5	Larson & Mutschler, 1971
	O-D	+16.5	-75.5	Recalculated from Creer, 1970, giving unit weight to each of 4 formations
	Cm	-33	-55	Creer, 1970
	Cu	-40	-54	
	P	-47	-65	
	Tr	-63.5	-8.0	Recalculated from Creer, 1970, giving unit weight to each of 12 formations
	J	-63	-2	Creer, 1970
	K	-75	+18	
	T	-82	+47	
4. W. Europe				
	€O	-11.5	-8	Recalculated from Creer, 1970, giving unit weight to each of 6 formations W of Urals
	D1	+3	-44	Creer, 1970
	D-Cm	-18	-19	
	Cu	-39	-23	
	P	-41	-17	
	Tr	-53	-38	
	J	-83	-49	
	K	-87	-165	
	T	-78	-23	

Table 8.2 contd

Age	Lat	Long	Source
5. Australia			
PC-O1	-12	+4	McElhinny & Briden, 1971
Su-C1	-76	-52	
Cu	-73	+147	
Cu-P	-44	+135	
Tr	-53	+152	Creer, 1970
J	-49	+150	
K	-53	+149	
T	-69	+130	
Q	-83	-123	
6. India			
€1	-28	+32	McElhinny & Briden, 1971
Cu-Pu	+26	+131	
PTr	-13	+127	Creer, 1970
J	-14	+117	
K	-28	+107	
KT	-33	+101	

Age	Lat	Long	Source
7. Antartica			
O1	-28	+10	Zijderveld, 1968
J	-54	-141	Creer, 1970
T	-88	+152	

Part II

Experiments on the alternating field demagnetisation of sediments, and investigations into the effects of asymmetries in the wave-form of the applied field

CHAPTER 9. EXPERIMENTS ON THE ALTERNATING FIELD DEMAGNETISATION OF SEDIMENTS

9.1 The technique of A.F. demagnetisation

The partial demagnetisation of rocks by alternating fields is now an established procedure in palaeomagnetism. It is used for investigating the stability of remanent magnetisations and for the removal of unwanted secondary components of remanence. The latter are frequently viscous magnetisations with low coercive forces, which can be preferentially demagnetised so as to isolate the underlying more-stable primary components. Sometimes, however, secondary components have considerable stability themselves, as in the case of chemical remanences (C.R.M.'s) produced by weathering, or secondary thermal remanences (T.R.M.'s) produced, for example, by heating during deep burial, orogenesis, or the emplacement of nearby igneous bodies. In such cases the stability of the secondary component may be comparable to that of the primary component, rendering its removal by partial A.F. demagnetisation difficult, if not impossible.

The A.F. demagnetisation technique was first used for palaeomagnetic work by Thellier and Rimbert (1954, 1955), and has subsequently been developed and described by Brynjolfsson (1957), As and Zijderveld (1958), Rimbert (1959), Creer (1959), Cox (1961), and Irving, Stott and Ward (1961), amongst others. The basic method consists of placing the specimen under study in the centre of a coil, through which an alternating current of peak value. I_{max} is passed. This current is then smoothly and uniformly

reduced to zero. In order to prevent the Earth's magnetic field from inducing an anhysteretic component (A.R.M.) in the sample, the demagnetising coil is placed in a field-free space, produced either by a set of three orthogonal Helmholtz coils, or by a mu-metal shield. It is essential that the alternating current supplied to the coil should have as pure a sinusoidal wave-form as possible, and should be free from harmonic distortion. To achieve this a bank of capacitors is connected in series with the coil, and its value adjusted until the coil reaches resonance. This also ensures minimal inductive losses in the coil, so that the maximum possible field can be obtained for a given coil and supply voltage. Some authors (e.g. As and Zijderveld, 1958) have employed an additional rejection filter tuned to the second harmonic frequency (100 Hz in the case of the 50 Hz mains).

For reasons discussed later in this chapter, it is important that the current should be reduced to zero as smoothly and uniformly as possible, and various methods have been employed to ensure this. Creer (1959) used a variable electrolytic resistance, whereas Irving et al (1961) withdrew the coil from the specimen, and Cox and Doell (1963) used a variable inductance. All of these methods appear to produce comparable results.

Two different types of technique have been used to ensure that demagnetisation is effectively performed along all directions in the sample. In the first the specimen is demagnetised separately along each of three orthogonal axes (e.g. As and Zijderveld, 1958) whereas in the second it is is made to rotate simultaneously about two (or three) mutually perpendicular axes within the demagnetising

coil (e.g. Creer, 1959). In the latter method, to prevent the production of A.R.M.s. it is important that the rates of rotation about each of the axes is independent of the others and of the supply frequency. This method has the advantage that only one sequence of treatment is necessary, compared with at least three sequences of treatment using the non-rotational system. It has the further advantage that any A.R.M.s which may be produced by small direct fields or asymmetries in the supply current can be averaged out. Hutchings (1966) has shown that the efficiency of the tumbling motion in averaging out the effects of A.R.M. depends on the speeds of rotation about the vertical and horizontal axes only, and that the optimum ratio of these two speeds is 0.62:1. The principal disadvantage of this method is that since the amount of decrease in current must be small over the time interval, t, required for the specimen to execute a complete sequence of rotations, the current must be reduced more slowly than in the case of non-rotational systems. Furthermore, variations in the rate of reduction of the current over time-intervals comparable with t may themselves produce an A.R.M. in the sample. Such small-scale variations in the rate of reduction of the current are less important in the case of non-rotational systems.

9.2 Theoretical Treatment of A.F. Demagnetisation

9.2.1. The Rayleigh Laws

A theoretical explanation of A.F. demagnetisation has been given by Néel (1942, 1943, and 1955), using the Preisach diagram (Preisach, 1935), and involving Rayleigh's laws (Rayleigh 1887).

The Rayleigh laws govern the magnetisation of ferromagnetic materials in fields which are weak compared with the coercive forces of the materials. They are applicable in rock magnetism because the Earth's magnetic field is always weak compared with the coercive forces of rocks.

The first law relates the magnetisation, J, of a previously demagnetised body to the applied field, H,

$$J = AH + BH^2 \qquad (9.1)$$

where A and B are constants.

The second law states that when the magnetic field is reduced by an amount ΔH after it has reached a value H_m, producing a magnetisation J_m, the magnetisation changes by ΔJ, having the same sign as ΔH, and given by:

$$\Delta J = A\,|\Delta H| + \tfrac{1}{2} B\,|\Delta H|^2 \qquad (9.2)$$

provided H remains within the interval $-H_m$ to $+H_m$. When removed, the magnetic field, H_m, leaves a remanent magnetisation, Jr, given by:

$$J_r = 1/2\, B\, H_m^2 \qquad (9.3)$$

Thus the second term in equations (9.1) and (9.2) represents the irreversible magnetisation, and the first term the reversible magnetisation. The coefficient, A, corresponds to the reversible susceptibility.

9.2.2. <u>The Preisach diagram</u>

T.R.M. is acquired by multi-domain grains as a result of enlargement of domains with one orientation at the expense of adjacent domains with opposite magnetisation. Demagnetisation of

the grains therefore involves the movement of domain walls to positions which give each grain zero total moment (Stacey, 1963). According to Néel's theory each wall displacement requires the application of critical fields, of value 'a' corresponding to increasing fields, and 'b' corresponding to decreasing fields. When an alternating field is applied to the grain the following two cycles of magnetisation can be envisaged for individual domains, depending on whether 'a' is greater than or less than 'b'

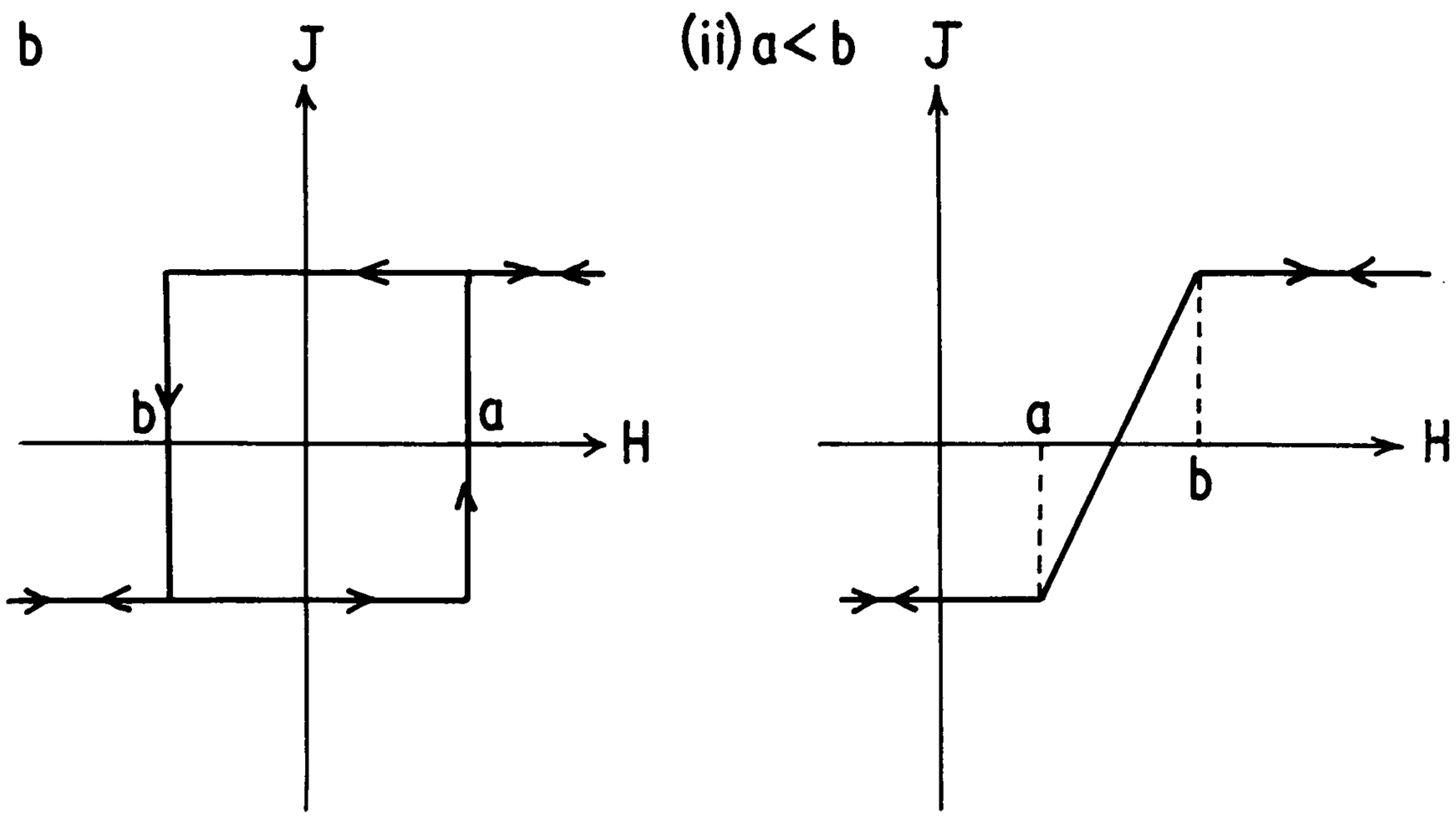


Fig. 9.1

The first cycle (a > b) represents irreversible changes in magnetisation, corresponding to the term BH^2 in Rayleigh's expression, whereas the second cycle (a < b) represents reversible changes in magnetisation, corresponding to the term AH.

Each of a large number of domain walls in a rock sample can therefore be represented by a point with coordinates (a, b) plotted on a plane as in Fig 9.2. This is known as a Preisach diagram (Preisach, 1935)

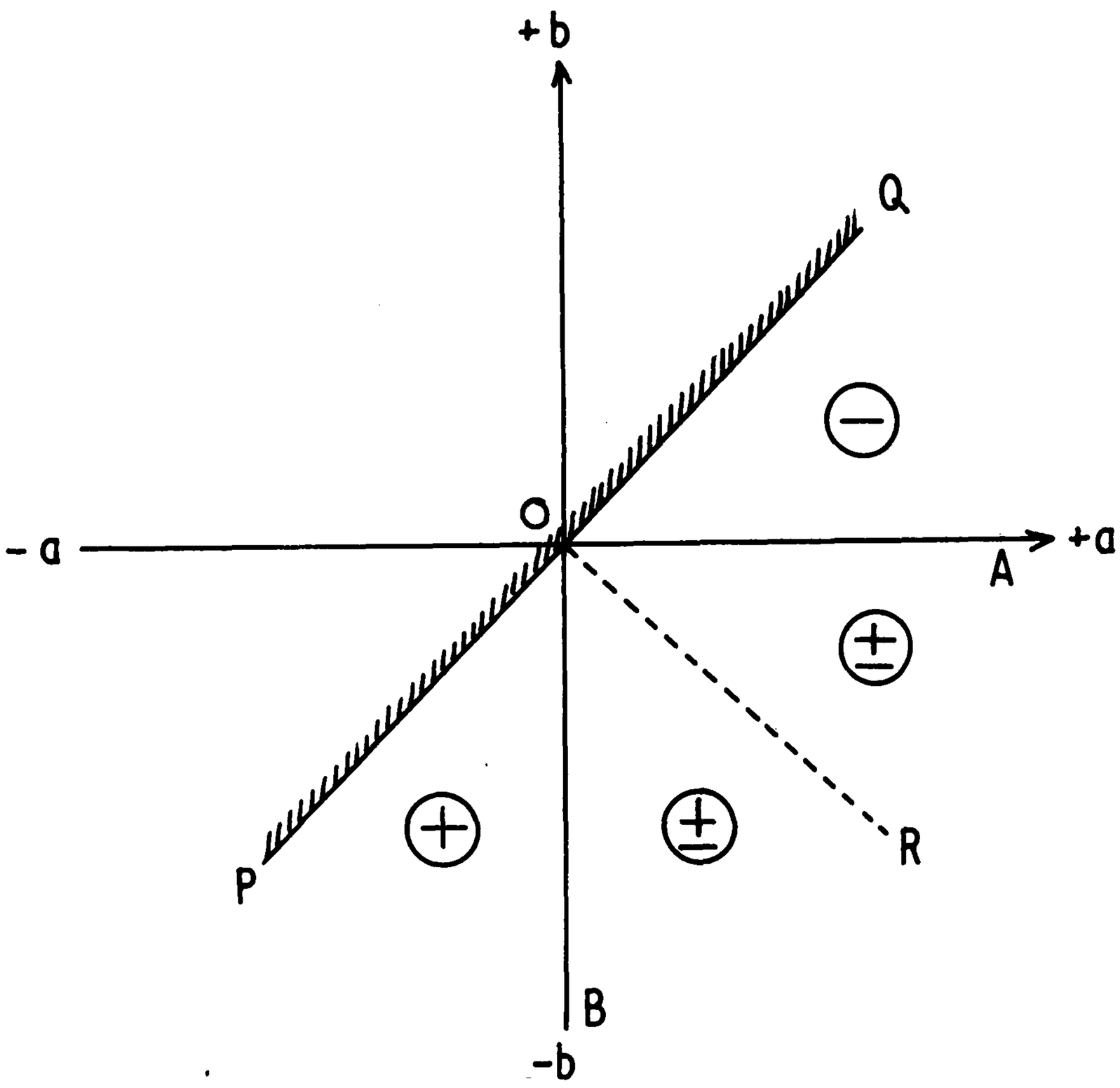


Fig. 9.2

9.2.3. Application to A.F. demagnetisation

In the case of A.F. demagnetisation we are concerned only with remanent magnetisation, i.e. with cycles for which $a > b$. The representative points of all such cycles are situated in the lower half plane, bounded by the first bisector. There are three regions to consider in this half-plane.

(i) Domains whose representative points are situated in the sector PoB, i.e. for which $b < a < o$. The cycle for such domains is indicated in Fig 9.3(a), and it is clear that they are always positively magnetised in zero applied field.

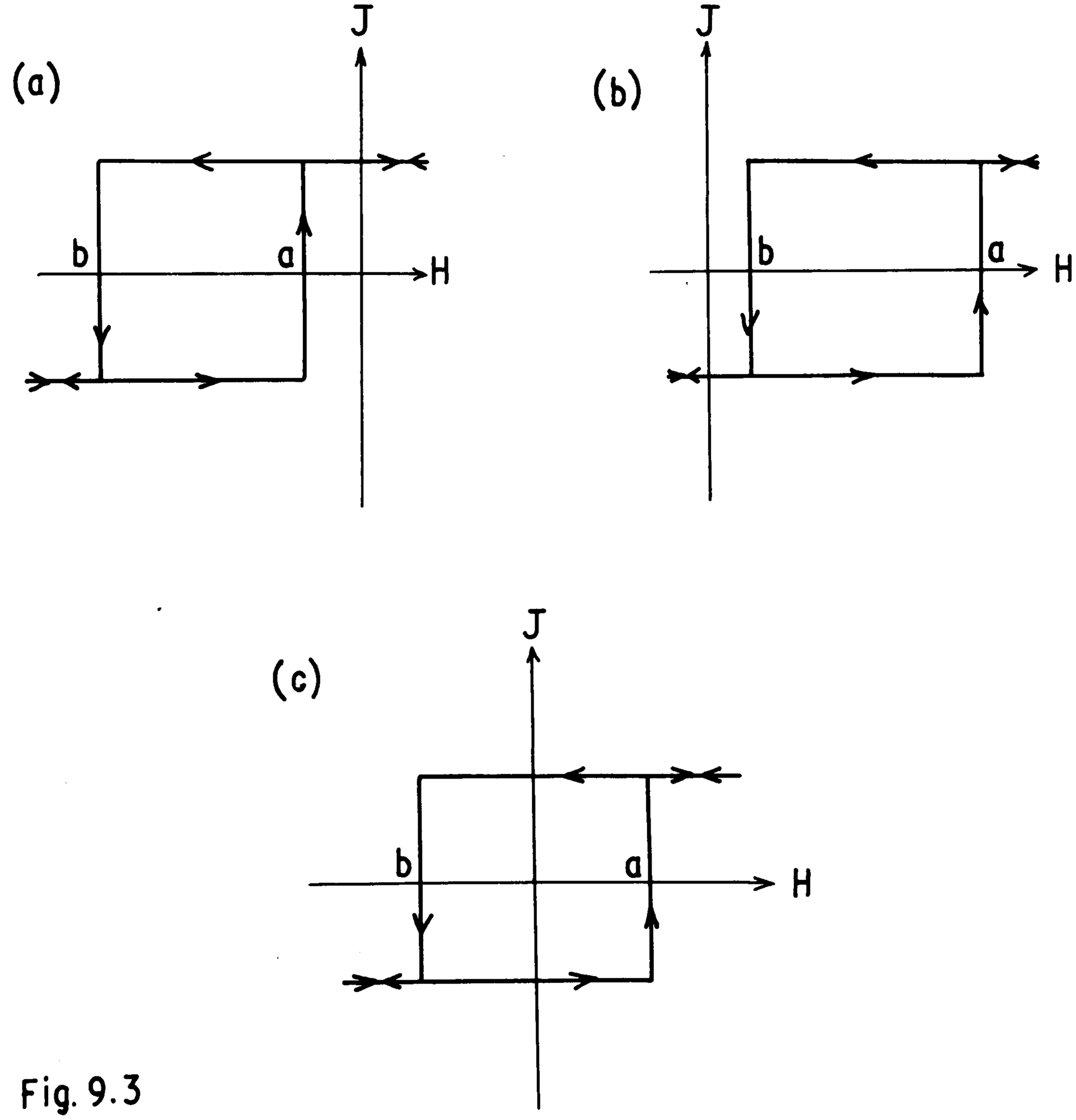


Fig. 9.3

(ii) Domains whose representative points are situated in the sector QoA, i.e. for which $a > b > o$. These are illustrated in Fig 9.3(b), and will clearly retain a negative magnetisation in zero applied field.

(iii)Domains represented by points in the quadrant BoA. These can have either sign, depending on the initial conditions. The quadrant is divided by the line OR into two groups of points having cycles of opposite asymmetry, and it is assumed that the distribution on either side of OR is identical.

The results of the application of an alternating field are as follows. Positive half-cycles of the applied field, H, cause all the negatively magnetised domains for which $a \leqslant H$ to reverse in sign, and negative half-cycles cause all the positively magnetised domains for which $b < H$ to reverse in sign. The effect of gradually reducing this alternating field to zero is shown in Fig 9.4, where $\hat{H}$ represents the peak applied field, and $-H_1$, $+H_2$, $-H_3$ etc., are successive half-cycle maximum values. The end result is an equal number of positively and negatively magnetised domains, i.e. a net magnetisation of zero, as in Fig 9.4(e). If the decrement in field (i.e. the difference, $\Delta H/2$, between two successive half-cycles) is infinitesimally small, the end result is as represented in Fig 9.4(f).

9.3 Application of A.F. Demagnetisation to Sediments

The most commonly used method for the removal of unwanted secondary components of remanence from sediments is that of thermal demagnetisation. This involves heating the sample to a temperature exceeding the blocking temperature of the grains carrying the

secondary magnetisation, and then cooling in field-free space. Frequently this necessitates heating samples to temperatures approaching the Curie Point of magnetite (570°C), and it is possible for the mineralogical composition and phase-relationships of the mineral assemblage to be affected by these high temperatures. The risk of oxidation or reduction taking place may be decreased by heating the sample in a vacuum or an inert atmosphere, or encasing it in plaster of paris, but this is a lengthy process, and does not eliminate the possible occurrence of other important changes such as exsolution, annealing, or the break-down of silicates such as felspars.

For this reason it is desirable to extend the technique of A.F. demagnetisation, now widely used on igneous rocks, to sediments. There are two main problems involved in doing this. The first of these concerns the mineral responsible for carrying the magnetic remanence. In the case of igneous rocks this is usually magnetite, or a member of the titanomagnetite series, whereas in sediments it is usually fine-grained haematite. The coercive forces of titanomagnetite grains are commonly a few hundred Oersteds or less, and these are easily attainable by normal A.F. demagnetisation apparatuses, but the coercive forces of fine-grained haematite particles are of the order of several thousand Oersteds, and are well beyond the upper limits of most A.F. demagnetisers.

The second main problem is that the remanence of most rocks is carried by only a small proportion of the total magnetic material present. Thus it is very easy to build up a spurious magnetisation in the previously randomly magnetised grains, as

a result of imperfect experimental conditions (e.g. the presence of small superimposed direct fields, asymmetries in the wave-form of the applied alternating field etc). Owing to the typical low intensity of NRM of sediments, spurious magnetisations of this sort rapidly become significant, and may exceed the NRM intensity by several orders of magnitude.

Previous attempts at the A.F. demagnetisation of sediments have met with varying degrees of success. Creer (1959) found that he was able to successfully remove an unstable component of remanence from the Triassic Keuper Marls of S.W. England using a peak field of only 1200 Oe., whereas Snape (1965), using peak fields of 1500 Oe., found that only one group of sediments out of twelve that he studied, responded to A.F. demagnetisation treatment. Snape concluded that fields of at least 3000 to 4000 Oe. would be needed to effectively 'clean' most groups of sediments.

9.4. Design of Apparatus

9.4.1. General Considerations

In order to meet the experimental requirements for the successful A.F. demagnetisation of sediments suggested by previous authors it was decided to design and construct a demagnetising coil capable of producing peak alternating fields of 5,000 Oe. Particular attention was paid to the placing of the apparatus in a magnetically quiet environment, to the careful cancellation of the Earth's field, and to the smooth and continuous reduction of the alternating field to zero.

Further requirements were that the field at the centre of the demagnetising coil should be uniform over at least the dimensions of the rock samples to be treated (2.54 cm), and that the inner diameter of the coil should be sufficiently large to accommodate these samples.

The power for the coil was to be drawn from the 50 Hz mains, via a transformer and heavy-duty variac, and a maximum current of 45 amps could be supplied at 120 volts.

9.4.2. Design of Coil

The basic theory for the design of high-field coils was developed by Maxwell (1881), who showed that for a given available electric power the greatest possible field is obtained from a uniformly wound coil when a longitudinal section through the coil containing the axis of symmetry exhibits the profile $r^2 = \sin\theta$, the line $\theta = o$ being the axis of symmetry. Because of difficulties in construction, and the fact that in such a system the windings extend right to the origin, rendering access to the centre of the coil very difficult, this shape was regarded as unsuitable.

The alternative to this design is a coil with a rectangular section winding-space. Such a design has neither of the previously mentioned disadvantages, and was therefore adopted.

Fabry (1898) and Cockcroft (1928) have shown that the field at the centre of such a coil is given by

$$H = G \left(\frac{W\eta}{a\rho} \right)^{\frac{1}{2}} \qquad (9.4)$$

where W is the power dissipated by the coil in Watts, ρ is the resistivity of the winding material in Ω -cm., a is the inner radius of the winding-space in cm, G is a dimensionless factor depending only on the shape of the winding space, and η is the 'filling factor', given by

$$\eta = \frac{\text{vol. of winding space occupied by conductor}}{\text{total vol. of winding space}} \qquad (9.5)$$

The experimental conditions require an extremely uniform field over a space having dimensions of at least 2.6 cm. Maxwells electro-magnetic equations indicate that if the field is uniform along the axis

of a solenoid then it is also uniform away from this axis. Thus it is only necessary to ensure that the field is uniform along the axis.

The greatest uniformity of field is achieved by using a 'Helmholtz pair' arrangement, i.e. by omitting a slice from the centre of the coil. Daniels (1950) has shown that for such a system, having a rectangular section winding-space with length 6a, outer radius 3a, and central gap 0.18a, the value of G is 0.16. This value is only 10% less than the theoretical maximum for a coil of similar shape, having no central gap, and Daniel's system was therefore adopted.

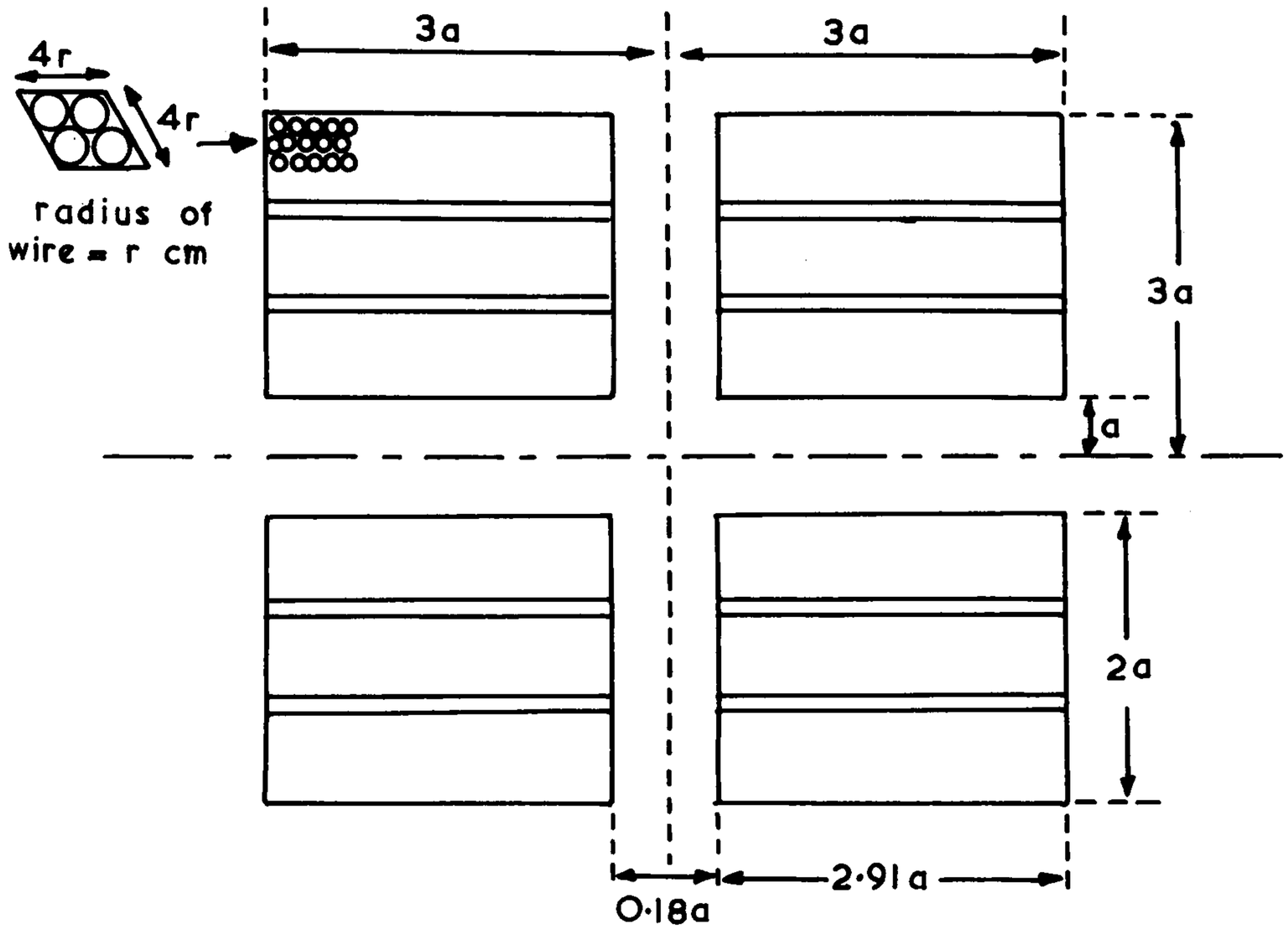
The production of high fields of the order of 5000 Oe necessitates the dissipation of large amounts of electrical energy, and it was therefore decided to incorporate a cooling-system in the coil. Air-cooling was chosen in preference to water-cooling, since this obviates the necessity for complicated water-tight joints, and eliminates the safety hazards associated with passing water over conductors carrying high electric currents.

To allow the air to circulate freely through the system, the coils were wound in three layers separated by 2mm gaps. Using equation (9.5), the value of the filling factor, η , for close-packed winding is reduced to 0.8, compared with 0.9 for a similar system without the gaps for air-cooling.

It can be seen from equation (9.4) that the maximum field is achieved when the inner radius of the coil, a, is as small as possible. It was decided, therefore, to use the single-axis demagnetising system, thereby eliminating the additional space necessary for a specimen rotation mechanism.

Fig. 9.5

Dimension of winding-space



The limiting value of a is then given by the overall dimensions of the specimen and holder, viz 2cm. Following this, the other dimensions are given from Fig 9.5 as

Overall length of coil = 12 cm

Width of central gap = 0.36 cm

Outer radius = 6 cm

Considering one of the four cross-sectional winding-spaces of Fig 9.5, the effective cross-sectional area of one piece of wire is

$$\frac{4r \times 4r \cos 30}{4} = 2\sqrt{3}\, r^2 \text{ cm}^2,$$

and the total cross-sectional area of this winding space is

$$(2a \times 2.91a) - (2 \times 0.2 \times 2.91) \text{ cm}^2 = 22.12 \text{ cm}^2$$

Hence the number of turns per half-coil $= \frac{22.12}{3.465r^2} = 6.4/r^2$

and the total number of turns $= 12.8/r^2$ (9.6)

If the total length of wire in the coil is ℓ cm, and the resistance per cm. of this wire is P, then the total resistance, R of the coil is given by

$$R = P\ell \qquad (9.7)$$

But length of wire = No. of turns x mean length per turn

$$= 12.8/r^2 \times 2\pi \times \text{mean radius}$$

$$\text{i.e. } \ell = 322/r^2$$

Hence total resistance of coil, $R = 322\ (P/r^2)$ (9.8)

Referring to equation (9.4), the power required to produce a field of 5000 Oe, using the values of G, η and a quoted above, and a value of 1.75×10^{-6} ohm-cm for the resistivity of the winding material (copper), is

$$W = \frac{H^2 a \rho}{G^2 \eta} = 4.26 \text{ killowatt}$$

The current which must be drawn from a 120 volt supply to produce this power is 35.5 amps, from which the optimum value of the coil resistance is given as 120/35.5 = 3.38 ohms.

Thus in order to produce a peak field of 5000 Oe with this coil, the value of the parameter r^2/P of the winding material, given from equation (9.8), must be

$$r^2/P = 322/R \simeq 100$$

The values of this parameter were calculated for different gauge copper wires, and are listed in Table 9.1

Table 9.1. Values of the Parameter $r^2/_P$ for copper wire

S.W.G.	$r^2/_P$	P (Resist per cm)
1	39,000	3.781×10^{-6}
5	9,500	7.571×10^{-6}
10	1,300	2.076×10^{-5}
15	130	6.563×10^{-5}
16	80	8.307×10^{-5}
17	47	1.085×10^{-4}
18	25	1.477×10^{-4}

It can be seen from this table that the optimum gauge wire, for which the value of $r^2/_p$ is closest to 100 is 16 gauge.

The coil was therefore wound from 16 gauge wire, and the total length required was calculated from

$$\ell = {}^{322}/_{r^2} \quad = 485 \text{ metres}$$

The total number of turns is given from $N = 12.8/_{r^2}$

$$= 1930 \text{ turns}$$

9.4.3. Practical Details of Coil

A detailed diagram of the coil former is given in Fig 9.6. Each set of windings was wound separately on a temporary former of appropriate diameter, and a thin coating of fibreglass resin was applied to each layer of wire to give additional insulation, and to bind the set of windings rigidly together. The six sets of windings were then assembled, the three sets in each half-coil being separated by 2mm diameter silica spacing rods. Connections between the sets of windings were made externally, using non-magnetic brass connectors.

The coil was mounted on aluminium runners with its axis horizontal and pointing in an E-W direction, in the centre of a 5 ft. diameter Helmholtz cage. The Earth's field could be cancelled at the centre of the system to within $\pm$ 5 γ in the vertical and N-S directions, and to $\pm$ 1 γ in the E-W direction.

Air for cooling was supplied by a BVC model BE500 blower unit, situated several feet away from the Helmholtz cage, and connected to the end housing of the coil at end A by a 12 ft. length of 1½ ins. diameter flexible P.V.C. hose.

The aluminium runners allowed the coil to be moved clear of the centre of the system to permit the positioning of fluxgate probes for cancelling the Earth's field prior to each run. The specimen holder, illustrated in Fig 9.7, was inserted at end B of the coil, and allowed 2.54 cm cylindrical specimens to be located accurately at the centre of the coil along any one of three mutually perpendicular axes. A thermocouple was situated in the central windings so that the temperature of the coil could be constantly monitored during use at high field value.

The measured total resistance of the coil was found to be 3.8Ω , in good agreement with the theoretical optimum value of 3.4Ω .

9.4.4. Tuning of Coil

For the reasons discussed in section 9.1 it was necessary to bring the coil to resonance by connecting a bank of capacitors in series with it. A theoretical value for the required capacitance was first derived so that resonance could be approximately achieved. Fine tuning was then performed by trial and error.

In order to calculate the required capacitance it was necessary to know the approximate inductance, L, of the coil. This was measured by means of an inductance meter, and found to be 64mH.

The required capacitance, C, is given by equating the inductive and capacitive reactance, viz.

$$2\pi f L = \frac{1}{2\pi fc}$$

From which $C = \frac{1}{4\pi^2 f^2 L}$

where f is the frequency of the applied current.

For f = 50 Hz and L = 64mH the required value of C is 158 μF.

The capacitors selected for use were Dubilier Nitrogol oil-filled 750V AC units. These were available in 8, 1 and 0.5 μ F values.

Fine tuning was then achieved by applying a constant voltage to the circuit, and varying the value of the capacitance in series with the coil from 130μF to 165μF, whilst monitoring the current. The results of this experiment are plotted in Fig 9.8, from which it can be seen that the optimum value of the capacitance is 153μF.

9.4.5. Calibration

Having accurately tuned the coil, it was then calibrated to find the field produced at its centre by unit current. This was done by placing a test-coil of 100 turns of wire wound on a paper former with mean radius r = 0.85 cm, in the centre of the demagnetising coil. The voltage induced in the test-coil was then measured on an oscilloscope, and a series of readings were taken for different values of current in the demagnetising coil. These are plotted in Fig 9.9.

The voltage, V., induced by a field of peak intensity H Oersteds, in a coil with cross-sectional area A metre^2 and N turns, is given by

$$V = HAN\omega \times 10^{-8} \text{ volts}$$

where $\omega = 2\pi f = 100\pi$ Hz, in this case.

Hence the calibration factor of the coil is given by

$$\frac{H}{I} = \frac{V}{I} \times \frac{1}{AN\omega} \times 10^{8} \text{ Oe per amp}$$

The value of $\frac{V}{I}$ is given from the graph in Fig 9.9 as 0.13 volts per amp, so that

$$\frac{H}{I} = \frac{0.13 \times 10^{8}}{\pi^{2} \times 0.85^{2} \times 10^{4}} = \underline{182 \text{ Oe per amp}}$$

The uniformity of the field along the axis of the coil was checked by means of a Newport model G fluxgate magnetometer. The probe of this instrument was placed at the centre of the demagnetising coil, and the field produced by a current of 2 amps was measured as the probe was moved progressively along the axis of the coil away from the centre, in both directions. The results are plotted in Fig 9.10 from which it can be seen that the field is uniform to within 0.3% over a total distance of 3 cm. at the centre of the coil. This was considered to be satisfactory for the purposes required.

9.4.6. Field Reduction Mechanism

The current through the coil was reduced smoothly and uniformly to zero by means of a motor-driven variable inductance unit. The principal of this unit is the variation in flux-linkage between two sets of heavy-duty windings as the angle between their axes is gradually increased from 0^{o} to 90^{o}. One of the sets of windings was fixed, and the other was attached to a rotating armature, connected via a gear-box to a variable-speed reversible electric motor. Using this system the current could be increased to the required maximum value very rapidly and then reduced at any desired rate. The variable inductance could be programmed to stop at the required maximum value by means of an adjustable cut-out switch actuated by the rotating

armature, and the same system was used for switching the drive-motor off when the current through the coil reached zero. The drive-motor control circuit is shown in Fig 9.11.

With the variable inductance in the 'maximum' position, the current through the coil circuit was adjusted to the required value by means of the heavy-duty variac RV1 indicated in Fig 9.12

Since demagnetisation was performed successively along each of three mutually perpendicular axes in the samples, it was important that the peak field value should be accurately reproducible. The automatic cut-out system described above was found to meet this requirement satisfactorily once the coil had been run for a few minutes and reached an equilibrium temperature.

9.4.7. Performance of Apparatus

When construction of the apparatus was complete, a series of test-runs were performed at gradually increasing currents, to check the efficiency of the coil cooling system. It was found that the coil would operate satisfactorily, without the blower switched on for forced air cooling, at fields up to 1500 Oe. With the blower on, the maximum desired field of 5000 Oe could be achieved without excessive over-heating, provided it was maintained for only a few seconds, and that the blower was left switched on for several minutes after the current had been reduced to zero.

9.5. Results of experiments on sediments

Having established that the coil was capable of producing the required maximum peak alternating fields, two test samples were selected for treatment. Both of these samples were sediments, and were known to carry an appreciable secondary component of remanence,

which could be removed by thermal demagnetisation at 300°C, leaving a stable underlying component with a shallow negative south-easterly direction.

It was accepted that there was a high probability of at least small components of anhysteretic remanence being induced in the samples as a result of imperfect experimental conditions (irregularities in rate of reduction of field, asymmetries of waveform etc.) A method suggested by Snape (1965) was therefore used, in an attempt to cancel out such components.

The specimen was first demagnetised along one axis at a peak field H_{max}, and was then turned through 180° and demagnetised at $\frac{1}{2} H_{max}$. If the induced ARM is directly proportional to the peak field, then demagnetisation at H_{max} will result in the production of an ARM of intensity J_A, along the axis of the coil. Subsequent demagnetisation at $\frac{1}{2} H_{max}$ in the opposite direction (ie - $\frac{1}{2} H_{max}$) will remove half of this ARM, reducing its intensity to $\frac{1}{2} J_A$, and will add a component of intensity $-\frac{1}{2} J_A$ in the opposite direction. The net ARM will then be zero.

The sequence of operations at each peak field value was:

1. Demagnetise along + x axis at H_{max}. Measure this component.
2. Demagnetise along -x axis at $\frac{1}{2} H_{max}$, and remeasure.
3. Demagnetise along +y axis at H_{max}, and measure.
4. Demagnetise along -y axis at $\frac{1}{2} H_{max}$, and remeasure.
5. Demagnetise along +z axis at H_{max}, and measure.
6. Demagnetise along -z axis at $\frac{1}{2} H_{max}$, and remeasure.

The mean direction and intensity of remanence of the sample was then calculated, firstly from the three sets of readings corresponding to $+ H_{max}$, and then from the three sets of readings corresponding to $-\frac{1}{2} H_{max}$.

The first sample (2073 C1) was treated at 180 Oe intervals up to a maximum peak field of 5040 Oe, and the results are listed in Table 9.2, and illustrated in Figs. 9.13 and 9.14. It can be seen from Fig 9.14(a) that after treatment at $+H_{max}$ only, the intensity of magnetisation changes erratically throughout the whole range of treatment, and rarely drops below its original value; treatment above 4,500 Oe results in very large increases. The direction of magnetisation (Fig 9.13(a)) shows similar erratic changes, although an overall pattern of fluctuation between north westerly and south easterly declinations is evident.

After treatment at both $+H_{max}$ and $-\frac{1}{2}H_{max}$, variations in intensity are a lot smaller (Fig 9.14(b)), but the directions of magnetisation undergo larger and more erratic changes. (Fig 9.13(a)).

It is clear that anhysteretic components were produced in the sample over the whole range of treatment. The intensity of the induced component is very variable over the range 1800 to 3800 Oe, and increases rapidly above 4,500 Oe. Thus although treatment by Snape's method, aimed at cancelling the ARM, does reduce its intensity, a substantial part of this component remains.

In order to check that the above behaviour was not peculiar to one sample only, a second sample was demagnetised at several values over the same range. The behaviour of this sample was broadly similar to that of 2073 C1.

The failure of Snape's method to cancel the induced ARM is probably due to the intensity of the latter not being directly proportional to H_{max}. The probable source of the ARM is discussed in the next chapter, together with suggestions for reducing or elminating it. This is clearly necessary before the apparatus can be successfully used for effective high-field demagnetisation.

References

As, J.A. and J.D.A. Zijderveld, 1958. Magnetic cleaning of rocks in palaeomagnetic research. Geophys. J., 1, 308

Brynjolfsson, A. 1957. Studies of remanent magnetism and viscous magnetism in the basalts of Iceland. Adv. Phys., 6, 247

Cockcroft, J.D. 1928. Phil. Trans. A., 227, 317

Cox, A., 1961. Anomalous remanent magnetisation of basalt. U.S. Geol. Surv. Bull., 1083-E, 131-160

Cox, A., and Doell, R.R., 1963. J. Geophys. Res., 68, p1997

Creer, K.M., 1959. A.C. demagnetisation of unstable Triassic Keuper Marls from S.W. England. Geophys. J.R. astr. Soc., 2, 261.

Daniels, J.M., 1950. A 100-killowatt water-cooled solenoid. Proc. Phys. Soc., B63, 1028-1034

Fabry, C., 1898., Elairage Electrique, 17, 133

Hutchings, A.M.J. 1966. A note on alternating field demagnetising apparatus. Geophys. J.R. astr. Soc., 11, 555-556.

Irving, E., P.M. Stott, and M.A. Ward, 1961. Demagnetisation of igneous rocks by alternating magnetic fields. Phil. Mag., 6, 225-241

Maxwell, J.C. 1881. Treatise on Electricity and Magnetism, 2nd Ed. Vol II (Oxford: Clarendon Press), p331

Néel, L. 1942. Cahiers Phys. No. 12, 2

Néel, L. 1943. Cahiers Phys. No. 13, 18

Néel, L. 1955. Some theoretical aspects of rock magnetism Adv. Phys., 4, 191

Preisach, F. 1935. Z. Phys., 94, 277

Lord Rayleigh, 1887, Adv. Phys., 4, P191-241

Rimbert, F. 1959. Contribution a l'étude de l'action de champs alternatifs sur les aimantations rémanentes des roches. Extr. Rev. de l'Inst. Francais du Petrole, 14, 1

Snape, C., 1965. Alternating field demagnetisation of sediments. Ph.D. Thesis. Univ. of Newcastle upon Tyne.

Stacey, F.D., 1963. The Physical theory of rock magnetism. Adv. Phys. 12, 45-133

Thellier, E., and F. Rimbert, 1954. Sur l'analyse d'aimantations fossiles par action de champs magnétique alternatifs. C.R. Acad. Sci. Paris, 239, 1399-1401

Thellier, E., and F. Rimbert, 1955. Sur l'utilisation en palaéomagnétisme de la désaimantation par champs alternatifs. C.R. Acad. Sci. Paris, 240, 1404-1406.

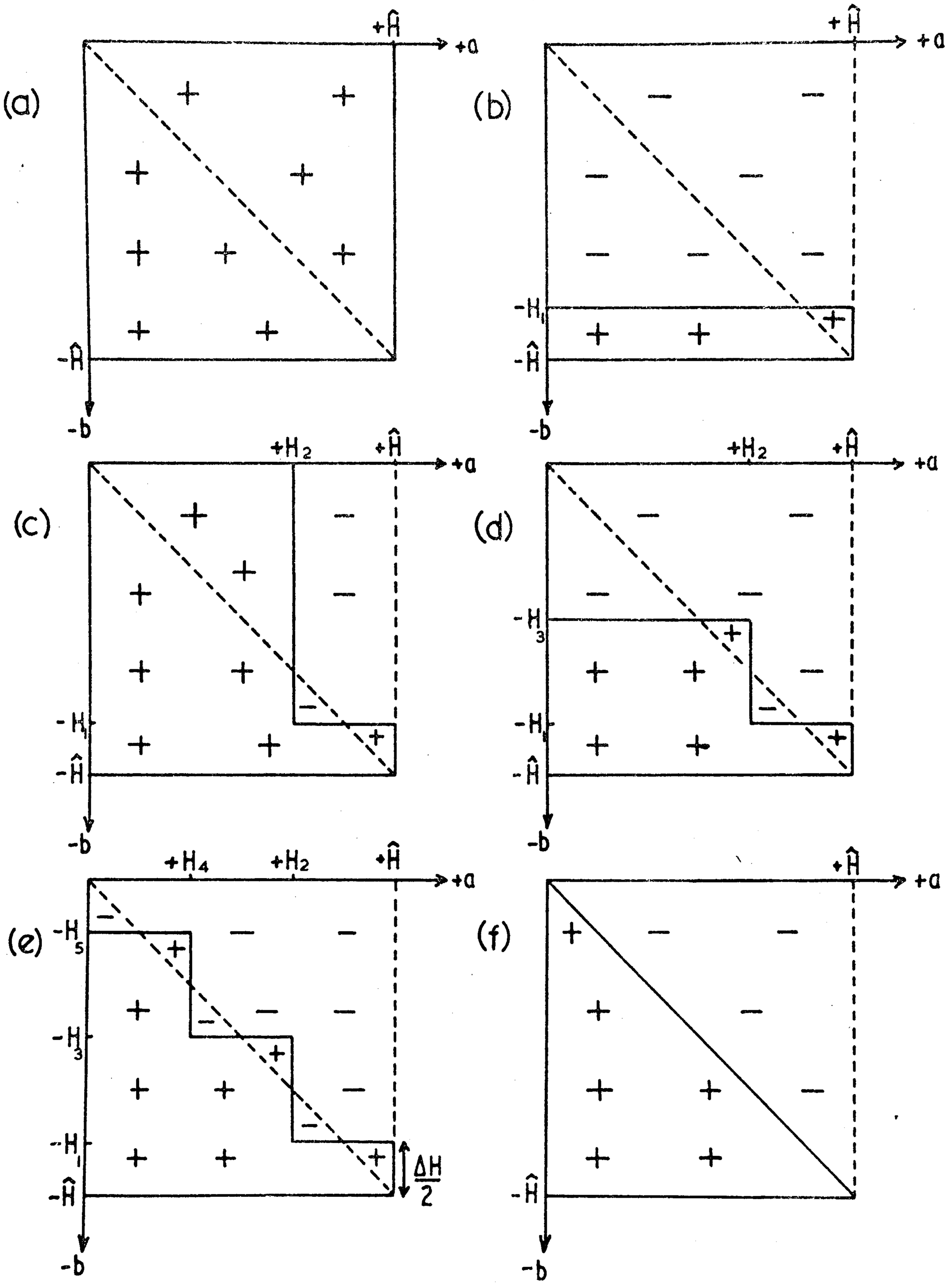


Fig 9.4 Explanation of AF demagnetisation by means of Preisach diagrams. (a) to (d) Magnetic states of rocks during successive half cycles of decreasing applied alternating field. (e) and (f) Magnetic state after field reduced to zero.

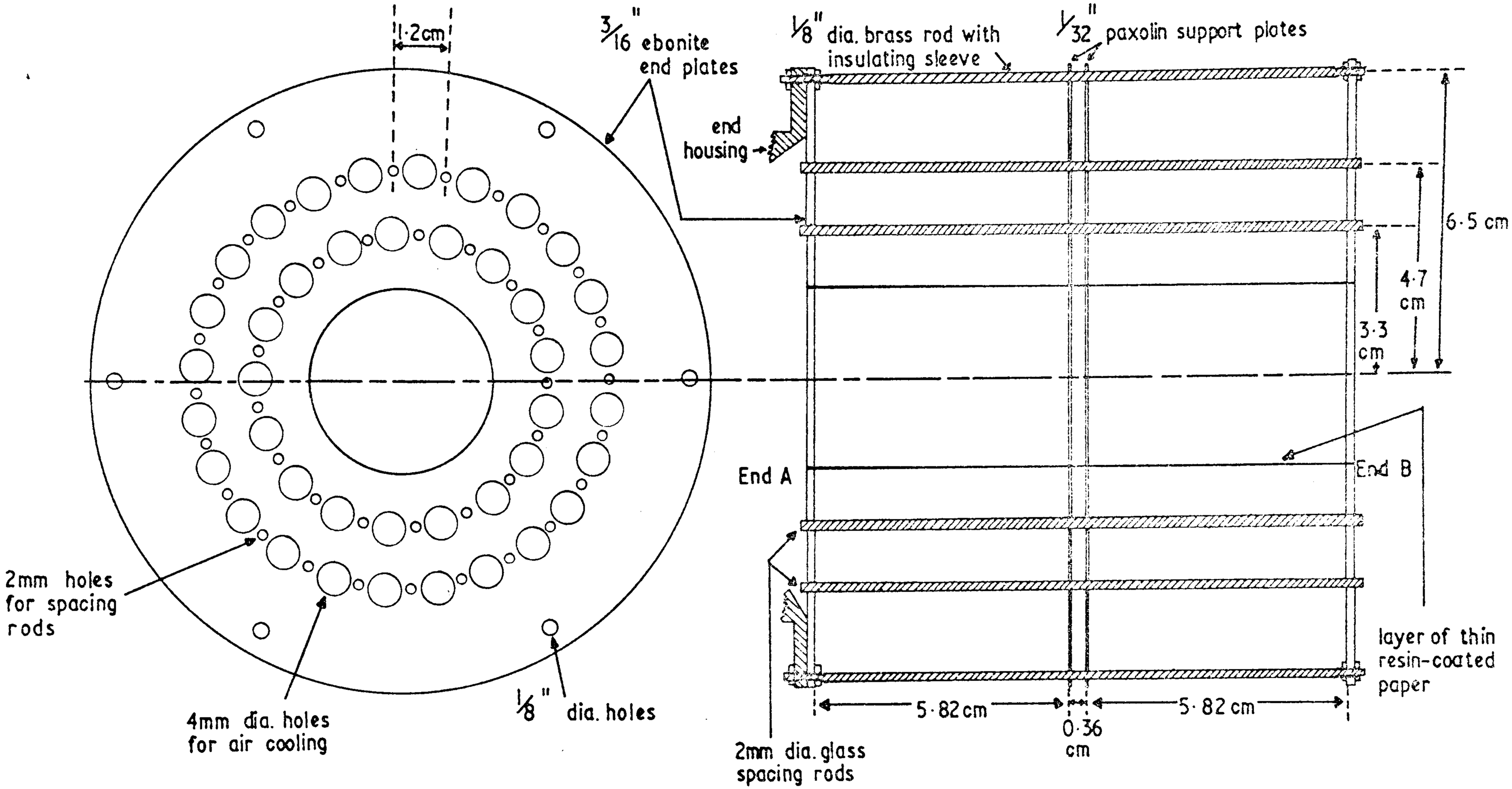


Fig 9.6 Construction of coil former.

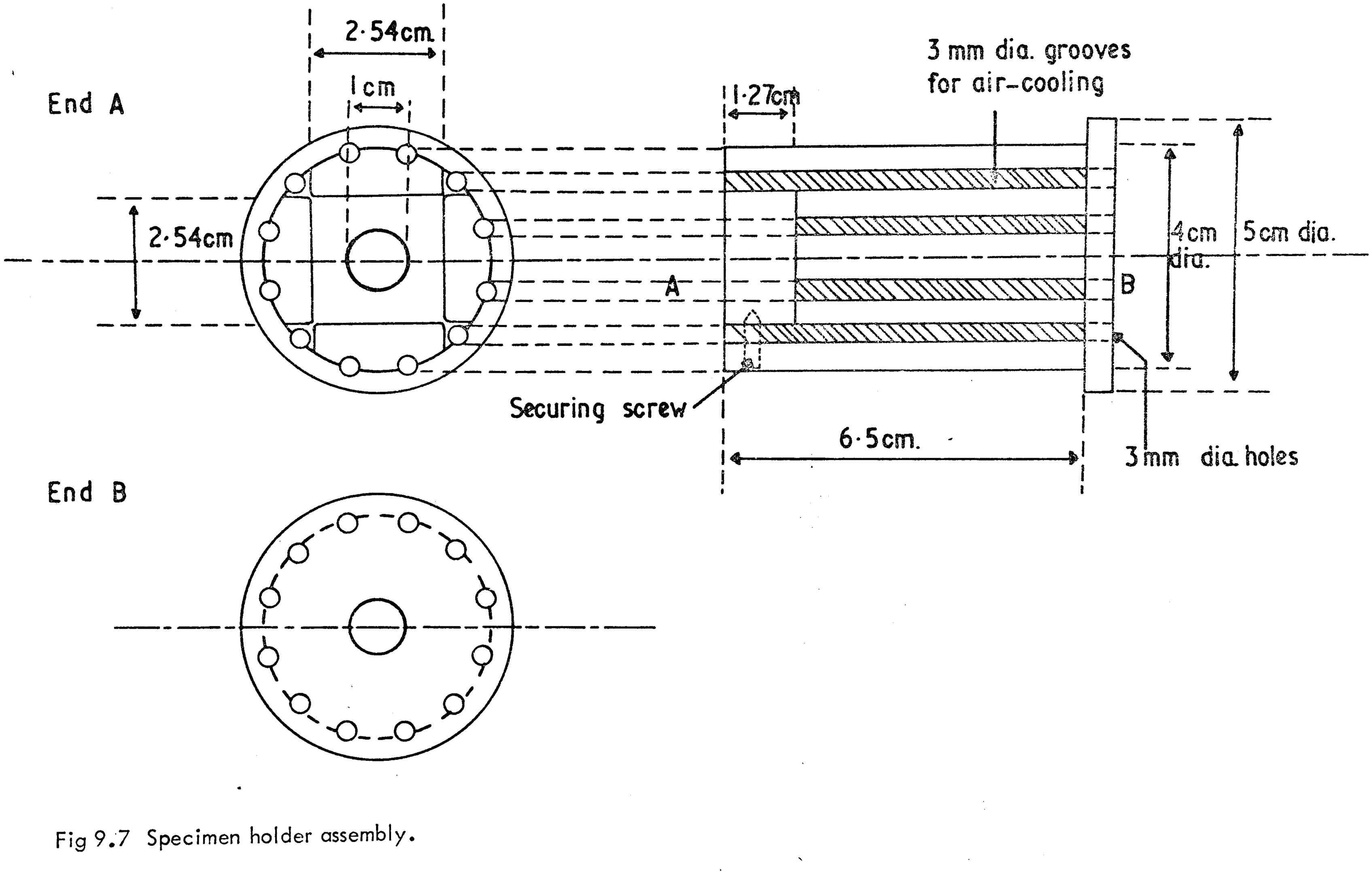


Fig 9.7 Specimen holder assembly.

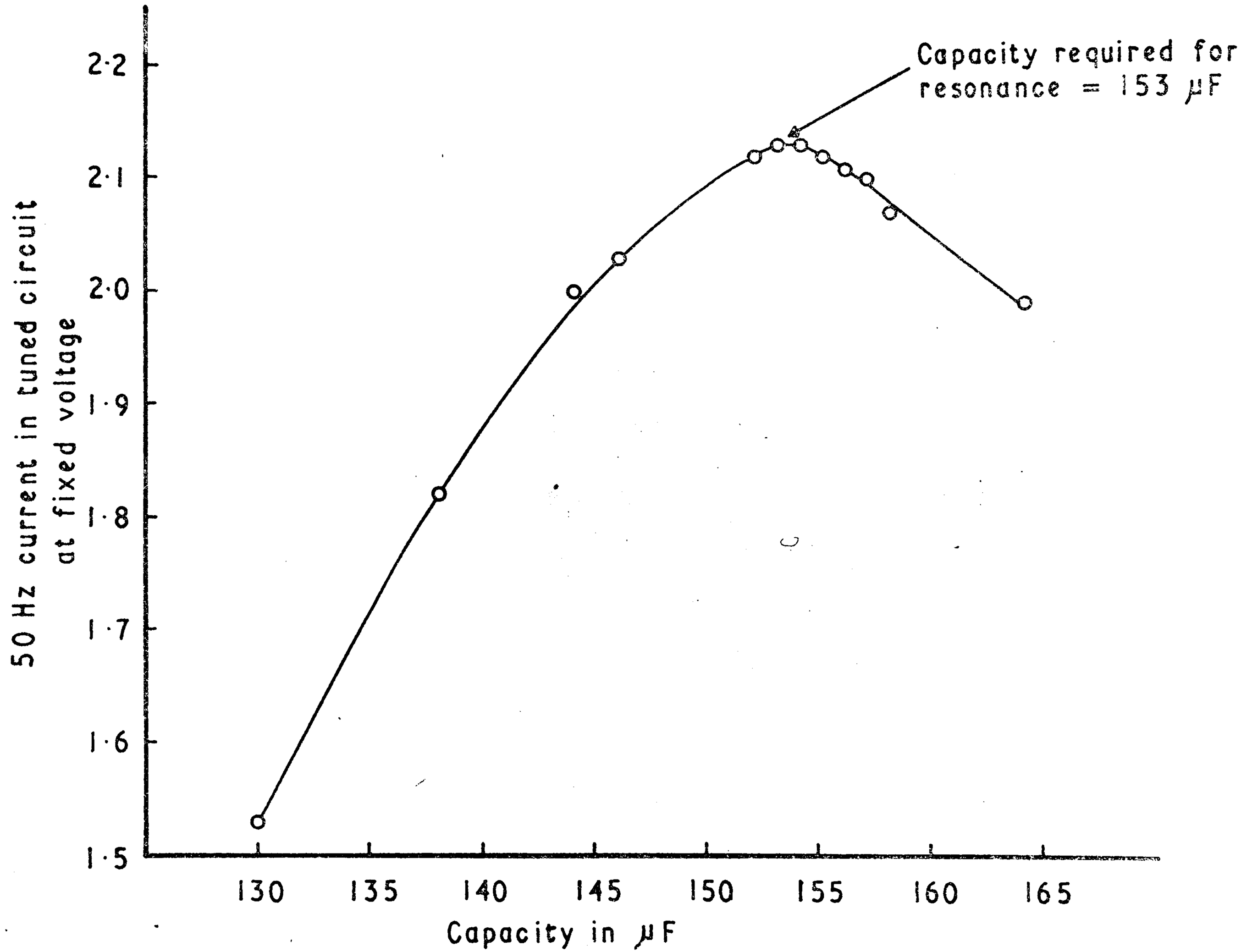


Fig 9.8 Coil tuning.

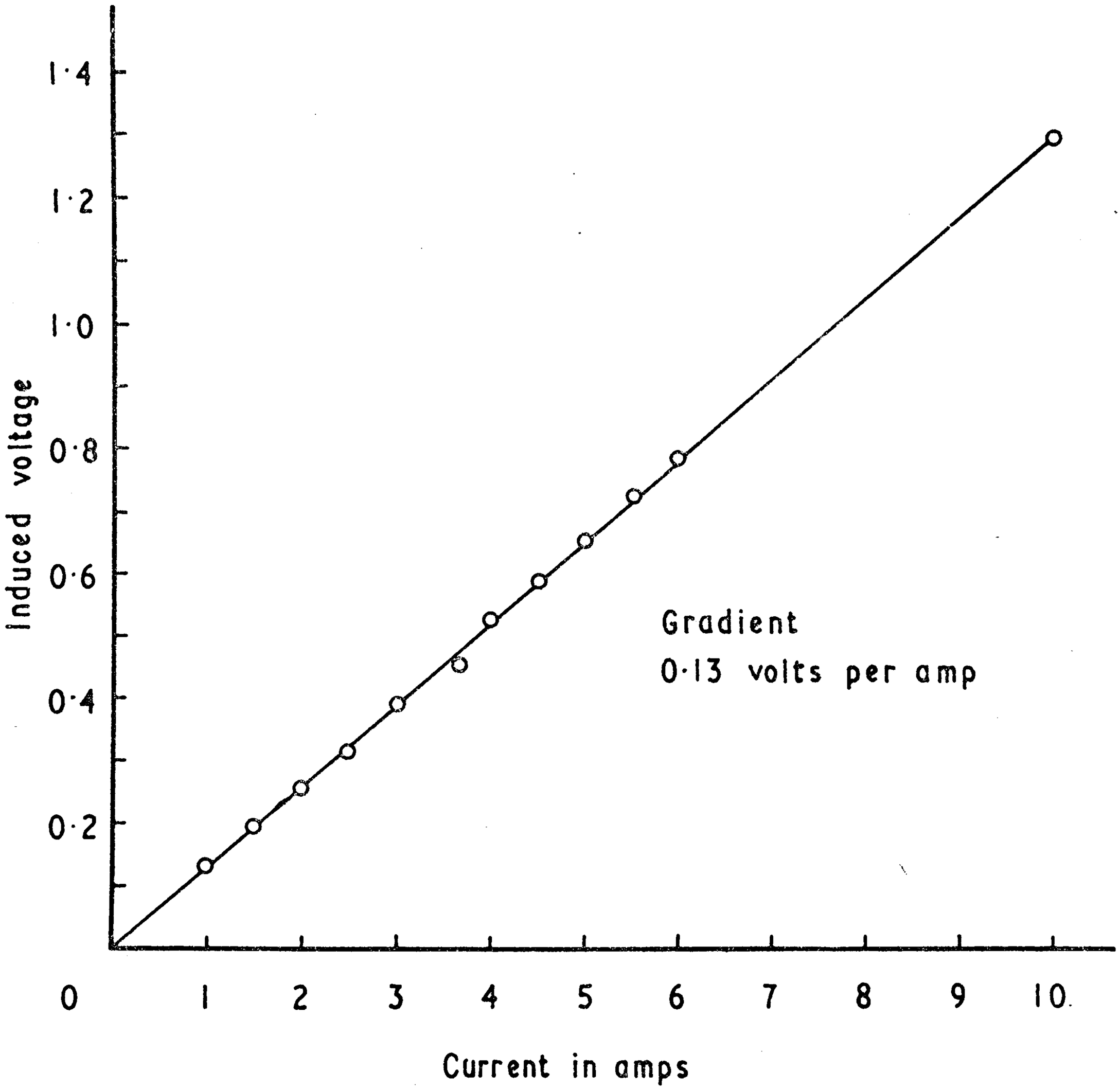


Fig 9.9 Coil calibration.

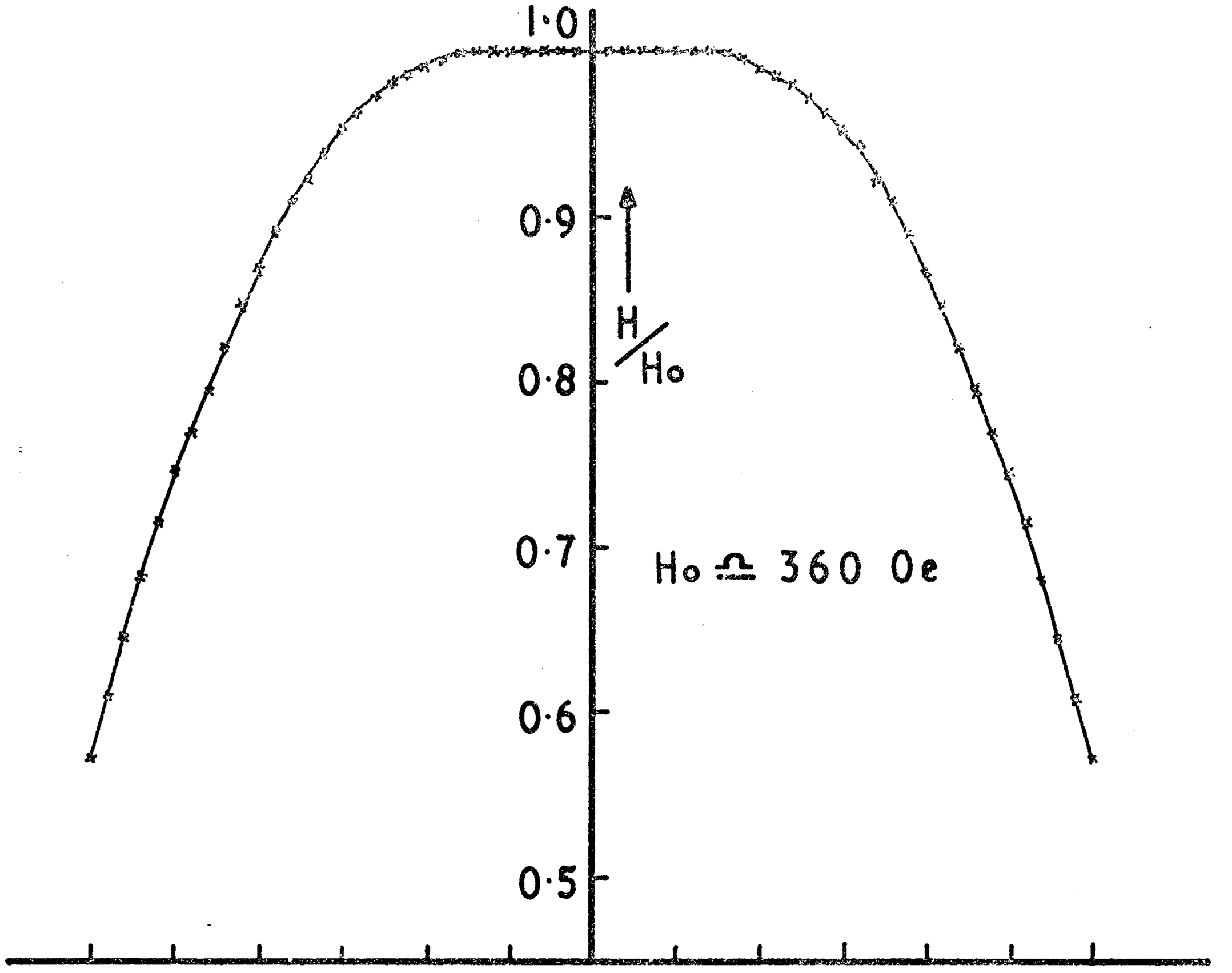


Fig 9.10 Variation of field along axis of coil.

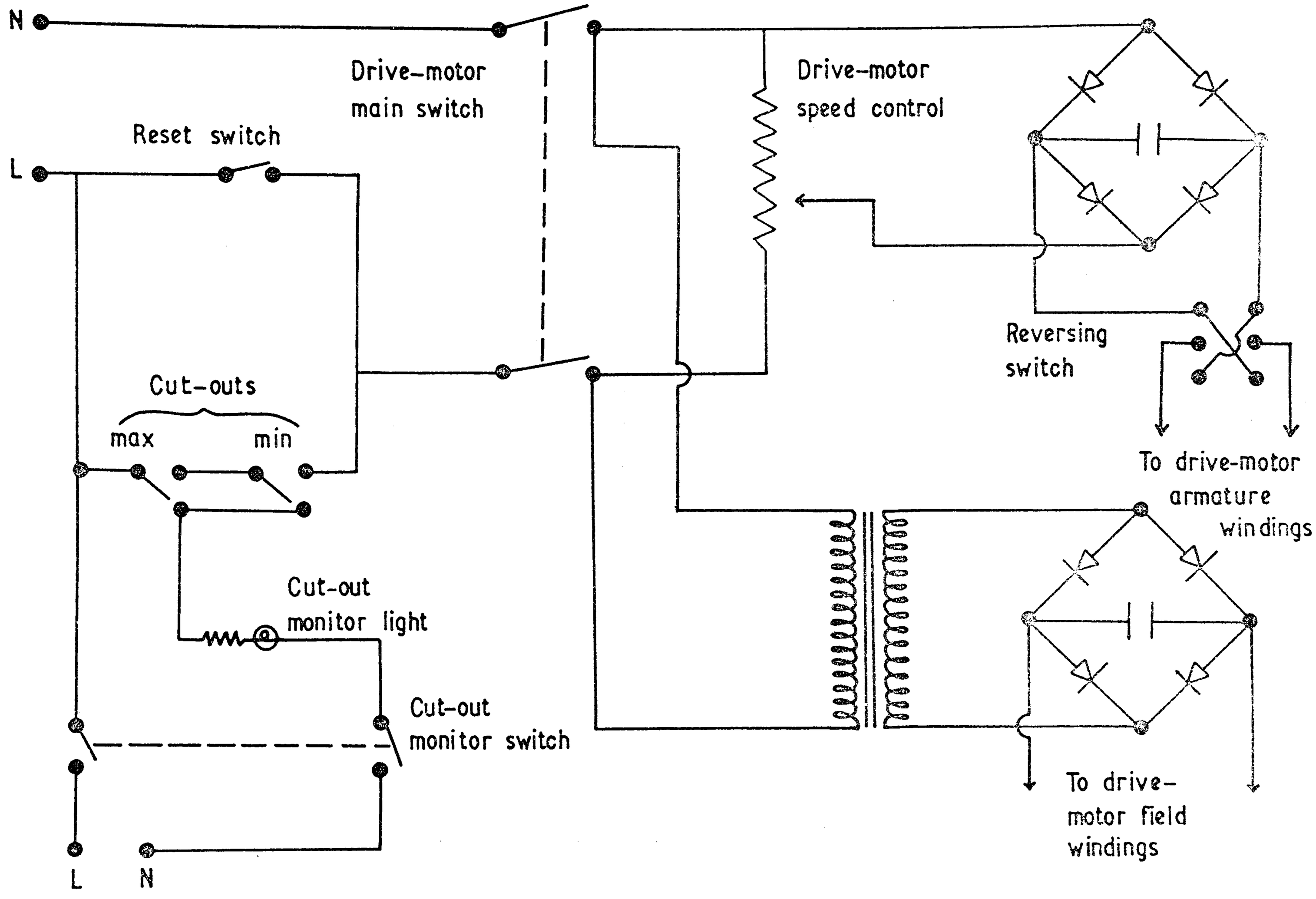


Fig 9.11 Variable inductance drive motor circuit.

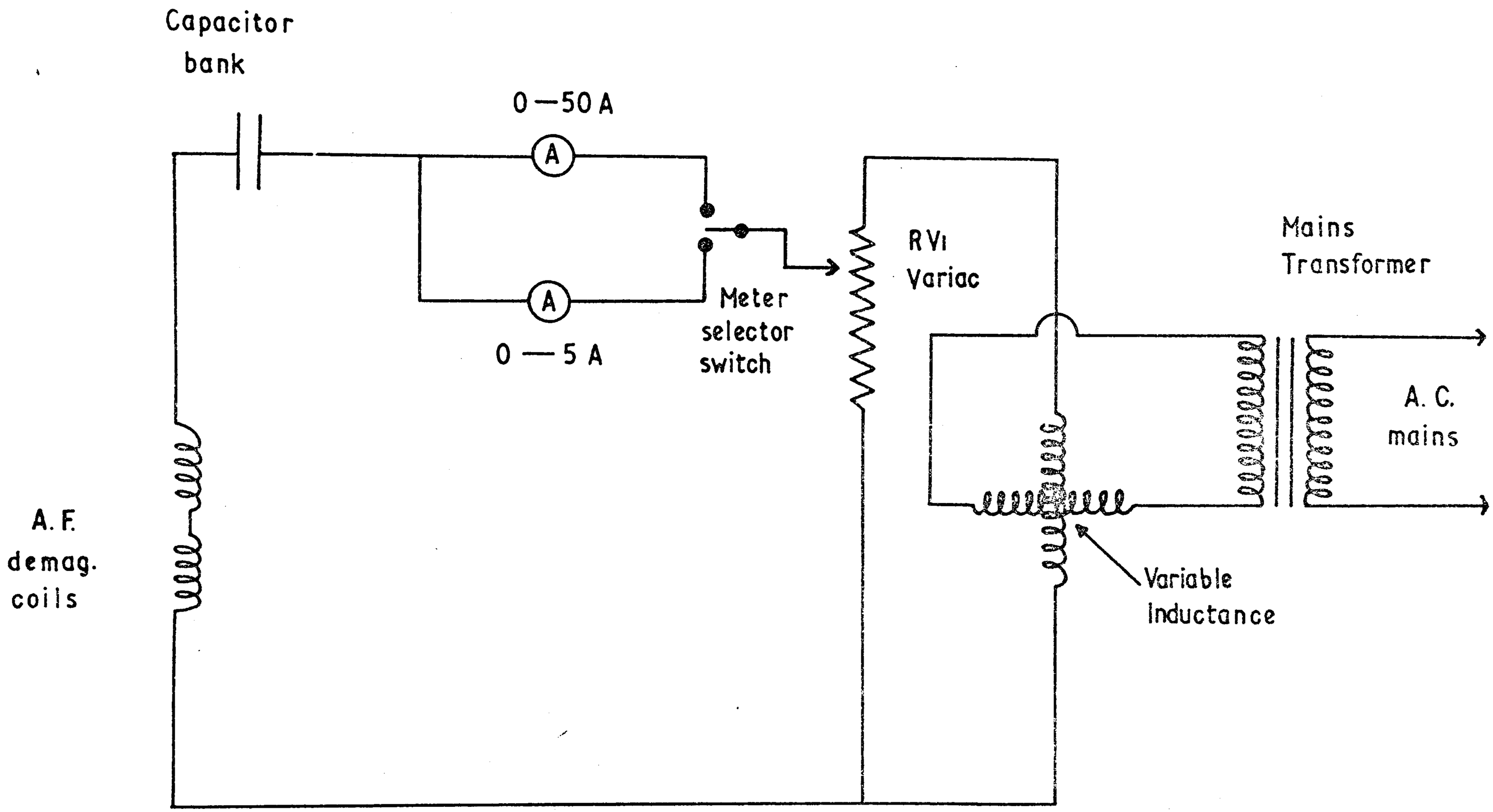


Fig 9.12 Demagnetising coil circuit.

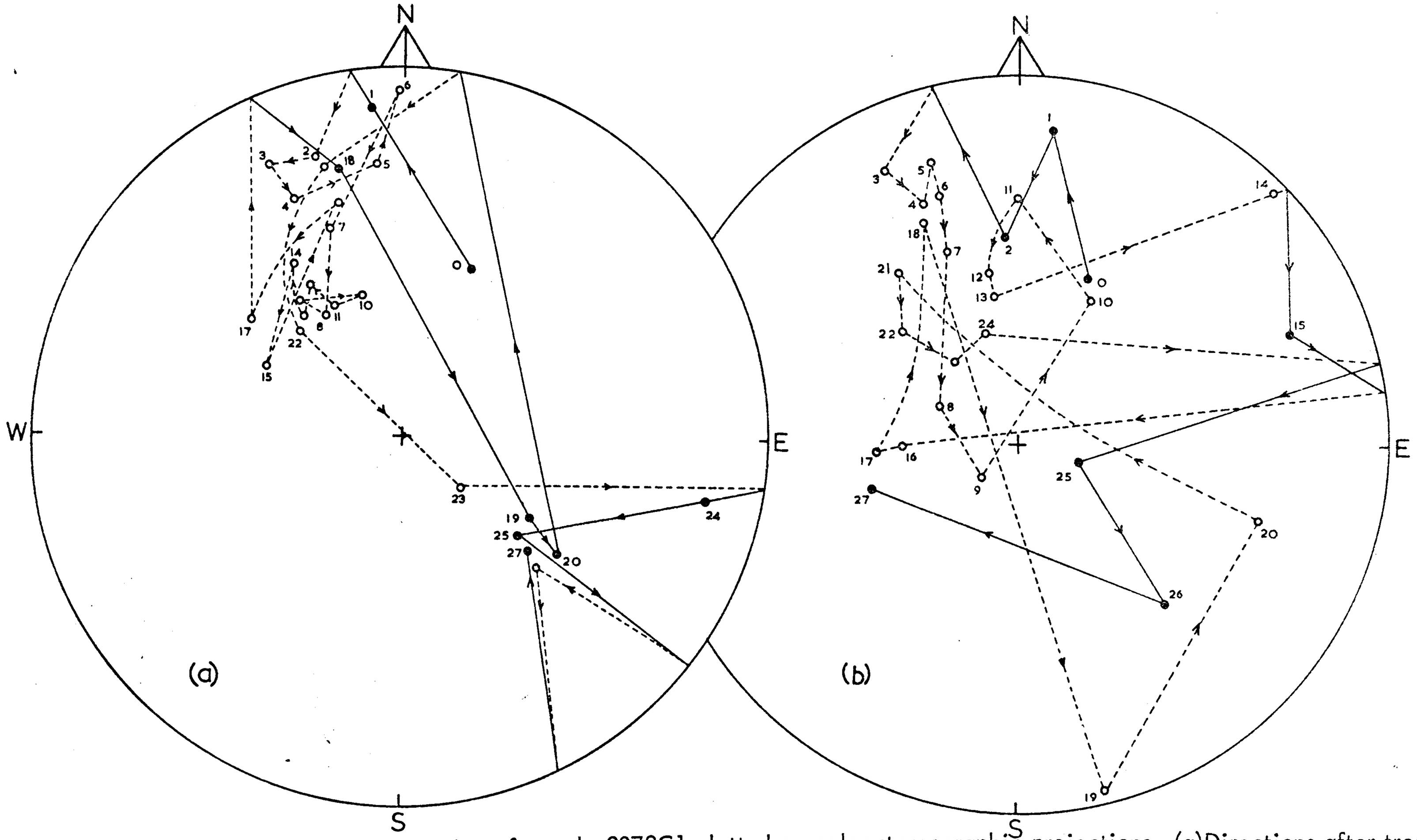


Fig 9.13 Results of AF demagnetisation of sample 2073C1 plotted on polar stereographic projections. (a)Directions after treatment at $+h_{max}$ only. (b) After treatment at $+h$ max and $-\frac{1}{2}h$ max. Numbers refer to field values in Table 9.2.

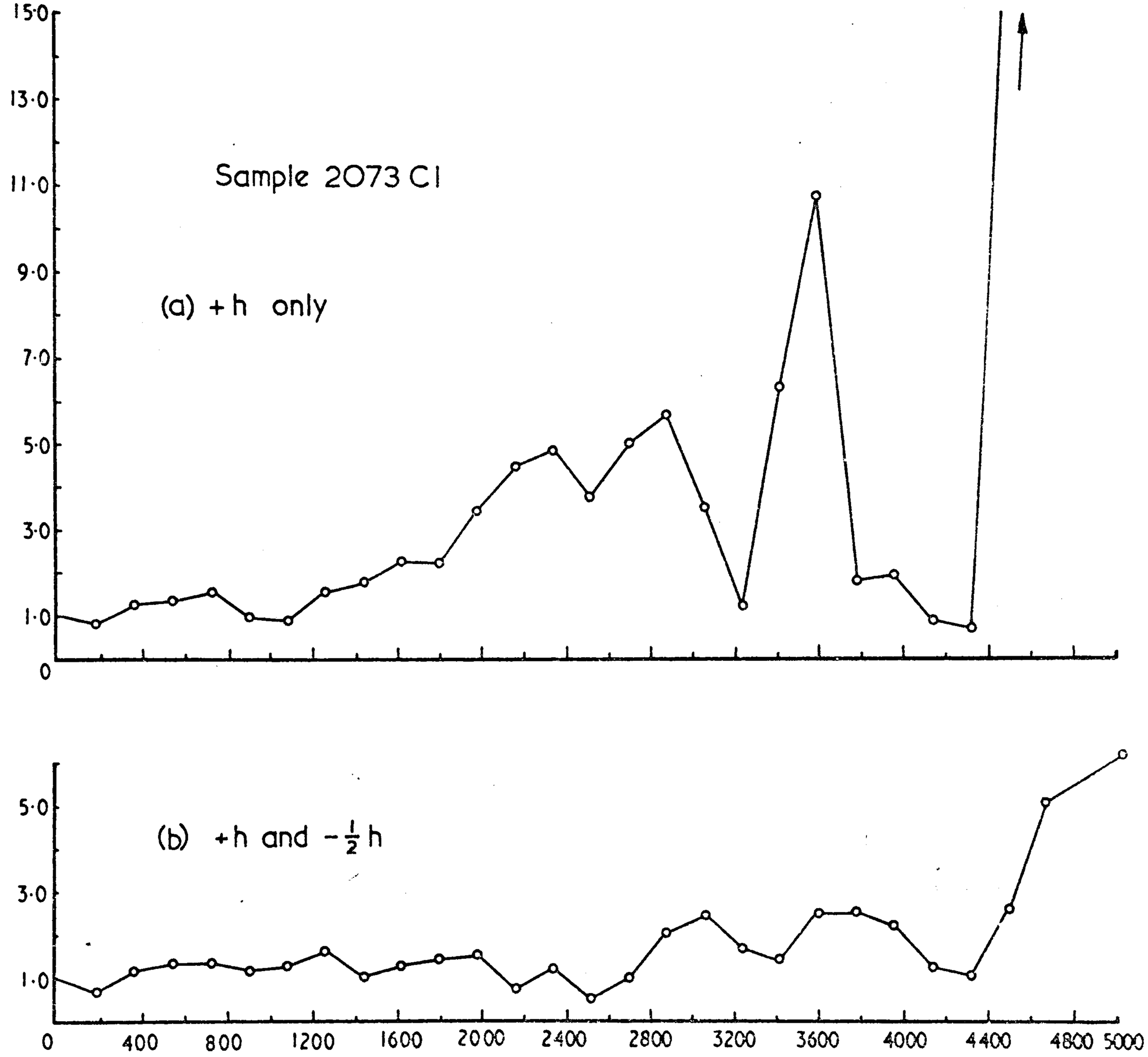


Fig 9.14 Variation of intensity of sample 2073C1 during progressive demagnetisation. (a) After treatment at $+h_{max}$ only. (b) After treatment at +h and $-\frac{1}{2}h$.

Table 9.2 Results of A.F. demagnetisation on Sample No. 2073 C1

Ref.No (Fig 9.6)	Treatment pk.AF in Oe) H	+h only x	y x10^{-5}	z	Dec	Inc	Int(x10^{-6})	M/M_o	+h and -$h/2$ x	y x10^{-5}	z	Dec	Inc	Int(x10^{-6})	M/M_o
0	NRM	+3.00	-1.27	-2.58	23	+38	3.39	1.00	+3.00	-1.27	-2.58	23	+38	3.39	1.00
1	180	+3.37	+0.33	-0.39	354	+7	2.78	0.82	+2.95	-0.31	-0.49	6	+9	2.45	0.72
2	360	+4.80	+1.59	+1.31	342	-15	4.25	1.25	+4.19	+0.26	-2.61	356	+32	4.03	1.19
3	540	+4.92	+2.47	+1.21	333	-12	4.60	1.36	+4.83	+2.48	+1.09	333	-11	4.51	1.33
4	720	+5.40	+2.60	+2.20	335	-20	5.22	1.54	+4.90	+1.90	+1.90	338	-20	4.58	1.35
5	900	+3.80	+0.40	+1.10	354	-17	3.20	0.94	+4.30	+1.40	+1.00	342	-13	3.82	1.13
6	1080	+3.75	+0.08	+0.26	359	-4	3.06	0.90	+4.77	+1.54	+1.85	342	-20	4.35	1.28
7	1260	+1.90	+1.90	+3.10	340	-29	5.23	1.54	+5.40	+2.00	+3.60	339	-32	5.51	1.62
8	1440	+4.11	+2.66	+5.40	327	-48	5.94	1.75	+0.77	+1.65	+3.75	295	-64	3.39	1.00
9	1620	+5.58	+4.30	+6.04	322	-41	7.56	2.23	-0.90	+0.95	+5.03	226	-75	4.24	1.25
10	1800	+6.00	+1.70	+6.80	344	-47	7.54	2.22	+3.90	-2.00	+4.10	27	-43	4.88	1.44
11	1980	+8.60	+4.60	+10.60	332	-47	11.62	3.43	+5.80	-0.02	+2.50	360	-23	5.14	1.52
12	2160	+12.20	+7.60	+11.60	328	-39	15.11	4.46	+2.26	+0.04	+1.91	350	-40	2.43	0.72
13	2340	+10.60	+9.50	+14.20	318	-45	16.42	4.85	+3.43	+0.63	+3.64	349	-46	4.11	1.21
14	2520	+11.20	+7.20	+8.30	327	-32	12.77	3.77	+1.47	-1.46	+0.27	45	-2	1.69	0.50
15	2700	+6.50	+13.20	+14.70	296	-45	16.93	5.00	+1.47	-3.55	-0.92	68	+13	3.22	0.95

Table 9.2 contd.

Ref.No (Fig 9.6)	Treatment pk.AF in Oe) H	+h only x	y x10^{-5}	z	Dec	Inc	Int(x10^{-6})	M/M_o	+h and - $h/2$ x	y x10^{-5}	z	Dec	Inc	Int(x10^{-6})	M/M_o
16	2880	+20.80	+5.80	+9.40	344	-24	19.23	5.68	-0.15	+4.93	+7.10	268	-55	7.05	2.08
17	3060	+7.20	+9.40	+8.30	307	-35	11.80	3.48	-0.46	+6.84	+7.71	266	-48	8.40	2.48
18	3240	+4.70	+1.10	-1.50	346	+17	4.13	1.22	+5.90	+2.50	+2.90	336	-24½	5.73	1.69
19	3420	-10.00	-15.90	-18.50	122	+45	21.50	6.35	-5.60	-1.50	+0.20	165	-2	4.71	1.39
20	3600	-22.50	-30.00	-24.90	127	+34	36.58	10.80	-2.82	-9.23	+3.68	107	-21	8.40	2.48
21	3780	+7.40	+2.20	+2.20	343	-16	6.20	1.77	+7.80	+5.70	+5.70	324	-31	8.60	2.53
22	3960	+4.00	+4.10	+6.20	315	-47	6.50	1.91	+4.90	+5.20	+6.70	313	-43	7.50	2.21
23	4140	-1.00	-1.20	+3.40	130	-66	2.88	0.85	+2.30	+1.80	+4.80	322	-59	4.30	1.26
24	4320	-0.55	-2.80	-0.45	101	+9	2.21	0.65	+2.56	+0.82	+3.90	343	-55	3.62	1.06
25	4500	-36.80	-44.50	-57.00	130	+45	62.5	18.40	-1.02	-3.75	-10.90	105	+70	8.90	2.62
26	4680	-62.00	-66.00	+65.00	133	-36	86.0	25.30	-14.30	-13.60	-10.90	137	+29	17.30	5.10
27	5040	-80.00	-91.00	-100.00	132	+40	121.0	35.60	-6.00	+18.60	-19.70	252	+45	21.30	6.20

CHAPTER 10. INVESTIGATIONS INTO THE EFFECTS OF ASYMMETRICAL ALTERNATING FIELD ON A.F. DEMAGNETISATION

10.1 Introduction

The attempts at high field A.F. demagnetisation of sediments described in the previous chapter were unsuccessful mainly because of the production of large Anhysteretic Remanent Magnetisations (A.R.M.s) in the samples. The possible sources of these ARMs are as follows:

1. The presence of small direct fields, superimposed on the alternating field, and resulting from inadequate cancellation of the earth's magnetic field.
2. Sharp irregularities in the rate of reduction of the alternating field to zero.
3. Deviations of the applied alternating field waveform from a perfectly symmetrical sinusoidal pattern.

The first of these possibilities is unlikely to contribute a significant ARM because the field was always cancelled to within $\pm$ 1γ along the axis of the coil. Cancellation at right angles to the axis was less-perfect ($\pm$ 5γ), but this is unimportant, since even if it were sufficient to produce an ARM in the sample, the direction of this ARM would be the same as that of the steady field, i.e. at right angles to the axis (Rimbert 1959). The component of magnetisation of the sample along any particular axis was always measured immediately after demagnetisation along that axis, to guard against the possibility of subsequent treatment along the other two orthogonal axes affecting the magnetic component along the first axis.

The second possible source of ARMs, viz sharp irregularities in the rate of reduction of the alternating field to zero, may be more significant. All possible precautions were taken to reduce the

current through the coil as smoothly as possible, but sharp drops still occurred.

Fig 10.1 shows the typical form of variation of current through the coil, as it was gradually reduced from its maximum value to zero. This plot was obtained by passing the current through a rectifier, and developing a direct voltage across a resistance. This voltage was fed to one channel of an X-Y recorder, and the other channel recorded time. Several runs were performed, both at the same rate of reduction of current, and at different rates, and, as can be seen from Fig 10.1, numerous sharp kinks occur at similar points on each curve. This indicates that the sharp drops in current are not due to transient effects in the mains supply, but are functions of the position of the rotating armature of the variable inductance. They are probably related to the geometry of the windings in this unit.

The magnitude of these drops are of the order of 0.5 to 1.0%, and they occur over time intervals of a fraction of a second. This means that if a peak alternating field of 5000 Oe is being produced by the coil, the magnitude of the drop will be 50 Oe. If this drop occurs in a time interval of half a second (which seems likely from Fig. 10.1), then it will correspond to a drop of 1 Oe in half a cycle at 50 Hz mains supply frequency.

If a three-axis rotation system had been used, there would have been a significant change in the field value during the time taken to execute one complete sequence of rotation. All directions in the rock would not then have "seen" the same demagnetising field, and an ARM would have resulted. However in the case of a single-axis

demagnetising system it is less clear whether drops in field of the order of one oersted in half a cycle are significant. It will depend largely on the number of grains present with coercive forces in the appropriate interval. The presence of these irregularities in the current reduction curves is clearly undesirable, and the 'Inductrol' variable inductance unit must be regarded as being far from ideal for the purpose used. Solid-state current reduction devices such as that used in the commercially built "Schonstedt" A.C. demagnetizer are far more suitable, but the upper limit of operation of these devices is at present only ten to fifteen amps. Further development is required before the very high currents required for the demagnetisation of sediments, can be successfully handled.

Although it is possible that ARMs were produced in the samples as a result of these sharp decreases in current, they are unlikely to be large, and would certainly not approach the order of magnitude observed in the samples described in Chapter 9.

The third possible source of ARMs is the presence of distortions in the wave-form of the applied alternating field. These are likely to be more important than small-scale fluctuations in the rate of reduction of field, since they will be present throughout the whole period of reduction of field, and will therefore affect grains of all coercive forces up to the maximum applied field.

Various authors, e.g. As and Zijderveld, 1958, have discussed the effects of distorted waveforms, and have concluded that even harmonics, particularly second harmonics, are likely to be harmful, since they produce asymmetrical distortion, whereas odd harmonics are unimportant, since they produce symmetrical distortion. Although this is true in general, it is also possible for there to be a

substantial second harmonic component in a waveform which is symmetrical about the axis. This is illustrated in Fig 10.2, which represents a plot of the function sin θ + 0.05 sin 2θ, i.e. a sine wave with 5% second harmonic content. Despite the high second harmonic, the curve is symmetrical about the axis, the reason for this lying in the phase difference between the fundamental and second harmonic components. In the waveform illustrated the two components are in phase, and there is no asymmetry, whereas maximum asymmetry would occur if there was a 45^{o} phase difference.

The factor of importance in the production of ARMs is the effective steady field superimposed on the alternating field, and this is related directly to the percentage asymmetry of the field. As illustrated above, it is not necessarily directly related to the percentage second harmonic content of the waveform. Quantitative measurements of the effects of asymmetrical waveforms have not been previously reported in the literature, and the work described in the remainder of this chapter was therefore carried out for two reasons. Firstly, the effects of a wide range of values of asymmetry on a variety of different rocks was investigated, to evaluate the importance of this quantity in general terms. The results were then inspected, to see if they could explain the observed behaviour of the samples during high field demagnetisation, described in Chapter 9.

10.2 Measurement of Asymmetry

10.2.1. Definition of percentage asymmetry

The term 'percentage asymmetry' as used in the following sections, represents the percentage ratio of the difference between the amplitudes of the positive and negative half-cycles to the mean amplitude, i.e.

$$\text{asym} = \frac{H_A - H_B}{(H_A + H_B)/2} \times 100$$

$$= \frac{2\,(H_A - H_B)}{H_A + H_B} \times 100 \qquad (10.1)$$

where H_A is the amplitude of the largest half-cycle and H_B is the amplitude of the smallest half-cycle, as illustrated in Fig 10.3.

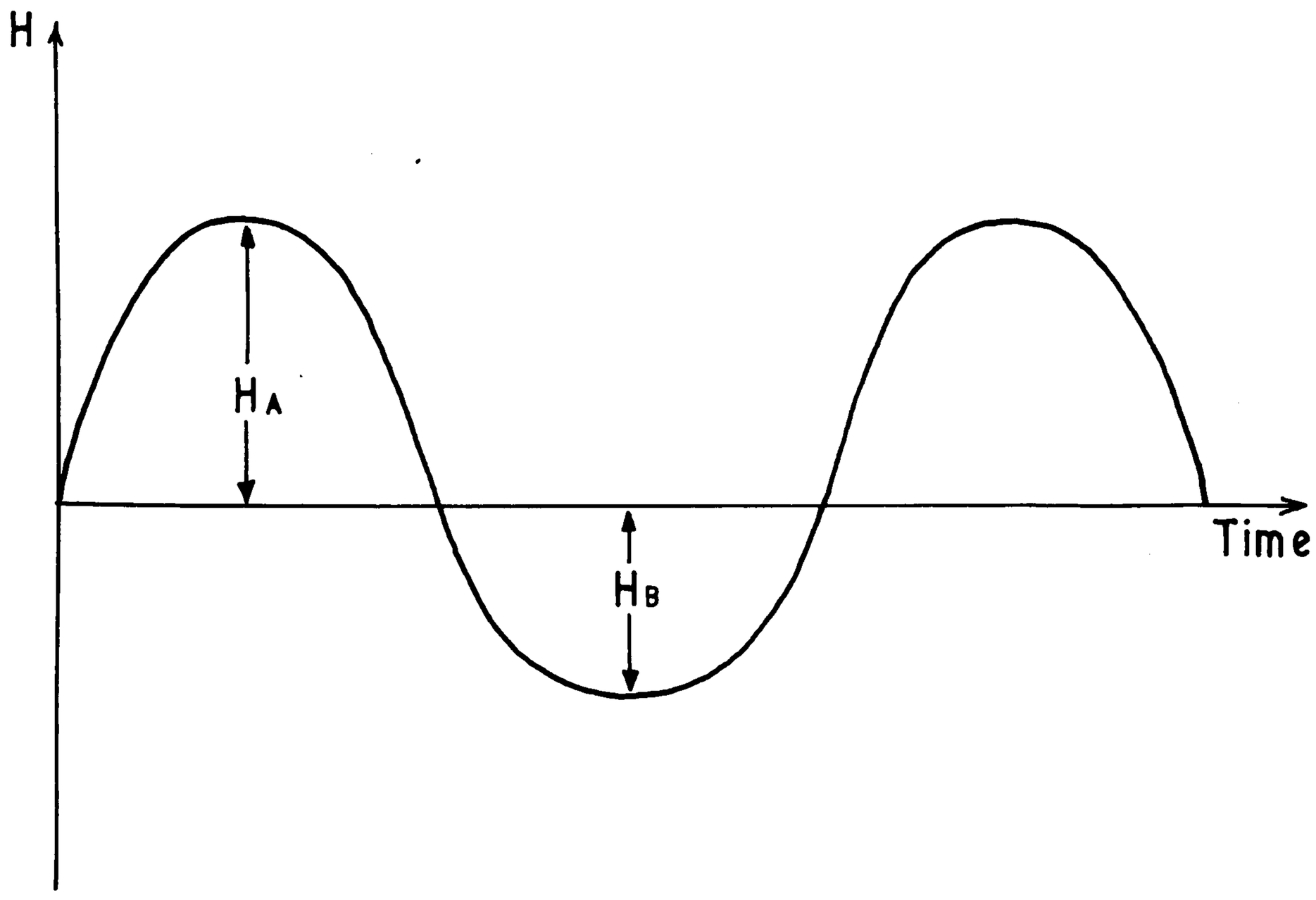
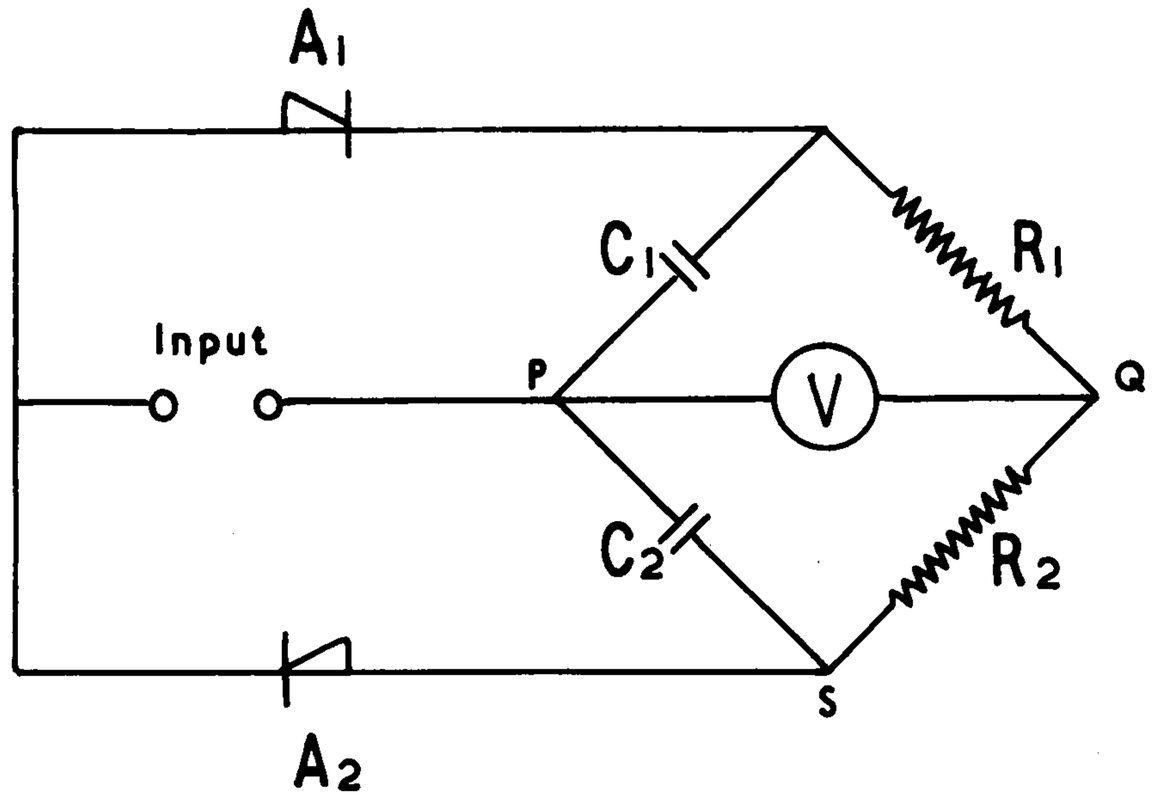


Fig 10.3

10.2.2. Asymmetry meter

The value of the asymmetry was measured by means of a new instrument designed by Dr. L. Molyneux. This instrument consists essentially of two rectifiers connected back to back, and the current entering the instrument is divided so that exactly half passes through each rectifier. The difference between the mean peak values of the positive and negative half-cycles is then measured and displayed on a centre-zero output meter as a fraction of the input voltage. The principle of the circuit is illustrated in Fig 10.4(a).

Fig 10.4(a)



If it is supposed that A_1 and A_2 are perfect rectifiers (i.e. the forced voltage drop is zero and the reverse impedance infinite), then the voltage across the capacitor C_1 will change to the peak value of the positive half-cycle, and that across C_2 to the peak value of the negative half-cycle. If the resistances R_1 and R_2 have identical values, which, combined with the capacitances C_1 and C_2 give a time constant which is long compared with the period of the input waveform, then, if the peak value of the negative half-cycle is equal to that of the positive half-cycle, the voltmeter (assumed to have infinite impedance) will register zero volts. If the peak values of the positive and negative half-cycles are not equal, then a potential difference will result across PQ, and the voltmeter will register a deflection.

Suppose for example that the positive peak value is 2.1 volts and the negative peak value is 2.0 volts. Then if point S in the circuit is taken as zero potential, point P will be at 2 volts, and the potential at point Q will be given by

$$V_Q = \frac{R_2}{R_1+R_2} \times (2 + 2.1) = \frac{4.1}{2} = 2.05 \text{ volts}$$

The potential difference registered by the meter will then be 0.05 volts.

Using the definition of percentage asymmetry given in Section 10.2.1, i.e. the percentage ratio of the difference between the amplitudes of the positive and negative half-cycles to the mean amplitude, it follows in this case that:

$$\% \text{ asym} = \frac{0.1}{2.05} \times 100 \simeq 5\%$$

Thus if a setting up procedure is used to adjust the mean peak height to 2 volts, the percentage asymmetry will be given by the voltmeter reading multiplied by 100

In practise perfect rectifiers do not exist, but these were simulated in this instrument by the use of operational amplifiers. High sensitivity was achieved by using an output amplifier to increase the strength of the signal applied to the output meter. A 'set zero' control was provided, to compensate for the offset voltage and current of the output amplifier, and the complete circuit is shown in Fig 10.4(b). The instrument was calibrated for a fixed input voltage of 2 volts (peak to peak) by injecting a signal of known asymmetry, produced by the method described in Section 10.3, and adjusting the attenuation of the output amplifier by means of the pre-set control VR_3. The circuit is arranged so that when the 'Set 20' switch, S_3, is closed the output meter should read 20 μ A. This enables the calibration to be checked each time before use.

The balance point of the circuit is affected slightly by temperature variations and the condition of the battery supply, and compensation can be achieved by adjustment of the balance control VR_2. Alternatively the polarity of the input can be reversed by means of the input reversing switch S_1, and the mean of the two readings of the output meter is then taken.

In its present form, asymmetries of between 0 and 2.5% can be measured with an accuracy of 0.02% on this instrument.

10.2.3. Measurements of natural asymmetry of mains supply

Prior to its direct use in the experiments described in Sections 10.3 and 10.9, the asymmetry meter was used to monitor the natural asymmetry of the A.C. mains at the Close House Laboratory. Readings were taken at irregular intervals over a total period of three months, and a striking pattern of variation emerges from the results. These are plotted in Fig 10.5.

Each day, the asymmetry remains low ($< 0.05\%$) from 08.00 to 11.00 hours, after which it gradually rises to a value of about 0.4% at 16.00 hours. Between 16.00 and 19.00 hours it increases very rapidly, and from 19.00 to 22.00 hours it remains high, but very variable, with values ranging from 1.3 to 1.8%. No readings were

taken between 22.00 and 08.00 hours, but the value seems to begin to decrease at 22.00 hours, so that if the curve is extrapolated symmetrically about a peak value at 20.30 hours it will decrease to 0.4% by 24.00 hours, and to 0.05% by 05.00 hours.

This curve suggests that the lowest values of natural mains asymmetrical distortion occur between 05.00 and 11.00 hours. The reasons for this daily variation are not obvious. The peak value does not occur at a time when local industrial machinery is likely to be in maximum use. The most likely source of such asymmetrical distortion is the effect of rectifiers, passing small components of D.C. back into the A.C. mains. The peak period of asymmetry appears to coincide with the time at which domestic television sets and radios are likely to be in maximum use, and since these devices incorporate rectifiers, they may well be the source of the asymmetrical distortion detected.

10.2.4. Measurements of natural asymmetry in the coil circuit

Following the measurements on the natural asymmetry of the mains described above, the asymmetry meter was connected into the demagnetising coil circuit, and a second series of readings was taken. It was immediately noticed that the values were much lower than those measured directly from the mains. Most of the values were near the minimum limit of measurement of the meter (0.02%), and the highest value recorded was 0.05%. This reading was taken at 19.00 hours, i.e. during the period of maximum distortion mentioned above.

The reason for this reduction in the asymmetry is the attenuating effect of the tuned coil circuit. The value of the 'effective attenuation factor' was calculated from subsequent readings, and is discussed in Section 10.4.

10.3. Production of artificial asymmetry

The following experiments were aimed at investigating the effects of known amounts of asymmetrical distortion during the A.F. demagnetisation of different rock types. The distortion was produced by drawing off a small proportion of the current to the demagnetising coil and passing it through a rectifier, using the circuit shown in Fig 10.6. The amount of distortion could be controlled by varying the proportion of current drawn off with the variable resistance Rv (max 40Ω).

If the demagnetising coil had infinite resistance, then the percentage asymmetry would be given by the ratio of the standard 1Ω resistance, R, to the variable resistance, R_v, multiplied by 100. This condition was used during the initial calibration of the asymmetry meter, when the demagnetising coil was replaced by a very high resistance. With the demagnetising coil in circuit, the resistance is finite, and this relationship becomes only approximate, but the percentage asymmetry is still directly related to the value of R_v.

The circuit was calibrated by connecting the asymmetry meter across a load resistance, R_m, and adjusting the current until the required potential difference of 2 volts (peak) was developed across R_m. The value of R_v was then varied, and a series of readings of the corresponding asymmetry were taken on the meter, It was necessary to readjust the current through the circuit at each new setting of R_v, to maintain a constant p.d. of 2 volts (peak) across R_m. The calibration curve is given in Fig 10.7, and this curve could be used to set the percentage asymmetry of the circuit to any required value between 0.05 and 1.30% in subsequent experiments.

10.4. Attenuation of asymmetry by tuned coil circuit

As discussed in Section 10.2.4, the tuned coil circuit has the effect of considerably reducing the magnitude of any asymmetry present in the mains supply to the coil. It was considered important to obtain a quantitative estimate of the amount of attenuation produced by the tuned circuit, so that the range of daily variation of natural asymmetry represented by Fig 10.5 could be calculated for the coil-circuit after attenuation. It was not possible to do this by direct readings of natural asymmetry in the coil circuit, since these were generally close to the limit of sensitivity of the asymmetry meter.

The 'theoretical' asymmetry in the current supply to the coil was calculated for each of the values of R_v listed in Table 10.1, by means of the approximate relationship discussed in Section 10.3, viz:

$$\text{Percentage asymmetry} = {}^{100}/_{R_v}$$

The results are listed in Table 10.2.

This 'theoretical' asymmetry is the approximate value that would have been measured in the coil circuit if it had not been tuned. The measured asymmetry in the coil circuit is plotted against the corresponding 'theoretical' values in Fig 10.8, which indicates an approximately linear relationship between these two quantities over the range of values studied. The effective attenuation factor of the tuned circuit is given by the gradient of this line as 50.

Reference to Fig 10.5 indicates that the corresponding natural asymmetry in the tuned coil circuit during the "minimum" period from 05.00 to 11.00 hours will be 0.001%, but that during the "maximum" period from 19.00 to 22.00 hours it will rise to 0.03%.

As indicated in the following sections, this amount of asymmetry may be sufficient to produce significant ARM's during A.F. demagnetisation.

10.5. Effect of varying asymmetry at constant peak field value

In the following experiments, aimed at investigating the effects of applying artificial asymmetries to rock samples, all treatment and measurements were performed along a single axis (the z-axis) in the sample. The samples were standard 2.5cm diameter and length cylinders, but the volume is not taken into account in the values of remanence quoted, i.e. these measurements are of the total magnetic moment along one axis, expressed in gauss cm^3, and not of intensity.

To reduce the complicating factor of natural mains asymmetry, measurements were always performed at times of 'low' to 'intermediate' natural asymmetry, i.e. between 08.00 and 14.00 hours. The period of 'high' natural asymmetry, from 14.00 to 22.00 hours was strictly avoided. Measurements involving very small applied asymmetries at low peak A.F. values were always performed between 08.00 and 11.00 hours.

In the first experiment a sample of dolerite was demagnetised at a peak field of 180 Oe and measured. An asymmetry of 0.05% was then applied by switching on the asymmetry circuit, and adjusting R_v to the appropriate value, and the sample was treated again at 180 Oe. The difference between these two measurements gave the component of ARM produced by this value of asymmetry, and listed in Table 10.3. The sample was then demagnetised a second time at 180 Oe, with the asymmetry circuit switched off, and the moment along this axis was found to decrease to a value similar to the original moment. This is in agreement with the observations of Rimbert (1959),

that an ARM produced by a steady field, h , superimposed on a peak alternating field H, will be destroyed by the same peak field if h is removed.

The above procedure was repeated twice, and the mean of the three values of induced ARM component corresponding to an asymmetry of 0.05% at a peak field of 180 Oe, was calculated. An estimate of the repeatability of these three values was obtained by calculating the standard error σ_m, in the mean of the three measurements, using the formula

$$\sigma_{\bar{m}} \left[\sum_{1} \frac{(M_i - \bar{M})^2}{n(n-1)} \right]^{1/2} \qquad (10.2)$$

The percentage asymmetry was then increased in steps up to a maximum of 0.5%, and at each stage the above procedure was repeated, so that three separate values of the induced ARM component were obtained for each value of asymmetry. The results are plotted in Fig 10.9, in which the 'error-bars' represent the standard error in the mean.

It can be seen from this diagram that increase in the percentage asymmetry results in a corresponding increase in the induced ARM component, and that there seems to be a tendency towards 'saturation' at higher asymmetry values. This diagram also indicates that an asymmetry of 0.03%, the maximum likely value in the tuned coil circuit due to natural mains distortion, will produce an induced ARM component of approximately 0.3×10^{-3} gauss cm^3 along this axis. The component of remanence along this axis after treatment at 180 Oe during the initial demagnetisation of this sample was 12.6×10^{-3} gauss cm^3, so that the induced ARM produced by an asymmetry of 0.03% would represent approximately 2.5% of the total

moment. Demagnetisation at higher peak field values is likely to produce larger ARMs, and since this treatment also reduces the intensity of the natural remanence, such ARMs will rapidly become a significant proportion of the total remanence of the sample.

To verify that this is the case, a series of experiments were performed in which samples were demagnetised at three different asymmetry values, over a wide range of peak applied alternating fields.

10.6. Effect of varying peak field value at constant asymmetry

Samples of dolerite, gabbro and red sandstone were subjected to this treatment, and were first completely demagnetised by thermal treatment at 650°C. The applied asymmetry was then set at 0.1% using the method described in Section 10.3, and each sample was progressively 'demagnetised' along one axis at 90 Oe intervals up to a maximum of 900 Oe, the remanence along this axis being measured after each step. This procedure was then repeated for 0.25% and 0.5% asymmetry, and the results are plotted in Figs 10.10, 10.11 and 10.12.

It is immediately clear from these results that at any particular value of asymmetry the induced ARM component in all three samples increases progressively as the peak alternating field is increased. By varying the amount of asymmetry, families of curves result, higher values of asymmetry producing larger ARMs.

Because of practical difficulties in maintaining very low applied asymmetries close to the limit of measurement of the asymmetry meter, investigations were not carried out below 0.1% asymmetry. Such investigations would be possible if the sensitivity

of the asymmetry meter could be increased by one order of magnitude, and it is hoped to do this in the near future.

However, if the results obtained are extrapolated, a position of the curve corresponding to 0.03% asymmetry, the maximum likely value in the tuned coil circuit due to natural mains asymmetry, can be postulated below the 0.1% curve, as indicated in Fig 10.12. This diagram refers to the sample of red sandstone which was subjected to high-field A.F. demagnetisation, described in Chapter 9. The NRM moment of this sample along the z-axis was 0.025 $x10^{-3}$ gauss cm^3, and Fig 10.12 indicates that the induced ARM due to an asymmetry of 0.03% will probably exceed this value after peak A.F. treatment above 500 Oe. By analogy with the other curves in Fig 10.12, the value of the induced ARM is likely to increase rapidly at higher peak A.F. values, becoming many times larger than the N.R.M., and this could well explain the anomalous results described in Chapter 9.

The diurnal variation of asymmetry in the mains supply at Close House had not yet been observed at the time the experiments on the high-field demagnetisation of sediments were performed, and no record was therefore kept of the time of day at which each reading was taken. It is known with certainty, however that the readings at 3400 to 3600 and 4500 to 5000 Oe were all taken in the evening, i.e. during the period of maximum mains asymmetry, whereas the readings at 3000 to 3200 and 3800 to 4300 were taken in the morning, during the period of low to intermediate asymmetry. The former correspond with peaks in the induced ARM curve (Fig 9.7) whereas the latter correspond with troughs, and this is strong evidence of the influence of the level of natural mains asymmetry on the induced ARM component.

It has long been known that ARMs can be approximately randomised by rotating the sample during demagnetisation (e.g. Hutchings, 1967). Such a system was not used on this apparatus because it was necessary to keep the internal diameter of the demagnetising coil as small as possible to enable the desired high fields to be produced. However a compromise could be achieved by using a single-axis rotation system perpendicular to the axis of the demagnetising coil. This would require slight enlargement of the internal diameter of the coil, and a consequent small reduction in the maximum peak field obtainable, but would have the advantage that only two sequences of operation would be necessary instead of the six described in Section 9.4.8. A.R.M.s introduced by asymmetrical distortions of the applied A.F. would then be randomised in the plane perpendicular to the rotation axis. The effectiveness of such a system for the averaging out of A.R.M.s could be assessed by performing experiments with artificial asymmetries, using the techniques described in this chapter.

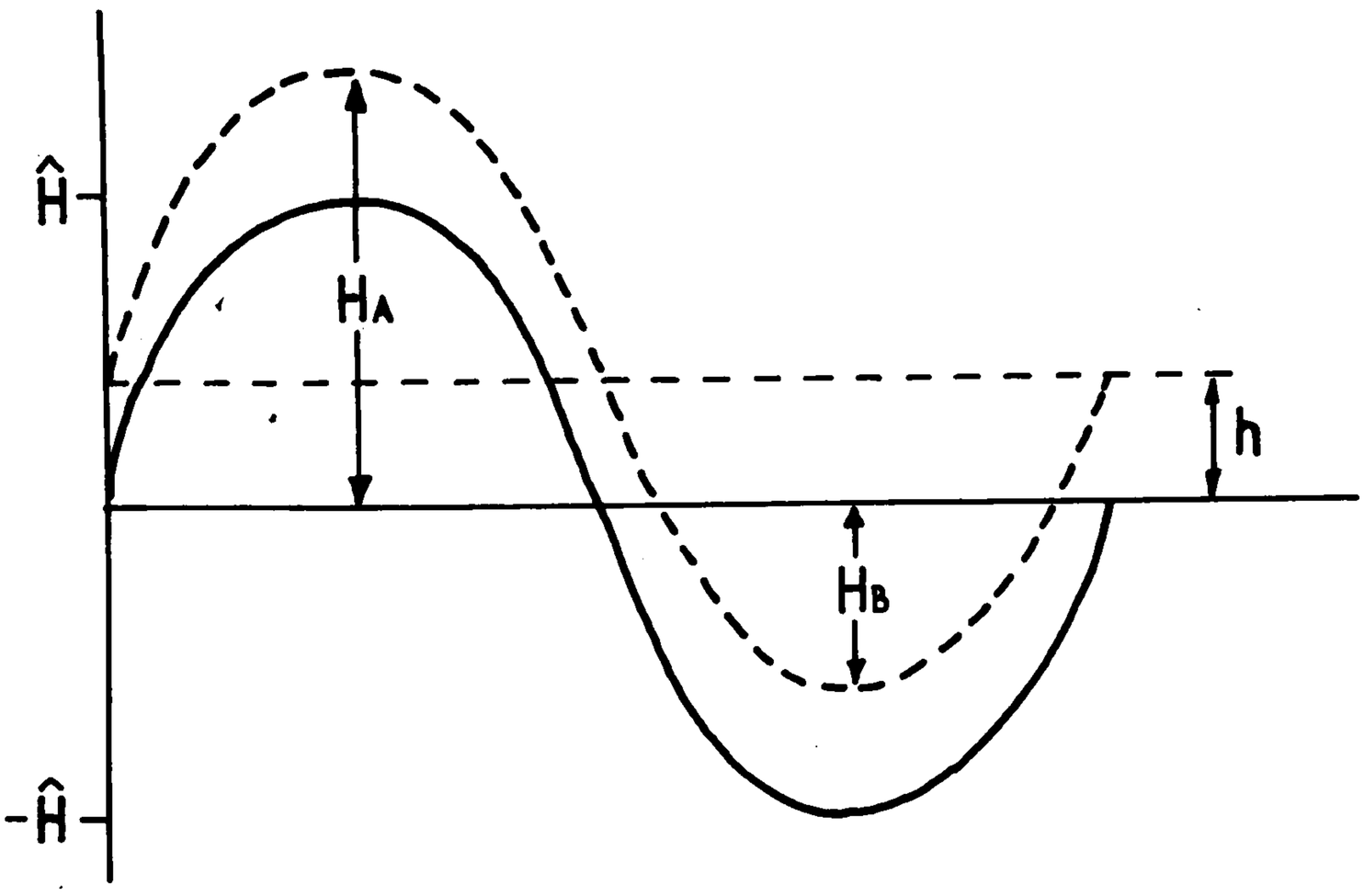
10.7. Comparison between ARMs produced by asymmetry and by superimposed steady fields

Further investigations into the nature of ARMs produced by asymmetrically distorted waveforms were carried out by comparing these with ARMs produced by superimposed direct fields. To do this, the samples of red sandstone and dolerite used in the previous experiments were completely demagnetised again by thermal treatment at 650°C, and were then subjected to A.F. treatment in the range 90 to 540 Oe., with a superimposed direct field of 0.5Oe. The results are listed in Table 10.5, and plotted in Figs 10.3 and 10.14. In both cases there is a linear relationship between the induced

ARM component and the peak A.F. demagnetising field up to 400 Oe, but in the red sandstone sample (2073 C1) the ARM begins to drop off above this field.

In order to compare these results with ARMs produced by asymmetrical fields, it is necessary to calculate the direct field, equivalent to a particular asymmetry value, at a given peak alternating field. The situation is illustrated in Fig 10.15.

Fig 10.15



If a direct field, + h, is superimposed on an alternating field of peak intensity, $\hat{H}$, the amplitude, H_A, of the positive half-cycle increases to $\hat{H} + h$, and that of the negative half-cycle, H_B, decreases to $\hat{H} - h$. Hence the difference, ΔH between the positive and negative half-cycles is given by

$$\Delta H = H_A - H_B = 2h$$

$$\text{i.e. } h = \Delta H/2 \qquad (10.3)$$

The percentage asymmètry, A, of the waveform is given from equation (10.1) as

$$A = \frac{\Delta H}{\hat{H}} \times 100$$

$$\text{i.e. } A = \frac{200h}{\hat{H}}$$

and the direct field equivalent, h, of a percentage asymmetry, A, is given by

$$h = \frac{\hat{H}}{200} \times A \qquad (10.4)$$

where $\hat{H}$ is the peak applied field.

This relationship can be used to calculate the peak applied fields at which asymmetries of 0.1%, 0.25%, and 0.5% are equivalent to a superimposed direct field of 0.5 Oe. These are listed in Table 10.6 below:

Table 10.6

Asymmetry	Peak field at which asymmetry is equivalent to direct field of 0.5 Oe
0.1%	1000 Oe
0.25%	400 Oe
0.50%	200 Oe

The ARMs equivalent to these peak fields can then be read from Figs 10.10 and 10.12, and are listed in Table 10.7:

Table 10.7 ARMs produced by asymmetries equivalent to a superimposed direct field of 0.5 Oe

Peak A.F. (Oe)	Dolerite sample MC1.1	Red sandstone sample 2073 C1
200	0.50×10^{-2} gauss cm^3	0.15×10^{-4} gauss cm^3
400	1.60×10^{-2} gauss cm^3	0.70×10^{-4} gauss cm^3
1000	4.80×10^{-2} gauss cm^3	2.15×10^{-4} gauss cm^3

The values in the appropriate range from Table 10.7 have been plotted in Figs 10.13 and 10.14. It can be seen from these diagrams that the ARM produced by a superimposed steady field of 0.5 Oe is substantially higher than that produced by an asymmetry of equivalent value. The reason for this will be discussed in the next section.

10.8 Theoretical explanation of A.R.M.s

The theoretical explanation of A.F. demagnetisation described in Section 9.2 can be extended to explain the acquisition of A.R.M.s.

If a steady field, +h, is superimposed on an alternating field of peak intensity $\hat{H}$, and if the critical fields corresponding to increasing and decreasing applied fields are 'a' and 'b' respectively (Section 9.2.2), then on each positive half-cycle all negatively magnetised domains for which $a \leqslant \hat{H} + h$ will reverse in sign, and on each negative half-cycle all positively magnetised domains for which $b \leqslant \hat{H}-h$ will reverse in sign. The effect of gradually reducing the alternating field to zero is shown by means of Preisach diagrams in Fig 10.16. The end result is an unequal number of positively and negatively magnetised domains, i.e. an A.R.M.

As $\Delta H/2$, the difference between two successive half-cycles, tends to zero, the form shown in Fig 10.16(f) results, and the ARM may be represented by a strip of approximately $\sqrt{2}\ \hat{H}$ in length and $\sqrt{2}\ h$ in width.

Similar reasoning may be applied to explain the acquisition of ARMs as a result of asymmetrical distortion of the applied alternating field. In this case, if the percentage asymmetry, A, remains constant during the period of reduction of the field, then from equation (10.4), the equivalent direct field, h, must decrease continuously as thealternating field, $\hat{H}$, is reduced to zero. This is the basic difference between the two types of ARM, and its effect is shown in Fig 10.17.

As the equivalent direct field decreases, represented by the sequence h_1, h_2, h_3 etc., the situation shown in Fig 10.17(e) is approached, and if $\Delta H/2$ tends to zero, the form shown in Fig 10.17(f) is reached. In this case the ARM may be represented by a triangle, approximately $\sqrt{2}$ $\hat{H}$ in length and $\sqrt{2}$ h in height. The total area is half that representing an ARM produced by a steady direct field, h.

If the distribution of domains in the a, b plane is uniform, then this area will be proportional to the difference between the number of domains magnetised positively and the number magnetised negatively. This will in turn be proportional to the intensity of ARM induced in the sample (Rimbert, 1959). The ARM produced by a steady direct field will then be double that produced by an equivalent asymmetry, for the same peak field value.

Figs 10.13 and 10.14 show that although the effect of a superimposed direct field is much larger than that of the equivalent asymmetry, it is not double the latter. There are two possible explanations for this. Firstly, the lines on these graphs may be inaccurate, either because of the small number of readings represented, or because of inaccuracies in measurement and in reading the value of the ARM's from the curves in Figs 10.10 and 10.12. Alternatively, this difference may be due to a non-uniform distribution of domains in the a, b plane. Rimbert (1959) has suggested that the density may be higher nearer the origin and weaker in the range of high coercive fields, so that a Gaussian distribution such as

$$n = \int_{a_1}^{a_2}\int_{b_1}^{b_2} e^{-(a^2+b^2)}\, da\, db \qquad (10.5)$$

would be more applicable, where n is the number of grains with critical fields in the intervals a_1 to a_2 and b_1 to b_2.

10.9 Discussion of the direct field equivalents of asymmetries

Various authors, e.g. Patton and Fitch, 1962, have observed that the intensity of ARM produced by a steady direct field, h, superimposed on an alternating field $\hat{H}$, is a linear function of the strength of the direct field h. The results of the above experiments were therefore inspected to see if a similar relationship was evident in the case of ARMs produced by asymmetries.

The peak direct field equivalent of each of the values of asymmetry studied (0.1%, 0.25% and 0.5%) was calculated for each peak alternating field value between 90 and 900 Oe., using equation (10.4). These are listed in Table 10.8. The results listed in Table 10.4 were then replotted, this time with the equivalent peak direct fields as abscissae. These are shown in Figs 10.18, 10.19 and 10.20. Although there are only three points for each peak alternating field, and the scatter of these points is often high, they do, in general, lie on sets of straight lines. The gradients of these lines increase as the peak alternating field value increases.

This may be explained by reference to Fig 10.17. If the induced ARM, I_A, is proportional to the area of the triangle bounding the first bisector, then

$$I_A \propto \frac{\sqrt{2} \quad h \quad x\sqrt{2}\ \hat{H}}{2}$$

$$\text{i.e.} \quad I_A \propto h\ \hat{H}$$

Hence if the induced ARM component is plotted against the equivalent direct field, h, the gradient of the line should be proportional to the peak alternating field value $\hat{H}$.

In the gabbro and red sandstone samples the gradient increases progressively with the peak applied field over the whole range of values studied. However in the dolerite sample large changes in gradient occur over the range of peak applied fields from 180 to 450 Oe,

but above this the gradient remains approximately constant. This indicates that the induced ARM is not directly proportional to the area of the triangle bounding the first bisector in the Preisach diagram, and probably reflects the influence of other factors, such as non-uniform grain-size distribution.

10.10. Conclusions

The results discussed in this chapter have shown that values of asymmetry likely to be present in the current through the demagnetising coil at certain times of the day, are sufficient to produce significant ARMs in a wide variety of samples. This is probably the source of the spurious magnetisations observed in the samples subjected to high-field demagnetisation and described in chapter 9., and it should be possible to randomise such ARMs by rotating the sample about an axis perpendicular to that of the coil during demagnetisation treatment. This will entail slight enlargement of the inner diameter of the coil, and consequent reduction in the maximum peak field obtainable with this apparatus.

Further studies on the nature of the ARMs suggest that they are analagous to ARMs produced by superimposed direct fields, and have broadly similar properties to these, but differ from the latter in having lower intensities for the same peak alternating field values.

References

As, J.A. and J.D.A. Zijderveld, 1958. Magnetic cleaning of rocks in palaeomagnetic research. Geophys. J.R. Astro.Soc., 1, 308-319.

Hutchings, A., 1967. Computations of the behaviour of two and three axis rotation systems. Methods in Palaeomagnetism. Elsevier Pub. Co.

Patton, R.J., and J.L. Fitch, 1962. Anhysterestic remanent magnetisation in small steady fields. J. Geophys. Res., 67, 1, 307-311

Rimbert, F. 1959. Contribution a l'étude de l'action de champs alternatifs sur les aimantations remanentes des roches. Extrait de la Revue de l'Institut Francais du Pétrole et Annales des Combustibles Liquides. Vol XIV Nos. 1 and 2.

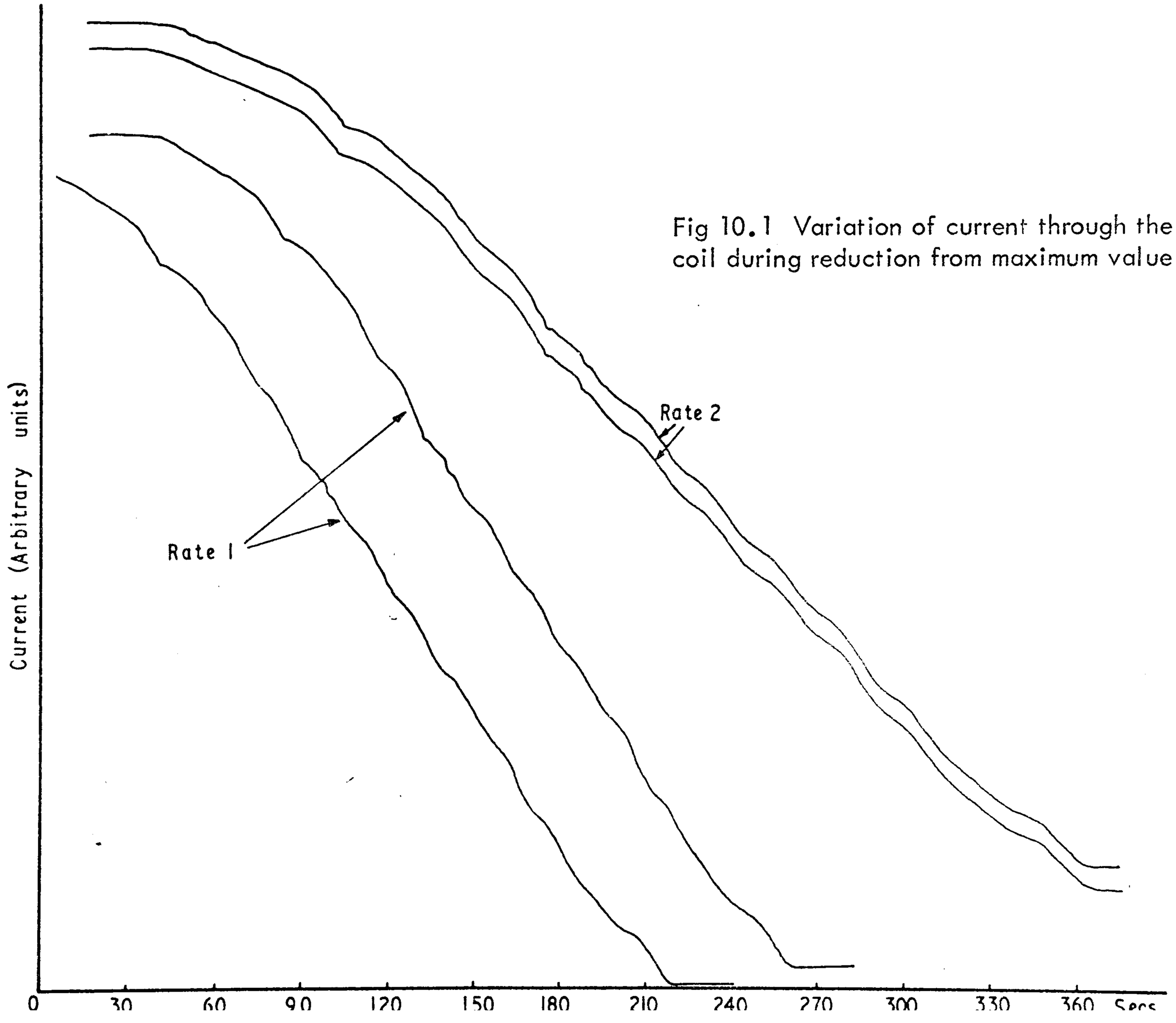


Fig 10.1 Variation of current through the demagnetisation coil during reduction from maximum value to zero.

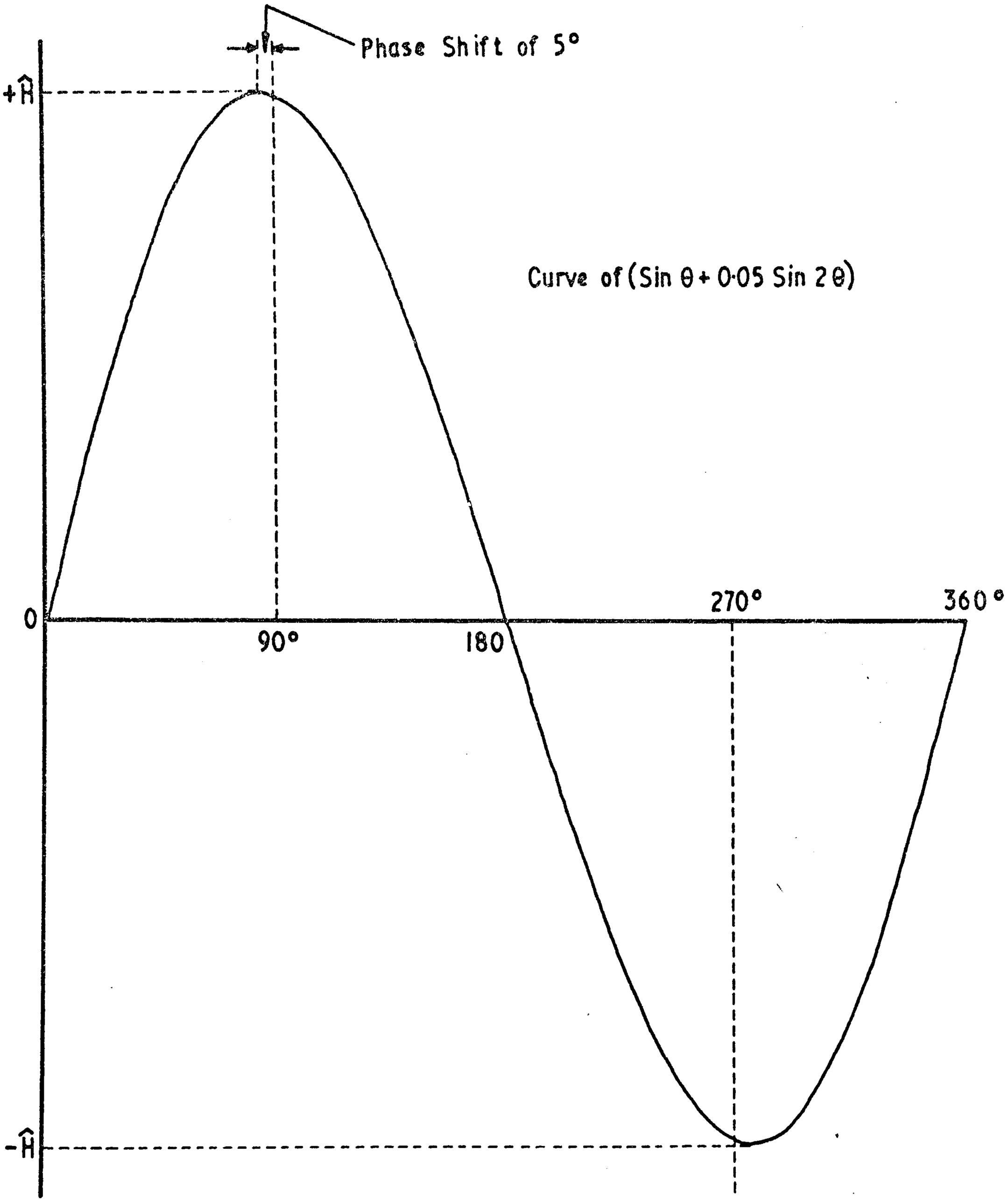


Fig 10.2 Example of sine wave containing 5% second harmonic distortion, but having no asymmetry.

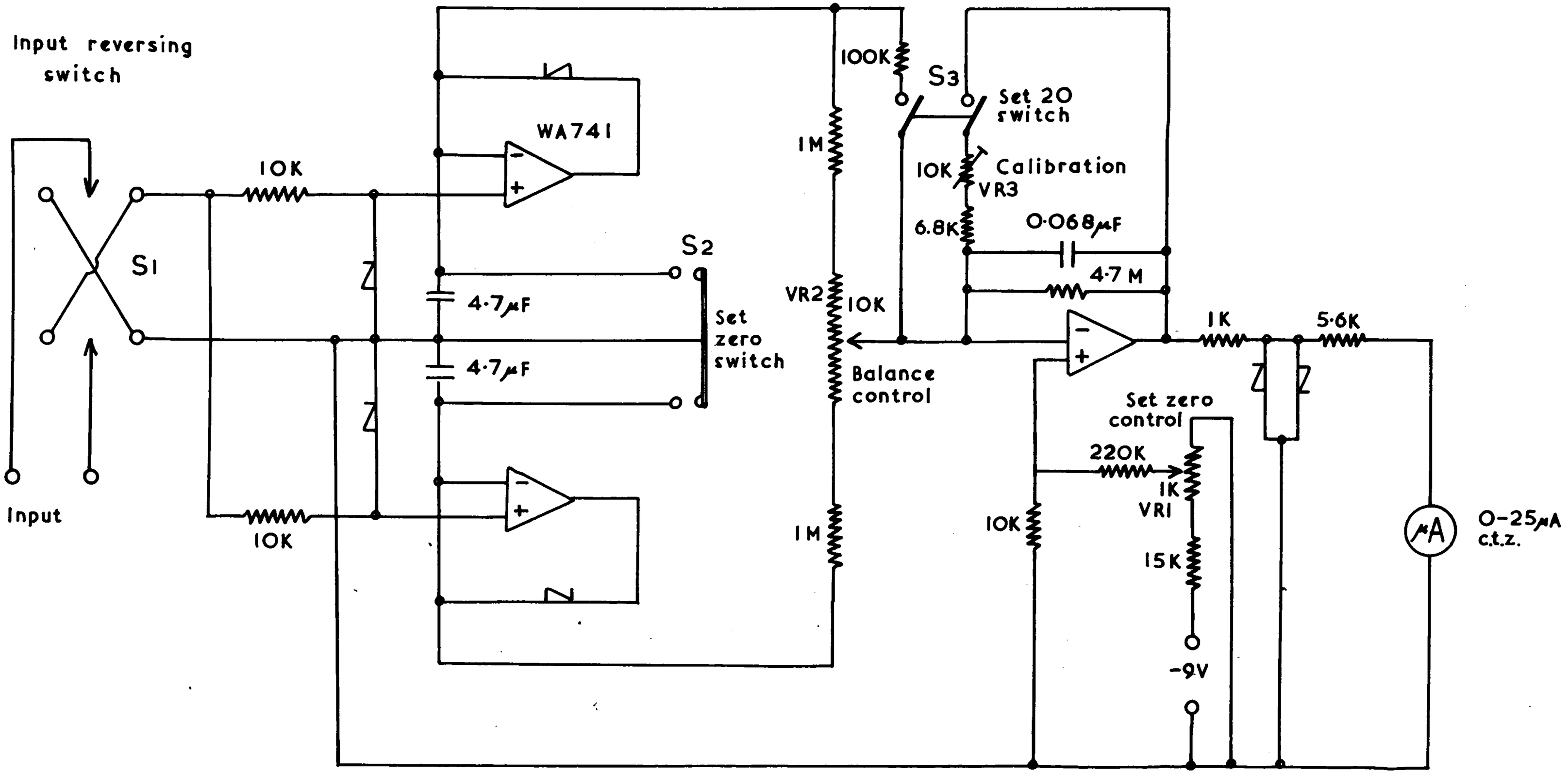


Fig 10.4(b) Circuit diagram of asymmetry meter.

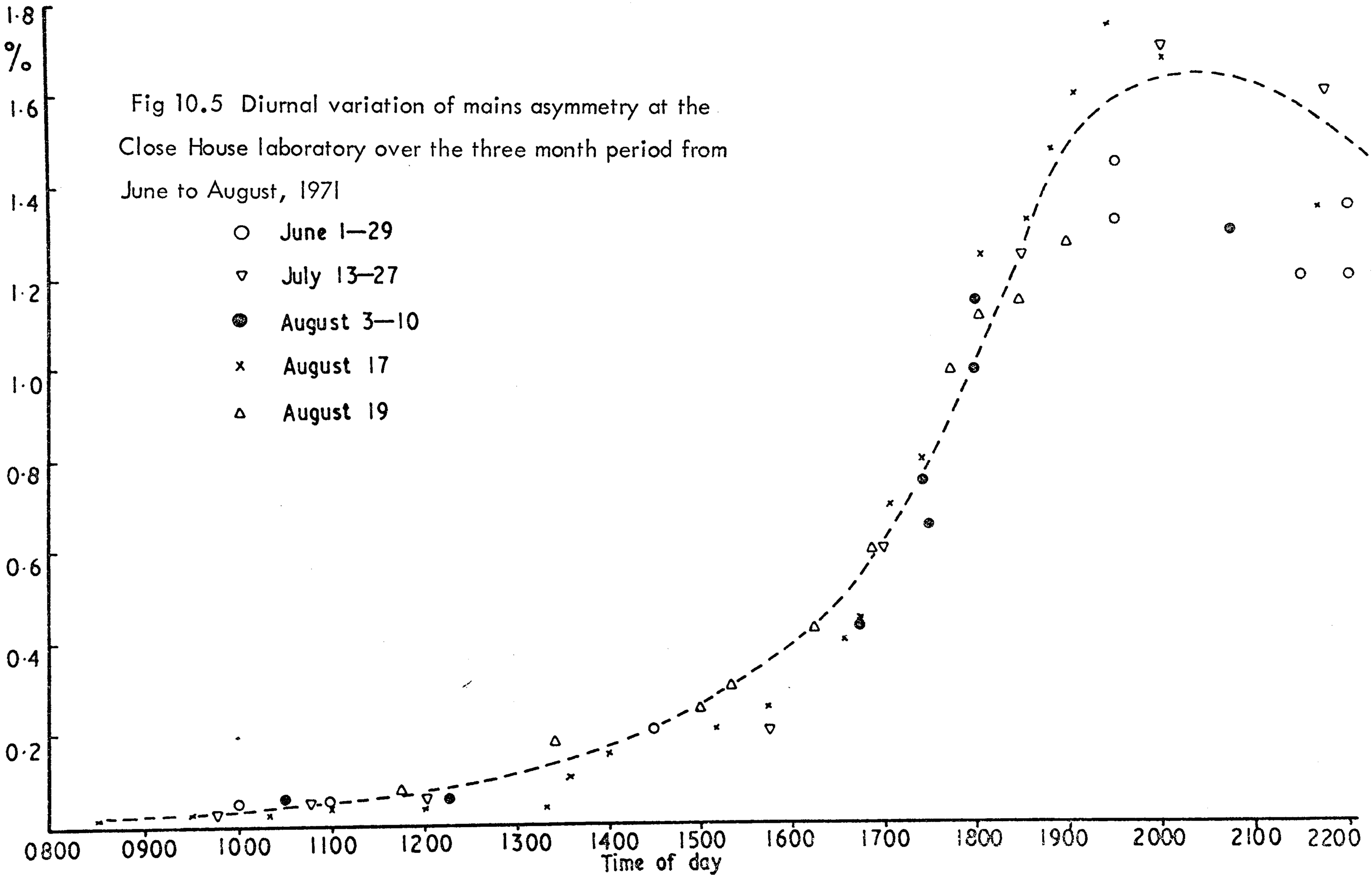


Fig 10.5 Diurnal variation of mains asymmetry at the Close House laboratory over the three month period from June to August, 1971

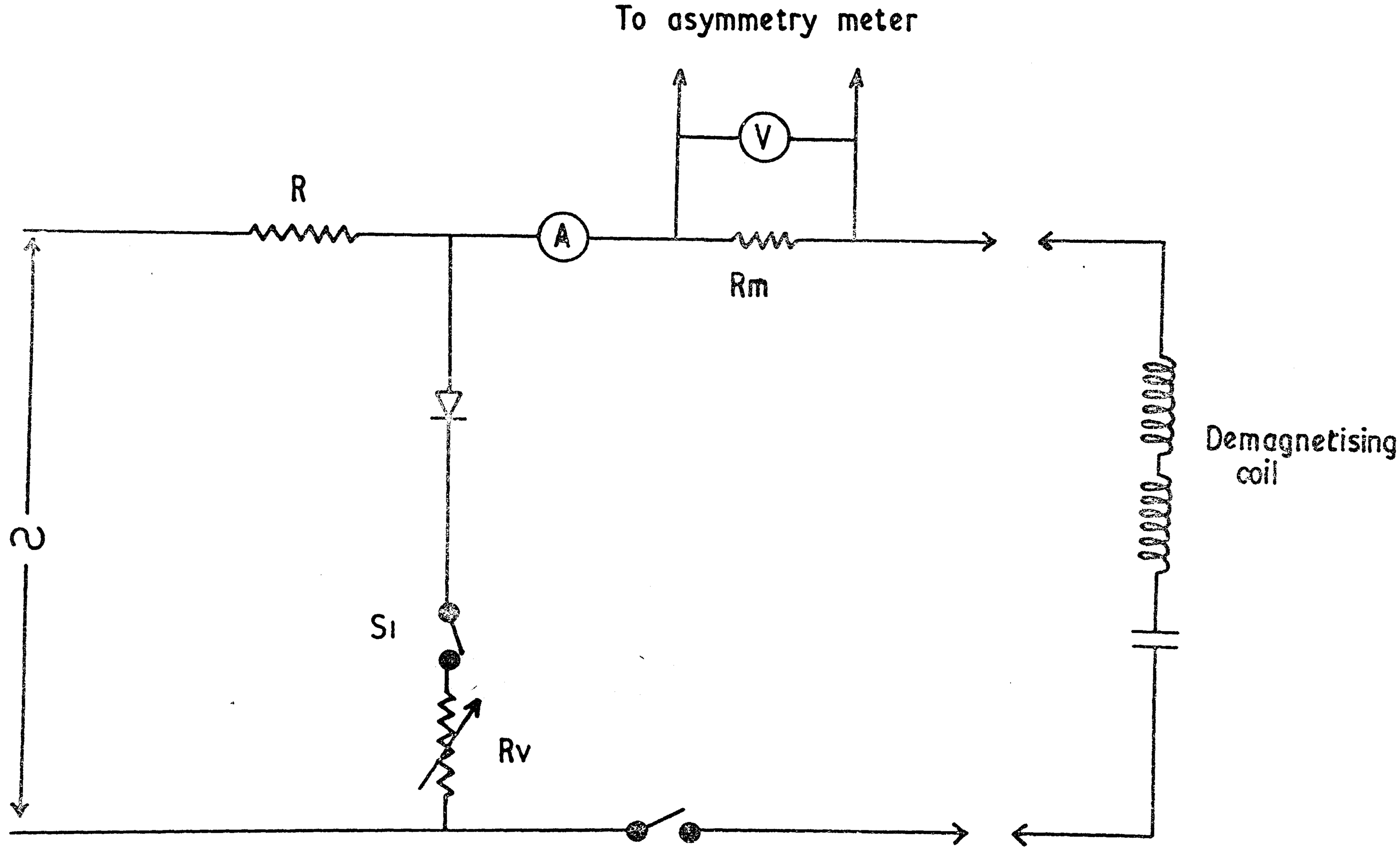


Fig. 10.6 Circuit used for production of artificial assymetry.

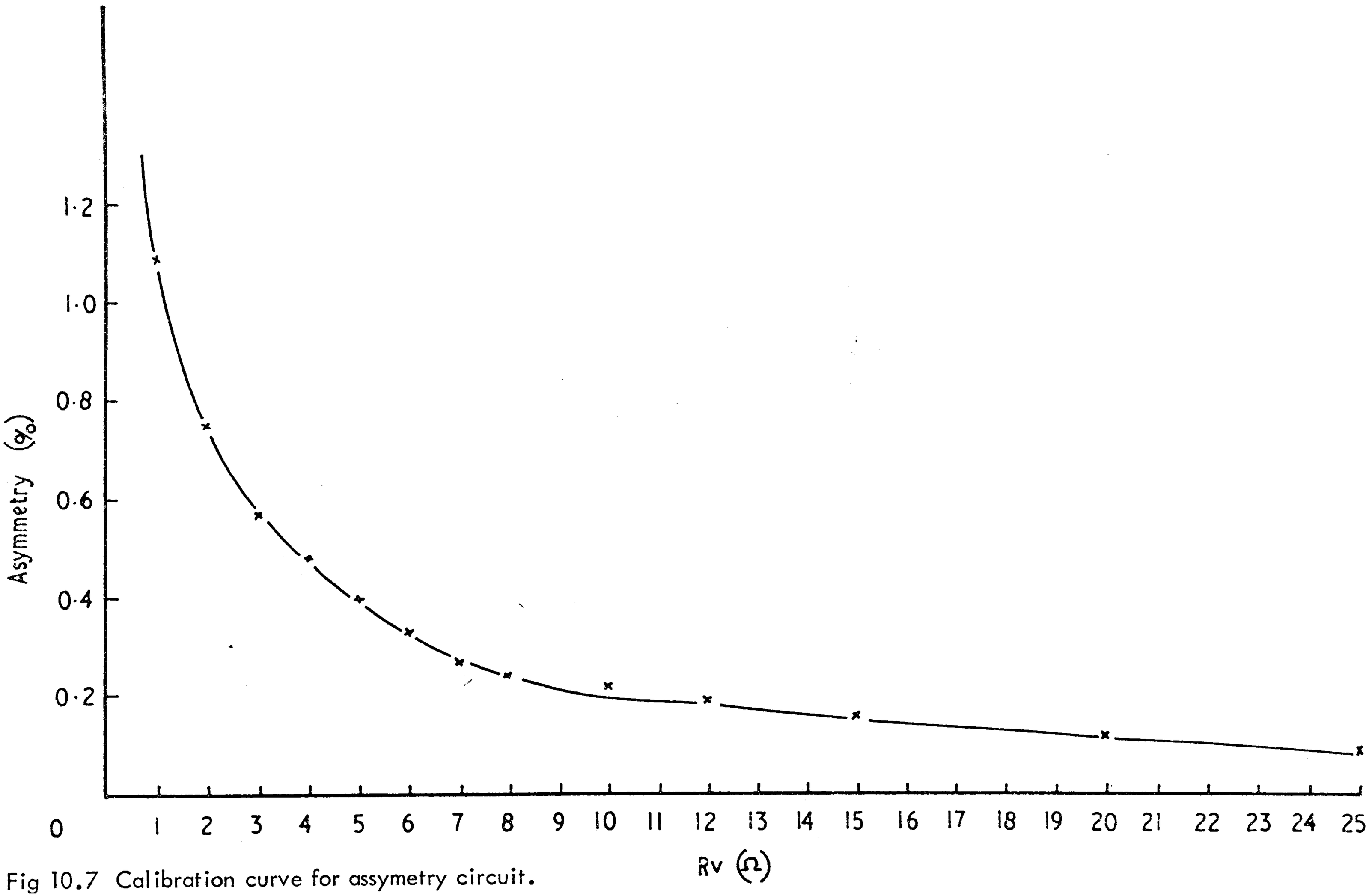
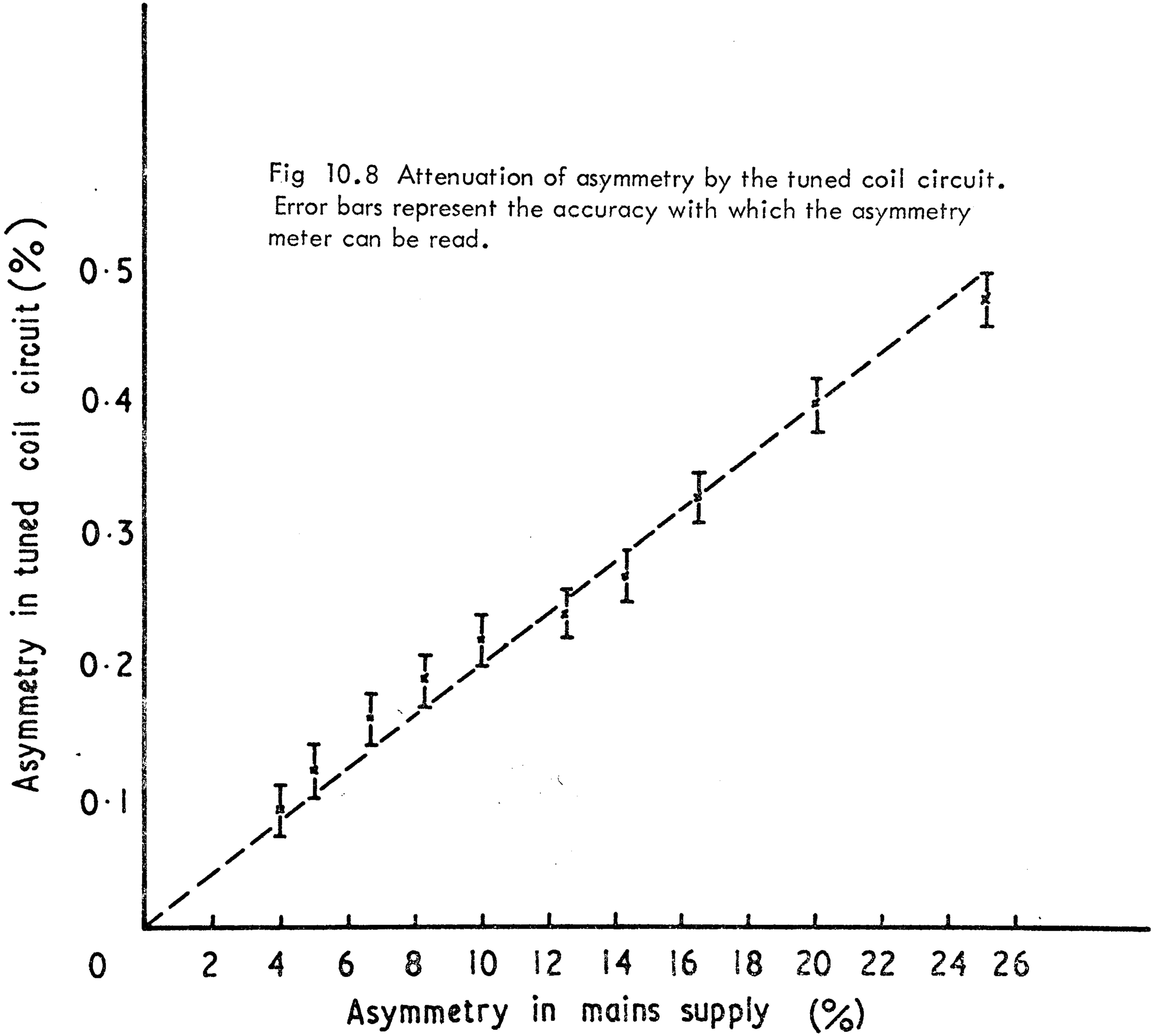


Fig 10.7 Calibration curve for assymetry circuit.

Fig 10.8 Attenuation of asymmetry by the tuned coil circuit. Error bars represent the accuracy with which the asymmetry meter can be read.



Sample No MC 6.1

Treated at 180 Oe. pk. A.F.

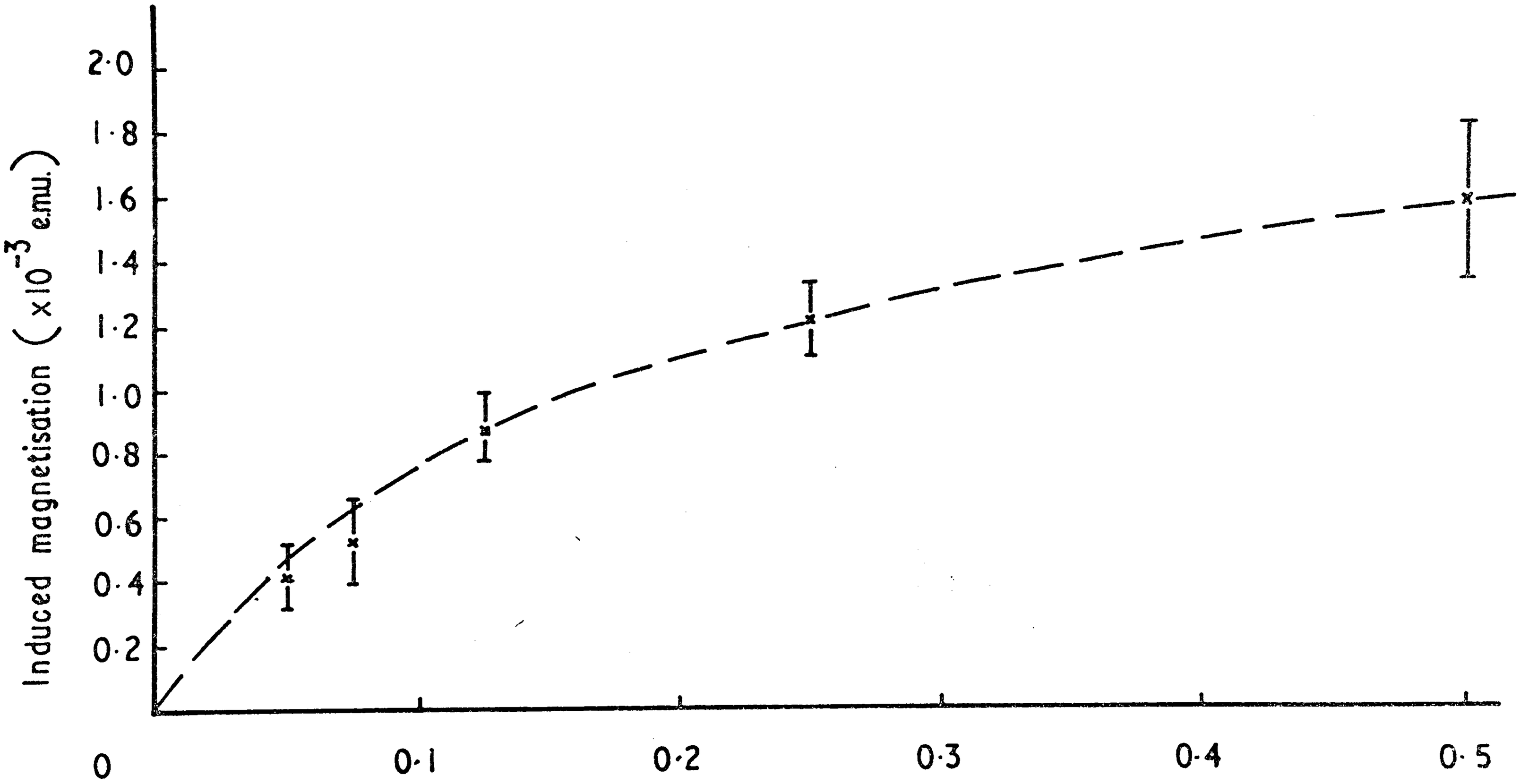


Fig 10.9 Effect of varying asymmetry from 0.05 to 0.5% at a

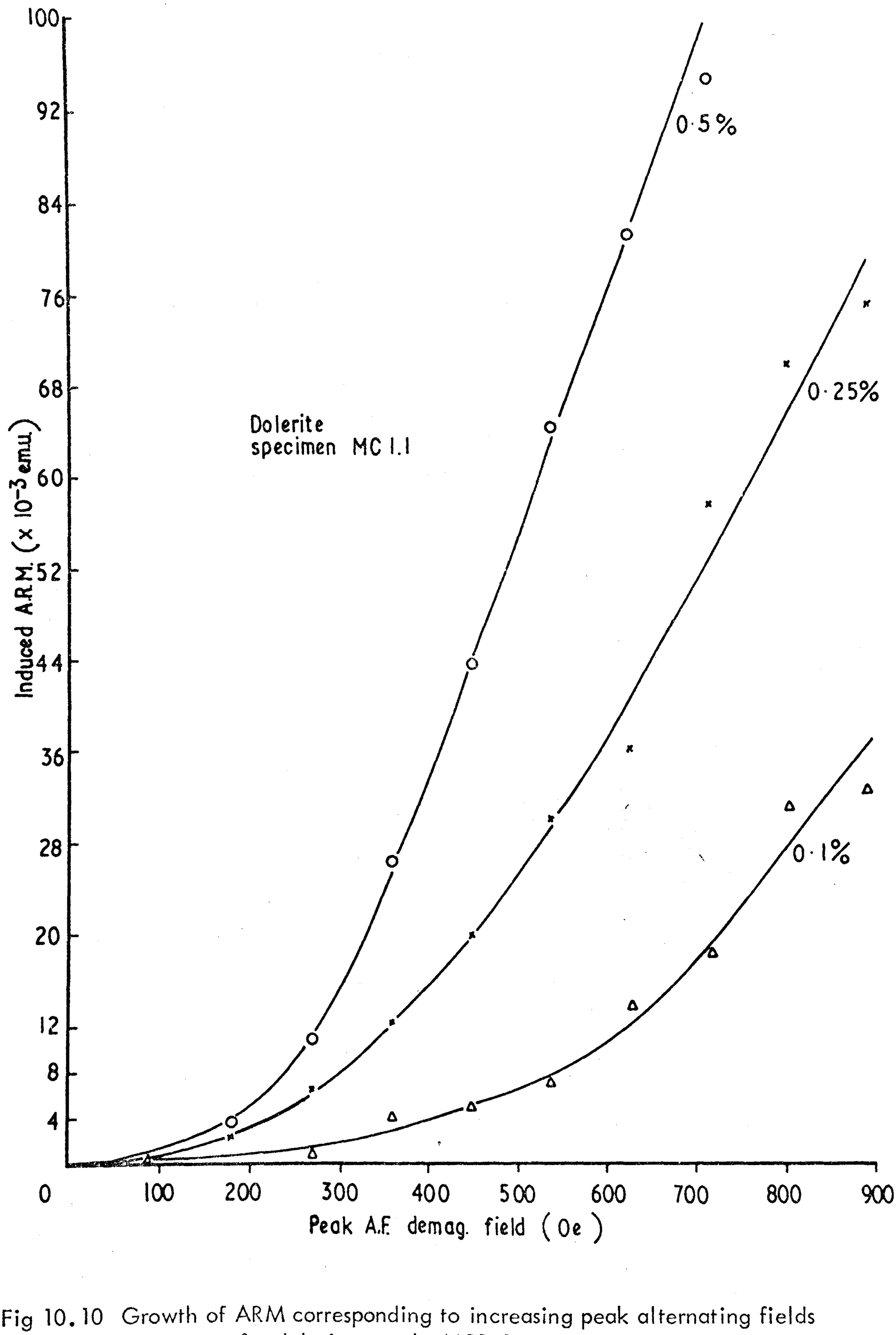


Fig 10.10 Growth of ARM corresponding to increasing peak alternating fields at constant asymmetry for dolerite sample MC1.1.

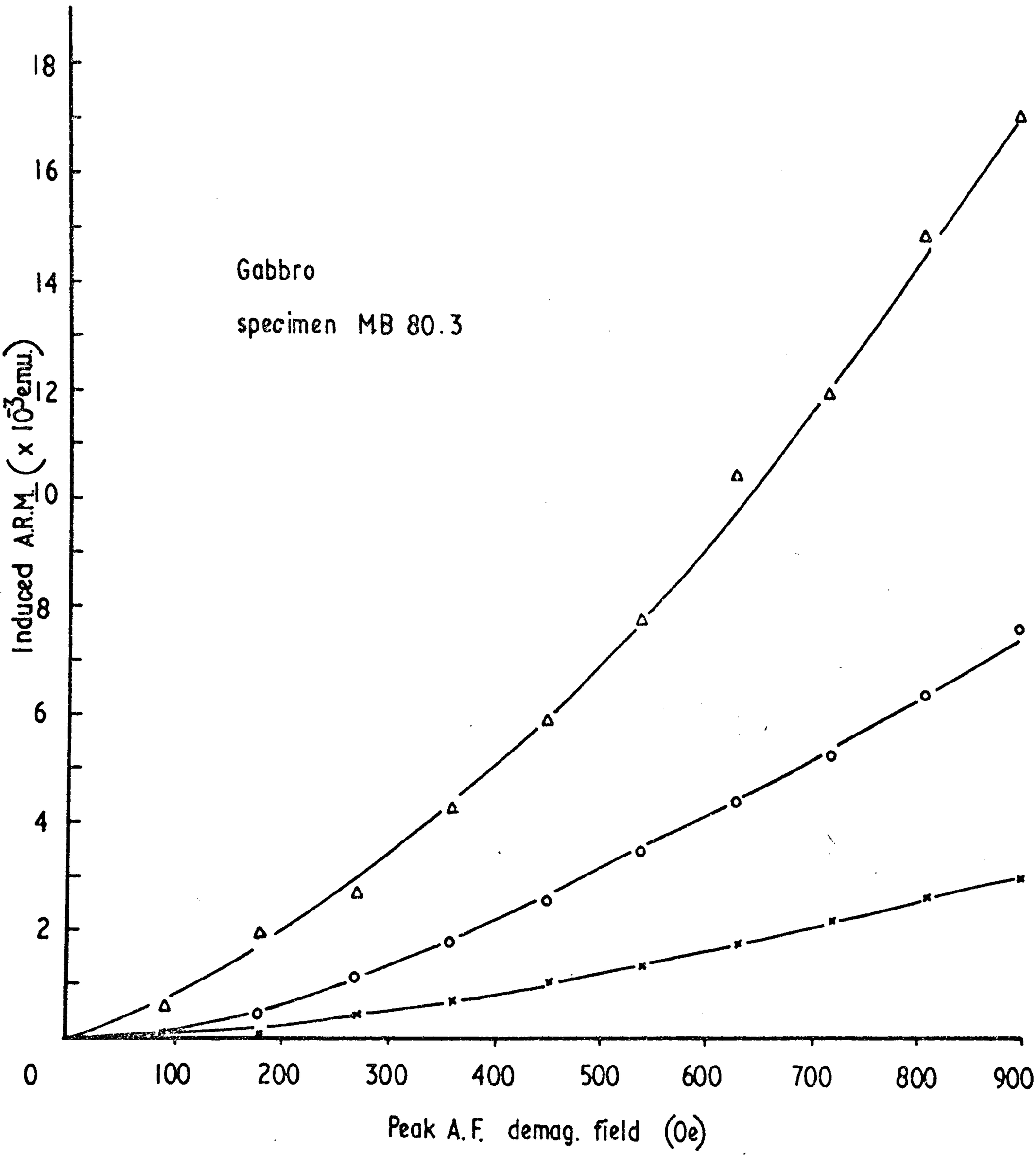


Fig 10.11 Growth of ARM corresponding to increasing peak alternating fields at constant asymmetry for gabbro sample MB80.3.

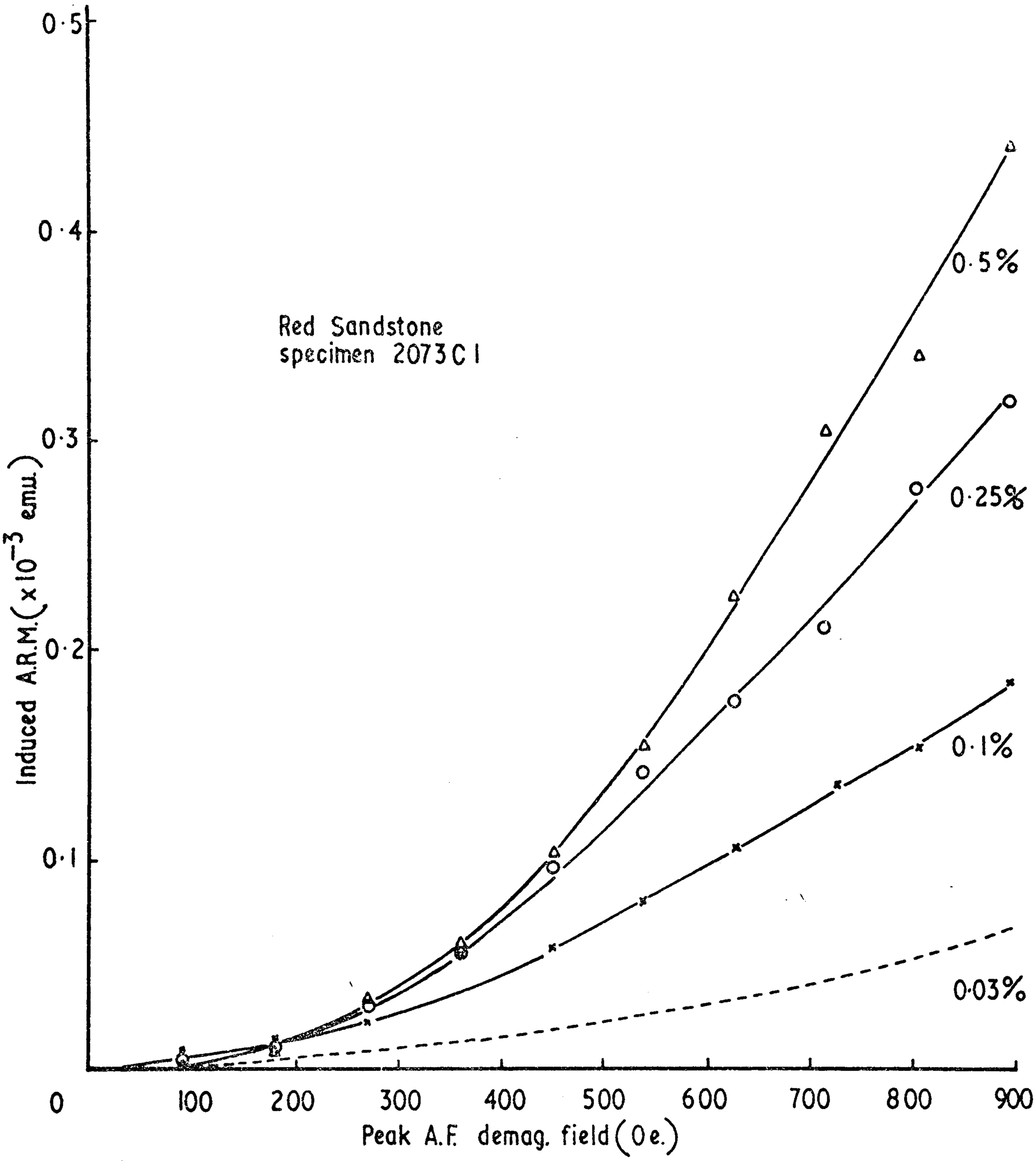


Fig 10.12 Growth of ARM corresponding to increasing peak alternating fields at constant asymmetry for red sandstone sample 2073C1 Broken line is postulated curve for 0.03% asymmetry.

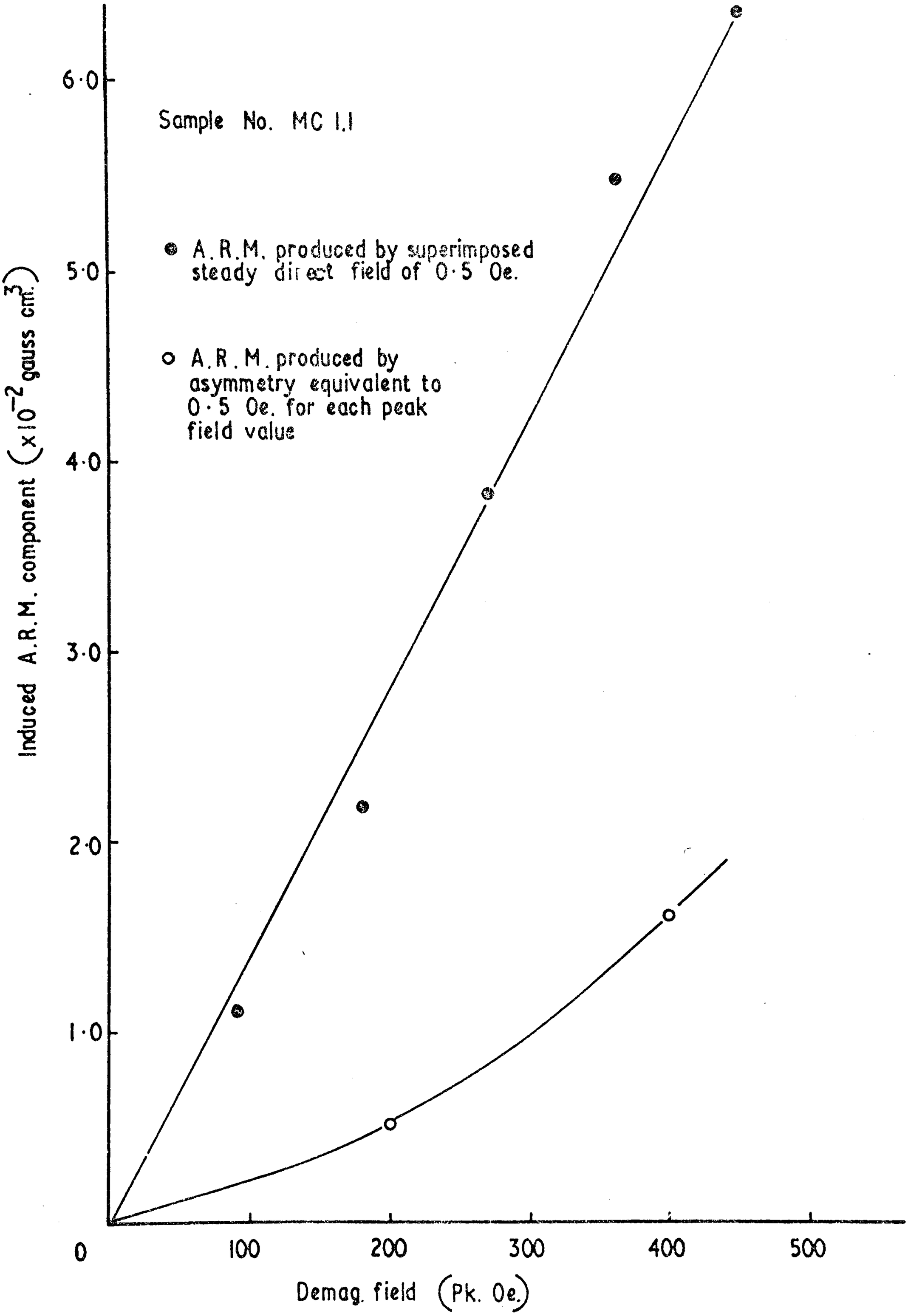


Fig 10.13 Comparison between ARM's produced by asymmetry and by superimposed direct fields on dolerite sample MC1.1.

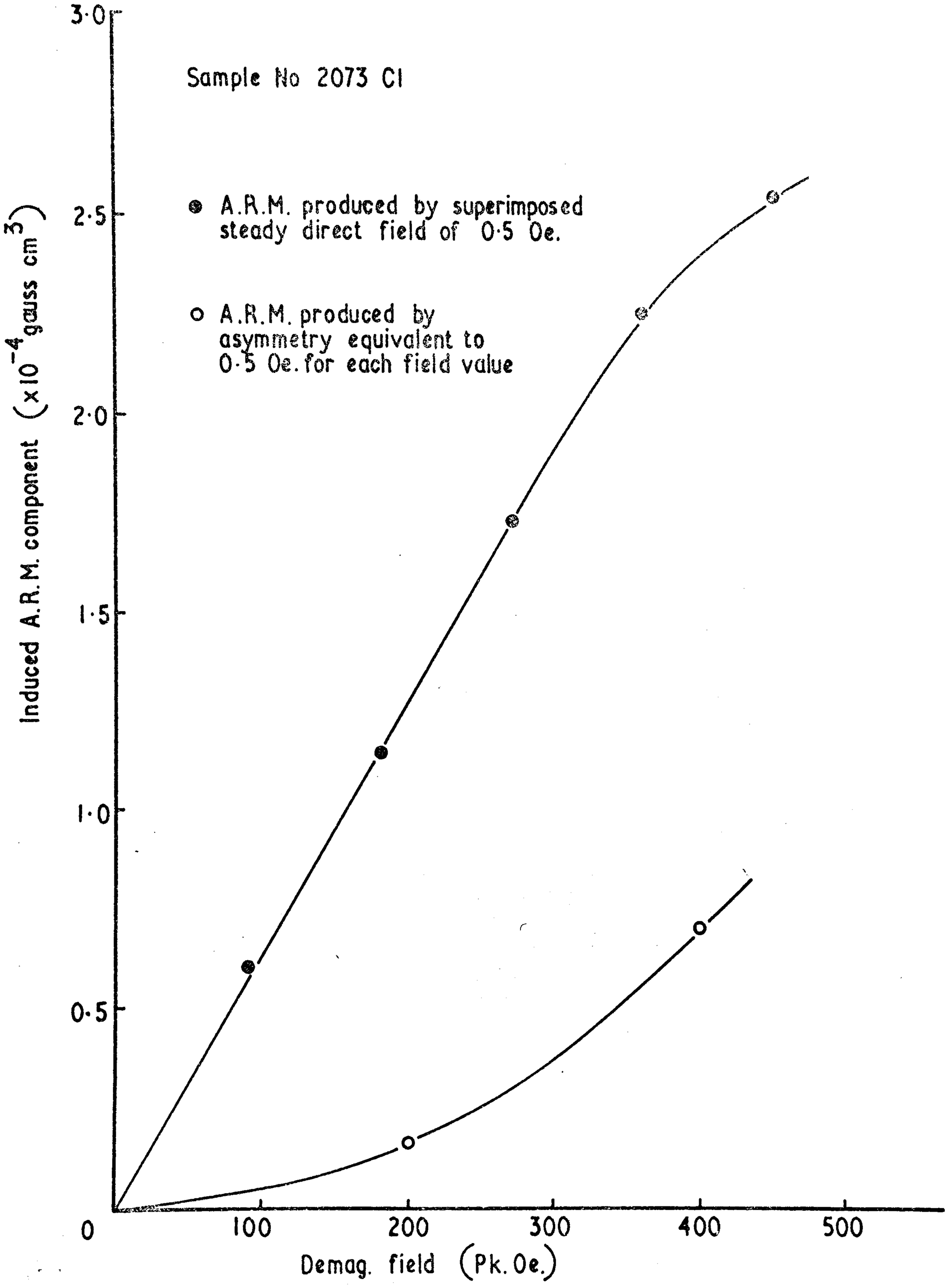


Fig 10.14 Comparison between ARM's produced by asymmetry and by superimposed direct fields on red sandstone sample 2073C1.

PAGE NUMBERING AS ORIGINAL

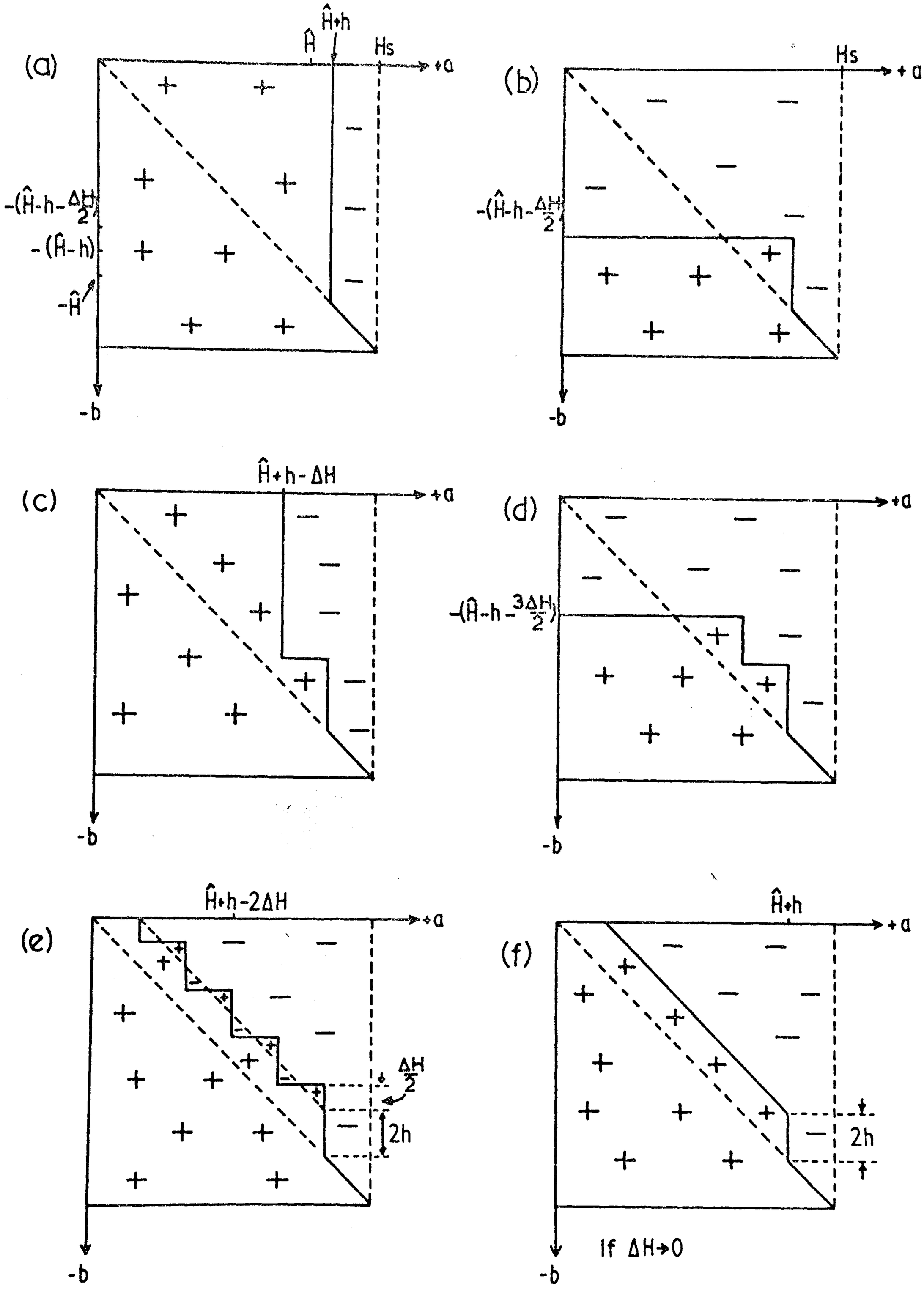


Fig 10.16 Production of ARM by superimposed direct field, h, on peak alternating field, $\hat{H}$, represented on Preisach diagrams. Hs is the saturation magnetisation, and $\Delta H/2$ the reduction in field at each half-cycle.

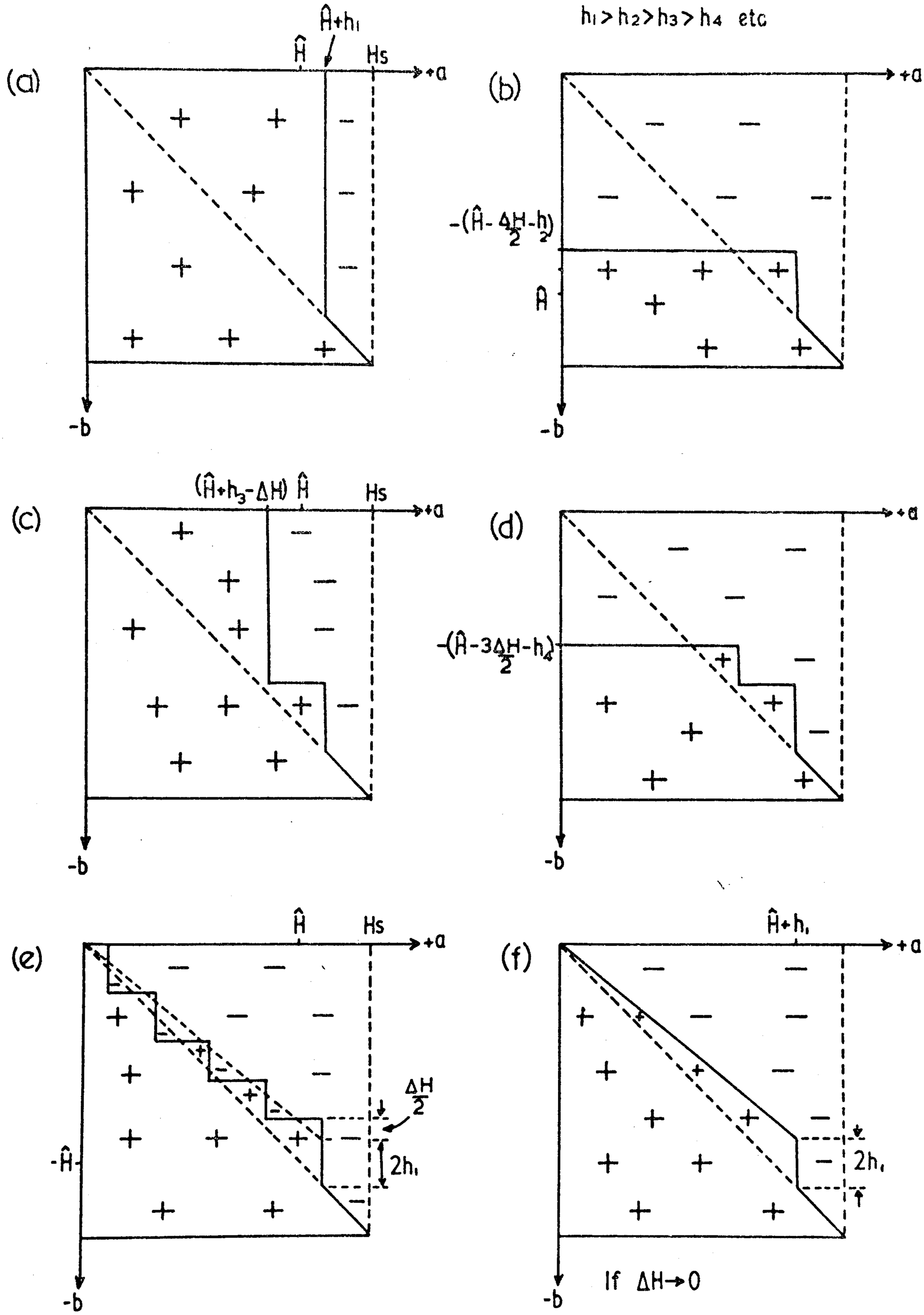


Fig 10.17 Production of ARM by asymmetrical alternating field, represented on Preisach diagrams. For explanation of nomenclature see text.

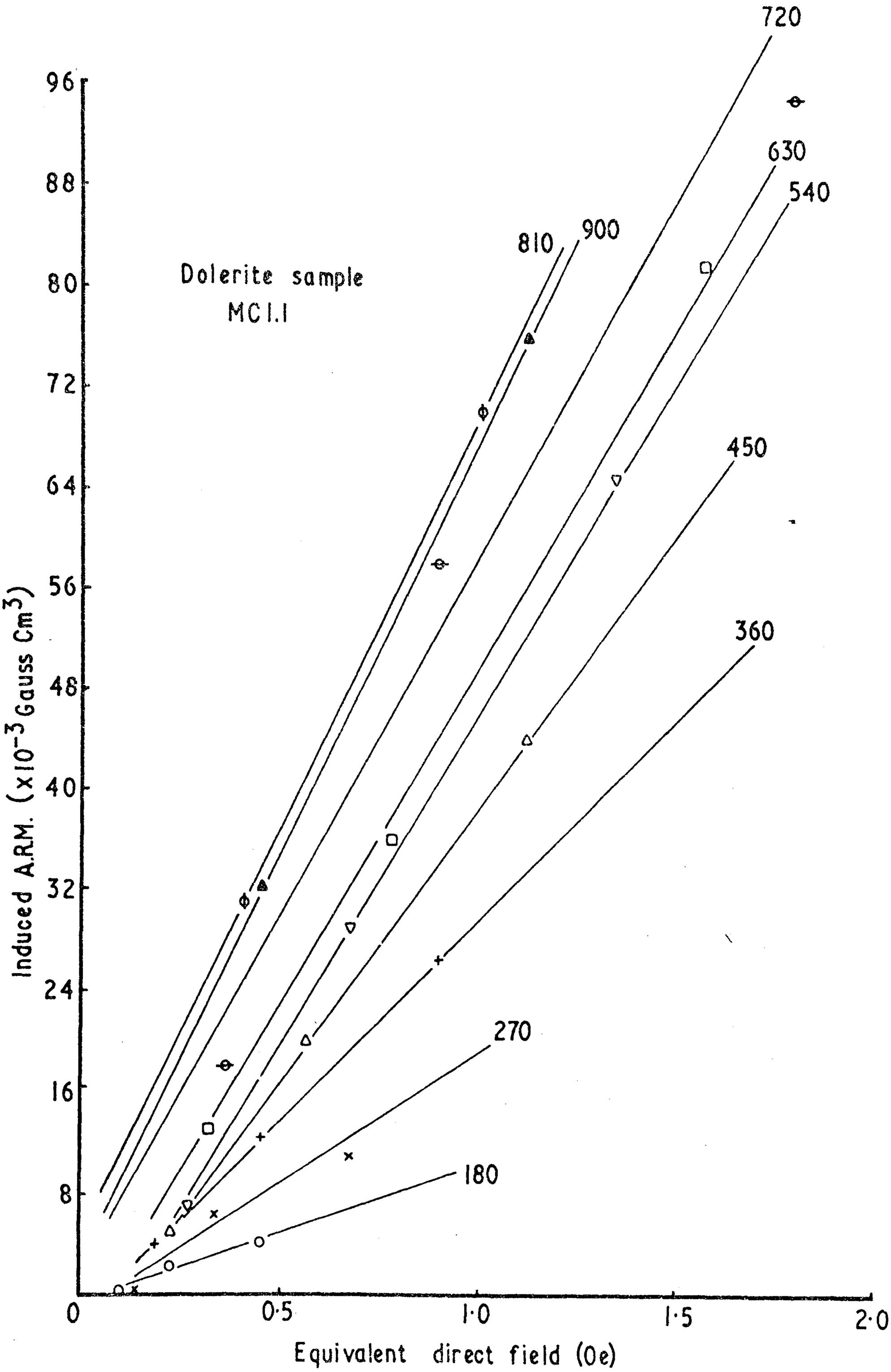


Fig 10.18 Induced ARM component plotted against equivalent peak direct field of asymmetry for sample MC1.1. Symbols refer to TAble 10.4. Numbers are peak altemating field values in Oe.

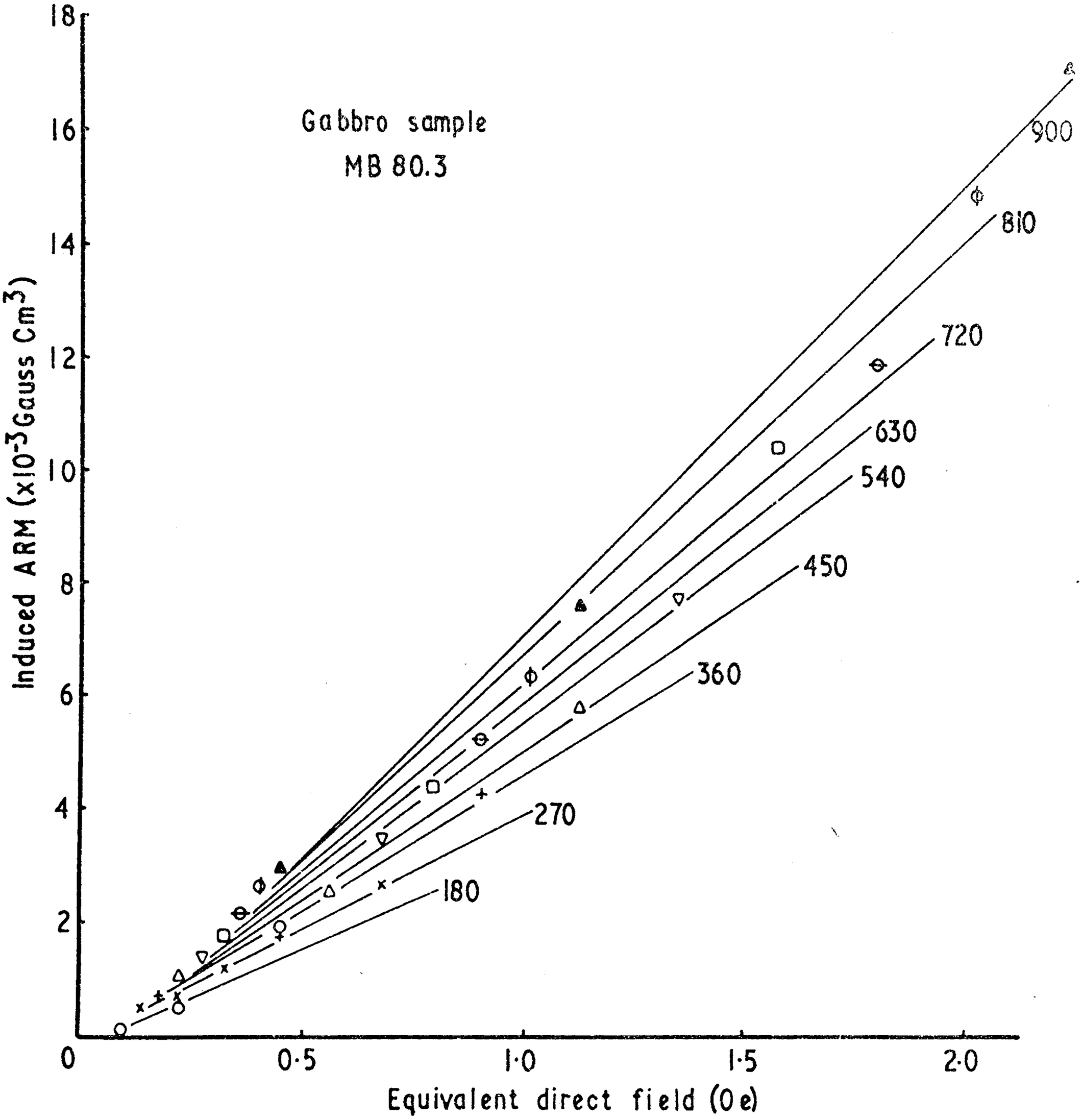


Fig 10.19 Induced ARM component plotted against equivalent peak direct field of asymmetry for sample MB80.3. Nomenclature as Fig 10,18.

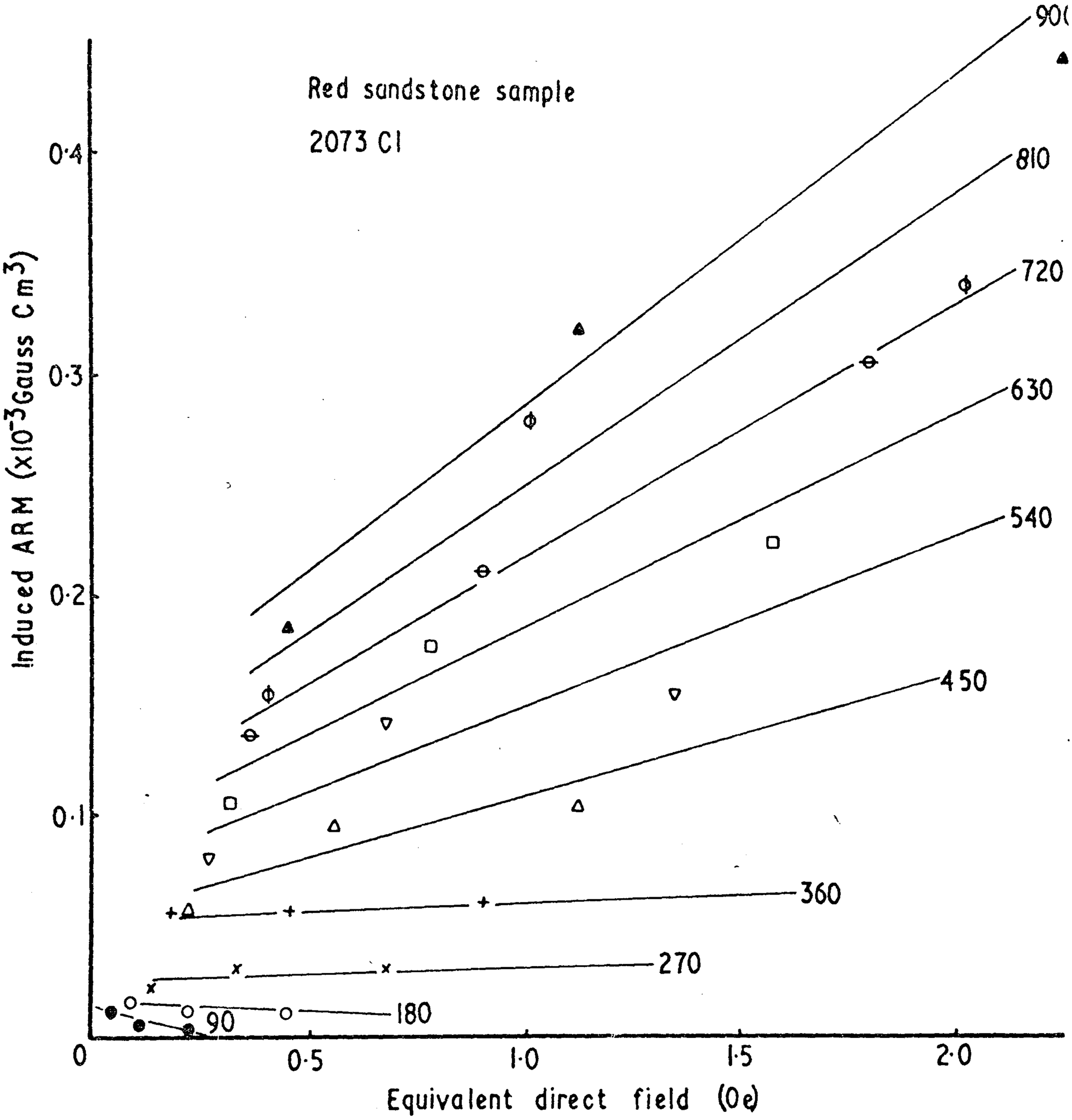


Fig 10.20 Induced ARM component plotted against equivalent peak direct field of asymmetry for sample 2073C1. Nomenclature as in Fig 10.20.

Table 10.1 Calibration of asymmetry circuit

$R_v(\Omega)$	Asym (%)	$R_v(\Omega)$	Asym (%)
1	1.09	7	0.27
2	0.75	8	0.24
3	0.57	10	0.22
4	0.48	12	0.19
5	0.40	15	0.16
6	0.33	20	0.13
		25	0.09

Table 10.2 Attenuation of asymmetry by tuned coil circuit

Asym. in tuned coil circuit (%)	Asym. in mains supply (%)
0.09	4.0
0.12	5.0
0.16	6.7
0.19	8.3
0.22	10.0
0.24	12.5
0.27	14.3
0.33	16.5
0.40	20.0
0.48	25.0

Table 10.3 Sample MC6.1 (dolerite). Induced ARM component along z-axis produced by different percentage asymmetries at peak field of 180 Oe.

Asym	Run No.	Measured component* No. Asym.	With Asym.	Induced* component	Mean induced* component	σm
0.05	1	-0.36	-0.61	-0.25	-0.42	$\pm$0.10
	2	-0.19	-0.79	-0.60		
	3	-0.46	-0.87	-0.41		
0.07	1	-0.24	-0.87	-0.63	-0.53	$\pm$0.13
	2	-0.40	-1.10	-0.70		
	3	-0.57	-0.84	-0.27		
0.12	1	-0.79	-1.45	-0.66	-0.88	+0.11
	2	-0.67	-1.65	-0.98		
	3	-0.65	-1.67	-1.01		
0.25	1	-0.71	-2.04	-1.33	-1.22	$\pm$0.11
	2	-0.78	-2.11	-1.33		
	3	-0.89	-1.90	-1.01		
0.50	1	-0.84	-2.87	-2.03	-1.58	$\pm$0.24
	2	-1.04	-2.55	-1.51		
	3	-0.89	-2.11	-1.22		

* $x10^{-3}$ gauss cm^3

Table 10.4 Variation of induced ARM component along z-axis of sample with asymmetry of applied A.F.

Sample No.		MC1.1(dolerite)			MB80.3(gabbro)			2073C1(red sandstone)		
Symbol Fig.	Peak AF demag.field (Oe)	0.1%	0.25%	0.5%	0.1%	0.25%	0.5%	0.1%	0.25%	0.5%
	90	0.33	0.21	0.30*	0.11	0.05	0.60*	0.11	0.03	0.02+
	180	0.37	2.27	3.57	0.10	0.47	1.90	0.16	0.11	0.09
	270	0.61	6.37	10.91	0.48	1.19	2.67	0.22	0.30	0.28
	360	4.04	12.29	26.39	0.69	1.79	4.24	0.55	0.56	0.58
	450	5.01	19.76	43.87	1.01	2.56	5.82	0.57	0.96	1.03
	540	6.89	28.96	64.70	1.31	3.46	7.75	0.80	1.42	1.55
	630	13.78	36.20	81.70	1.75	4.39	10.43	1.06	1.77	2.24
	720	18.07	57.90	94.90	2.16	5.24	11.95	1.37	2.11	3.07
	810	30.91	70.20	124.00	2.62	6.38	14.96	1.54	2.79	3.41
	900	32.51	75.60	153.10	2.95	7.60	17.19	1.85	3.21	4.44

* $\times 10^{-3}$ cm^3 + $\times 10^{-4}$ gauss cm^3

Table 10.5 ARMs produced by superimposed direct fields of 0.5 Oe

Peak A.F. (Oe)	Dolerite sample MC1.1	Red sandstone sample 2073 C1
90	1.10×10^{-2} gauss cm^3	0.62×10^{-4} gauss cm^3
180	2.17	1.14
270	3.82	1.73
360	5.49	2.26
450	6.36	2.54
540	7.47	2.68

Table 10.8 Peak direct field equivalents of percentage asymmetries

Peak H	0.1%	0.25%	0.5%
90	0.045	0.110	0.220
180	0.090	0.225	0.450
270	0.135	0.335	0.675
360	0.180	0.450	0.900
450	0.225	0.560	1.125
540	0.270	0.675	1.350
630	0.315	0.785	1.575
720	0.360	0.900	1.800
810	0.405	1.010	2.025
900	0.450	1.125	2.250